

Doctoral thesis:

Greenhouse gases in reservoirs: from watersheds to functional genes

Elizabeth León Palmero

Granada, 2021

Doctoral Thesis:

Greenhouse gases in reservoirs:
from watersheds to functional genes

Elizabeth León Palmero

Departamento de Ecología



Universidad de Granada

Programa de Doctorado en Biología Fundamental y de Sistemas

Granada, 2021

Editor: Universidad de Granada. Tesis Doctorales
Autor: Elizabeth León Palmero
ISBN: 978-84-1306-769-8
URI: <http://hdl.handle.net/10481/66668>

This thesis has been carried out at the Departamento de Ecología and Instituto del Agua of the Universidad de Granada. The research was funded by the project HERA (CGL2014-52362-R) to I.Reche and R. Morales-Baquero of the Spanish Ministry of Economy and Competitiveness, the Modeling Nature Scientific Unit (UCE.PP2017.03) of the Universidad de Granada – Unidades de Excelencia to I. Reche; and the European Regional Development Fund (ERDF; grant no. SOMM17/6109/UGR). E. León Palmero was supported by a PhD fellowship FPU (Formación del Profesorado Universitario: 014/02917) from the Ministry of Education, Culture y Sports. The research stays at the Geosciences Department of Princeton University (NJ, EEUU), hosted by Dr. B.B. Ward, were funded by a PhD International Mobility scholarship from the Universidad de Granada (2017), and a short stay grant for FPU grant holders from the Spanish Ministry of Science, Innovation and Universities (2018).

Agradecimientos

En primer lugar, me gustaría agradecer a mis directores Isabel y Rafa por darme la oportunidad de desarrollar esta investigación, por guiarme en este duro proceso, por enseñarme tanto y por darme siempre la libertad para desarrollar mis propias ideas y madurar como científica. Gracias, Rafa, porque has estado conmigo en la barca en cada muestreo. Gracias, Isabel, por todas las veces que te has sentado conmigo a explicarme los entresijos de la ciencia. Esta tesis no se podría haber desarrollado sin la inconmensurable ayuda de todo el personal técnico involucrado: Eulogio, alias MacGyver, Gustavo en citometría, y Ana durante los análisis genéticos. Por supuesto Alba, con quien me he reído y trabajado a partes iguales, y con quien he compartido fatigas y alguna noche de muestreo en Iznájar. También gracias a María del Mar y a Gerardo por ayudarme en los muestreos. Y gracias a Elo por echarme una mano con la docencia, y en aquel primer muestreo en el que estaba tan perdida...

También me gustaría mostrar mi más sincero agradecimiento a Ana, Dori y Jesús, del grupo de Química Física de la Universidad de Cádiz, por acogerme en vuestro laboratorio, por todo lo que me habéis enseñado durante este tiempo, y, sobre todo, por la amabilidad con la que siempre me habéis tratado.

To Hans-Peter Grossart, and his research group, thanks for you help introducing me in the greenhouse gas sampling and analysis. Thanks to the members of the Ward Lab at Princeton University, for teaching me so much about nitrogen, and about science. To Bess, for letting me be part of the *N babes* for a while. To Amal, for your help with the genetic analysis. To Claudia, for your knowledge sharing, and for being such a kind and cool person and scientist. I absolutely loved working with you, and the spare time we spent together =D. To Xin, for being so nice to me. I will never forget your master class on Chinese food at the Cantonese restaurant. What a nice way to say *see you soon!*

A mis compis del Instituto del Agua y del Departamento de Ecología, por todo el tiempo que hemos compartido, por las veces que nos hemos apoyado, por la aventura que pasamos en Holanda y las veces que hemos intentado arreglar el mundo entre cervezas. A Gema, que tanto me ha enseñado. A Ada, me es imposible resumir aquí todo lo que te debo. A Dani con su vitalidad y las risas que hemos

compartido, a Juanma y su eterno buen humor, a Marco y el tiempo que pasamos en Coimbra, y Alba y su amor por los gatos...

A Juani y a Esther, habéis aparecido en mi vida como un oasis en mitad del desierto.

A Agustín, por todas las historias que acumulamos juntos, por la confianza y complicidad que solo los mejores amigos entienden. Ojalá algún día volver a coger el coche y escaparnos.

A Elena, por acogerme siempre con los brazos abiertos en Cádiz, por tu dulzura, por tu optimismo contagioso, por los paseos científicos a pie de playa y por tantos buenos momentos que hemos compartido durante estos años. Todo el mundo debería tener a alguien como tú en su vida, eres una fuente de inspiración para mí.

A Ecologistas en Acción Baena, por alimentar mi pasión por la naturaleza, a todos los profes que he tenido y que tanto me han enseñado, a Cándido por ser un referente moral...

A Nico, por estar siempre ahí, por guiarme y ayudarme tanto con la tesis, por quererme y apoyarme, por aguantar tantos malos ratos y compartir conmigo tan buenos momentos.

Gracias a mi familia: a mis padres, mis abuelos, mi hermana, mi cuñado, y mi Elías, sois un pilar fundamental en mi vida, y el anclaje que me mantiene con los pies en el suelo. Día a día me enseñáis el valor del esfuerzo y el trabajo duro. Gracias, Estela, por escucharme sin entenderme, y apoyarme siempre. Y a mi Elías, que es el único capaz de sacarme de mi propia cabeza.

A todAs las que pasaron por aquí antes que yo, y me han permitido ser y estar.

A todas las personas que he nombrado, y a las que no, pero igualmente me habéis ayudado durante estos años de alguna manera u otra. A todas, os dedico la tesis a todas vosotras.

“Science and everyday life cannot and should not be separated”

Rosalind Franklin

“Reserve your right to think, for even to think wrongly is better than not to think at all.”

Hypatia

Table of contents

Resumen	15
Summary	19
Graphical abstract	23
Glossary of abbreviations	25
Chapter 1: General Introduction	27
1. 1. Greenhouse gases: CO ₂ , CH ₄ and N ₂ O	29
1. 2. The role of inland waters in CO ₂ and CH ₄ global budgets	31
1. 3. The role of inland waters in N ₂ O global budget	37
1. 4. Emissions of CO ₂ , CH ₄ , and N ₂ O from reservoirs	48
1. 5. Objectives and structure of the thesis	55
1. 6. References	56
Chapter 2: Material and methods	73
2. 1. Study reservoirs, morphometry and watershed characterization	75
2. 1. 1. Study reservoirs	75
2. 1. 2. Morphometry characterization	79
2. 1. 3. Watershed characterization	81

Table of contents

2. 1. 4. Reservoir samplings	84
2. 2. Greenhouse gas fluxes quantification	85
2. 2. 1. Greenhouse gas fluxes quantification	85
2. 2. 2. Discriminative algorithm for CH ₄ ebullitive and diffusive fluxes	89
2. 3. Physico-chemical analysis in the water column	92
2. 3. 1. Vertical profiles of the water column	92
2. 3. 2. CH ₄ and N ₂ O concentration in the water column.	94
2. 3. 3. Dissolved inorganic carbon (DIC) and dissolved organic carbon (DOC) concentration	96
2. 3. 4. Chromophoric dissolved organic matter (CDOM) analysis	96
2. 3. 5. Total nitrogen (TN), total dissolved nitrogen (TDN) and dissolved inorganic nitrogen (DIN) concentration	97
2. 3. 6. Total phosphorus (TP), total dissolved phosphorus (TDP) and soluble reactive phosphorus (SRP) concentration	98
2. 4. Biological analyses	98
2. 4. 1. Chlorophyll- <i>a</i> concentration and Reservoir metabolism	98
2. 4. 2. Abundance of prokaryotes, cyanobacteria and picoeukaryotes	102
2. 4. 3. Functional genes	103
2. 5. Experiments	108
2. 5. 1. Photoproduction of CO ₂ , CH ₄ , and N ₂ O	108
2. 5. 2. Microbial N ₂ O production using ¹⁵ N tracers	109
2. 6. Statistical tests	110
2. 7. References	111
Chapter 3: Greenhouse gas fluxes from reservoirs determined by watershed lithology, morphometry, and anthropogenic pressure	119
Chapter 4: Daily patterns of greenhouse gas emissions in reservoirs: evidence of CO ₂ and N ₂ O photoproduction	147
Chapter 5: Dissolved CH ₄ coupled to photosynthetic picoeukaryotes in oxic waters and to cumulative chlorophyll <i>a</i> in anoxic waters of reservoirs	187
Chapter 6: Dissolved N ₂ O driven by nitrogen and the <i>nirS</i> gene abundance in the water column of reservoirs	237

Table of contents

Chapter 7: Nitrous oxide production from ammonium and nitrate in the water column of two reservoirs	273
Chapter 8: General Discussion	317
Conclusiones Generales	341
General Conclusions	345
Peer review and scientific outreach publications	349
Appendixes	351
Appendix 1: Publication Atenuación de la luz en embalses del sur-este de la Península Ibérica (Light attenuation in Southern Iberian Peninsula reservoirs) .	353
Appendix 2: El uso del suelo en las cuencas de captación condiciona la calidad del agua en embalses del sudeste peninsular ibérico (Land-use on the watershed determines the quality of water in Southern Iberian Peninsula reservoirs)	371
Appendix 3: Supplementary material for Chapter 3	385
Appendix 4: Supplementary material for Chapter 4	429
Appendix 5: Supplementary material for Chapter 5	439
Appendix 6: Supplementary material for Chapter 6	457
Appendix 7: Supplementary material for Chapter 7	471
Appendix 8: Supplementary material for Chapter 8	483

Table of contents

Resumen:

Los embalses son fuentes significativas de gases de efecto invernadero (GEI), como dióxido de carbono (CO_2), metano (CH_4) y óxido nitroso (N_2O). Sin embargo, nuestro conocimiento sobre los flujos de GEI de los embalses es muy limitado a escala latitudinal y temporal (Deemer *et al.*, 2016) y hay aún muchas incertidumbres sobre la producción de GEI y los factores ambientales que la determinan. Además, el CH_4 y el N_2O absorben la radiación infrarroja con mayor intensidad que el CO_2 (IPCC, 2013) y, en consecuencia, su contribución al forzamiento radiativo deber evaluarse con mayor frecuencia.

En esta tesis doctoral hemos cuantificado los flujos, concentraciones y producción de CO_2 , CH_4 y N_2O en embalses mediterráneos, con un particular énfasis en el CH_4 y el N_2O . Seleccionamos doce embalses en el sur de España, situados en cuencas con diversas litologías y usos del suelo, y que cubren un amplio rango de variabilidad en edad, morfometría y características químicas y tróficas.

Medimos los flujos de CO_2 , CH_4 y N_2O en doce embalses durante la estratificación estival y la mezcla invernal. Los flujos de GEI presentaron una alta variabilidad entre sistemas y entre estaciones, de más de tres órdenes de magnitud. Algunos embalses fueron sumideros y otros fuentes de CO_2 y N_2O , pero todos los

Resumen

embalses fueron fuentes de CH₄. Los embalses ubicados en cuencas calcáreas actuaron como fuentes de CO₂ y como sumideros cuando la litología de la cuenca era predominantemente silíceas. Los embalses que actuaron como fuentes de N₂O están localizados en cuencas dominadas por zonas agrícolas y urbanas, mientras que los embalses que actuaron como sumideros de N₂O están localizados en cuencas con más de un 40 % de cobertura forestal. Las emisiones de CH₄ estuvieron determinadas por la profundidad media del embalse y la temperatura del agua. El forzamiento radiativo fue sustancialmente mayor durante la estratificación estival (125 - 31.884 mg CO₂ equivalentes m⁻² d⁻¹) que durante la mezcla invernal (29 - 722 mg mg CO₂ equivalentes m⁻² d⁻¹).

Exploramos los patrones diarios en los flujos de CO₂, N₂O y los componentes difusivo y ebullitivo de las emisiones de CH₄ en dos embalses eutróficos (Cubillas e Iznájar). Encontramos una variabilidad diaria significativa en los tres flujos de GEI, con emisiones más elevadas durante el día que durante la noche y patrones similares para los flujos de CO₂, N₂O y el CH₄ difusivo. Estas emisiones de GEI estuvieron acopladas con el ciclo solar diario, la velocidad del viento, la temperatura del agua y la saturación de oxígeno. Detectamos experimentalmente la producción fotoquímica de carbono inorgánico disuelto y N₂O, que fue responsable de una fracción relevante de la producción diaria de CO₂ y N₂O en las aguas superficiales.

A continuación, cuantificamos las concentraciones de CH₄ y N₂O disueltos en la columna de agua de estos doce embalses. El CH₄ disuelto varió hasta cuatro órdenes de magnitud (0.02 – 213.64 μmol L⁻¹), y tanto las profundidades oxigénicas como las anóxicas, estuvieron consistentemente supersaturadas de CH₄. La biomasa de fitoplancton y la producción primaria estuvieron relacionadas con la concentración de CH₄ en estos embalses. En las aguas anóxicas, la concentración de CH₄ estuvo significativamente correlacionada con la concentración de clorofila-*a* acumulada en profundidad, que es una aproximación para medir la biomasa fitoplanctónica exportada de toda la columna de agua hacia los sedimentos. En las aguas oxigénicas, la concentración de CH₄ disuelto estuvo significativamente correlacionada con la abundancia de picoeucariotas fotosintéticos durante ambos períodos. La profundidad media de los embalses, como indicador del transporte vertical del CH₄ producido en el sedimento a las aguas oxigénicas, también

contribuyó inversamente a determinar la concentración de CH₄ en las aguas oxigénicas.

La concentración de N₂O disuelto en la columna de agua varió hasta tres órdenes de magnitud (4.7 - 2441.2 nmol L⁻¹). Detectamos subsaturación y supersaturación de N₂O a diferentes profundidades de la misma columna de agua. La concentración de N₂O se correlacionó con la concentración de nitrógeno total (TN) y el hipolimnion anóxico de los embalses actuó como un sumidero o fuente de N₂O dependiendo de esta concentración de TN. Las arqueas oxidadoras de amonio (es decir, que contienen el gen *arch-amoA*) dominaron sobre las bacterias oxidadoras de amonio (es decir, que contienen el gen *bac-amoA*), pero su abundancia no estuvo relacionada con la concentración de N₂O. En cambio, la concentración de N₂O estuvo significativamente relacionada la abundancia de las bacterias desnitrificantes (es decir, que contienen el gen *nirS*). Detectamos el gen *nirS* de forma consistente en la columna de agua de todos los embalses, tanto en condiciones anóxicas como oxigénicas. La abundancia del gen *nirS* se correlacionó con la concentración de fósforo total y la clorofila-*a* acumulada en profundidad. Juntas, la concentración de TN y la abundancia de *nirS* explicaron la concentración de N₂O disuelto en los embalses estudiados. Estos resultados indican que la columna de agua de los embalses es un lugar activo para la producción de N₂O, que puede producirse tanto en condiciones oxigénicas como anóxicas por desnitrificación.

Finalmente, usamos isótopos estables como trazadores (¹⁵N-NH₄⁺ and ¹⁵N-NO₃⁻) para cuantificar la producción de N₂O en dos embalses eutróficos al comienzo y al final de la estratificación estival. La producción de N₂O a partir de amonio varió entre 0.3 y 22.2 nmol-N L⁻¹ d⁻¹ en el embalse de Cubillas, y entre 0.1 y 38.0 nmol-N L⁻¹ d⁻¹ en el embalse de Iznájar. La producción de N₂O a partir de nitrato varió entre 6.2 y 12.5 nmol-N L⁻¹ d⁻¹ en el embalse de Cubillas, y entre 3.2 y 117.7 nmol-N L⁻¹ d⁻¹ en el embalse de Iznájar. También detectamos elevadas tasas de nitrificación y de reducción de nitrato a nitrito. La producción de N₂O a partir de amonio estuvo significativamente relacionada con las tasas de nitrificación, y fue una función de la abundancia *in situ* del gen *nirS* y la concentración de carbono orgánico disuelto. Este hecho sugiere un acoplamiento entre la nitrificación y la desnitrificación en la columna de agua. También encontramos que la producción de N₂O podría estar

Resumen

promovida por la materia orgánica autóctona exportada en la columna de agua (es decir, la concentración de clorofila-*a* acumulada en profundidad).

En general, esta tesis doctoral ha contribuido al inventario global de los flujos de GEI de los embalses del bioma mediterráneo, mostrando la gran variabilidad entre sistemas, entre estaciones y diaria de los flujos, que debe considerarse en las estimaciones de GEI a escala global. Nuestros resultados también indican que la futura construcción de embalses puede reducir su forzamiento radiativo mediante la selección de ubicaciones óptimas en cuencas de roca silíceas, en paisajes forestales y cañones profundos. Demostramos que la eutrofización promueve la producción de metano y óxido nítrico y, por lo tanto, aumenta el forzamiento radiativo de los embalses. Por lo tanto, la reducción de la entrada de N y P a las aguas continentales podría prevenir la degradación de los recursos hídricos y reducir las emisiones de GEI de los embalses ya construidos.

Summary:

Reservoirs are significant sources of the greenhouse gases (GHGs), as carbon dioxide (CO₂), methane (CH₄), and nitrous oxide (N₂O). However, our knowledge on the GHG fluxes from reservoirs is still very limited at latitudinal and temporal scales (Deemer *et al.*, 2016), and there are many uncertainties on the GHG production and environmental drivers. In addition, CH₄, and N₂O absorb infrared radiation more intensely than CO₂ (IPCC, 2013) and, consequently, their contribution to the radiative forcing should be assessed more often.

In this PhD dissertation, we have quantified the fluxes, concentrations, and production of CO₂, CH₄, and N₂O in Mediterranean reservoirs, with a particular emphasis on the CH₄ and N₂O. We selected twelve reservoirs in the southern Spain, located in watersheds with diverse lithologies and land-uses, and covering a wide range of variability in age, morphometry, and chemical and trophic characteristics.

We measured the fluxes of CO₂, CH₄, and N₂O in twelve reservoirs during the summer stratification and the winter mixing. GHGs fluxes presented a high inter-system and inter-season variability ranging more than three orders of magnitude. Some reservoirs were sinks, and other sources for CO₂ and N₂O fluxes, but all reservoirs were CH₄ sources. The reservoirs located in calcareous watersheds were

Summary

CO₂ sources, and were sinks of CO₂ when the lithology of the watershed was predominantly siliceous. We found that reservoirs acting as N₂O sources were located in watersheds dominated by agricultural and urban areas, while the reservoirs acting as N₂O sinks were located in watersheds with more than 40 % of forestal coverage. The CH₄ emissions were determined by the reservoir mean depth and the water temperature. The radiative forcing was substantially higher during the summer stratification (125 - 31,884 mg CO₂ equivalents m⁻² d⁻¹) than during the winter mixing (29 - 722 mg CO₂ equivalents m⁻² d⁻¹).

We explored the daily patterns in the fluxes of CO₂, N₂O, and the diffusive and the ebullitive components of CH₄ in two eutrophic reservoirs (i.e. Cubillas and Iznájar). We found a significant daily variability in the GHG fluxes with higher emissions during the daytime than during the nighttime and similar daily patterns for CO₂, N₂O, and diffusive CH₄ fluxes. These GHG emissions were coupled with the daily solar cycle, wind speed, water temperature, and oxygen saturation. We experimentally detected photochemical production of dissolved inorganic carbon and N₂O, that can be responsible for a relevant fraction of the daily CO₂ and N₂O production in surface waters.

Next, we quantified the dissolved CH₄ and N₂O concentrations in the water column of these twelve reservoirs. The dissolved CH₄ varied up to 4 orders of magnitude (0.02 – 213.64 μmol L⁻¹), and both oxic and anoxic depths were consistently supersaturated. The CH₄ concentration was related to phytoplankton biomass and primary production in these reservoirs. In anoxic waters, the CH₄ concentration was significantly correlated to the depth-cumulative chlorophyll-*a* concentration, that is a proxy for the phytoplanktonic biomass exported from the whole water column toward the sediment. In oxic waters, the dissolved CH₄ concentration was significantly correlated to the photosynthetic picoeukaryotes abundance during both periods. The mean depth of the reservoirs, as a surrogate of the vertical transport of the CH₄ produced in the sediment to the oxic waters, also contributed inversely to the CH₄ concentration in oxic waters.

The dissolved N₂O concentration in the water column varied up to three orders of magnitude (4.7 - 2441.2 nmol L⁻¹). We detected N₂O undersaturation and supersaturation at different depths of the same water column. The concentration of N₂O was correlated to the total nitrogen (TN) concentration. The anoxic

hypolimnion of reservoirs acted as a N₂O sink or source depending on this TN concentration. The ammonia-oxidizing archaea (i.e., the occurrence of arch-*amoA* gene) dominated over the ammonia-oxidizing bacteria (i.e., the occurrence of bac-*amoA* gene), but their abundance was not related to the N₂O concentration. In contrast, the abundance of the denitrifying bacteria (i.e., the occurrence of the *nirS* gene) was significantly related to the N₂O concentration. We detected the *nirS* gene consistently in the water column of all reservoirs, both in anoxic and oxic conditions. The abundance of the gene *nirS* was correlated to the concentration of total phosphorus and the depth-cumulative chlorophyll-*a*. Together, the TN concentration and the *nirS* abundance explained the dissolved N₂O concentration in the study reservoirs. These results indicate that the water column in reservoirs is an active site for N₂O production, that may occur both in oxic and anoxic conditions by denitrification.

Finally, we used stable isotope tracers (¹⁵N-NH₄⁺ and ¹⁵N-NO₃⁻) to quantify the N₂O production in two eutrophic reservoirs at the beginning and at the end of the stratification process. The N₂O production from ammonium ranged from 0.3 to 22.2 nmol-N L⁻¹ d⁻¹ in the Cubillas reservoir, and from 0.1 to 38.0 nmol-N L⁻¹ d⁻¹ in the Iznájar reservoir. The N₂O production from nitrate varied from 6.2 to 12.5 nmol-N L⁻¹ d⁻¹ in the Cubillas reservoir, and from 3.2 to 117.7 nmol-N L⁻¹ d⁻¹ in the Iznájar reservoir. We also detected high rates of nitrification and nitrate reduction to nitrite. The N₂O production from ammonium was significantly related to the nitrification rates, and was a function of the *in situ* abundance of the *nirS* gene and dissolved organic carbon concentration, suggesting a coupled nitrification-denitrification in the water column. We also found that N₂O production may be promoted by the autochthonous organic matter exported in the water column (i.e., depth-cumulative chlorophyll-*a* concentration).

Overall, this dissertation contributed to the global inventory of GHG fluxes from reservoirs in the Mediterranean biome, and we showed the great variability at inter-system, inter-season, and daily scales of the fluxes, which must be considered in GHG estimates at global scale. Our results also indicate that future construction of reservoirs may reduce their radiative forcing by selecting optimal locations with siliceous bedrock, in forestal landscapes, and deep canyons. We demonstrated that eutrophication promotes the production of methane and nitrous oxide, and,

Summary

therefore, increases the radiative forcing of the reservoirs. Thus, the reduction of N and P loading into inland waters may prevent water resources degradation, and reduce the GHG emissions from the already constructed reservoirs.

References:

- Deemer, B. R., Harrison, J. A., Li, S., Beaulieu, J. J., DelSontro, T., Barros, N., Bezerra-Neto, J. F., Powers, S. M., dos Santos, M. A. and Vonk, J. A. (2016). Greenhouse gas emissions from reservoir water surfaces: a new global synthesis, *BioScience*, 66(11), pp. 949–964. doi: 10.1093/biosci/biw117.
- IPCC. (2013). *Climate Change 2013: The Physical Science Basis. Contribution of Working Group I to the Fifth Assessment Report of the Intergovernmental Panel on Climate Change* Cambridge, United Kingdom and New York, NY, USA: Cambridge University Press. Edited by T. F. Stocker, D. Qin, G.-K. Plattner, M. Tignor, S. K. Allen, J. Boschung, A. Nauels, Y. Xia, V. Bex, and P. M. Midgley. Available at: <https://www.ipcc.ch/report/ar5/wg1/>.

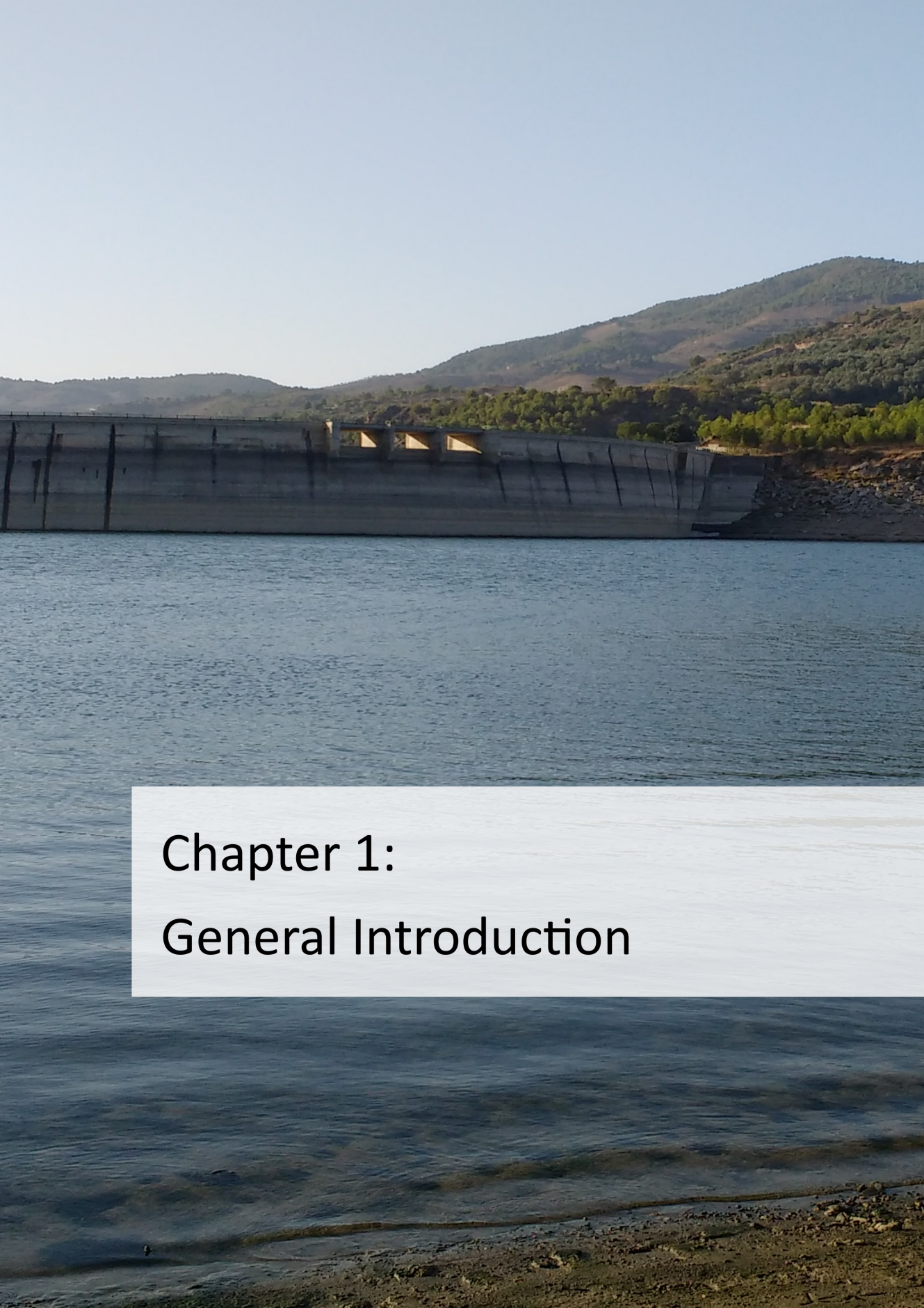
Graphical abstract

Glossary of abbreviations:

a ₃₂₅	Absorption coefficient at 325 nm
AIC	Akaike Information Criterion
AO	Ammonia Oxidation
AOA	Ammonia-Oxidizing Archaea
AOB	Ammonia-Oxidizing Bacteria
APHA	American Public Health Association
bp	base pair
C	Carbon
CDOM	Chromophoric Dissolved Organic Matter
CFCs	Chlorofluorocarbons
Chl-a	Chlorophyll-a
Comammox	COMplete AMMonia Oxidiser
CRDS	Cavity Ring-Down Spectroscopy
CTD	Conductivity Temperature Depth profiler
Cum Chl-a	Depth-cumulative chlorophyll-a concentration
CYA	Cyanobacteria
DIC	Dissolved Inorganic Carbon
DIN	Dissolved Inorganic Nitrogen
D _L	Shoreline development ratio
DNRA	Dissimilatory Nitrate Reduction to Ammonium
DO	Dissolved Oxygen
DOC	Dissolved Organic Carbon
F	Flux
FL1	Green fluorescence of the DNA stained with SYBR Green I
FL2	Orange fluorescence, phycoerythrin
FL3	Red fluorescence, chlorophyll-a
FL4	Blue fluorescence, phycocyanin
FTU	Formazin Turbidity Unit
GAM	Generalized Additive Model
GC	Gas Chromatograph
GC-IRMS	Gas Chromatography-Isotope Ratio Mass Spectrometry
GCV	Generalized Cross Validation criterion
GHG	Greenhouse Gases
GPP	Gross Primary Production
GW	GigaWatt

Glossary of abbreviations

GWP	Global Warming Potential
HCFCs	Hydrochlorofluorocarbons
ICP-OES	Inductively Coupled Plasma Optical Emission Spectrometry
IPCC	The Intergovernmental Panel on Climate Change
K	Kelvin, unit of temperature
k	Gas transfer coefficient/velocity
MPn's	Methyl-Phosphonates
N	Nitrogen
NEP	Net Ecosystem Production
NOAA	National Oceanic and Atmospheric Administration
NOB	Nitrite-Oxidizing Bacteria
P	Phosphorus
PA	Total Prokaryotes
Pa	Pascal, unit of pressure
PCR	Polymerase Chain Reaction
ppb	Parts per billion, unit of concentration
PPEs	Photosynthetic Picoeukaryotes
ppm	Parts per million, unit of concentration
qPCR	quantitative PCR
R	Respiration
$S_{275-295}$	Spectral slopes from 275 to 295 nm
$S_{350-400}$	Spectral slopes from 350 to 400 nm
SD	Standard Deviation
SE	Standard Error
S_R	Ratio of the spectral slopes from 275-295 nm and 350-400 nm
SRP	Soluble Reactive Phosphorus
SSC	Side Scatter
TDN	Total Dissolved Nitrogen
TDP	Total Dissolved Phosphorus
TN	Total Nitrogen
TOC	Total Organic Carbon
TP	Total phosphorus
WCD	World Commission on Dams
WMO	World Meteorological Organization
$\delta^{15}\text{N}$	Delta-N-15, a measure of the ratio of the two stable isotopes of nitrogen (15N:14N)



Chapter 1: General Introduction

Chapter 1 | Introduction

Chapter 1:

General Introduction

1. 1. Greenhouse gases: CO₂, CH₄ and N₂O

The increase in the concentration of greenhouse gases (GHG) in the atmosphere associated to anthropogenic activities is a major driver of climate change in the last century (IPCC, 2013; Murphy and Ravishankara, 2018). Carbon dioxide (CO₂), methane (CH₄), and nitrous oxide (N₂O), are the three main long-lived greenhouse gases in the troposphere, and they have increase by 147 %, 259 % and 123 % since the preindustrial era, respectively (IPCC, 2013; WMO, 2019) (Table 1.1). Carbon dioxide is the most important anthropogenic GHG in the atmosphere, contributing approximately by 66 % of the increase in the global radiative forcing, in 2018, since pre-industrial times. Methane and nitrous oxide are the second and the third anthropogenic GHG in relevance, and they contribute by 17 % and 6 %, respectively (Butler and Montzka, 2019). Other relevant GHG contributing to the global warming are the halogenated compounds, mainly chlorofluorocarbons (CFCs), as CFC-11, CFC-12, and also the hydrochlorofluorocarbons (HCFCs), as HCFC-22, and HCF-134a (Butler and Montzka, 2019). The increase in the concentration of these gases since 1979 is shown in Figure 1.1.

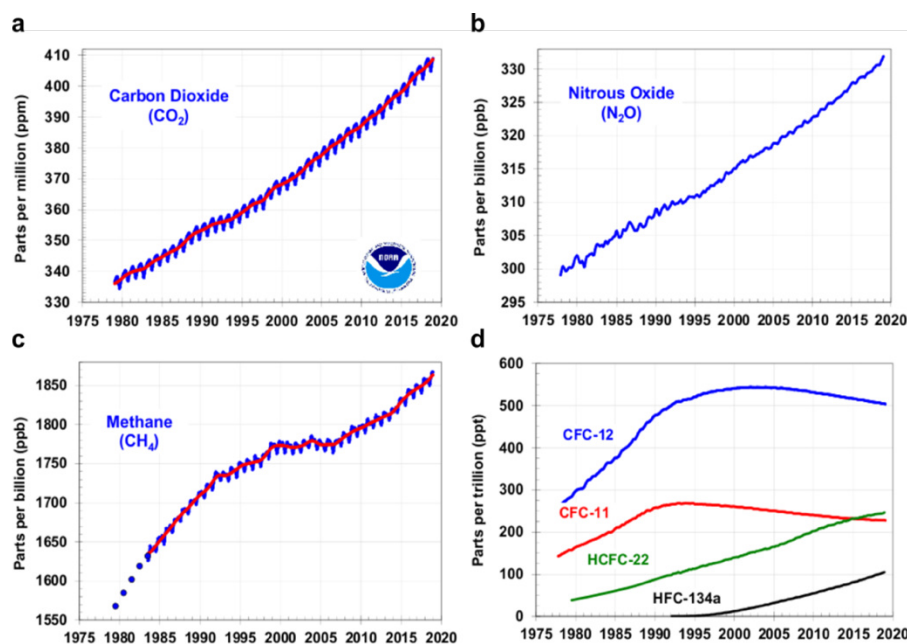


Figure 1.1. Global average concentrations of the major, well-mixed, long-lived greenhouse gases since 1979. (a) Carbon dioxide, (b) nitrous oxide, (c) methane, (d) CFC-12, CFC-11, HCFC-22, and HCF-134a. Modified from Butler and Montzka (2019).

Despite their lower concentrations in the atmosphere, CH₄ and N₂O absorb infrared radiation more intensely than CO₂ (Lashof and Ahuja, 1990), and they present a global warming potential (GWP) of 34, and 298 times, respectively, that of CO₂ for a 100-year timescale (IPCC, 2013). In addition, CH₄ and N₂O are ozone-depleting gases. N₂O, with a lifetime of 121 years in the troposphere, is the main driver of ozone depletion when it is transported toward the stratosphere (Ravishankara *et al.*, 2009). Therefore, we need a comprehensive knowledge of global sinks and sources of CO₂, CH₄, and N₂O to understand their changes over time and role in the climate change. However, there are still large uncertainties in the global balance of GHGs.

Table 1.1. Global trends in GHG since pre-industrial era (WMO, 2019). Units are dry air mole fractions.

	CO ₂	CH ₄	N ₂ O
Pre-industrial era mole fraction (before 1750)	278 ppm	772 ppb	270 ppb
2018 global mean abundance	407.8 ± 0.1 ppm	1869 ± 2 ppb	331.1 ± 0.1 ppb
2018 concentration relative to year 1750	147 %	259 %	123 %
Mean annual absolute increase over the last 10 years	2.26 ppm yr ⁻¹	7.1 ppb yr ⁻¹	0.95 ppb yr ⁻¹

1. 2. The role of inland waters in CO₂ and CH₄ global budgets

Inland waters (rivers, lakes and reservoirs) contribute significantly to the global carbon cycle, despite they only cover 5 - 8 % of the Earth's surface (Tranvik *et al.*, 2009; Mitsch *et al.*, 2012; Raymond *et al.*, 2013). They are an active part of carbon cycle in the landscape, and receive, process, emit, and store carbon in sediments in globally significant quantities (Cole *et al.*, 2007; Tranvik *et al.*, 2009; DelSontro *et al.*, 2018a) (Figure 1.2). The CO₂ emissions from inland waters have been estimated in 2.1 Pg C yr⁻¹ (Raymond *et al.*, 2013) (Figure 1.2), which are similar in magnitude to the global uptake of CO₂ by the global ocean (2.4 Pg C yr⁻¹) (Le Quéré *et al.*, 2018). The burial of organic carbon in the sediments of lakes and reservoirs at the global scale (0.15 Pg C yr⁻¹) (Mendonça *et al.*, 2017) (Figure 1.2) is similar to the organic carbon burial in the ocean floor (0.2 Pg C yr⁻¹) (IPCC, 2013).

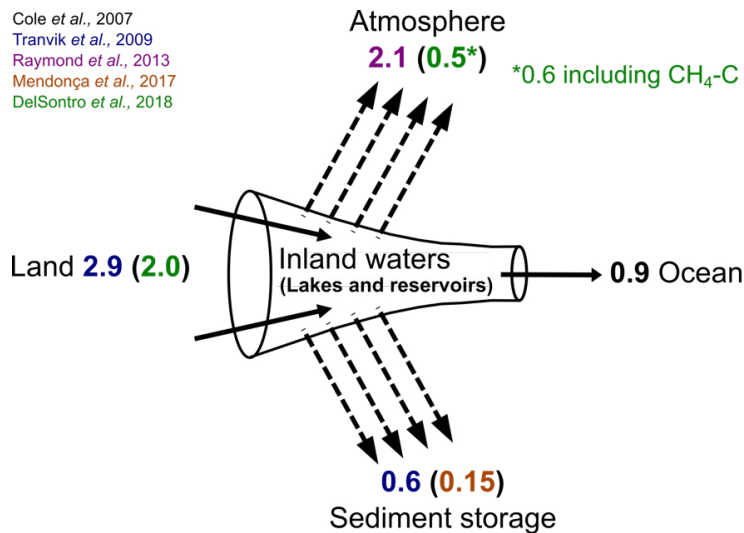
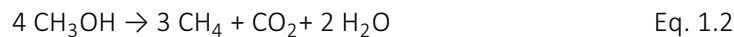


Figure 1.2. Inland waters as “an active pipe”. Schematic view of the “active pipe” hypothesis advanced by Cole *et al.* (2007), and revised by Tranvik *et al.* (2009), and DelSontro *et al.* (2018a). We also included the estimations from Raymond *et al.* (2013) and Mendonça *et al.* (2017). We included the estimations for inland waters, and for lakes and reservoirs inside the parentheses. Data are provided in Pg C yr⁻¹. Re-elaborated.

Lakes and reservoirs are usually supersaturated in CO₂ (Cole *et al.*, 1994), and they release 0.32 Pg C yr⁻¹ to the atmosphere (Raymond *et al.*, 2013). These systems are often heterotrophic, where the CO₂ production by microbial mineralization of dissolved organic carbon (DOC) exceeds the CO₂ uptake by photosynthesis. DOC is the most abundant form of organic carbon in most lakes and reservoirs, and it is

commonly dominated by terrestrial import from the watershed (i.e., allochthonous DOC) (Tranvik *et al.*, 2018). Consequently, the supersaturation in CO₂ is frequently attributed to the net heterotrophy of the system, but this explanation remains still insufficient, because we know now that there are other sources of CO₂ in aquatic systems. For instance, DOC mineralization also occurs by photochemical reactions. Sunlight decomposes dissolved organic matter in inorganic molecules, releasing CO₂ (Johannessen and Miller, 2001; Reche, 2003). Besides, photobleaching reactions break complex and recalcitrant organic molecules in smaller ones that enhances microbial DOC mineralization and, consequently, CO₂ production (Reche *et al.*, 1998; Ortega-Retuerta *et al.*, 2007). Koehler *et al.* (2014) calculated that up to 10 % of the global CO₂ emissions from inland waters are sunlight induced. On the other hand, the studies on lake metabolism have been traditionally conducted in carbonate-poor lakes, and they ignored the lakes located in calcareous watersheds, where the loadings of inorganic carbon during the weathering contribute significantly to CO₂ supersaturation (López *et al.*, 2011; McDonald *et al.*, 2013; Marcé *et al.*, 2015; Weyhenmeyer *et al.*, 2015).

Rivers, lakes and reservoirs are also supersaturated in CH₄, and they emit up to 77.5 – 134.4 Tg C yr⁻¹ (Bastviken *et al.*, 2011; Deemer *et al.*, 2016; Stanley *et al.*, 2016). That emission from inland waters represents more CH₄ than the emitted from the ocean surface (Saunio *et al.*, 2016). Traditionally, methanogenesis is considered as the formation of methane during the microbial decomposition of organic matter in anoxic conditions, such as lake sediments, and the intestinal tract of animals. Anoxic sediments are a primary source of CH₄ in inland waters (Segers, 1998) (Figure 1.3). The bacterial community ferments the organic matter to smaller organic compounds, as organic acids and alcohols, and then, these smaller organic compounds are converted into methane by methanogens from the domain of Archaea (Thauer, 1998). Archaeal methanogens produce methane by the hydrogenotrophic, acetoclastic, and methylotrophic pathways. The hydrogenotrophic pathway uses the CO₂ as terminal electron acceptor (Eq. 1.1), the methylotrophic pathway uses methyl-containing substances (i.e., methanol) as electron acceptors (Eq. 1.2), and the acetoclastic pathway uses the acetic acid as electron acceptor (Eq. 1.3) (Kampmann *et al.*, 2012):



Despite the differences in the electron acceptor, all known methanogens from the Archaea domain have the *methyl coenzyme-M reductase*, which is the enzyme responsible for the conversion of a methyl group to CH₄, and a widespread genetic marker for *Archaeal* methanogen studies (Grabarse *et al.*, 2001) (Figure 1.3). The methane produced in the anoxic sediment diffuses up to the water overlaying the sediment, and it is rapidly oxidized by methanotrophs to CO₂ in the presence of oxygen (Oswald *et al.*, 2015, 2016; Tang *et al.*, 2016; Schubert and Wehrli, 2018; Thalasso *et al.*, 2020). Therefore, the net production of CH₄ is determined by archaeal methanogenesis in anoxic conditions, and by methanotrophs, which consume CH₄ in oxic conditions (Schubert and Wehrli, 2018).

Archaeal methanogens are very sensitive to temperature, and quantity and quality of the organic substrate (Thanh-Duc *et al.*, 2010; West *et al.*, 2012; Marotta *et al.*, 2014; Yvon-Durocher *et al.*, 2014; Rasilo *et al.*, 2015; Sepulveda-Jauregui *et al.*, 2018). They are also affected by the extent of anoxia in the sediments, as far as they are obligate anaerobes and will not survive and produce CH₄ under aerobic conditions (Chistoserdova *et al.*, 1998; Schubert and Wehrli, 2018). However, many observations both in inland and marine waters have detected CH₄ supersaturation in the oxic layers. These observations are a widespread phenomenon called “*the methane paradox*” (Kiene, 1991; Owens *et al.*, 1991; Schmidt and Conrad, 1993; Schulz *et al.*, 2001; Murase *et al.*, 2003; Damm *et al.*, 2010; Grossart *et al.*, 2011; Bogard *et al.*, 2014; Tang *et al.*, 2014; Donis *et al.*, 2017).

The persistent CH₄ supersaturation in oxic layers of marine and inland waters requires alternative sources to compensate for the CH₄ losses by methanotrophy, and the emissions toward the atmosphere. These CH₄ sources might come from the anoxic sediments of the bottom and littoral zones, or from *in situ* sources in the oxic waters. The transport of CH₄ from the bottom and littoral sediments has been proposed as a plausible explanation of the supersaturation in several lakes (Rudd and Hamilton, 1978; Michmerhuizen *et al.*, 1996; Murase *et al.*, 2003; Bastviken *et al.*, 2004; Encinas Fernández *et al.*, 2016; Peeters *et al.*, 2019) (Figure 1.3). The vertical

and horizontal transport appears to be relevant in small lakes, but in deep and thermally stratified systems, the vertical diffusion of dissolved gases across the thermocline are too low, and apparently there is not upward movements of CH₄ from the hypolimnion (Rudd and Hamilton, 1978; Peeters *et al.*, 1996). CH₄ diffusion from shallow sediments in littoral zones may be a significant source in the open surface of small lakes and reservoirs (Encinas Fernández *et al.*, 2016; Peeters *et al.*, 2019) (Figure 1.3). However, lateral transport does not fully explain CH₄ supersaturation in the open ocean and large reservoirs and lakes. Therefore, other alternative CH₄ sources likely occur (Scranton and Brewer, 1977; Owens *et al.*, 1991; Schmidt and Conrad, 1993; Tilbrook and Karl, 1995; Schulz *et al.*, 2001; Damm *et al.*, 2010; Grossart *et al.*, 2011; Tang *et al.*, 2014; DelSontro *et al.*, 2018b).

Previous works demonstrated the CH₄ production in oxic waters using stable isotope techniques in experiments, mesocosms, and field samples (Bogard *et al.*, 2014; Tang *et al.*, 2016; DelSontro *et al.*, 2018b; Bižić *et al.*, 2020; Hartmann *et al.*, 2020) and using molecular approaches (Grossart *et al.*, 2011; Yao *et al.*, 2016; Khatun *et al.*, 2020) (Figure 1.3). There are different alternatives proposed as CH₄ sources in the literature. On the one hand, some studies have reported the occurrence of methanogenesis in micro-anoxic zones in the guts of fishes and zooplankton, in faecal pellets, and within sinking particles (Oremland, 1979; Bianchi *et al.*, 1992; de Angelis and Lee, 1994; Karl and Tilbrook, 1994) (Figure 1.3). However, the CH₄ production was too low to sustain the CH₄ supersaturation of the oxic waters (Tang *et al.*, 2014; Schmale *et al.*, 2018). On the other hand, there is a consistent link between dissolved CH₄ concentration and autotrophic organisms, primary production, and chlorophyll-*a* concentration (Owens *et al.*, 1991; Schmidt and Conrad, 1993; Grossart *et al.*, 2011; Bogard *et al.*, 2014; Tang *et al.*, 2014) (Figure 1.4). Grossart *et al.* (2011) detected potential methanogenic *Archaea* attached to photoautotrophs as Chlorophyta (Eukarya), and Cyanobacteria (Bacteria) in the epilimnion of an oligotrophic lake, and they confirmed the production of CH₄ in the presence of oxygen in laboratory incubations (Figure 1.3). If occurring, that symbiosis would require that the methanogens tolerate the oxygen exposure, in contrast to general belief (Jarrell, 1985; Angel *et al.*, 2011; Angle *et al.*, 2017).

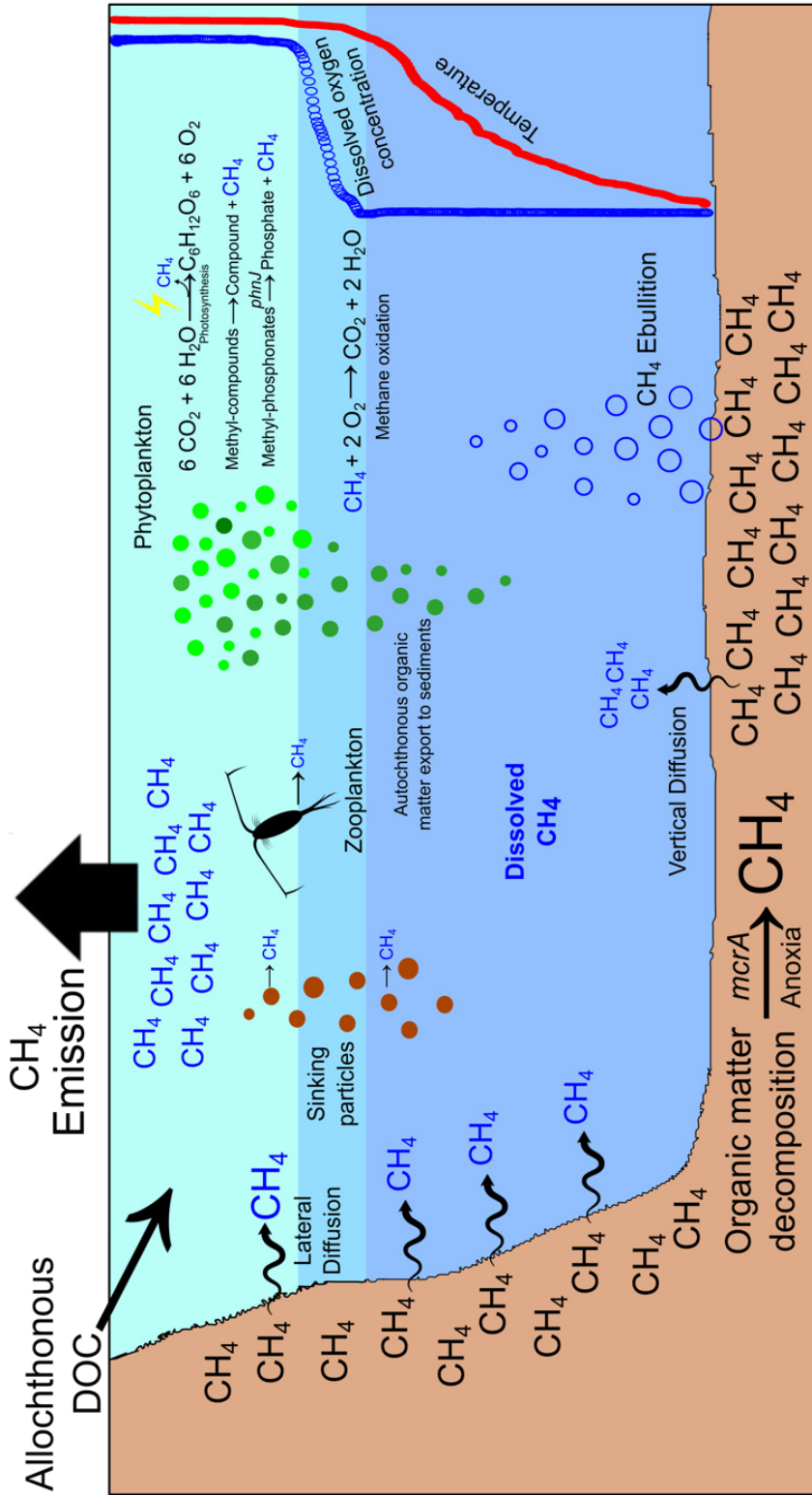


Figure 1.3. Main pathways of CH₄ production and transportation in a lake or reservoir. We show the classical production of CH₄ in sediments in anoxia, and the transportation of this CH₄ to the water column through diffusion (from bottom and lateral sediments), and ebullition. We also show the production of CH₄ in oxic waters from sinking particles, zooplankton, and phytoplankton related sources.

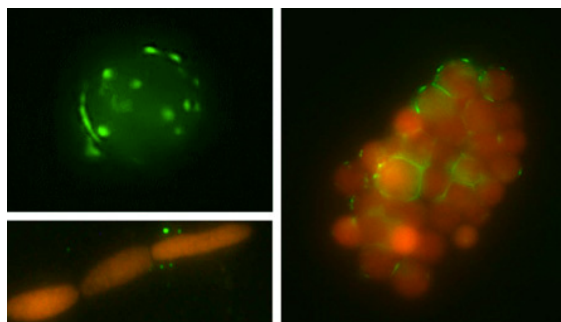


Figure 1.4. Direct attachment of methanogenic *Archaea* (green, FITC-labeled oligonucleotide probe) to autotrophs (red, autofluorescence) observed by FISH. (Upper Left) A single *Chlorella*-like algal cell. (Right) A colony of *Chlorella*-like green alga. (Lower Left) A filament of the cyanobacterium *A. flos-aquae*. Taken from Grossart *et al.* (2011).

New findings suggest that the link between phytoplankton and dissolved CH₄ may rely on diverse metabolic pathways in Bacteria and Eukarya. These metabolic pathways contribute to the dissolved CH₄ in oxic waters due to the degradation of methylated compounds. In the open ocean, archaea and bacteria appear to metabolize the abundant algal osmolyte dimethylsulfoniopropionate producing methane as a by-product (Damm *et al.*, 2008, 2010, 2015; Zindler *et al.*, 2013) (Figure 1.3). Common methyl-containing substances as methionine produce methane in algae, saprotrophic fungi, and plants (Lenhart *et al.*, 2012, 2015, 2016). Another reported pathway is the degradation of methyl-phosphonates (MPn's) as an alternative source of phosphorus (P) in phosphate-starved bacterioplankton. The hydrolysis of these compounds, using the enzyme C–P lyase, also releases methane as a by-product. This pathway appears in environments chronically P starved, as the ocean gyres, oligotrophic lakes, and microbial mats (Karl *et al.*, 2008; Beversdorf *et al.*, 2010; Gomez-Garcia *et al.*, 2011; Carini *et al.*, 2014; del Valle and Karl, 2014; Repeta *et al.*, 2016; Yao *et al.*, 2016; Wang *et al.*, 2017; Teikari *et al.*, 2018) (Figure 1.3). Recent studies using phytoplankton cultures and stable isotope techniques proposed that the production of CH₄ is directly related to photosynthesis in algae and cyanobacteria (Lenhart *et al.*, 2016; Klintzsch *et al.*, 2019; Bižić *et al.*, 2020; Hartmann *et al.*, 2020). All these alternative sources of CH₄ in oxic waters, however, still have not been tested simultaneously in reservoirs, despite the known high contribution of these aquatic ecosystems to global CH₄ emissions. We summarized all the explained pathways of CH₄ production and transportation in a lake or reservoir in Figure 1.3.

1. 3. The role of inland waters in N₂O global budget

The nitrogen (N) cycle is the most complex biogeochemical cycle on Earth (Thamdrup, 2012). N appears in diverse chemical forms with different valence states, and gaseous forms (Figure 1.5), and undergoes a variety of transformations that are mediated by specialized microorganisms (Thamdrup, 2012; Stein and Klotz, 2016). N cycle involves different compounds in the atmosphere, ocean, soil and sediment, the crust, and the biota. The most important pool of nitrogen is the dinitrogen gas (N₂) in the atmosphere.

Molecule	Name	Oxidation state
C-NH ₂	Organic-N	Reduced
NH ₃ , NH ₄ ⁺	Ammonia, Ammonium	-3
N ₂ H ₄	Hydrazine	-2
NH ₂ OH	Hydroxylamine	-1
N ₂	Dinitrogen	0
N ₂ O	Nitrous oxide	+1
NO	Nitric oxide	+2
HNO ₂ , NO ₂ ⁻	Nitrous acid, Nitrite	+3
NO ₂	Nitrogen dioxide	+4
HNO ₃ , NO ₃ ⁻	Nitric acid, Nitrate	+5
		Oxidized

Figure 1.5. Nitrogen intermediates and their oxidation states. Modified from Stein and Klotz (2016).

N is a limiting element for the biota, with a critical role in controlling primary production in the biosphere (Gruber and Galloway, 2008). Nitrogen-fixing microorganisms introduce the atmospheric N₂ into the biosphere, where N is assimilated and recycled and, eventually, other microbial processes as denitrification determine its return to the atmosphere. The generation and recycling of reactive nitrogen in the biosphere was exclusively a matter of microorganisms, until human beings developed the artificial synthesis of fertilizers by the Haber-Bosch process (i.e., the industrial fixation of N₂ into ammonia, NH₄⁺). The anthropogenic production of nitrogen fertilizer has doubled the inputs of this element into the Earth's surface, changing the nitrogen cycle at local, regional, and global scales (Gruber and Galloway, 2008; Battye *et al.*, 2017) (Figure 1.6). This change likely exceeds all the other human interventions in the cycles of nature (Gruber and Galloway, 2008; Schlesinger, 2009), but in comparison with the carbon cycle has received less attention (Battye *et al.*, 2017). In addition, other human activities also add fixed nitrogen by the cultivation of legumes with associated nitrogen-fixing bacteria, and by burning fossil fuels (Canfield *et al.*, 2010) (Figure 1.6). According to the planetary boundaries, which

describe a safe operating space for humanity, we have reached the dangerous level (i.e., high risk of serious impacts) in the nitrogen biogeochemical cycle (Steffen *et al.*, 2015) (Figure 1.7).

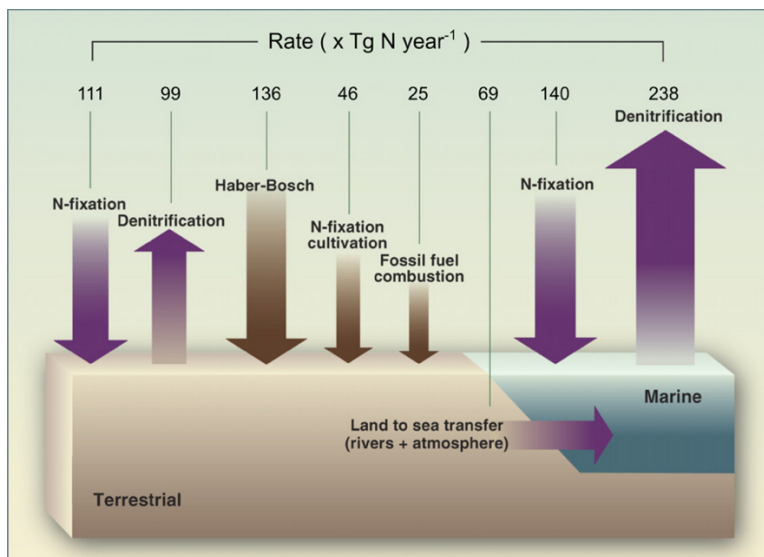


Figure 1.6. Rates of nitrogen flux in the modern nitrogen cycle. Arrow size reflects relative size of the flux. The dark brown arrows represent anthropogenic inputs. Modified from Canfield *et al.* (2010).

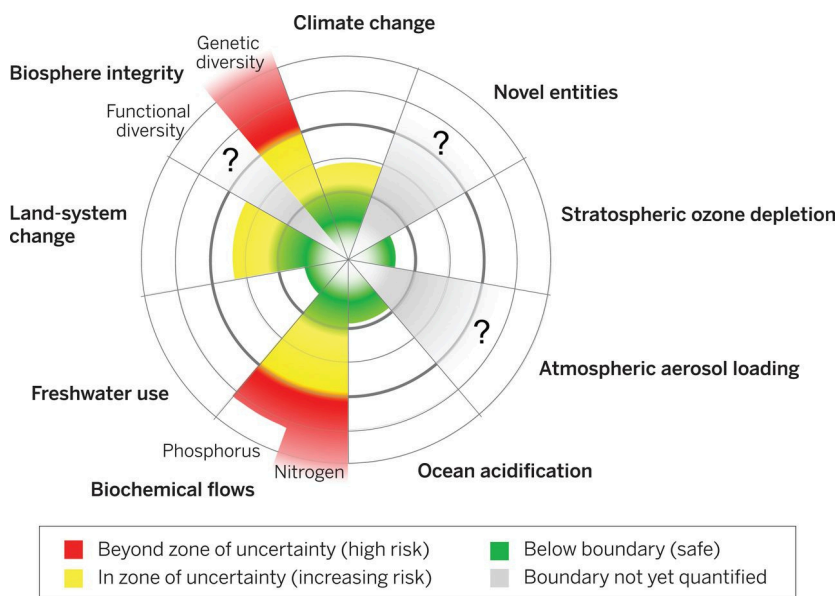


Figure 1.7. Current status of the control variables for seven of the planetary boundaries. The green zone is the safe operating space, the yellow represents the zone of uncertainty (increasing risk), and the red is a high-risk zone. The planetary boundary itself lies at the intersection of the green and yellow zones. Taken from Steffen *et al.* (2015)

Anthropogenic addition of bioavailable nitrogen to the biosphere has increased the inputs of nitrogen into inland waters (Vitousek, 1994; Howarth *et al.*, 1996; Gruber and Galloway, 2008), promoting eutrophication (Canfield *et al.*, 2010; Heathcote and Downing, 2012), and boosting the N₂O production, a potent GHG (Seitzinger *et al.*, 2000; Mulholland *et al.*, 2008; Beaulieu *et al.*, 2011).

N₂O is a by-product of nitrification in oxic environments, and an intermediate during denitrification in anoxic environments (Canfield *et al.*, 2010). Nitrification is a chemolithoautotrophic process that consists of the oxidation of ammonia to nitrite (i.e., ammonia oxidation step), and then to nitrate (i.e., nitrite oxidation step) (Figure 1.8a). Ammonia oxidation is the first and rate-limiting step during nitrification, and it is performed by ammonia-oxidizing bacteria (AOB), and ammonia-oxidizing archaea (AOA). AOB and AOA present physiological differences, and a niche differentiation determined by environmental conditions (Hink *et al.*, 2018). The global significance of ammonia oxidation and the relative contribution of AOB and AOA have been inferred from the abundance of the bacterial and the archaeal *amoA* genes, which encode the subunit A of the key enzyme ammonia monooxygenase (Kowalchuk and Stephen, 2001; Francis *et al.*, 2005).

During the ammonia oxidation, the intermediate compound hydroxylamine (NH₂OH) can decompose to form N₂O (Anderson, 1964; Vajjala *et al.*, 2013) (Figure 1.8a). Recently, new evidences of an obligate intermediate (i.e., nitric oxide, NO) to N₂O formation have appeared, but the details about N₂O formation are still controversial (Caranto and Lancaster, 2017; Carini *et al.*, 2018). N₂O can be also produced by hybrid N₂O formation. That is, one N atom comes from NO₂⁻ and the other one from NH₄⁺ or an intermediate of ammonia oxidation (Stieglmeier *et al.*, 2014; Frame *et al.*, 2017; Terada *et al.*, 2017) (Figure 1.8a). The nitrite oxidation to nitrate is the second step of nitrification, and it is carried out by nitrite-oxidizing bacteria (NOB) (Kowalchuk and Stephen, 2001; Könneke *et al.*, 2005). Recently, the existence of bacteria with the capacity to perform the complete nitrification, that is, from ammonia to nitrate (complete ammonia oxidation; comammox) has been demonstrated (Daims *et al.*, 2015; van Kessel *et al.*, 2015).

Ammonia oxidizers can perform the ammonia oxidation (i.e., ammonia to nitrite) or the nitrifier denitrification depending on the oxygen concentration (Figure 1.8). Nitrifier denitrification consists on the NH₄⁺ oxidation to NO₂⁻ followed by their

reduction to NO, and N₂O. This process was detected in cultures of AOB (Frame and Casciotti, 2010) and AOA (Santoro *et al.*, 2011) (Figure 1.8b) and occurs at low oxygen concentration, increasing the yield of N₂O produced relative to the ammonia oxidized (Goreau *et al.*, 1980; Yoshida, 1988) (Figure 1.8b). Nitrifier denitrification is an important pathway of N₂O production in soils, and hypoxic waters in the ocean (Wrage *et al.*, 2001; Frame and Casciotti, 2010; Löscher *et al.*, 2012). In fact, AOA are present in marine waters and soils (Francis *et al.*, 2005; Könneke *et al.*, 2005; Leininger *et al.*, 2006; Wuchter *et al.*, 2006; Prosser and Nicol, 2008; Hu *et al.*, 2014) contributing significantly to N₂O production (Francis *et al.*, 2005; Santoro *et al.*, 2011; Löscher *et al.*, 2012; Trimmer *et al.*, 2016). However, few studies have addressed the nitrification process or the abundance of AOA and AOB in lakes (Carini and Joye, 2008; Auguet *et al.*, 2012; Pajares *et al.*, 2017; Palacin-Lizarbe *et al.*, 2019) and, as far as we know, there are not studies in reservoirs.

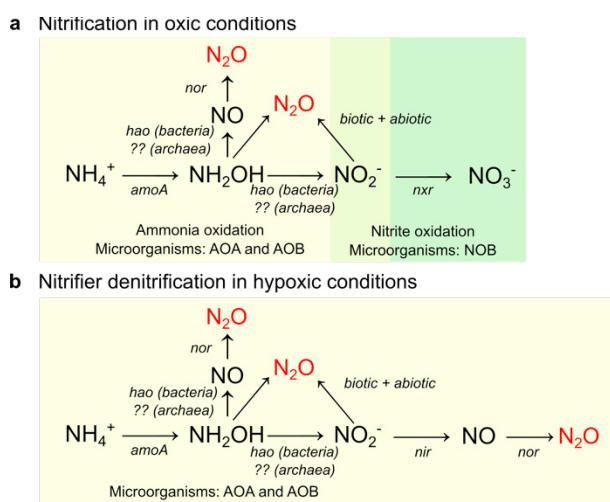


Figure 1.8. Production of N₂O from (a) nitrification, and (b) nitrifier denitrification. Genes encoding enzymes that conduct the important transformations are: *amoA* (ammonia monooxygenase), *hao* (hydroxylamine oxidoreductase), *nxr* (nitrite oxidoreductases), *nir* (nitrite reductase), *nor* (nitric oxide reductase). Genes and enzymes according to Frame *et al.* (2017).

Denitrification is the primary biological reduction of nitrate in aquatic environments, with high rates in rivers and lakes in comparison with estuaries, coastal areas, and open ocean (Ward 1996; Piña-Ochoa and Álvarez-Cobelas 2006). Denitrifiers obtain energy from organic matter oxidation, and the subsequent reduction of nitrate to nitrite, nitric oxide, nitrous oxide, and dinitrogen (Figure 1.9a). Due to denitrification, lakes and reservoirs reduce the excess of nitrogen that they

received through microbially mediated emissions of dinitrogen gas (N_2), and also through anaerobic ammonium oxidation (anammox) (Brezonik and Lee, 1968; Seitzinger, 1988; Harrison *et al.*, 2009; Rissanen *et al.*, 2013; Wenk *et al.*, 2014; Roland *et al.*, 2018) (Figure 1.9), with denitrification representing up to 87 – 100 % of the total N_2 production in the anoxic lake water column (Roland *et al.*, 2018). Denitrification also produces significant amounts of N_2O , that can accumulate in the waters if the rate of N_2O production exceeds the N_2O reduction to N_2 (Schlesinger, 2009). On the other hand, denitrification can be an N_2O sink or source depending on the rate of N_2 formation. When the nitrate used by denitrifiers directly comes from nitrification, there is a spatial coupling nitrification–denitrification. The abundances of the genes that coded for the nitrite reductases (i.e., *nirS/nirK*) and the nitrous oxide reductase (i.e., *nosZ*) are widely used to infer the contribution of denitrifying bacteria to the concentration of dissolved N_2O (Hallin *et al.*, 2018). Although most studies focused on bacterial denitrification, fungi and foraminifera can also denitrify (Wankel *et al.*, 2017; Woehle *et al.*, 2018).

Denitrification is usually considered as facultative anaerobic respiration. Oxygen concentration appears to regulate the sequence of the denitrification enzymes, especially the *nosZ*, which is inhibited even at very low oxygen concentrations (Bonin *et al.*, 1989; Zumft, 1997). Consequently, the studies on denitrification in inland waters have been performed in anoxic waters and, particularly, in sediments (Piña-Ochoa and Álvarez-Cobelas, 2006). Denitrification can produce up to 87 – 100 % of the total N_2 in the anoxic lake water (Roland *et al.*, 2018). However, denitrifiers also occur in oxic waters of lakes and reservoirs (e.g., Junier *et al.*, 2008; Kim *et al.*, 2011; Pajares *et al.*, 2017). Some studies pointed out that the influence of O_2 concentration on the denitrifying activity differed from one bacterium to another (Lloyd *et al.*, 1987; Lloyd, 1993; Hayatsu *et al.*, 2008). Denitrifying bacteria are taxonomically, and physiologically diverse, and the existence of aerobic denitrifying bacteria has been demonstrated in laboratory cultures, and described across diverse environments (Robertson and Kuenen, 1984; Lloyd *et al.*, 1987; Robertson *et al.*, 1989, 1995; Lloyd, 1993; Hayatsu *et al.*, 2008). Furthermore, many bacteria can denitrify also in oxic conditions, with the highest N_2O/N_2 ratios in these conditions (Hochstein *et al.*, 1984; Lloyd *et al.*, 1987; Lloyd, 1993). Thus, although some studies have addressed the production of N_2 by denitrification in

anoxic lake waters (Goering and Dugdale, 1966; Brezonik and Lee, 1968; Chan and Campbell, 1980; Hamersley *et al.*, 2009; Wenk *et al.*, 2013; Roland *et al.*, 2018), we still lack direct measurements on the production of N₂O by denitrifiers in the water column of lakes and reservoirs in oxic conditions.

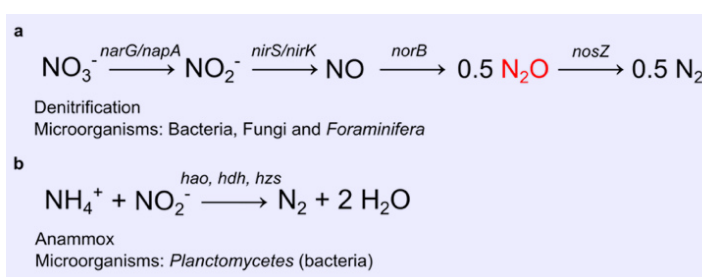


Figure 1.9. (a) Denitrification and (b) anammox pathways and the genes that code for the main enzymes. Genes encoding enzymes that conduct the important transformations during denitrification are: *narG* and *napA* (dissimilatory nitrate reductases), *nirS* and *nirK* (nitrite reductases), *norB* (nitric oxide reductase), and *nosZ* (nitrous oxide reductase); and during anammox is the *hao* (hydroxylamine oxidoreductase), *hdh* (hydrazine dehydrogenase), *hzs* (hydrazine synthase). Genes and enzymes according to Canfield *et al.* (2010) and Kuypers *et al.* (2018).

Dissimilatory nitrate reduction to ammonium (DNRA) is another heterotrophic process of nitrate reduction coupled to organic carbon oxidation (Figure 1.10). Unlike denitrification, DNRA leads to N retention in the ecosystem. DNRA is a strict anaerobic process that reduces nitrate to nitrite and then to ammonium, with concomitant formation of small amounts of N₂O (Stremińska *et al.*, 2012). In the second step, the nitrite reduction to ammonium is the critical reaction catalyzed by the enzyme nitrite reductase coded by the gene *nrfA* (Tiedje and Zehnder, 1988). DNRA is an important process in marine and lake sediments, where competes for nitrate with denitrification. DNRA dominates in environments with high content in organic matter in comparison to N availability. In contrast, high nitrate concentrations in proportion to organic matter availability may favor denitrification (Nizzoli *et al.*, 2010; Dong *et al.*, 2011; Roland *et al.*, 2018).

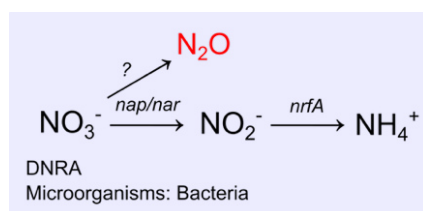


Figure 1.10. DNRA pathway and the genes that code for the main enzymes. The genes that code for the enzymes are: *nar* and *nap* (dissimilatory nitrate reductases), and *nrfA* (nitrite reductases). Genes and enzymes according to Canfield *et al.* (2010) and Kuypers *et al.* (2018).

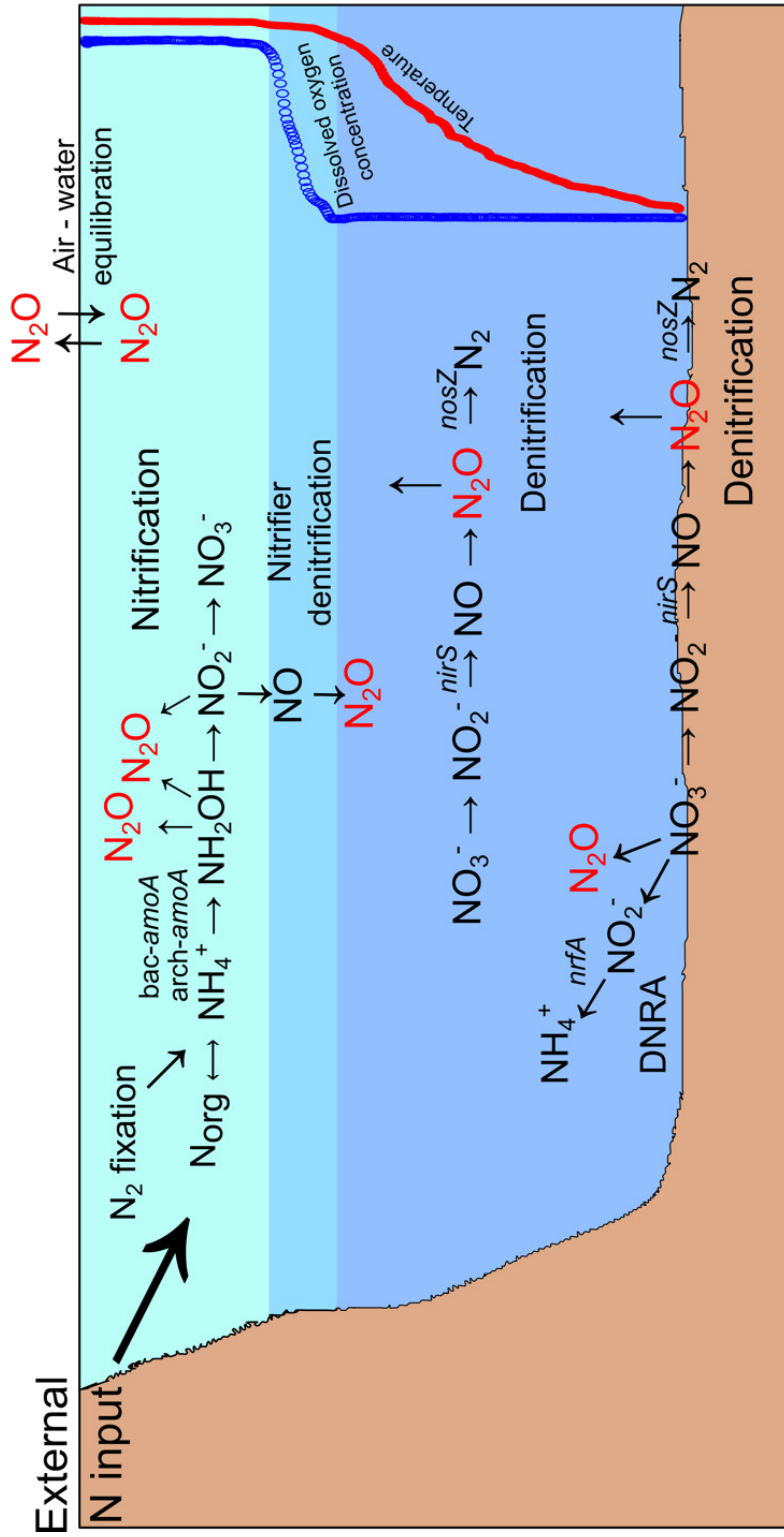
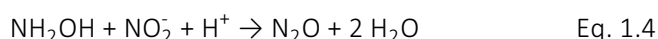


Figure 1.11. Main pathways in the microbial production of N_2O in a lake or reservoir. We show the nitrification, nitrifier denitrification, denitrification, and DNRA, and the target genes.

In addition to the biological production of N₂O, some studies have also focused on the abiotic production of N₂O, that may occur by two main pathways: the NH₂OH decomposition to N₂O, and by chemodenitrification to N₂O (Heil *et al.*, 2014; Zhu-Barker *et al.*, 2015; Soler-Jofra *et al.*, 2016; Liu *et al.*, 2017; Wankel *et al.*, 2017). The decomposition of NH₂OH to N₂O is a coupled biotic–abiotic reaction, that requires the extracellular ammonia-oxidation intermediate NH₂OH, and other substrates such as NO₂⁻, MnO₂ and Fe³⁺ (Heil *et al.*, 2014; Zhu-Barker *et al.*, 2015; Soler-Jofra *et al.*, 2016; Liu *et al.*, 2017). Recently, Liu *et al.* (2017) demonstrated the occurrence of extracellular NH₂OH in cultures of AOB, AOA, and comammox bacteria. Then, the extracellular NH₂OH may react with the NO₂⁻ abiotically to form N₂O, following the Eq. 1.4 (Soler-Jofra *et al.*, 2016):



The extracellular NH₂OH oxidation may be also coupled to the reduction of iron (Fe III) or manganese (Mn IV) (Zhu-Barker *et al.*, 2015) (Figure 1.12). During chemodenitrification, NO₃⁻, NO₂⁻, NO are reduced by Fe²⁺ to N₂O. This reaction has been demonstrated in low O₂ conditions and high organic supply (Zhu-Barker *et al.*, 2015; Wankel *et al.*, 2017) (Figure 1.12).

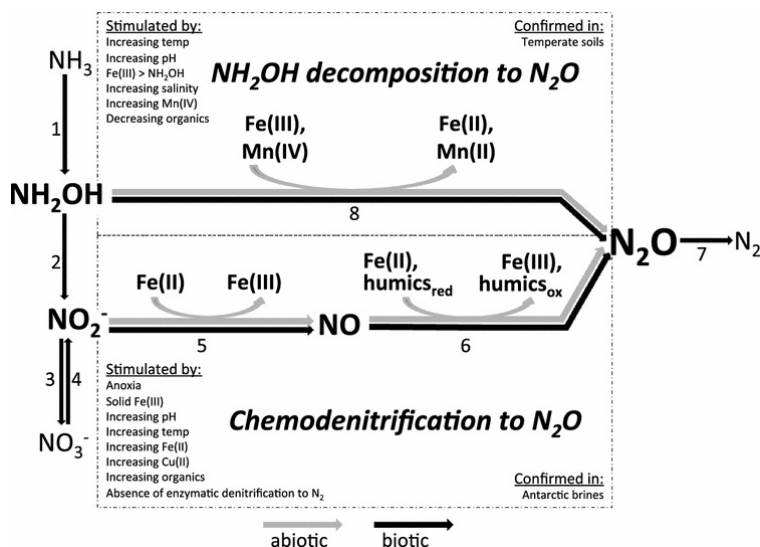


Figure 1.12. Abiotic processes that produce N₂O by hydroxylamine decomposition and chemodenitrification. The conditions, elements involved, and studies that confirmed each process are included. Biological processes are labeled with numbers: 1 + 2 + 3 = Nitrification; 1 + 2 + 5 + 6 = Nitrifier denitrification; 1 + 2 + 3 + 4 + 5 + 6 + 7 = Nitrification-coupled denitrification; 4 + 5 + 6 + 7 = Denitrification; 8 = Hydroxylamine oxidation. From Zhu-Barker *et al.* (2015).

These biotic and abiotic N transformations produce different degrees of isotopic fractionation. The preference for the lighter isotopic specie (^{14}N), results in a significant fractionation between the substrate, which remains heavier, and the product, which becomes lighter (Kendall and Caldwell, 1998; Sigman *et al.*, 2009) (More details in Box 1.1). In the ocean water column, denitrifiers strongly discriminate against the heavier isotope in the nitrate pool (i.e., $^{15}\text{N-NO}_3^-$), with a fractionation factor of ϵ between 25 and 35 ‰, that determines the progressive enrichment in ^{15}N of the remaining nitrate pool, while nitrate is consumed by denitrification (Sigman *et al.*, 2009; Ryabenko, 2013) (Figure 1.13). Similarly, denitrification from NO_2^- also enriches in ^{15}N the remaining NO_2^- pool, with different fractionation according to the enzyme for the nitrite reduction: $\epsilon = 22\text{‰}$ for the copper(Cu)-containing enzyme encoded by the *nirK* gene, and $\epsilon = 8\text{‰}$ for the cytochrome cd1 (iron, Fe)-containing enzyme encoded by the *nirS* gene (Martin and Casciotti, 2016). During abiotic nitrite reduction by Fe(II) to N_2O the isotope fractionation (ϵ) varied from 6 to 45 ‰ (Buchwald *et al.*, 2016). The production of N_2O produces gas depleted in ^{15}N and ^{18}O relative to their substrates. At the same time, the reduction of N_2O to N_2 by denitrification leaves the residual N_2O pool enriched in ^{15}N and ^{18}O , with a $\delta^{15}\text{N-N}_2\text{O}$ (Sigman *et al.*, 2009). This explains that a strong maximum in the $\delta^{15}\text{N-N}_2\text{O}$ can be observed in denitrifying waters of the ocean, presumably due to isotope fractionation associated with N_2O reduction to N_2 (Sigman *et al.*, 2009). Then, the analysis of the natural isotopic composition of the nitrogen compounds (i.e., the $\delta^{15}\text{N}$ method) can provide useful information about the predominant processes affecting nitrogen at the ecosystem level (Robinson, 2001; Bedard-Haughn *et al.*, 2003). In addition, specific processes can be examined and precisely quantified using ^{15}N -enriched tracers (i.e., ^{15}N -enriched method).

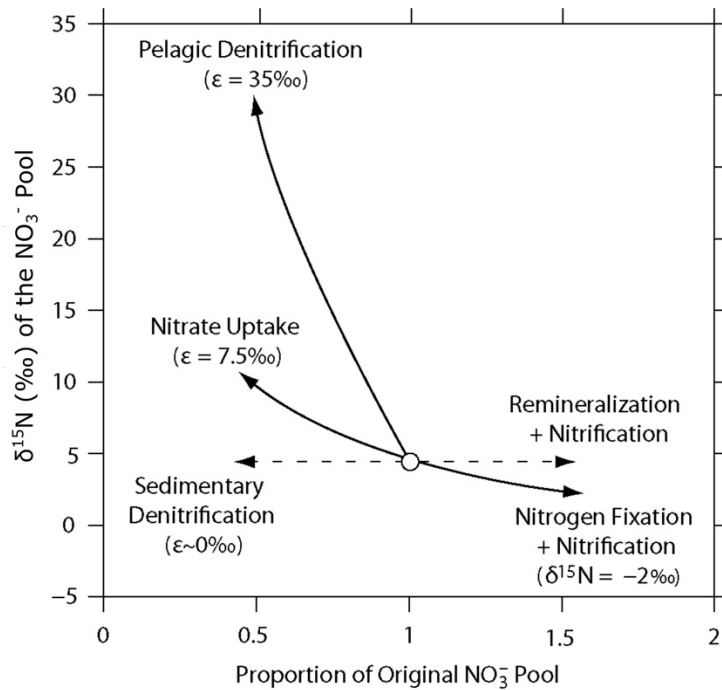


Figure 1.13. The impact of different processes on the $\delta^{15}\text{N}$ signature of oceanic pool of nitrate. Axes show deviation of $\delta^{15}\text{N}$ signal from oceanic average and loss/input of nitrogen due to different processes. From Ryabenko (2013).

In general, the nitrogen-processing microorganisms, and the biotic production of N_2O have been extensively studied in the ocean and soils, some investigations in inland waters have focused on streams and rivers (Beaulieu *et al.*, 2008, 2011; Mulholland *et al.*, 2008; Rosamond *et al.*, 2011), but less attention have been paid to lakes and reservoirs. McCrackin and Elser (2011) suggested that lakes and reservoirs may play an important role in the N removal at the landscape scale, acting as sources of N_2O , especially in areas submitted to high N inputs. However, few studies have explored the role of reservoirs removing N, and producing N_2O vs N_2 , and these few ones have focused on the sediments rather than in the water column (Piña-Ochoa and Álvarez-Cobelas, 2006). Therefore, a better understanding on the N cycle in reservoirs is needed to determine their role as sinks or sources of N_2O .

Box 1.1. Definitions and measurements of ^{15}N abundance

N atoms in nature appears in two stable isotopes: ^{14}N and ^{15}N , with atomic masses of 14 and 15, respectively. The lighter isotope, ^{14}N , makes about the 99.6337 % of the natural N, while the remaining 0.3663 % is ^{15}N . These atom % abundances (A) are calculated as follows (Eq. 1) (Robinson, 2001):

$$A (\%) = 100 \times \left(\frac{n_{15}}{n_{15} + n_{14}} \right) = 100 \times \left(\frac{R_{\text{sample}}}{R_{\text{sample}} + 1} \right) \quad \text{Eq. 1}$$

n_{15} and n_{14} are the numbers of ^{15}N and ^{14}N atoms present in a sample, respectively. R_{sample} is the $^{15}\text{N} : ^{14}\text{N}$ isotope ratio ($n_{15} : n_{14}$). This equation (Eq. 1) is used in the studies in which ^{15}N is used as tracer, when A exceeds 0.5 atoms %.

In samples that only contain slight ^{15}N enrichments and in all natural abundances studies, isotope ratios are reported on the $\delta^{15}\text{N}$ scale, which is defined as follows (Sigman *et al.*, 2009):

$$\delta^{15}\text{N} (\text{‰}) = 1000 \times \left(\frac{\left(\frac{^{15}\text{N}/^{14}\text{N}}{\text{sample}} \right)}{\left(\frac{^{15}\text{N}/^{14}\text{N}}{\text{standard}} \right)} - 1 \right) \quad \text{Eq. 2}$$

where $\left(\frac{^{15}\text{N}/^{14}\text{N}}{\text{sample}} \right)$ is the $^{15}\text{N}/^{14}\text{N}$ ratio for the sample, and $\left(\frac{^{15}\text{N}/^{14}\text{N}}{\text{standard}} \right)$ is the $^{15}\text{N}/^{14}\text{N}$ ratio for the standard. The standard reference for N isotopes is atmospheric N_2 , with an $^{15}\text{N}/^{14}\text{N}$ ratio of $0.36765 \text{‰} \pm 0.00081\text{‰}$ and $\delta^{15}\text{N} = 0 \text{‰}$. According to $\delta^{15}\text{N}$, the more ^{15}N -enriched a sample is, the more positive (or less negative) its $\delta^{15}\text{N}$ is.

^{14}N and ^{15}N have slightly different chemical and physical properties because of their mass differences. A molecule containing a heavy isotope is more stable (i.e., has a higher dissociation energy) than the same molecule with the lighter isotope. These differences produce isotope fractionation during many physical, chemical, and biological processes. The isotopic fractionation is the change in the relative proportions of various isotopes, and it is caused by both equilibrium processes (i.e., equilibrium fractionation) and unidirectional reactions (i.e., kinetic fractionation) (Kendall and Caldwell, 1998; Sigman *et al.*, 2009). Biological processes are generally unidirectional and excellent examples of kinetic isotope reactions, because organisms preferentially use lighter isotopic species (Kendall and Caldwell,

1998; Sigman *et al.*, 2009). The kinetic isotope effect of a reaction (ϵ , ‰) is calculated using the rates of the reactions (Eq. 3) (Sigman *et al.*, 2009):

$$\epsilon (\text{‰}) = 1000 \times \left(\frac{{}^{14}k}{{}^{15}k} - 1 \right) \quad \text{Eq. 3}$$

where the ${}^{14}k$ and the ${}^{15}k$ are the rate coefficients of the reaction for the ${}^{14}\text{N}$ - and ${}^{15}\text{N}$ -containing reactant, respectively. In the reactions where $\epsilon \ll 1000$ ‰, it can be also computed as the difference in the $\delta^{15}\text{N}$ between the substrate and its product. For example, if a reaction has a fractionation of 10 ‰, the $\delta^{15}\text{N}$ of the product will be about 10 ‰ lower than the $\delta^{15}\text{N}$ of the substrate (Sigman *et al.*, 2009).

1. 4. Emissions of CO₂, CH₄, and N₂O from reservoirs

The human development has promoted the construction of dams and impoundments for water supply, irrigation, flood control, and the generation of hydropower (WCD, 2000). The number of reservoirs has increased significantly worldwide since the 1950s, reaching over 2.8 millions of impoundments larger than 0.001 km², and 16.7 million larger than 100 m², with a total storage volume over 8000 km³ (Lehner *et al.*, 2011). Large reservoirs are more abundant between 30° and 55° North, reflecting major dam constructions in the United States, southern Canada, Europe, Russia and China (Lehner and Döll, 2004) (Figure 1.14: green and blue dots). About the 50 percent of the world's large dams were built exclusively or primarily for irrigation (WCD, 2000). Nevertheless, the need of more clean energy have moved the main purpose to hydropower dams, especially in countries with emerging economies, where over 3500 reservoirs are either planned or under construction (Zarfl *et al.*, 2015) (Figure 1.14: orange and red dots). These new reservoirs are predicted to increase the global hydropower capacity by 73 % to about 1,700 GW (Zarfl *et al.*, 2015).

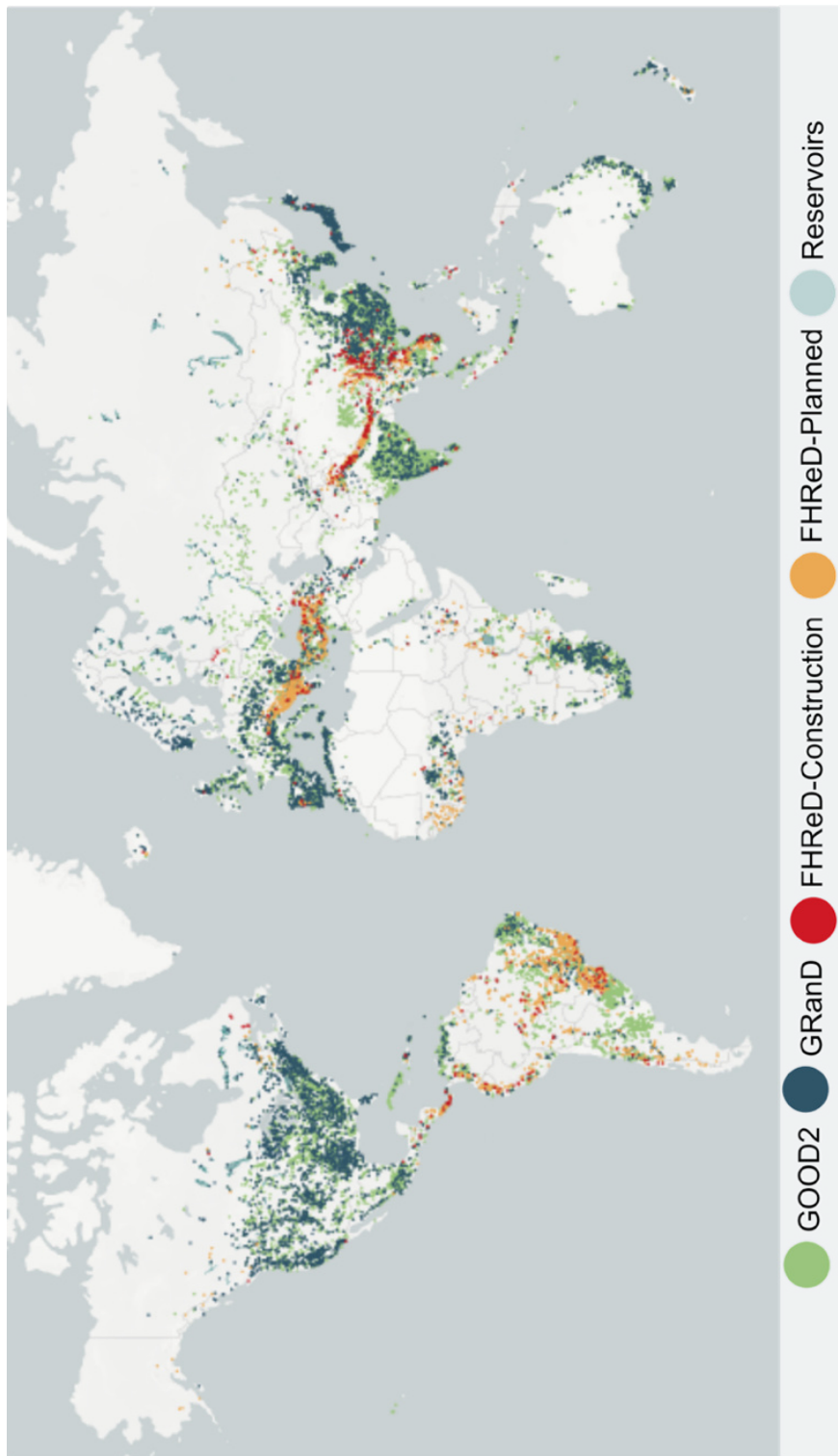


Figure 1.14. Global spatial distribution of constructed (green and blue dots), and future hydropower dams, either under construction (red dots) or planned (orange dots). The database included in the map are: GOOD2 (Global Geo-Referenced Database of Dams), GRand (Global Reservoir and Dam Database), and FHReD (Future Hydropower Reservoirs and Dams). Modified from GDW (2020) (<http://globaldamwatch.org/data/>).

On the other hand, the construction of reservoirs has an important social and environmental impact. Reservoirs have forced the displacement of human societies, and fragmented rivers, affecting the river biodiversity, flow regulation, and delivery of nutrients and sediments downstream (Lehner *et al.*, 2011). The damming determines the reduction in the flow and the increase in the residence time, with the subsequent changes in the temperature, stratification, reduction in the turbulence by particle settling, and sometimes an increase in autochthonous primary production, and anoxia events in the deep waters. Dam construction also affects carbon, phosphorus, and nitrogen biogeochemical cycles (Friedl and Wüest, 2002). Reservoirs can be seen as digesters that metabolize the elements that they receive; exchange the gaseous forms with the atmosphere (i.e., CO₂, CH₄, N₂O, and N₂); store one part in the sediments; and export another part downstream. Reservoirs process the autochthonous and allochthonous organic matter, producing greenhouse gases, as CO₂, and CH₄. They also process a disproportionately high fraction of the total nitrogen in comparison to lakes, due to their higher drainage ratio (i.e., the catchment area : lake or reservoir surface area), the higher apparent settling velocities for N, and the greater average N loading rates in reservoirs than in lakes (Harrison *et al.*, 2009). The processes involved in the N cycle may determine the emission of N₂O and N₂ toward the atmosphere. At the same time, reservoirs have larger rates of organic carbon burial in sediments than lakes, as a result of catchment instability and high erosion rates (Mendonça *et al.*, 2017; Anderson *et al.*, 2020). Therefore, the net effect of reservoirs as sources or sinks of elements will depend on the balance of these processes. In our work, we study the effect of reservoirs on the variation in concentrations of greenhouse gases that we are currently observing in the atmosphere. CO₂, CH₄ and N₂O are increasing their concentrations in the atmosphere in such a way that it can be measured annually. This is the time scale we will focus on, regardless of whether the reservoirs are net sources or sinks of C or N.

There is an increasing concern about the magnitude of the greenhouse gas emissions from reservoirs, that contribute significantly to global budgets (Barros *et al.*, 2011; Deemer *et al.*, 2016). Barros *et al.* (2011) estimated that hydroelectric reservoirs emit about 48 Tg C yr⁻¹ as CO₂ and 3 Tg C yr⁻¹ as CH₄, and that corresponds to 4 % of global carbon emissions from inland waters. Reservoirs presented the

highest emissions of GHG during the first years after the flooding event, due to the decomposition of the flooded vegetation and soil organic matter (Abril *et al.*, 2005; Barros *et al.*, 2011) (Figure 1.15 a, c). Carbon emissions were also related to the latitude, with the highest emission rates in the tropical Amazon region (Barros *et al.*, 2011) (Figure 1.15). Later, Deemer *et al.* (2016) estimated that reservoirs emit 36.8 Tg C yr⁻¹ of CO₂, 13.3 Tg C yr⁻¹ of CH₄, and 0.03 Tg N yr⁻¹ of N₂O. Regionally, the emissions of CH₄ were correlated to Chl-*a* concentration, and the emissions of N₂O to NO₃⁻ concentration (Deemer *et al.*, 2016). CH₄ emissions from reservoirs appear to be responsible for the majority of the radiative forcing of these ecosystems (ca. 80 % of the CO₂ equivalents), and they are comparable to emissions from paddies or biomass burning (Deemer *et al.*, 2016; Samiotis *et al.*, 2018). Although previous studies linked reservoir GHG emissions to reservoir age and latitude, Deemer *et al.* (2016) reported that reservoir productivity was a better predictor for the CH₄ emissions.

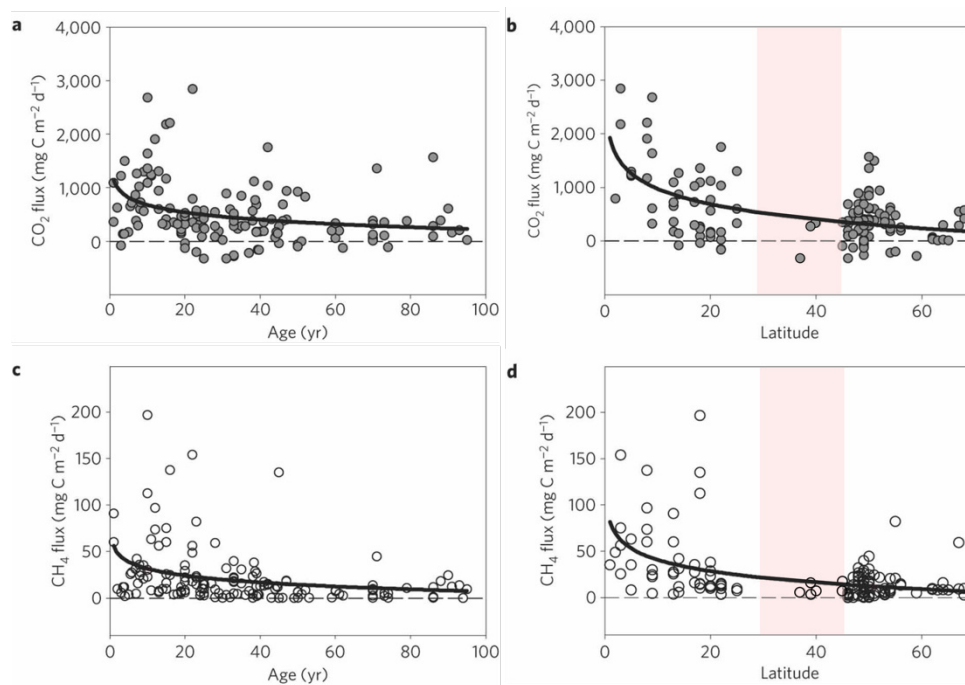


Figure 1.15. Fluxes of CO₂ and CH₄ versus age (a, c), and latitude (b, d). (a) CO₂ versus age, (b) CO₂ versus latitude, (c) CH₄ versus age, and (d) CH₄ versus latitude. Red areas stand for the latitudinal band 30° – 45° (Mediterranean biome). Modified from Barros *et al.* (2011).

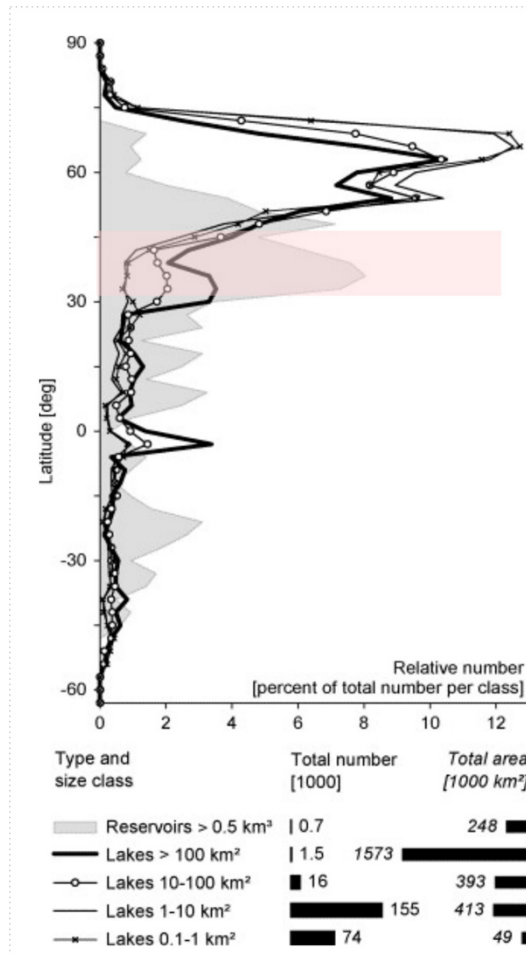


Figure 1.16. Latitudinal distribution of global lake and reservoir numbers according to Global Lakes and Wetlands Database. Red area stands for the latitudinal band 30° – 45° (Mediterranean biome). Modified from Lehner and Döll (2004).

Nevertheless, the existing estimations are highly uncertain, because they are based on very limited data sets. Fluxes of CO₂, CH₄, and N₂O have been reported mostly for tropical and boreal reservoirs, lacking data for the Mediterranean biome from 30°N to 45°N, where reservoirs are the preponderant aquatic ecosystems (Lehner and Döll, 2004) (Red area in Figure 1.16). This latitudinal gap is evident in the work of Barros *et al.* (2011) (red area in Figure 1.15). More recently, Deemer *et al.* (2016) showed measurements for the three main GHGs in a few reservoirs (Figure 1.17). This lack of data on GHG fluxes from reservoirs seriously limits the confidence on the global estimates of GHG emissions.

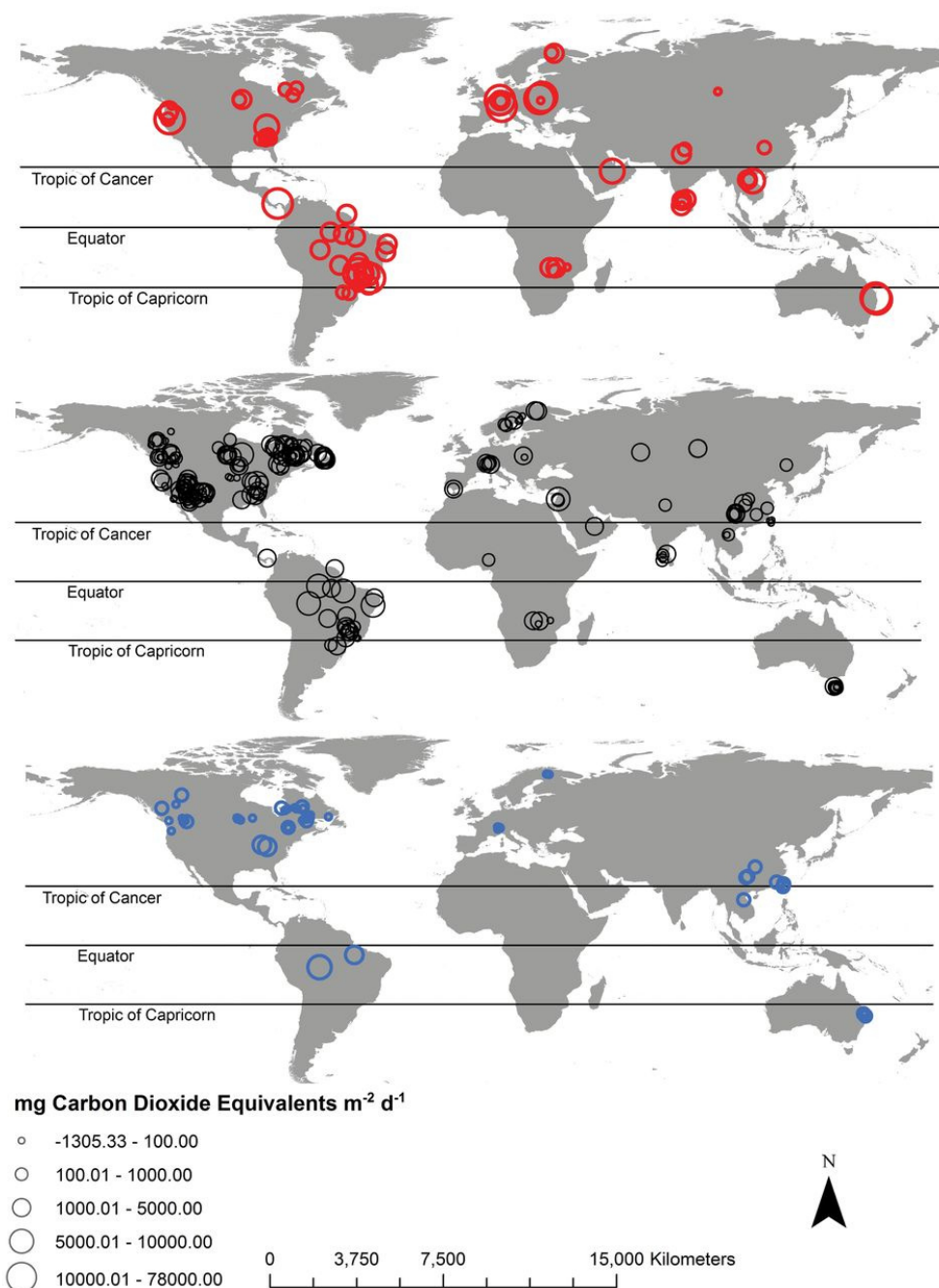


Figure 1.17. Fluxes of CH_4 , CO_2 and N_2O from reservoirs. Diffusive and ebullitive methane (top), carbon dioxide (middle), and nitrous oxide (bottom) emissions from reservoirs on a CO_2 -equivalent basis. The annual CO_2 equivalents were calculated by multiplying the mass-based flux (in units of Tg CH_4 , CO_2 or N_2O per year) by the 100-year global warming potential of each gas (1 for CO_2 , 34 for CH_4 and 298 for N_2O). Few reservoirs had measurements for all three gases. Taken from Deemer *et al.* (2016).

The studies on GHG emissions are also very limited in their temporal coverage, despite seasonal and diel changes represents an important part of the total GHG variability in reservoirs (Liu *et al.*, 2016). Environmental drivers that affects the microbial production of GHG change at seasonal and daily scales. This is the case of the water temperature or the oxygen availability in aquatic systems. Water temperature affects the microbial production and the emission of GHG (Marotta *et al.*, 2014; Yvon-Durocher *et al.*, 2014; Rasilo *et al.*, 2015; Aben *et al.*, 2017; Sepulveda-Jauregui *et al.*, 2018). Therefore, daily and seasonal changes in the water temperature may determine differences in the GHG emissions. The mixing and thermal stratification in the water column also influence the production and emission of the GHGs. The suboxic conditions in the hypolimnion of reservoirs during the thermal stratification stimulate the production of CH₄ and N₂O (Downes, 1988; Almeida *et al.*, 2013; Salk *et al.*, 2016). The amplitude of diel changes in GHG emissions can be much larger than the amplitude occurring on a monthly timescale (Zhang *et al.*, 2019). However, current estimations for GHG emissions in reservoirs are based on the upscaling of discrete samplings during daytime that do not account for nighttime emissions (Liu *et al.*, 2016) or the changes of the water column between the thermal stratification and the mixing period. The few studies on daily patterns of GHG emissions have focused on CO₂ and CH₄ (Liu *et al.*, 2016; Erkkilä *et al.*, 2018). To the best of our knowledge, there are no studies in lakes or reservoirs characterizing diurnal changes in N₂O emissions. Therefore, we need a more comprehensive analysis of the GHG emissions in reservoirs, that focus on the latitudinal gap of Mediterranean reservoirs, temporal scales, and on the biotic and abiotic processes of production of CH₄ and N₂O in reservoirs.

1. 5. Objectives and structure of the thesis

The general objective of this PhD dissertation is to determine the concentrations and fluxes of CO₂, CH₄, and N₂O in Mediterranean reservoirs, with special emphasis on late two. By analyzing the spatial and temporal variability of the reservoirs we will be able to assess their role as a sinks or sources of greenhouse gases to the atmosphere, and their potential contribution to climate forcing. In this study we will also explore the abiotic and biotic origin of the CH₄ and the N₂O through in situ measurements, experiments, and the analysis of functional genes.

The specific objectives of this PhD dissertation are:

1. To measure the fluxes of CO₂, CH₄, and N₂O in twelve Mediterranean reservoirs during the stratification and mixing periods covering a broad spectrum of landscape and reservoir intrinsic properties, to determine the inter-system variability and its drivers.
2. To quantify daily variability in the fluxes of CO₂, CH₄, and N₂O in two Mediterranean reservoirs, and determine the environmental drivers responsible of this variability.
3. To explore the effect of sunlight on the production of greenhouse gases and assess its quantitative relevance.
4. To quantify the concentration of dissolved CH₄ in the water column of twelve Mediterranean reservoirs during the stratification and the mixing period, and determine the origin of the CH₄ supersaturation in oxic waters.
5. To quantify the concentration of the dissolved N₂O in the water column of the twelve Mediterranean reservoirs during the stratification and the mixing period, and explore the origin of this dissolved N₂O using the functional genes involved in the nitrification and denitrification pathways.
6. To determine the production rates of N₂O by nitrification and denitrification using stable isotope techniques in a shallow and a deep reservoir over the summer to explore the effect of morphometry and oxygen availability in the production rates.

We show the chapter structure of this dissertation, and the relationship among the contents, the chapters, and the specific objectives in Figure 1.18.

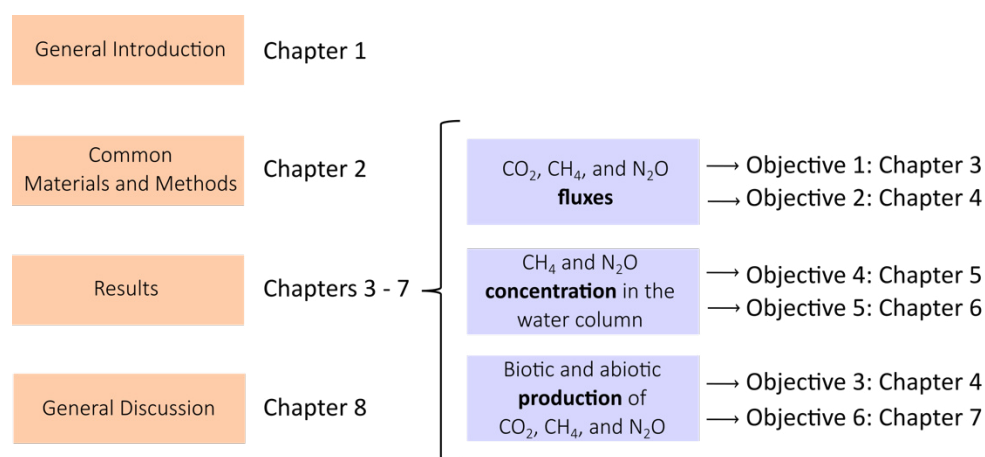


Figure 1.18. Structure of this dissertation. Relationship among the contents, the chapters, and the objectives of this dissertation.

1. 6. References

- Aben, R. C. H., Barros, N., Donk, E. van, Frenken, T., Hilt, S., Kazanjian, G., Lamers, L. P. M., Peeters, E. T. H. M., Roelofs, J. G. M., Domis, L. N. S., Stephan, S., Velthuis, M., Waal, D. B. V. de, Wik, M., Thornton, B. F., Wilkinson, J., DelSontro, T. and Kosten, S. (2017). Cross continental increase in methane ebullition under climate change, *Nature Communications*, 8(1), p. 1682. doi: 10.1038/s41467-017-01535-y.
- Abril, G., Guérin, F., Richard, S., Delmas, R., Galy-Lacaux, C., Gosse, P., Tremblay, A., Varfalvy, L., Santos, M. A. D. and Matvienko, B. (2005). Carbon dioxide and methane emissions and the carbon budget of a 10-year old tropical reservoir (Petit Saut, French Guiana), *Global Biogeochemical Cycles*, 19(4). doi: 10.1029/2005GB002457.
- Almeida, R. M., Barros, N., Cole, J. J., Tranvik, L. and Roland, F. (2013). Emissions from Amazonian dams, *Nature Climate Change*, 3(12), pp. 1005–1005. doi: 10.1038/nclimate2049.
- Anderson, J. H. (1964). The metabolism of hydroxylamine to nitrite by Nitrosomonas, *Biochemistry Journal*, 91(1948), pp. 8–17. doi: 10.1042/bj0910008.
- Anderson, N. J., Heathcote, A. J., Engstrom, D. R. and Globocarb data contributors. (2020). Anthropogenic alteration of nutrient supply increases the global freshwater carbon sink, *Science Advances*, 6(16), p. eaaw2145. doi: 10.1126/sciadv.aaw2145.
- Angel, R., Matthies, D. and Conrad, R. (2011). Activation of methanogenesis in arid biological soil crusts despite the presence of oxygen, *PLOS ONE*, 6(5), p. e20453. doi: 10.1371/journal.pone.0020453.
- de Angelis, M. A. and Lee, C. (1994). Methane production during zooplankton grazing on marine phytoplankton, *Limnology and Oceanography*, 39(6), pp. 1298–1308. doi:

10.4319/lo.1994.39.6.1298.

- Angle, J. C., Morin, T. H., Solden, L. M., Narrowe, A. B., Smith, G. J., Borton, M. A., Rey-Sanchez, C., Daly, R. A., Mirfenderesgi, G., Hoyt, D. W., Riley, W. J., Miller, C. S., Bohrer, G. and Wrighton, K. C. (2017). Methanogenesis in oxygenated soils is a substantial fraction of wetland methane emissions, *Nature Communications*, 8, pp. 1–9. doi: 10.1038/s41467-017-01753-4.
- Auguet, J.-C., Triadó-Margarit, X., Nomokonova, N., Camarero, L. and Casamayor, E. O. (2012). Vertical segregation and phylogenetic characterization of ammonia-oxidizing Archaea in a deep oligotrophic lake, *The ISME Journal*, 6(9), pp. 1786–1797. doi: 10.1038/ismej.2012.33.
- Barros, N., Cole, J. J., Tranvik, L. J., Prairie, Y. T., Bastviken, D., Huszar, V. L. M., del Giorgio, P. and Roland, F. (2011). Carbon emission from hydroelectric reservoirs linked to reservoir age and latitude, *Nature Geoscience*, 4(9), pp. 593–596. doi: 10.1038/ngeo1211.
- Bastviken, D., Cole, J., Pace, M. and Tranvik, L. (2004). Methane emissions from lakes: Dependence of lake characteristics, two regional assessments, and a global estimate, *Global Biogeochemical Cycles*, 18(4), pp. 1–12. doi: 10.1029/2004GB002238.
- Bastviken, D., Tranvik, L. J., Downing, J. A., Crill, P. M. and Enrich-Prast, A. (2011). Freshwater methane emissions offset the continental carbon sink, *Science*, 331(6013), pp. 1–12. doi: 10.1126/science.1196808.
- Battye, W., Aneja, V. P. and Schlesinger, W. H. (2017). Is nitrogen the next carbon?, *Earth's Future*, 5(9), pp. 894–904. doi: 10.1002/2017EF000592.
- Beaulieu, J. J., Arango, C. P., Hamilton, S. K. and Tank, J. L. (2008). The production and emission of nitrous oxide from headwater streams in the Midwestern United States, *Global Change Biology*, 14(4), pp. 878–894.
- Beaulieu, J. J., Tank, J. L., Hamilton, S. K., Wollheim, W. M., Hall, R. O., Mulholland, P. J., Peterson, B. J., Ashkenas, L. R., Cooper, L. W., Dahm, C. N., Dodds, W. K., Grimm, N. B., Johnson, S. L., McDowell, W. H., Poole, G. C., Valett, H. M., Arango, C. P., Bernot, M. J., Burgin, A. J., Crenshaw, C. L., Helton, A. M., Johnson, L. T., O'Brien, J. M., Potter, J. D., Sheibley, R. W., Sobota, D. J. and Thomas, S. M. (2011). Nitrous oxide emission from denitrification in stream and river networks, *Proceedings of the National Academy of Sciences*, 108(1), pp. 214–219. doi: 10.1073/pnas.1011464108.
- Bedard-Haughn, A., van Groenigen, J. W. and van Kessel, C. (2003). Tracing ¹⁵N through landscapes: Potential uses and precautions, *Journal of Hydrology*, 272(1), pp. 175–190. doi: 10.1016/S0022-1694(02)00263-9.
- Beversdorf, L. J., White, A. E., Björkman, K. M., Letelier, R. M. and Karl, D. M. (2010). Phosphonate metabolism by *Trichodesmium* IMS101 and the production of greenhouse gases, *Limnology and Oceanography*, 55(4), pp. 1768–1778. doi: 10.4319/lo.2010.55.4.1768.
- Bianchi, M., Marty, D., Teyssié, J.-L. and Fowler, S. W. (1992). Strictly aerobic and anaerobic bacteria associated with sinking particulate matter and zooplankton fecal pellets, *Marine Ecology Progress Series*, 88(1), pp. 55–60.

- Bižić, M., Klintzsch, T., Ionescu, D., Hindiyeh, M. Y., Günthel, M., Muro-Pastor, A. M., Eckert, W., Ulrich, T., Keppler, F. and Grossart, H.-P. (2020). Aquatic and terrestrial cyanobacteria produce methane, *Science Advances*, 6(3), p. 3aax5343. doi: 10.1126/sciadv.aax5343.
- Bogard, M. J., del Giorgio, P. A., Boutet, L., Chaves, M. C. G., Prairie, Y. T., Merante, A. and Derry, A. M. (2014). Oxic water column methanogenesis as a major component of aquatic CH₄ fluxes, *Nature Communications*, 5, p. 5350. doi: 10.1038/ncomms6350.
- Bonin, P., Gilewicz, M. and Bertrand, J. C. (1989). Effects of oxygen on each step of denitrification on *Pseudomonas nautica*, *Canadian Journal of Microbiology*, 35(11), pp. 1061–1064. doi: 10.1139/m89-177.
- Brezonik, P. L. and Lee, G. F. (1968). Denitrification as a nitrogen sink in Lake Mendota, Wisconsin, *Environmental Science & Technology*, 2(2), pp. 120–125.
- Buchwald, C., Grabb, K., Hansel, C. M. and Wankel, S. D. (2016). Constraining the role of iron in environmental nitrogen transformations: Dual stable isotope systematics of abiotic NO₂⁻ reduction by Fe(II) and its production of N₂O, *Geochimica et Cosmochimica Acta*, 186, pp. 1–12. doi: 10.1016/j.gca.2016.04.041.
- Butler, J. H. and Montzka, S. A. (2019). *The NOAA Annual Greenhouse Gas Index (AGGI), The NOAA Annual Greenhouse Gas Index (AGGI)*. Available at: <https://www.esrl.noaa.gov/gmd/aggi/aggi.html> (Accessed: 3 March 2020).
- Canfield, D. E., Glazer, A. N. and Falkowski, P. G. (2010). The evolution and future of Earth's nitrogen cycle, *Science*, 330(6001), pp. 192–196. doi: 10.1126/science.1186120.
- Caranto, J. D. and Lancaster, K. M. (2017). Nitric oxide is an obligate bacterial nitrification intermediate produced by hydroxylamine oxidoreductase, *Proceedings of the National Academy of Sciences*, 114(31), pp. 8217–8222. doi: 10.1073/pnas.1704504114.
- Carini, P., White, A. E., Campbell, E. O. and Giovannoni, S. J. (2014). Methane production by phosphate-starved SAR11 chemoheterotrophic marine bacteria, *Nature Communications*, 5, p. 4346. doi: 10.1038/ncomms5346.
- Carini, P., Dupont, C. L. and Santoro, A. E. (2018). Patterns of thaumarchaeal gene expression in culture and diverse marine environments, *Environmental Microbiology*, 20(6), pp. 2112–2124. doi: 10.1111/1462-2920.14107.
- Carini, S. A. and Joye, S. B. (2008). Nitrification in Mono Lake, California: Activity and community composition during contrasting hydrological regimes, *Limnology and Oceanography*, 53(6), pp. 2546–2557. doi: 10.4319/lo.2008.53.6.2546.
- Chan, Y. K. and Campbell, N. E. R. (1980). Denitrification in Lake 227 during summer stratification, *Canadian Journal of Fisheries and Aquatic Sciences*, 37(3), pp. 506–512. doi: 10.1139/f80-065.
- Chistoserdova, L., Vorholt, J. A., Thauer, R. K. and Lidstrom, M. E. (1998). C1 transfer enzymes and coenzymes linking methylotrophic bacteria and methanogenic archaea, *Science*, 281(5373), pp. 99–102. doi: 10.1126/science.281.5373.99.
- Cole, J. J., Caraco, N. F., Kling, G. W. and Kratz, T. K. (1994). Carbon dioxide supersaturation in the surface waters of lakes, *Science*, 265(5178), pp. 1568–1570. doi:

10.1126/science.265.5178.1568.

- Cole, J. J., Prairie, Y. T., Caraco, N. F., McDowell, W. H., Tranvik, L. J., Striegl, R. G., Duarte, C. M., Kortelainen, P., Downing, J. A., Middelburg, J. J. and Melack, J. (2007). Plumbing the global carbon cycle: Integrating inland waters into the terrestrial carbon budget, *Ecosystems*, 10(1), pp. 172–185. doi: 10.1007/s10021-006-9013-8.
- Daims, H., Lebedeva, E. V., Pjevac, P., Han, P., Herbold, C., Albertsen, M., Jehmlich, N., Palatinszky, M., Vierheilig, J., Bulaev, A., Kirkegaard, R. H., von Bergen, M., Rattei, T., Bendinger, B., Nielsen, P. H. and Wagner, M. (2015). Complete nitrification by *Nitrospira* bacteria, *Nature*, 528(7583), pp. 504–509. doi: 10.1038/nature16461.
- Damm, E., Kiene, R. P., Schwarz, J., Falck, E. and Dieckmann, G. (2008). Methane cycling in Arctic shelf water and its relationship with phytoplankton biomass and DMSP, *Marine Chemistry*, 109(1–2), pp. 45–59. doi: 10.1016/j.marchem.2007.12.003.
- Damm, E., Helmke, E., Thoms, S., Schauer, U., Nöthig, E., Bakker, K. and Kiene, R. P. (2010). Methane production in aerobic oligotrophic surface water in the central Arctic Ocean, *Biogeosciences*, 7(3), pp. 1099–1108. doi: 10.5194/bg-7-1099-2010.
- Damm, E., Thoms, S., Beszczynska-Möller, A., Nöthig, E. M. and Kattner, G. (2015). Methane excess production in oxygen-rich polar water and a model of cellular conditions for this paradox, *Polar Science*, 9(3), pp. 327–334. doi: 10.1016/j.polar.2015.05.001.
- Deemer, B. R., Harrison, J. A., Li, S., Beaulieu, J. J., DelSontro, T., Barros, N., Bezerra-Neto, J. F., Powers, S. M., dos Santos, M. A. and Vonk, J. A. (2016). Greenhouse gas emissions from reservoir water surfaces: a new global synthesis, *BioScience*, 66(11), pp. 949–964. doi: 10.1093/biosci/biw117.
- DelSontro, T., Beaulieu, J. J. and Downing, J. A. (2018a). Greenhouse gas emissions from lakes and impoundments: Upscaling in the face of global change, *Limnology and Oceanography Letters*, 3(3), pp. 64–75. doi: 10.1002/lol2.10073.
- DelSontro, T., del Giorgio, P. A. and Prairie, Y. T. (2018b). No longer a paradox: The interaction between physical transport and biological processes explains the spatial distribution of surface water methane within and across lakes, *Ecosystems*, 21(6), pp. 1073–1087. doi: 10.1007/s10021-017-0205-1.
- Dong, L. F., Sobey, M. N., Smith, C. J., Rusmana, I., Phillips, W., Stott, A., Osborn, A. M. and Nedwell, D. B. (2011). Dissimilatory reduction of nitrate to ammonium, not denitrification or anammox, dominates benthic nitrate reduction in tropical estuaries, *Limnology and Oceanography*, 56(1), pp. 279–291. doi: 10.4319/lo.2011.56.1.0279.
- Donis, D., Flury, S., Stöckli, A., Spangenberg, J. E., Vachon, D. and McGinnis, D. F. (2017). Full-scale evaluation of methane production under oxic conditions in a mesotrophic lake, *Nature Communications*, 8(1), p. 1661. doi: 10.1038/s41467-017-01648-4.
- Downes, M. T. (1988). Aquatic nitrogen transformations at low oxygen concentrations., *Applied and Environmental Microbiology*, 54(1), pp. 172–175.
- Encinas Fernández, J., Peeters, F. and Hofmann, H. (2016). On the methane paradox: Transport from shallow water zones rather than in situ methanogenesis is the major source of CH₄ in the open surface water of lakes, *Journal of Geophysical Research*:

- Biogeosciences*, 121(10), pp. 2717–2726. doi: 10.1002/2016JG003586.
- Erkkilä, K.-M., Ojala, A., Bastviken, D., Biermann, T., Heiskanen, J. J., Lindroth, A., Peltola, O., Rantakari, M., Vesala, T. and Mammarella, I. (2018). Methane and carbon dioxide fluxes over a lake: comparison between eddy covariance, floating chambers and boundary layer method, *Biogeosciences*, 15(2), pp. 429–445. doi: 10.5194/bg-15-429-2018.
- Frame, C. H. and Casciotti, K. L. (2010). Biogeochemical controls and isotopic signatures of nitrous oxide production by a marine ammonia-oxidizing bacterium, *Biogeosciences*, 7(9), pp. 2695–2709. doi: <https://doi.org/10.5194/bg-7-2695-2010>.
- Frame, C. H., Lau, E., Nolan, E. J., Goepfert, T. J. and Lehmann, M. F. (2017). Acidification enhances hybrid N₂O production associated with aquatic ammonia-oxidizing microorganisms, *Frontiers in Microbiology*, 7, p. 2104. doi: 10.3389/fmicb.2016.02104.
- Francis, C. A., Roberts, K. J., Beman, J. M., Santoro, A. E. and Oakley, B. B. (2005). Ubiquity and diversity of ammonia-oxidizing archaea in water columns and sediments of the ocean, *Proceedings of the National Academy of Sciences*, 102(41), pp. 14683–14688. doi: 10.1073/pnas.0506625102.
- Friedl, G. and Wüest, A. (2002). Disrupting biogeochemical cycles - Consequences of damming, *Aquatic Sciences*, 64(1), pp. 55–65. doi: 10.1007/s00027-002-8054-0.
- GDW. (2020). *Global Reservoir and Dam (GRanD) Database, Global Dam Watch*. Available at: <http://globaldamwatch.org/data/> (Accessed: 9 March 2020).
- Goering, J. J. and Dugdale, V. A. (1966). Estimates of the rates of denitrification in a subarctic lake, *Limnology and Oceanography*, 11(1), pp. 113–117. doi: 10.4319/lo.1966.11.1.0113.
- Gomez-Garcia, M. R., Davison, M., Blain-Hartnung, M., Grossman, A. R. and Bhaya, D. (2011). Alternative pathways for phosphonate metabolism in thermophilic cyanobacteria from microbial mats, *The ISME journal*, 5(1), pp. 141–149. doi: 10.1038/ismej.2010.96.
- Goreau, T. J., Kaplan, W. A., Wofsy, S. C., McElroy, M. B., Valois, F. W. and Watson, S. W. (1980). Production of NO₂⁻ and N₂O by nitrifying bacteria at reduced concentrations of oxygen, *Appl. Environ. Microbiol.*, 40(3), pp. 526–532.
- Grabarse, W., Mahlert, F., Duin, E. C., Goubeaud, M., Shima, S., Thauer, R. K., Lamzin, V. and Ermler, U. (2001). On the mechanism of biological methane formation: structural evidence for conformational changes in methyl-coenzyme M reductase upon substrate binding, *Journal of Molecular Biology*, 309(1), pp. 315–330. doi: 10.1006/jmbi.2001.4647.
- Grossart, H.-P., Frindte, K., Dziallas, C., Eckert, W. and Tang, K. W. (2011). Microbial methane production in oxygenated water column of an oligotrophic lake, *Proceedings of the National Academy of Sciences*, 108(49), pp. 19657–19661. doi: 10.1073/pnas.1110716108.
- Gruber, N. and Galloway, J. N. (2008). An Earth-system perspective of the global nitrogen cycle, *Nature*, 451(7176), pp. 293–296. doi: 10.1038/nature06592.

- Hallin, S., Philippot, L., Löffler, F. E., Sanford, R. A. and Jones, C. M. (2018). Genomics and ecology of novel N₂O-reducing microorganisms, *Trends in Microbiology*, 26(1), pp. 43–55. doi: 10.1016/j.tim.2017.07.003.
- Hamersley, M. R., Woebken, D., Boehrer, B., Schultze, M., Lavik, G. and Kuypers, M. M. M. (2009). Water column anammox and denitrification in a temperate permanently stratified lake (Lake Rassnitzer, Germany), *Systematic and Applied Microbiology*, 32(8), pp. 571–582. doi: 10.1016/j.syapm.2009.07.009.
- Harrison, J. A., Maranger, R. J., Alexander, R. B., Giblin, A. E., Jacinthe, P.-A., Mayorga, E., Seitzinger, S. P., Sobota, D. J. and Wollheim, W. M. (2009). The regional and global significance of nitrogen removal in lakes and reservoirs, *Biogeochemistry*, 93(1–2), pp. 143–157. doi: 10.1007/s10533-008-9272-x.
- Hartmann, J. F., Günthel, M., Klintzsch, T., Kirillin, G., Grossart, H.-P., Keppler, F. and Isenbeck-Schröter, M. (2020). High spatiotemporal dynamics of methane production and emission in oxic surface water, *Environmental Science & Technology*, 54(3), pp. 1451–1463. doi: 10.1021/acs.est.9b03182.
- Hayatsu, M., Tago, K. and Saito, M. (2008). Various players in the nitrogen cycle: Diversity and functions of the microorganisms involved in nitrification and denitrification, *Soil Science and Plant Nutrition*, 54(1), pp. 33–45. doi: 10.1111/j.1747-0765.2007.00195.x.
- Heathcote, A. J. and Downing, J. A. (2012). Impacts of eutrophication on carbon burial in freshwater lakes in an intensively agricultural landscape, *Ecosystems*, 15(1), pp. 60–70. doi: 10.1007/s10021-011-9488-9.
- Heil, J., Wolf, B., Brüggemann, N., Emmenegger, L., Tuzson, B., Vereecken, H. and Mohn, J. (2014). Site-specific ¹⁵N isotopic signatures of abiotically produced N₂O, *Geochimica et Cosmochimica Acta*, 139, pp. 72–82.
- Hink, L., Gubry-Rangin, C., Nicol, G. W. and Prosser, J. I. (2018). The consequences of niche and physiological differentiation of archaeal and bacterial ammonia oxidisers for nitrous oxide emissions, *The ISME Journal*, 12(4), pp. 1084–1093. doi: 10.1038/s41396-017-0025-5.
- Hochstein, L. I., Betlach, M. and Kritikos, G. (1984). The effect of oxygen on denitrification during steady-state growth of *Paracoccus halodenitrificans*, *Archives of Microbiology*, 137(1), pp. 74–78. doi: 10.1007/BF00425811.
- Howarth, R. W., Billen, G., Swaney, D., Townsend, A., Jaworski, N., Lajtha, K., Downing, J. A., Elmgren, R., Caraco, N., Jordan, T., Berendse, F., Freney, J., Kudryarov, V., Murdoch, P. and Zhao-Liang, Z. (1996). Regional nitrogen budgets and riverine N & P fluxes for the drainages to the North Atlantic Ocean: Natural and human influences, *Biogeochemistry*, 35(1), pp. 75–139. doi: 10.1007/BF02179825.
- Hu, H.-W., Xu, Z.-H. and He, J.-Z. (2014). Ammonia-oxidizing archaea play a predominant role in acid soil nitrification, in Sparks, D. L. (ed.) *Advances in Agronomy*, Vol 125, pp. 261–302.
- IPCC. (2013). *Climate Change 2013: The Physical Science Basis. Contribution of Working Group I to the Fifth Assessment Report of the Intergovernmental Panel on Climate Change* Cambridge, United Kingdom and New York, NY, USA: Cambridge University

Press. Edited by T. F. Stocker, D. Qin, G.-K. Plattner, M. Tignor, S. K. Allen, J. Boschung, A. Nauels, Y. Xia, V. Bex, and P. M. Midgley. Available at: <https://www.ipcc.ch/report/ar5/wg1/>.

- Jarrell, K. F. (1985). Extreme oxygen sensitivity in methanogenic archaeobacteria, *BioScience*, 35(5), pp. 298–302. doi: 10.2307/1309929.
- Johannessen, S. C. and Miller, W. L. (2001). Quantum yield for the photochemical production of dissolved inorganic carbon in seawater, *Marine Chemistry*, 76(4), pp. 271–283. doi: 10.1016/S0304-4203(01)00067-6.
- Junier, P., Kim, O.-S., Witzel, K.-P., Imhoff, J. F. and Hadas, O. (2008). Habitat partitioning of denitrifying bacterial communities carrying *nirS* or *nirK* genes in the stratified water column of Lake Kinneret, Israel, *Aquatic Microbial Ecology*, 51(2), pp. 129–140. doi: 10.3354/ame01186.
- Kampmann, K., Ratering, S., Baumann, R., Schmidt, M., Zerr, W. and Schnell, S. (2012). Hydrogenotrophic methanogens dominate in biogas reactors fed with defined substrates, *Systematic and Applied Microbiology*, 35(6), pp. 404–413. doi: 10.1016/j.syapm.2012.07.002.
- Karl, D. M. and Tilbrook, B. D. (1994). Production and transport of methane in oceanic particulate organic matter, *Nature*, 368(6473), pp. 732–734. doi: 10.1038/368732a0.
- Karl, D. M., Beversdorf, L., Björkman, K. M., Church, M. J., Martinez, A. and Delong, E. F. (2008). Aerobic production of methane in the sea, *Nature Geoscience*, 1(7), pp. 473–478. doi: 10.1038/ngeo234.
- Kendall, C. and Caldwell, E. A. (1998). Chapter 2: Fundamentals of isotope geochemistry, in Kendall, C. and McDonnell, J. J. (eds) *Isotope tracers in catchment hydrology*, pp. 51–86. Available at: <https://wwwrcamnl.wr.usgs.gov/isoig/isopubs/itchch2.html#2.2.2>.
- van Kessel, M. A. H. J., Speth, D. R., Albertsen, M., Nielsen, P. H., Op den Camp, H. J. M., Kartal, B., Jetten, M. S. M. and Lücker, S. (2015). Complete nitrification by a single microorganism, *Nature*, 528(7583), pp. 555–559. doi: 10.1038/nature16459.
- Khatun, S., Iwata, T., Kojima, H., Ikarashi, Y., Yamanami, K., Imazawa, D., Kenta, T., Shinohara, R. and Saito, H. (2020). Linking stoichiometric organic carbon–nitrogen relationships to planktonic cyanobacteria and subsurface methane maximum in deep freshwater lakes, *Water*, 12(2), p. 402. doi: 10.3390/w12020402.
- Kiene, R. P. (1991). Production and consumption of methane in aquatic systems, in Rogers, J. E. and Whitman, W. B. (eds) *Microbial Production and Consumption of Greenhouse Gases: Methane, Nitrogen Oxides, and Halomethanes*, pp. 111–146.
- Kim, O.-S., Imhoff, J. F., Witzel, K.-P. and Junier, P. (2011). Distribution of denitrifying bacterial communities in the stratified water column and sediment–water interface in two freshwater lakes and the Baltic Sea, *Aquatic Ecology*, 45(1), pp. 99–112. doi: 10.1007/s10452-010-9335-7.
- Klitzsch, T., Langer, G., Nehrke, G., Wieland, A., Lenhart, K. and Keppler, F. (2019). Methane production by three widespread marine phytoplankton species: release rates, precursor compounds, and potential relevance for the environment, *Biogeosciences*, 16(20), pp. 4129–4144. doi: 10.5194/bg-16-4129-2019.

- Koehler, B., Landelius, T., Weyhenmeyer, G. A., Machida, N. and Tranvik, L. J. (2014). Sunlight-induced carbon dioxide emissions from inland waters, *Global Biogeochemical Cycles*, 28(7), pp. 696–711. doi: 10.1002/2014GB004850.
- Könneke, M., Bernhard, A. E., de la Torre, J. R., Walker, C. B., Waterbury, J. B. and Stahl, D. A. (2005). Isolation of an autotrophic ammonia-oxidizing marine archaeon, *Nature*, 437(7058), pp. 543–546. doi: 10.1038/nature03911.
- Kowalchuk, G. A. and Stephen, J. R. (2001). Ammonia-oxidizing bacteria: A model for molecular microbial ecology, *Annual Review of Microbiology*, 55(1), pp. 485–529. doi: 10.1146/annurev.micro.55.1.485.
- Kuypers, M. M. M., Marchant, H. K. and Kartal, B. (2018). The microbial nitrogen-cycling network, *Nature Reviews Microbiology*, 16(5), pp. 263–276. doi: 10.1038/nrmicro.2018.9.
- Lashof, D. A. and Ahuja, D. R. (1990). Relative contributions of greenhouse gas emissions to global warming, *Nature*, 344(6266), pp. 529–531. doi: 10.1038/344529a0.
- Le Quéré, C. L., Andrew, R. M., Friedlingstein, P., Sitch, S., Hauck, J., Pongratz, J., Pickers, P. A., Korsbakken, J. I., Peters, G. P., Canadell, J. G., Arneeth, A., Arora, V. K., Barbero, L., Bastos, A., Bopp, L., Chevallier, F., Chini, L. P., Ciais, P., Doney, S. C., Gkritzalis, T., Goll, D. S., Harris, I., Haverd, V., Hoffman, F. M., Hoppema, M., Houghton, R. A., Hurtt, G., Ilyina, T., Jain, A. K., Johannessen, T., Jones, C. D., Kato, E., Keeling, R. F., Goldewijk, K. K., Landschützer, P., Lefèvre, N., Lienert, S., Liu, Z., Lombardozzi, D., Metzl, N., Munro, D. R., Nabel, J. E. M. S., Nakaoka, S., Neill, C., Olsen, A., Ono, T., Patra, P., Peregon, A., Peters, W., Peylin, P., Pfeil, B., Pierrot, D., Poulter, B., Rehder, G., Resplandy, L., Robertson, E., Rocher, M., Rödenbeck, C., Schuster, U., Schwinger, J., Séférian, R., Skjelvan, I., Steinhoff, T., Sutton, A., Tans, P. P., Tian, H., Tilbrook, B., Tubiello, F. N., Laan-Luijckx, I. T. van der, Werf, G. R. van der, Viovy, N., Walker, A. P., Wiltshire, A. J., Wright, R., Zaehle, S. and Zheng, B. (2018). Global Carbon Budget 2018, *Earth System Science Data*, 10(4), pp. 2141–2194. doi: 10.5194/essd-10-2141-2018.
- Lehner, B. and Döll, P. (2004). Development and validation of a global database of lakes, reservoirs and wetlands, *Journal of Hydrology*, 296(1), pp. 1–22. doi: 10.1016/j.jhydrol.2004.03.028.
- Lehner, B., Liermann, C. R., Revenga, C., Vörösmarty, C., Fekete, B., Crouzet, P., Döll, P., Endejan, M., Frenken, K., Magome, J., Nilsson, C., Robertson, J. C., Rödel, R., Sindorf, N. and Wisser, D. (2011). High-resolution mapping of the world's reservoirs and dams for sustainable river-flow management, *Frontiers in Ecology and the Environment*, 9(9), pp. 494–502. doi: 10.1890/100125.
- Leininger, S., Urlich, T., Schloter, M., Schwark, L., Qi, J., Nicol, G. W., Prosser, J. I., Schuster, S. C. and Schleper, C. (2006). Archaea predominate among ammonia-oxidizing prokaryotes in soils, *Nature*, 442(7104), pp. 806–809. doi: 10.1038/nature04983.
- Lenhart, K., Bunge, M., Ratering, S., Neu, T. R., Schüttmann, I., Greule, M., Kammann, C., Schnell, S., Müller, C., Zorn, H. and Keppler, F. (2012). Evidence for methane production by saprotrophic fungi, *Nature Communications*, 3, p. 1046. doi: 10.1038/ncomms2049.

- Lenhart, K., Althoff, F., Greule, M. and Keppler, F. (2015). Technical Note: Methionine, a precursor of methane in living plants, *Biogeosciences*, 12(6), pp. 1907–1914. doi: 10.5194/bg-12-1907-2015.
- Lenhart, K., Klintzsch, T., Langer, G., Nehrke, G., Bunge, M., Schnell, S. and Keppler, F. (2016). Evidence for methane production by the marine algae *Emiliana huxleyi*, *Biogeosciences*, 13(10), pp. 3163–3174. doi: 10.5194/bg-13-3163-2016.
- Liu, H., Zhang, Q., Katul, G. G., Cole, J. J., Chapin, F. S. and MacIntyre, S. (2016). Large CO₂ effluxes at night and during synoptic weather events significantly contribute to CO₂ emissions from a reservoir, *Environmental Research Letters*, 11(6), p. 064001. doi: 10.1088/1748-9326/11/6/064001.
- Liu, S., Han, P., Hink, L., Prosser, J. I., Wagner, M. and Brüggemann, N. (2017). Abiotic conversion of extracellular NH₂OH contributes to N₂O emission during ammonia oxidation, *Environmental Science & Technology*, 51(22), pp. 13122–13132. doi: 10.1021/acs.est.7b02360.
- Lloyd, D., Boddy, L. and Davies, K. J. P. (1987). Persistence of bacterial denitrification capacity under aerobic conditions: The rule rather than the exception, *FEMS Microbiology Ecology*, 3(3), pp. 185–190. doi: 10.1111/j.1574-6968.1987.tb02354.x.
- Lloyd, D. (1993). Aerobic denitrification in soils and sediments: From fallacies to factx, *Trends in Ecology & Evolution*, 8(10), pp. 352–356. doi: 10.1016/0169-5347(93)90218-E.
- López, P., Marcé, R. and Armengol, J. (2011). Net heterotrophy and CO₂ evasion from a productive calcareous reservoir: Adding complexity to the metabolism-CO₂ evasion issue, *Journal of Geophysical Research: Biogeosciences*, 116(G2). doi: 10.1029/2010JG001614.
- Löscher, C. R., Kock, A., Könneke, M., LaRoche, J., Bange, H. W. and Schmitz, R. A. (2012). Production of oceanic nitrous oxide by ammonia-oxidizing archaea, *Biogeosciences*, 9(7), pp. 2419–2429. doi: <https://doi.org/10.5194/bg-9-2419-2012>.
- Marcé, R., Obrador, B., Morguí, J.-A., Riera, J. L., López, P. and Armengol, J. (2015). Carbonate weathering as a driver of CO₂ supersaturation in lakes, *Nature Geoscience*, 8(2), pp. 107–111. doi: 10.1038/ngeo2341.
- Marotta, H., Pinho, L., Gudas, C., Bastviken, D., Tranvik, L. J. and Enrich-Prast, A. (2014). Greenhouse gas production in low-latitude lake sediments responds strongly to warming, *Nature Climate Change*, 4(6), pp. 467–470. doi: 10.1038/nclimate2222.
- Martin, T. S. and Casciotti, K. L. (2016). Nitrogen and oxygen isotopic fractionation during microbial nitrite reduction, *Limnology and Oceanography*, 61(3), pp. 1134–1143. doi: 10.1002/lno.10278.
- McCrackin, M. L. and Elser, J. J. (2011). Greenhouse gas dynamics in lakes receiving atmospheric nitrogen deposition, *Global Biogeochemical Cycles*, 25(4), p. GB4005. doi: 10.1029/2010GB003897.
- McDonald, C. P., Stets, E. G., Striegl, R. G. and Butman, D. (2013). Inorganic carbon loading as a primary driver of dissolved carbon dioxide concentrations in the lakes and reservoirs of the contiguous United States, *Global Biogeochemical Cycles*, 27(2), pp.

- 285–295. doi: 10.1002/gbc.20032.
- Mendonça, R., Müller, R. A., Clow, D., Verpoorter, C., Raymond, P., Tranvik, L. J. and Sobek, S. (2017). Organic carbon burial in global lakes and reservoirs, *Nature Communications*, 8(1), p. 1694. doi: 10.1038/s41467-017-01789-6.
- Michmerhuizen, C. M., Striegl, R. G. and McDonald, M. E. (1996). Potential methane emission from north-temperate lakes following ice melt, *Limnology and Oceanography*, 41(5), pp. 985–991. doi: 10.4319/lo.1996.41.5.0985.
- Mitsch, W. J., Bernal, B., Nahlik, A. M., Mander, Ü., Zhang, L., Anderson, C. J., Jørgensen, S. E. and Brix, H. (2012). Wetlands, carbon, and climate change, *Landscape Ecology*, 28(4), pp. 583–597. doi: 10.1007/s10980-012-9758-8.
- Mulholland, P. J., Helton, A. M., Poole, G. C., Hall, R. O., Hamilton, S. K., Peterson, B. J., Tank, J. L., Ashkenas, L. R., Cooper, L. W., Dahm, C. N., Dodds, W. K., Findlay, S. E. G., Gregory, S. V., Grimm, N. B., Johnson, S. L., McDowell, W. H., Meyer, J. L., Valett, H. M., Webster, J. R., Arango, C. P., Beaulieu, J. J., Bernot, M. J., Burgin, A. J., Crenshaw, C. L., Johnson, L. T., Niederlehner, B. R., O'Brien, J. M., Potter, J. D., Sheibley, R. W., Sobota, D. J. and Thomas, S. M. (2008). Stream denitrification across biomes and its response to anthropogenic nitrate loading, *Nature*, 452(7184), p. 202. doi: 10.1038/nature06686.
- Murase, J., Sakai, Y., Sugimoto, A., Okubo, K. and Sakamoto, M. (2003). Sources of dissolved methane in Lake Biwa, *Limnology*, 4(2), pp. 91–99. doi: 10.1007/s10201-003-0095-0.
- Murphy, D. M. and Ravishankara, A. R. (2018). Trends and patterns in the contributions to cumulative radiative forcing from different regions of the world, *Proceedings of the National Academy of Sciences of the United States of America*, 115(52), pp. 13192–13197. doi: 10.1073/pnas.1813951115.
- Nizzoli, D., Carraro, E., Nigro, V. and Viaroli, P. (2010). Effect of organic enrichment and thermal regime on denitrification and dissimilatory nitrate reduction to ammonium (DNRA) in hypolimnetic sediments of two lowland lakes, *Water Research*, 44(9), pp. 2715–2724. doi: 10.1016/j.watres.2010.02.002.
- Oremland, R. S. (1979). Methanogenic activity in plankton samples and fish intestines: A mechanism for in situ methanogenesis in oceanic surface waters, *Limnology and Oceanography*, 24(6), pp. 1136–1141. doi: 10.4319/lo.1979.24.6.1136.
- Ortega-Retuerta, E., Pulido-Villena, E. and Reche, I. (2007). Effects of dissolved organic matter photoproducts and mineral nutrient supply on bacterial growth in Mediterranean inland waters, *Microbial Ecology*, 54(1), pp. 161–169. doi: 10.1007/s00248-006-9186-x.
- Oswald, K., Milucka, J., Brand, A., Littmann, S., Wehrli, B., Kuypers, M. M. M. and Schubert, C. J. (2015). Light-dependent aerobic methane oxidation reduces methane emissions from seasonally stratified lakes, *PLoS one*, 10(7), pp. e0132574–e0132574. doi: 10.1371/journal.pone.0132574.
- Oswald, K., Jegge, C., Tischer, J., Berg, J., Brand, A., Miracle, M. R., Soria, X., Vicente, E., Lehmann, M. F., Zopfi, J. and Schubert, C. J. (2016). Methanotrophy under versatile conditions in the water column of the ferruginous meromictic lake La Cruz (Spain), *Frontiers in microbiology*, 7, p. 1762. doi: 10.3389/fmicb.2016.01762.

- Owens, N. J. P., Law, C. S., Mantoura, R. F. C., Burkill, P. H. and Llewellyn, C. A. (1991). Methane flux to the atmosphere from the Arabian Sea, *Nature*, 354(6351), pp. 293–296. doi: 10.1038/354293a0.
- Pajares, S., Merino-Ibarra, M., Macek, M. and Alcocer, J. (2017). Vertical and seasonal distribution of picoplankton and functional nitrogen genes in a high-altitude warm-monomictic tropical lake, *Freshwater Biology*, 62(7), pp. 1180–1193. doi: 10.1111/fwb.12935.
- Palacin-Lizarbe, C., Camarero, L., Hallin, S., Jones, C. M., Cáliz, J., Casamayor, E. O. and Catalan, J. (2019). The DNRA-Denitrification Dichotomy Differentiates Nitrogen Transformation Pathways in Mountain Lake Benthic Habitats, *Frontiers in Microbiology*, 10. doi: 10.3389/fmicb.2019.01229.
- Peeters, F., Wüest, A., Piepke, G. and Imboden, D. M. (1996). Horizontal mixing in lakes, *Journal of Geophysical Research: Oceans*, 101(C8), pp. 18361–18375. doi: 10.1029/96JC01145.
- Peeters, F., Fernandez Encinas, J. and Hofmann, H. (2019). Sediment fluxes rather than oxic methanogenesis explain diffusive CH₄ emissions from lakes and reservoirs, *Scientific Reports*, 9(1), pp. 1–10. doi: 10.1038/s41598-018-36530-w.
- Piña-Ochoa, E. and Álvarez-Cobelas, M. (2006). Denitrification in aquatic environments: A cross-system analysis, *Biogeochemistry*, 81(1), pp. 111–130. doi: 10.1007/s10533-006-9033-7.
- Prosser, J. I. and Nicol, G. W. (2008). Relative contributions of archaea and bacteria to aerobic ammonia oxidation in the environment, *Environmental Microbiology*, 10(11), pp. 2931–2941. doi: 10.1111/j.1462-2920.2008.01775.x.
- Rasilo, T., Prairie, Y. T. and del Giorgio, P. A. (2015). Large-scale patterns in summer diffusive CH₄ fluxes across boreal lakes, and contribution to diffusive C emissions, *Global Change Biology*, 21(3), pp. 1124–1139. doi: 10.1111/gcb.12741.
- Ravishankara, A. R., Daniel, J. S. and Portmann, R. W. (2009). Nitrous oxide (N₂O): The dominant ozone-depleting substance emitted in the 21st century, *Science*, 326(5949), pp. 123–125. doi: 10.1126/science.1176985.
- Raymond, P. A., Hartmann, J., Lauerwald, R., Sobek, S., McDonald, C., Hoover, M., Butman, D., Striegl, R., Mayorga, E., Humborg, C., Kortelainen, P., Dürr, H., Meybeck, M., Ciais, P. and Guth, P. (2013). Global carbon dioxide emissions from inland waters, *Nature*, 503(7476), pp. 355–359. doi: 10.1038/nature12760.
- Reche, I., Pace, M. L. and Cole, J. J. (1998). Interactions of Photobleaching and Inorganic Nutrients in Determining Bacterial Growth on Colored Dissolved Organic Carbon, *Microbial Ecology*, 36(3), pp. 270–280. doi: 10.1007/s002489900114.
- Reche, I. (2003). Sensibilidad de los ecosistemas acuáticos a la radiación ultravioleta: el papel de la materia orgánica disuelta, *Revista Ecosistemas*, 12(1). doi: 10.7818/re.2014.12-1.00.
- Repeta, D. J., Ferrón, S., Sosa, O. A., Johnson, C. G., Repeta, L. D., Acker, M., DeLong, E. F. and Karl, D. M. (2016). Marine methane paradox explained by bacterial degradation of dissolved organic matter, *Nature Geoscience*, 9(12), pp. 884–887. doi:

10.1038/ngeo2837.

- Rissanen, A. J., Tirola, M., Hietanen, S. and Ojala, A. (2013). Interlake variation and environmental controls of denitrification across different geographical scales, *Aquatic Microbial Ecology*, 69(1), pp. 1–16. doi: 10.3354/ame01619.
- Robertson, L. A. and Kuenen, J. G. (1984). Aerobic denitrification — old wine in new bottles?, *Antonie van Leeuwenhoek*, 50(5), pp. 525–544. doi: 10.1007/BF02386224.
- Robertson, L. A., Cornelisse, R., De Vos, P., Hadjioetomo, R. and Kuenen, J. G. (1989). Aerobic denitrification in various heterotrophic nitrifiers, *Antonie van Leeuwenhoek*, 56(4), pp. 289–299. doi: 10.1007/BF00443743.
- Robertson, L. A., Dalsgaard, T., Revsbech, N.-P. and Kuenen, J. G. (1995). Confirmation of ‘aerobic denitrification’ in batch cultures, using gas chromatography and ^{15}N mass spectrometry, *FEMS Microbiology Ecology*, 18(2), pp. 113–119. doi: 10.1111/j.1574-6941.1995.tb00168.x.
- Robinson, D. (2001). $\delta^{15}\text{N}$ as an integrator of the nitrogen cycle, *Trends in Ecology & Evolution*, 16(3), pp. 153–162. doi: 10.1016/S0169-5347(00)02098-X.
- Roland, F. A. E., Darchambeau, F., Borges, A. V., Morana, C., Brabandere, L. D., Thamdrup, B. and Crowe, S. A. (2018). Denitrification, anaerobic ammonium oxidation, and dissimilatory nitrate reduction to ammonium in an East African Great Lake (Lake Kivu), *Limnology and Oceanography*, 63(2), pp. 687–701. doi: 10.1002/lno.10660.
- Rosamond, M. S., Thuss, S. J., Schiff, S. L. and Elgood, R. J. (2011). Coupled Cycles of Dissolved Oxygen and Nitrous Oxide in Rivers along a Trophic Gradient in Southern Ontario, Canada, *Journal of Environmental Quality*, 40(1), pp. 256–270. doi: 10.2134/jeq2010.0009.
- Rudd, J. W. M. and Hamilton, R. D. (1978). Methane cycling in a eutrophic shield lake and its effects on whole lake metabolism, *Limnology and Oceanography*, 23(2), pp. 337–348. doi: 10.4319/lo.1978.23.2.0337.
- Ryabenko, E. (2013). Stable isotope methods for the study of the nitrogen cycle, *Topics in Oceanography*, pp. 1–40. doi: 10.5772/56105.
- Salk, K. R., Ostrom, P. H., Biddanda, B. A., Weinke, A. D., Kendall, S. T. and Ostrom, N. E. (2016). Ecosystem metabolism and greenhouse gas production in a mesotrophic northern temperate lake experiencing seasonal hypoxia, *Biogeochemistry*, 131(3), pp. 303–319. doi: 10.1007/s10533-016-0280-y.
- Samiotis, G., Pekridis, G., Kaklidis, N., Trikoilidou, E., Taousanidis, N. and Amanatidou, E. (2018). Greenhouse gas emissions from two hydroelectric reservoirs in Mediterranean region, *Environmental Monitoring and Assessment*, 190(6), p. 363. doi: 10.1007/s10661-018-6721-4.
- Santoro, A. E., Buchwald, C., McIlvin, M. R. and Casciotti, K. L. (2011). Isotopic Signature of N_2O Produced by Marine Ammonia-Oxidizing Archaea, *Science*, 333, pp. 1282–1285. doi: 10.1126/science.1208239.
- Saunio, M., Bousquet, P., Poulter, B., Peregón, A., Ciais, P., Canadell, J. G., Dlugokencky, E. J., Etiope, G., Bastviken, D., Houweling, S., Janssens-Maenhout, G., Tubiello, F. N., Castaldi, S., Jackson, R. B., Alexe, M., Arora, V. K., Beerling, D. J., Bergamaschi, P.,

- Blake, D. R., Brailsford, G., Brovkin, V., Bruhwiler, L., Crevoisier, C., Crill, P., Covey, K., Curry, C., Frankenberg, C., Gedney, N., Höglund-Isaksson, L., Ishizawa, M., Ito, A., Joos, F., Kim, H.-S., Kleinen, T., Krummel, P., Lamarque, J.-F., Langenfelds, R., Locatelli, R., Machida, T., Maksyutov, S., McDonald, K. C., Marshall, J., Melton, J. R., Morino, I., Naik, V., O'Doherty, S., Parmentier, F.-J., Patra, P. K., Peng, C., Peng, S., Peters, G. P., Pison, I., Prigent, C., Prinn, R., Ramonet, M., Riley, W. J., Saito, M., Santini, M., Schroeder, R., Simpson, I. J., Spahni, R., Steele, P., Takizawa, A., Thornton, B. F., Tian, H., Tohjima, Y., Viovy, N., Voulgarakis, A., van Weele, M., van der Werf, G. R., Weiss, R., Wiedinmyer, C., Wilton, D. J., Wiltshire, A., Worthy, D., Wunch, D., Xu, X., Yoshida, Y., Zhang, B., Zhang, Z. and Zhu, Q. (2016). The global methane budget 2000–2012, *Earth System Science Data*, 8, pp. 697–751.
- Schlesinger, W. H. (2009). On the fate of anthropogenic nitrogen, *Proceedings of the National Academy of Sciences*, 106(1), pp. 203–208. doi: 10.1073/pnas.0810193105.
- Schmale, O., Wäge, J., Mohrholz, V., Wasmund, N., Gräwe, U., Rehder, G., Labrenz, M. and Loick-Wilde, N. (2018). The contribution of zooplankton to methane supersaturation in the oxygenated upper waters of the central Baltic Sea, *Limnology and Oceanography*, 63(1), pp. 412–430. doi: 10.1002/lno.10640.
- Schmidt, U. and Conrad, R. (1993). Hydrogen, carbon monoxide, and methane dynamics in Lake Constance, *Limnology and Oceanography*, 38(6), pp. 1214–1226. doi: 10.4319/lo.1993.38.6.1214.
- Schubert, C. J. and Wehrli, B. (2018). Contribution of methane formation and methane oxidation to methane emission from freshwater systems, *Biogenesis of Hydrocarbons*. Edited by A. J. M. Stams and D. Sousa. Available at: https://doi.org/10.1007/978-3-319-53114-4_18-1.
- Schulz, M., Faber, E., Hollerbach, A., Schröder, H. G. and Güde, H. (2001). The methane cycle in the epilimnion of Lake Constance, *Archiv für Hydrobiologie*, pp. 157–176. doi: 10.1127/archiv-hydrobiol/151/2001/157.
- Scranton, M. I. and Brewer, P. G. (1977). Occurrence of methane in the near-surface waters of the western subtropical North-Atlantic, *Deep Sea Research*, 24(2), pp. 127–138. doi: 10.1016/0146-6291(77)90548-3.
- Segers, R. (1998). Methane production and methane consumption: a review of processes underlying wetland methane fluxes, *Biogeochemistry*, 41(1), pp. 23–51. doi: 10.1023/A:1005929032764.
- Seitzinger, S. P. (1988). Denitrification in freshwater and coastal marine ecosystems: Ecological and geochemical significance, *Limnology and Oceanography*, 33(4part2), pp. 702–724. doi: 10.4319/lo.1988.33.4part2.0702.
- Seitzinger, S. P., Kroeze, C. and Styles, R. V. (2000). Global distribution of N₂O emissions from aquatic systems: natural emissions and anthropogenic effects, *Chemosphere - Global Change Science*, 2(3), pp. 267–279. doi: 10.1016/S1465-9972(00)00015-5.
- Sepulveda-Jauregui, A., Hoyos-Santillan, J., Martinez-Cruz, K., Walter Anthony, K. M., Casper, P., Belmonte-Izquierdo, Y. and Thalasso, F. (2018). Eutrophication exacerbates the impact of climate warming on lake methane emission, *Science of The Total Environment*, 636, pp. 411–419. doi: 10.1016/j.scitotenv.2018.04.283.

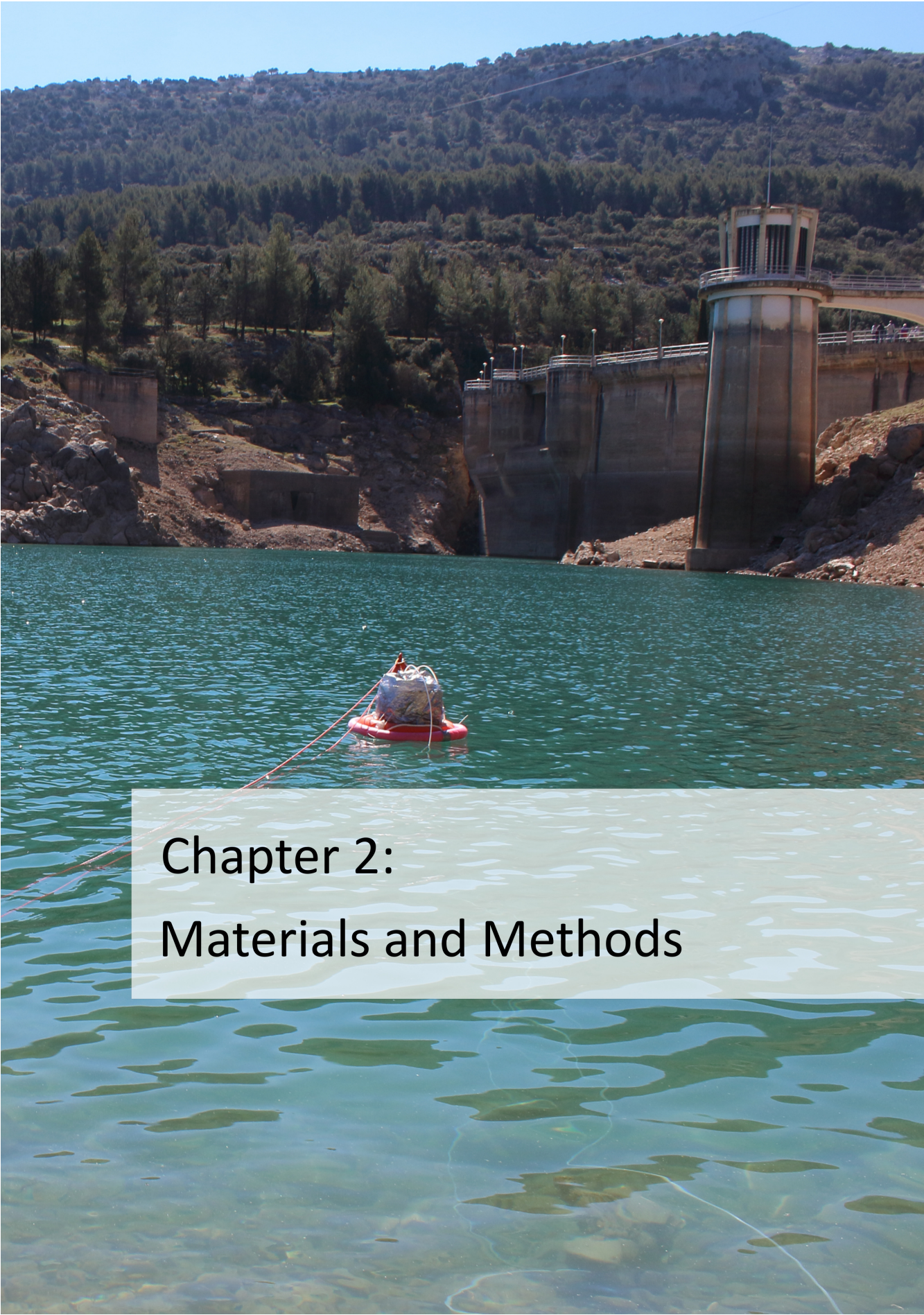
- Sigman, D. M., Karsh, K. L. and Casciotti, K. L. (2009). Nitrogen isotopes in the ocean, in Steele, J. H. (ed.) *Encyclopedia of Ocean Sciences (Second Edition)*, pp. 40–54. doi: 10.1016/B978-012374473-9.00632-9.
- Soler-Jofra, A., Stevens, B., Hoekstra, M., Piciooreanu, C., Sorokin, D., van Loosdrecht, M. C. and Pérez, J. (2016). Importance of abiotic hydroxylamine conversion on nitrous oxide emissions during nitrification of reject water, *Chemical Engineering Journal*, 287, pp. 720–726.
- Stanley, E. H., Casson, N. J., Christel, S. T., Crawford, J. T., Loken, L. C. and Oliver, S. K. (2016). The ecology of methane in streams and rivers: patterns, controls, and global significance, *Ecological Monographs*, 86(2), pp. 146–171. doi: 10.1890/15-1027.
- Steffen, W., Richardson, K., Rockström, J., Cornell, S. E., Fetzer, I., Bennett, E. M., Biggs, R., Carpenter, S. R., Vries, W. de, Wit, C. A. de, Folke, C., Gerten, D., Heinke, J., Mace, G. M., Persson, L. M., Ramanathan, V., Reyers, B. and Sörlin, S. (2015). Planetary boundaries: Guiding human development on a changing planet, *Science*, 347(6223). doi: 10.1126/science.1259855.
- Stein, L. Y. and Klotz, M. G. (2016). The nitrogen cycle, *Current Biology*, 26(3), pp. R94–R98. doi: 10.1016/j.cub.2015.12.021.
- Stieglmeier, M., Mooshammer, M., Kitzler, B., Wanek, W., Zechmeister-Boltenstern, S., Richter, A. and Schleper, C. (2014). Aerobic nitrous oxide production through N-nitrosating hybrid formation in ammonia-oxidizing archaea, *The ISME Journal*, 8(5), pp. 1135–1146. doi: 10.1038/ismej.2013.220.
- Stremińska, M. A., Felgate, H., Rowley, G., Richardson, D. J. and Baggs, E. M. (2012). Nitrous oxide production in soil isolates of nitrate-ammonifying bacteria, *Environmental Microbiology Reports*, 4(1), pp. 66–71. doi: 10.1111/j.1758-2229.2011.00302.x.
- Tang, K. W., McGinnis, D. F., Frindte, K., Brüchert, V. and Grossart, H.-P. (2014). Paradox reconsidered: Methane oversaturation in well-oxygenated lake waters, *Limnology and Oceanography*, 59(1), pp. 275–284. doi: 10.4319/lo.2014.59.1.0275.
- Tang, K. W., McGinnis, D. F., Ionescu, D. and Grossart, H.-P. (2016). Methane production in oxic lake waters potentially increases aquatic methane flux to air, *Environmental Science & Technology Letters*, 3(6), pp. 227–233. doi: 10.1021/acs.estlett.6b00150.
- Teikari, J. E., Fewer, D. P., Shrestha, R., Hou, S., Leikoski, N., Mäkelä, M., Simojoki, A., Hess, W. R. and Sivonen, K. (2018). Strains of the toxic and bloom-forming *Nodularia spumigena* (cyanobacteria) can degrade methylphosphonate and release methane, *The ISME Journal*, 12(6), pp. 1619–1630. doi: 10.1038/s41396-018-0056-6.
- Terada, A., Sugawara, S., Hojo, K., Takeuchi, Y., Riya, S., Harper, W. F., Yamamoto, T., Kuroiwa, M., Isobe, K., Katsuyama, C., Suwa, Y., Koba, K. and Hosomi, M. (2017). Hybrid nitrous oxide production from a partial nitrifying bioreactor: Hydroxylamine interactions with nitrite, *Environmental Science & Technology*, 51(5), pp. 2748–2756. doi: 10.1021/acs.est.6b05521.
- Thalasso, F., Sepulveda-Jauregui, A., Gandois, L., Martinez-Cruz, K., Gerardo-Nieto, O., Astorga-España, M. S., Teisserenc, R., Lavergne, C., Tananaev, N., Barret, M. and Cabrol, L. (2020). Sub-oxycline methane oxidation can fully uptake CH₄ produced in sediments: case study of a lake in Siberia, *Scientific Reports*, 10(1), pp. 1–7. doi:

10.1038/s41598-020-60394-8.

- Thamdrup, B. (2012). New pathways and processes in the global nitrogen cycle, *Annual Review of Ecology, Evolution, and Systematics*, 43(1), pp. 407–428. doi: 10.1146/annurev-ecolsys-102710-145048.
- Thanh-Duc, N., Crill, P. and Bastviken, D. (2010). Implications of temperature and sediment characteristics on methane formation and oxidation in lake sediments, *Biogeochemistry*, 100(1), pp. 185–196. doi: 10.1007/s10533-010-9415-8.
- Thauer, R. K. (1998). Biochemistry of methanogenesis: a tribute to Marjory Stephenson: 1998 Marjory Stephenson Prize Lecture, *Microbiology*, 144(9), pp. 2377–2406. doi: 10.1099/00221287-144-9-2377.
- Tiedje, J. M. and Zehnder, A. J. B. (1988). Biology of anaerobic microorganisms, *Ecology of Denitrification and Dissimilarity Nitrate Reduction to Ammonium*. New York: John Wiley, p. 179.
- Tilbrook, B. D. and Karl, D. M. (1995). Methane sources, distributions and sinks from California coastal waters to the oligotrophic North Pacific gyre, *Marine Chemistry*, 49(1), pp. 51–64. doi: 10.1016/0304-4203(94)00058-L.
- Tranvik, L. J., Downing, J. A., Cotner, J. B., Loiselle, S. A., Striegl, R. G., Ballatore, T. J., Dillon, P., Finlay, K., Fortino, K., Knoll, L. B., Kortelainen, P. L., Kutser, T., Larsen, Soren., Laurion, I., Leech, D. M., McCallister, S. L., McKnight, D. M., Melack, J. M., Overholt, E., Porter, J. A., Prairie, Y., Renwick, W. H., Roland, F., Sherman, B. S., Schindler, D. W., Sobek, S., Tremblay, A., Vanni, M. J., Verschoor, A. M., von Wachenfeldt, E. and Weyhenmeyer, G. A. (2009). Lakes and reservoirs as regulators of carbon cycling and climate, *Limnology and Oceanography*, 54(6part2), pp. 2298–2314. doi: 10.4319/lo.2009.54.6_part_2.2298.
- Tranvik, L. J., Cole, J. J. and Prairie, Y. T. (2018). The study of carbon in inland waters—from isolated ecosystems to players in the global carbon cycle, *Limnology and Oceanography Letters*, 3(3), pp. 41–48. doi: 10.1002/lol2.10068.
- Trimmer, M., Chronopoulou, P.-M., Maanoja, S. T., Upstill-Goddard, R. C., Kitidis, V. and Purdy, K. J. (2016). Nitrous oxide as a function of oxygen and archaeal gene abundance in the North Pacific, *Nature Communications*, 7(1), pp. 1–10. doi: 10.1038/ncomms13451.
- Vajjala, N., Martens-Habbena, W., Sayavedra-Soto, L. A., Schauer, A., Bottomley, P. J., Stahl, D. A. and Arp, D. J. (2013). Hydroxylamine as an intermediate in ammonia oxidation by globally abundant marine archaea, *Proceedings of the National Academy of Sciences*, 110(3), pp. 1006–1011. doi: 10.1073/pnas.1214272110.
- del Valle, D. A. and Karl, D. M. (2014). Aerobic production of methane from dissolved water-column methylphosphonate and sinking particles in the North Pacific Subtropical Gyre, *Aquatic Microbial Ecology*, 73(2), pp. 93–105. doi: 10.3354/ame01714.
- Vitousek, P. M. (1994). Beyond global warming: Ecology and global change, *Ecology*, 75(7), pp. 1861–1876. doi: 10.2307/1941591.
- Wang, Q., Dore, J. E. and McDermott, T. R. (2017). Methylphosphonate metabolism by *Pseudomonas* sp. populations contributes to the methane oversaturation paradox in

- an oxic freshwater lake, *Environmental Microbiology*, 19(6), pp. 2366–2378. doi: 10.1111/1462-2920.13747.
- Wankel, S. D., Ziebis, W., Buchwald, C., Charoenpong, C., Beer, D. de, Dentinger, J., Xu, Z. and Zengler, K. (2017). Evidence for fungal and chemodenitrification based N₂O flux from nitrogen impacted coastal sediments, *Nature Communications*, 8, p. 15595. doi: 10.1038/ncomms15595.
- Ward, B. B. (1996). Nitrification and denitrification: Probing the nitrogen cycle in aquatic environments, *Microbial Ecology*, 32(3), pp. 247–261. doi: 10.1007/BF00183061.
- WCD. (2000). *Dams and development: A new framework for decision-making: The report of the World Commission on Dams* London: Earthscan Publications Ltd.
- Wenk, C. B., Bles, J., Zopfi, J., Veronesi, M., Bourbonnais, A., Schubert, C. J., Niemann, H. and Lehmann, M. F. (2013). Anaerobic ammonium oxidation (anammox) bacteria and sulfide-dependent denitrifiers coexist in the water column of a meromictic south-alpine lake, *Limnology and Oceanography*, 58(1), pp. 1–12. doi: 10.4319/lo.2013.58.1.0001.
- Wenk, C. B., Zopfi, J., Gardner, W. S., McCarthy, M. J., Niemann, H., Veronesi, M. and Lehmann, M. F. (2014). Partitioning between benthic and pelagic nitrate reduction in the Lake Lugano south basin, *Limnology and Oceanography*, 59(4), pp. 1421–1433. doi: 10.4319/lo.2014.59.4.1421.
- West, W. E., Coloso, J. J. and Jones, S. E. (2012). Effects of algal and terrestrial carbon on methane production rates and methanogen community structure in a temperate lake sediment, *Freshwater Biology*, 57(5), pp. 949–955. doi: 10.1111/j.1365-2427.2012.02755.x.
- Weyhenmeyer, G. A., Kosten, S., Wallin, M. B., Tranvik, L. J., Jeppesen, E. and Roland, F. (2015). Significant fraction of CO₂ emissions from boreal lakes derived from hydrologic inorganic carbon inputs, *Nature Geoscience*, 8(12), pp. 933–936. doi: 10.1038/ngeo2582.
- Woehle, C., Roy, A.-S., Glock, N., Wein, T., Weissenbach, J., Rosenstiel, P., Hiebenthal, C., Michels, J., Schönfeld, J. and Dagan, T. (2018). A novel eukaryotic denitrification pathway in foraminifera, *Current Biology*, 28(16), pp. 2536–2543.e5. doi: 10.1016/j.cub.2018.06.027.
- World Meteorological Organization (WMO). (2019). *The State of Greenhouse Gases in the Atmosphere Based on Global Observations through 2018* p. 8 15. Geneva: WMO, p. 8. Available at: https://library.wmo.int/index.php?lvl=notice_display&id=3030#.Xv9OrZMzb6Z.
- Wrage, N., Velthof, G. L., van Beusichem, M. L. and Oenema, O. (2001). Role of nitrifier denitrification in the production of nitrous oxide, *Soil Biology and Biochemistry*, 33(12), pp. 1723–1732. doi: 10.1016/S0038-0717(01)00096-7.
- Wuchter, C., Abbas, B., Coolen, M. J. L., Herfort, L., Bleijswijk, J. van, Timmers, P., Strous, M., Teira, E., Herndl, G. J., Middelburg, J. J., Schouten, S. and Damsté, J. S. S. (2006). Archaeal nitrification in the ocean, *Proceedings of the National Academy of Sciences*, 103(33), pp. 12317–12322. doi: 10.1073/pnas.0600756103.

- Yao, M., Henny, C. and Maresca, J. A. (2016). Freshwater bacteria release methane as a byproduct of phosphorus acquisition, *Applied and Environmental Microbiology*, 82(23), pp. 6994–7003. doi: 10.1128/AEM.02399-16.
- Yoshida, N. (1988). ¹⁵N-depleted N₂O as a product of nitrification, *Nature*, 335(6190), pp. 528–529. doi: 10.1038/335528a0.
- Yvon-Durocher, G., Allen, A. P., Bastviken, D., Conrad, R., Gudasz, C., St-Pierre, A., Thanh-Duc, N. and del Giorgio, P. A. (2014). Methane fluxes show consistent temperature dependence across microbial to ecosystem scales, *Nature*, 507(7493), pp. 488–491. doi: 10.1038/nature13164.
- Zarfl, C., Lumsdon, A. E., Berlekamp, J., Tydecks, L. and Tockner, K. (2015). A global boom in hydropower dam construction, *Aquatic Sciences*, 77(1), pp. 161–170. doi: 10.1007/s00027-014-0377-0.
- Zhang, C., Cheng, S., Li, Y., Zhang, W. and Xiao, S. (2019). Diel methane flux from a subtropical eutrophic pond in November based on continuous monitoring, *Acta Geochimica*. doi: 10.1007/s11631-019-00317-1.
- Zhu-Barker, X., Cavazos, A. R., Ostrom, N. E., Horwath, W. R. and Glass, J. B. (2015). The importance of abiotic reactions for nitrous oxide production, *Biogeochemistry*, 126(3), pp. 251–267. doi: 10.1007/s10533-015-0166-4.
- Zindler, C., Bracher, A., Marandino, C. A., Taylor, B., Torrecilla, E., Kock, A. and Bange, H. W. (2013). Sulphur compounds, methane, and phytoplankton: interactions along a north–south transit in the western Pacific Ocean, *Biogeosciences*, 10(5), pp. 3297–3311. doi: 10.5194/bg-10-3297-2013.
- Zumft, W. G. (1997). Cell biology and molecular basis of denitrification., *Microbiology and Molecular Biology Reviews*, 61(4), pp. 533–616.



Chapter 2:
Materials and Methods

Chapter 2 | Materials and Methods

Chapter 2: Materials and Methods

2. 1. Study reservoirs, morphometry and watershed characterization

2. 1. 1. Study reservoirs

In this study, we selected twelve reservoirs located in the Southeastern of Spain trying to cover the regional heterogeneity (Figure 2.1). This region has an exceptional geological, tectonic and lithological heterogeneity, like a “collage” of materials from all the geological periods, from the Precambrian (i.e., about 600 million years ago) to the present day (Villalobos Megía and Pérez Muñoz, 2006; Jódar, 2009). These materials include sedimentary, igneous and metamorphic rocks, with great abundance and variety of fossil records (Villalobos Megía and Pérez Muñoz, 2006). We found three large morpho-structural units, that corresponds to geological domains, and each one of them presents its own geological history: the Iberian Massif (i.e., Sierra Morena), the Baetic System, and the neogenic depressions (i.e., the Guadalquivir River Basin, and Baetic Neogene Basins). The Baetic System is divided into the Penibaetic System, the Subbaetic System, and the Prebaetic System (Villalobos Megía and Pérez Muñoz, 2006; Jódar, 2009).

In general, the region is submitted to the Mediterranean climate, which is characterized by dry summers, mild, wet winters, and low precipitation rates.

However, the complex geography and topography determines a certain climatic regionalization with different bioclimatic zones. According to the Köppen climate classification for the Iberian Peninsula, the climate often referred as “Mediterranean” correspond to the subtypes Csa (temperate with dry or hot summer) and Csb (temperate with dry or temperate summer). The Csa climate covers most of the Iberian Peninsula and present an average temperature in the hottest month above 22 °C. The Csa appear in numerous mountainous regions within the Peninsula, and it characterized by an average temperature in the hottest month below or equal to 22 °C, and with four months or more with average temperatures above 10 °C. In the Southeastern of Spain, we also detected areas of dry climates (type B) coinciding with the minimum rainfall values for the Peninsula. In these areas the annual precipitation is in the range of 50 – 100 % of the threshold for potential evapotranspiration (subtypes BSh: hot steppe; and BSk: cold steppe), or less than 50 % of the threshold for potential evapotranspiration (subtypes BWh: hot desert; and BWk: cold desert). The average annual temperature is above 18 °C in hot climates (letter “h”), and below 18 °C in cold climates (letter “k”). In small areas of the mountainous regions we also found cold climates (type D), where the average temperature for the coldest month is lower than 0 °C, and the average temperature of the hottest month is higher than 10 °C. In particular, we found the subtypes Dsb (cold with temperate and dry summer) and Dsc (cold with dry and fresh summer) at higher altitudes in the Sierra Nevada mountains (Agencia Estatal de Meteorología de España and Instituto de Meteorología de Portugal, 2011).

The water scarcity of the region led to the construction of many reservoirs dedicated to water supply and agriculture irrigation during the last century. Secondary, some reservoirs also produce hydropower. Many of these reservoirs have an extra economic, social, and cultural value as recreational area. These twelve reservoirs cover a wide spectrum of age, morphometry, chemical, trophic, and landscape characteristics (Table 2.1.). The study reservoirs were built between 1932 and 2003, in the provinces of Granada, Jaén, and Córdoba. The Jándula reservoir was built in 1932, and it is one of the oldest in the region, whereas the Rules reservoir is the youngest reservoir and was built in 2003. The study reservoirs belong to the hydrological demarcations of Guadalquivir and Mediterránea Andaluza. We show the

location of the study reservoirs in Figure 2.1., and the geographical coordinates, hydrological demarcation, and construction year of the study reservoirs in Table 2.1.

Table 2.1. Location, and construction year of the study reservoirs.

Reservoir	Latitude (°, decimal degrees)	Longitude (°, decimal degrees)	Altitude (m)	Construction year
Cubillas	37.27	-3.68	640	1956
Colomera	37.40	-3.72	810	1990
Negratín	37.56	-2.95	618	1984
La Bolera	37.76	-2.90	950	1967
Los Bermejales	36.99	-3.89	852	1958
Iznájar	37.26	-4.33	425	1969
Francisco Abellán	37.31	-3.27	942	1991
Béznar	36.92	-3.55	486	1986
San Clemente	37.86	-2.65	1050	1990
El Portillo	37.81	-2.79	920	1999
Jándula	38.23	-3.97	350	1932
Rules	36.86	-3.49	239	2003

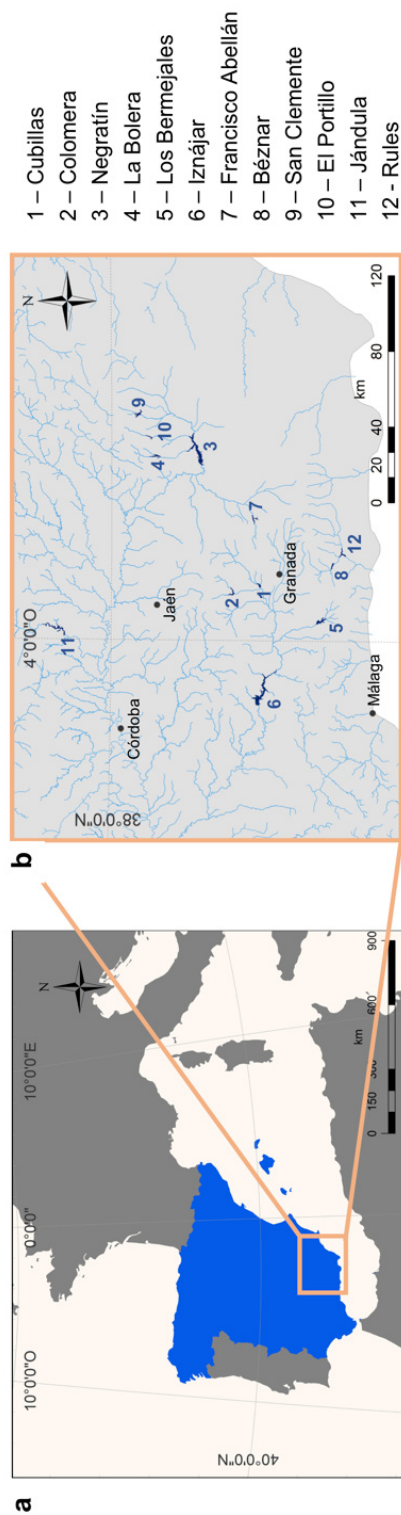


Figure 2.1.1. Study site. (a) The orange square delimited the region where the reservoirs are located; (b) the twelve study reservoirs are numbered and listed on the side.

2. 1. 2. Morphometry characterization

We obtained the data on age, location, reservoir perimeter, area and capacity from open databases: the Infraestructura de Datos Espaciales de Andalucía (IDEAndalucía; <http://www.ideandalucia.es/portal/web/ideandalucia/>) and the Ministerio para la Transición Ecológica (<https://www.embalses.net/>), and the Confederación Hidrográfica del Guadalquivir (CHG; <https://www.chguadalquivir.es/saih/>).

The reservoir volume (m^3) divided by its surface area (m^2) yields its mean depth (m) (Eq. 2.1):

$$\text{Mean depth} = \frac{\text{Volume}}{\text{Surface area}} \quad \text{Eq. 2.1}$$

The shoreline development ratio (D_L , unitless) (Aronow, 1982) is a comparative index relating the shoreline length (i.e., the perimeter of the reservoir, m) to the circumference of a circle that has the same area (m^2) (Eq. 2.2).

$$D_L = \frac{\text{Length of the shoreline}}{2\sqrt{\pi \times \text{area}}} \quad \text{Eq. 2.2}$$

The closer this ratio is to 1, the more circular the reservoir is. A large ratio ($\gg 1$) indicates the shoreline is more scalloped than a low ratio (Figure 2.2).

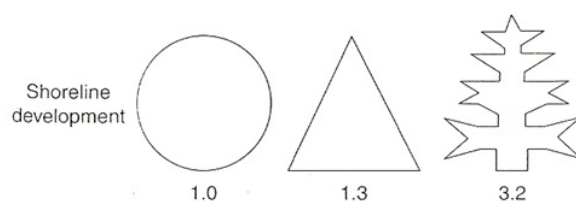


Figure 2.2. Graphical representation of shoreline development for three lakes of different shape. Taken from Timms (2009).

The shallowness index (m^{-1}) was obtained by dividing the shoreline development index by the mean depth (m), as follows in Eq. 2.3:

$$\text{Shallowness index} = \frac{D_L}{\text{Mean depth}} \quad \text{Eq. 2.3}$$

The hydraulic residence time (d) was obtained by dividing the mean volume during the study period (hm^3) by the mean water inflow or the mean disbursed volume per day ($hm^3 d^{-1}$), whichever is larger. The hydraulic residence time depended on the study period.

$$\text{Hydraulic residence time} = \frac{\text{Mean volume}}{\text{Flow per day}} \quad \text{Eq. 2.4}$$

The surface area of the study reservoirs varied from 1.18 km² of El Portillo reservoir to 26.13 km² of Iznájar reservoir. The volume of the reservoirs ranged from 18.74 hm³ of Cubillas reservoir to 981.12 hm³ of Iznájar reservoir. In fact, Iznájar reservoir is the biggest reservoir in Andalucía. The shoreline development index reached up to 7.10 in Jándula reservoir, which is an elongated and dendritic reservoir; whereas Cubillas was the most circular reservoir with a shoreline development index of 2.00. These morphometric characteristics are shown in Table 2.2.

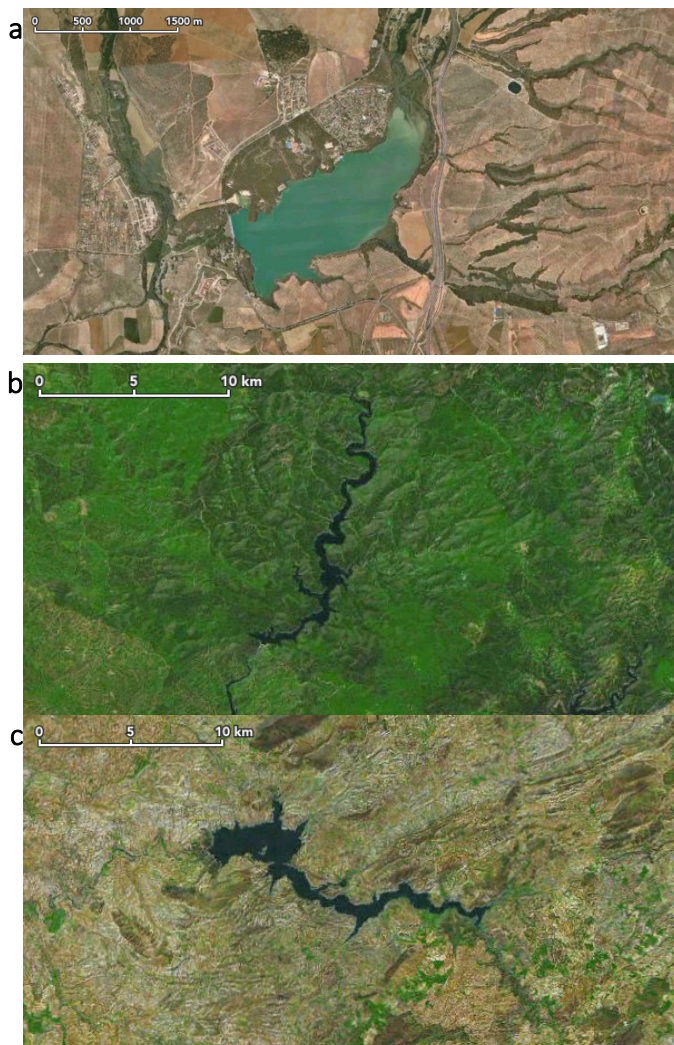


Figure 2.3. Aerial photographs of (a) Cubillas, (b) Jándula, and (c) Iznájar reservoirs. Obtained from Apple Maps.

Table 2.2. Morphometric description of the study reservoirs.

Reservoir	Reservoir area (km ²)	Reservoir volume (hm ³)	Mean depth (m)	Shoreline development index (D _L)	Shallowness index (m ⁻¹)
Cubillas	1.94	18.74	9.66	2.00	0.21
Colomera	2.76	40.18	14.56	3.35	0.23
Negratín	23.51	567.12	24.12	5.90	0.24
La Bolera	2.89	53.19	18.40	4.05	0.22
Los Bermejales	5.95	103.12	17.33	2.90	0.17
Iznájar	26.13	981.12	37.55	5.76	0.15
Francisco Abellán	2.43	58.21	23.95	3.80	0.16
Béznar	1.60	52.90	33.06	2.65	0.08
San Clemente	3.76	117.92	31.36	3.43	0.11
El Portillo	1.18	32.90	27.88	3.69	0.13
Jándula	8.43	321.99	38.20	7.10	0.19
Rules	3.06	110.78	36.20	3.09	0.09

2. 1. 3. Watershed characterization

We studied the lithology and land-use of the watersheds of the twelve reservoirs using ArcGIS® 10.2 software (ESRI, 2012) under Universidad de Granada license. First, we delimited the watershed of each reservoir using the rivers and hydrographical demarcations, and, second, we calculated the area for each different type of lithology and land-use. We used the following databases: Infraestructura de Datos Espaciales (IDE) from the Ministerio de Agricultura, Pesca y Alimentación (MAPA; <https://www.mapa.gob.es/es/cartografia-y-sig/ide/default.aspx>); the Infraestructura de Datos Espaciales de Andalucía (IDEAndalucía; <http://www.ideandalucia.es/portal/web/ideandalucia/>); the Instituto Geológico y Minero de España (IGME; <http://www.igme.es/default.asp>); the Confederación Hidrográfica del Segura (CHSEGURA; <https://www.chsegura.es/chs/>); and The Junta de Comunidades de Castilla-La Mancha (IDE-JCCM; <https://castillalamanca.maps.arcgis.com/home/index.html>).

We defined the next lithological categories: water-covered area; carbonate-rich rocks; limestones, marls, and dolomites; gravels, conglomerates, sands and silts; and non-calcareous rocks. The soils with high capacity to solubilize dissolved

inorganic carbon are carbonate-rich rocks and limestones, marls, and dolomites. In contrast, non-calcareous rocks include igneous rocks like basalt and metamorphic rocks like marble, schist, quartzite, phyllite, gneiss, and slate have less capacity to leach dissolved inorganic carbon. We compiled the lithological data of the study reservoirs in Table 2.3. The land-use categories were: crops, forest, urban, treeless area, and water covered area. The forestry area includes trees, plantation trees, sparse trees, and dispersed trees. We compiled the land-use analysis in the watershed of the study reservoirs in Table 2.3. The lithological and land-use maps of each reservoir are shown in Supplementary Figures from 3.1 to 3.24 in Appendix 3.

Table 2.3. Lithological and land-use analysis in the watershed of the study reservoirs

Reservoir	Non-calcareous rocks (km ²)	Limestones, marls and dolomites (km ²)	Carbonate-rich rocks (km ²)	Gravels, conglomerates, sands and silts (km ²)	Urban areas (km ²)	Crops (km ²)	Forest (km ²)	Treeless areas (km ²)	Water covered areas (km ²)	Watershed area (km ²)
Cubillas	3.98	623.60	15.57	0.00	6.46	416.83	166.14	55.14	1.99	646.57
Colomera	11.91	224.65	0.00	0.00	2.23	145.90	64.98	20.82	2.61	236.56
Negratín	218.42	2506.13	284.59	750.80	21.91	1698.15	1303.95	708.15	32.46	3764.62
La Bolera	0.00	79.39	77.96	0.00	0.00	4.76	138.81	16.73	2.48	162.78
Los Bermejales	132.8	85.24	0.00	56.16	1.07	83.63	133.37	57.13	5.83	281.03
Iznájar	531.95	3704.91	115.22	323.36	153.00	2751.98	983.64	787.82	37.43	4713.87
Francisco Abellán	43.14	93.42	53.59	2.68	1.80	27.33	116.67	45.21	1.82	192.82
Béznar	182.09	57.39	51.70	56.05	8.62	109.85	122.46	104.09	2.22	347.23
San Clemente	0.00	111.26	36.35	5.35	0.19	18.03	101.38	31.61	1.75	152.95
El Portillo	0.00	81.94	31.19	0.00	0.04	4.04	62.48	45.16	1.40	113.12
Jándula	2026.32	210.89	0.00	0.00	25.36	427.42	1350.03	416.03	25.95	2244.8
Rules	786.38	155.86	80.08	56.05	12.06	254.13	349.91	456.69	5.57	1078.36

2. 1. 4. Reservoir samplings

We performed two types of samplings from 2015 to 2018: an extensive sampling of the twelve reservoirs, and intensive 24h-samplings in the Cubillas and Iznájar reservoirs. During the extensive sampling we studied the twelve reservoirs once during the summer stratification and once during the winter mixing between July 2016 and August 2017 to determine the cross-system variability. We measured the greenhouse gases fluxes, and we characterized the water column in both periods. The results of this extensive sampling appear in the Chapter 3, 5, and 6.

We also performed an intensive sampling in the Cubillas reservoir in the summer 2016, and in Cubillas and Iznájar in the summer 2018 to explore the daily variability in GHG fluxes, and to perform experiments of photoproduction of GHG during the summer 2018 (Chapter 4). In the summer 2018, we also sampled twice Cubillas and Iznájar reservoirs at the beginning (July) and the end (September) of the stratification period to measure N₂O production rates (Chapter 7).

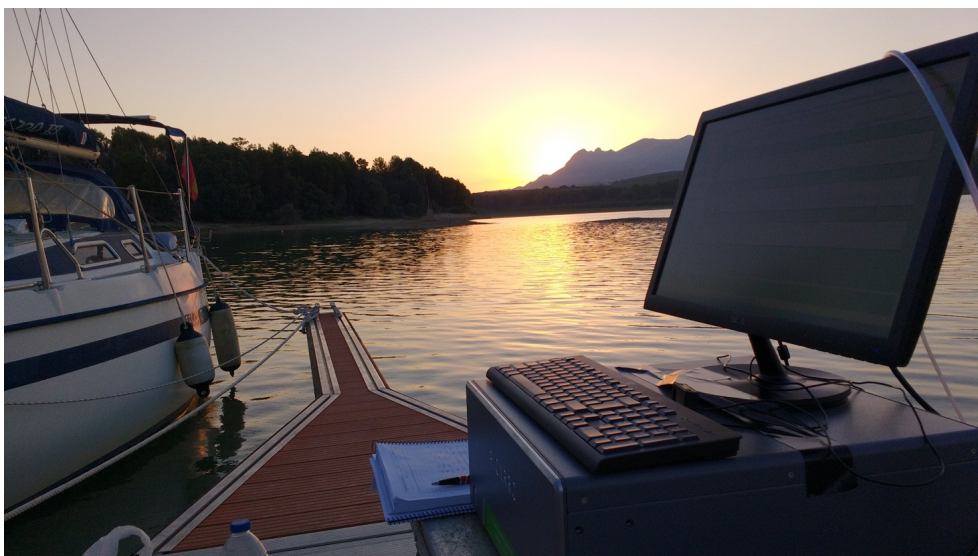


Figure 2.4. Picarro G2508 Cavity Ring-Down Spectroscopy gas analyzer at dawn during an intensive 24 hours sampling in Cubillas reservoir.

2. 2. Greenhouse gas fluxes quantification

2. 2. 1. Greenhouse gas fluxes quantification

We measured CO₂, CH₄, and N₂O fluxes using a high-resolution laser-based Cavity Ring-Down Spectrometer (CRDS PICARRO G2508) (more details in Box 2.1). The Picarro G2508 gas analyzer measures simultaneous, and precisely the concentration of dry CO₂, CH₄, and N₂O at parts-per-billion (ppb) sensitivity with negligible drift, and with automatic water correction. The precision at 1 minute and 5 minutes is < 300 and < 200 ppb for CO₂, < 7 and < 5 ppb for CH₄, and < 10 and < 5 ppb for N₂O (PICARRO, 2020). The spectrometer was connected to a vacuum pump, and to a floating chamber in a closed cycle. We also connected a monitor to the spectrometer to follow the measurements in real time (Figure 2.6). We set up the system by making a floating chamber with a double floater, and a thermal cover to prevent the chamber from heating up (Figure 2.7). We also added a water trap to prevent that water goes inside the system.



Figure 2.6. A picture of the Picarro G2508 analyzer including the monitor, and the vacuum pump.

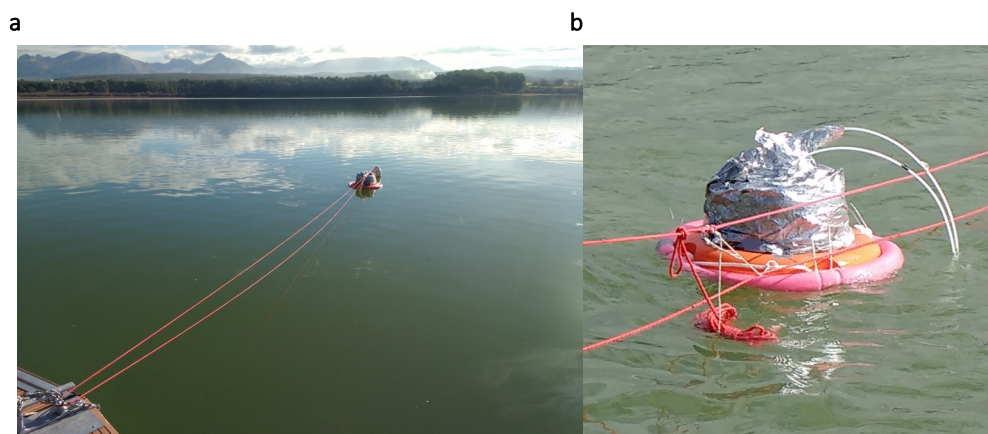


Figure 2.7. Floating chamber connected to the Picarro G2508 analyzer. (a) Floating chamber during a measurement, connected to the Picarro analyzer and to the platform; (b) detail of the floating chamber showing the double floater, the thermal fabric, and the connections.

The analyzer registered the change over time in the concentration of the CO_2 , CH_4 , and N_2O in the headspace of the floating chamber. We ventilated the floating chamber by flipping it over to avoid gas saturation in the headspace of the chamber between two measurements. In Figure 2.8 we represented the cycle between the increase in the concentration of the CO_2 in the chamber, and the ventilation events. At the point (1) we placed the floating chamber in the water, and the concentration of CO_2 started to increase linearly inside the chamber. Instead of a linear increase (i.e., outflow), we may find a linear decrease, in case of GHG inflow. We finished the measurement at the point (2), when we flipped the chamber over for ventilation. At the point (3) we reached the atmospheric concentration of CO_2 , so we placed again the floating chamber in the water and started the following measurement. We made the slope calculation from the section between (1) and (2), that lasted about 30 – 40 minutes. The section between (2) and (3) is considered the death band, and that was applied to the beginning of each flux measurement to exclude measurement artefacts caused by the ventilation of the floating chamber.

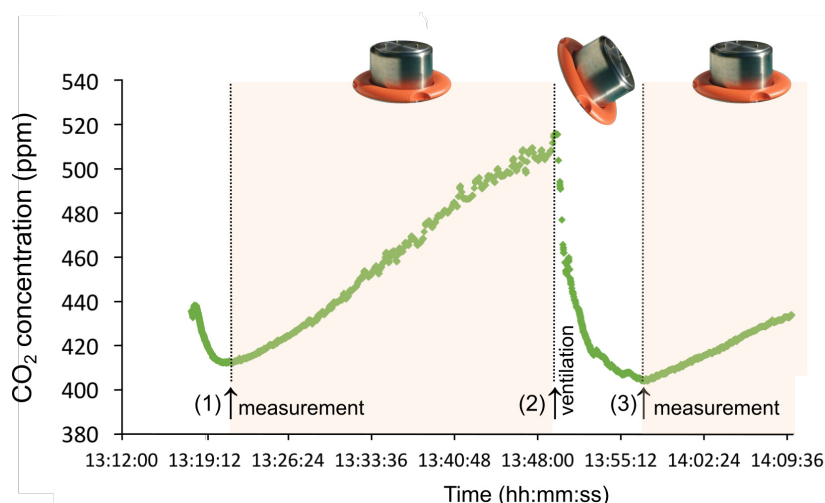


Figure 2.8. Concentration of the CO₂ in the floating chamber over measurement and ventilation times.

During the extensive sampling, we took 3-5 measurements for 40 min for each reservoir (from 10 am to 4 pm) during the stratification and mixing periods. For the daily cycles of GHG fluxes, we took at least 24 measurements. We obtained the flux calculation using the equation 2.5 (Zhao *et al.*, 2015):

$$\text{Flux}_{\text{air-water}} = \frac{b \times V \times P_0}{A \times R \times T_0} \quad \text{Eq. 2.5}$$

Where $\text{Flux}_{\text{air-water}}$ ($\mu\text{mol m}^{-2} \text{s}^{-1}$) is the flux from the water surface to the atmosphere; the b (ppm s^{-1}) value is the slope of the linear regression between the time and the concentration of each gas inside the floating chamber; the V (m^3) is the floating chamber volume that was 0.018 m^3 ; the A (m^2) is the floating chamber area that was 0.08 m^2 ; the P_0 (Pa) is the atmospheric pressure; the R is the gas constant ($8.314, \text{ m}^3 \text{ Pa K}^{-1} \text{ mol}^{-1}$); and the T_0 (K) is the ambient temperature. We checked that the slope was significantly different from zero for each measurement using a two-tailed t-Student test. We also calculated the coefficient of determination (R^2) for each measurement, accepting those whose $R^2 > 0.85$ (Moseman-Valtierra *et al.*, 2016). We measured ambient temperature, atmospheric pressure (HANNA HI 9828), and wind speed (MASTECH MS6252A) at the beginning of each flux measurement.

Determination coefficients (R^2) for CO₂ fluxes were always > 0.85 . For CH₄ fluxes, most cases R^2 were > 0.85 , but it decreased until 0.65 when ebullition events

were relevant. Each ebullition event (bubble) produces an abrupt change in the accumulation of methane inside the floating chamber and, consequently, in the slope of CH₄ concentration vs time. In contrast, diffusion increased linearly over time (Figure 2.9). In case of the occurrence of ebullition events, we computed the b value using the end-point concentrations and the time interval between them as it was proposed by Zhao *et al.* (2015) (Eq. 2.6):

$$b = \frac{[\text{CH}_4]_f - [\text{CH}_4]_i}{t_f - t_i} \quad \text{Eq. 2.6}$$

Where [CH₄]_f and [CH₄]_i are the CH₄ concentration (ppm) in the floating chamber at the end and the beginning of the time considered; t_f and t_i are the time (s) at the end and the beginning of the measurement.

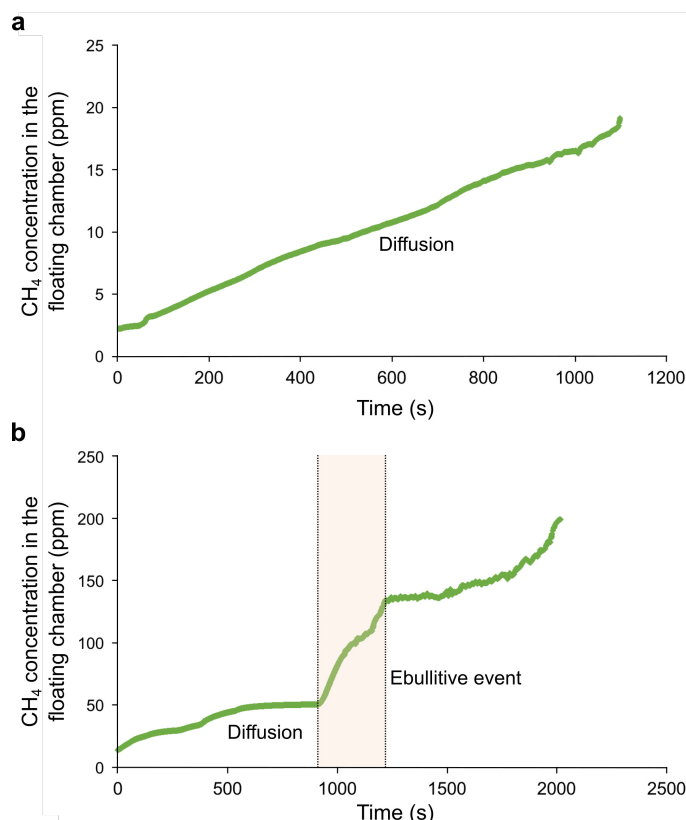


Figure 2.9. CH₄ accumulation inside the space of the floating chamber. (a) Linear increase in the CH₄ concentration inside the floating chamber by diffusion; (b) linear and abrupt increase in CH₄ concentration inside the floating chamber by diffusion and an abrupt ebullitive event, respectively.

For N₂O flux measurements, most of the R² values were low (even when the regression was significantly different from zero). For those cases, we first checked

the analyzer precision (< 25 ppb). If the changes were larger than the analyzer precision, we assumed these fluxes were different from zero. We also compared the N₂O fluxes with the percentage of saturation of the dissolved N₂O in the water column. N₂O undersaturated waters and negative slopes mean N₂O influxes (i.e., N₂O sinks). By contrast, N₂O supersaturated waters and positive slopes mean N₂O outfluxes (i.e., N₂O sources).

2. 2. 2. Discriminative algorithm for CH₄ ebullitive and diffusive fluxes

We discriminated the total CH₄ fluxes (i.e., CH_{4total}) in two components: the CH₄ emitted by diffusion (CH_{4diffusion}) and the CH₄ emitted by ebullition (CH_{4ebullition}) in the data of the 24 hours intensive sampling in the Cubillas and the Iznájar reservoirs. The CH_{4total} was calculated following the equation 2.5. The slope (b) was calculated following the equation 2.6.

The CH₄ flux discrimination between diffusion and ebullition in CH_{4diffusion} and in CH_{4ebullition} components was performed using the algorithm proposed by Hoffmann *et al.* (2017), but adapting the procedure to higher data frequency. Briefly, the algorithm sets a variable moving window to generate several data subsets per each measurement, calculating the slope of a linear regression and different statistics for each subset. We established the moving window with a size of 50 data. The resulting slopes for each measurement are evaluated according to strict exclusion criteria to keep only the slopes for the diffusion component. These inclusion criteria included: a significant regression slope between CH₄ concentration and time ($p < 0.05$); determination coefficients $R^2 > 0.5$; non-abrupt changes within each data subset (slope < 0.012, determined by manual inspection); and the interquartile range test to discharge the slopes outside of the range between the upper and the lower quartile. Finally, we calculated the mean value for the resulting slopes that passed all the statistical tests. The resulting slope is used to calculate the diffusive component of the flux following the equation 2.5. The ebullitive component CH_{4ebullition} is estimated by subtracting the identified CH_{4diffusion} from the CH_{4total} calculated before (Eq. 2.7):

$$\text{CH}_{4\text{ebullition}} = \sum_{i=1}^n (\text{CH}_{4\text{total}} - \text{CH}_{4\text{diffusion}}) \quad \text{Eq. 2.7}$$

Box 2.1. Cavity Ring-Down Spectroscopy

Infrared spectroscopy analyses the interaction between infrared light and molecules, based on the specific ability of the molecules to absorb at different wavelengths of light according to their structures. Nearly every small gas-phase molecule has a unique near-infrared absorption spectrum. Therefore, we can identify the chemical substances and their concentration by measuring the specific absorption peaks. Infrared spectroscopy has widely used in environmental sciences, in air, water and soil analysis. Common applications include the measurement of greenhouse gases concentration, as CO₂, CH₄, and N₂O (Stuart, 2005). However, conventional infrared spectrometers have limited sensitivity, and they are not able to measure trace gases. Cavity Ring-Down Spectroscopy (CRDS) uses an effective path length of many kilometers, that enables gases to be monitored in seconds or less at the parts per million level, and some gases at the parts per billion level. A Picarro cavity of only 25 cm in length has an effective path length within the cavity over 20 kilometers. That path length is achieved including three high reflectivity mirrors in the cavity, and that support a continuous traveling light wave. These mirrors have slightly less than 100% reflectivity (99.999%) (Figure B.2.1).

When the laser is on, the cavity fills with the laser light, and that is detected by the photodetector (Figure B.2.1a). The laser is turned off when the photodetector signal reaches a threshold level (in a few tens of microseconds). Although the laser is off, the light continues to bounce between the high reflectivity mirrors within the cavity. The light intensity inside the cavity decays to zero in an exponential function. This decay, or "ring down", is measured in real-time by the photodetector, and this time for the ring down depends on the reflectivity of the mirrors. If a gas that absorbs the laser light is introduced into the cavity, the ring down time is accelerated Figure B.2.1b and Figure B.2.1d compare the ring down time without an absorbing gas. By changing the laser to different wavelengths where the gas absorbs light, and then to wavelengths where the gas does not absorb light, the "cavity only" ring down time can be compared to the ring down time when a target gas is contributing to the optical loss within the cavity. Picarro automatically and constantly calculate and compare the ring down time of the cavity with and without absorption due to the target gas species, and

that produces precise and quantitative measurements. That accounts for any intra-cavity loss that may be changing over time, and permits to discriminate the loss due to absorption and the loss due to the cavity mirrors (PICARRO, 2020).

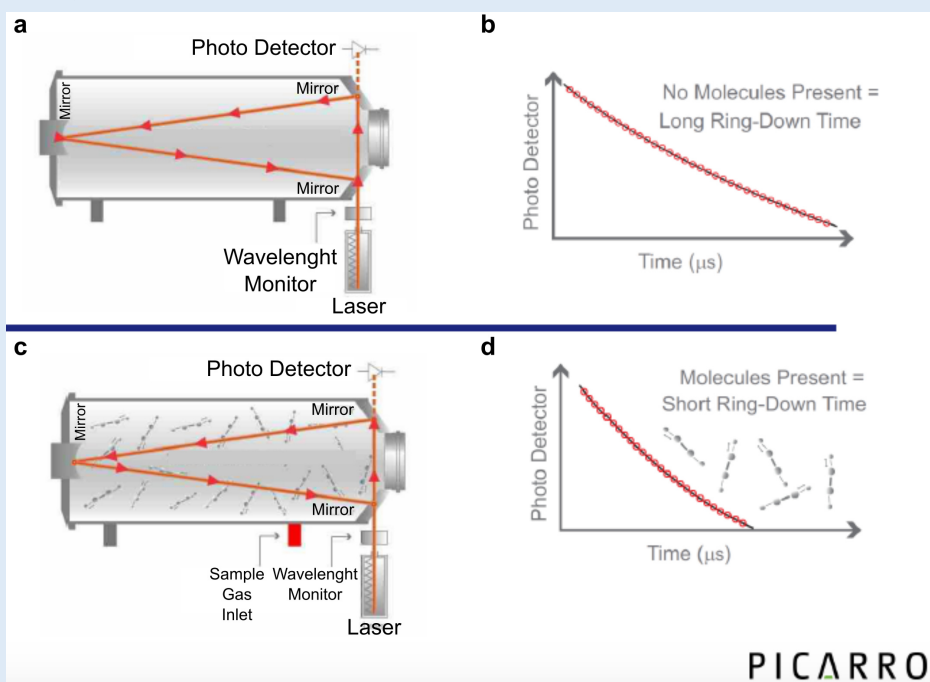


Figure B.2.1. Picarro three mirror cavity and ring-down effect. Three mirror cavity with the laser, wavelength monitor, and photo detector without sample (a) and with sample (c); (b) light intensity as a function of time in a CRDS system without sample (b) and with sample (d) having a resonant absorbance. Modified from PICARRO (2020).

2. 3. Physico-chemical analysis in the water column

2. 3. 1. Vertical profiles of the water column

We performed the vertical profiles of the water column of the reservoirs using a Sea-Bird 19 plus CTD profiler, coupled to Spherical Underwater Quantum Sensor (LI-193R) and to a fluorimeter Turner® SCUFA (model CYCLOPS-7) (Figure 2.10). We obtained continuous measurements of temperature ($^{\circ}\text{C}$), dissolved oxygen ($\mu\text{mol L}^{-1}$), conductivity ($\mu\text{S cm}^{-1}$), turbidity (FTU), density (kg m^{-3}), photosynthetic active radiation, chlorophyll-*a* fluorescence ($\mu\text{g L}^{-1}$), specific conductance ($\mu\text{S cm}^{-1}$), and salinity (psu - practical salinity units). We calculated the saturation values (%) for dissolved oxygen as the ratio of the dissolved gas measured and the gas concentration expected in equilibrium. We calculated the gas concentration in equilibrium, taking into account the differences in temperature, salinity, and barometric pressure (Mortimer, 1956). Then, based on the temperature and oxygen profiles obtained, we selected six to nine depths along the water column representative of the oxic and anoxic layers and the transition between them in each reservoirs during the stratification period. We also selected six to nine representative depths during the mixing period. From each discrete point, we collected the water samples using a UWITEC sampling bottle of 5 liters with a self-closing mechanism. These samples were used for the chemical and biological analysis which are described below.



Figure 2.10. Sea-Bird 19 plus CTD profiler in the Bézinar reservoir.

2. 3. 2. CH₄ and N₂O concentration in the water column

We collected samples for dissolved CH₄ and N₂O analysis in 125 or 250 mL air-tight Winkler bottles by duplicate (250 mL) or triplicate (125 mL). We filled up the bottles very carefully from the bottom to avoid the formation of bubbles and minimize the loss of CH₄ and N₂O during field sampling. We preserved the samples with a solution of HgCl₂ (final concentration 1 mmol L⁻¹) to inhibit biological activity and sealed the bottles with Apiezon® grease to prevent gas exchanges. We stored the samples in the dark at room temperature until analysis. We measured dissolved CH₄ and N₂O using headspace equilibration in a 50 ml air-tight glass syringe (Agilent P/N 5190–1547) (Figure 2.11) by duplicate (in 125 mL bottles) or triplicate (in 250 mL bottles) from each Winkler bottle in the laboratory of the Department of Physical Chemistry at the University of Cádiz (Sierra *et al.*, 2017a, 2017b).

We took a quantity of 25 g of water (\pm 0.01 g) using the air-tight syringe and added a quantity of 25 mL of a standard gas mixture that has a methane and nitrous oxide concentration similar to atmospheric values (1.8 and 0.3 ppmv, respectively) to complete the volume of the syringe. The syringes were shaken for 5 min (VIBROMATIC Selecta) to ensure a complete mixing, and we waited for 5 min to reach the equilibrium. Finally, the gas in the syringe was injected manually in the gas chromatograph (Bruker® GC-450). The gas chromatograph was equipped with Hydrogen Flame Ionization Detector and Electron Capture Detector to measure the concentration of CH₄ and N₂O simultaneously (Figure 2.12).

We daily calibrated the detectors using three standard gas mixtures with CH₄ concentrations of 1952, 10064, and 103829 ppbv, and N₂O concentrations of 305, 474, 2000 ppbv, made and certified by Air Liquide (France). We calculated the gas concentration in the water samples from the concentration measured in the headspace using the Bunsen functions for CH₄ (Yamamoto *et al.*, 1976; Wiesenburg and Guinasso, 1979), and for the N₂O solubility (Weiss and Price, 1980). The precision in the quantification of the gas mixture of CH₄ used in the headspace equilibrium (1.8 ppmv) expressed as the coefficient of variation was 3.7% (n = 123). The precision for the gas mixture of N₂O used in the headspace equilibrium (0.3 ppmv) was 7.8 % (n = 108). The precision of the measurement of the dissolved CH₄ and N₂O concentration, that included the analytical processing of the samples and the equilibration step, was

3.6% (CH_4) and 3.1% (N_2O) for four to six replicates of each sample. We calculated the saturation values (%) as the ratio between the concentration of the dissolved gas measured and the gas concentration expected in equilibrium considering the temperature, salinity, and barometric pressure of each reservoir. We used the atmospheric gas concentrations provided by *The Global Greenhouse Gas Reference Network* website (<https://www.esrl.noaa.gov/gmd/ccgg/index.html>), which is part of the National Oceanic and Atmospheric Administration (NOAA) Earth System Research Laboratory in Boulder, Colorado. We calculated the 2016 global mean atmospheric concentrations for CH_4 (Dlugokencky, 2019) and for N_2O (Elkins *et al.*, 2017) from the 2016 global monthly mean.

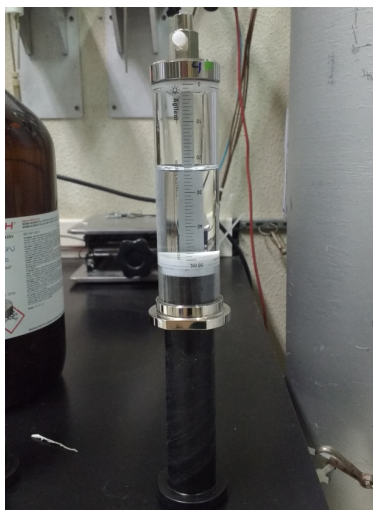


Figure 2.11. The 50 ml air-tight glass syringe (Agilent P/N 5190-1547) during headspace equilibration.



Figure 2.12. Gas chromatograph Bruker® GC-450 at the Department of Physical Chemistry at the University of Cádiz

2. 3. 3. Dissolved inorganic carbon (DIC) and dissolved organic carbon (DOC) concentration

We took the samples for dissolved organic carbon (DOC) and dissolved inorganic carbon (DIC) analysis after filtered through pre-combusted (2 hours 500 °C) Whatman GF/F glass-fiber filters, and stored at 4 °C until analysis. Samples for dissolved organic carbon (DOC) were acidified with phosphoric acid (final pH<2). We measured DOC, and DIC concentrations by high-temperature catalytic oxidation using a Shimadzu total organic carbon (TOC) analyzer (Model TOC-V CSH). The instrument was calibrated using a four-point standard curve of dried potassium hydrogen phthalate for DOC, and dried sodium bicarbonate and sodium carbonate for DIC. We analyzed two replicates and three to five injections per replicate for each sample. Samples for DOC analysis were purged with phosphoric acid for 20 min to eliminate any residue of dissolved inorganic carbon. The detection limit for DIC and DOC concentration was 0.3 $\mu\text{mol-C L}^{-1}$.

2. 3. 4. Chromophoric dissolved organic matter (CDOM) analysis

We measured the absorbance of chromophoric dissolved organic matter (CDOM) from 200 to 700 nm with 1 nm interval in 10-cm quartz cuvettes using a Perkin-Elmer Lambda 40 spectrophotometer connected to a computer equipped with Lambda 35 software. The detection limit of the spectrophotometer (0.001 Absorbance) corresponds to a CDOM absorption coefficient detection limit of 0.02 m^{-1} . CDOM absorption coefficients (a_λ) were calculated using the following equation:

$$a_\lambda = 2.303 \frac{\text{Absorbance } (\lambda) - \text{Absorbance } (600-700)}{l} \quad \text{Eq. 2.8}$$

Where a_λ is the absorption coefficients in m^{-1} at each λ wavelength, Absorbance (λ) is the absorbance at the wavelength λ , Absorbance (600-700) is the average absorbance from 600 to 700 nm, 2.303 is the factor that converts decadic to natural logarithms, and l is the cuvette path length in m^{-1} . The Absorbance (600-700) is the scan corrections due to residual scattering by fine size particle fractions, micro-air bubbles, or colloidal material present in the sample (Green and Blough, 1994). The absorption coefficient at 325 nm (a_{325}) was used to measure the CDOM quantity, since this wavelength is the most common in the literature (Nelson and Siegel, 2013;

Catalá *et al.*, 2015). Using the absorption coefficients, we also computed the spectral slopes to describe the shape decay of absorption coefficients vs. wavelengths that gives information about the quality (size and lability) of CDOM. Slopes were calculated from the linear regression of log-transformed absorption coefficients in the wavelength bands 275-295 nm ($S_{275-295}$) and 350-400 nm ($S_{350-400}$) (Helms *et al.*, 2008). The spectral slopes for both wavelength ranges were calculated as in equation 2.9:

$$a_{\lambda} = a_{\lambda_{\text{ref}}} e^{-S(\lambda - \lambda_{\text{ref}})} \quad \text{Eq. 2.9}$$

Where λ is the selected wavelength in nm, a_{λ} (m^{-1}) is the absorption coefficient at a wavelength of λ , $a_{\lambda_{\text{ref}}}$ is the absorption coefficient at a reference wavelength λ_{ref} , and S is the spectral slope. The spectral slope ratio (S_R) was calculated as the ratio of the spectral slope from 275 nm to 295 nm ($S_{275-295}$) to the spectral slope from 350 nm to 400 nm ($S_{350-400}$).

2. 3. 5. Total nitrogen (TN), total dissolved nitrogen (TDN) and dissolved inorganic nitrogen (DIN) concentration

We took the samples for total nitrogen (TN) analysis from unfiltered water, and the samples for dissolved nitrogen analysis from water filtered through pre-combusted (2 hours 500 °C) Whatman GF/F glass-fiber filters. All the samples were stored at 4 °C until analysis. We measured TN and TDN concentrations by high-temperature catalytic oxidation using a Shimadzu total organic carbon analyzer (Model TOC-V CSH) coupled to nitrogen analyzer (TNM-1) (Álvarez-Salgado and Miller, 1998). The instrument was calibrated using a four-point standard curve of dried potassium nitrate for TN and TDN. We analyzed two replicates and three to five injections per replicate for each sample. The detection limit for TN and TDN concentration was 0.4 $\mu\text{mol-N L}^{-1}$.

We measured the nitrate (NO_3^-) concentration using the ultraviolet spectrophotometric method, using a Perkin Elmer UV-Lambda 40 spectrophotometer at wavelengths of 220 nm and correcting for DOC absorbance at 275 nm (APHA, 1992). The detection limit for the NO_3^- concentration was 0.1 $\mu\text{mol L}^{-1}$. We measured ammonia (NH_4^+), and nitrite (NO_2^-) concentrations by Inductively Coupled Plasma Optical Emission Spectrometry (ICP-OES) at the Centro de Instrumentación Científica of the University of Granada. Dissolved inorganic nitrogen

(DIN) is the addition of the NO_3^- , NH_4^+ , and NO_2^- concentrations. The detection limits for the NH_4^+ , and NO_2^- concentrations were $3.6 \mu\text{mol L}^{-1}$ and $1.4 \mu\text{mol L}^{-1}$, respectively.

2. 3. 6. Total phosphorus (TP), total dissolved phosphorus (TDP) and soluble reactive phosphorus (SRP) concentration

We collected the samples for total phosphorus (TP) analysis from unfiltered water, and samples for total dissolved phosphorus (TDP), and soluble reactive phosphorus (SRP) analysis from water filtered through pre-combusted (2 hours 500 °C) Whatman GF/F glass-fiber filters. All the samples were stored at -20 °C until analysis. We measured SRP concentration by triplicate using the molybdenum blue method (Murphy and Riley, 1962). We measured TP and TDP concentrations as SRP after digestion with a mixture of potassium persulphate and boric acid at 120 °C for 30 min following the standard protocol (APHA, 1992). During the protocol, the antimony potassium tartrate and ammonium molybdate reacted in an acid medium with dilute solutions of phosphorus to form an antimony-phosphomolybdate complex, which was reduced to a blue-colored complex by ascorbic acid. The color intensity was measured by spectrophotometry at a wavelength of 885 nm. The detection limit of this method for TP and TDP concentration was $0.03 \mu\text{mol-P L}^{-1}$, and for SRP concentration was $0.02 \mu\text{mol-P L}^{-1}$.

2. 4. Biological analyses

2. 4. 1. Chlorophyll-*a* concentration and Reservoir metabolism

Chlorophyll-*a* concentration

We determined chlorophyll-*a* (Chl-*a*) concentration by filtering the particulate material of 500 to 2000 ml of water through pre-combusted (2 hours 500 °C) Whatman GF/F glass-fiber filters. Filters were frozen at -20 °C until analysis. Once thawed, each filter was kept in a glass vial with 7mL 95% methanol in the dark at 4 °C for 24 hours for pigments extraction (APHA, 1992). Then, we measured the absorbance of the extracts from 400 to 800 nm using a Perkin Elmer UV-Lambda 40 spectrophotometer connected to a computer equipped with UV-WINLAB software. The chlorophyll-*a* concentration ($\mu\text{g L}^{-1}$) was estimated according to the expression proposed by Marker (1980):

$$\text{Chl-}a = \frac{13.9 (A665-A750) V}{B} \quad \text{Eq. 2.10}$$

Where 13.9 is the absorbance specific coefficient for Chl-*a* in methanol; A665 is the absorbance of the extract at 665 nm; A750 is the absorbance of the extract at 750 nm, used for scattering correction; V is the volume of the methanol used (L); and B is the volume of sample filtered (L). The detection limit was 0.1 µg L⁻¹.

To obtain the integrated mean of chlorophyll-*a* (µg Chl-*a* L⁻¹), from the discrete points along the water column, we calculated the weighted average of the Chl-*a* concentration along the water column using the trapezoidal rule (León-Palmero *et al.*, 2019), and dividing by the maximum depth, as indicated in Equation 2.11:

$$\text{Integrated Chl-}a = \frac{1}{Z} \sum_{k=1}^n X_{ik} \times (Z_{k+1} - \frac{Z_{k-1}}{2}) \quad \text{Eq. 2.11}$$

Where Z stands for the maximum depth considered, and n is the number of depths sampled. Z_k stands for the n sampled depth; X_{ij} is the Chl-*a* concentration (µg L⁻¹) at the depth Z_k. To obtain the cumulative chlorophyll-*a* concentration in the whole water column (mg Chl-*a* m⁻²), we summed the concentration of Chl-*a* from each stratum using the trapezoidal rule, as indicated in Eq. 2.12 (León-Palmero *et al.*, 2020):

$$\text{Cumulative Chl-}a = \sum_{k=1}^n X_{ik} (Z_{k+1} - \frac{Z_{k-1}}{2}) \quad \text{Eq. 2.12}$$

Reservoir metabolism

We estimated the gross primary production (GPP), reservoir respiration (R), and net ecosystem production (NEP) from diel changes in dissolved oxygen concentration. We recorded the time, the date, the dissolved oxygen concentration, and the water temperature every 10 minutes during a period of 24 - 48 hours using a miniDOT (PME) submersible water logger during the same sampling days. The oxygen sensor is an optode that measures dissolved oxygen concentration in water through a fluorescence method. Data are recorded to an internal SD card. We placed the sensor in each study reservoir during the stratification period hanging from a buoy at 1 m to 4 m deep. An example of the daily cycle of dissolved oxygen

concentration and temperature obtained in La Bolera reservoir is shown in Figure 2.13.

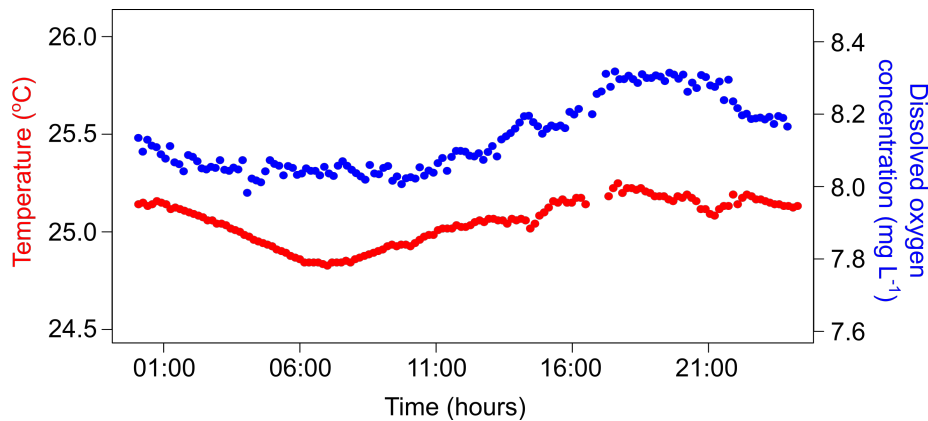


Figure 2.13. Daily cycle of the dissolved oxygen concentration and the water temperature in La Bolera reservoir.

We calculated the GPP, R and NEP of the reservoir with the measurements of dissolved oxygen concentration and the water temperature using the diel dissolved oxygen technique. The diel dissolved oxygen technique assumes that changes in oxygen concentration of a body of water reflect the biological balance between photosynthetic production and respiratory consumption and the physical exchange of oxygen between air and water (Staeher *et al.*, 2010). Briefly, the equation for estimating free-water metabolism from measurements of dissolved oxygen was established by Odum (1956) (Eq. 2.13):

$$\Delta O_2 / \Delta t = GPP - R - F - A \quad \text{Eq. 2.13}$$

Where $\Delta O_2 / \Delta t$ is the change in dissolved oxygen concentration through time; F is the exchange of O_2 with the atmosphere; and A is a term that combines all other processes that may cause changes in the dissolved oxygen concentration as horizontal or vertical advection, and it is often assumed to be negligible. The calculations were performed as in Staeher *et al.* (2010). The physical gas flux was modelled as follows (Eq. 2.14):

$$F = k (O_{2 \text{ meas}} - O_{2 \text{ sat}}) \quad \text{Eq. 2.14}$$

Where F ($g O_2 m^{-2} h^{-1}$) is the physical gas flux, and k ($m h^{-1}$) is the piston velocity estimated following the equation of Jähne *et al.* (1987) and the indications of Staeher *et al.* (2010). $O_{2 \text{ meas}}$ is the actual oxygen concentration ($mg L^{-1}$), and $O_{2 \text{ sat}}$ is the

oxygen concentration (mg L^{-1}) in water in equilibrium with the atmosphere at ambient temperature and salinity.

We calculated the hourly net ecosystem production (NEP_{hr}) and the daytime net ecosystem production ($\text{NEP}_{\text{daytime}}$) following the equations 2.15 (Cole *et al.*, 2000) and 2.16:

$$\text{NEP}_{\text{hr}} = \Delta\text{O}_2 - F/Z_{\text{mix}} \quad \text{Eq. 2.15}$$

$$\text{NEP}_{\text{daytime}} = \text{mean NEP}_{\text{hr}} \text{ during daylight} \times \text{Light hours} \quad \text{Eq. 2.16}$$

NEP_{hr} ($\text{g O}_2 \text{ m}^{-3} \text{ h}^{-1}$) is directly derived from the changes in dissolved oxygen (ΔO_2 , $\text{g O}_2 \text{ m}^{-3} \text{ h}^{-1}$) after accounting for physical gas flux with the atmosphere (F). Z_{mix} is the depth of the mixed layer (m), and that was inferred from the temperature profile as the upper mixed zone where the temperature remains constant. $\text{NEP}_{\text{daytime}}$ ($\text{g O}_2 \text{ m}^{-3} \text{ daylight period}^{-1}$) is the portion of NEP between sunrise and sunset, when the photosynthesis is taking place. We obtained the exact light hours from an online solar calculator (<https://es.calcuworld.com/calendarios/calcular-salida-y-puesta-del-sol/>). We established the start and the end time for photosynthesis as 30 minutes before sunrise and 30 minutes after dawn (Schlesinger and Bernhardt, 2013). We obtained hourly R (R_{hr} , $\text{g O}_2 \text{ m}^{-3} \text{ h}^{-1}$), R during the daytime (R_{daytime} , $\text{g O}_2 \text{ m}^{-3} \text{ daylight period}^{-1}$), and R during all the day (R_{day} , $\text{g O}_2 \text{ m}^{-3} \text{ d}^{-1}$) following equation 2.17, 2.18, and 2.19, respectively:

$$R_{\text{hr}} = \text{mean NEP}_{\text{hr}} \text{ during darkness} \quad \text{Eq. 2.17}$$

$$R_{\text{daytime}} = R_{\text{hr}} \times \text{Light hours} \quad \text{Eq. 2.18}$$

$$R_{\text{day}} = R_{\text{hr}} \times 24 \quad \text{Eq. 2.19}$$

We calculated the respiration rate during the night (the period between 60 minutes after dawn and 60 minutes before sunrise) (Staehr *et al.*, 2010), and we assumed that the respiration rate overnight was similar to the respiration rate over the day. Finally, we obtained the GPP and NEP for the day ($\text{g O}_2 \text{ m}^{-3} \text{ d}^{-1}$) (Eq. 2.20 and 2.21):

$$\text{GPP} = \text{NEP}_{\text{daytime}} + R_{\text{daytime}} \quad \text{Eq. 2.20}$$

$$\text{NEP} = \text{GPP} - R_{\text{day}} \quad \text{Eq. 2.21}$$

2. 4. 2. Abundance of prokaryotes, cyanobacteria and picoeukaryotes

We determined the abundances of total prokaryotes (PA), cyanobacteria (CYA), and photosynthetic picoeukaryotes (PPEs) using flow cytometry in unfiltered water following the procedures proposed by Gasol and Giorgio (2000). We collected and fixed the samples with a mixture of 1 % paraformaldehyde and 0.05 % glutaraldehyde for 30 min in the dark at 4 °C. Then, we froze the samples in liquid nitrogen and stored them at –80 °C until analysis. We analyzed the samples by triplicate in a FACScalibur flow cytometer equipped with the BD CellQuest Pro software for data analysis. The flow cytometer was located at the Centro de Instrumentación Científica of the University of Granada. In the laboratory, we thawed the samples and diluted them ≥ 10 -fold with double-distilled water to avoid coincidence of cell counts when it was necessary. Before analysis, we stained the PA samples (500 μ L) for 10 min in the dark with a DMSO diluted SYBR Green I (Molecular Probes) stock (1:200) at 10 μ mol L⁻¹ final concentration. We used yellow-green 0.92 μ m latex beads (Polysciences) as an internal standard to control the cytometer performance every day. The beads solution was sonicated for 10 min before adding to the sample. We used different signals for groups determination: the side scatter (SSC), chlorophyll-*a* (red fluorescence, FL3), phycoerythrin (the orange fluorescence, FL2), and phycocyanin (the blue fluorescence, FL4); following the protocols and indications for data previously published (Corzo *et al.*, 1999; Collier, 2000; Gasol and Giorgio, 2000; Cellamare *et al.*, 2010; Liu *et al.*, 2014). Samples for PA analysis were run at low speed for 2 min, and we detected them by their signature in bivariate plots SSD vs. FL1 (green fluorescence of the DNA stained with SYBR Green I). Samples for CYA and PPEs analysis were run at high speed for 4 min. The signature of CYA and PPEs were detected in bivariate plots as SSC vs FL3; FL4 vs FL3; and FL2 vs FL3.

In Figure 2.14, we show a cytogram of the populations of CYA and PPEs. We analyzed the cell number of the subpopulations by drawing windows around the cells of interest that were consistent over the whole study. We determined the cell abundance (cells mL⁻¹) using the following equation (Eq. 2.22):

$$\text{Cell abundance} = \frac{\text{cell number}}{t \times \text{FR}} \quad \text{Eq. 2.22}$$

Where the cell number is determined by selecting a subpopulation in the cytogram; t is the time (2 or 4 min); and FR is the flow rate ($\mu\text{L min}^{-1}$), determined daily at low speed for PA and a high speed for CYA and PPEs.

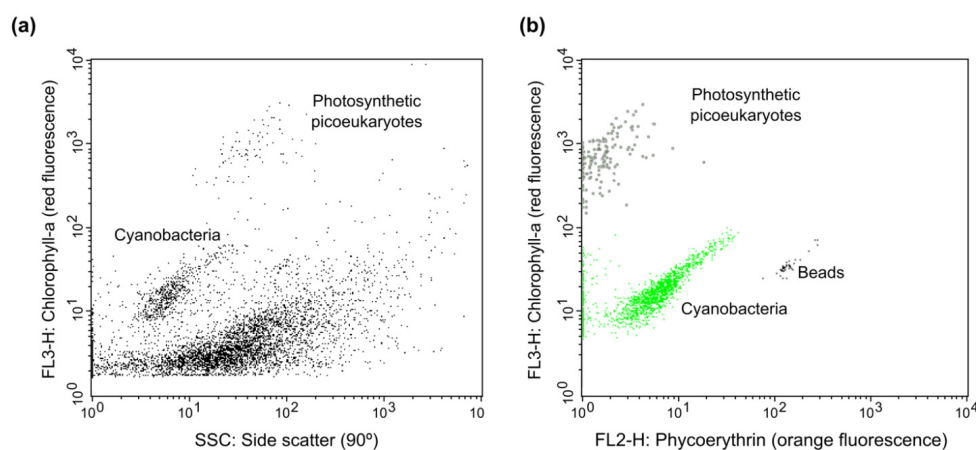


Figure 2.14. Flow cytometric signatures of cyanobacteria and photosynthetic picoeukaryotes populations in the epilimnion of Bézna reservoir. (a) Side scatter (SSC) on the x-axis and chlorophyll- a (red fluorescence, FL3) on the y-axis. (b) Phycoerythrin (the orange fluorescence, FL2) on the x-axis and chlorophyll- a (red fluorescence, FL3) on the y-axis. Populations selected in the plot A were colored on the plot B. We used yellow-green $0.92 \mu\text{m}$ latex beads (Polysciences) as an internal standard.

2. 4. 3. Functional genes

From the extensive sampling, we selected 3 or 4 representative depths of epilimnion, metalimnion (oxycline), and hypolimnion and bottom layers during the stratification period for determining the abundance of the functional genes. We also selected 3 or 4 similar depths during the mixing period.

We studied unique functional genes involved in the specific microbial transformations of interest using PCR for detection and quantitative PCR (qPCR) as a proxy for the abundance of these groups in the water column (Table 2.4). First, we pre-filtered the water through $3.0 \mu\text{m}$ pore-size filter and extracted DNA following the procedure developed for environmental samples (Boström *et al.*, 2004). During the DNA extraction protocol, we combined a cell recovery step by centrifugation of 12 - 20 mL of the pre-filtered water, a cell lysis step with enzyme treatment (lysozyme and proteinase K), and finally, the DNA recovery step with a co-precipitant (yeast tRNA) to improve the precipitation of low-concentration DNA. Extracted DNA served

as the template for PCR and qPCR analysis to test the presence and abundance of the different functional genes. For PCR analysis, we used the recombinant Taq DNA Polymerase (Thermo Fisher Scientific) using the Mastercycler X50 thermal cycler (Eppendorf). We checked the result of the amplification by running 1.5 % (w/v) agarose gel electrophoresis. We ran the qPCR plates using SYBR Green as the reporter dye (PowerUp™ SYBR™ Green Master Mix, Thermo Fisher Scientific) in the Applied Biosystems 7500 Real-Time PCR System and the 7500 Software. In both cases, PCR and qPCR, we designed the standard reaction mix recipes and the thermocycling conditions using the provider specifications and primer requirements. We chose specific primers for each gene from similar studies in freshwaters (see below). If we did not detect amplification in the PCR or qPCR samples, we changed the standard procedure by increasing the DNA amount and the primers concentration to warranty the negative results. We used pure cultures as positive controls.

In the experiments performed in Cubillas and Iznájar reservoirs, we analyzed all the abundance of nitrogen functional genes at all the depths sampled.

CH₄ related genes

To determine the occurrence and abundance of methanogenic *Archaea*, we targeted the alpha subunit of methyl-coenzyme reductase (*mcrA*) as a genetic marker in our samples. This gene is considered an excellent marker since all known methanogens have the *methyl coenzyme-M reductase*, which is the enzyme responsible for the conversion of a methyl group to CH₄ (Grabarse *et al.*, 2001). We used the specific primers as in West *et al.* (2012) adapting their procedure. The forward primer was mcrAqF (5'-AYGGTATGGARCAGTACGA-3'), and the reverse primer was mcrAqR (5'- TGVAGRTCCTABCCGWAGAA -3'), and the annealing temperature was 54 °C. We used a culture of *Methanosarcina acetivorans* (ATCC 35395) as a positive control.

To determine the occurrence and abundance of the *phnJ* gene, which encodes a subunit of the C-P lyase complex (White and Metcalf, 2007; Seweryn *et al.*, 2015). This enzyme cleaves C-P bonds in phosphonate compounds releasing methane, and changes in response to the phosphate availability (Yao *et al.*, 2016). We ran the amplification with a pair of primers previously used (Fox *et al.*, 2014; Yao *et al.*, 2016). The forward primer was PhnJoc1 (5'-AARGTRATMGAYCARGG-3') and the reverse

PhnJoc2 (5'-CATYTTYGGATTRTCRAA-3') adapting the PCR procedure from Yao *et al.* (2016). The annealing temperature was 52.5 °C, and the positive controls were run using a pure culture of *Rhodopseudomonas palustris* (ATCC 33872). We checked the result of the amplification by running 1.5 % (w/v) agarose gel electrophoresis. If we did not detect amplification in the PCR or qPCR samples, we changed the standard procedure by increasing the DNA amount and the primers concentration to corroborate the negative results.

N₂O related genes

We prepared the standards for PCR quantification of each functional gene by amplifying a pure culture of a strain containing the gene fragment, followed by fragment purification, quantification, and serial dilution. In the case of the *nirS* gene, we used a constructed plasmid containing the respective gene fragment. We used these standards to build a standard curve for the absolute quantification of the gene copies in the environmental samples. DNA from water column samples (2-3 µL) was analyzed by triplicate, together with triplicates of the no-template control, a no-primer control, and four standards also in triplicate. We used automatic analysis settings to determine the threshold cycle (C_T) values. We checked the dissociation curves and the melting temperature of the qPCR products to ensure the purity of the products. Before qPCR analysis, we quantified the environmental DNA and the standards using a DNA quantitation kit (Sigma-Aldrich) based on the fluorescent dye bisBenzimide (Hoechst 33258). In each plate assay, we calculated a standard curve between the copy number of the standards and the C_T obtained for them during the qPCR run. We calculated the copy number in the standards following equation (Eq. 2.23):

$$\text{Copy number} = \frac{\text{DNA in the reaction} \times 6.022 \times 10^{23}}{\text{Length of the amplicon} \times 650 \times 10^9} \quad \text{Eq. 2.23}$$

Where we obtained the DNA in the reaction (ng) from the DNA concentration of each sample and the volume used in the qPCR reaction, 6.022×10^{23} is the Avogadro's constant (molecules mol⁻¹), 650 is the average mass of one base pairs (bp) of DNA (g mol⁻¹ per bp), and 10^9 is a conversion factor. Note that the length of the amplicon (bp) is different for each gene and pair of primers. We used the standard curve to calculate the copy number of each sample using the C_T obtained during the

qPCR run. Then, we normalized to copy number per volume of water (copy number mL⁻¹), assuming 100 % recovery, as follows:

$$\text{Copy number per volume} = \frac{\text{copy number} \times \text{DNA extracted}}{\text{DNA in the reaction} \times \text{volume of water}} \quad \text{Eq. 2.24}$$

Where the DNA extracted, and the DNA in the reaction are in nanograms (ng), and the volume of water (mL) is the water used for the DNA extraction.

We targeted the gene *amoA*, which encodes the catalytic subunit of ammonia monooxygenase, the first and rate-limiting step of the nitrification (Kowalchuk and Stephen, 2001). We studied the ammonia-oxidizing bacteria (AOB, *bacterial amoA*) and the ammonia-oxidizing archaea (AOA, *archaeal amoA*). For the bacterial *amoA*, we used specific primers tested in various aquatic and terrestrial environments (Rotthauwe *et al.*, 1997). The forward primer was amoA-1F (5'-GGGGTTTCTACTGGTGGT-3'), and the reverse primer was amoA-2R (5'-CCCCTCKGSAAAGCCTTCTTC - 3'). The specific amplicon length was 491 bp, and the annealing temperature was 60 °C. We used a pure culture of *Nitrosomonas europaea* Winogradsky 1892 (ATCC 25978) as positive control for bacterial *amoA* standard quantification. For the archaeal *amoA*, we used the specific primers described in Francis *et al.* (2005). The forward primer was Arch-amoAF (5'-STAATGGTCTGGCTTAGACG-3'), and the reverse primer was Arch-amoAR (5'-GCGGCCATCCATCTGTATGT-3') at a final concentration of 0.4 μmol L⁻¹. The specific amplicon length was 635 bp, and the annealing temperature was 53 °C. We used a pure culture of *Nitrososphaera viennensis* (Stieglmeier *et al.*, 2014) (strain EN76^T) for standard preparation.

We also studied the presence of the comammox *amoA* genes using two degenerate PCR primer pairs to target the clade A or the clade B of comammox bacteria. We used specific primers from Pjevac *et al.* (2017) adapting their procedure. We used these two pairs of primers: comaA-244F (5'-TAYAAYTGGTSAAYTA-3') and comaA-659R (5'-ARATCATSGTGCTRTG-3') for the clade A; and comaB-244F (5'-TAYTTCTGGACRTTYTA-3') and comaB-659R (5'-ARATCCARACDGTGTG-3') for the clade B. The annealing temperature was 52 °C. The expected amplicon length was 415 bp.

To determine the denitrifier abundance, we targeted the gene *nirS* in all the depths of the water column and the gene *nosZ* in the bottom layer. The gene *nirS* encodes the nitrite reductase that catalyzes the transformation of nitrite to NO during denitrification. We used the primers from Braker *et al.* (1998). The forward primer was nirS-1F (5'-CCTAYTGCCCGCCRCART-3'), and the reverse primer was nirS-3R (5'-GCCGCCGTCRTGVAGGAA-3') at a final concentration of 2 $\mu\text{mol L}^{-1}$. The specific amplicon length was 260 bp, and the annealing temperature was 62 °C. We used a pure culture of *Escherichia coli* transformed with a constructed plasmid containing the *nirS* gene fragment for the standard preparation. The gene *nosZ* encodes the enzyme nitrous oxide reductase, responsible for the last step in denitrification: the N₂O reduction to N₂. We used the primers from Henry *et al.* (2006) at a final concentration of 2 $\mu\text{mol L}^{-1}$. The forward primer was nosZ1F (5'-WCSYTGTTTCMTCGACAGCCAG-3'), and the reverse primer was nosZ1R (5'-ATGTCGATCARCTGVKCRTTYTC-3'). The specific amplicon length was 259 bp and the annealing temperature was 63 °C. We used a pure culture of *Paracoccus denitrificans* (Beijerinck and Minkman 1910) Davis 1969 (ATCC 17741) as a positive control for the standard quantification.

We also studied in the bottom layer the gene *nrfA* that encodes for the nitrite reduction to ammonium, the second step in the DNRA. We used the primers established by Takeuchi (2006) at a final concentration of 0.5 $\mu\text{mol L}^{-1}$. The forward primer was nrfA6F (5'-GAYTGCCAYATGCCRAAAGT-3'), and the reverse primer was nrfA6R (5'-GCBKCTTTYGCTTCRAAGTG-3'). The annealing temperature was 54.5 °C, and the amplicon length was 222 bp. We used a pure culture of *Escherichia coli* as a positive control.

Table 2.4. Summary of the target genes analyzed, the strains used for the positive control, annealing temperature during the PCR and qPCR, and the references for the selected primers.

Process	Target gene	Positive control	Annealing temperature (°C)	Primers reference
Archaeal Methanogenesis	<i>mcrA</i>	<i>Methanosarcina acetivorans</i> (ATCC 35395)	54.0	(West <i>et al.</i> , 2012)
Phosphonate degradation	<i>phnJ</i>	<i>Rhodopseudomonas palustris</i> (ATCC 33872)	52.5	(Yao <i>et al.</i> , 2016)
Ammonia oxidation	Bacterial <i>amoA</i>	<i>Nitrosomonas europaea</i> (ATCC 25978)	60.0	(Rotthauwe <i>et al.</i> , 1997)
Ammonia oxidation	Archaeal <i>amoA</i>	<i>Nitrososphaera viennensis</i> (strain EN76 ^T)	53.0	(Francis <i>et al.</i> , 2005)
Comammox nitrification	<i>comammox amoA</i>		52.0	(Pjevac <i>et al.</i> , 2017)
Denitrification	<i>nirS</i>	<i>Escherichia coli</i> transformed with a constructed plasmid containing the <i>nirS</i> gene	62.0	(Braker <i>et al.</i> , 1998)
Denitrification	<i>nosZ</i>	<i>Paracoccus denitrificans</i> (ATCC 17741)	63.0	(Henry <i>et al.</i> , 2006)
Dissimilatory nitrate reduction (DNRA)	<i>nrfA</i>	<i>Escherichia coli</i>	54.5	(Takeuchi, 2006)

2. 5. Experiments

2. 5. 1. Photoproduction of CO₂, CH₄, and N₂O

We tested the effect of sunlight on the production of greenhouse gases using water from the Cubillas and Iznájar reservoirs. We performed two sets of experiments to determine the photoproduction of dissolved inorganic carbon (DIC), photomineralization of dissolved organic carbon (DOC), and photobleaching of chromophoric dissolved organic matter (CDOM); and three sets to determine the photoproduction of dissolved CH₄ and N₂O. We performed the experiment using quartz bottles that allow the transmission of ultraviolet light and included dark bottles as controls. The experiments were incubated in situ using small floating

platforms, as shown in Figure 2.15. More details on the experiment set up are provided in Chapter 4.



Figure 2.15. Incubation of quartz bottles during the photochemical experiments in the Cubillas reservoir.

2. 5. 2. Microbial N₂O production using ¹⁵N tracers

We analyzed the production of N₂O in the study reservoirs using ¹⁵N tracers. We used two different tracers: ¹⁵N-NH₄⁺ and ¹⁵N-NO₃⁻. We measured the N₂O production, the ammonia oxidation to nitrite (nitrite oxidation), and the ammonia oxidation to nitrate (complete nitrification) with additions of ¹⁵N-NH₄⁺. In separate bottles, we measured the N₂O production during denitrification, and the reduction of nitrate to nitrite with additions of ¹⁵N-NO₃⁻. We measured the samples using a gas chromatograph coupled to isotope ratio mass spectrometry (GC-IRMS, Delta V Plus, Thermo) in the Department of Geosciences at Princeton University (NJ, EEUU). We performed the experiments in the Cubillas and Iznájar reservoirs at the beginning of the stratification in July and the end of stratification in September 2018. We chose three depths in each reservoir to measure the production rates in the epilimnion, oxycline, and hypolimnion. We incubated a set of nine bottles per depth and treatment: two bottles at t₀ (≈ 0.25 h), two at t₁ (≈ 3 h), two at t₂ (≈ 12 h), and three at t₃ (≈ 24 h), to determine a single rate. We incubated the samples at the in situ

temperature from 13 °C up to 26 °C. We finished the incubations adding 0.1 mL saturated mercuric chloride (HgCl₂). Besides incubations, we also took two serum bottles per depth without headspace or any treatment to analyze the natural isotopic composition ($\delta^{15}\text{N}$) of the nitrate, nitrite and nitrous oxide. All samples were stored at room temperature in the dark and shipped to the laboratory at Princeton University, where we measured the production rates. We provided more details on the set-up and the rate calculations in Chapter 7.

2. 6. Statistical tests

We conducted most of the statistical analysis using the free software R (R Core Team, 2019), using the packages *car* (Fox and Weisberg, 2011), *mgcv* (Wood, 2011), *nortest* (Gross and Ligges, 2015), *outliers* (Komsta, 2011), *Rcmdr* (Fox and Bouchet-Valat, 2019), *readxl* (Wickham and Bryan, 2019), and *rpart* (Therneau and Atkinson, 2019). We also used R to plot the results and create the Figures, using the packages *ggplot2* (Wickham, 2016), *plotrix* (Lemon, 2006), and *rpart.plot* (Milborrow, 2019); and the software Inkscape™ (Inkscape Project, 2017).

We performed the Shapiro-Wilk ($n < 30$) or the Kolmogorov-Smornov tests ($n > 30$) for normality analysis. We used the Levene's test for homogeneity of variance across groups. We also performed correlation analysis to study the association between paired samples. We used the Pearson product-moment correlation in normally distributed data, and the Spearman correlation in non-normally distributed data. We performed a one-way analysis of variance test (ANOVA), or the t-test when the data were normally distributed. In case the data did not meet the assumptions of normality, we used the Kruskal-Wallis rank sum test (K-W) or the Wilcoxon test (V). We also used simple and multiple linear regression analysis and generalized additive models (GAMs) (Wood, 2006). In multiple regression analysis we tested the multicollinearity using the variable inflation factor (VIF). GAM is a generalized model with a linear predictor involving a sum of smooth functions of covariates (Hastie and Tibshirani, 1986, 1990). The model structure is detailed in equation 2.25:

$$y_i = f_1(x_{1i}) + f_2(x_{2i}) + \dots + f_n(x_{ni}) + \epsilon_i \quad \text{Eq. 2.25}$$

Where the $f_{1,2,\dots,n}$ are the smooth functions, and the ϵ_i are independent identically distributed $N(0, \sigma^2)$ random variables. We fit smoothing functions by

penalized cubic regression splines. The cross-validation method (Generalized Cross Validation criterion, GCV) estimates the smoothness of the functions. Before model fitting, we examined the concavity among predictors. We fitted the models to minimize the Akaike Information Criterion (AIC) and the GCV values. We calculated the percentage of variance explained by the model ($\text{adj } R^2$) and the quality of the fit (deviance explained). We also fixed the effect of each predictor to assess the contribution of the other predictors to the total deviance explained. Then, the sum of the deviance explained by two predictors can be different from the deviance explained by the model due to interactive effects.

We used the software Oriana (Kovach, 2011) to analyze and plot the circular data. Oriana performs analyses designed specifically for circular data, distributed on a daily cycle during the 24-hour cycles, where the time is a circular variable measured in a closed and cyclical scale. Because classical statistical analysis does not work for circular variables, we decided to use linear-circular regression, also known as periodic regression. We performed linear-circular correlation (Fisher, 1993; Zar, 1998; Mardia and Jupp, 2000) between a circular variable (solar time, h) and a linear one (the fluxes or environmental variables). This correlation coefficient ranges from 0 to 1, so there is no negative correlation. The calculation of the significance of the correlation follows Mardia and Jupp (2000) in using their approximation of the F distribution. Linear-circular regression is a simple, sensitive and robust alternative for the detection of cyclical patterns of known period, considering the independent variable as an angular representation of time (Batschelet, 1981). Other authors have used linear-circular regression to detect cyclical patterns in marine ecology (e.g., deBruyn and Meeuwig, 2001)

2. 7. References

- Agencia Estatal de Meteorología de España and Instituto de Meteorología de Portugal (eds). (2011). *Atlas climático ibérico - Iberian climate atlas - Agencia Estatal de Meteorología - AEMET. Gobierno de España*. Available at: http://www.aemet.es/es/conocermas/recursos_en_linea/publicaciones_y_estudios/publicaciones/detalles/Atlas-climatologico (Accessed: 19 April 2020).
- Álvarez-Salgado, X. A. and Miller, A. E. J. (1998). Simultaneous determination of dissolved organic carbon and total dissolved nitrogen in seawater by high temperature catalytic oxidation: conditions for precise shipboard measurements, *Marine Chemistry*, 62(3), pp. 325–333. doi: 10.1016/S0304-4203(98)00037-1.

- American Public Health Association (APHA). (1992). *Standard methods for the examination of water and wastewater*. 18th edn. Edited by A. E. Greenberg, L. S. Clesceri, and A. D. Eaton.
- Aronow, S. (1982). Shoreline development ratio, in *Beaches and Coastal Geology*, pp. 754–755. doi: 10.1007/0-387-30843-1_417.
- Batschelet, E. (1981). *Circular statistics in biology*.
- Boström, K. H., Simu, K., Hagström, Å. and Riemann, L. (2004). Optimization of DNA extraction for quantitative marine bacterioplankton community analysis, *Limnology and Oceanography: Methods*, 2(11), pp. 365–373. doi: 10.4319/lom.2004.2.365.
- Braker, G., Fesefeldt, A. and Witzel, K.-P. (1998). Development of PCR primer systems for amplification of nitrite reductase genes (*nirK* and *nirS*) to detect denitrifying bacteria in environmental samples, *Applied and Environmental Microbiology*, 64(10), pp. 3769–3775. doi: 10.1128/AEM.64.10.3769-3775.1998.
- Catalá, T. S., Reche, I., Álvarez, M., Khatiwala, S., Guallart, E. F., Benítez-Barrios, V. M., Fuentes-Lema, A., Romera-Castillo, C., Nieto-Cid, M., Pelejero, C., Fraile-Nuez, E., Ortega-Retuerta, E., Marrasé, C. and Álvarez-Salgado, X. A. (2015). Water mass age and aging driving chromophoric dissolved organic matter in the dark global ocean, *Global Biogeochemical Cycles*, 29(7), pp. 917–934. doi: 10.1002/2014GB005048.
- Cellamare, M., Rolland, A. and Jacquet, S. (2010). Flow cytometry sorting of freshwater phytoplankton, *Journal of Applied Phycology*, 22(1), pp. 87–100. doi: 10.1007/s10811-009-9439-4.
- Cole, J. J., Pace, M. L., Carpenter, S. R. and Kitchell, J. F. (2000). Persistence of net heterotrophy in lakes during nutrient addition and food web manipulations, *Limnology and Oceanography*, 45(8), pp. 1718–1730. doi: 10.4319/lo.2000.45.8.1718.
- Collier, J. L. (2000). Flow cytometry and the single cell in phycology, *Journal of Phycology*, 36(4), pp. 628–644. doi: 10.1046/j.1529-8817.2000.99215.x.
- Corzo, A., Jimenez-Gomez, F., Gordillo, F., Garcia-Ruiz, R. and Niell, F. (1999). *Synechococcus* and *Prochlorococcus*-like populations detected by flow cytometry in a eutrophic reservoir in summer, *Journal of Plankton Research*, 21(8), pp. 1575–1581. doi: 10.1093/plankt/21.8.1575.
- deBruyn, A. M. H. and Meeuwig, J. J. (2001). Detecting lunar cycles in marine ecology: periodic regression versus categorical ANOVA, *Marine Ecology Progress Series*, 214, pp. 307–310. doi: 10.3354/meps214307.
- Dlugokencky, E. J. (2019). *Trends in Atmospheric Methane. Globally averaged marine surface monthly mean data*. Available at: www.esrl.noaa.gov/gmd/ccgg/trends_ch4/.
- Elkins, J. W., Hall, B. D. and Nance, J. D. (2017). Nitrous Oxide data from the NOAA/ESRL halocarbons in situ program. Mauna Loa, Hawaii (MLO). Available at: <http://www.esrl.noaa.gov/gmd/obop/>.
- ESRI. (2012). *ArcGIS*. Available at: www.esri.com.
- Fisher, N. I. (1993). in *Statistical analysis of circular data*, p. 277.

- Fox, A., Kwapinski, W., Griffiths, B. S. and Schmalenberger, A. (2014). The role of sulfur- and phosphorus-mobilizing bacteria in biochar-induced growth promotion of *Lolium perenne*, *FEMS Microbiology Ecology*, 90(1), pp. 78–91. doi: 10.1111/1574-6941.12374.
- Fox, J. and Bouchet-Valat, M. (2019). *Rcmdr: R Commander*. Available at: <http://socserv.socsci.mcmaster.ca/jfox/Misc/Rcmdr/>.
- Fox, J. and Weisberg, S. (2011). *An R Companion to Applied Regression*. Second. Available at: <http://socserv.socsci.mcmaster.ca/jfox/Books/Companion>.
- Francis, C. A., Roberts, K. J., Beman, J. M., Santoro, A. E. and Oakley, B. B. (2005). Ubiquity and diversity of ammonia-oxidizing archaea in water columns and sediments of the ocean, *Proceedings of the National Academy of Sciences*, 102(41), pp. 14683–14688. doi: 10.1073/pnas.0506625102.
- Gasol, J. M. and Giorgio, P. A. del. (2000). Using flow cytometry for counting natural planktonic bacteria and understanding the structure of planktonic bacterial communities, *Scientia Marina*, 64(2), pp. 197–224. doi: 10.3989/scimar.2000.64n2197.
- Grabarse, W., Mahlert, F., Duin, E. C., Goubeaud, M., Shima, S., Thauer, R. K., Lamzin, V. and Ermler, U. (2001). On the mechanism of biological methane formation: structural evidence for conformational changes in methyl-coenzyme M reductase upon substrate binding, *Journal of Molecular Biology*, 309(1), pp. 315–330. doi: 10.1006/jmbi.2001.4647.
- Green, S. A. and Blough, N. V. (1994). Optical absorption and fluorescence properties of chromophoric dissolved organic matter in natural waters, *Limnology and Oceanography*, 39(8), pp. 1903–1916. doi: 10.4319/lo.1994.39.8.1903.
- Gross, J. and Ligges, U. (2015). *nortest: Tests for Normality*. Available at: <https://CRAN.R-project.org/package=nortest> (Accessed: 3 June 2018).
- Hastie, T. and Tibshirani, R. (1986). Generalized Additive Models, *Statistical Science*, 1(3), pp. 297–310. doi: 10.1214/ss/1177013604.
- Hastie, T. and Tibshirani, R. J. (1990). *Generalized additive models*. 1st ed.
- Helms, J. R., Stubbins, A., Ritchie, J. D., Minor, E. C., Kieber, D. J. and Mopper, K. (2008). Absorption spectral slopes and slope ratios as indicators of molecular weight, source, and photobleaching of chromophoric dissolved organic matter, *Limnology and Oceanography*, 53(3), pp. 955–969. doi: 10.4319/lo.2008.53.3.0955.
- Henry, S., Bru, D., Stres, B., Hallet, S. and Philippot, L. (2006). Quantitative detection of the *nosZ* gene, encoding nitrous oxide reductase, and comparison of the abundances of 16S rRNA, *narG*, *nirK*, and *nosZ* genes in soils, *Applied and Environmental Microbiology*, 72(8), pp. 5181–5189. doi: 10.1128/AEM.00231-06.
- Hoffmann, M., Schulz-Hanke, M., Garcia Alba, J., Jurisch, N., Hagemann, U., Sachs, T., Sommer, M. and Augustin, J. (2017). A simple calculation algorithm to separate high-resolution CH₄ flux measurements into ebullition- and diffusion-derived components, *Atmospheric Measurement Techniques*, 10(1), pp. 109–118. doi: <https://doi.org/10.5194/amt-10-109-2017>.

- Inkscape Project. (2017). *Inkscape: Open Source Scalable Vector Graphics Editor*. Available at: <https://inkscape.org>.
- Jähne, B., Münnich, K. O., Bösinger, R., Dutzi, A., Huber, W. and Libner, P. (1987). On the parameters influencing air-water gas exchange, *Journal of Geophysical Research: Oceans*, 92(C2), pp. 1937–1949. doi: 10.1029/JC092iC02p01937.
- Jódar, G. (2009). *Contextualización Geológica de Andalucía, una aproximación a la Geodiversidad andaluza*. Edited by Consejería de Medio Ambiente. Available at: http://www.juntadeandalucia.es/medioambiente/portal_web/web/temas_ambientales/geodiversidad/geodiversidad_andalucia/contextualizacion_geologica.pdf (Accessed: 19 April 2020).
- Komsta, L. (2011). *outliers: Tests for outliers*. Available at: <https://CRAN.R-project.org/package=outliers>.
- Kovach, W. L. (2011). Oriana—circular statistics for windows, ver. 4, *Kovach Computing Services, Pentraeth, Wales, UK*.
- Kowalchuk, G. A. and Stephen, J. R. (2001). Ammonia-oxidizing bacteria: A model for molecular microbial ecology, *Annual Review of Microbiology*, 55(1), pp. 485–529. doi: 10.1146/annurev.micro.55.1.485.
- Lemon, J. (2006). Plotrix: a package in the red light district of R, *R-News*, 6(4), pp. 8–12.
- León-Palmero, E., Contreras-Ruiz, A., Sierra, A., Morales-Baquero, R. and Reche, I. (2020). Dissolved CH₄ coupled to photosynthetic picoeukaryotes in oxic waters and to cumulative chlorophyll *a* in anoxic waters of reservoirs, *Biogeosciences*, 17(12), pp. 3223–3245. doi: 10.5194/bg-17-3223-2020.
- León-Palmero, E., Reche, I. and Morales-Baquero, R. (2019). Atenuación de luz en embalses del sur-este de la Península Ibérica, *Ingeniería del agua*, 23(1), pp. 65–75. doi: 10.4995/ia.2019.10655.
- Liu, H., Jing, H., Wong, T. H. C. and Chen, B. (2014). Co-occurrence of phycocyanin- and phycoerythrin-rich *Synechococcus* in subtropical estuarine and coastal waters of Hong Kong, *Environmental Microbiology Reports*, 6(1), pp. 90–99. doi: 10.1111/1758-2229.12111.
- Mardia, K. V. and Jupp, P. E. (2000). in *Statistics of directional data*. 2nd edn, p. 429.
- Marker, A. F. (1980). Methanol and acetone as solvents for estimating chlorophyll *a* and phaeopigments by spectrophotometry, *Arch. Hydrobiol. Beih., Ergebnisseder Limnologie*, 14, pp. 52–69.
- Milborrow, S. (2019). *rpart.plot: Plot 'rpart' Models: An Enhanced Version of 'plot.rpart'*. Available at: <https://CRAN.R-project.org/package=rpart.plot>.
- Mortimer, C. H. (1956). *The oxygen content of air-saturated fresh waters, and aids in calculating percentage saturation*. Available at: http://www.schweizerbart.de/publications/detail/isbn/9783510520060/Mitteilunge_n_IVL_Nr_6.
- Moseman-Valtierra, S., Abdul-Aziz, O. I., Tang, J., Ishtiaq, K. S., Morkeski, K., Mora, J., Quinn, R. K., Martin, R. M., Egan, K., Brannon, E. Q., Carey, J. and Kroeger, K. D. (2016).

- Carbon dioxide fluxes reflect plant zonation and belowground biomass in a coastal marsh, *Ecosphere*, 7(11), p. e01560. doi: 10.1002/ecs2.1560.
- Murphy, J. and Riley, J. P. (1962). A modified single solution method for the determination of phosphate in natural waters, *Analytica Chimica Acta*, 27(Supplement C), pp. 31–36. doi: 10.1016/S0003-2670(00)88444-5.
- Nelson, N. B. and Siegel, D. A. (2013). The Global Distribution and Dynamics of Chromophoric Dissolved Organic Matter, *Annual Review of Marine Science*, 5(1), pp. 447–476. doi: 10.1146/annurev-marine-120710-100751.
- Odum, H. T. (1956). Primary production in flowing waters, *Limnology and Oceanography*, 1(2), pp. 102–117. doi: 10.4319/lo.1956.1.2.0102.
- PICARRO. (2020). *Picarro website*. Available at: <https://www.picarro.com/company/technology/crds> (Accessed: 1 March 2020).
- Pjevac, P., Schauburger, C., Poghosyan, L., Herbold, C. W., van Kessel, M. A. H. J., Daebeler, A., Steinberger, M., Jetten, M. S. M., Lückner, S., Wagner, M. and Daims, H. (2017). *amoA*-targeted polymerase chain reaction primers for the specific detection and quantification of comammox *Nitrospira* in the Environment, *Frontiers in Microbiology*, 8. doi: 10.3389/fmicb.2017.01508.
- R Core Team. (2019). *R: A Language and Environment for Statistical Computing*. Available at: <https://www.R-project.org/>.
- Rotthauwe, J. H., Witzel, K. P. and Liesack, W. (1997). The ammonia monooxygenase structural gene *amoA* as a functional marker: molecular fine-scale analysis of natural ammonia-oxidizing populations., *Applied and Environmental Microbiology*, 63(12), pp. 4704–4712.
- Schlesinger, W. H. and Bernhardt, E. S. (2013). *Biogeochemistry: An Analysis of Global Change*.
- Seweryn, P., Van, L. B., Kjeldgaard, M., Russo, C. J., Passmore, L. A., Hove-Jensen, B., Jochimsen, B. and Brodersen, D. E. (2015). Structural insights into the bacterial carbon–phosphorus lyase machinery, *Nature*, 525(7567), pp. 68–72. doi: 10.1038/nature14683.
- Sierra, A., Jiménez-López, D., Ortega, T., Ponce, R., Bellanco, M. J., Sánchez-Leal, R., Gómez-Parra, A. and Forja, J. (2017a). Spatial and seasonal variability of CH₄ in the eastern Gulf of Cadiz (SW Iberian Peninsula), *Science of The Total Environment*, 590–591, pp. 695–707. doi: 10.1016/j.scitotenv.2017.03.030.
- Sierra, A., Jiménez-López, D., Ortega, T., Ponce, R., Bellanco, M. J., Sánchez-Leal, R., Gómez-Parra, A. and Forja, J. (2017b). Distribution of N₂O in the eastern shelf of the Gulf of Cadiz (SW Iberian Peninsula), *Science of The Total Environment*, 593–594, pp. 796–808. doi: 10.1016/j.scitotenv.2017.03.189.
- Staehr, P. A., Bade, D., Bogert, M. C. V. de, Koch, G. R., Williamson, C., Hanson, P., Cole, J. J. and Kratz, T. (2010). Lake metabolism and the diel oxygen technique: State of the science, *Limnology and Oceanography: Methods*, 8(11), pp. 628–644. doi: 10.4319/lom.2010.8.0628.
- Stieglmeier, M., Mooshammer, M., Kitzler, B., Wanek, W., Zechmeister-Boltenstern, S.,

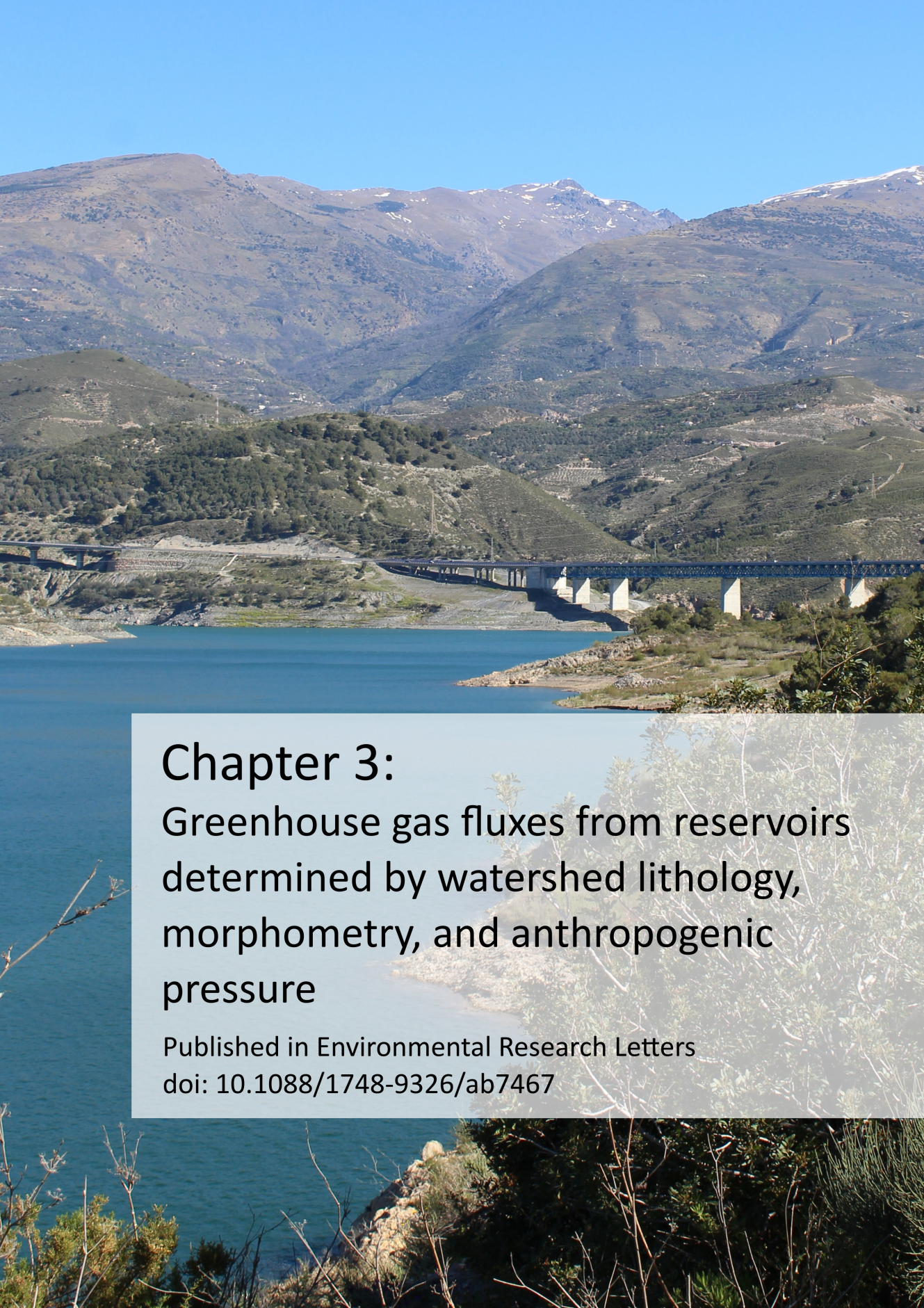
- Richter, A. and Schleper, C. (2014). Aerobic nitrous oxide production through N-nitrosating hybrid formation in ammonia-oxidizing archaea, *The ISME Journal*, 8(5), pp. 1135–1146. doi: 10.1038/ismej.2013.220.
- Stuart, B. H. (2005). Industrial and Environmental Applications, in *Infrared Spectroscopy: Fundamentals and Applications*, pp. 167–186. doi: 10.1002/0470011149.ch8.
- Takeuchi, J. (2006). Habitat segregation of a functional gene encoding nitrate ammonification in estuarine sediments, *Geomicrobiology Journal*, 23(2), pp. 75–87. doi: 10.1080/01490450500533866.
- Therneau, T. and Atkinson, B. (2019). *rpart: Recursive Partitioning and Regression Trees*. Available at: <https://CRAN.R-project.org/package=rpart>.
- Timms, B. (2009). Geomorphology of Lake Basins, in Likens, G. E. (ed.) *Lake Ecosystem Ecology: A Global Perspective*, p. 438.
- Villalobos Megía, M. and Pérez Muñoz, A. B. (2006). *Geodiversidad y patrimonio geológico de Andalucía: itinerario geológico por Andalucía, guía didáctica de campo*. Edited by Consejería de Medio Ambiente, Junta de Andalucía.
- Weiss, R. F. and Price, B. A. (1980). Nitrous oxide solubility in water and seawater, *Marine Chemistry*, 8(4), pp. 347–359. doi: 10.1016/0304-4203(80)90024-9.
- West, W. E., Coloso, J. J. and Jones, S. E. (2012). Effects of algal and terrestrial carbon on methane production rates and methanogen community structure in a temperate lake sediment, *Freshwater Biology*, 57(5), pp. 949–955. doi: 10.1111/j.1365-2427.2012.02755.x.
- White, A. K. and Metcalf, W. W. (2007). Microbial metabolism of reduced phosphorus compounds, *Annual Review of Microbiology*, 61(1), pp. 379–400. doi: 10.1146/annurev.micro.61.080706.093357.
- Wickham, H. (2016). *ggplot2: Elegant Graphics for Data Analysis*. Available at: <https://ggplot2.tidyverse.org>.
- Wickham, H. and Bryan, J. (2019). *readxl: Read Excel Files*. Available at: <https://CRAN.R-project.org/package=readxl>.
- Wiesenburg, D. A. and Guinasso, N. L. (1979). Equilibrium solubilities of methane, carbon monoxide, and hydrogen in water and sea water, *Journal of Chemical & Engineering Data*, 24(4), pp. 356–360. doi: 10.1021/je60083a006.
- Wood, S. N. (2006). *Generalized additive models: an introduction with R*.
- Wood, S. N. (2011). Fast stable restricted maximum likelihood and marginal likelihood estimation of semiparametric generalized linear models, *Journal of the Royal Statistical Society: Series B (Statistical Methodology)*, 73(1), pp. 3–36. doi: 10.1111/j.1467-9868.2010.00749.x.
- Yamamoto, S., Alcauskas, J. B. and Crozier, T. E. (1976). Solubility of methane in distilled water and seawater, *Journal of Chemical & Engineering Data*, 21(1), pp. 78–80. doi: 10.1021/je60068a029.
- Yao, M., Henny, C. and Maresca, J. A. (2016). Freshwater bacteria release methane as a byproduct of phosphorus acquisition, *Applied and Environmental Microbiology*,

82(23), pp. 6994–7003. doi: 10.1128/AEM.02399-16.

Zar, J. H. (1998). Biostatistical analysis, in *Prentice-hall*. 4th edn, p. 663.

Zhao, Y., Sherman, B., Ford, P., Demarty, M., DelSontro, T., Harby, A., Tremblay, A., Øverjordet, I. B., Zhao, X., Hansen, B. H. and Wu, B. (2015). A comparison of methods for the measurement of CO₂ and CH₄ emissions from surface water reservoirs: Results from an international workshop held at Three Gorges Dam, June 2012, *Limnology and Oceanography: Methods*, 13(1), pp. 15–29. doi: 10.1002/lom3.10003.

Chapter 2 | Materials and Methods



Chapter 3: Greenhouse gas fluxes from reservoirs determined by watershed lithology, morphometry, and anthropogenic pressure

Published in Environmental Research Letters
doi: [10.1088/1748-9326/ab7467](https://doi.org/10.1088/1748-9326/ab7467)

Chapter 3: Greenhouse gas fluxes from reservoirs determined by watershed lithology, morphometry, and anthropogenic pressure

Elizabeth León-Palmero¹, Rafael Morales-Baquero¹ and Isabel Reche^{1,2}

¹Instituto del Agua and Departamento de Ecología, Universidad de Granada, E-18071 Granada, Spain

²Research Unit Modeling Nature (MNat), Universidad de Granada, E-18071 Granada, Spain

The Supplementary Material is available in Appendix 3

Abstract

Human population growth has increased the demand for water and clean energy, leading to the massive construction of reservoirs. Reservoirs can emit greenhouse gases (GHG) affecting the atmospheric radiative budget. The radiative forcing due to CO₂, CH₄, and N₂O emissions and the relative contribution of each GHG in terms of CO₂ equivalents to the total forcing is practically unknown. We determined simultaneously the CO₂, CH₄, and N₂O fluxes in reservoirs from diverse watersheds and under variable human pressure to cover the vast idiosyncrasy of temperate Mediterranean reservoirs. We obtained that GHG fluxes ranged more than three orders of magnitude. The reservoirs were sources of CO₂ and N₂O when the watershed lithology was mostly calcareous, and the crops and the urban areas dominated the landscape. By contrast, reservoirs were sinks of CO₂ and N₂O when the watershed lithology was predominantly siliceous, and the landscape had more than 40 % of forestal coverage. All reservoirs were sources of CH₄, and emissions were determined mostly by reservoir mean depth and water temperature. The radiative forcing was substantially higher during the stratification than during the mixing. During the stratification the radiative forcings ranged from 125 mg CO₂

equivalents $\text{m}^{-2} \text{d}^{-1}$ to 31,884 mg CO₂ equivalents $\text{m}^{-2} \text{d}^{-1}$ and were dominated by the CH₄ emissions; whereas during the mixing the radiative forcings ranged from 29 mg CO₂ equivalents $\text{m}^{-2} \text{d}^{-1}$ to 722 mg CO₂ equivalents $\text{m}^{-2} \text{d}^{-1}$ and were dominated by CO₂ emissions. The N₂O contribution to the radiative forcing was minor except in one reservoir with a landscape dominated by crops and urban areas. Future construction of reservoirs should consider that siliceous bedrocks, forestal landscapes, and deep canyons could minimize their radiative forcings.

3. 1. Introduction

Human population growth has increased the need for water and clean energy, promoting the construction of reservoirs for irrigation, consumption, and hydropower. The number of reservoirs has increased significantly over the past 60 years, reaching over 16.7 million dams globally (Lehner *et al.*, 2011). This trend is still ongoing, especially in countries with emerging economies, where over 3,000 major hydropower dams are either planned or under construction (Zarfl *et al.*, 2015). Now it widely is accepted that inland waters, including reservoirs, despite their small global surface area, contribute much in proportion to the global carbon cycle (Tranvik *et al.*, 2009; Raymond *et al.*, 2013). Reservoirs have a radiative forcing dependent on their greenhouse gas (GHG) emissions (Barros *et al.*, 2011; Deemer *et al.*, 2016). The CO₂ emissions from inland waters (ca. 2.1 Pg C yr⁻¹) are similar in magnitude to the estimate of the global uptake of CO₂ by the global ocean (2.4 Pg C yr⁻¹) (Le Quéré *et al.*, 2018). Lakes and reservoirs are usually CO₂ supersaturated (Cole *et al.*, 1994), releasing 0.32 Pg C yr⁻¹ (Raymond *et al.*, 2013). In carbonate-poor lakes, an excess of respiration over primary production produces supersaturation, whereas, in calcareous watersheds, supersaturation is due to the loadings of inorganic carbon during the weathering (López *et al.*, 2011; McDonald *et al.*, 2013; Marcé *et al.*, 2015; Weyhenmeyer *et al.*, 2015). Inland waters are not only sources of CO₂, but they can be significant sources of CH₄ and N₂O (Tranvik *et al.*, 2009; Bastviken *et al.*, 2011; Soued *et al.*, 2015) with warming potential of 34 and 298 times higher than CO₂ in a 100-year timescale (IPCC, 2013).

CH₄ emissions from reservoirs appear to be responsible for the majority of their radiative forcings (ca. 80 % of the CO₂ equivalents) and are comparable to emissions from paddies or biomass burning (Deemer *et al.*, 2016; Samiotis *et al.*,

2018). Reservoirs, collectively considered, emit $13.3 \text{ Tg C yr}^{-1}$ of CH_4 , although there is an astonishing lack of data, which severely limits our confidence in this global estimation (Deemer *et al.*, 2016). Methanogenesis is a microbial process more sensitive to temperature than other processes as, for instance, methanotrophy, respiration, and photosynthesis (Marotta *et al.*, 2014; Yvon-Durocher *et al.*, 2014; Rasilo *et al.*, 2015; Aben *et al.*, 2017; Sepulveda-Jauregui *et al.*, 2018). Therefore, the current rising temperatures can particularly intensify CH_4 emissions (Marotta *et al.*, 2014; Rasilo *et al.*, 2015; Aben *et al.*, 2017) due to changes both in CH_4 solubility and in the methanogenesis vs. methanotrophy balance. On the other hand, the eutrophic reservoirs emit at least one order of magnitude more CH_4 than the oligotrophic ones. Indeed CH_4 emissions seem to be closely linked to primary productivity (Schmidt and Conrad, 1993; Grossart *et al.*, 2011; Bogard *et al.*, 2014; Tang *et al.*, 2014; Deemer *et al.*, 2016). Phytoplankton-derived organic carbon appears to fuel higher rates of methane production than terrestrial-derived organic carbon (West *et al.*, 2012, 2016). Reservoir eutrophication is increasing worldwide as a result of the intensification of agriculture and the use of fertilizers (Canfield *et al.*, 2010; Heathcote and Downing, 2012). Then, the expected increase in global temperatures along with reservoirs eutrophication might exacerbate CH_4 emissions.

The anthropogenic production of nitrogen fertilizer has doubled the inputs of this element to the Earth's surface, changing the nitrogen cycle. This change likely exceeds all the other human interventions in the cycles of nature (Gruber and Galloway, 2008; Schlesinger, 2009), but in comparison with the carbon cycle has received less attention (Battye *et al.*, 2017). Changes in land-use from forestal to agricultural or urban can boost the production of N_2O due to nitrogen loadings into the aquatic systems (Seitzinger *et al.*, 2000; Mulholland *et al.*, 2008; Beaulieu *et al.*, 2011). N_2O is produced aerobically by nitrification and anaerobically by denitrification depending on oxygen availability (Canfield *et al.*, 2010). In reservoirs, the few available data suggest that they are relevant in agricultural landscapes (Beaulieu *et al.*, 2015). Unfortunately, the importance of the reservoirs in global N_2O emissions is practically unknown. Deemer *et al.* (2016) estimated, using a very scarce database, that the global N_2O emission from reservoirs is $0.03 \text{ Tg N yr}^{-1}$ accounting for 4% of the radiative forcing in a 100-year timescale.

Fluxes of CO₂, CH₄, and N₂O have been reported mostly for tropical and boreal reservoirs, lacking the data of these fluxes in the Mediterranean biome, where the reservoirs are the preponderant aquatic ecosystems (Naselli-Flores, 2003; Barros *et al.*, 2011; Lehner *et al.*, 2011; Morales-Pineda *et al.*, 2014; Deemer *et al.*, 2016). In this region, reservoirs provide drinking and irrigation water (Naselli-Flores, 2003; Morales-Pineda *et al.*, 2014); consequently, they are close to agriculture and urban areas having high human pressure. Therefore, we need more simultaneous measurements of CO₂, CH₄, and N₂O emissions in Mediterranean reservoirs submitted to contrasting anthropogenic pressure to get more accurate estimates of the global reservoir radiative forcing.

Here, we simultaneously measured the fluxes of CO₂, CH₄, and N₂O in a group of Mediterranean reservoirs. We covered the vast idiosyncrasy of temperate reservoirs to obtain their radiative forcings in terms of CO₂ equivalents. We hypothesized that reservoirs located in anthropogenic landscapes would have higher radiative forcings than forestal reservoirs. Besides, we postulated that CH₄ emissions would be the main responsible for the positive radiative forcings.

3. 2. Material and Methods

3. 2. 1. Study reservoirs

We sampled 12 reservoirs between July 2016 and August 2017 in the South of Spain (Figure 3.1a, b). The reservoirs are located in watersheds with diverse lithology (Figure 3.1c, d; Supplementary Figures 3.1 - 3.12), different land-use (Figure 3.1e, f; Supplementary Figures 3.13 – 3.24), morphometries, and ages (Supplementary Table 3.1). We quantified the CO₂, CH₄, and N₂O fluxes using a PICARRO Cavity Ring-Down Spectroscopy (CRDS) gas analyzer connected to a floating chamber during the stratification (summer) and mixing (fall-winter) periods at one representative location. The reservoirs were built between 1932 and 2003, and they also differ in chemical and trophic characteristics with a range of chlorophyll-*a* concentration from 0.6 µg l⁻¹ to 18.6 µg l⁻¹ and a range of dissolved organic carbon concentration from 0.79 mg l⁻¹ to 4.95 mg l⁻¹. More basic details on the study reservoirs in León-Palmero *et al.* (2019) and Supplementary Table 3.1 and Table 3.4. We collected data on reservoir area, capacity, age, watershed lithology, and land use from open databases (more details in Supplementary methods).

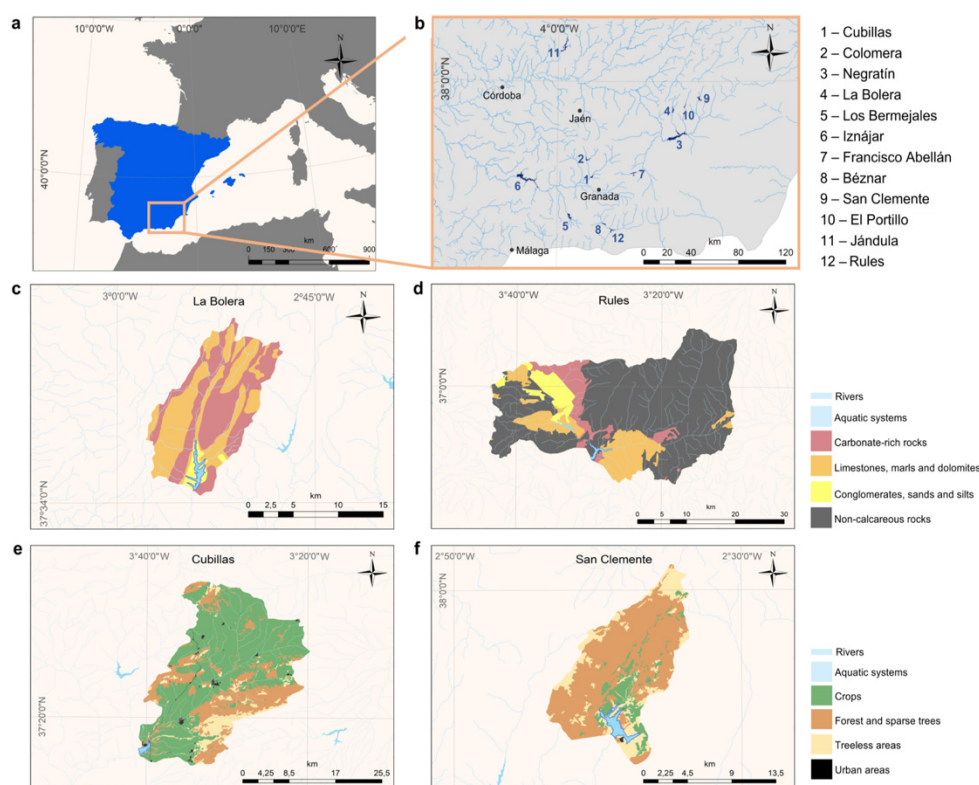


Figure 3.1. Geographical location of the study reservoirs and two examples of contrasting lithologies and land-uses. (a) The location area of the study reservoirs in the South of the Iberian Peninsula delimited by an orange box. (b) Detailed location of the twelve reservoirs with their corresponding numbers (# 1 - 12) and names are listed on the side. (c), (d), Contrasting lithology in the watersheds of La Bolera (mostly carbonate-rich rocks) and Rules (mostly non-calcareous rocks) reservoirs. (e), (f), Contrasting land-use in the watersheds of Cubillas (mostly agricultural) and San Clemente (mostly forestal) reservoirs. Lithology and land-use maps for the twelve reservoirs are provided as Supplementary Figures 3.1 – 3.12 and Supplementary Figures 3.13 – 3.24, respectively. Details about the lithology and land-use composition in the watersheds of the study reservoirs are shown in Supplementary Table 3.1.

3. 2. 2. Quantification of CO₂, CH₄ and N₂O fluxes

We measured CO₂, CH₄, and N₂O fluxes using a high-resolution laser-based Cavity Ring-Down Spectrometer (CRDS PICARRO G2508) coupled to a floating chamber. For each reservoir in each sampling period, we took 3-5 measurements for 40 min. We calculated the daily (from 10 am to 4 pm) average and the standard error from these measurements. We obtained the flux calculation using the equation 3.1 (Zhao *et al.*, 2015):

$$\text{Flux}_{\text{water-air}} = \frac{b \times V \times P_0}{A \times R \times T_0} \quad \text{Eq. 3.1}$$

Where $\text{Flux}_{\text{water-air}}$ ($\mu\text{mol m}^{-2} \text{s}^{-1}$) is the flux from the water surface to the atmosphere; the b (ppm s^{-1}) value is the slope of the linear regression between the time and the concentration of each gas inside the chamber; the V (m^3) is the floating chamber volume; the A (m^2) is the floating chamber area; the P_0 (Pa) is the atmospheric pressure; the R is the gas constant ($8.314 \text{ m}^3 \text{ Pa K}^{-1} \text{ mol}^{-1}$); and T_0 (K) is the ambient temperature. We checked that the slope was significantly different from zero for each measurement using a two-tailed t-Student test. We also calculated the coefficient of determination (R^2) for each measurement, accepting those whose $R^2 > 0.85$ (Moseman-Valtierra *et al.*, 2016). We measured ambient temperature, atmospheric pressure (HANNA HI 9828), and wind speed (MASTECH MS6252A) at the beginning of each flux measurement.

Determination coefficients (R^2) for CO_2 fluxes were always > 0.85 . For CH_4 fluxes, most cases R^2 were > 0.85 , but it decreased until 0.65 when ebullition events were relevant. In these cases, we computed the b value using the end-point concentrations and the time interval between them (equation 3.2) (Zhao *et al.*, 2015):

$$b = \frac{[\text{CH}_4]_f - [\text{CH}_4]_i}{t_f - t_i} \quad \text{Eq. 3.2}$$

Where $[\text{CH}_4]_f$ and $[\text{CH}_4]_i$ are the CH_4 concentration (ppm) in the floating chamber at the end and the beginning of the time considered; t_f and t_i are the time at the end and the beginning of the measurement.

For N_2O flux measurements, most of R^2 values were low (even when the regression was significantly different from zero). For those cases, we first checked the analyzer precision (< 25 ppb). If the changes were larger than the analyzer precision, we assumed these fluxes were different from zero. We also compared the N_2O fluxes with the percentage of saturation of dissolved N_2O in the water column. Details for the measurements of dissolved N_2O are in Supplementary methods. N_2O undersaturated waters and negative slopes mean N_2O influxes (i.e., N_2O sinks). By contrast, N_2O supersaturated waters and positive slopes mean N_2O outfluxes (i.e., N_2O sources).

To obtain the reservoir radiative forcings we summed the corresponding forcing due to CO_2 emissions, the warming potential (GWP) of CH_4 in terms of CO_2 equivalents, and the warming potential of N_2O in terms of CO_2 equivalents. We used

34 to convert CH₄ in CO₂ equivalent and 298 to convert N₂O in CO₂ equivalent in a 100-year time horizon, including the climate-carbon feedbacks (IPCC, 2013).

3. 2. 3. C, N and P analysis in the water column

We sampled the epilimnion of each reservoir for C, N and, P analysis. We measured total nutrient concentrations using unfiltered water, while we filtered through 0.7 µm pore-size Whatman GF/F glass-fiber filters samples for dissolved nutrients. We acidified with phosphoric acid (final pH < 2) the samples for dissolved organic carbon (DOC), total dissolved nitrogen (TDN), and total nitrogen (TN). We measured DOC, dissolved inorganic carbon (DIC), TN, and TDN by high-temperature catalytic oxidation using a Shimadzu total organic carbon (TOC) analyzer (Model TOC-V CSH) coupled to nitrogen analyzer (TNM-1) (Álvarez-Salgado and Miller, 1998). The instrument was calibrated using a four-point standard curve of dried potassium hydrogen phthalate for DOC, dried sodium bicarbonate and sodium carbonate for DIC, and dried potassium nitrate for TN and TDN. We analyzed two replicates and three to five injections per replicate for each sample. Samples for DOC analysis were purged with phosphoric acid for 20 min to eliminate DIC.

We measured the NO₃⁻ concentration using the ultraviolet spectrophotometric method, using a Perkin Elmer UV-Lambda 40 spectrophotometer at wavelengths of 220 nm and correcting for DOC absorbance at 275 nm (APHA, 1992). We measured NH₄⁺ and NO₂⁻ concentrations by Inductively Coupled Plasma Optical Emission Spectrometry (ICP-OES). Total phosphorus (TP) concentration was measured by triplicate using the molybdenum blue method (Murphy and Riley, 1962) after digestion with a mixture of potassium persulphate and boric acid at 120 °C for 30 min (APHA, 1992).

We also measured dissolved CH₄ and N₂O by headspace equilibration in a 50 ml air-tight glass syringe by duplicate in the water column (Sierra *et al.*, 2017a, 2017b). We analyzed simultaneously the concentration of dissolved CH₄ and N₂O using gas chromatography (more details in Supplementary methods).

3. 2. 4. Biological analyses and reservoir metabolism

We determined chlorophyll-*a* concentration by collecting the particulate material of 500 to 2000 ml of water by filtering through 0.7 µm pore-size Whatman GF/F glass-fiber filters, then extracting the filters with 95% methanol in the dark at 4

°C for 24 h (APHA, 1992). We measured pigment absorption using a Perkin Elmer UV-Lambda 40 spectrophotometer at wavelengths of 665 nm and 750 nm for scattering correction.

We recorded dissolved oxygen concentration and temperature using a miniDOT (PME) submersible water logger during the stratification period. We got measurements every 10 minutes for 24-48 hours. We established the start and ended time for photosynthesis as 30 minutes before sunrise and 30 minutes after dawn (Schlesinger and Bernhardt, 2013). We calculated the respiration rate during the night (the period between 60 minutes after dawn and 60 minutes before sunrise) (Staeher *et al.*, 2010), and we assumed that the respiration rate overnight was similar to the respiration rate over the day. The equations used to calculate lake metabolism were taken from Staeher *et al.* (2010).

3. 2. 5. Statistical tests

We performed all the statistical analysis in R (R Core Team, 2014) using the packages *car* (Fox and Weisberg, 2011), *nortest* (Gross and Ligges, 2015), and *mgcv* (Wood, 2011). More details on T-test and generalized additive models (GAMs) (Wood, 2006) in Supplementary Methods.

3. 3. Results and Discussion

3. 3. 1. CO₂, CH₄, and N₂O fluxes

We found that some reservoirs were sinks (fluxes < 0) and other sources (fluxes > 0) for CO₂ and N₂O fluxes, but all reservoirs were CH₄ sources (Figure 3.2, Supplementary Table 3.2). The daily average of CO₂ fluxes ranged from -131.97 to 393.11 mg C m⁻² day⁻¹ during the stratification period (Figure 3.2a, orange dots) and from -52.51 to 149.62 mg C m⁻² day⁻¹ during the mixing period (Figure 3.2a, blue dots). We measured the lower value in the Jándula reservoir (# 11) consistently in both periods. We did not find significant differences between the stratification and mixing periods (Figure 3.2b; Supplementary Table 3.3). The median of these fluxes in both periods was 114.00 mg C m⁻² day⁻¹, similar to previous data for northern temperate reservoirs (Barros *et al.*, 2011) and smaller than the fluxes measured in other Mediterranean reservoirs (Morales-Pineda *et al.*, 2014; Samiotis *et al.*, 2018), and the global average estimated by Deemer *et al.* (2016).

The daily average of CH₄ fluxes varied more than three orders of magnitude from 0.51 to 678.84 mg C m⁻² day⁻¹ during the stratification period (Figure 3.2c, orange dots) and from 0.10 to 4.41 mg C m⁻² day⁻¹ during the mixing period (Figure 3.2c, blue dots). The maximum values were reached in Cubillas (# 1), a shallow reservoir with evident ebullition fluxes. The median value during the stratification period was 5.27 mg C m⁻² day⁻¹, whereas during the mixing period was 0.63 mg C m⁻² day⁻¹. Emissions were significantly higher during the summer stratification than during the winter mixing (Figure 3.2d; Supplementary Table 3.3) as it has been found in previous works (Beaulieu *et al.*, 2014; Musenze *et al.*, 2014) and emphasized the need to perform seasonal studies to obtain accurate annual rates of CH₄ emissions. This wide range in CH₄ emissions covers from typical values found in tropical reservoirs to values found in northern temperate reservoirs (Barros *et al.*, 2011), although lower than in other Mediterranean reservoirs (Samiotis *et al.*, 2018).

The daily average of N₂O fluxes ranged from -154.03 to 3,600.88 µgN m⁻² day⁻¹ during the stratification period (Figure 3.2e, orange dots) and from -238.08 to 313.44 µgN m⁻² day⁻¹ during the mixing period (Figure 3.2e, blue dots). In both periods, we obtained the maximum values in the Iznájar reservoir (# 6). We did not find significant differences between stratification and mixing periods (Figure 3.2f; Supplementary Table 3.3). The median value was 0.00 µgN m⁻² day⁻¹ acting globally as neutral systems. In the particular case of the Iznájar reservoir (# 6), however, it acted as a relevant source of N₂O with values similar to those found in tropical reservoirs (Guérin *et al.*, 2006). N₂O flux variability in these Mediterranean reservoirs was more comprehensive than the variability found in boreal lakes and reservoirs (Soued *et al.*, 2015).

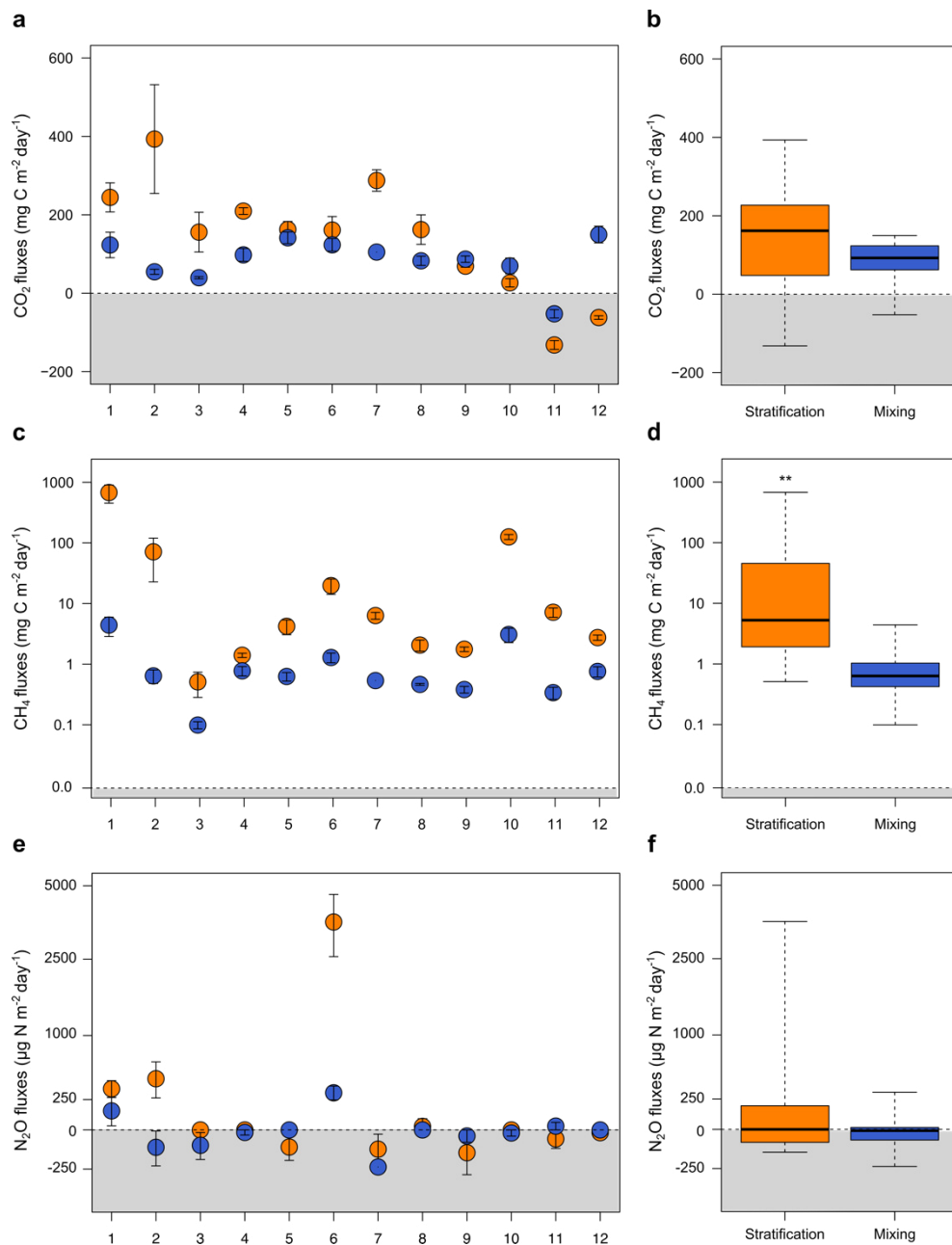


Figure 3.2. Fluxes of CO₂, CH₄ and N₂O fluxes in the study reservoirs during the stratification and mixing periods. (a), (c), (e), The CO₂, CH₄, and N₂O fluxes (mean ± SE) measured during the stratification (orange dots) and mixing (blue dots) periods in the twelve study reservoirs (listed # 1 - 12 in x-axis). (b), (d), (f), Boxplots (median, 25 – 75 % percentile, maximum and minimum values) of the CO₂, CH₄, and N₂O fluxes during the stratification (orange boxes) and mixing (blue boxes) periods. Note the log-scale in CH₄ and N₂O fluxes. Grey zone stands for greenhouse gas sinks. ** Stands for statistically significant differences (p-value < 0.01) between both periods.

3. 3. 2. CO₂ flux drivers

To determine the main drivers (predictors) of GHG fluxes in the study reservoirs, we used generalized additive models (GAMs, see Supplementary Methods, Supplementary Tables 3.4 and 3.5). The inputs of dissolved inorganic and organic carbon and net ecosystem metabolism (i.e., the budget between photosynthesis and respiration) are considered the main drivers of CO₂ fluxes in lakes and reservoir (Tranvik *et al.*, 2009; McDonald *et al.*, 2013; Marcé *et al.*, 2015; Weyhenmeyer *et al.*, 2015). In fact, the non-calcareous area in the watershed and the reservoir respiration were the main drivers of CO₂ fluxes during the stratification period with a fit deviance of 93.4 % ($\text{Log}_{10}(\text{CO}_2 + 150) = -6.6 \cdot 10^{-4} \text{ non-calcareous area} + 1.70 \log_{10}(\text{Respiration rate})^{0.35}$) and an explained variance of 91 % (Figure 3.3a; Supplementary Table 3.5). The non-calcareous area in the watershed was a linear function inversely related to CO₂ fluxes (Figure 3.3b), and explained most of the deviance (i.e., 90.7 %), whereas respiration only explained the 9.4 %. Unlike this linear function, reservoir respiration showed a power function with the CO₂ flux (Figure 3.3c). The smaller the calcareous watershed, the lower the export of dissolved inorganic carbon (DIC) is. Indeed, we found a significant and negative relationship between non-calcareous area and the DIC concentration in the reservoirs irrespectively of the sampling period (linear regression results $n = 24$, $R^2 = 0.50$, $p\text{-value} < 0.001$) (Figure 3.3d).

This result agrees with previous studies showing that a significant fraction of CO₂ emissions in boreal lakes is related to inorganic carbon loading from watershed (Weyhenmeyer *et al.*, 2015). In other Mediterranean reservoirs, carbonate weathering was also related to CO₂ supersaturation and, consequently, to CO₂ evasion (López *et al.*, 2011; Marcé *et al.*, 2015). We obtained a significant and positive function between reservoir respiration and the concentration of chlorophyll-*a* during the stratification period (linear regression results $n = 12$, $R^2 = 0.43$, $p\text{-value} < 0.05$) (Figure 3.3e), but not with the concentration of dissolved organic carbon (linear regression results $n = 12$, $p\text{-value} = 0.64$). Overall, we show, for the first time, a remarkable and direct link between watershed lithology and the CO₂ fluxes from reservoirs.

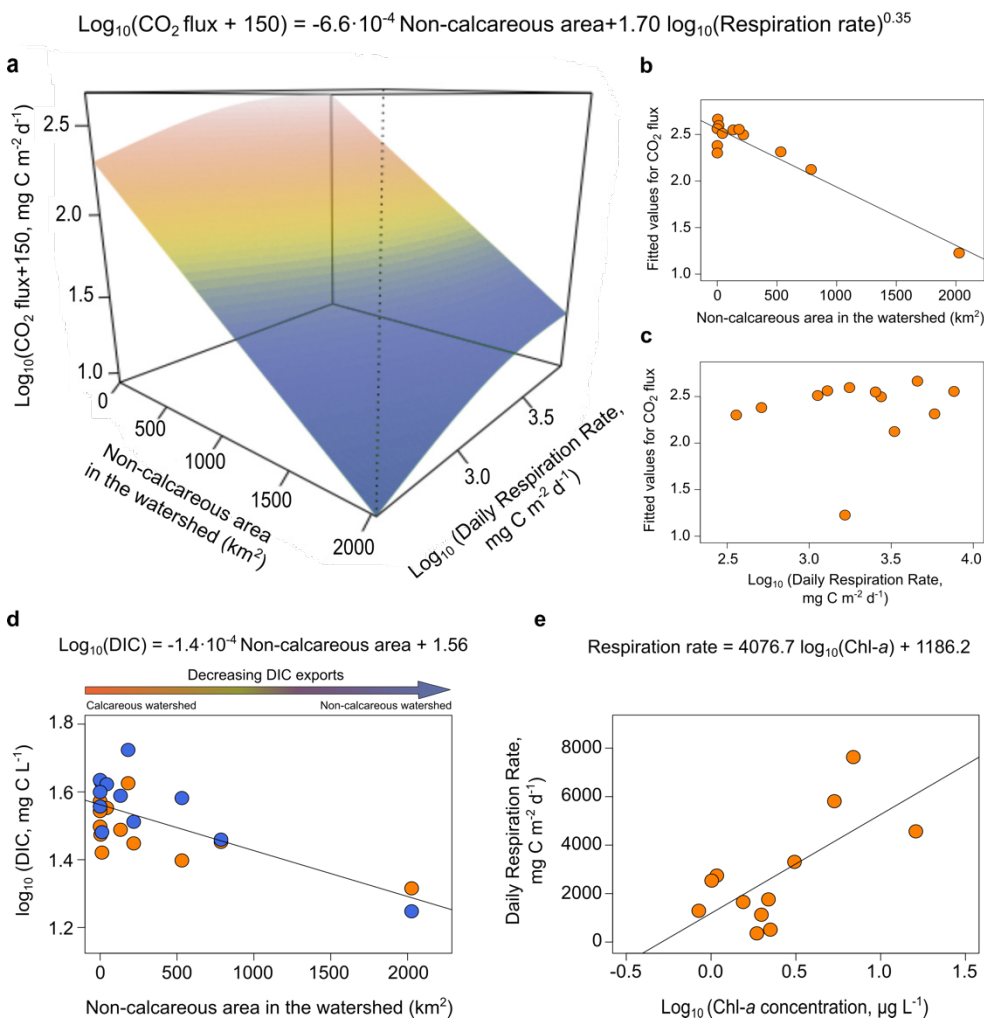


Figure 3.3. 3D-model for the main drivers of the CO_2 fluxes during the stratification period. The non-calcareous area in the watershed (x-axis) and the daily respiration rates (y-axis) determined CO_2 fluxes (z-axis). (b), Partial response plot showing the linear relationship between the fitted GAM values for CO_2 flux and the non-calcareous surface in the watershed. (c), Partial response plot showing the power relationship between the fitted GAM values for CO_2 flux and the daily respiration rates. More statistical details provided in Supplementary Table 3.3. (d), Linear relationship between the non-calcareous area in the watershed and the dissolved inorganic carbon concentration in the reservoirs ($n = 24$, $\text{adj } R^2 = 0.50$, $p\text{-value} < 0.001$). (e), Linear relationship between the chlorophyll-a concentration in the surface waters and the daily respiration rate ($n = 12$, $\text{adj } R^2 = 0.47$, $p\text{-value} < 0.05$).

3. 3. 3. CH₄ flux drivers

CH₄ emissions from a reservoir depend on its net production (i.e., the budget between methanogenesis and methanotrophy) and its storage capacity into the water column. Dissolved CH₄ storage is related to water mean depth (i.e., the higher the hydrostatic pressure, the higher storage capacity is) and temperature (i.e., the lower temperature, the higher solubility is) (Keller and Stallard, 1994; West *et al.*, 2016). Shallow systems are prone to have warmer waters, higher sediment exposure enhancing significantly CH₄ ebullition rates, and, consequently, less capacity to store CH₄ (Keller and Stallard, 1994; Marotta *et al.*, 2014; Aben *et al.*, 2017). In the study reservoirs, we obtained that water temperature and reservoir mean depth were the main drivers of the CH₄ emissions with a fit deviance of 65.0 % and an explained variance of 59 % ($\text{Log}_{10}(\text{CH}_4 \text{ flux} + 1) = 6.6 \cdot 10^{-2} \text{ Temperature} - 0.82 + 2.5 \cdot 10^{-4} e^{(8.44/\log_{10}(\text{mean depth}))}$) (Figure 3.4 a; Supplementary Table 3.3).

CH₄ emission rate was a linear and positive function of water temperature (Figure 3.4b) and accounted for 38.1 % of the fit deviance. CH₄ emission rate resulted in a negative exponential function of the reservoir mean depth (Figure 3.4c) with fit deviance of 27.6 %. At mean depths shallower than 16 meters, the CH₄ emissions increased exponentially (i.e., 1.2 in Figure 3.4c). CH₄ emissions depended on concentration of CH₄ in the surface waters following a power function (Figure 3.4d) ($n = 24$, $R^2 = 0.87$, $p\text{-value} < 0.001$). Previous studies have shown that CH₄ concentration in the water column is related to chlorophyll-*a* concentration (Schmidt and Conrad, 1993; Grossart *et al.*, 2011; Bogard *et al.*, 2014; Tang *et al.*, 2014). We also found a positive and power relationship between the concentration of chlorophyll-*a* and the concentration of CH₄ in the surface waters ($n = 24$, $R^2 = 0.19$, $p\text{-value} < 0.05$) (Figure 3.4e), but not directly with the emissions. Recent studies point out the eutrophication as the primary driver of CH₄ emissions (Deemer *et al.*, 2016; Beaulieu *et al.*, 2019).

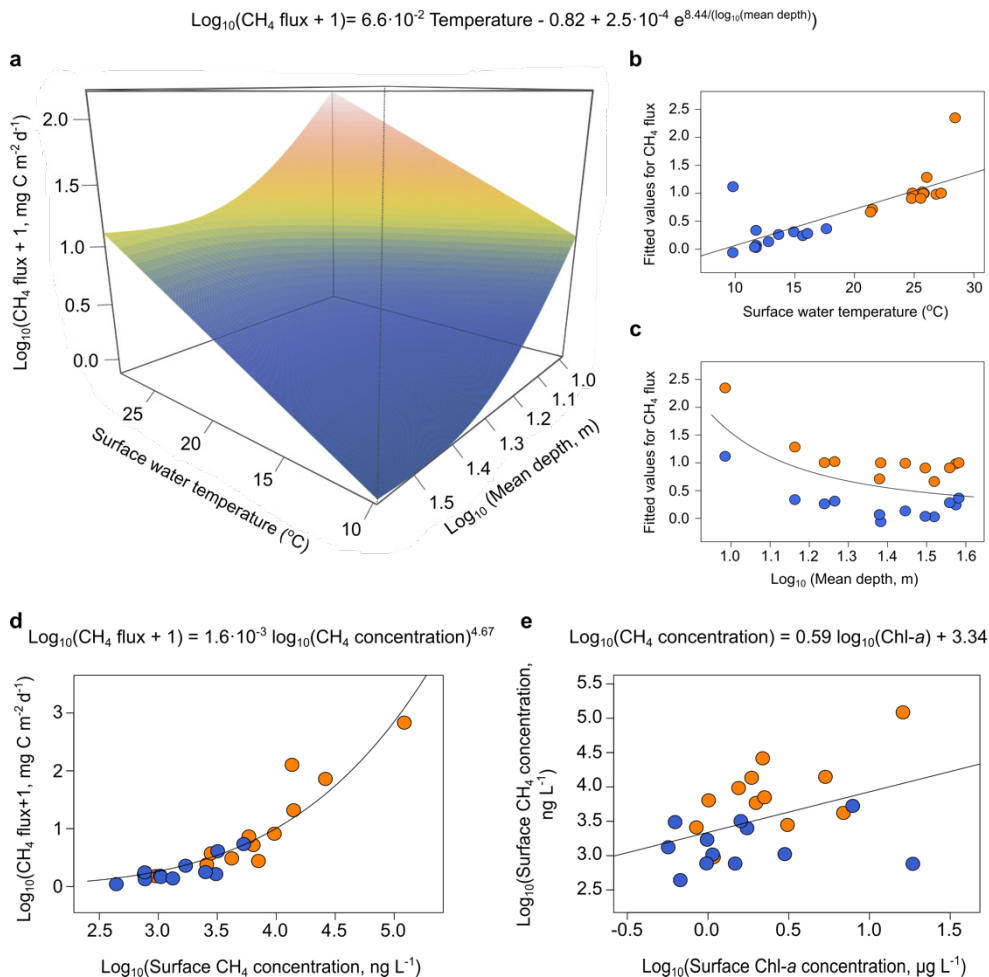


Figure 3.4. 3D-model for the main drivers of the CH₄ fluxes during stratification and mixing periods. The surface water temperature (x-axis) and the mean depth in the reservoir (y-axis) determined CH₄ fluxes (z-axis). (b), Partial response plot showing the linear relationship between the fitted GAM values for CH₄ flux and the surface water temperature. (c), Partial response plot showing the exponential relationship between the fitted GAM values for CH₄ flux and the mean depth. More statistical details provided in Supplementary Table 3.3 (d), Exponential relationship between surface CH₄ concentration and the CH₄ flux ($n = 24$, $\text{adj } R^2 = 0.87$, $p\text{-value} < 0.001$). (e), Linear relationship between the chlorophyll-*a* concentration in the surface waters and the surface CH₄ concentration ($n = 24$, $\text{adj } R^2 = 0.15$, $p\text{-value} < 0.05$). Orange dots stand for the fluxes during the stratification period and blue dots stand for fluxes during the mixing period.

3. 3. 4. N₂O flux drivers

Nitrogen loading derived from human activities affects N₂O emissions from inland waters (Seitzinger *et al.*, 2000; Mulholland *et al.*, 2008; Baulch *et al.*, 2011; Beaulieu *et al.*, 2011). It is widely acknowledged that the N₂O production increases in streams and reservoirs located in agricultural and urban landscapes as a

consequence of nitrate loading (Mulholland *et al.*, 2008; Baulch *et al.*, 2011; Beaulieu *et al.*, 2011, 2015). In the study reservoirs, consistently, the GAMs result showed that the total nitrogen (TN) concentration was the main driver of N₂O fluxes along with the wind speed ($\text{Log}_{10}(\text{N}_2\text{O flux} + 240) = 0.64 e^{0.21 \text{ TN}} + 1.30 \text{ Wind speed}^{0.21}$) with a fit deviance of 72.9 % and an explained variance of 69.4 % (Figure 3.5a; Supplementary Table 3.5). N₂O fluxes were an exponential function of TN concentration and explained most of the deviance 42.7 % (Figure 3.5b). Wind speed showed a positive power function with the fluxes and only explained 18.3 % (Figure 3.5c). We determined the anthropogenic pressure in the reservoir watershed as the ratio of the area with crops plus the urban area divided by the forest area (i.e., the anthropogenic land-use ratio). We found a significant and positive relationship between this land-use ratio and the concentration of total nitrogen (TN) in the reservoir waters ($n = 24$, $R^2 = 0.60$, $p\text{-value} < 0.001$) (Figure 3.5d; Supplementary Table 3.6). Both crops and urban areas increased the nitrogen concentration in their different compounds (total nitrogen, total dissolved nitrogen, NO₃⁻ and NO₂⁻) (Supplementary Table 3.6). The urban area, in square kilometer or in its percentage relative in the watershed, showed a higher slope than the slope in the crop areas (Figure 3.5e). Therefore, the impact of urban development on nitrogen inputs is even higher than the influence of crop areas.

N₂O fluxes were a non-linear function of the anthropogenic land-use ratio (Figure 3.5f). For anthropogenic land-use ratios higher than 1 (i.e., crops and urban areas predominance over the forest area), the N₂O fluxes increased exponentially (Figure 3.5f). In contrast, we observed that for watersheds with forestal coverage more extensive than ~40% of watershed, the N₂O emissions decreased drastically, even becoming an N₂O sink (Figure 3.5g). Other authors also found that boreal forest reservoirs acted as N₂O sinks (Hendzel *et al.*, 2005). Therefore, the relevance of the nitrogen inputs from watershed on N₂O fluxes is mostly dependent on the anthropogenic land-use. Our results suggest an exponential influence of the agricultural and, mainly, urban areas in the watershed on the N₂O emissions. However, most of the previous studies have been mainly focused on the agricultural effects (Baulch *et al.*, 2011; Musenze *et al.*, 2014; Beaulieu *et al.*, 2015), relegating the urban influence on the background.

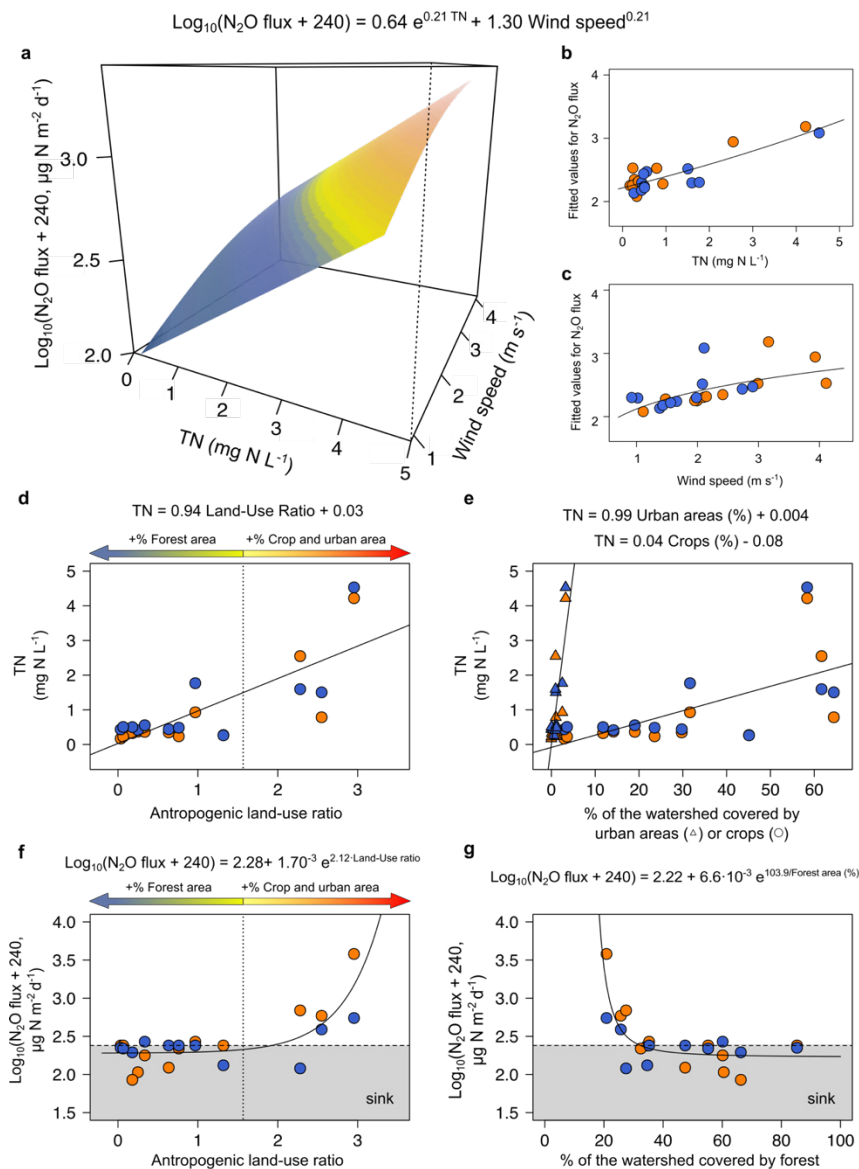


Figure 3.5. 3D-model for the main drivers of the N₂O flux during stratification and mixing periods. The total nitrogen concentration (TN) in the epilimnion (x-axis) and the wind speed (y-axis) determined N₂O fluxes (z-axis). (b), Partial response plot showing the exponential relationship between the fitted GAM values for N₂O flux and the TN concentration. (c), Partial response plot showing the exponential relationship between the fitted GAM values for N₂O flux and the wind speed. More statistical details provided in Supplementary Table 3.3 (d), Lineal relationship between the land-use ratio and the TN concentration (n = 24, adj R² = 0.60, p-value < 0.001). (e), Linear relationships between the coverage of the watershed in percentage of urban area (triangles) and crops (circles). (f), Exponential relationship between the land-use ratio and the N₂O fluxes (n = 23, adj R² = 0.60). (g), Exponential decay relationship between the coverage of the watershed in percentage of forest and the N₂O fluxes (n = 23, adj R² = 0.60). Orange dots stand for the fluxes during the stratification period and blue dots stand for fluxes during the mixing period.

3. 3. 5. Reservoir radiative forcings in CO₂ equivalents

We obtained a variability range in the GHG fluxes larger than the latitudinal variability reported in previous works (Barros *et al.*, 2011). The radiative forcings due to the GHG emissions from the reservoirs differed substantially between the stratification (summer) and the mixing (fall-winter) (Figure 3.6). Radiative forcings were substantially higher during the stratification than during the mixing. This difference could be related to the significantly higher emissions of CH₄ during the stratification than mixing (Figure 3.2). Methanogenesis is a microbial process particularly sensitive to temperature (Marotta *et al.*, 2014; Yvon-Durocher *et al.*, 2014; Rasilo *et al.*, 2015; Aben *et al.*, 2017; Sepulveda-Jauregui *et al.*, 2018) that increase during summer. In addition, water mean depth decrease during this season and these factors also affect to the CH₄ emissions (Figure 3.4). Radiative forcings ranged from 124.53 mg CO₂ equivalents m⁻² d⁻¹ in Rules reservoir (# 12) to 31,884.03 mg CO₂ equivalents m⁻² d⁻¹ in Cubillas reservoir (# 1) (Supplementary Table 3.2). These last values were even higher than those found for tropical plantations (Laine *et al.*, 2016). In stratification, CH₄ emissions contributed significantly to the total radiative forcing (in terms of CO₂ equivalent), ranging from 3.90 to 98.32 % (Figure 3.6a purple sector). In contrast, the CO₂ emissions contributed to the total radiative forcing mostly during the mixing (fall and winter), accounting for up to 97 % (Figure 3.6b blue sector). During the mixing, the radiative forcing ranged from 28.68 mg CO₂ equivalents m⁻² d⁻¹ in Jándula reservoir (# 11) to 721.65 mg CO₂ equivalents m⁻² d⁻¹ in Cubillas reservoir (# 1) (Supplementary Table 3.2). The contribution of N₂O emissions to the radiative forcing in the study reservoirs was secondary (Supplementary Table 3.2) with the exception of the Iznájar reservoir (# 6) in both periods (Figure 3.6) and the Cubillas and Jándula reservoirs (# 1 and 11) during the mixing (Figure 3.6b). In the Iznájar reservoir, the N₂O emissions accounted for up to 53.10 % of the radiative forcing during the stratification, whereas during the mixing period was 22.32 % (Supplementary Table 3.2). CO₂ and N₂O emissions were driven by external factors as lithology and land-use without significant differences between mixing and stratification. In contrast, CH₄ emissions were driven by internal factors as water temperature and mean depth with higher emissions during stratification, which affected the total radiative forcings of the reservoirs.

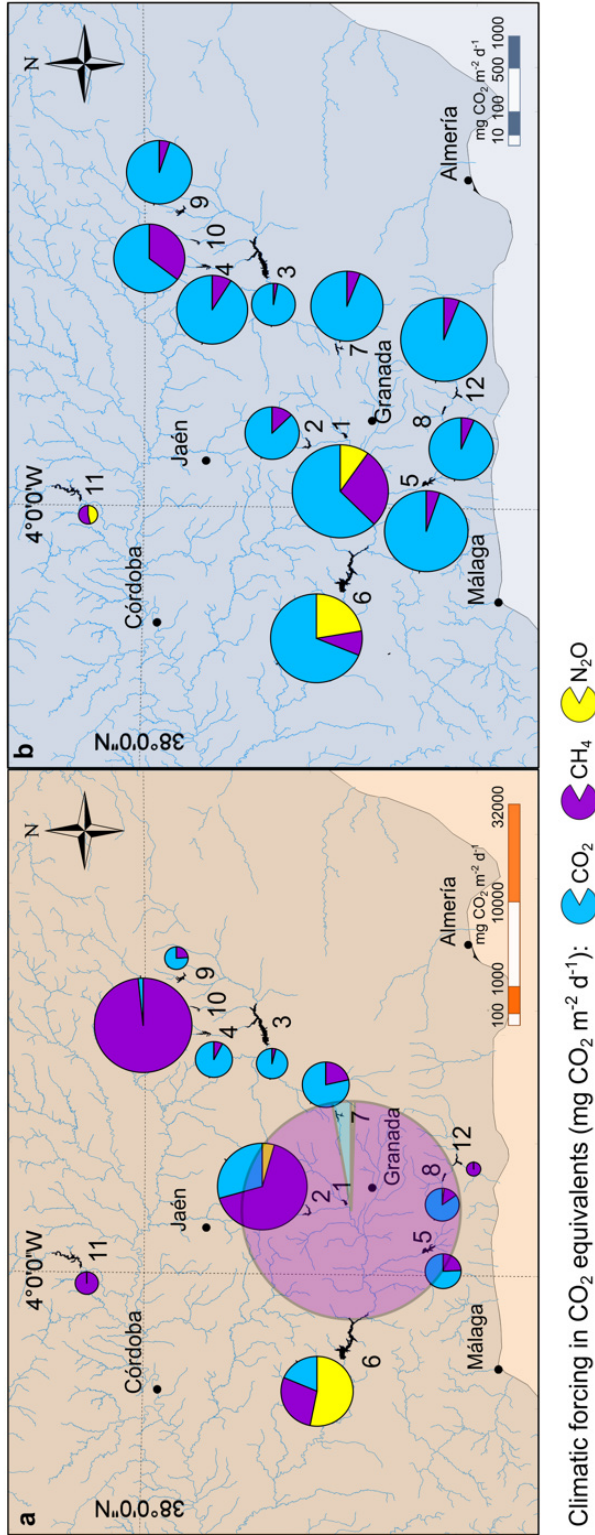


Figure 3.6. Climatic forcing due to CO₂, CH₄ and N₂O emissions in CO₂ equivalents in the study reservoirs in stratification (a) and mixing (b) periods. The diameter of the pie charts stands for the total climatic forcing of each reservoir. Note that scales are different for the stratification and mixing periods. Cubillas reservoir (# 1) during stratification is drawn with low opacity for a better visualization of the other pie charts.

Future climatic scenarios for the Mediterranean biome suggest substantial warming, a decrease in total precipitation, and extreme heat-waves and heavy precipitations (Giorgi and Lionello, 2008) that likely will enhance the CH₄ emissions due to a reduction in reservoir depth (i.e., lower precipitation and higher evaporation) and an increase in the water temperatures. Climatic change may also affect nutrient loading by runoff to the reservoirs. Hydrological models for Mediterranean watersheds suggest that nutrient concentrations in reservoirs may increase despite a runoff reduction (Molina-Navarro *et al.*, 2014). The potential increase in the N and P concentrations will boost water eutrophication and the resulting emissions of N₂O (Mulholland *et al.*, 2008; Baulch *et al.*, 2011; Beaulieu *et al.*, 2015) and CH₄ (Deemer *et al.*, 2016; Beaulieu *et al.*, 2019). Temperature increases and eutrophication may also have synergic effects on CH₄ emissions (Davidson *et al.*, 2018; Sepulveda-Jauregui *et al.*, 2018).

Policies to reduce the fertilizers used in agricultural areas and, in particular, to promote the tertiary wastewater treatment in urban areas may decrease N and P loading to prevent water resources degradation and reduce GHG emissions and their subsequent radiative forcings from the already constructed reservoirs. For the construction of the projected reservoirs, the selection of optimal locations should consider that siliceous bedrock, in forestal locations, and deep canyons can minimize or even offset the GHG emissions and, consequently, reduce their radiative forcings.

Acknowledgements

This research was funded by the project HERA (CGL2014-52362-R) to IR and RM-B of the Spanish Ministry of Economy and Competitiveness and the Modeling Nature Scientific Unit (UCE.PP2017.03) to IR co-financed with FEDER funds. E.L-P was supported by a PhD fellowship FPU (Formación del Profesorado Universitario: 014/02917) from the Ministry of Education, Culture y Sports. We specially thank to Jesús Forja, Teodora Ortega and Ana Sierra for helping with gas chromatography analysis and Eulogio Corral Arredondo for sampling support.

3. 4. References

- Aben, R. C. H., Barros, N., Donk, E. van, Frenken, T., Hilt, S., Kazanjian, G., Lamers, L. P. M., Peeters, E. T. H. M., Roelofs, J. G. M., Domis, L. N. S., Stephan, S., Velthuis, M., Waal, D. B. V. de, Wik, M., Thornton, B. F., Wilkinson, J., DelSontro, T. and Kosten, S. (2017). Cross continental increase in methane ebullition under climate change, *Nature*

Communications, 8(1), p. 1682. doi: 10.1038/s41467-017-01535-y.

- Álvarez-Salgado, X. A. and Miller, A. E. J. (1998). Simultaneous determination of dissolved organic carbon and total dissolved nitrogen in seawater by high temperature catalytic oxidation: conditions for precise shipboard measurements, *Marine Chemistry*, 62(3), pp. 325–333. doi: 10.1016/S0304-4203(98)00037-1.
- American Public Health Association (APHA). (1992). *Standard methods for the examination of water and wastewater*. 18th edn. Edited by A. E. Greenberg, L. S. Clesceri, and A. D. Eaton. Washington, DC, USA: American Public Health Association.
- Barros, N., Cole, J. J., Tranvik, L. J., Prairie, Y. T., Bastviken, D., Huszar, V. L. M., del Giorgio, P. and Roland, F. (2011). Carbon emission from hydroelectric reservoirs linked to reservoir age and latitude, *Nature Geoscience*, 4(9), pp. 593–596. doi: 10.1038/ngeo1211.
- Bastviken, D., Tranvik, L. J., Downing, J. A., Crill, P. M. and Enrich-Prast, A. (2011). Freshwater Methane Emissions Offset the Continental Carbon Sink, *Science*, 331(6013), pp. 1–12. doi: 10.1126/science.1196808.
- Battye, W., Aneja, V. P. and Schlesinger, W. H. (2017). Is nitrogen the next carbon?, *Earth's Future*, 5(9), pp. 894–904. doi: 10.1002/2017EF000592.
- Baulch, H. M., Schiff, S. L., Maranger, R. and Dillon, P. J. (2011). Nitrogen enrichment and the emission of nitrous oxide from streams, *Global Biogeochemical Cycles*, 25(4), p. 15. doi: 10.1029/2011GB004047.
- Beaulieu, J. J., DelSontro, T. and Downing, J. A. (2019). Eutrophication will increase methane emissions from lakes and impoundments during the 21st century, *Nature Communications*, 10(1), p. 1375. doi: 10.1038/s41467-019-09100-5.
- Beaulieu, J. J., Nietch, C. T. and Young, J. L. (2015). Controls on nitrous oxide production and consumption in reservoirs of the Ohio River Basin, *Journal of Geophysical Research-Biogeosciences*, 120(10), pp. 1995–2010. doi: 10.1002/2015JG002941.
- Beaulieu, J. J., Smolenski, R. L., Nietch, C. T., Townsend-Small, A. and Elovitz, M. S. (2014). High Methane Emissions from a Midlatitude Reservoir Draining an Agricultural Watershed, *Environmental Science & Technology*, 48(19), pp. 11100–11108. doi: 10.1021/es501871g.
- Beaulieu, J. J., Tank, J. L., Hamilton, S. K., Wollheim, W. M., Hall, R. O., Mulholland, P. J., Peterson, B. J., Ashkenas, L. R., Cooper, L. W., Dahm, C. N., Dodds, W. K., Grimm, N. B., Johnson, S. L., McDowell, W. H., Poole, G. C., Valett, H. M., Arango, C. P., Bernot, M. J., Burgin, A. J., Crenshaw, C. L., Helton, A. M., Johnson, L. T., O'Brien, J. M., Potter, J. D., Sheibley, R. W., Sobota, D. J. and Thomas, S. M. (2011). Nitrous oxide emission from denitrification in stream and river networks, *Proceedings of the National Academy of Sciences*, 108(1), pp. 214–219. doi: 10.1073/pnas.1011464108.
- Bogard, M. J., del Giorgio, P. A., Boutet, L., Chaves, M. C. G., Prairie, Y. T., Merante, A. and Derry, A. M. (2014). Oxic water column methanogenesis as a major component of aquatic CH₄ fluxes, *Nature Communications*, 5, p. 5350. doi: 10.1038/ncomms6350.
- Canfield, D. E., Glazer, A. N. and Falkowski, P. G. (2010). The Evolution and Future of Earth's Nitrogen Cycle, *Science*, 330(6001), pp. 192–196. doi: 10.1126/science.1186120.

- Cole, J. J., Caraco, N. F., Kling, G. W. and Kratz, T. K. (1994). Carbon Dioxide Supersaturation in the Surface Waters of Lakes, *Science*, 265(5178), pp. 1568–1570. doi: 10.1126/science.265.5178.1568.
- Davidson, T. A., Audet, J., Jeppesen, E., Landkildehus, F., Lauridsen, T. L., Søndergaard, M. and Syväranta, J. (2018). Synergy between nutrients and warming enhances methane ebullition from experimental lakes, *Nature Climate Change*, 8(2), pp. 156–160. doi: 10.1038/s41558-017-0063-z.
- Deemer, B. R., Harrison, J. A., Li, S., Beaulieu, J. J., DelSontro, T., Barros, N., Bezerra-Neto, J. F., Powers, S. M., dos Santos, M. A. and Vonk, J. A. (2016). Greenhouse Gas Emissions from Reservoir Water Surfaces: A New Global Synthesis, *BioScience*, 66(11), pp. 949–964. doi: 10.1093/biosci/biw117.
- Fox, J. and Weisberg, S. (2011). *An R Companion to Applied Regression*. Second. Thousand Oaks CA: Sage. Available at: <http://socserv.socsci.mcmaster.ca/jfox/Books/Companion>.
- Giorgi, F. and Lionello, P. (2008). Climate change projections for the Mediterranean region, *Global and Planetary Change*. (Mediterranean climate: trends, variability and change), 63(2), pp. 90–104. doi: 10.1016/j.gloplacha.2007.09.005.
- Gross, J. and Ligges, U. (2015). *nortest: Tests for Normality*. Available at: <https://CRAN.R-project.org/package=nortest> (Accessed: 3 June 2018).
- Grossart, H.-P., Frindte, K., Dziallas, C., Eckert, W. and Tang, K. W. (2011). Microbial methane production in oxygenated water column of an oligotrophic lake, *Proceedings of the National Academy of Sciences*, 108(49), pp. 19657–19661. doi: 10.1073/pnas.1110716108.
- Gruber, N. and Galloway, J. N. (2008). An Earth-system perspective of the global nitrogen cycle, *Nature*, 451(7176), pp. 293–296. doi: 10.1038/nature06592.
- Guérin, F., Abril, G., Richard, S., Burban, B., Reynouard, C., Seyler, P. and Delmas, R. (2006). Methane and carbon dioxide emissions from tropical reservoirs: Significance of downstream rivers, *Geophysical Research Letters*, 33(21). doi: 10.1029/2006GL027929.
- Heathcote, A. J. and Downing, J. A. (2012). Impacts of Eutrophication on Carbon Burial in Freshwater Lakes in an Intensively Agricultural Landscape, *Ecosystems*, 15(1), pp. 60–70. doi: 10.1007/s10021-011-9488-9.
- Henzel, L. L., Matthews, C. J. D., Venkiteswaran, J. J., St. Louis, V. L., Burton, D., Joyce, E. M. and Bodaly, R. A. (2005). Nitrous Oxide Fluxes in Three Experimental Boreal Forest Reservoirs, *Environmental Science & Technology*, 39(12), pp. 4353–4360. doi: 10.1021/es049443j.
- IPCC. (2013). *Climate Change 2013: The Physical Science Basis. Contribution of Working Group I to the Fifth Assessment Report of the Intergovernmental Panel on Climate Change*. Edited by T. F. Stocker, D. Qin, G.-K. Plattner, M. Tignor, S. K. Allen, J. Boschung, A. Nauels, Y. Xia, V. Bex, and P. M. Midgley. Cambridge: Cambridge University Press.
- Keller, M. and Stallard, R. F. (1994). Methane emission by bubbling from Gatun Lake,

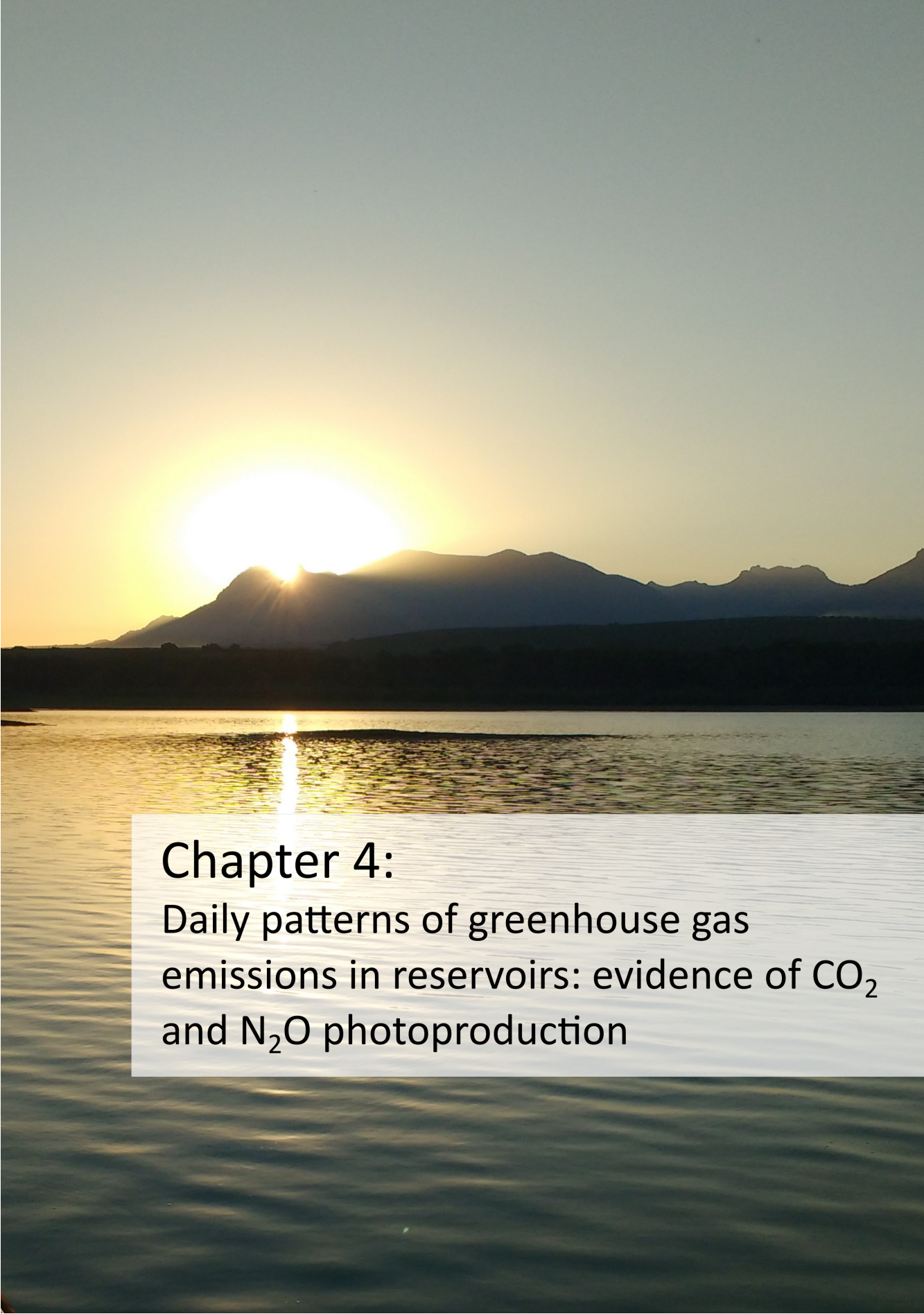
- Panama, *Journal of Geophysical Research: Atmospheres*, 99(D4), pp. 8307–8319. doi: 10.1029/92JD02170.
- Laine, J., Joosten, H., Sirin, A., Couwenberg, J. and Smith, P. (2016). Chapter Four: The role of peatlands in climate regulation, in Bonn, A., Allott, T., Evans, M., Joosten, H., and Stoneman, R. (eds) *Peatland Restoration and Ecosystem Services: Science, Policy and Practice*. Cambridge University Press.
- Le Quéré, C. L., Andrew, R. M., Friedlingstein, P., Sitch, S., Hauck, J., Pongratz, J., Pickers, P. A., Korsbakken, J. I., Peters, G. P., Canadell, J. G., Arneeth, A., Arora, V. K., Barbero, L., Bastos, A., Bopp, L., Chevallier, F., Chini, L. P., Ciais, P., Doney, S. C., Gkritzalis, T., Goll, D. S., Harris, I., Haverd, V., Hoffman, F. M., Hoppema, M., Houghton, R. A., Hurtt, G., Ilyina, T., Jain, A. K., Johannessen, T., Jones, C. D., Kato, E., Keeling, R. F., Goldewijk, K. K., Landschützer, P., Lefèvre, N., Lienert, S., Liu, Z., Lombardozzi, D., Metzl, N., Munro, D. R., Nabel, J. E. M. S., Nakaoka, S., Neill, C., Olsen, A., Ono, T., Patra, P., Peregon, A., Peters, W., Peylin, P., Pfeil, B., Pierrot, D., Poulter, B., Rehder, G., Resplandy, L., Robertson, E., Rocher, M., Rödenbeck, C., Schuster, U., Schwinger, J., Séférian, R., Skjelvan, I., Steinhoff, T., Sutton, A., Tans, P. P., Tian, H., Tilbrook, B., Tubiello, F. N., Laan-Luijckx, I. T. van der, Werf, G. R. van der, Viovy, N., Walker, A. P., Wiltshire, A. J., Wright, R., Zaehle, S. and Zheng, B. (2018). Global Carbon Budget 2018, *Earth System Science Data*, 10(4), pp. 2141–2194. doi: 10.5194/essd-10-2141-2018.
- Lehner, B., Liermann, C. R., Revenga, C., Vörösmarty, C., Fekete, B., Crouzet, P., Döll, P., Endejan, M., Frenken, K., Magome, J., Nilsson, C., Robertson, J. C., Rödel, R., Sindorf, N. and Wisser, D. (2011). High-resolution mapping of the world's reservoirs and dams for sustainable river-flow management, *Frontiers in Ecology and the Environment*, 9(9), pp. 494–502. doi: 10.1890/100125.
- León-Palmero, E., Reche, I. and Morales-Baquero, R. (2019). Atenuación de luz en embalses del sur-este de la Península Ibérica, *Ingeniería del agua*, 23(1), pp. 65–75. doi: 10.4995/ia.2019.10655.
- López, P., Marcé, R. and Armengol, J. (2011). Net heterotrophy and CO₂ evasion from a productive calcareous reservoir: Adding complexity to the metabolism-CO₂ evasion issue, *Journal of Geophysical Research: Biogeosciences*, 116(G2). doi: 10.1029/2010JG001614.
- Marcé, R., Obrador, B., Morguí, J.-A., Riera, J. L., López, P. and Armengol, J. (2015). Carbonate weathering as a driver of CO₂ supersaturation in lakes, *Nature Geoscience*, 8(2), pp. 107–111. doi: 10.1038/ngeo2341.
- Marotta, H., Pinho, L., Gudas, C., Bastviken, D., Tranvik, L. J. and Enrich-Prast, A. (2014). Greenhouse gas production in low-latitude lake sediments responds strongly to warming, *Nature Climate Change*, 4(6), pp. 467–470. doi: 10.1038/nclimate2222.
- McDonald, C. P., Stets, E. G., Striegl, R. G. and Butman, D. (2013). Inorganic carbon loading as a primary driver of dissolved carbon dioxide concentrations in the lakes and reservoirs of the contiguous United States, *Global Biogeochemical Cycles*, 27(2), pp. 285–295. doi: 10.1002/gbc.20032.
- Molina-Navarro, E., Trolle, D., Martínez-Pérez, S., Sastre-Merlín, A. and Jeppesen, E. (2014). Hydrological and water quality impact assessment of a Mediterranean limno-

- reservoir under climate change and land use management scenarios, *Journal of Hydrology*, 509, pp. 354–366. doi: 10.1016/j.jhydrol.2013.11.053.
- Morales-Pineda, M., Cózar, A., Laiz, I., Úbeda, B. and Gálvez, J. Á. (2014). Daily, biweekly, and seasonal temporal scales of pCO₂ variability in two stratified Mediterranean reservoirs, *Journal of Geophysical Research: Biogeosciences*, 119(4), p. 2013JG002317. doi: 10.1002/2013JG002317.
- Moseman-Valtierra, S., Abdul-Aziz, O. I., Tang, J., Ishtiaq, K. S., Morkeski, K., Mora, J., Quinn, R. K., Martin, R. M., Egan, K., Brannon, E. Q., Carey, J. and Kroeger, K. D. (2016). Carbon dioxide fluxes reflect plant zonation and belowground biomass in a coastal marsh, *Ecosphere*, 7(11), p. e01560. doi: 10.1002/ecs2.1560.
- Mulholland, P. J., Helton, A. M., Poole, G. C., Hall, R. O., Hamilton, S. K., Peterson, B. J., Tank, J. L., Ashkenas, L. R., Cooper, L. W., Dahm, C. N., Dodds, W. K., Findlay, S. E. G., Gregory, S. V., Grimm, N. B., Johnson, S. L., McDowell, W. H., Meyer, J. L., Valett, H. M., Webster, J. R., Arango, C. P., Beaulieu, J. J., Bernot, M. J., Burgin, A. J., Crenshaw, C. L., Johnson, L. T., Niederlehner, B. R., O'Brien, J. M., Potter, J. D., Sheibley, R. W., Sobota, D. J. and Thomas, S. M. (2008). Stream denitrification across biomes and its response to anthropogenic nitrate loading, *Nature*, 452(7184), p. 202. doi: 10.1038/nature06686.
- Murphy, J. and Riley, J. P. (1962). A modified single solution method for the determination of phosphate in natural waters, *Analytica Chimica Acta*, 27(Supplement C), pp. 31–36. doi: 10.1016/S0003-2670(00)88444-5.
- Musenze, R. S., Grinham, A., Werner, U., Gale, D., Sturm, K., Udy, J. and Yuan, Z. (2014). Assessing the spatial and temporal variability of diffusive methane and nitrous oxide emissions from subtropical freshwater reservoirs, *Environmental Science & Technology*, 48(24), pp. 14499–14507. doi: 10.1021/es505324h.
- Naselli-Flores, L. (2003). Man-made lakes in Mediterranean semi-arid climate: the strange case of Dr Deep Lake and Mr Shallow Lake, *Hydrobiologia*, 506–509(1–3), pp. 13–21. doi: 10.1023/B:HYDR.0000008550.34409.06.
- R Core Team. (2014). *R: A Language and Environment for Statistical Computing*. Vienna, Austria: R Foundation for Statistical Computing. Available at: <http://www.R-project.org/>.
- Rasilo, T., Prairie, Y. T. and del Giorgio, P. A. (2015). Large-scale patterns in summer diffusive CH₄ fluxes across boreal lakes, and contribution to diffusive C emissions, *Global Change Biology*, 21(3), pp. 1124–1139. doi: 10.1111/gcb.12741.
- Raymond, P. A., Hartmann, J., Lauerwald, R., Sobek, S., McDonald, C., Hoover, M., Butman, D., Striegl, R., Mayorga, E., Humborg, C., Kortelainen, P., Dürr, H., Meybeck, M., Ciais, P. and Guth, P. (2013). Global carbon dioxide emissions from inland waters, *Nature*, 503(7476), pp. 355–359. doi: 10.1038/nature12760.
- Samiotis, G., Pekridis, G., Kaklidis, N., Trikoilidou, E., Taousanidis, N. and Amanatidou, E. (2018). Greenhouse gas emissions from two hydroelectric reservoirs in Mediterranean region, *Environmental Monitoring and Assessment*, 190(6), p. 363. doi: 10.1007/s10661-018-6721-4.
- Schlesinger, W. H. (2009). On the fate of anthropogenic nitrogen, *Proceedings of the*

- National Academy of Sciences*, 106(1), pp. 203–208. doi: 10.1073/pnas.0810193105.
- Schlesinger, W. H. and Bernhardt, E. S. (2013). *Biogeochemistry: An Analysis of Global Change*. Academic Press.
- Schmidt, U. and Conrad, R. (1993). Hydrogen, carbon monoxide, and methane dynamics in Lake Constance, *Limnology and Oceanography*, 38(6), pp. 1214–1226. doi: 10.4319/lo.1993.38.6.1214.
- Seitzinger, S. P., Kroeze, C. and Styles, R. V. (2000). Global distribution of N₂O emissions from aquatic systems: natural emissions and anthropogenic effects, *Chemosphere - Global Change Science*. (Atmospheric Nitrous Oxide), 2(3), pp. 267–279. doi: 10.1016/S1465-9972(00)00015-5.
- Sepulveda-Jauregui, A., Hoyos-Santillan, J., Martinez-Cruz, K., Walter Anthony, K. M., Casper, P., Belmonte-Izquierdo, Y. and Thalasso, F. (2018). Eutrophication exacerbates the impact of climate warming on lake methane emission, *Science of The Total Environment*, 636, pp. 411–419. doi: 10.1016/j.scitotenv.2018.04.283.
- Sierra, A., Jiménez-López, D., Ortega, T., Ponce, R., Bellanco, M. J., Sánchez-Leal, R., Gómez-Parra, A. and Forja, J. (2017a). Spatial and seasonal variability of CH₄ in the eastern Gulf of Cadiz (SW Iberian Peninsula), *Science of The Total Environment*, 590–591, pp. 695–707. doi: 10.1016/j.scitotenv.2017.03.030.
- Sierra, A., Jiménez-López, D., Ortega, T., Ponce, R., Bellanco, M. J., Sánchez-Leal, R., Gómez-Parra, A. and Forja, J. (2017b). Distribution of N₂O in the eastern shelf of the Gulf of Cadiz (SW Iberian Peninsula), *Science of The Total Environment*, 593–594, pp. 796–808. doi: 10.1016/j.scitotenv.2017.03.189.
- Soued, C., del Giorgio, P. A. and Maranger, R. (2015). Nitrous oxide sinks and emissions in boreal aquatic networks in Québec, *Nature Geoscience*, 9(2), p. 116. doi: 10.1038/ngeo2611.
- Staehr, P. A., Bade, D., Bogert, M. C. V. de, Koch, G. R., Williamson, C., Hanson, P., Cole, J. J. and Kratz, T. (2010). Lake metabolism and the diel oxygen technique: State of the science, *Limnology and Oceanography: Methods*, 8(11), pp. 628–644. doi: 10.4319/lom.2010.8.0628.
- Tang, K. W., McGinnis, D. F., Frindte, K., Brüchert, V. and Grossart, H.-P. (2014). Paradox reconsidered: Methane oversaturation in well-oxygenated lake waters, *Limnology and Oceanography*, 59(1), pp. 275–284. doi: 10.4319/lo.2014.59.1.0275.
- Tranvik, L. J., Downing, J. A., Cotner, J. B., Loiselle, S. A., Striegl, R. G., Ballatore, T. J., Dillon, P., Finlay, K., Fortino, K., Knoll, L. B., Kortelainen, P. L., Kutser, T., Larsen, Soren., Laurion, I., Leech, D. M., McCallister, S. L., McKnight, D. M., Melack, J. M., Overholt, E., Porter, J. A., Prairie, Y., Renwick, W. H., Roland, F., Sherman, B. S., Schindler, D. W., Sobek, S., Tremblay, A., Vanni, M. J., Verschoor, A. M., von Wachenfeldt, E. and Weyhenmeyer, G. A. (2009). Lakes and reservoirs as regulators of carbon cycling and climate, *Limnology and Oceanography*, 54(6part2), pp. 2298–2314. doi: 10.4319/lo.2009.54.6_part_2.2298.
- West, W. E., Coloso, J. J. and Jones, S. E. (2012). Effects of algal and terrestrial carbon on methane production rates and methanogen community structure in a temperate lake sediment, *Freshwater Biology*, 57(5), pp. 949–955. doi: 10.1111/j.1365-

2427.2012.02755.x.

- West, W. E., Creamer, K. P. and Jones, S. E. (2016). Productivity and depth regulate lake contributions to atmospheric methane: Lake productivity fuels methane emissions, *Limnology and Oceanography*, 61(S1), pp. S51–S61. doi: 10.1002/lno.10247.
- Weyhenmeyer, G. A., Kosten, S., Wallin, M. B., Tranvik, L. J., Jeppesen, E. and Roland, F. (2015). Significant fraction of CO₂ emissions from boreal lakes derived from hydrologic inorganic carbon inputs, *Nature Geoscience*, 8(12), pp. 933–936. doi: 10.1038/ngeo2582.
- Wood, S. N. (2006). *Generalized additive models: an introduction with R*. New York, USA: Chapman and Hall/CRC.
- Wood, S. N. (2011). Fast stable restricted maximum likelihood and marginal likelihood estimation of semiparametric generalized linear models, *Journal of the Royal Statistical Society: Series B (Statistical Methodology)*, 73(1), pp. 3–36. doi: 10.1111/j.1467-9868.2010.00749.x.
- Yvon-Durocher, G., Allen, A. P., Bastviken, D., Conrad, R., Gudas, C., St-Pierre, A., Thanh-Duc, N. and del Giorgio, P. A. (2014). Methane fluxes show consistent temperature dependence across microbial to ecosystem scales, *Nature*, 507(7493), pp. 488–491. doi: 10.1038/nature13164.
- Zarfl, C., Lumsdon, A. E., Berlekamp, J., Tydecks, L. and Tockner, K. (2015). A global boom in hydropower dam construction, *Aquatic Sciences*, 77(1), pp. 161–170. doi: 10.1007/s00027-014-0377-0.
- Zhao, Y., Sherman, B., Ford, P., Demarty, M., DelSontro, T., Harby, A., Tremblay, A., Øverjordet, I. B., Zhao, X., Hansen, B. H. and Wu, B. (2015). A comparison of methods for the measurement of CO₂ and CH₄ emissions from surface water reservoirs: Results from an international workshop held at Three Gorges Dam, June 2012, *Limnology and Oceanography: Methods*, 13(1), pp. 15–29. doi: 10.1002/lom3.10003.

A photograph of a sunset over a large body of water, likely a reservoir. The sun is low on the horizon, partially obscured by a range of dark mountains. The sky is a gradient of light yellow to pale blue. The water in the foreground is dark with gentle ripples, and a bright reflection of the sun is visible on the water's surface.

Chapter 4:
Daily patterns of greenhouse gas
emissions in reservoirs: evidence of CO₂
and N₂O photoproduction

Chapter 4:

Daily patterns of greenhouse gas emissions in reservoirs: evidence of CO₂ and N₂O photoproduction

The Supplementary Material is available in Appendix 4

Abstract

Greenhouse gas (GHG) emissions from reservoirs are quantitatively relevant for atmospheric climatic forcing. Eutrophic reservoirs produce significant emissions of methane (CH₄) and nitrous oxide (N₂O), that are responsible for most of this climatic forcing. Most current emission data come from daytime, but nighttime emissions could affect GHG budgets. However, daily patterns in GHG fluxes in reservoirs have been scarcely studied. Here, we explored the daily patterns of CO₂, N₂O, and diffusive and ebullitive CH₄ fluxes in two eutrophic reservoirs with contrasted morphometries. Besides, we experimentally explored the abiotic production of CO₂, N₂O, and CH₄ due to sunlight. We found similar daily patterns for CO₂, N₂O, and diffusive CH₄ fluxes with higher emissions during the daytime than during the nighttime. These emissions were coupled with the daily solar cycle, wind speed, and water temperature. The daily emissions of the CO₂, N₂O, and CH₄ were also positive and significantly related to oxygen saturation. We experimentally detected photochemical production of dissolved inorganic carbon likely mediated by CO₂ photoproduction during the photodegradation of the organic matter. We also show evidence of the abiotic production of N₂O induced by sunlight. Our data

suggest that photochemical processes can be responsible for a relevant fraction of the daily CO₂ and N₂O production.

4. 1. Introduction

Greenhouse gas (GHG) emissions from reservoirs are quantitatively relevant for atmospheric climatic forcing (Deemer *et al.*, 2016; León-Palmero *et al.*, 2020a). Eutrophic reservoirs are responsible for most of this climatic forcing (Deemer *et al.*, 2016; León-Palmero *et al.*, 2020a). GHG emissions have a large temporal (seasonal and daily) variability in reservoirs (Xiao *et al.*, 2013; Liu *et al.*, 2016; Lin *et al.*, 2019). Daily changes can represent an important part of the total GHG variability (Xiao *et al.*, 2013; Morales-Pineda *et al.*, 2014; Liu *et al.*, 2016; Lin *et al.*, 2019; Sieczko *et al.*, 2020). However, there is still an astonishing lack of data on GHG daily emissions, which severely limits our confidence in the global estimates of GHG emissions using upscaling approaches (Liu *et al.*, 2016; Sieczko *et al.*, 2020). The underlying problem is that most of the measurements that exist were collected during daylight hours, and under good weather conditions, which cannot fully resolve the real temporal variability of fluxes within any given system. Given the apparent mismatch between sampling and natural temporal patterns of gas fluxes, serious biases could affect the global estimates of GHG emissions from reservoirs (Deemer *et al.*, 2016). The daily variability in GHG emissions can be larger than the variability occurring on a monthly timescale during daytime (Zhang *et al.*, 2019). However, most estimations for GHG fluxes are based on the upscaling of discrete measurements during the daytime, and, in general, they did not account for the nighttime emissions (Liu *et al.*, 2016; Sieczko *et al.*, 2020).

Daily patterns of the GHG fluxes depend on the biological activity inside the reservoirs, and the physical-chemical processes that determine the CO₂, CH₄, and N₂O concentrations and solubility, and their subsequent emission to the atmosphere (Donelan, 1990; Laursen and Seitzinger, 2004; Bastviken *et al.*, 2010; Wang *et al.*, 2015; Liu *et al.*, 2016). These environmental drivers change considerably on a daily scale, likely affecting the daily patterns of GHG emissions. The wind is a significant driver affecting water turbulence and promoting gas exchange across the air-water interface (Wang *et al.*, 2015; Liu *et al.*, 2016). For this reason, gas transfer coefficients (k) are frequently parameterized as a function of

the wind speed in emission estimates (Cole and Caraco, 1998; Crusius and Wanninkhof, 2003; Cole *et al.*, 2010). Liu *et al.* (2016) measured that CO₂ emissions at nighttime were approximately 70 % greater than those occurring in the daytime due to the wind events at night. In contrast, the higher wind-induced turbulence at daytime increased the emissions of diffusive and ebullitive CH₄ during the day in wetlands, reservoirs, and lakes (Edwards *et al.*, 1994; Keller and Stallard, 1994; Bastviken *et al.*, 2010). Temperature is another crucial environmental driver that affects both GHG production (i.e., stimulating the microbial metabolism) and emission (i.e., changing the gas solubility). Daily changes in air and water temperature were positively correlated to the daily pattern of the diffusive CH₄ emission (Zhang *et al.*, 2019). The studies on daily patterns in N₂O emissions in rivers showed that air and water temperature determined a higher N₂O production and emission at daytime (Laursen and Seitzinger, 2004; Yang *et al.*, 2011; Xia *et al.*, 2013). Besides, wind speed and cooling events can also promote upwelling motions and waterside convection events in shallow systems that can bring CO₂ and CH₄ rich waters from deeper layers to the surface water, promoting emissions during the nighttime (Godwin *et al.*, 2013; Podgrajsek *et al.*, 2014).

Solar radiation determines the daily cycle of photosynthesis and photochemistry in surface waters. Whereas photosynthesis (CO₂ uptake) only occurs during daytime, respiration (CO₂ release) occurs throughout the day. The respiration of primary producers and heterotrophs may determine higher emissions of CO₂ at nighttime than at daytime depending on photosynthesis rates (Liu *et al.*, 2016). Moreover, CH₄ emissions seem to be closely linked to photosynthesis in lakes and reservoirs (Schmidt and Conrad, 1993; Grossart *et al.*, 2011; Bogard *et al.*, 2014; Tang *et al.*, 2014; Deemer *et al.*, 2016; León-Palmero *et al.*, 2020b). Recently, Bižić *et al.* (2020) demonstrated that the production of CH₄ by cyanobacteria is associated with the photosynthetic activity, following a daily cycle dependent on solar radiation. N₂O fluxes also exhibit daily variations (Harrison *et al.*, 2005; Clough *et al.*, 2007; Xia *et al.*, 2013). The daily changes in the dissolved oxygen affect the rates of microbial nitrogen processing during the nitrification and the coupling nitrification-denitrification (Lorenzen *et al.*, 1998; Laursen and Seitzinger, 2004; Baulch *et al.*, 2012) contributing to the diurnal patterns of N₂O concentration and emission found in rivers (Harrison *et al.*, 2005; Clough *et al.*, 2007; Xia *et al.*, 2013).

Photochemical processes also vary on a daily scale. Solar radiation, mostly in the ultraviolet band, catalyzes photochemical reactions that decompose chromophoric and recalcitrant organic molecules in smaller ones, like carboxylic acids (oxalic, malonic, formic, and acetic acid), that can be further completely mineralized to CO₂ (contributing to the pool of dissolved inorganic carbon). Indirectly, these smaller organic molecules can also enhance microbial mineralization and, consequently, the CO₂ production (Allard *et al.*, 1994; Bertilsson and Tranvik, 1998; Reche *et al.*, 1998; Bertilsson and Tranvik, 2000; Johannessen and Miller, 2001; Ortega-Retuerta *et al.*, 2007). Koehler *et al.* (2014) calculated that approximately 12 % of the CO₂ emissions from Swedish lakes were directly induced by sunlight, and up to 10 % of the global CO₂ emissions from inland waters are sunlight-induced. More recently, Zhang and Xie (2015) demonstrated the CH₄ photoproduction associated with photobleaching of chromophoric dissolved organic matter. This CH₄ photoproduction appears to be quantitatively relevant in the open ocean, accounting for up to 20 - 60-% of the CH₄ emissions (Li *et al.*, 2020). However, this photochemical process has not been studied in inland waters.

In this chapter, we measured the fluxes of CO₂, N₂O, and CH₄ in three 24-hour cycles in two eutrophic reservoirs of contrasting morphometric properties during the summer stratification. We split the total CH₄ emissions into the diffusive and ebullitive components to better understand the daily CH₄ patterns. We described the daily patterns in the fluxes of CO₂, N₂O, and CH₄, and determine the environmental drivers explaining these patterns. Finally, we also performed experiments to measure the photoproduction of CO₂, N₂O, and CH₄, and we assessed the contribution of GHG photoproduction to the daily variability.

4. 2. Material and Methods

4. 2. 1. Study Reservoirs

We performed three 24-hour sampling campaigns in two eutrophic reservoirs (Cubillas and Iznájar) located in southeastern Spain during the stratification period. Both reservoirs were built for irrigation and water supply purposes. We sampled the Cubillas reservoir in 2016 (from July 14th to July 15th) and 2018 (from June 21st to June 22nd), and the Iznájar reservoir in 2018 (July 8th to July 9th). The Cubillas reservoir is a small and shallow system with a maximum capacity of 19 hm³, in

which temporal variation in volume and maximum depth are related to annual rainfall. The year 2016 was dry (326.6 mm of rainfall and 7.0 meters of maximum depth) with an extreme summer, whereas the year 2018 was wet (509.4 mm of rainfall and 8.9 meters of maximum depth). The Iznájar reservoir is a bigger and deeper system than the Cubillas reservoir, with a maximum capacity of 981 hm³ and a mean depth of 22.4 m. We collected these data from The Confederación Hidrográfica del Guadalquivir (CHG; <https://www.chguadalquivir.es/>), and Infraestructura de Datos Espaciales de Andalucía (IDEAndalucía; <http://www.ideandalucia.es/portal/web/ideandalucia/>). We show more information about the morphometry and other characteristics of the study reservoirs in Chapter 2 (see subsection 2. 1. Study reservoirs, morphometry and watershed characterization).

4. 2. 2. Quantification of CO₂, N₂O and CH₄ fluxes

We measured CO₂, N₂O, and CH₄ fluxes from 13 to 24 times along the 24-hour sampling using a high-resolution laser-based Cavity Ring-Down Spectrometer (CRDS PICARRO G2508) coupled to a floating chamber. We performed the CH₄ separation in the diffusive and ebullitive components based on the algorithm proposed by Hoffmann *et al.* (2017) adapted to our data. We performed the calculations as detailed in Chapter 2 (see subsection 2. 2. Greenhouse gas fluxes quantification).

4. 2. 3. Physico-chemical analysis in the water column

We measured ambient temperature, and barometric pressure using a multiparametric probe (HANNA HI 9828), and wind speed using an anemometer (MASTECH MS6252A) at the beginning of each flux measurement. We recorded the dissolved oxygen concentration, and the water temperature in the epilimnion every 10 minutes during the 24-hour sampling using a miniDOT (PME) submersible water logger. More details are provided in Chapter 2 (see subsection 2. 4. Biological analysis, Reservoir metabolism).

4. 2. 4. Experiment set up and analysis

We performed five experiments with water from the reservoirs to test the effect of solar radiation on the greenhouse gas production: two experiments to

measure DIC photoproduction and three experiments to measure CH₄ and N₂O photoproduction. We collected surface water (0.5 - 1 m) from Cubillas and Iznájar reservoir. We filled UV-VIS transparent quartz spherical bottles with frosted closure, preserved with a solution of HgCl₂ (final concentration 1 mmol L⁻¹) to inhibit biological activity, and sealed with Apiezon® grease to prevent gas exchange.

We performed the experiments in June (only in Cubillas) and September 2018 using bottles with different volumes (250 mL, 100 mL, or 50 mL) according to the quartz bottle availability, but using the same volume in each incubation set. We selected two bottles (replicates) at time 0 (t_0), 2 or 3 UV-VIS transparent bottles (replicates) at time 1 (t_1), and 2 or 3 UV-VIS transparent bottles (replicates) at time 2 (t_2), besides we included a dark control at time 1, and time 2 that were incubated in the same floating platforms that the UV-VIS transparent bottles. We covered the control bottles with black tape to avoid solar radiation. The t_1 was incubated for one to three days, while the t_2 was incubated for seven days. We calculated the exact hours of sunlight during the incubations, by considering the time of sunrise and sunset on each day during the experiment running. We stored the samples in the dark at room temperature in the laboratory until analysis. The details of the incubations are in Figure 4.1.

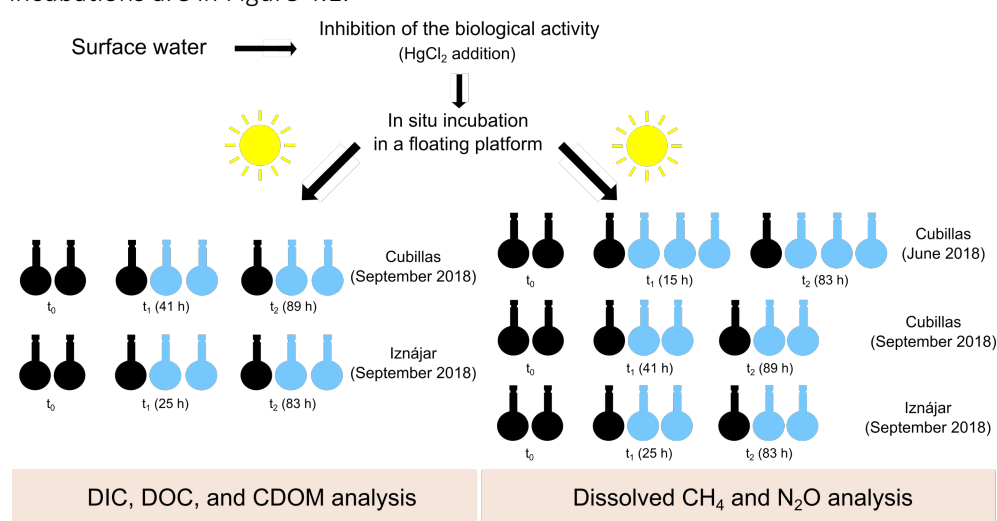


Figure 4.1. Scheme of the experimental design to determine the GHG photoproduction

We performed the first experiment to measure CH₄ and N₂O photoproduction in June 2018 using water from the Cubillas reservoir and 250 mL UV-VIS transparent bottles. In September 2018, we repeated the experiment to

measure CH₄ and N₂O photoproduction using water from Cubillas and Iznájar reservoirs and 100 mL UV-VIS transparent bottles. As a consequence of the different volumes, the ratio of surface to volume was smaller in June (73 m⁻¹) than in the September experiments (98 m⁻¹).

We performed the two experiments to measure the photoproduction of dissolved inorganic carbon (DIC), and the photobleaching of chromophoric dissolved organic matter (CDOM) using water from Cubillas and Iznájar reservoirs in 50 mL UV-VIS transparent bottles. We took two pseudo-replicates per each replicate. After sunlight incubations, we filtered the water through 0.7 µm pore-size Whatman GF/F glass-fiber filters to measure the dissolved inorganic carbon (DIC) and dissolved organic carbon (DOC) by high-temperature catalytic oxidation using a Shimadzu total organic carbon (TOC) analyzer (Model TOC-V CSH) (Álvarez-Salgado and Miller, 1998). We also measured the chromophoric dissolved organic matter (CDOM) by absorbance scans from 200 to 700 nm in 10-cm quartz cuvettes using a Perkin-Elmer Lambda 40 spectrophotometer. We calculated the absorption coefficients at 325 nm (a_{325}), the spectral slopes from 275 to 295 nm ($S_{275-295}$) and from 350 to 400 nm ($S_{350-400}$), and the spectral ratio (S_R) as in Catalá *et al.* (2015).

We measured the dissolved CH₄ and N₂O in unfiltered water by performing a headspace equilibration in a 50 ml air-tight glass by duplicate or triplicate. We analyzed simultaneously the concentration of dissolved CH₄ and N₂O of each sample using a gas chromatograph (GC; Bruker® GC-450) equipped with Hydrogen Flame Ionization Detector, and Electron Capture Detector. We provided more details on these chemical analyses and calculations in Chapter 2 (see subsection 2.3.2. CH₄ and N₂O concentration in the water column).

If we detected significant differences between the treatments, we calculated the DIC, CH₄ or N₂O (GHG) production rates for each incubation from the slope of the increase in the quantity of DIC, CH₄ or N₂O (moles) over time (incubation light hours), respectively. We calculated the slope of the increase between the t_0 and t_1 incubation, and between the t_0 and t_2 incubation. The error for each production rate was calculated as the standard error of the slope. We calculated the production rate per area following the equation 4.1:

$$R_{\text{GHG-Area}} = \frac{\Delta \text{GHG}}{\Delta t} \times \frac{12 \text{ h light per day}}{\text{Area of the incubation bottle}} \quad \text{Eq. 4.1}$$

Where $R_{\text{GHG-Area}}$ (moles $\text{m}^{-2} \text{d}^{-1}$) is the production rate of DIC, CH_4 or N_2O . ΔGHG represents the slope of the variation in the amount of GHG (moles) over the incubation time (Δt , exact hours of sunlight during the incubations). To upscale from hours to days, we assumed 12 hours of light per day. The area of the incubation bottles (m^2) varied in the different experiments. We also determined the production rate per volume following the equation 4.2:

$$R_{\text{GHG-Volume}} = \frac{\Delta\text{GHG}}{\Delta t} \times \frac{12 \text{ h light per day}}{\text{Volume of the incubation bottle}} \quad \text{Eq. 4.2}$$

Where $R_{\text{GHG-Volume}}$ (moles $\text{m}^{-3} \text{d}^{-1}$) is the production rate of DIC, CH_4 or N_2O . The volume of the incubation bottles (m^3) varied in the different experiments. We also determined the percentage of the increase in GHG per day following the equation 4.3:

$$\text{Percentage of increase per day} = \left(\frac{R_{\text{GHG-Volume}} \times 1 \text{ day}}{[\text{GHG concentration}]_{\text{initial}}} \right) \times 100 \quad \text{Eq. 4.3}$$

Where the % of increase per day is the production in relation to the initial concentration of GHG in a day.

4. 2. 5. Statistical tests and rates determination

We used the software Oriana to perform circular statistics and plot the circular data in rose diagrams (Kovach, 2011). Circular statistics have been designed to analyze the variables with a cyclical nature and for which classical statistical analysis is not appropriate (Mendoza, 2020). Our circular data are distributed on a 24-hour cycle, where the time is a circular variable measured at a closed and cyclical scale. Therefore, the difference between 23:00 h and 00:00 h is only one hour on a circular scale, while on a linear scale the difference would be 24 hours. We performed linear-circular correlation (Fisher, 1993; Zar, 1998; Mardia and Jupp, 2000) between a circular variable (solar time, h) and a linear one (the fluxes or environmental variables). This correlation coefficient ranges from 0 to 1, so there is no negative correlation. We performed the calculation of the significance of the correlation following (Mardia and Jupp, 2000) and using their approximation of the F distribution. We also used R (R Core Team, 2014) for the rest of the statistical analysis and plots, using the packages car (Fox and Weisberg, 2011), nortest (Gross and Ligges, 2015), and mgcv (Wood, 2011). We used the Spearman's rank

correlation analysis to study the synchrony between the greenhouse gases fluxes. We used simple linear regression, and correlation analysis to study the environmental drivers of the fluxes.

To examine the results of the experiment on the sunlight effect on CO₂, N₂O, and CH₄ production, we performed the Shapiro-Wilk test of normality analyses and the Levene's test for homogeneity of variance across groups. When the dataset was normally distributed, we performed the one-way analysis of variance test (ANOVA). In case the data did not meet the assumptions of normality, we used the Kruskal-Wallis rank sum test (K-W).

4. 3. Results

4. 3. 1. Daily patterns in CO₂, N₂O, and CH₄ fluxes

Circular plots and statistics describe better daily patterns than traditional one. In Figure 4.2, we show the daily patterns of the CO₂, N₂O, and CH₄ fluxes in circular plots (i.e., rose diagrams) and the statistical significance of the circular-linear correlation between the solar time and the GHG fluxes. The values of the CO₂ emissions ranged from 0.10 to 0.42 $\mu\text{mol m}^{-2} \text{s}^{-1}$ in Cubillas 2016, from 0.17 to 1.46 $\mu\text{mol m}^{-2} \text{s}^{-1}$ in Cubillas 2018, and from -0.01 to 0.35 $\mu\text{mol m}^{-2} \text{s}^{-1}$ in Iznájar. The Cubillas reservoir always acted as a source of CO₂. Similarly, the Iznájar reservoir acted mostly as a source, although punctually was a sink. We measured the maximum values at daytime, and the minimum values at nighttime (Figure 4.2a, b, and c, and Supplementary Table 4.1). We detected significant correlations, using circular-linear analysis, between the solar time and the CO₂ fluxes in the 24-hour cycles performed in Cubillas and Iznájar reservoirs in 2018 (Figure 4.2b and c, and Supplementary Table 4.2).

The values of N₂O fluxes ranged more than one order of magnitude from 0.03 to 0.31 $\text{nmol m}^{-2} \text{s}^{-1}$ in Cubillas 2016, from 0.08 to 1.13 $\text{nmol m}^{-2} \text{s}^{-1}$ in Cubillas 2018, and from -0.09 to 0.46 $\text{nmol m}^{-2} \text{s}^{-1}$ in Iznájar, acting mostly as N₂O sources, although the Iznájar reservoir acted punctually as a sink at nighttime. Like in the CO₂ emissions, we also measured the maximum values at daytime, and the minimum values at nighttime (Figure 4.2d, e, and f, and Supplementary Table 4.1). We detected significant circular correlations between the solar time and the N₂O

fluxes in the three 24-hour cycles performed (Figure 4.2d, e, and f, and Supplementary Table 4.2).

In the case of the total CH₄ emissions, we discriminated two fractions: diffusive fluxes (Figure 4.2g, h, and i) and ebullitive fluxes (Figure 4.2j, k, and l). The daily values of CH₄ diffusive fluxes ranged from 0.00 to 989.15 nmol m⁻² s⁻¹ in Cubillas 2016, from 11.31 to 142.89 nmol m⁻² s⁻¹ in Cubillas 2018, and from 0.00 to 14.61 nmol m⁻² s⁻¹ in Iznájar, acting consistently as sources throughout the day (Supplementary Table 4.1). We also detected significant circular correlations between solar time and the diffusive CH₄ emissions in Cubillas 2018 and Iznájar reservoir (Figure 4.2h, and i, and Supplementary Table 4.2). For the ebullitive fraction, the values varied more than two orders of magnitude from 0.00 to 1815.32 nmol m⁻² s⁻¹ in Cubillas 2016, from 1.05 to 206.79 nmol m⁻² s⁻¹ in Cubillas 2018, and from 0.00 to 27.06 nmol m⁻² s⁻¹ in Iznájar. We did not find any significant correlation between solar time and the ebullitive CH₄ emissions (Supplementary Table 4.2). The contribution of the ebullitive fraction to the total CH₄ emission was very variable. The mean contribution ranged between 33 and 55 % during the day, and between 17 and 81 % during the night. At some moments in the Cubillas reservoir in 2016, the ebullition represented almost 100 % of the CH₄ emission. Ebullitive fluxes contributed more to the total emissions in the shallower reservoir (Cubillas in 2016) than in the deeper one (Iznájar in 2018) (Supplementary Table 4.1).

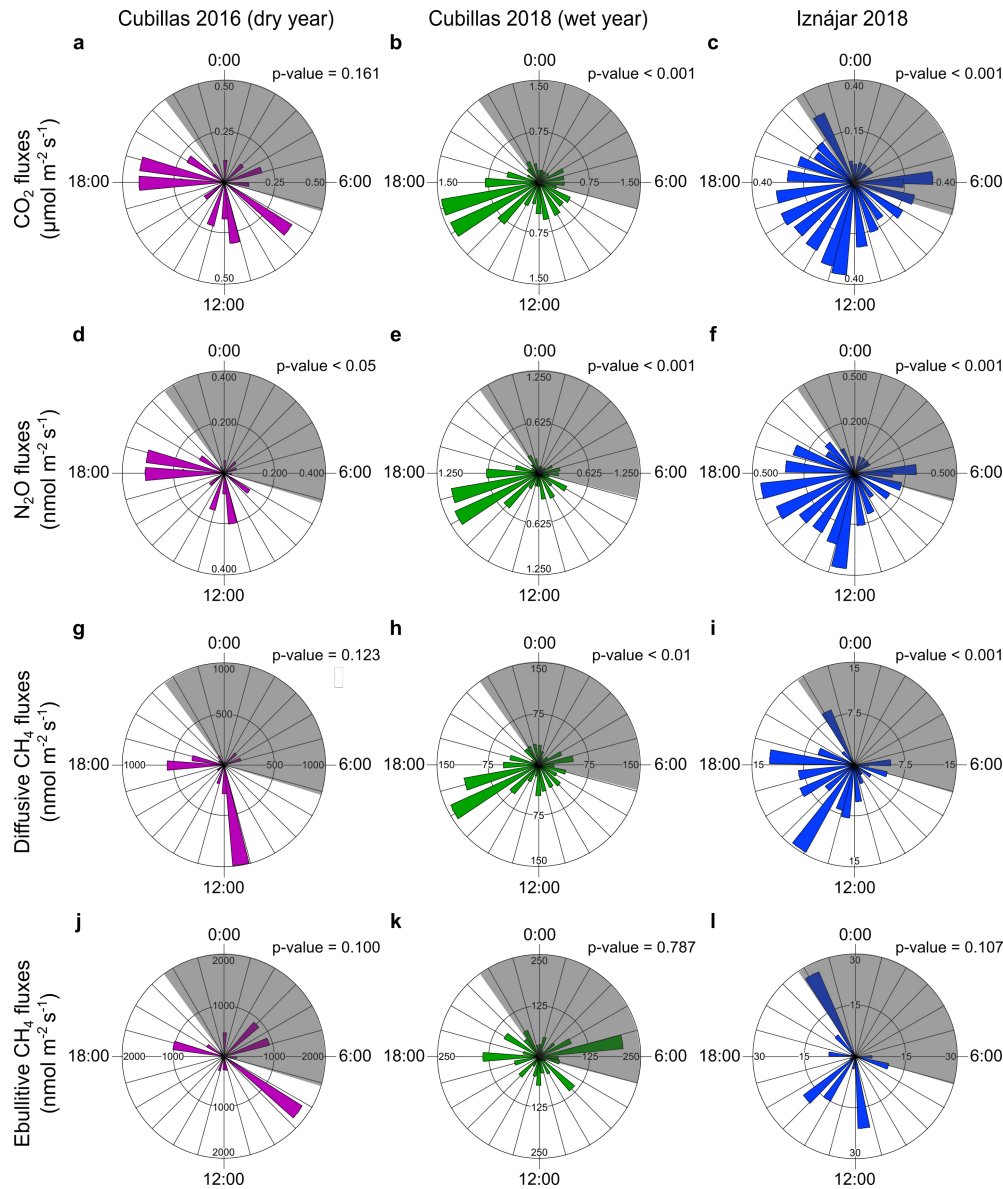


Figure 4.2. Rose diagrams of daily GHG fluxes in relation to solar time. We show the CO_2 (a, b, c), N_2O (d, e, f), diffusive CH_4 (g, h, i), and ebullitive CH_4 (j, k, l) fluxes in the Cubillas reservoir in 2016 (purple color), in the Cubillas reservoir in 2018 (green color), and in the Iznájár reservoir in 2018 (blue color). Solar time is shown with numbers outside the circle, and numbers inside the circle show the GHG emission thresholds. The shaded areas refer to the night hours. We also provided the p-value for the circular-linear correlation between solar time (h, circular variable) and greenhouse gas fluxes (linear variable).

We tested the existence of daily synchrony in the GHG emissions using correlation analysis among GHG fluxes (Supplementary Table 4.3). We found that CO_2 and N_2O fluxes were strongly synchronous in the three 24-hour measurement

cycles performed. We also found that CO₂ and N₂O fluxes were higher in the Cubillas reservoir in 2018 than in 2016. In contrast, CH₄ emissions were higher in Cubillas 2016 than in Cubillas 2018. Diffusive CH₄ emissions were also significantly correlated to N₂O fluxes in the three daily cycles and correlated to CO₂ fluxes in the Cubillas and Iznájar reservoirs in 2018. In contrast, the ebullitive component of CH₄ fluxes correlated to the CO₂ fluxes only in the Iznájar reservoir in 2018.

4. 3. 2. Drivers of daily patterns of GHG fluxes

GHG fluxes are the result of the production and gas exchange with the atmosphere. Wind speed (m s⁻¹) and water temperature (°C) are the main physical drivers affecting the GHG fluxes with the atmosphere. On the other hand, the percentage of oxygen saturation in the surface waters (%) can be considered a biological indicator of the net photosynthesis (i.e., O₂ production that leads to supersaturation with respect to gas solubility) vs. respiration (i.e., O₂ consumption that lead to undersaturation with respect to gas solubility). The mean, minimum, and maximum values for wind speed, surface water temperature, air temperature, and oxygen saturation during the 24-hour sampling are shown in Supplementary Table 4.4. These environmental drivers were significantly correlated to solar time based on a circular-linear correlation analysis (Supplementary Table 4.5). We show the daily cycle of the wind speed, water temperature, oxygen saturation, and the GHG fluxes of the Cubillas reservoir in Figure 4.3 and of the Iznájar reservoir in Figure 4.4. We also show the results of the linear regressions between these environmental drivers and the GHG fluxes in Table 4.1.

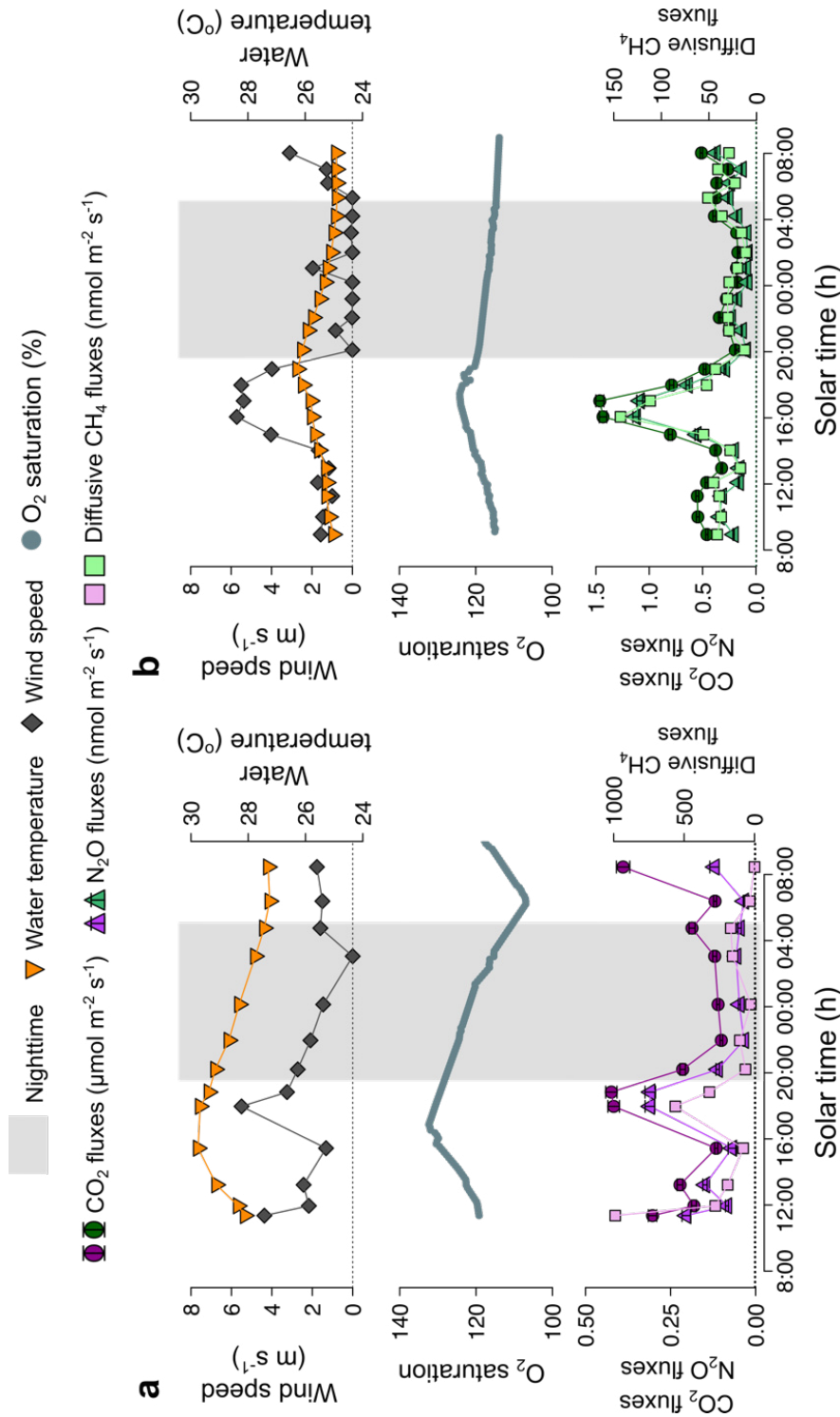


Figure 4.3. Wind speed, water temperature, and oxygen saturation as drivers for the variability of GHG fluxes at daily scales in Cubillas reservoir. We show the drivers in the upper part of the Figures and the GHG fluxes in the lower part, in relation to the solar time (x-axis) 2016 (a), 2018 (b). The shaded areas stand for the nighttime. Note the different scales.

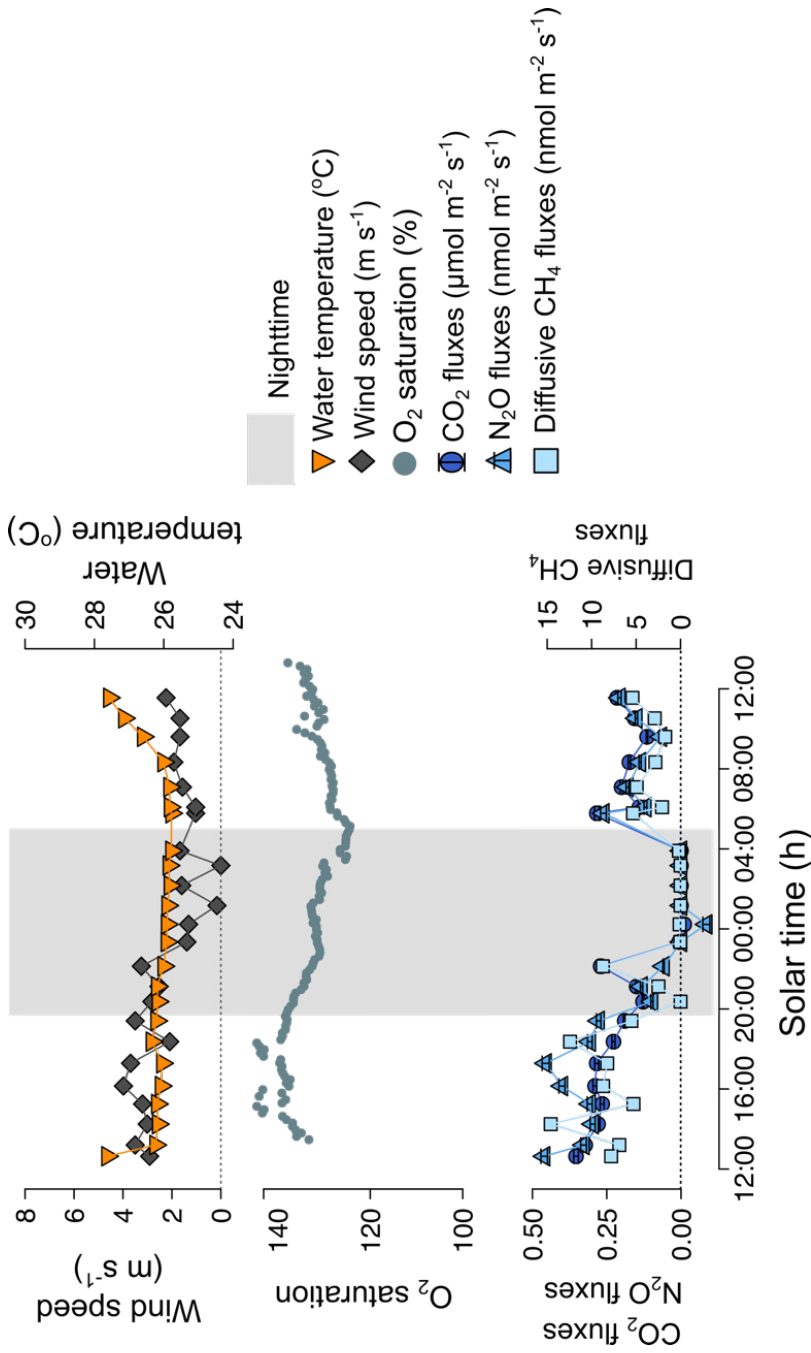


Figure 4.4. Wind speed, water temperature, and oxygen saturation as drivers for the variability of GHG fluxes at daily scales in Iznájar reservoir. We show the drivers in the upper part of the Figures and the GHG fluxes in the lower part, in relation to the solar time (x-axis) 2018. The shaded areas stand for the nighttime. Note the different scales.

Wind speed varied from 0.0 to 5.5 m s⁻¹ in Cubillas 2016, from 0.0 to 5.7 m s⁻¹ in Cubillas 2018, and from 0.0 to 4.0 m s⁻¹ in Iznájar 2018. The water temperature ranged from 27.3 to 29.8 °C in Cubillas 2016, from 25.0 to 26.9 °C in Cubillas 2018, and from 25.0 to 28.8 °C in Iznájar 2018 (Supplementary Table 4.4). Wind speed was the main driver of the CO₂, N₂O, and diffusive CH₄ fluxes in the Cubillas reservoir (2016 and 2018), and the maximum emissions coincided with the maximum wind speeds (Figure 4.3, Table 4.1). We found that the water temperature showed a slightly better relationship to the CO₂, N₂O, and diffusive CH₄ fluxes than the wind speed in the Iznájar reservoir in 2018 (Figure 4.4, and Table 4.1). Wind speed in the Cubillas reservoir was higher than in the Iznájar reservoir. In contrast, we detected a higher variability in the water temperature in the Iznájar reservoir than in the Cubillas reservoir.

The oxygen saturation (%) also showed a daily cycle presumably determined by the photosynthesis and respiration activity. This variable changed in the Cubillas reservoir from 107 to 132 % in 2016 and from 114 to 125 % in 2018. In the Iznájar reservoir in 2018 changed from 124 to 141 % (Figures 4.3 and 4.4, and Supplementary Table 4.4). The maximum values for the oxygen saturation in the three daily cycles were closed to the maximum values for the emissions (Figures 4.3 and 4.4). We found that the oxygen saturation was positively related to the fluxes in most cases, with the fits more significant for the N₂O fluxes (Table 4.1). We did not find any significant relationship with the ebullitive component of CH₄ emission, only a marginally significant relationship to the water temperature in Cubillas 2016. In the linear regression models reported in Table 4.1, we detected that the slopes (estimate ± std. error) that explained the effect of the wind speed, the water temperature, and the oxygen saturation were similar for the same 24-hour cycle for the CO₂ and the N₂O fluxes. In contrast, the slopes for the diffusive CH₄ emissions were different from the CO₂ and N₂O (Table 4.1).

Table 4.1. Results of the linear regressions between wind speed (m s^{-1}), water temperature (water temp., $^{\circ}\text{C}$), or oxygen saturation (oxygen sat, %), and the GHG fluxes. CO_2 emissions are provided in $\mu\text{mol m}^{-2} \text{s}^{-1}$, and N_2O and CH_4 are provided in $\text{nmol m}^{-2} \text{s}^{-1}$.

Sampling	GHG flux (y)	Driver (x)	n	Equation (estimate \pm std. error)	Adj R^2	p-value
Cubillas 2016	CO_2 emissions	Wind speed	13	$y = 0.08 (\pm 0.05) + 0.06 (\pm 0.02) x$	0.46	< 0.01
Cubillas 2018			24	$y = 0.20 (\pm 0.05) + 0.16 (\pm 0.02) x$	0.70	< 0.001
Iznájar 2018			24	$y = 0.00 (\pm 0.04) + 0.08 (\pm 0.02) x$	0.49	< 0.001
Cubillas 2016	CO_2 emissions	Water temp.	13	not significant		0.548
Cubillas 2018			24	$y = -8.41 (\pm 2.52) + 0.35 (\pm 0.10) x$	0.33	< 0.01
Iznájar 2018			24	$y = -1.79 (\pm 0.37) + 0.07 (\pm 0.01) x$	0.54	< 0.001
Cubillas 2016	CO_2 emissions	Oxygen sat.	13	not significant		0.354
Cubillas 2018			24	$y = -8.90 (\pm 2.04) + 0.08 (\pm 0.02) x$	0.47	< 0.001
Iznájar 2018			24	$y = -1.84 (\pm 0.66) + 0.02 (\pm 0.00) x$	0.26	< 0.01
Cubillas 2016	N_2O emissions	Wind speed	13	$y = -0.01 (\pm 0.03) + 0.06 (\pm 0.01) x$	0.65	< 0.001
Cubillas 2018			24	$y = 0.08 (\pm 0.04) + 0.13 (\pm 0.02) x$	0.71	< 0.001
Iznájar 2018			24	$y = -0.04 (\pm 0.05) + 0.10 (\pm 0.02) x$	0.46	< 0.001
Cubillas 2016	N_2O emissions	Water temp.	13	marginally significant		0.082
Cubillas 2018			24	$y = -7.37 (\pm 2.02) + 0.30 (\pm 0.08) x$	0.37	< 0.001
Iznájar 2018			24	$y = -2.59 (\pm 0.45) + 0.10 (\pm 0.02) x$	0.61	< 0.001
Cubillas 2016	N_2O emissions	Oxygen sat.	13	$y = -0.76 (\pm 0.40) + 0.01 (\pm 0.00) x$	0.25	< 0.05
Cubillas 2018			24	$y = -7.45 (\pm 1.67) + 0.07 (\pm 0.01) x$	0.47	< 0.001
Iznájar 2018			24	$y = -3.12 (\pm 0.78) + 0.02 (\pm 0.01) x$	0.42	< 0.001
Cubillas 2016	Diffusive CH_4 emissions	Wind speed	13	$y = -107.09 (\pm 105.10) + 144.65 (\pm 39.06) x$	0.51	< 0.01
Cubillas 2018			24	$y = 20.18 (\pm 5.76) + 11.68 (\pm 2.27) x$	0.53	< 0.001
Iznájar 2018			24	$y = -0.68 (\pm 1.53) + 2.37 (\pm 0.64) x$	0.36	< 0.01
Cubillas 2016	Diffusive CH_4 emissions	Water temp.	13	not significant		0.617
Cubillas 2018			24	$y = -702.92 (\pm 219.97) + 28.95 (\pm 8.57) x$	0.31	< 0.01
Iznájar 2018			24	$y = -57.08 (\pm 14.78) + 2.31 (\pm 0.56) x$	0.42	< 0.001
Cubillas 2016	Diffusive CH_4 emissions	Oxygen sat.	13	not significant		0.478
Cubillas 2018			24	$y = -674.19 (\pm 192.96) + 6.07 (\pm 1.64) x$	0.36	< 0.01
Iznájar 2018			24	$y = -76.74 (\pm 21.87) + 0.61 (\pm 0.16) x$	0.36	< 0.01

4. 3. 3. GHG photoproduction

We performed two experiments to measure CO₂ photoproduction quantifying the increase in the concentration of dissolved inorganic carbon (DIC) and the decrease of chromophoric dissolved organic matter (CDOM) after sunlight exposure (i.e., photobleaching). Figure 4.5 shows the sunlight effect (UV-VIS transparent vs. dark control treatment) on the DIC concentration and CDOM. The statistical results are shown in Supplementary Table 4.6. The DIC photoproduction rate ($R_{\text{DIC-Area}}$ in Supplementary Table 4.7) was $0.74 \pm 0.31 \text{ mmol-C m}^{-2} \text{ d}^{-1}$ for the incubation t_1 , and $0.17 \pm 0.03 \text{ mmol-C m}^{-2} \text{ d}^{-1}$ for the incubation t_2 . These DIC photoproduction rates represented the 1 - 4 % per day of the initial DIC pool (Supplementary Table 4.7). Concerning photobleaching, we found a significant decrease in the absorption coefficients at 325 nm (a_{325}) in the UV-VIS treatment in both reservoirs (Figure 4.5 c and d). Besides, in Iznájar the incubation time had a significant effect on the a_{325} ; the more prolonged the incubation, the higher the photobleaching at 325 nm was. The spectral slope from 275 nm to 295 nm ($S_{275-295}$) increased significantly over the sunlight incubation in both experiments (Figure 4.5 e and f), whereas the spectral slope from 350 nm to 400 nm ($S_{350-400}$) decreased in both reservoirs (Supplementary Table 4.6). The spectral slope ratios (S_R), a surrogate of the molecular mean size of CDOM, also showed a significant increase in the UV-VIS treatment in both reservoirs (Supplementary Table 4.6), suggesting a reduction in the mean size of CDOM molecules.

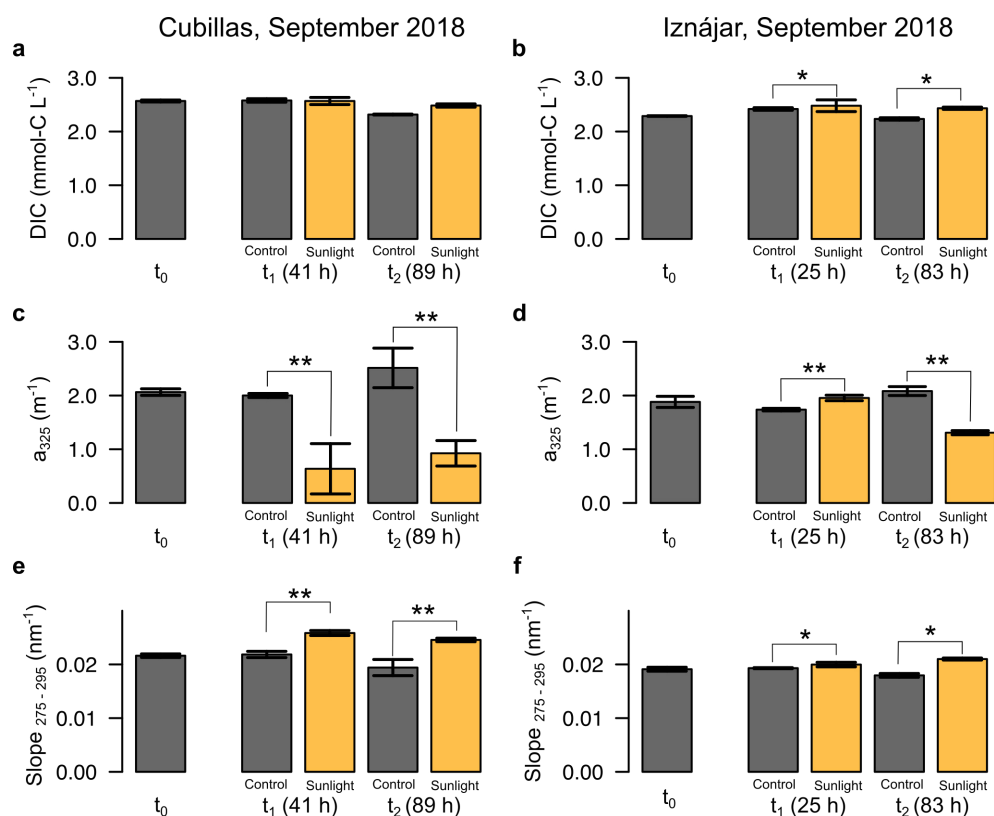


Figure 4.5. Results of the experiment on the sunlight effect on DIC concentration and CDOM characteristics. We show the DIC concentration (a, b), the a_{325} (c, d) and the spectral slope 275 - 295 (e, f) for the CDOM analysis during the incubation experiments in Cubillas (a, c, e) and Iznájar reservoir (b, d, f). The mean value \pm standard error is shown for each treatment (t_0 , t_1 , t_2 and their dark controls). The significant effect of the light treatment was included in each experiment: * stands for p-value < 0.05; ** stands for p-value < 0.01. More statistical details are provided in Supplementary Table 4.6. The production rates are provided in Supplementary Table 4.7.

In Figure 4.6, we show the results of the sunlight effect on N_2O and CH_4 photoproduction, and in Supplementary Table 4.6, we show the statistical analysis. We found a significant increase in the N_2O concentration in the UV-VIS treatment in the three experiments (Figure 4.6a, b, and c). Furthermore, the more prolonged the UV-VIS exposition, the larger the increases in the N_2O concentrations were (Supplementary Table 4.6). The N_2O photoproduction rates ($R_{N_2O-Area}$) were $18.5 \pm 4.0 \text{ nmol m}^{-2} \text{ d}^{-1}$ for the incubation t_1 , and $16.7 \pm 1.7 \text{ nmol m}^{-2} \text{ d}^{-1}$ for the incubation t_2 in the experiment performed in the Cubillas reservoir in June. The rates in the Cubillas reservoir in September were $168.1 \pm 91.7 \text{ nmol m}^{-2} \text{ d}^{-1}$ for the incubation t_1 , and $335.4 \pm 7.8 \text{ nmol m}^{-2} \text{ d}^{-1}$ for the incubation t_2 . In September, the rates in Iznájar were $126.7 \pm 13.9 \text{ nmol m}^{-2} \text{ d}^{-1}$ for the incubation t_1 , and $224.5 \pm 120.1 \text{ nmol m}^{-2} \text{ d}^{-1}$

for the incubation t_2 (Supplementary Table 4.8). The N_2O produced per day in the first experiment of June in the Cubillas reservoir accounted for 4 % of the initial N_2O pool, whereas this value increased up to 19 - 39 % per day in the Cubillas reservoir in September. The N_2O produced per day accounted for 15 - 26 % in the experiment of the Iznájar reservoir in September (Supplementary Table 4.8). The initial N_2O concentration was higher in September in both reservoirs (i.e., 84.6 nmol L^{-1} in Cubillas, and 83.4 nmol L^{-1} in Iznájar) than in June in Cubillas (i.e., 33.0 nmol L^{-1}) (Supplementary Table 4.4). We did not find significant changes in the dissolved CH_4 concentration due to the direct effect of solar radiation.

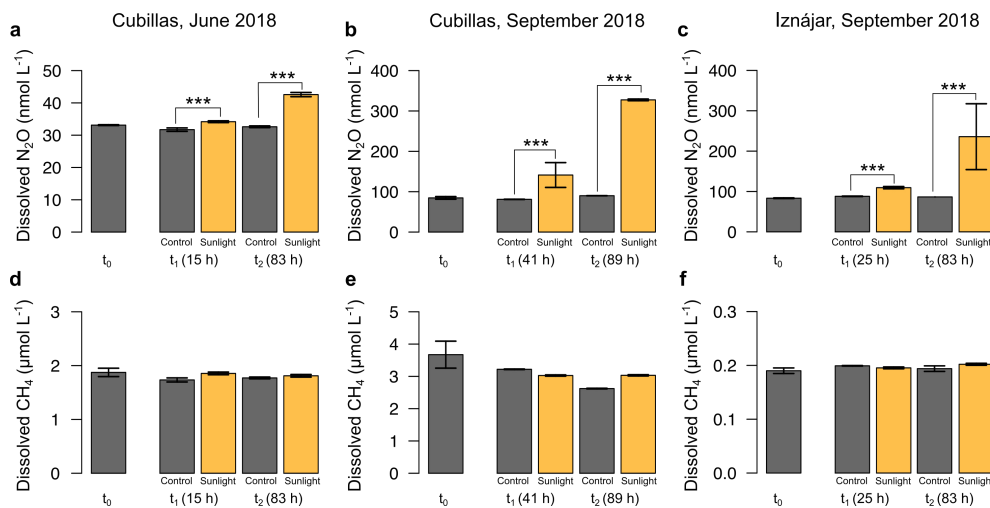


Figure 4.6. Results of the experiment on the sunlight effect on N_2O and CH_4 production. We show the dissolved N_2O concentration (a, b, c) and the dissolved CH_4 concentration (d, e, f) in the incubation experiments in Cubillas in June (a, d), in Cubillas in September (b, e), and Iznájar reservoir in September (c, f). The mean value \pm standard error is shown for each treatment (t_0 , t_1 , t_2 , and their dark controls). The significant effect of the light treatment was included for each experiment: *** stands for p -value < 0.001 . More statistical details are provided in Supplementary Table 4.6. The production rates are provided in Supplementary Table 4.8.

4. 4. Discussion

Daily and interannual variability

Our data reveal that the daily variability is a relevant component of the variability in the GHG fluxes of a system. In Table 4.2, we compared the variability detected inter-seasons (mixing vs. stratification) in Cubillas and Iznájar reservoirs (León-Palmero *et al.*, 2020a), and the daily variability reported in these two reservoirs in this study. Daily emissions varied up to one order of magnitude for

CO₂, two orders of magnitude for N₂O, and three orders of magnitude for CH₄ (Table 4.2). We found that the daily variability in CO₂ and N₂O fluxes were higher than the inter-season variability (León-Palmero *et al.*, 2020a) (Table 4.2). We found that variability in the total CH₄ emissions was higher inter-seasons than at a daily scale in the Cubillas reservoir, but we found the opposite in Iznájar (Table 4.2). The total CH₄ emissions showed the highest variability inter seasons in the reservoir Cubillas, reaching up to two orders of magnitude in Cubillas 2016 (Table 4.2).

Table 4.2. Variability detected in Cubillas and Iznájar reservoirs at seasonal (winter - summer) and at daily scales. Seasonal values corresponded to the winter (minimum) and summer (maximum) fluxes, and they were reported in León-Palmero *et al.* (2020a).

	Inter-season variability	Daily variability
CO ₂ ($\mu\text{mol m}^{-2} \text{s}^{-1}$)	Cubillas: 0.12 - 0.24 Iznájar: 0.12 - 0.16	Cubillas 2016: 0.10 - 0.42 Cubillas 2018: 0.17 - 1.46 Iznájar: -0.01 - 0.35
N ₂ O ($\text{nmol m}^{-2} \text{s}^{-1}$)	Cubillas: 0.06 - 0.15 Iznájar: 0.13 - 1.49	Cubillas 2016: 0.03 - 0.31 Cubillas 2018: 0.08 - 1.13 Iznájar: -0.09 - 0.46
CH ₄ ($\text{nmol m}^{-2} \text{s}^{-1}$, total emissions)	Cubillas: 4.25 - 654.16 Iznájar: 1.24 - 19.06	Cubillas 2016: 150.51 - 1815.32 Cubillas 2018: 26.98 - 257.80 Iznájar: 0.00 - 35.80

The few studies have focused on the daily variability of the GHG emissions in reservoirs and lakes are summarized in Table 4.3. We also included data from rivers, wetlands, and soils, due to the lack of data in lakes and reservoirs. Previous studies found a similar variability of the CO₂ fluxes at daily scales in a deep reservoir and lakes (Xiao *et al.*, 2013; Martínez-Cruz *et al.*, 2020), but a higher variability of the CO₂ fluxes in systems shallower than the study reservoirs (Podgrajsek *et al.*, 2015; Rey-Sánchez *et al.*, 2018) (Table 4.3). In rivers and soils, the daily variability of the N₂O fluxes was up to one order of magnitude (Du *et al.*, 2006; Clough *et al.*, 2007; Yang *et al.*, 2011; Yan *et al.*, 2012) (Table 4.3). Concerning the variability of the CH₄ emissions, it was up to one order of magnitude in reservoirs and lakes (Bastviken *et al.*, 2010; Xiao *et al.*, 2013; Martínez-Cruz *et al.*, 2020), increasing this variability range in the shallow systems (Podgrajsek *et al.*, 2014; Rey-Sánchez *et al.*, 2018) (Table 4.3).

Table 4.3. Summary Table of published studies on the variability of CO₂, N₂O, and CH₄ fluxes at daily scales in different ecosystems and using different methods. We classified these methods in direct measurement, by eddy covariance technique (EC); closed/floating chamber (FC) and bubble traps for ebullitive fluxes (BT); and the indirect method that predicted the fluxes (PF) based on gas transfer velocities (k). The transfer velocities are traditionally based on wind-speed, as k_{CC} (Cole and Caraco, 1998) and k_{CW} for low wind speeds (Crusius and Wanninkhof, 2003). Other gas transfer velocities also include the effects of water-side cooling to the gas transfer besides shear-induced turbulence, as k_{HE} (Heiskanen *et al.*, 2014) and k_{TE} (Tedford *et al.*, 2014). Other authors preferred an empirical model for k, derived from laboratory experiments. We provided the daytime and nighttime mean (value ± standard error); or the range of variation (minimum - maximum). We provided the daily values when the data for daytime/nighttime are not supplied in the reference study. The results of this study are included in the Table as C1 (Cubillas 2016), C2 (Cubillas 2018), and Iz (Iznájar 2018).

GHG	Ecosystem, mean depth, and state	Method	Daytime flux	Nighttime flux	Study
CO ₂ ($\mu\text{mol m}^{-2} \text{s}^{-1}$)	Reservoir (70 - 130 m)	Direct: FC	August: 0.74 - 2.71 October: 0.27 - 1.46 February: 0.12 - 0.53 April: 0.14 - 1.74		Xiao <i>et al.</i> (2013)
	Reservoir (5 m, 1 year period)	Direct: EC	0.23	0.39	Liu <i>et al.</i> (2016)
	Reservoir (littoral zone)	Direct: FC	0.06 ± 0.04	0.13 ± 0.05	Lin <i>et al.</i> (2019)
	Lake (1.3 m, 2 years period)	Direct: EC	-0.78 - 1.62 Higher fluxes at nighttime		Podgrajsek <i>et al.</i> (2015)
	Lake (8 m, several seasons)	Direct: EC	0.35	0.31	Czikowsky <i>et al.</i> (2018)
		Indirect: PF (k _{TE} or k _{CC})	k _{TE} : 0.31 k _{CC} : 0.28	k _{TE} : 0.23 k _{CC} : 0.23	
	Lake (6.3 m, stratified)	Direct: EC and FC	EC: 0.31 ± 0.04 FC: 0.62 ± 0.80	EC: 0.28 ± 0.08 FC: 0.29 ± 0.04	Erkkilä <i>et al.</i> (2018)
		Indirect: PF	k _{HE} : 0.305 ± 0.009 k _{TE} : 0.545 ± 0.014 k _{CC} : 0.201 ± 0.004	k _{HE} : 0.410 ± 0.008 k _{TE} : 0.396 ± 0.010 k _{CC} : 0.180 ± 0.004	
	Lake (6.3 m, mixed)	Direct: EC	1.3 ± 0.2	0.88 ± 0.14	
		Indirect: PF (k _{HE} , k _{TE} or k _{CC})	k _{HE} : 2.15 ± 0.06 k _{TE} : 2.37 ± 0.06 k _{CC} : 1.11 ± 0.04	k _{HE} : 1.43 ± 0.05 k _{TE} : 1.54 ± 0.05 k _{CC} : 0.58 ± 0.02	
	Lakes (stratified): Dagow (6 m, oligo-mesotrophic), Stechlin (21 m, eutrophic)	Direct: FC	Dw: 0.03 - 0.13 Higher daytime fluxes St: - 0.10 - (- 0.04) No differences found		Martinez-Cruz <i>et al.</i> (2020)
Wetland (0.5 m)	Direct: EC	- 3.58	3.24	Rey-Sanchez <i>et al.</i> (2018)	
Reservoirs (stratified):	Direct: FC	C1: 0.12 - 0.42 C2: 0.26 - 1.46	C1: 0.10 - 0.21 C2: 0.17 - 0.39	This study	

	C1 (7.0 m), C2, (8.9 m), and Iz (22.4 m)		Iz: 0.11 - 0.35	Iz: -0.01 - 0.27		
N ₂ O (nmol m ⁻² s ⁻¹)	River (0.01 - 0.15 m)	Indirect: PF	Daily mean: 5.96 Mean at daytime : 9.69		Harrison <i>et al.</i> (2005)	
	River (1.2 m)	Direct: FC Indirect: PF	FC: 0.52 - 1.39 PF: 0.13 - 0.25 Higher fluxes at daytime		Clough <i>et al.</i> (2007)	
	Rivers (FLR, HBR, NFR)	Direct: FC	FLR: 0.05 - 0.10 HBR: 0.04 - 0.11 NFR: 0.45 - 0.94	FLR: 0.05 - 0.06 HBR: 0.08 - 0.09 NFR: 0.70 - 1.03	Yang <i>et al.</i> (2011)	
	10 Streams (0.10 - 0.60 m)	Indirect: PF	0.94	0.86	Baulch <i>et al.</i> (2012)	
	River (23 sites, < 1 m)	Indirect: PF	Higher fluxes at nighttime, numbers not provided		Rosamond <i>et al.</i> (2012)	
	River (3 sites, 13 - 19 m)	Indirect: PF	Daily mean S1: 0.08 - 0.25 Daily mean S2: 0.02 - 0.35 Daily mean S3: 0.08- 0.40 Peak of emission at daytime		Yan <i>et al.</i> (2012)	
	River (2.5 m)	Direct: FC	0.41 - 0.87		Xia <i>et al.</i> (2013)	
			0.61	0.50		
		Grassland soil (0.15 m, different season)	Direct: FC	June: 0.01 - 0.11 July: 0.05 - 0.62 August: 0.03 - 0.11 September: 0.00 - 0.03 Peaks of emission at daytime		Du <i>et al.</i> (2006)
		Soil Mesocosms	Direct: FC	Treatments presented different daily means and ranges, but all treatments had higher fluxes at daytime		Xu <i>et al.</i> (2016)
	Reservoirs (stratified): C1 (7.0 m), C2, (8.9 m), and Iz (22.4 m)	Direct: FC	C1: 0.03 - 0.31 C2: 0.13 - 1.13 Iz: 0.07 - 0.47	C1: 0.03 - 0.11 C2: 0.08 - 0.24 Iz: -0.09 - 0.28	This study	
CH ₄ (nmol m ⁻² s ⁻¹)	Reservoir (1 - 10 m)	Direct: FC and BT	FC: 523 ± 479 (4 - 1502) BT: 849 ± 192	FC: 336 ± 442 BT: 260 ± 77	Keller and Stallard (1994)	
	Reservoir (70 - 130 m)	Direct: FC	August: 0.5 - 2.1 October: 0.2 - 2.3 February: 0.0 - 0.5 April: 0.2 - 5.5		Xiao <i>et al.</i> (2013)	
	73 Lakes	Direct: FC	9 - 158 % greater emissions during the day		Bastviken <i>et al.</i> (2004)	
	16 Lakes (0.5 - 3.4 m)	Direct: FC	The daily means ranged from 45 - 859 Daytime fluxes were significantly higher		Bastviken <i>et al.</i> (2010)	
	Lake (1.3 m)	Direct: EC	0 - 300 Highest values during night and early morning		Podgrajsek <i>et al.</i> (2014)	

Lake (6.3 m, stratified)	Direct: EC and FC	EC: 0.41 ± 0.04 FC: 2.4 ± 0.3	EC: 0.34 ± 0.04 FC: 1.1 ± 0.2	Erkkilä <i>et al.</i> (2018)
	Indirect: PF (k_{HE} , k_{TE} or k_{CC})	k_{HE} : 0.177 ± 0.005 k_{TE} : 0.370 ± 0.011 k_{CC} : 0.128 ± 0.003	k_{HE} : 0.431 ± 0.008 k_{TE} : 0.439 ± 0.007 k_{CC} : 0.186 ± 0.004	
Lake (6.3 m, mixed)	Direct: EC	5.9 ± 0.3	5.0 ± 0.4	
	Indirect: PF (k_{HE} , k_{TE} or k_{CC})	k_{HE} : 7.1 ± 0.6 k_{TE} : 7.7 ± 0.6 k_{CC} : 3.7 ± 0.3	k_{HE} : 6.6 ± 0.5 k_{TE} : 7.1 ± 0.5 k_{CC} : 2.8 ± 0.2	
Lakes (stratified): Dagow (6 m, oligo- mesotrophic), Stechlin (21 m, eutrophic)	Direct: FC	D: 7.7 - 49.3 S: 0.7 - 1.5 No differences found between daytime fluxes and nighttime fluxes		Martinez-Cruz <i>et al.</i> (2020)
4 lakes ($<0.5 - 8$ m)	Direct: FC	Higher emissions at daytime than at nighttime		Sieczko <i>et al.</i> (2020)
Wetland: bog (0.2 m)	Direct: EC	15.0 ± 18.7	6.9 ± 6.2	Edwards <i>et al.</i> (1994)
Wetland (0.16 - 0.32 m)	Indirect: PF	126 ± 21	75 ± 11	Poindexter <i>et al.</i> (2016)
Wetland (0.5 m)	Direct: EC	30 - 1600 Peak of emission at daytime		Rey-Sanchez <i>et al.</i> (2018)
Pond (1.45 m)	Direct: FC	Diffusive: 3.1 Ebullitive: 8.1	Diffusive: 3.1 Ebullitive: 5.0	Zhang <i>et al.</i> (2019)
Reservoirs (stratified): C1 (7.0 m), C2, (8.9 m), and Iz (22.4 m)	Direct: FC	Diffusive fluxes C1: 0 - 989 C2: 17 - 143 Iz: 2 - 15 Ebullitive fluxes C1: 0 - 1815 C2: 1 - 207 Iz: 0 - 21	Diffusive fluxes C1: 27 - 169 C2: 11 - 36 Iz: 0 - 9 Ebullitive fluxes C1: 133 - 920 C2: 16 - 97 Iz: 0 - 27	This study

The daily patterns of the CO_2 , N_2O , and diffusive CH_4 fluxes were recurrent, despite the flux magnitudes between years and reservoirs. However, ebullitive fluxes, which are a relevant fraction of total CH_4 emissions, did not show the same pattern. These differences in the magnitude of the fluxes in the Cubillas reservoir in 2016 and 2018 are similar to the differences detected in the DIC, N_2O , and CH_4 concentration in the surface waters (Supplementary Table 4.4). In the study reservoirs, the DIC and N_2O concentrations depended on the carbonates and nitrogen inputs from their watersheds (León-Palmero *et al.*, 2020a). The year 2018 was wetter than 2016, involving a higher runoff and DIC and nitrogen inputs into the reservoir. The higher concentration of dissolved inorganic carbon in 2018 than in 2016 (i.e., $2.48 \text{ mmol-C L}^{-1}$ in 2016, and $2.86 \text{ mmol-C L}^{-1}$ in 2018; Supplementary

Table 4.4), could produce the higher concentration and fluxes of CO₂ in 2018 than in 2016. The higher concentration of nitrate in 2018 than in 2016 (i.e., 42.2 μmol-N L⁻¹ in 2016, and 375.5 μmol-N L⁻¹ in 2018; Supplementary Table 4.4), could determine the higher concentration of N₂O (i.e., 17.4 nmol L⁻¹ in 2016, and 33.0 nmol L⁻¹ in 2018; Supplementary Table 4.4), and the higher fluxes of N₂O (León-Palmero *et al.*, 2020a). In contrast, the CH₄ fluxes were an order of magnitude higher in 2016 than in 2018, reflecting the differences in the CH₄ concentration in surface waters (i.e., 8.87 μmol L⁻¹ in 2016, and 1.80 μmol L⁻¹ in 2018; Supplementary Table 4.4). In the year 2016, Cubillas had warmer and shallower waters, and a higher concentration of Chl-*a* than in 2018 (Supplementary Table 4.4), and that could explain the higher concentration and emission of CH₄ in the year 2016 than in 2018. Previous studies showed that the concentration and emission of CH₄ are related to the concentration of Chl-*a*, the mean depth of the system, and the water temperature (Keller and Stallard, 1994; Marotta *et al.*, 2014; West *et al.*, 2016; Aben *et al.*, 2017; León-Palmero *et al.*, 2020a, 2020b). In addition, the lower mean depth in 2016 than in 2018 also promoted the ebullition of CH₄, because of the reduction in the hydrostatic pressure in the water column (Harrison *et al.*, 2017; Beaulieu *et al.*, 2018). Keller and Stallard (1994) also described higher ebullitive fluxes of CH₄ in the shallow sites of their study lake compared to the deep sites.

The synchrony of the fluxes and environmental drivers

The three diffusive fluxes showed evident daily synchrony among them with higher fluxes at daytime than at nighttime coupled to the environmental drivers. This synchrony arises from extrinsic forces acting outside the system, which drives the GHG emissions and/or production. GHG fluxes were strongly correlated among them, especially the CO₂ and N₂O fluxes (Supplementary Table 4.3). In addition, the CO₂, N₂O, and diffusive CH₄ fluxes were significantly related to the solar time, except for the CO₂ and diffusive CH₄ fluxes in the Cubillas reservoir in 2016. We think that the lower number of measurements in 2016 (*n* = 13) than in 2018 (*n* = 24) could have caused the absence of statistically significant results (Supplementary Table 4.2). The fluxes of N₂O were always significantly related to solar time. The environmental drivers (i.e., wind speed, water and air temperature, and dissolved

oxygen saturation) were also significantly related to the solar time (Supplementary Table 4.5).

Drivers of the CO₂, N₂O and CH₄ fluxes

Environmental drivers can increase the GHG emissions by producing turbulence and changing gas solubility (i.e., wind and temperature), while other drivers act increasing directly on the GHG production in surface waters. Water temperature, besides changing gas solubility, also regulates microbial metabolism, and determines the biological GHG production. Solar radiation promotes photosynthesis and the abiotic GHG photoproduction.

We found that the wind speed was the main driver of CO₂, N₂O, and diffusive CH₄ daily fluxes in Cubillas, while the water temperature was the main driver in Iznájar. We detected a higher range of wind speed in Cubillas (2016 and 2018) than in Iznájar, and a higher range of variation in the water temperature in Iznájar than in Cubillas. These differences in the variation range of the environmental drivers may explain the differences between the corresponding drivers of the GHG fluxes in these two reservoirs. It is noteworthy that the wind speed affected with similar intensity to CO₂ and N₂O emissions, as suggested by the fact that the slopes of these relationships were similar (Table 4.1). The slope for the diffusive fluxes of CH₄ was variable between years and reservoirs (Table 4.1). In contrast, ebullitive CH₄ fluxes did not show a clear relationship to the environmental drivers considered in this study.

The higher CO₂ emissions during the daytime than during the nighttime are counterintuitive, considering that photosynthesis (i.e., CO₂ uptake) occurs in the daytime. Previous works found larger CO₂ emissions at nighttime in shallow systems disturbed by high winds and convective processes (Podgrajsek *et al.*, 2015; Liu *et al.*, 2016; Rey-Sanchez *et al.*, 2018). However, studies performed in deep systems found higher CO₂ emissions at daytime than nighttime (Czikowsky *et al.*, 2018; Erkkilä *et al.*, 2018; Martinez-Cruz *et al.*, 2020). Czikowsky *et al.* (2018) found that CO₂ emissions at daytime were 35 % higher than at nighttime using eddy covariance and diffusion models (Table 4.3). Erkkilä *et al.* (2018) also found higher CO₂ emissions during the day than during the night using a floating chamber in a stratified lake. They obtained different results using diffusion models, depending on the gas transfer velocity used (*k*) (Table 4.3). Martinez-Cruz *et al.* (2020) found

significant differences in the CO₂ emission in a eutrophic lake, but they did not find significant differences in an oligo-mesotrophic one (Table 4.3). In addition, other processes occurring at daytime, such as direct CO₂ photoproduction and indirect promotion of bacterial mineralization throughout photobleaching, can increase the surface concentration of CO₂ and could explain, to some extent, the higher CO₂ emissions at daytime (Allard *et al.*, 1994; Bertilsson and Tranvik, 1998; Reche *et al.*, 1998; Bertilsson and Tranvik, 2000; Johannessen and Miller, 2001; Ortega-Retuerta *et al.*, 2007; Koehler *et al.*, 2014).

The N₂O emissions were also higher during the daytime than at nighttime. We did not find studies on N₂O fluxes at daily scales in lakes or reservoirs, although we found studies in rivers and soils, which we compiled in Table 4.3. These previous studies also reported higher N₂O emissions at daytime in rivers (Harrison *et al.*, 2005; Clough *et al.*, 2007; Yang *et al.*, 2011; Baulch *et al.*, 2012; Yan *et al.*, 2012; Xia *et al.*, 2013), and in soils (Du *et al.*, 2006; Xu *et al.*, 2016) (Table 4.3). In the study reservoirs, the daily pattern in the N₂O emissions was driven by wind speed, water temperature, and oxygen saturation. In rivers, Yan *et al.* (2012) also found a strong correlation between the N₂O emissions and the wind speed, whereas Xia *et al.* (2013) determined that the temperature and the dissolved oxygen were the environmental factors controlling N₂O fluxes. Water temperature was also significantly related to N₂O fluxes in Yang *et al.* (2011). The daily changes in the dissolved oxygen can affect microbial nitrogen processing rates during the nitrification and coupled nitrification-denitrification (Lorenzen *et al.*, 1998; Laursen and Seitzinger, 2004; Baulch *et al.*, 2012). In this study, we demonstrated that solar radiation induced N₂O production in abiotic conditions. This fact can also contribute to the daily pattern of N₂O emission, as we explain more extensively below.

We also detected higher emissions of diffusive CH₄ in the daytime than at nighttime. Previous studies found similar results in stratified and mixed lakes (Bastviken *et al.*, 2004; Erkkilä *et al.*, 2018), and in a savannah floodplain (Bastviken *et al.*, 2010). In contrast, Martinez-Cruz *et al.* (2020) did not detect differences in the CH₄ emissions at the daily scale (Table 4.3). Erkkilä *et al.* (2018) observed that wind speed was higher during the daytime causing more effective turbulent transfer, especially during the mixing period. In very shallow lakes and wetlands, the higher wind-induced turbulence at daytime increases the emissions of diffusive CH₄

(Edwards *et al.*, 1994; Bastviken *et al.*, 2010; Poindexter *et al.*, 2016). However, the opposite trend was also found in the shallow systems affected by convective mixing at nighttime, which brought CH₄ rich waters from deep layers to the surface waters (Godwin *et al.*, 2013; Podgrajsek *et al.*, 2014). Besides, microbial CH₄ production in sediments is temperature-dependent (Yvon-Durocher *et al.*, 2014). Therefore, the daily changes in air and water temperature can determine a daily CH₄ production pattern. In fact, Zhang *et al.* (2019) detected that daily changes in air and water temperature were positively correlated to daily changes in the diffusive CH₄ emissions in a eutrophic pond.

On the other hand, in the case of the CH₄ ebullitive emissions, we did not find a clear daily pattern. These emissions were not correlated to the other GHG emissions either to the environmental variables considered in this study. Unlike our results, Keller and Stallard (1994) and Zhang *et al.* (2019) measured higher ebullitive fluxes in the daytime. Keller and Stallard (1994) found that the higher winds during the day and the associated water movements appeared to promote CH₄ bubbling. Ebullitive emissions can represent a relevant fraction of total CH₄ emissions (Keller and Stallard, 1994; Bastviken *et al.*, 2010; Zhang *et al.*, 2019). For this reason, to determine the environmental factors that control these ebullition events is challenging and needs further studies.

GHG photoproduction depends directly on solar radiation. Therefore, it could affect the daily pattern by increasing CO₂, N₂O, and CH₄ concentrations in surface waters in the daytime. Moreover, by acting on surface waters, this production could affect GHG emissions more directly than other processes, which occur at deep layers in the water column. The photoproduction signature in the daily GHG emissions will depend on the magnitude of this contribution to the total production. In this study, we performed experiments to measure the effect of solar radiation on CO₂, N₂O, and CH₄ production and quantify its contribution to total emissions.

Recent studies found that CDOM photochemical transformation produces CH₄ (Zhang and Xie, 2015) and could account for 20 - 60 % of the open-ocean CH₄ emissions (Li *et al.*, 2020). However, we did not find a significant CH₄ photoproduction in our experiments. Therefore, in the study reservoirs, the higher emissions of diffusive CH₄ at daytime than at nighttime appear to be related to the

biological activity rather than photoproduction. Daily changes in temperature may promote different rates of biological CH₄ production (Yvon-Durocher et al., 2014). Besides, dissolved CH₄ is closely linked to phytoplankton dynamics in lakes and reservoirs (Schmidt and Conrad, 1993; Grossart *et al.*, 2011; Bogard *et al.*, 2014; Tang *et al.*, 2014; Deemer *et al.*, 2016; León-Palmero *et al.*, 2020b). Recently, Bižić *et al.* (2020) described the existence of a daily pattern of CH₄ production associated with the photosynthetic activity in cyanobacteria cultures. In fact, we also found that cyanobacteria abundance was related to dissolved CH₄ in oxic waters of reservoirs (León-Palmero *et al.*, 2020b).

In contrast, we detected CDOM photobleaching in both reservoirs. We found a significant reduction in the a_{325} coefficients in the UV-VIS treatments (Figure 4.5). Spectral slopes $S_{275-295}$ and $S_{350-400}$ and the spectral slope ratio (S_R) are related to the DOM molecular weight (Helms *et al.*, 2008). The $S_{275-295}$ and S_R are inversely related to molecular weight of CDOM in water samples. Therefore, in our experiments, sunlight decomposed the CDOM into smaller molecules. Moreover, we obtained a significant increase in DIC concentration in the treatments receiving solar radiation in the Iznájar reservoir, but not in Cubillas experiments. This increase is caused by direct DOM photomineralization since the experiments were in abiotic conditions. Bertilsson and Tranvik (2000) also found that the light-induced decomposition of DOM produced dissolved inorganic carbon and low molecular weight carboxylic acids. The DIC production found in our experiments reached up to $0.74 \text{ mmol-C m}^{-2} \text{ d}^{-1}$, which is similar to the production obtained by Koehler *et al.* (2014) (i.e., $0.87 \text{ mmol-C m}^{-2} \text{ d}^{-1}$). If we compared the DIC photoproduction rate in the September experiment in Iznájar with the mean CO₂ emission measured in July, we obtained that represents at least the 7 % of the CO₂ daytime emission. This calculation is an underestimation because the direct CO₂ photoproduction in July is presumably higher than in September due to higher solar radiation. In addition, in this calculation, we only considered the direct CO₂ photoproduction, but in the natural environment, it is necessary to consider also the CO₂ indirectly produced by the microbial mineralization of the CDOM photoproducts. Vachon *et al.* (2016) determined that on an annual cycle, the DOC photomineralization rates were similar across lakes, averaging $12.1 \text{ mg C m}^{-2} \text{ d}^{-1}$, with a mean contribution of DOC photomineralization to total pelagic CO₂ production of 14 %. Koehler *et al.* (2014)

also calculated that up to 10 % of the global CO₂ emissions from inland waters are sunlight-induced.

In this study, we reported, for the first time, the N₂O photoproduction in aquatic ecosystems. The results were consistent in the three experiments, with maximum rates of 18.5 nmol m⁻² d⁻¹ in Cubillas in June, 335.4 nmol m⁻² d⁻¹ in Cubillas in September, and 224.5 nmol m⁻² d⁻¹ in Iznájar in September (Supplementary Table 4.8). These rates of N₂O photoproduction were lower to those found for N₂O production by denitrification in rivers (Laursen and Seitzinger, 2004; Beaulieu *et al.*, 2011), but higher than the N₂O production by ammonia oxidation or denitrification in the ocean (Ji *et al.*, 2015). The higher emissions of N₂O at daytime is a widespread phenomenon in rivers (Harrison *et al.*, 2005; Clough *et al.*, 2007; Yang *et al.*, 2011; Baulch *et al.*, 2012; Yan *et al.*, 2012; Xia *et al.*, 2013), but daily patterns in emissions are frequently attributed to biological activity. Liu *et al.* (2011) found that the seasonal pattern in N₂O fluxes in Antarctica lakes was positively related to daily radiation, but they attributed this pattern to algal activity.

We detected a net N₂O production in these experiments, but we do not know the chemical mechanism underlying this N₂O photoproduction. We have hypothesized several plausible pathways involved in the abiotic N₂O photoproduction. These pathways are the decomposition of the NH₂OH to N₂O catalyzed by singlet oxygen (¹O₂), superoxide (O₂⁻), or other reactive oxygen species (ROS) associated with oxygen photoionization and nitrate-induced photooxidation, or the NO₂⁻ chemodenitrification catalyzed by the photoreduced Fe²⁺. We show these chemical reactions in Figure 4.7. The decomposition of NH₂OH is a coupled biotic-abiotic reaction that requires the extracellular ammonia-oxidation intermediate NH₂OH and other substrates such as NO₂⁻, MnO₂, and Fe³⁺. This process was confirmed in laboratory experiments and in temperate soils (Heil *et al.*, 2014; Zhu-Barker *et al.*, 2015; Soler-Jofra *et al.*, 2016; Liu *et al.*, 2017). We hypothesize that sunlight may act directly, increasing the rate of decomposition of NH₂OH to N₂O through the production of reactive oxygen species, which are the byproducts of the oxygen photoionization (Figure 4.7a). Interestingly, we detected that the maxima for the oxygen saturation in the three daily cycles were closed to the maxima values for the N₂O emissions, and the oxygen saturation was positively related to the fluxes in most of the cases, with the best results for N₂O fluxes. It is

also known that the nitrate photolysis produces reactive oxygen species that are potent oxidants (Zepp *et al.*, 1987; Mopper and Zhou, 1990).

On the other hand, during the chemodenitrification, the NO_2^- is reduced to N_2O , and this reaction is coupled to the oxidation of metals such as Fe^{2+} (Heil *et al.*, 2014; Zhu-Barker *et al.*, 2015; Wankel *et al.*, 2017; Otte *et al.*, 2019). The sunlight reduction of Fe^{3+} to Fe^{2+} in lakes has been previously demonstrated (Pehkonen *et al.*, 1993; Emmenegger *et al.*, 2001; Song *et al.*, 2005). We suggest that the photoreduced Fe^{2+} can also intervene on the chemodenitrification of NO_2^- to N_2O (Figure 4.7b).

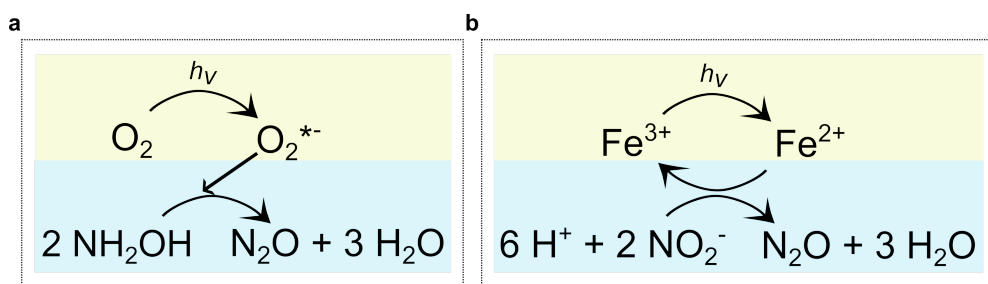


Figure 4.7. Possible mechanisms of photoproduction of N_2O . (a) Decomposition of the NH_2OH to N_2O catalyzed by superoxide, (b) chemodenitrification of NO_2^- to N_2O catalyzed by the photoreduced Fe^{2+} .

Regardless of the ultimate mechanism, N_2O photoproduction represented a relevant contribution to the N_2O pool, reaching up to 39 % of the initial N_2O pool per day. The N_2O photoproduction reported in the June experiment in Cubillas represented 0.1 % of the mean emission at daytime, and represented up to the 2 % of the mean emission of N_2O at daytime in Iznájar (calculated with the rate of photoproduction in Iznájar). Therefore, the N_2O photoproduction may be an essential and overlooked process responsible for a significant part of the N_2O emissions at daily scales in aquatic systems globally, and it should be considered in future works on N_2O production and emissions.

Overall, we show that the daily patterns of GHG emissions are a relevant component of the GHG flux variability. We demonstrated the existence of a similar and consistent pattern in CO_2 , N_2O , and diffusive CH_4 emissions in two eutrophic reservoirs, despite the differences in magnitude among years and reservoirs. Emissions were consistently higher at daytime than at nighttime, and they were significantly related to wind speed, water temperature, and oxygen saturation. GHG photoproduction also contributed to the daily patterns, increasing the

concentration of CO₂ and N₂O in surface waters during the daytime. We found that light catalyzed the N₂O production. The N₂O photoproduction is a relevant process that has been overlooked and can contribute significantly to the global N₂O emissions. Since many aquatic ecosystems are highly impacted with nitrogen inputs from human activities, the N₂O photoproduction may contribute significantly to the GHG budget in ecosystems receiving more UV radiation, as high altitudes, equatorial latitudes and regions with reduced stratospheric ozone concentration.

4. 5. References

- Aben, R. C. H., Barros, N., Donk, E. van, Frenken, T., Hilt, S., Kazanjian, G., Lamers, L. P. M., Peeters, E. T. H. M., Roelofs, J. G. M., Domis, L. N. S., Stephan, S., Velthuis, M., Waal, D. B. V. de, Wik, M., Thornton, B. F., Wilkinson, J., DelSontro, T. and Kosten, S. (2017). Cross continental increase in methane ebullition under climate change, *Nature Communications*, 8(1), p. 1682. doi: 10.1038/s41467-017-01535-y.
- Allard, B., Borén, H., Pettersson, C. and Zhang, G. (1994). Degradation of humic substances by UV irradiation, *Environment International*, 20(1), pp. 97–101. doi: 10.1016/0160-4120(94)90072-8.
- Álvarez-Salgado, X. A. and Miller, A. E. J. (1998). Simultaneous determination of dissolved organic carbon and total dissolved nitrogen in seawater by high temperature catalytic oxidation: conditions for precise shipboard measurements, *Marine Chemistry*, 62(3), pp. 325–333. doi: 10.1016/S0304-4203(98)00037-1.
- Bastviken, D., Cole, J., Pace, M. and Tranvik, L. (2004). Methane emissions from lakes: Dependence of lake characteristics, two regional assessments, and a global estimate, *Global Biogeochemical Cycles*, 18(4), pp. 1–12. doi: 10.1029/2004GB002238.
- Bastviken, D., Santoro, A. L., Marotta, H., Pinho, L. Q., Calheiros, D. F., Crill, P. and Enrich-Prast, A. (2010). Methane emissions from Pantanal, South America, during the low water season: toward more comprehensive sampling, *Environmental Science & Technology*, 44(14), pp. 5450–5455. doi: 10.1021/es1005048.
- Baulch, H. M., Dillon, P. J., Maranger, R., Venkiteswaran, J. J., Wilson, H. F. and Schiff, S. L. (2012). Night and day: short-term variation in nitrogen chemistry and nitrous oxide emissions from streams, *Freshwater Biology*, 57(3), pp. 509–525. doi: 10.1111/j.1365-2427.2011.02720.x.
- Beaulieu, J. J., Tank, J. L., Hamilton, S. K., Wollheim, W. M., Hall, R. O., Mulholland, P. J., Peterson, B. J., Ashkenas, L. R., Cooper, L. W., Dahm, C. N., Dodds, W. K., Grimm, N. B., Johnson, S. L., McDowell, W. H., Poole, G. C., Valett, H. M., Arango, C. P., Bernot, M. J., Burgin, A. J., Crenshaw, C. L., Helton, A. M., Johnson, L. T., O'Brien, J. M., Potter, J. D., Sheibley, R. W., Sobota, D. J. and Thomas, S. M. (2011). Nitrous oxide emission from denitrification in stream and river networks, *Proceedings of the National Academy of Sciences*, 108(1), pp. 214–219. doi: 10.1073/pnas.1011464108.
- Beaulieu, J. J., Balz, D. A., Birchfield, M. K., Harrison, J. A., Nietch, C. T., Platz, M. C., Squier, W. C., Waldo, S., Walker, J. T., White, K. M. and Young, J. L. (2018). Effects of an

experimental water-level drawdown on methane emissions from a eutrophic reservoir, *Ecosystems (New York, N.y.)*, 21(4), pp. 657–674. doi: 10.1007/s10021-017-0176-2.

Bertilsson, S. and Tranvik, L. J. (1998). Photochemically produced carboxylic acids as substrates for freshwater bacterioplankton, *Limnology and Oceanography*, 43(5), pp. 885–895. doi: 10.4319/lo.1998.43.5.0885.

Bertilsson, S. and Tranvik, L. J. (2000). Photochemical transformation of dissolved organic matter in lakes, *Limnology and Oceanography*, 45(4), pp. 753–762. doi: 10.4319/lo.2000.45.4.0753.

Bižić, M., Klintzsch, T., Ionescu, D., Hindiyeh, M. Y., Günthel, M., Muro-Pastor, A. M., Eckert, W., Urich, T., Keppler, F. and Grossart, H.-P. (2020). Aquatic and terrestrial cyanobacteria produce methane, *Science Advances*, 6(3), p. 3aax5343. doi: 10.1126/sciadv.aax5343.

Bogard, M. J., del Giorgio, P. A., Boutet, L., Chaves, M. C. G., Prairie, Y. T., Merante, A. and Derry, A. M. (2014). Oxic water column methanogenesis as a major component of aquatic CH₄ fluxes, *Nature Communications*, 5, p. 5350. doi: 10.1038/ncomms6350.

Catalá, T. S., Reche, I., Álvarez, M., Khaliwala, S., Guallart, E. F., Benítez-Barrios, V. M., Fuentes-Lema, A., Romera-Castillo, C., Nieto-Cid, M., Pelejero, C., Fraile-Nuez, E., Ortega-Retuerta, E., Marrasé, C. and Álvarez-Salgado, X. A. (2015). Water mass age and aging driving chromophoric dissolved organic matter in the dark global ocean, *Global Biogeochemical Cycles*, 29(7), pp. 917–934. doi: 10.1002/2014GB005048.

Clough, T. J., Buckthought, L. E., Kelliher, F. M. and Sherlock, R. R. (2007). Diurnal fluctuations of dissolved nitrous oxide (N₂O) concentrations and estimates of N₂O emissions from a spring-fed river: implications for IPCC methodology, *Global Change Biology*, 13(5), pp. 1016–1027. doi: 10.1111/j.1365-2486.2007.01337.x.

Cole, J. J. and Caraco, N. F. (1998). Atmospheric exchange of carbon dioxide in a low-wind oligotrophic lake measured by the addition of SF₆, *Limnology and Oceanography*, 43(4), pp. 647–656. doi: 10.4319/lo.1998.43.4.0647.

Cole, J. J., Bade, D. L., Bastviken, D., Pace, M. L. and Bogert, M. V. de. (2010). Multiple approaches to estimating air-water gas exchange in small lakes, *Limnology and Oceanography: Methods*, 8(6), pp. 285–293. doi: 10.4319/lom.2010.8.285.

Crusius, J. and Wanninkhof, R. (2003). Gas transfer velocities measured at low wind speed over a lake, *Limnology and Oceanography*, 48(3), pp. 1010–1017. doi: 10.4319/lo.2003.48.3.1010.

Czikowsky, M. J., MacIntyre, S., Tedford, E. W., Vidal, J. and Miller, S. D. (2018). Effects of Wind and Buoyancy on Carbon Dioxide Distribution and Air-Water Flux of a Stratified Temperate Lake, *Journal of Geophysical Research: Biogeosciences*, 123(8), pp. 2305–2322. doi: 10.1029/2017JG004209.

Deemer, B. R., Harrison, J. A., Li, S., Beaulieu, J. J., DelSontro, T., Barros, N., Bezerra-Neto, J. F., Powers, S. M., dos Santos, M. A. and Vonk, J. A. (2016). Greenhouse gas emissions from reservoir water surfaces: a new global synthesis, *BioScience*, 66(11), pp. 949–964. doi: 10.1093/biosci/biw117.

- Donelan, M. A. (1990). Air-sea interaction, *The sea*, 9, pp. 239–292.
- Du, R., Lu, D. and Wang, G. (2006). Diurnal, seasonal, and inter-annual variations of N₂O fluxes from native semi-arid grassland soils of inner Mongolia, *Soil Biology and Biochemistry*, 38(12), pp. 3474–3482. doi: 10.1016/j.soilbio.2006.06.012.
- Edwards, G. C., Neumann, H. H., den Hartog, G., Thurtell, G. W. and Kidd, G. (1994). Eddy correlation measurements of methane fluxes using a tunable diode laser at the Kinosheo Lake tower site during the Northern Wetlands Study (NOWES), *Journal of Geophysical Research*, 99(D1), p. 1511. doi: 10.1029/93JD02368.
- Emmenegger, L., Schönenberger, R., Sigg, L. and Sulzberger, B. (2001). Light-induced redox cycling of iron in circumneutral lakes, *Limnology and Oceanography*, 46(1), pp. 49–61. doi: 10.4319/lo.2001.46.1.0049.
- Erkkilä, K.-M., Ojala, A., Bastviken, D., Biermann, T., Heiskanen, J. J., Lindroth, A., Peltola, O., Rantakari, M., Vesala, T. and Mammarella, I. (2018). Methane and carbon dioxide fluxes over a lake: comparison between eddy covariance, floating chambers and boundary layer method, *Biogeosciences*, 15(2), pp. 429–445. doi: 10.5194/bg-15-429-2018.
- Fisher, N. I. (1993). in *Statistical analysis of circular data*, p. 277.
- Fox, J. and Weisberg, S. (2011). *An R Companion to Applied Regression* Thousand Oaks CA: Sage. Second. Available at: <http://socserv.socsci.mcmaster.ca/jfox/Books/Companion>.
- Godwin, C. M., McNamara, P. J. and Markfort, C. D. (2013). Evening methane emission pulses from a boreal wetland correspond to convective mixing in hollows, *Journal of Geophysical Research: Biogeosciences*, 118(3), pp. 994–1005. doi: 10.1002/jgrg.20082.
- Gross, J. and Ligges, U. (2015). *nortest: Tests for Normality*. Available at: <https://CRAN.R-project.org/package=nortest> (Accessed: 3 June 2018).
- Grossart, H.-P., Frindte, K., Dziallas, C., Eckert, W. and Tang, K. W. (2011). Microbial methane production in oxygenated water column of an oligotrophic lake, *Proceedings of the National Academy of Sciences*, 108(49), pp. 19657–19661. doi: 10.1073/pnas.1110716108.
- Harrison, J. A., Matson, P. A. and Fendorf, S. E. (2005). Effects of a diel oxygen cycle on nitrogen transformations and greenhouse gas emissions in a eutrophied subtropical stream, *Aquatic Sciences*, 67(3), pp. 308–315. doi: 10.1007/s00027-005-0776-3.
- Harrison, J. A., Deemer, B. R., Birchfield, M. K. and O'Malley, M. T. (2017). Reservoir water-level drawdowns accelerate and amplify methane emission, *Environmental Science & Technology*, 51(3), pp. 1267–1277. doi: 10.1021/acs.est.6b03185.
- Heil, J., Wolf, B., Brüggemann, N., Emmenegger, L., Tuzson, B., Vereecken, H. and Mohn, J. (2014). Site-specific ¹⁵N isotopic signatures of abiotically produced N₂O, *Geochimica et Cosmochimica Acta*, 139, pp. 72–82.
- Heiskanen, J. J., Mammarella, I., Haapanala, S., Pumpanen, J., Vesala, T., MacIntyre, S. and Ojala, A. (2014). Effects of cooling and internal wave motions on gas transfer coefficients in a boreal lake, *Tellus B: Chemical and Physical Meteorology*, 66(1), p.

22827. doi: 10.3402/tellusb.v66.22827.

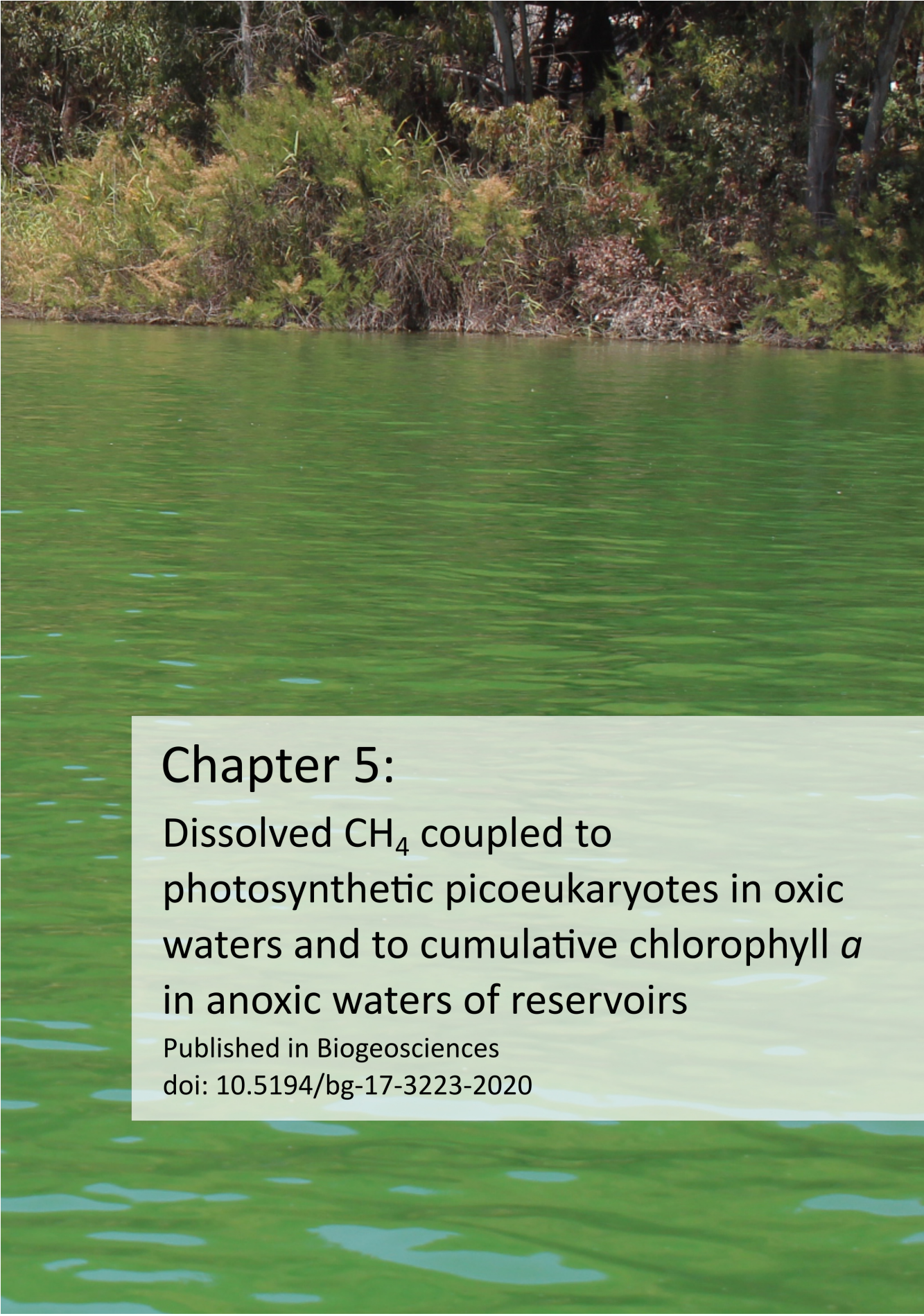
- Helms, J. R., Stubbins, A., Ritchie, J. D., Minor, E. C., Kieber, D. J. and Mopper, K. (2008). Absorption spectral slopes and slope ratios as indicators of molecular weight, source, and photobleaching of chromophoric dissolved organic matter, *Limnology and Oceanography*, 53(3), pp. 955–969. doi: 10.4319/lo.2008.53.3.0955.
- Hoffmann, M., Schulz-Hanke, M., Garcia Alba, J., Jurisch, N., Hagemann, U., Sachs, T., Sommer, M. and Augustin, J. (2017). A simple calculation algorithm to separate high-resolution CH₄ flux measurements into ebullition- and diffusion-derived components, *Atmospheric Measurement Techniques*, 10(1), pp. 109–118. doi: <https://doi.org/10.5194/amt-10-109-2017>.
- Ji, Q., Babbin, A. R., Jayakumar, A., Oleynik, S. and Ward, B. B. (2015). Nitrous oxide production by nitrification and denitrification in the Eastern Tropical South Pacific oxygen minimum zone, *Geophysical Research Letters*, 42(24), p. 10,755–10,764. doi: 10.1002/2015GL066853.
- Johannessen, S. C. and Miller, W. L. (2001). Quantum yield for the photochemical production of dissolved inorganic carbon in seawater, *Marine Chemistry*, 76(4), pp. 271–283. doi: 10.1016/S0304-4203(01)00067-6.
- Keller, M. and Stallard, R. F. (1994). Methane emission by bubbling from Gatun Lake, Panama, *Journal of Geophysical Research: Atmospheres*, 99(D4), pp. 8307–8319. doi: 10.1029/92JD02170.
- Koehler, B., Landelius, T., Weyhenmeyer, G. A., Machida, N. and Tranvik, L. J. (2014). Sunlight-induced carbon dioxide emissions from inland waters, *Global Biogeochemical Cycles*, 28(7), pp. 696–711. doi: 10.1002/2014GB004850.
- Kovach, W. L. (2011). Oriana—circular statistics for windows, ver. 4, *Kovach Computing Services, Pentraeth, Wales, UK*.
- Laursen, A. E. and Seitzinger, S. P. (2004). Diurnal patterns of denitrification, oxygen consumption and nitrous oxide production in rivers measured at the whole-reach scale, *Freshwater Biology*, 49(11), pp. 1448–1458. doi: 10.1111/j.1365-2427.2004.01280.x.
- León-Palmero, E., Morales-Baquero, R. and Reche, I. (2020a). Greenhouse gas fluxes from reservoirs determined by watershed lithology, morphometry, and anthropogenic pressure, *Environmental Research Letters*, 15(4), p. 044012. doi: 10.1088/1748-9326/ab7467.
- León-Palmero, E., Contreras-Ruiz, A., Sierra, A., Morales-Baquero, R. and Reche, I. (2020b). Dissolved CH₄ coupled to photosynthetic picoeukaryotes in oxic waters and to cumulative chlorophyll *a* in anoxic waters of reservoirs, *Biogeosciences*, 17(12), pp. 3223–3245. doi: 10.5194/bg-17-3223-2020.
- Li, Y., Fichot, C. G., Geng, L., Scarratt, M. G. and Xie, H. (2020). The Contribution of Methane Photoproduction to the Oceanic Methane Paradox, *Geophysical Research Letters*, 47(14), p. e2020GL088362. doi: 10.1029/2020GL088362.
- Lin, L., Lu, X., Liu, S., Liang, S.-Y. and Fu, K. (2019). Physically controlled CO₂ effluxes from a reservoir surface in the upper Mekong River Basin: a case study in the Gongguoqiao

- Reservoir, *Biogeosciences*, 16(10), pp. 2205–2219. doi: <https://doi.org/10.5194/bg-16-2205-2019>.
- Liu, H., Zhang, Q., Katul, G. G., Cole, J. J., Chapin, F. S. and MacIntyre, S. (2016). Large CO₂ effluxes at night and during synoptic weather events significantly contribute to CO₂ emissions from a reservoir, *Environmental Research Letters*, 11(6), p. 064001. doi: [10.1088/1748-9326/11/6/064001](https://doi.org/10.1088/1748-9326/11/6/064001).
- Liu, S., Han, P., Hink, L., Prosser, J. I., Wagner, M. and Brüggemann, N. (2017). Abiotic conversion of extracellular NH₂OH contributes to N₂O emission during ammonia oxidation, *Environmental Science & Technology*, 51(22), pp. 13122–13132. doi: [10.1021/acs.est.7b02360](https://doi.org/10.1021/acs.est.7b02360).
- Liu, Y., Zhu, R., Ma, D., Xu, H., Luo, Y., Huang, T. and Sun, L. (2011). Temporal and spatial variations of nitrous oxide fluxes from the littoral zones of three alga-rich lakes in coastal Antarctica, *Atmospheric Environment*, 45(7), pp. 1464–1475. doi: [10.1016/j.atmosenv.2010.12.017](https://doi.org/10.1016/j.atmosenv.2010.12.017).
- Lorenzen, J., Larsen, L. H., Kjær, T. and Revsbech, N.-P. (1998). Biosensor determination of the microscale distribution of nitrate, nitrate assimilation, nitrification, and denitrification in a diatom-inhabited freshwater sediment, *Applied and Environmental Microbiology*, 64(9), pp. 3264–3269.
- Mardia, K. V. and Jupp, P. E. (2000). in *Statistics of directional data*. 2nd edn, p. 429.
- Marotta, H., Pinho, L., Gudas, C., Bastviken, D., Tranvik, L. J. and Enrich-Prast, A. (2014). Greenhouse gas production in low-latitude lake sediments responds strongly to warming, *Nature Climate Change*, 4(6), pp. 467–470. doi: [10.1038/nclimate2222](https://doi.org/10.1038/nclimate2222).
- Martinez-Cruz, K., Sepulveda-Jauregui, A., Greene, S., Fuchs, A., Rodriguez, M., Pansch, N., Gonsiorczyk, T. and Casper, P. (2020). Diel variation of CH₄ and CO₂ dynamics in two contrasting temperate lakes, *Inland Waters*, 0(0), pp. 1–15. doi: [10.1080/20442041.2020.1728178](https://doi.org/10.1080/20442041.2020.1728178).
- Mendoza, I. (2020). Estadística circular aplicada a la Ecología, *Revista Ecosistemas*, 29(2), p. 1995. doi: [10.7818/re.2014.29-2.00](https://doi.org/10.7818/re.2014.29-2.00).
- Mopper, K. and Zhou, X. (1990). Hydroxyl radical photoproduction in the sea and its potential impact on marine processes, *Science*, 250(4981), pp. 661–664. doi: [10.1126/science.250.4981.661](https://doi.org/10.1126/science.250.4981.661).
- Morales-Pineda, M., Cózar, A., Laiz, I., Úbeda, B. and Gálvez, J. Á. (2014). Daily, biweekly, and seasonal temporal scales of pCO₂ variability in two stratified Mediterranean reservoirs, *Journal of Geophysical Research: Biogeosciences*, 119(4), p. 2013JG002317. doi: [10.1002/2013JG002317](https://doi.org/10.1002/2013JG002317).
- Ortega-Retuerta, E., Pulido-Villena, E. and Reche, I. (2007). Effects of dissolved organic matter photoproducts and mineral nutrient supply on bacterial growth in Mediterranean inland waters, *Microbial Ecology*, 54(1), pp. 161–169. doi: [10.1007/s00248-006-9186-x](https://doi.org/10.1007/s00248-006-9186-x).
- Otte, J. M., Blackwell, N., Ruser, R., Kappler, A., Kleindienst, S. and Schmidt, C. (2019). N₂O formation by nitrite-induced (chemo)denitrification in coastal marine sediment, *Scientific Reports*, 9(1), pp. 1–12. doi: [10.1038/s41598-019-47172-x](https://doi.org/10.1038/s41598-019-47172-x).

- Pehkonen, S. O., Siefert, R., Erel, Y., Webb, S. and Hoffmann, M. R. (1993). Photoreduction of iron oxyhydroxides in the presence of important atmospheric organic compounds, *Environmental Science & Technology*, 27(10), pp. 2056–2062. doi: 10.1021/es00047a010.
- Podgrajsek, E., Sahlée, E. and Rutgersson, A. (2014). Diurnal cycle of lake methane flux, *Journal of Geophysical Research: Biogeosciences*, 119(3), pp. 236–248. doi: 10.1002/2013JG002327.
- Podgrajsek, E., Sahlée, E. and Rutgersson, A. (2015). Diel cycle of lake-air CO₂ flux from a shallow lake and the impact of waterside convection on the transfer velocity, *Journal of Geophysical Research: Biogeosciences*, 120(1), pp. 29–38. doi: 10.1002/2014JG002781.
- Poindexter, C. M., Baldocchi, D. D., Matthes, J. H., Knox, S. H. and Variano, E. A. (2016). The contribution of an overlooked transport process to a wetland's methane emissions, *Geophysical Research Letters*, 43(12), pp. 6276–6284. doi: 10.1002/2016GL068782.
- R Core Team. (2014). *R: A Language and Environment for Statistical Computing* Vienna, Austria: R Foundation for Statistical Computing. Available at: <http://www.R-project.org/>.
- Rasilo, T., Prairie, Y. T. and del Giorgio, P. A. (2015). Large-scale patterns in summer diffusive CH₄ fluxes across boreal lakes, and contribution to diffusive C emissions, *Global Change Biology*, 21(3), pp. 1124–1139. doi: 10.1111/gcb.12741.
- Reche, I., Pace, M. L. and Cole, J. J. (1998). Interactions of Photobleaching and Inorganic Nutrients in Determining Bacterial Growth on Colored Dissolved Organic Carbon, *Microbial Ecology*, 36(3), pp. 270–280. doi: 10.1007/s002489900114.
- Rey-Sanchez, A. C., Morin, T. H., Stefanik, K. C., Wrighton, K. and Bohrer, G. (2018). Determining total emissions and environmental drivers of methane flux in a Lake Erie estuarine marsh, *Ecological Engineering*, 114, pp. 7–15. doi: 10.1016/j.ecoleng.2017.06.042.
- Rosamond, M. S., Thuss, S. J. and Schiff, S. L. (2012). Dependence of riverine nitrous oxide emissions on dissolved oxygen levels, *Nature Geoscience*, 5(10), pp. 715–718. doi: 10.1038/ngeo1556.
- Schmidt, U. and Conrad, R. (1993). Hydrogen, carbon monoxide, and methane dynamics in Lake Constance, *Limnology and Oceanography*, 38(6), pp. 1214–1226. doi: 10.4319/lo.1993.38.6.1214.
- Sepulveda-Jauregui, A., Hoyos-Santillan, J., Martinez-Cruz, K., Walter Anthony, K. M., Casper, P., Belmonte-Izquierdo, Y. and Thalasso, F. (2018). Eutrophication exacerbates the impact of climate warming on lake methane emission, *Science of The Total Environment*, 636, pp. 411–419. doi: 10.1016/j.scitotenv.2018.04.283.
- Sieczko, A. K., Duc, N. T., Schenk, J., Pajala, G., Rudberg, D., Sawakuchi, H. O. and Bastviken, D. (2020). Diel variability of methane emissions from lakes, *Proceedings of the National Academy of Sciences*, 117(35), pp. 21488–21494. doi: 10.1073/pnas.2006024117.
- Soler-Jofra, A., Stevens, B., Hoekstra, M., Picioreanu, C., Sorokin, D., van Loosdrecht, M. C.

- and Pérez, J. (2016). Importance of abiotic hydroxylamine conversion on nitrous oxide emissions during nitrification of reject water, *Chemical Engineering Journal*, 287, pp. 720–726.
- Song, W., Ma, W., Ma, J., Chen, C., Zhao, J., Huang, Y. and Xu, Y. (2005). Photochemical oscillation of Fe(II)/Fe(III) ratio induced by periodic flux of dissolved organic matter, *Environmental Science & Technology*, 39(9), pp. 3121–3127. doi: 10.1021/es0483701.
- Tang, K. W., McGinnis, D. F., Frindte, K., Brüchert, V. and Grossart, H.-P. (2014). Paradox reconsidered: Methane oversaturation in well-oxygenated lake waters, *Limnology and Oceanography*, 59(1), pp. 275–284. doi: 10.4319/lo.2014.59.1.0275.
- Tedford, E. W., MacIntyre, S., Miller, S. D. and Czikowsky, M. J. (2014). Similarity scaling of turbulence in a temperate lake during fall cooling, *Journal of Geophysical Research: Oceans*, 119(8), pp. 4689–4713. doi: 10.1002/2014JC010135.
- Vachon, D., Lapierre, J.-F. and Giorgio, P. A. del. (2016). Seasonality of photochemical dissolved organic carbon mineralization and its relative contribution to pelagic CO₂ production in northern lakes, *Journal of Geophysical Research: Biogeosciences*, 121(3), pp. 864–878. doi: 10.1002/2015JG003244.
- Wang, B., Liao, Q., Fillingham, J. H. and Bootsma, H. A. (2015). On the coefficients of small eddy and surface divergence models for the air-water gas transfer velocity, *Journal of Geophysical Research: Oceans*, 120(3), pp. 2129–2146. doi: 10.1002/2014JC010253.
- Wankel, S. D., Ziebis, W., Buchwald, C., Charoenpong, C., Beer, D. de, Dentinger, J., Xu, Z. and Zengler, K. (2017). Evidence for fungal and chemodenitrification based N₂O flux from nitrogen impacted coastal sediments, *Nature Communications*, 8, p. 15595. doi: 10.1038/ncomms15595.
- West, W. E., Creamer, K. P. and Jones, S. E. (2016). Productivity and depth regulate lake contributions to atmospheric methane: Lake productivity fuels methane emissions, *Limnology and Oceanography*, 61(S1), pp. S51–S61. doi: 10.1002/lno.10247.
- Wood, S. N. (2011). Fast stable restricted maximum likelihood and marginal likelihood estimation of semiparametric generalized linear models, *Journal of the Royal Statistical Society: Series B (Statistical Methodology)*, 73(1), pp. 3–36. doi: 10.1111/j.1467-9868.2010.00749.x.
- Xia, Y., Li, Y., Li, X., Guo, M., She, D. and Yan, X. (2013). Diurnal pattern in nitrous oxide emissions from a sewage-enriched river, *Chemosphere*, 92(4), pp. 421–428. doi: 10.1016/j.chemosphere.2013.01.038.
- Xiao, S., Wang, Y., Liu, D., Yang, Z., Lei, D. and Zhang, C. (2013). Diel and seasonal variation of methane and carbon dioxide fluxes at Site Guojiaba, the Three Gorges Reservoir, *Journal of Environmental Sciences*, 25(10), pp. 2065–2071. doi: 10.1016/S1001-0742(12)60269-1.
- Xu, J., Wei, Q., Yang, S., Wang, Y. and Lv, Y. (2016). Diurnal pattern of nitrous oxide emissions from soils under different vertical moisture distribution conditions, *Chilean journal of agricultural research*, 76(1), pp. 84–92. doi: 10.4067/S0718-58392016000100012.

- Yan, W., Yang, L., Wang, F., Wang, J. and Ma, P. (2012). Riverine N₂O concentrations, exports to estuary and emissions to atmosphere from the Changjiang River in response to increasing nitrogen loads, *Global Biogeochemical Cycles*, 26(4), p. 15. doi: 10.1029/2010GB003984.
- Yang, L., Yan, W., Ma, P. and Wang, J. (2011). Seasonal and diurnal variations in N₂O concentrations and fluxes from three eutrophic rivers in Southeast China, *Journal of Geographical Sciences*, 21(5), p. 820. doi: 10.1007/s11442-011-0882-1.
- Yvon-Durocher, G., Allen, A. P., Bastviken, D., Conrad, R., Gudas, C., St-Pierre, A., Thanh-Duc, N. and del Giorgio, P. A. (2014). Methane fluxes show consistent temperature dependence across microbial to ecosystem scales, *Nature*, 507(7493), pp. 488–491. doi: 10.1038/nature13164.
- Zar, J. H. (1998). Biostatistical analysis, in *Prentice-hall*. 4th edn, p. 663.
- Zepp, R. G., Hoigne, J. and Bader, H. (1987). Nitrate-induced photooxidation of trace organic chemicals in water, *Environmental science & technology*, 21(5), pp. 443–450.
- Zhang, C., Cheng, S., Li, Y., Zhang, W. and Xiao, S. (2019). Diel methane flux from a subtropical eutrophic pond in November based on continuous monitoring, *Acta Geochimica*. doi: 10.1007/s11631-019-00317-1.
- Zhang, Y. and Xie, H. (2015). Photomineralization and photomethanification of dissolved organic matter in Saguenay River surface water, *Biogeosciences*, 12(22), pp. 6823–6836. doi: <https://doi.org/10.5194/bg-12-6823-2015>.
- Zhu-Barker, X., Cavazos, A. R., Ostrom, N. E., Horwath, W. R. and Glass, J. B. (2015). The importance of abiotic reactions for nitrous oxide production, *Biogeochemistry*, 126(3), pp. 251–267. doi: 10.1007/s10533-015-0166-4.

A photograph of a reservoir with green water and a vegetated shoreline. The water is a vibrant green color, and the shoreline is covered in dense green and brown vegetation. The background shows a line of trees.

Chapter 5:

Dissolved CH₄ coupled to
photosynthetic picoeukaryotes in oxic
waters and to cumulative chlorophyll *a*
in anoxic waters of reservoirs

Published in Biogeosciences

doi: [10.5194/bg-17-3223-2020](https://doi.org/10.5194/bg-17-3223-2020)

Chapter 5:

Dissolved CH₄ coupled to photosynthetic picoeukaryotes in oxic waters and to cumulative chlorophyll *a* in anoxic waters of reservoirs

Elizabeth León-Palmero¹, Alba Contreras-Ruiz¹, Ana Sierra², Rafael Morales-Baquero¹, and Isabel Reche^{1,3}

¹Departamento de Ecología and Instituto del Agua, Universidad de Granada, 18071, Granada, Spain

²Departamento de Química Física and Instituto Universitario de Investigación Marina (INMAR), Facultad de Ciencias del Mar y Ambientales, Universidad de Cádiz, Puerto Real, 11510, Cádiz, Spain

³Research Unit “Modeling Nature” (MNat), Universidad de Granada, 18071 Granada, Spain

The Supplementary material is available in Appendix 5

Abstract

Methane (CH₄) emissions from reservoirs are responsible for most of the atmospheric climatic forcing of these aquatic ecosystems, comparable to emissions from paddies or biomass burning. Primarily, CH₄ is produced during the anaerobic mineralization of organic carbon in anoxic sediments by methanogenic archaea. However, the origin of the recurrent and ubiquitous CH₄ supersaturation in oxic waters (i.e., the methane paradox) is still controversial. Here, we determined the dissolved CH₄ concentration in the water column of 12 reservoirs during summer stratification and winter mixing to explore CH₄ sources in oxic waters. Reservoir sizes ranged from 1.18 to 26.13 km². We found that dissolved CH₄ in the water column varied by up to 4 orders of magnitude (0.02 – 213.64 μmol L⁻¹), and all oxic depths were consistently supersaturated in both periods. Phytoplanktonic sources appear to determine the concentration of CH₄ in these reservoirs primarily. In anoxic waters, the depth-cumulative chlorophyll *a* concentration, a proxy for the phytoplanktonic biomass exported to sediments, was correlated to CH₄ concentration. In oxic waters,

the photosynthetic picoeukaryotes' abundance was significantly correlated to the dissolved CH₄ concentration during both the stratification and the mixing. The mean depth of the reservoirs, as a surrogate of the vertical CH₄ transport from sediment to the oxic waters, also contributed notably to the CH₄ concentration in oxic waters. Our findings suggest that photosynthetic picoeukaryotes can play a significant role in determining CH₄ concentration in oxic waters, although their role as CH₄ sources to explain the methane paradox has been poorly explored.

5. 1. Introduction

Lakes and reservoirs are significant sources of methane (CH₄), affecting the atmospheric climatic forcing (Deemer *et al.*, 2016). The estimated contribution of lakes to the global emission budget is ca. 71.6 Tg CH₄ yr⁻¹ (Bastviken *et al.*, 2011), and the specific contribution of reservoirs ranges between 4 and 70 Tg CH₄ yr⁻¹, representing up to 10 % of total CH₄ emissions (Deemer *et al.*, 2016). Although freshwater only covers about 5 % – 8 % of the Earth's surface (Mitsch *et al.*, 2012), it emits more CH₄ than the ocean surface (Saunio *et al.*, 2016). Traditionally, the net CH₄ production is determined by archaeal methanogenesis, which produces methane as an end product of organic matter degradation in anoxic conditions, and to methanotrophs, which consume it in oxic conditions (Schubert and Wehrli, 2018). In freshwater ecosystems, the anoxic sediments are a primary source of CH₄ (Segers, 1998), where methanogens are very sensitive to temperature and quantity and quality of the organic matter used as substrate (Thanh-Duc *et al.*, 2010; West *et al.*, 2012; Marotta *et al.*, 2014; Yvon-Durocher *et al.*, 2014; Rasilo *et al.*, 2015; Sepulveda-Jauregui *et al.*, 2018). They are also affected by the extent of anoxia in the sediments inasmuch as they are obligate anaerobes and will not survive and produce CH₄ under aerobic conditions (Chistoserdova *et al.*, 1998; Schubert and Wehrli, 2018). However, many observations from freshwater and marine water have detected CH₄ supersaturation in the oxic layers, a widespread phenomenon described as the "methane paradox" (Kiene, 1991; Owens *et al.*, 1991; Schmidt and Conrad, 1993; Schulz *et al.*, 2001; Murase *et al.*, 2003; Damm *et al.*, 2010; Grossart *et al.*, 2011; Bogard *et al.*, 2014; Tang *et al.*, 2014, 2016; Donis *et al.*, 2017).

This persistent CH₄ supersaturation in oxic layers of marine and freshwater ecosystems requires extra inputs to compensate for the CH₄ losses by

methanotrophy and the emissions toward the atmosphere. CH₄ inputs may come from anoxic sediments or from *in situ* sources in the oxic layers. The transport of CH₄ from the bottom and littoral sediments in shallow zones has been proposed to explain the supersaturation in the surface waters of some lakes (Rudd and Hamilton, 1978; Michmerhuizen *et al.*, 1996; Murase *et al.*, 2003; Bastviken *et al.*, 2004; Encinas Fernández *et al.*, 2016; Peeters *et al.*, 2019). The vertical transport may be relevant in small lakes, but in deep and thermally stratified systems, the vertical diffusion rates of dissolved gases across the thermocline are too low, and there is no apparent CH₄ upward movement from the hypolimnion (Rudd and Hamilton, 1978; Peeters *et al.*, 1996). In fact, Thalasso *et al.* (2020) determined that there was no exchange between the hypolimnion and the epilimnion in a Siberian lake. The CH₄ produced in the sediments and the hypolimnion was assimilated there. Consequently, the CH₄ in the epilimnion came from lateral transport and *in situ* production. Lateral CH₄ transport from shallow sediments of the littoral zones may be a significant source in the open surface of some lakes and reservoirs. DelSontro *et al.* (2018) found that CH₄ transport from littoral zones was relevant for the dissolved CH₄ in the epilimnion of small lakes. However, lateral transport does not fully explain CH₄ supersaturation in the open ocean, and large freshwater ecosystems, and, hence, other *in situ* CH₄ sources, likely occur (Scranton and Brewer, 1977; Owens *et al.*, 1991; Schmidt and Conrad, 1993; Tilbrook and Karl, 1995; Schulz *et al.*, 2001; Damm *et al.*, 2010; Grossart *et al.*, 2011; Tang *et al.*, 2014; DelSontro *et al.*, 2018; Khatun *et al.*, 2020).

Previous works demonstrated the *in situ* CH₄ production in oxic waters using stable isotope techniques in experiments, mesocosms, and field samples (Bogard *et al.*, 2014; Tang *et al.*, 2016; DelSontro *et al.*, 2018; Bižić *et al.*, 2020; Hartmann *et al.*, 2020) and using molecular approaches (Grossart *et al.*, 2011; Yao *et al.*, 2016a; Khatun *et al.*, 2020). In the literature, there are different alternatives proposed as CH₄ sources. On the one hand, there is the occurrence of methanogenesis in micro-anoxic niches in the guts of zooplankton and within sinking particles (de Angelis and Lee, 1994; Karl and Tilbrook, 1994). In both micro-anoxic niches, the CH₄ production appeared to be too low to sustain the total CH₄ supersaturation of the oxic waters (Tang *et al.*, 2014; Schmale *et al.*, 2018). On the other hand, there is a consistent link between dissolved CH₄ concentration and autotrophic organisms, primary

production, and chlorophyll *a* concentration (Owens *et al.*, 1991; Schmidt and Conrad, 1993; Grossart *et al.*, 2011; Bogard *et al.*, 2014; Tang *et al.*, 2014). Grossart *et al.* (2011) detected potential methanogenic Archaea attached to photoautotrophs as Chlorophyta (Eukarya) and cyanobacteria (Bacteria) in the epilimnion of an oligotrophic lake and confirmed the production of CH₄ in the presence of oxygen in laboratory incubations. If occurring, that symbiosis would require that the methanogenic microorganisms tolerate the oxygen exposure, as has been observed by several authors (Jarrell, 1985; Angel *et al.*, 2011; Angle *et al.*, 2017), in contrast to general belief.

New findings suggest that the link between phytoplankton and dissolved CH₄ may rely on diverse metabolic pathways in Bacteria and Eukarya. These metabolic pathways contribute to the dissolved CH₄ in oxic waters due to the degradation of methylated compounds. In the open ocean, archaea and bacteria appear to metabolize the algal osmolyte dimethylsulfoniopropionate, producing methane as a by-product (Damm *et al.*, 2008, 2010, 2015; Zindler *et al.*, 2013). Common methyl-containing substances like methionine produce methane in algae, saprotrophic fungi, and plants (Lenhart *et al.*, 2012, 2015, 2016). Another reported pathway is the degradation of methylphosphonates (MPn's) as an alternative source of phosphorus (P) in phosphate-starved bacterioplankton. The hydrolysis of these compounds, using the enzyme C–P lyase, also releases methane as a by-product. This pathway appears in chronically P-starved ecosystems as the ocean gyres, oligotrophic lakes, and microbial mats (Karl *et al.*, 2008; Beversdorf *et al.*, 2010; Gomez-Garcia *et al.*, 2011; Carini *et al.*, 2014; del Valle and Karl, 2014; Yao *et al.*, 2016a; Repeta *et al.*, 2016; Wang *et al.*, 2017; Teikari *et al.*, 2018). Recent studies using phytoplankton cultures and stable isotope techniques propose that the production of CH₄ may rely directly on the photoautotrophic carbon fixation of algae and cyanobacteria (Lenhart *et al.*, 2016; Klintzsch *et al.*, 2019; Bižić *et al.*, 2020; Hartmann *et al.*, 2020). These sources of CH₄ in oxic waters, however, still have not been tested simultaneously in reservoirs, despite the known high contribution of these freshwater ecosystems to global CH₄ emissions.

In this study, we measured the dissolved CH₄ concentration in the water column of 12 reservoirs that cover a broad spectrum of sizes, ages, morphometries, and trophic states during the summer stratification and winter mixing (León-Palmero

et al., 2020a). Our objective was to assess the relative contribution of different sources of CH₄ in the oxic waters and to shed light on the methane paradox depending on reservoir properties. We explored the following CH₄ sources in oxic waters: (1) vertical and lateral transport of CH₄ from hypolimnetic and littoral waters, (2) *in situ* production by methanogenic Archaea tolerant to oxygen, (3) *in situ* production by methylphosphonate degradation, and (4) *in situ* production by photosynthetic microorganisms. We used the concentration chlorophyll *a*, the primary production, and the abundance of photosynthetic picoeukaryotes and cyanobacteria as variables for the photosynthetic signatures. The photosynthetic picoeukaryotes are a relevant part of the freshwater phytoplankton, but their role in the methane paradox has been particularly little studied.

5. 2. Material and Methods

5. 2. 1. Studied reservoirs, morphometry, and vertical profiles

We sampled 12 reservoirs located in southern Spain (Figure 5.1) between July 2016 and August 2017 once during the summer stratification and once during winter mixing. In Table 5.1, we show the geographical coordinates, age, and the morphometric description of the studied reservoirs. The reservoirs were built between 1932 and 2003, for water supply and agriculture irrigation, and they are located in watersheds with different lithologies and land uses (more details can be found in León-Palmero *et al.* (2019, 2020a).

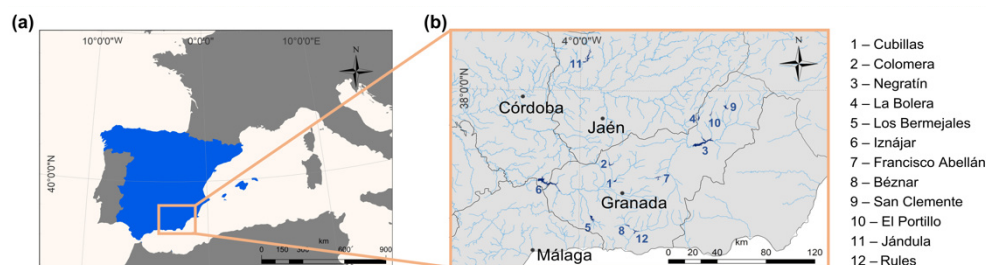


Figure 5.1. Geographical location of the studied reservoirs. (a) The location area of the studied reservoirs delimited by an orange box in the south of the Iberian Peninsula. (b) Detailed location of the 12 reservoirs with the numbers (1–12) and their corresponding names listed on the side. Geographical coordinates appear in Table 5.1. We obtained these maps using ArcGIS® 10.2 software (ESRI, 2012) under the Universidad de Granada license. ©ESRI: ArcGIS, Redlands, CA.

These reservoirs differ in morphometric, chemical, and trophic characteristics, covering a wide range of concentrations of dissolved organic carbon (DOC), total nitrogen (TN), total phosphorus (TP), and chlorophyll *a* (Table 5.2). All raw data for the water column were deposited in the PANGAEA database (<https://doi.org/10.1594/PANGAEA.912535>, last access: 14 May 2020.). We obtained the reservoir surface area, perimeter, and volume using the following open databases: Infraestructura de Datos Espaciales de Andalucía (IDEAndalucia; <http://www.ideandalucia.es/portal/web/ideandalucia/>, last access: 4 February 2018), and the Ministerio para la Transición Ecológica (<https://www.embalses.net/>, last access: 15 September 2019).

The mean depth was calculated using the reservoir volume (m³) and the reservoir surface area (m²) (Eq. 5.1):

$$\text{Mean depth} = \frac{\text{Volume}}{\text{Surface area}} \quad \text{Eq. 5.1}$$

The shoreline development ratio (D_L , unitless) (Aronow, 1982) is a comparative index relating the shoreline length (i.e., the perimeter of the reservoir, m) to the circumference of a circle that has the same area (m²). The closer this ratio is to 1, the more circular the lake. A large ratio ($\gg 1$) indicates the shoreline is more scalloped than a low ratio. The equation is as follows (Eq. 5.2):

$$D_L = \frac{\text{Length of the shoreline}}{2\sqrt{\pi \times \text{area}}} \quad \text{Eq. 5.2}$$

The shallowness index (m⁻¹) was obtained by dividing the shoreline development index (D_L) by the mean depth (m), as in Eq. 5.3:

$$\text{Shallowness index} = \frac{D_L}{\text{Mean depth}} \quad \text{Eq. 5.3}$$

We sampled the water column near the dam, in the open waters of the reservoir. During the stratification and the mixing period, we selected the same location. First, we performed a vertical profile of the reservoir using a Sea-Bird 19plus CTD profiler, coupled to a Spherical Underwater Quantum Sensor (LI-193R), and a fluorimeter Turner® SCUFA (model CYCLOPS-7) for continuous measurements of temperature (°C), dissolved oxygen (μmol L⁻¹), conductivity (μS cm⁻¹), turbidity (FTU - formazin turbidity unit), density (kg m⁻³), photosynthetic active radiation, chlorophyll *a* fluorescence (μg L⁻¹), specific conductance (μS cm⁻¹), and salinity (psu – practical

salinity units). Then, based on the temperature and oxygen profiles, we selected six to nine depths, representative of the oxic and anoxic layers and the transition between them in the different reservoirs. We took the water samples using a UWITEC sampling bottle of 5 L with a self-closing mechanism. We collected samples for the dissolved CH₄ analysis in 125 or 250mL airtight Winkler bottles in duplicate (250 mL) or in triplicate (125 mL). We filled up the bottles very carefully from the bottom to avoid the formation of bubbles and minimize the loss of CH₄ during field sampling. We preserved the samples with a solution of HgCl₂ (final concentration 1 mmol L⁻¹) to inhibit biological activity and sealed the bottles with Apiezon® grease to prevent gas exchanges. We also took samples from each depth from the chemical and biological analysis explained below. We also measured barometric pressure using a multi-parameter probe (Hanna HI 9828) for the gas saturation calculations. We calculated the saturation values (%) for dissolved oxygen as the ratio of the dissolved gas measured and the gas concentration expected in equilibrium. We calculated the gas concentration in equilibrium, taking into account the differences in temperature, salinity, and barometric pressure (Mortimer, 1956).

Table 5.1. Geographical location and morphometric description of the studied reservoirs.

Reservoir	Latitude (°, decimal degrees)	Longitude (°, decimal degrees)	Altitude (m)	Construction year	Reservoir area (km ²)	Reservoir capacity (hm ³)	Mean depth (m)	Shoreline development index	Shallow-ness index (m ⁻¹)
Cubillas	37.27	-3.68	640	1956	1.94	18.74	9.66	2.00	0.21
Colomera	37.40	-3.72	810	1990	2.76	40.18	14.56	3.35	0.23
Negratín	37.56	-2.95	618	1984	23.51	567.12	24.12	5.90	0.24
La Bolera	37.76	-2.90	950	1967	2.89	53.19	18.40	4.05	0.22
Los Bermejales	36.99	-3.89	852	1958	5.95	103.12	17.33	2.90	0.17
Iznájar	37.26	-4.33	425	1969	26.13	981.12	37.55	5.76	0.15
Francisco Abellán	37.31	-3.27	942	1991	2.43	58.21	23.95	3.80	0.16
Béznar	36.92	-3.55	486	1986	1.60	52.90	33.06	2.65	0.08
San Clemente	37.86	-2.65	1050	1990	3.76	117.92	31.36	3.43	0.11
El Portillo	37.81	-2.79	920	1999	1.18	32.90	27.88	3.69	0.13
Jándula	38.23	-3.97	350	1932	8.43	321.99	38.20	7.10	0.19
Rules	36.86	-3.49	239	2003	3.06	110.78	36.20	3.09	0.09

Table 5.2. Sampling date; mean values of the DOC, TN, and TP concentrations; DIN : TP ratio; and chlorophyll *a* concentration in the water column of the studied reservoirs during the stratification and the mixing period.

Reservoir	Period	Sampling Date	DOC ($\mu\text{mol-C}$ L^{-1})	TN ($\mu\text{mol-N}$ L^{-1})	TP ($\mu\text{mol-P}$ L^{-1})	DIN:TP ($\mu\text{mol-N}$: $\mu\text{mol-P}$)	Chl <i>a</i> ($\mu\text{g L}^{-1}$)
Cubillas	Stratification	July 15, 2016	172.1	60.4	1.84	23	17.8
	Mixing	February 6, 2017	240.5	115.4	0.78	111	8.4
Colomera	Stratification	July 22, 2016	99.4	181.4	0.78	236	2.1
	Mixing	March 7, 2017	123.3	112.4	0.44	291	0.7
Negratín	Stratification	June 27, 2016	109.7	21.2	0.80	23	1.2
	Mixing	February 16, 2017	148.9	19.7	0.24	65	0.6
La Bolera	Stratification	June 28, 2016	123.7	17.3	0.61	12	2.1
	Mixing	April 8, 2017	107.4	34.4	0.15	176	3.3
Los Bermejales	Stratification	September 7, 2016	94.2	30.4	0.42	52	1.8
	Mixing	March 17, 2017	101.5	30.6	0.31	88	1.1
Iznájar	Stratification	September 9, 2016	116.8	278.5	0.39	675	5.1
	Mixing	March 15, 2017	147.5	298.7	1.16	392	13.1
Francisco Abellán	Stratification	September 28, 2016	90.6	27.8	0.28	79	1.9
	Mixing	March 21, 2017	118.0	29.2	0.47	63	1.1
Béznar	Stratification	October 7, 2016	74.3	74.2	0.68	103	6.0
	Mixing	February 23, 2017	121.6	113.0	0.95	104	9.8
San Clemente	Stratification	July 17, 2017	104.1	32.0	0.39	39	3.5
	Mixing	March 28, 2017	119.4	35.9	0.21	145	3.8
El Portillo	Stratification	July 18, 2017	78.0	22.8	0.17	103	2.4
	Mixing	March 30, 2017	76.4	34.4	0.26	108	1.2
Jándula	Stratification	July 24, 2017	359.9	37.2	0.78	43	2.3
	Mixing	April 5, 2017	399.4	46.2	0.37	103	1.7
Rules	Stratification	July 10, 2017	81.2	23.2	0.21	82	3.7
	Mixing	April 7, 2017	68.5	38.0	0.43	143	1.2

5. 2. 2. Dissolved CH₄ in the water column

We stored the Winkler bottles in the dark at room temperature until analysis in the laboratory. We measured dissolved CH₄ using headspace equilibration in a 50 mL air-tight glass syringe (Agilent P/N 5190–1547) (Sierra *et al.*, 2017). We obtained two replicates for each 150 mL Winkler bottle and three replicates for each 250 mL

Winkler bottle. We took a quantity of 25 g of water (± 0.01 g) using the air-tight syringe and added a quantity of 25 mL of a standard gas mixture that had a methane concentration similar to atmospheric values (1.8 ppmv) to complete the volume of the syringe. The syringes were shaken for 5 min (Vibromatic, Selecta) to ensure mixing, and we waited 5 min to reach complete equilibrium. Then, the gas in the syringe was injected manually into the gas chromatograph (GC; Bruker® GC-450) equipped with a hydrogen flame ionization detector. We calibrated the detectors daily using three standard gas mixtures with CH₄ mixing ratios of 1952, 10 064, and 103 829 ppbv, made and certified by Air Liquide (France). We calculated the gas concentration in the water samples from the concentration measured in the headspace using the Bunsen functions for CH₄ (Yamamoto *et al.*, 1976; Wiesenburg and Guinasso, 1979). The precision in the quantification of the gas mixture of CH₄ used in the headspace equilibrium (1.8 ppmv) expressed as the coefficient of variation was 3.7% (n = 123). The precision of the measurement of the dissolved CH₄ concentration, which included the analytical processing of the samples and the equilibration step, was 3.6 % for four to six replicates of each sample. We calculated the saturation values (%) as the ratio of the concentration of the dissolved gas measured to the gas concentration expected in equilibrium considering the temperature, salinity, and barometric pressure of each reservoir. We used the atmospheric gas concentrations provided by the Global Greenhouse Gas Reference Network website (<https://www.esrl.noaa.gov/gmd/ccgg/index.html>, last access: 20 September 2019), which is part of the National Oceanic and Atmospheric Administration (NOAA) Earth System Research Laboratory in Boulder, Colorado. We calculated the 2016 global mean atmospheric concentrations for CH₄ (Dlugokencky, 2019) from the 2016 global monthly mean. The differences among these values and the local atmospheric concentrations are assumed to be small compared with the high dissolved concentrations obtained in the studied reservoirs.

5. 2. 3. Chemical analysis in the water column

From the discrete sampling, we selected three or four representative depths of the epilimnion, metalimnion (oxycline), and hypolimnion, and bottom layers for nutrient analysis during the stratification period. We also selected three or four

equivalent depths during the mixing period. In total, we analyzed 77 samples: 41 samples from the stratification period, and 36 samples from the mixing period. We determined total nutrients using unfiltered water, while we filtered the samples through pre-combusted 0.7 µm pore-size Whatman GF/F glass-fiber filters for the dissolved nutrients. We acidified the samples for dissolved organic carbon (DOC), total dissolved nitrogen (TDN), and total nitrogen (TN) with phosphoric acid (final pH<2). We measured DOC, TN, and TDN by high-temperature catalytic oxidation using a Shimadzu total organic carbon (TOC) analyzer (Model TOC-VCSH) coupled to a nitrogen analyzer (TNM-1). We calibrated the instrument using a four-point standard curve of dried potassium hydrogen phthalate for DOC and dried potassium nitrate for TN and TDN (Álvarez-Salgado and Miller, 1998). We analyzed two replicates and three to five injections per replicate for each sample. We purged the DOC samples with phosphoric acid for 20 min to eliminate all the dissolved inorganic carbon. The precision of the DOC measurements expressed as the mean coefficient of variation was 3.0 %. The mean precision for the TN and TDN was 8.2 % and 2.9 %, respectively.

We measured the NO₃⁻ concentration in duplicate with the ultraviolet spectrophotometric method, using a Perkin Elmer UV Lambda 40 spectrophotometer at wavelengths of 220 nm and correcting for DOC absorbance at 275 nm (APHA, 1992). The mean coefficient of variation was 0.5 %. We measured NO₂⁻ concentrations by inductively coupled plasma optical emission spectrometry (ICP-OES). Dissolved inorganic nitrogen (DIN) was calculated as the addition of the NO₃⁻ and NO₂⁻ concentrations. The detection limits for the NO₂⁻ concentration was 1.4 µmol L⁻¹. We measured total phosphorus (TP) concentration in triplicate using the molybdenum blue method (Murphy and Riley, 1962) after digestion with a mixture of potassium persulfate and boric acid at 120 °C for 30 min (APHA, 1992). The precision in the quantification of the TP concentration was 11.1 %.

5. 2. 4. Chlorophyll *a*, phytoplankton, and primary production in the water column

We determined the chlorophyll *a* concentration and the abundances of cyanobacteria and photosynthetic picoeukaryotes in all the depths sampled during the discrete samplings (n = 178). We determined the chlorophyll *a* concentration by

filtering the particulate material of 500 to 2000 mL of water through pre-combusted Whatman GF/F glass-fiber filters. Then, we extracted the pigments from the filters with 95 % methanol in the dark at 4 °C for 24 h (APHA, 1992). We measured chlorophyll *a* (Chl *a*) absorption using a Perkin Elmer UV Lambda 40 spectrophotometer at the wavelength of 665 nm and for scattering correction at 750 nm. The detection limit was 0.1 µg L⁻¹. To obtain the cumulative chlorophyll *a* in the whole water column (mg Chl *a* m⁻²), from the discrete depths, we summed the concentration of Chl *a* from each stratum using the trapezoidal rule (León-Palmero *et al.*, 2019), as indicated in Eq. 5.4:

$$\text{Cumulative Chl } a = \sum_{k=1}^n X_{ik} \left(Z_{k+1} - \frac{Z_{k-1}}{2} \right) \quad \text{Eq. 5.4}$$

Where *Z* stands for the depth considered, and *n* is the number of depths sampled. *Z_k* stands for the *n* sampled depth; *X_{ij}* is the Chl *a* concentration (µg L⁻¹) at the depth *Z_k*.

We determined in triplicate the abundances of cyanobacteria and photosynthetic picoeukaryotes using flow cytometry using unfiltered water. We collected and fixed the samples with a mixture of 1 % paraformaldehyde and 0.05 % glutaraldehyde for 30 min in the dark at 4 °C. Then, we froze the samples in liquid nitrogen and stored them at 80 °C until analysis. We analyzed the samples in the FACSCalibur flow cytometer equipped with the BD CellQuest Pro software for data analysis. We used yellow–green 0.92 µm latex beads (Polysciences) as an internal standard to control the cytometer performance every day. We used different signals for groups determination: the side scatter (SSC), chlorophyll *a* (red fluorescence - FL3), phycoerythrin (orange fluorescence - FL2), and phycocyanin (blue fluorescence - FL4), following the protocols and indications for data analysis of previous works (Corzo *et al.*, 1999; Collier, 2000; Gasol and Giorgio, 2000; Cellamare *et al.*, 2010; Liu *et al.*, 2014). In Supplementary Figure 5.13, we show a cytogram of the populations of cyanobacteria and photosynthetic picoeukaryotes. The mean coefficient of variation for the abundances of cyanobacteria and photosynthetic picoeukaryotes was 8.8 % and 11.4 %, respectively.

We estimated gross primary production (GPP), net ecosystem production (NEP), and ecosystem respiration (R) by measuring temporal changes in dissolved oxygen concentration and temperature using a miniDOT (PME) submersible waterlogger during the stratification period. We recorded measurements every 10 min for 24–48 h during the same sampling days. Briefly, the equation for estimating free-water metabolism from measurements of dissolved oxygen was established by Odum (1956) (Eq. 5.5):

$$\Delta O_2 / \Delta t = GPP - R - F - A \quad \text{Eq. 5.5}$$

Where $\Delta O_2 / \Delta t$ is the change in dissolved oxygen concentration through time; F is the exchange of O₂ with the atmosphere; and A is a term that combines all other processes that may cause changes in the dissolved oxygen concentration as horizontal or vertical advection, and it is often assumed to be negligible. The calculations were performed as in Staehr *et al.* (2010). The physical gas flux was modelled as follows (Eq. 5.6):

$$F = k (O_{2 \text{ meas}} - O_{2 \text{ sat}}) \quad \text{Eq. 5.6}$$

Where F (g O₂ m⁻² h⁻¹) is the physical gas flux, and k (m h⁻¹) is the piston velocity estimated following the equation of Jähne *et al.* (1987), and the indications of Staehr *et al.* (2010). $O_{2 \text{ meas}}$ is the actual oxygen concentration (mg mL⁻¹), and $O_{2 \text{ sat}}$ is the oxygen concentration (mg mL⁻¹) in water in equilibrium with the atmosphere at ambient temperature and salinity.

We calculated the hourly net ecosystem production (NEP_{hr}) and the daytime net ecosystem production (NEP_{daytime}) following the equations 5.7 (Cole *et al.*, 2000) and 5.8:

$$NEP_{hr} = \Delta O_2 - F / Z_{mix} \quad \text{Eq. 5.7}$$

$$NEP_{daytime} = \text{mean } NEP_{hr} \text{ during daylight} \times \text{Light hours} \quad \text{Eq. 5.8}$$

NEP_{hr} (g O₂ m⁻³ h⁻¹) is directly derived from the changes in dissolved oxygen (ΔO_2 , g O₂ m⁻³ h⁻¹) after accounting for physical gas flux with the atmosphere (F). Z_{mix} is the depth of the mixed layer (m), and that was inferred from the temperature profile as the upper mixed zone where the temperature remains constant. NEP_{daytime} (g O₂ m⁻³ daylight period⁻¹) is the portion of NEP between sunrise and sunset, when the photosynthesis is taking place. We obtained the exact light hours from an online

solar calculator (<https://es.calcuworld.com/calendarios/calcular-salida-y-puesta-del-sol/>). We established the start and the end time for photosynthesis as 30 minutes before sunrise and 30 minutes after dawn (Schlesinger and Bernhardt, 2013). We obtained hourly R (R_{hr} , g O₂ m⁻³ h⁻¹), R during the daytime ($R_{daytime}$, g O₂ m⁻³ daylight period⁻¹), and R during all the day (R_{day} , g O₂ m⁻³ d⁻¹) following equation 5.9, 5.10, and 5.11, respectively:

$$R_{hr} = \text{mean NEP}_{hr} \text{ during darkness} \quad \text{Eq. 5.9}$$

$$R_{daytime} = R_{hr} \times \text{Light hours} \quad \text{Eq. 5.10}$$

$$R_{day} = R_{hr} \times 24 \quad \text{Eq. 5.11}$$

We calculated the respiration rate during the night (the period between 60 minutes after dawn and 60 minutes before sunrise) (Staehr *et al.*, 2010), and we assumed that the respiration rate overnight was similar to the respiration rate over the day. Finally, we obtained the GPP and NEP for the day (g O₂ m⁻³ d⁻¹) (Eq. 5.12 and 5.13):

$$\text{GPP} = \text{NEP}_{daytime} + R_{daytime} \quad \text{Eq. 5.12}$$

$$\text{NEP} = \text{GPP} - R_{day} \quad \text{Eq. 5.13}$$

5. 2. 5. DNA analysis

We selected three or four representative depths for determining the abundance of the functional genes of the epilimnion, metalimnion (oxycline), and hypolimnion and bottom layers during the stratification period. We also selected three or four equivalent depths during the mixing period. In total, we analyzed 41 samples from the stratification period and 36 samples for the mixing period. We pre-filtered the water through 3.0 µm pore-size filters and extracted DNA following the procedure developed by Boström *et al.* (2004) for environmental samples. During the DNA extraction protocol, we combined a cell recovery step by centrifugation of 12 – 20 mL of the pre-filtered water, a cell lysis step with enzyme treatment (lysozyme and proteinase K), and, finally, the DNA recovery step with a co-precipitant (yeast tRNA) to improve the precipitation of low-concentration DNA. DNA was quantified using a DNA quantitation kit (Sigma-Aldrich) based on the fluorescent dye

bisbenzimidazole (Hoechst 33258). Extracted DNA served as the template for PCR and quantitative PCR (qPCR) analysis to test the presence and abundance of the *mcrA* gene and the *phnJ* gene. For PCR analysis, we used the recombinant Taq DNA Polymerase (Thermo Fisher Scientific) using the Mastercycler X50 thermal cycler (Eppendorf). We ran the qPCR plates using SYBR Green as the reporter dye (PowerUp™ SYBR™ Green Master Mix, Thermo Fisher Scientific) in the Applied Biosystems 7500 Real-Time PCR System and the 7500 Software. In both cases, PCR and qPCR, we designed the standard reaction mix recipes and the thermocycling conditions using the provider specifications and primer requirements. We chose specific primers from studies performed in natural samples of freshwater. We used pure cultures as positive controls (more details below).

We targeted the alpha subunit of methyl-coenzyme reductase (*mcrA*) as a genetic marker to determine the existence and abundance of methanogenic Archaea in our samples. This gene appears to be an excellent marker, since all known methanogens have the methyl-coenzyme M reductase, which is the enzyme responsible for the conversion of a methyl group to CH₄ (Grabarse *et al.*, 2001). We used specific primers from West *et al.* (2012), adapting their procedure. The forward primer was *mcrAqF* (5' – AYGGTATGGARCAGTACGA – 3'), the reverse primer was *mcrAqR* (5' – TGVAGRTCCTABCCGWAGAA – 3'), and the annealing temperature was 54 °C. The expected size of the PCR product was ~200 bp (bp – base pair). We used a culture of *Methanosarcina acetivorans* (ATCC 35395) as a positive control. We tested all the samples (n = 77). We also tested the presence of the *phnJ* gene, which encodes a subunit of the C–P lyase complex (White and Metcalf, 2007; Seweryn *et al.*, 2015). This enzyme cleaves C–P bonds in phosphonate compounds, releasing methane, and changes in response to the phosphate availability (Yao *et al.*, 2016a). We ran the amplification with a pair of primers previously used by Fox *et al.* (2014) and Yao *et al.* (2016). The forward primer was *PhnJoc1* (5' – AARGTRATMGAYCARGG – 3'), and the reverse was *PhnJoc2* (5' – CATYTTYGGATTRTCRAA – 3'), adapting the PCR procedure from Yao *et al.* (2016). The annealing temperature was 52.5 °C, and the positive controls were run using a pure culture of *Rhodospseudomonas palustris* (ATCC 33872). The expected size of the PCR product was ~400 bp. We checked the result of the amplification by running 1.5 % (w/v) agarose gel electrophoresis. If we did not detect amplification in the PCR or qPCR samples, we changed the standard procedure by

increasing the DNA amount and the primers' concentration to corroborate the negative results. We tested all the samples ($n = 77$).

5. 2. 6. Statistical tests

We conducted all the statistical analysis in R (R Core Team, 2014) using the packages “car” (Fox and Weisberg, 2011), “nortest” (Gross and Ligges, 2015), and “mgcv” (Wood, 2011). We performed the Shapiro-Wilk test of normality analysis and Levene's test for homogeneity of variance across groups. We performed a one-way analysis-of-variance test (ANOVA) when the data were normally distributed. In case the data did not meet the assumptions of normality, we used the paired Kruskal-Wallis rank-sum (K-W) or Wilcoxon (V) tests. We analyzed the potential sources of dissolved CH₄ using simple regression analysis and generalized additive models (GAMs) (Wood, 2006). GAM is a generalized model with a linear predictor involving a sum of smooth functions of covariates (Hastie and Tibshirani, 1986, 1990). The model structure is shown in Eq. 5.14:

$$y_i = f_1(x_{1i}) + f_2(x_{2i}) + \dots + f_n(x_{ni}) + \epsilon_i \quad \text{Eq. 5.14}$$

Where the f_j are the smooth functions, and the ϵ_i is independent identically distributed $N(0, \sigma^2)$ random variables. We fit smoothing functions by penalized cubic regression splines. The cross-validation method (Generalized Cross Validation criterion, GCV) estimates the smoothness of the functions. We fitted the models to minimize the Akaike Information Criterion (AIC) and the GCV values. We calculated the percentage of variance explained by the model (adjusted R^2) and the quality of the fit (deviance explained). We also fixed the effect of each predictor to assess the contribution of the other predictors on the total deviance explained. Then, the sum of the deviance explained by two predictors can be different from the deviance explained by the model due to interactive effects.

5. 3. Results and discussion

5. 3. 1. Profile description

We found pronounced differences in the concentration of dissolved CH₄ of the studied reservoirs among depths and seasonal periods (Figures 5.2 - 5.4, and Supplementary Figures 5.1 – 5.9). The concentration of dissolved CH₄ ranged up to 4

orders of magnitude from 0.06 to 213.64 $\mu\text{mol L}^{-1}$ during the summer stratification ($n = 96$), and it was less variable during the winter mixing ($n = 84$) ranging only from 0.02 to 0.69 $\mu\text{mol L}^{-1}$. All depths were consistently supersaturated in CH₄, during both the stratification and mixing period (Supplementary Table 5.1). The dissolved CH₄ concentration and the percentage of saturation values were significantly higher during the stratification period than during the mixing period ($V = 78$, $p\text{-value} < 0.001$; $V = 78$, $p\text{-value} < 0.001$, respectively). These differences in the concentration of dissolved CH₄ are coherent with the differences found in the CH₄ emissions from these reservoirs in the stratification and mixing periods (León-Palmero *et al.*, 2020a). The wide range in CH₄ concentrations found in this study covers values reported in temperate lakes (Grossart *et al.*, 2011; Tang *et al.*, 2014; West *et al.*, 2016; Donis *et al.*, 2017), to those found in tropical lakes and reservoirs (Murase *et al.*, 2003; Roland *et al.*, 2017; Naqvi *et al.*, 2018; Okuku *et al.*, 2019). In the surface mixing layer during the stratification period (i.e., epilimnion), we found values from 0.06 to 8.18 $\mu\text{mol L}^{-1}$ (Supplementary Table 5.1), which is about 80 times the maximum values found in the surface waters of Lake Kivu (Africa) by Roland *et al.* (2017) and similar to the concentrations reported in subtropical and tropical reservoirs (Musenze *et al.*, 2014 and references therein).

The dissolved CH₄ profiles showed considerable differences among depths during the summer stratification (Figures 5.2a – 5.4a, and Supplementary Figures 5.1a – 5.9a), but were very homogeneous during the winter mixing in all the reservoirs (Figures 5.2b – 5.4b, and Supplementary Figures 5.1b – 5.9b) (Supplementary Table 5.1). Based on the differences found during the stratification period in the dissolved CH₄ profiles, we sorted the reservoirs into three types. The first type of CH₄ profile included six reservoirs that were characterized by an increase in the dissolved CH₄ from the oxycline to the anoxic bottom, just above the sediments, where CH₄ concentration reached its maximum. In these reservoirs, the oxycline may be spatially coupled to the thermocline or not. When the oxycline and the thermocline were spatially coupled, the dissolved CH₄ concentration increased exponentially from the thermocline along the anoxic hypolimnion to the sediments. The reservoirs Béznař, San Clemente, and Iznájar showed this type of profile (Figure 5.2a and Supplementary Figures 5.1a and 5.2a). The existence of a sizeable almost-anoxic hypolimnion led to a massive accumulation of CH₄ in this layer. The differences

in the CH₄ concentration between the surface and bottom waters were up to 3 orders of magnitude, as we found in Béznar (from the 0.25 to 56.17 μmol L⁻¹; Figure 5.2a), San Clemente (from the 0.23 to 45.15 μmol L⁻¹; Supplementary Figure 5.1a), and Iznájar (from the 0.82 to 213.64 μmol L⁻¹; Supplementary Figure 5.2a). When the oxycline and the thermocline were not spatially coupled, the dissolved CH₄ concentration increased just above the sediments, where the anoxic-oxic interface was near to the bottom. The reservoirs Cubillas, La Bolera, and Francisco Abellán showed this profile type (Supplementary Figures 5.3a, 5.4a, and 5.5a). This accumulation of CH₄ in the hypolimnion and above sediments might be related to the high rates of methanogenesis in the sediments and its subsequent diffusion to the water column. Dissolved CH₄ concentration declines at the oxycline level, where the highest rates of CH₄ oxidation usually occur (Oswald *et al.*, 2015, 2016). The CH₄ profiles in this group were similar to the ones found in tropical eutrophic and temperate reservoirs (West *et al.*, 2016; Naqvi *et al.*, 2018).

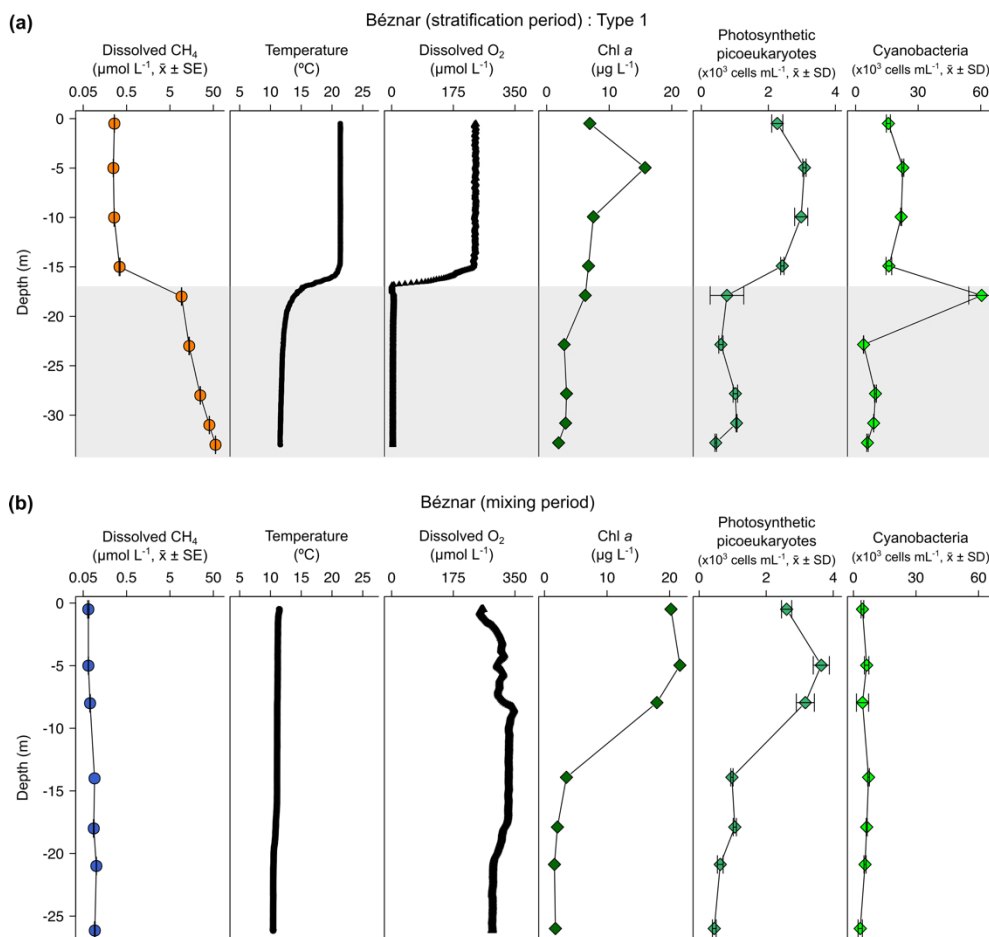


Figure 5.2. Vertical profiles of physicochemical and biological variables in Béznař reservoir. Dissolved methane (CH₄) concentration (μmol L⁻¹, mean ± standard error), temperature (°C), dissolved oxygen (DO) concentration (μmol L⁻¹), chlorophyll *a* (Chl *a*) concentration (μg L⁻¹), abundance of photosynthetic picoeukaryotes (x 10³ cells mL⁻¹, mean ± standard deviation) and abundance of cyanobacteria (x 10³ cells mL⁻¹, mean ± standard deviation) during the stratification period (a) and the mixing period (b). The grey area represents the anoxic zone (DO < 7.5 μmol L⁻¹). Note the logarithmic scales in the x axis of the dissolved CH₄ profiles. The sampling for the stratification period was on 7 October 2016 and 23 February 2017 for the mixing period.

The second profile type presents a small peak of metalimnetic CH₄, concomitant with peaks of dissolved oxygen, chlorophyll *a*, photosynthetic picoeukaryotes, and cyanobacteria (Figure 5.3a). In the Negratín reservoir, we found the maximum concentration of CH₄ in the oxic hypolimnion. Unlike several previous works in lakes (Murase *et al.*, 2003; Grossart *et al.*, 2011; Bles *et al.*, 2015; Khatun *et al.*, 2019), we did not find a metalimnetic CH₄ maximum. Khatun *et al.* (2019) described the existence of a metalimnetic CH₄ maximum in 10 out of 14 lakes. The metalimnetic CH₄ maximum may represent a physically driven CH₄ accumulation due

to solubility differences with the temperature at the thermocline, the epilimnetic CH₄ losses by emission, and the lateral inputs from the littoral zone (Hofmann *et al.*, 2010; Encinas Fernández *et al.*, 2016; Donis *et al.*, 2017). The metalimnetic CH₄ maximum can also be determined by biological factors, including the light inhibition of the methane oxidation (Murase and Sugimoto, 2005; Tang *et al.*, 2014) or the distinctive methane production by phytoplankton due to availability of nutrients, light or precursors at this layer (Khatun *et al.*, 2019).

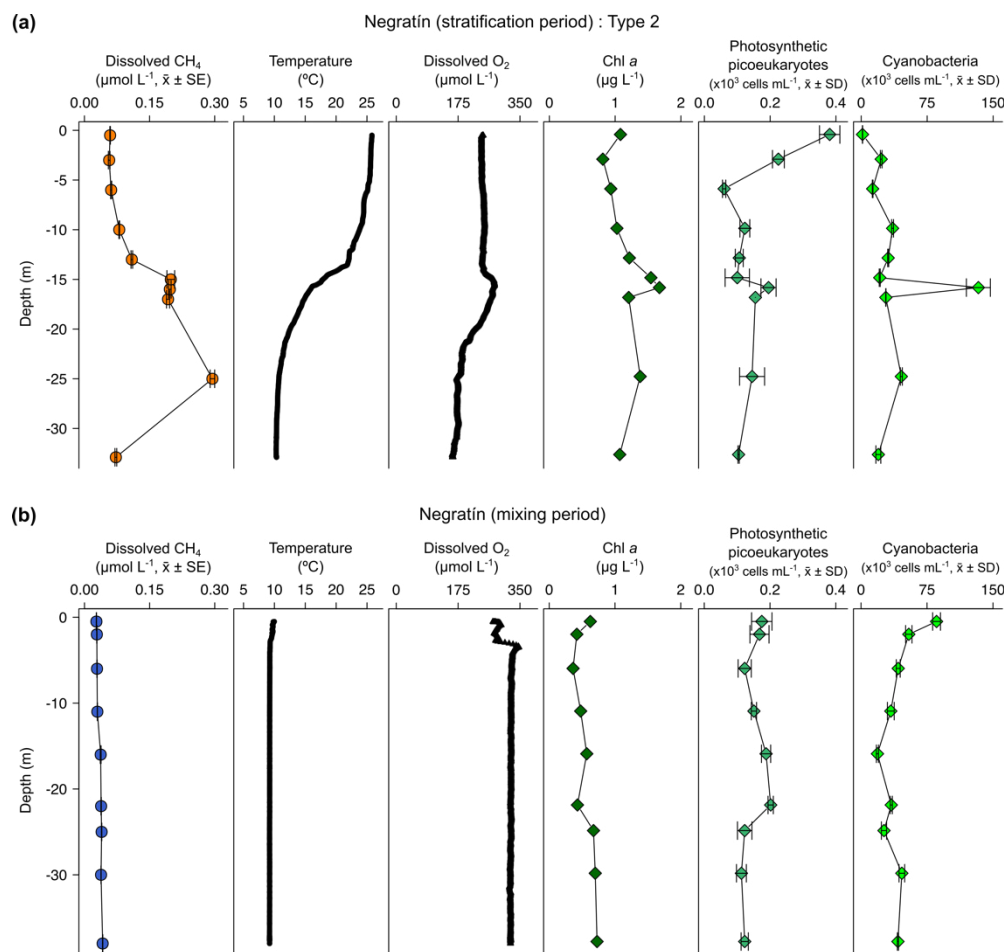


Figure 5.3. Vertical profiles of physicochemical and biological variables in Negratín reservoir. Dissolved methane (CH₄) concentration (μmol L⁻¹, mean ± standard error), temperature (°C), dissolved oxygen (DO) concentration (μmol L⁻¹), chlorophyll *a* (Chl *a*) concentration (μg L⁻¹), abundance of photosynthetic picoeukaryotes (x 10³ cells mL⁻¹, mean ± standard deviation) and abundance of cyanobacteria (x 10³ cells mL⁻¹, mean ± standard deviation) during the stratification period (a) and the mixing period (b). The sampling for the stratification period was on 27 July 2016 and 16 February 2017 for the mixing period.

The third profile type included five reservoirs, in which the dissolved CH₄ profile presented a CH₄ accumulation more significant in the epilimnion than in the hypolimnion. The reservoirs Jándula, Bermejales, Rules, El Portillo, and Colomera showed this profile type (Figure 5.4a, and Supplementary Figures 5.6a – 5.9a). These reservoirs had a mean CH₄ concentration in the water column significantly lower than the reservoirs from the first type. Similar profiles have been reported in temperate (Tang *et al.*, 2014) and tropical lakes (Murase *et al.*, 2003).

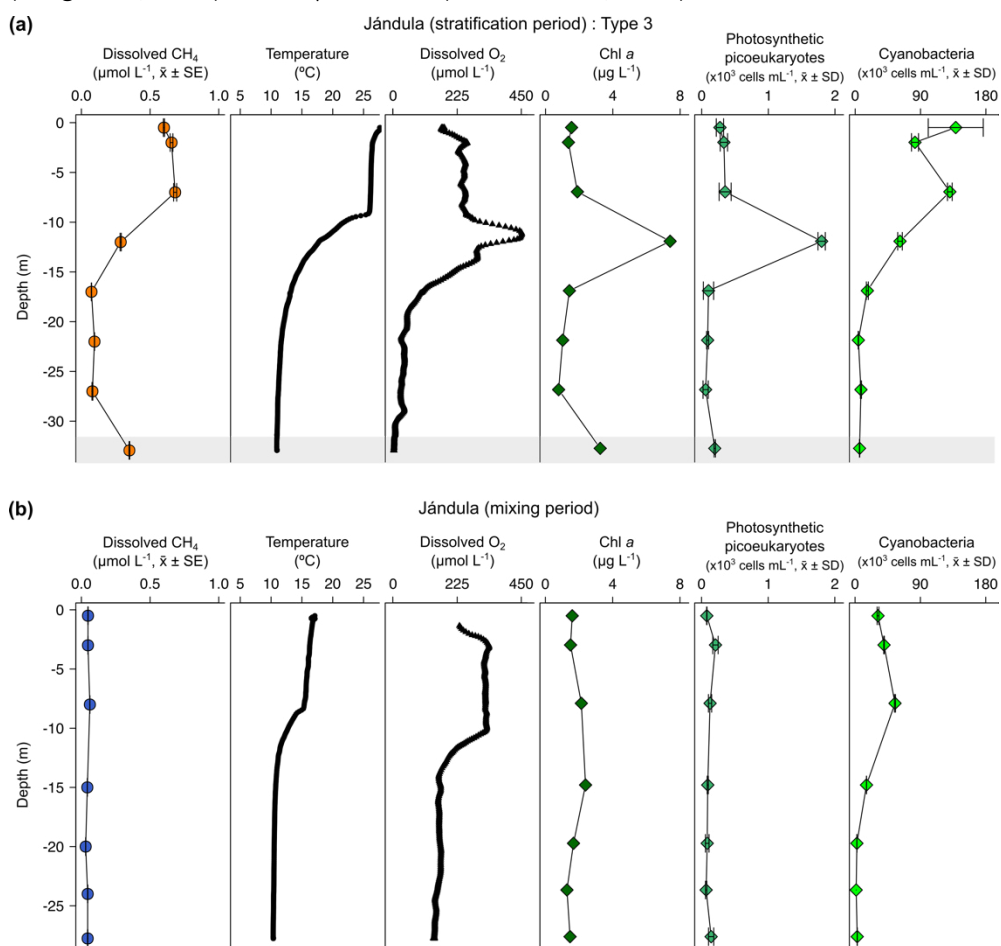


Figure 5.4. Vertical profiles of physicochemical and biological variables in Jándula reservoir. Dissolved methane (CH₄) concentration (μmol L⁻¹, mean ± standard error), temperature (°C), dissolved oxygen (DO) concentration (μmol L⁻¹), chlorophyll *a* (Chl *a*) concentration (μg L⁻¹), abundance of photosynthetic picoeukaryotes (x 10³ cells mL⁻¹, mean ± standard deviation) and abundance of cyanobacteria (x 10³ cells mL⁻¹, mean ± standard deviation) during the stratification period (a) and the mixing period (b). The grey area represents the anoxic zone (DO < 7.5 μmol L⁻¹). The sampling for the stratification period was on 24 July and 5 April 2017 for the mixing period.

5. 3. 2. CH₄ sources in the water column

We found two well-differentiated groups of CH₄ data sorted by the dissolved oxygen (DO) concentration (Supplementary Figure 5.10), as in previous studies (Tang *et al.*, 2014). The first dataset included the samples with a DO lower than 7.5 μmol L⁻¹ (n = 18, hereafter anoxic samples). These samples belong to the hypolimnion of the studied reservoirs during the stratification period. The second dataset included the samples with DO higher than 7.5 μmol L⁻¹ (n = 160, hereafter oxic samples). All the samples from the mixing period (n = 82) and most of the samples from the stratification period (n = 78) belong to this second dataset. We found significant differences (W = 2632, p-value < 0.001) between the concentration of CH₄ in the anoxic samples (median = 15.79 μmol L⁻¹, min = 0.35 μmol L⁻¹, max = 213.64 μmol L⁻¹) and in the oxic samples (median = 0.15 μmol L⁻¹, min = 0.02 μmol L⁻¹, max = 8.17 μmol L⁻¹). Since these two groups of samples are different, we determined their sources and drivers separately (Supplementary Table 5.2).

5. 3. 2. 1. CH₄ sources in anoxic samples

Archaeal methanogens are obligate anaerobes that decompose the organic matter and produce CH₄ in anoxic environments, as freshwater sediments. We analyzed the presence of the methanogenic Archaea in the anoxic samples of the water column by targeting the gene *mcrA*. From the 77 samples selected for genetic analysis, 12 of them were anoxic. We did not detect the amplification of the *mcrA* gene in the PCR or the qPCR analysis in these 12 samples. Therefore, we assumed that the methanogenic Archaea were not present, as free-living microorganisms, in the water column of the anoxic samples. However, they may still be present in micro-anoxic zones in the water column (i.e., in the guts of zooplankton or within exopolymeric particles). Methanogenesis is a microbial process particularly sensitive to temperature (Marotta *et al.*, 2014; Yvon-Durocher *et al.*, 2014; Sepulveda-Jauregui *et al.*, 2018). However, we did not find a significant relationship between the water temperature and the dissolved CH₄ concentration in the anoxic samples (n = 17, p-value = 0.66). The lack of a detection of the *mcrA* gene in the hypolimnetic waters and the absence of a relationship between the dissolved CH₄ and water temperature suggest that CH₄ production is not happening in the water column of the studied reservoirs. We think that most methanogenic Archaea must be present in the

sediments, where they produce CH₄ that diffuses up to the water column, producing vast accumulations of CH₄ in the hypolimnion.

Methanogenesis in the sediments may be affected by organic matter quantity and quality (West *et al.*, 2012). Organic matter quantity is measured as the dissolved organic carbon concentration, whereas the organic matter quality usually is related to their phytoplanktonic versus terrestrial origin. In the studied reservoirs, the dissolved organic carbon concentration did not show a significant relationship with the dissolved CH₄ concentration ($n = 12$, p -value = 0.10, Supplementary Table 5.2). We examined the importance of the autochthonous organic matter produced by primary producers using the total cumulative chlorophyll *a* (Chl *a*, mg m⁻²). The cumulative Chl *a* is considered to be a surrogate for the vertical export of the phytoplankton biomass in the whole water column. We found that the CH₄ concentrations in anoxic samples were correlated to the cumulative Chl *a* following a power function ($\text{CH}_4 = 3.0 \cdot 10^{-4} \text{ Cumulative Chl } a^{2.28}$; $n = 17$, adjusted $R^2 = 0.40$, p -value < 0.01, Supplementary Table 5.2) (Figure 5.5). The autochthonous organic matter appeared to be a better predictor for the concentration of CH₄ in anoxic waters than the dissolved organic matter concentration. In the studied reservoirs, the dissolved organic carbon concentration was significantly related to the age of the reservoirs and the forestry coverage in their watersheds (León-Palmero *et al.*, 2019). Therefore, in terms of quality, the total pool of dissolved organic carbon may be more representative of the carbon fraction that is allochthonous, recalcitrant, and more resistant to microbial degradation.

In contrast, the autochthonous organic matter may represent a more labile and biodegradable fraction. Previous experimental studies have demonstrated that the addition of algal biomass on sediment cores increases the CH₄ production more than the addition of terrestrial organic matter (Schwarz *et al.*, 2008; West *et al.*, 2012, 2015). The stimulation of the methanogenesis rates appears to be related to the lipid content in phytoplankton biomass (West *et al.*, 2015). West *et al.* (2016) found a significant relationship between the chlorophyll *a* concentration in the epilimnion and the potential methanogenesis rates from sediment incubations. In this study, we corroborate the importance of the autochthonous-derived organic matter determining the CH₄ concentrations in anoxic waters. Since we did not detect the existence of the *mcrA* gene in the water column, we considered that the production

of methane by methanogenic Archaea occurred primarily in the sediments and was affected by the sedimentation of organic matter derived from phytoplankton.

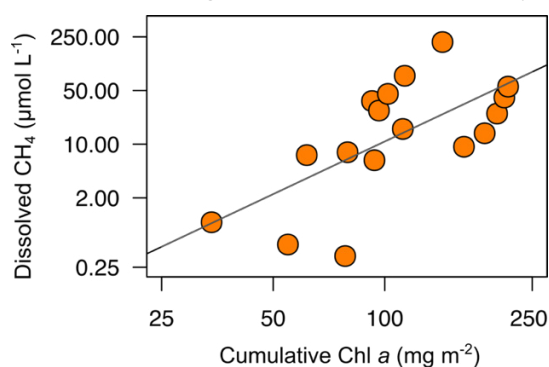


Figure 5.5. Power relationship between the depth-cumulative chlorophyll *a* concentration and the concentration of dissolved CH₄ in the anoxic waters during the stratification period (CH₄, μmol L⁻¹ = 3.0 10⁻⁴ Cumulative Chl *a*^{2.28}, *n* = 17, adj R² = 0.40). Note that both axes are in logarithmic scale. More statistical details in Supplementary Table 5.2.

5. 3. 2. 2. CH₄ sources in oxic samples

In this study, the concentration of dissolved CH₄ ranged from 0.02 to 8.18 μmol L⁻¹, and all the samples of the oxic waters were supersaturated, with values always above 800% and ranging more than 2 orders of magnitude (Supplementary Table 5.1). To determine the origin of this CH₄ supersaturation, we examined the following potential sources: (1) the vertical and lateral CH₄ transport from deep layers and littoral zones, (2) the *in situ* CH₄ production by methanogenic Archaea potentially tolerant to oxygen or by the methylphosphonate degradation under severe P limitation, and (3) the *in situ* CH₄ production by processes associated to the phytoplanktonic community.

Vertical and lateral CH₄-transport from anoxic sediments to oxic waters

Several previous works have pointed out that CH₄ supersaturation in oxic waters can be explained by the vertical transport from the bottom sediments and the lateral inputs from the littoral zones that are in contact with shallow sediments where methanogenesis occurs (Michmerhuizen *et al.*, 1996; Bastviken *et al.*, 2004; Encinas Fernández *et al.*, 2016). To test the importance of the lateral and vertical transport explaining the concentration of CH₄ in the oxic waters of the studied reservoirs, we used two morphometric parameters: the mean depth (m) as a proxy for the vertical transport and the shallowness index as a proxy for the lateral transport. The dissolved CH₄ concentration was an exponential decay function of the reservoir mean depth

(Figure 5.6a) both during the stratification period ($\text{CH}_4 = 4.0 \cdot 10^{-2} e^{(50.0/\text{mean depth})}$, adjusted $R^2 = 0.95$) and during the mixing period ($\text{CH}_4 = 3.7 \cdot 10^{-2} e^{(22.9/\text{mean depth})}$, adjusted $R^2 = 0.54$) (Figure 5.6a). We observed that in reservoirs with a mean depth shallower than 16 m, the dissolved CH₄ concentration increased exponentially (Figure 5.6a). Several studies have proposed that the vertical transport of CH₄ from bottom sediments explains the supersaturation in surface waters (Rudd and Hamilton, 1978; Michmerhuizen *et al.*, 1996; Murase *et al.*, 2003; Bastviken *et al.*, 2004; Encinas Fernández *et al.*, 2016). However, the vertical diffusion rates of dissolved gases across the thermocline are too low in deep and thermally stratified systems, and no movements of methane upwards from the hypolimnion have been detected (Rudd and Hamilton, 1978). However, in shallow reservoirs, the hydrostatic pressure might be reduced, promoting CH₄ diffusion from the anoxic layers.

The shallowness index increases in elongated and dendritic reservoirs, with a greater impact of the littoral zone, and decreases in near-circular reservoirs, with low shoreline length per surface. However, we did not find a significant relationship between the shallowness index and the dissolved CH₄ concentration (Figure 5.6b). One explanation for the absence of this relationship could be the relatively large size of the reservoirs. Although the reservoir size covered more than 1 order of magnitude (Table 5.1), all reservoirs have a size larger than 1 km². Previous studies have shown that CH₄ lateral diffusion may be an important process in areas near to the littoral zone and small lakes. Hofmann *et al.* (2010) found higher concentrations in the shallow littoral zones than in the open waters. DelSontro *et al.* (2018) predicted that lateral inputs from littoral zones to pelagic waters are more critical in small and round lakes than in large and elongated lakes. Nevertheless, the differences between the observations and predictions from the model suggested that these lateral inputs may not be enough to explain CH₄ concentration in open waters, where *in situ* production may prevail over lateral transport (DelSontro *et al.*, 2018).

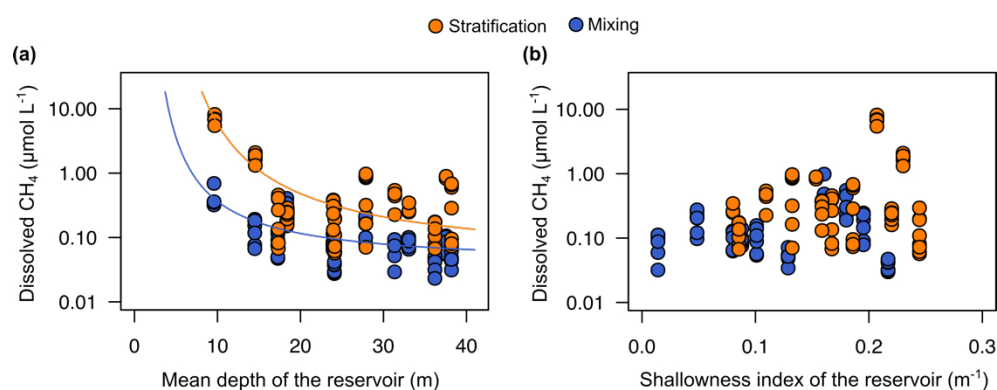


Figure 6: Reservoir morphometry and the dissolved CH₄ concentration in the oxic zone. (a) Exponential decay relationships of the dissolved CH₄ concentration and the mean depth (m) during the stratification period ($\text{CH}_4 = 0.04 e^{(50.0/\text{mean depth})}$, $n = 78$, adjusted $R^2 = 0.95$) and the mixing period ($\text{CH}_4 = 0.037 e^{(22.9/\text{mean depth})}$, $n = 82$, adjusted $R^2 = 0.54$). (b) Scatterplot of dissolved CH₄ concentration and the reservoir shallowness index during the stratification period ($p\text{-value} = 0.134$) and the mixing period ($n = 0.114$). More statistical details in Supplementary Table 5.2.

***In situ* CH₄-production by methanogenic Archaea or methyl-phosphonate degradation**

The ubiquitous CH₄ supersaturation found in oxic waters appears not to be fully explained by the vertical and lateral transport, underlining that there is an *in situ* production of CH₄, as proposed by Grossart *et al.* (2011); Bogard *et al.* (2014) and DelSontro *et al.* (2018). We studied the presence of the methanogenic Archaea in the oxic samples by targeting the gene *mcrA*, but we were unable to detect this gene (Supplementary Figure 5.11). This result indicates that methanogenic Archaea were not present, at least as free-living microorganisms, in a significant number in the water column of the oxic samples. The classical methanogens (i.e., Archaea with the *mcrA* gene) are obligate anaerobes without the capacity to survive and produce CH₄ under aerobic conditions (Chistoserdova *et al.*, 1998). Previous studies by Angel *et al.* (2011) and Angle *et al.* (2017) showed that methanogens might tolerate oxygen exposure in soils, and Grossart *et al.* (2011) detected potential methanogenic Archaea attached to photoautotrophs in oxic lake waters. Unfortunately, we did not test their occurrence in large particles, phytoplankton, or zooplankton guts, although some authors have detected them in these microsites' particles (de Angelis and Lee, 1994; Karl and Tilbrook, 1994).

We also considered the possibility of methylphosphonate degradation as an *in situ* CH₄ source. This metabolic pathway appears in the bacterioplankton under

chronic starvation for phosphorus (Karl *et al.*, 2008). Several pieces of evidence have shown that marine bacterioplankton can degrade the MPn's and produce CH₄ through the C-P lyase activity in typically phosphorus-starved environments, like the ocean gyres (Beversdorf *et al.*, 2010; Carini *et al.*, 2014; del Valle and Karl, 2014; Repeta *et al.*, 2016; Teikari *et al.*, 2018). Freshwater bacteria can also degrade the MPn's and produce CH₄, as has been demonstrated in Lake Matano (Yao *et al.*, 2016a, 2016b). Lake Matano is an ultra-oligotrophic lake with a severe P deficiency (below 0.050 $\mu\text{mol-P L}^{-1}$) due to the permanent stratification, iron content, and extremely low nutrient inputs (Crowe *et al.*, 2008; Sabo *et al.*, 2008). The ratio of dissolved inorganic nitrogen (DIN) to total phosphorus (TP) ($\mu\text{mol-N} : \mu\text{mol-P}$) is widely used to evaluate P limitation (Morris and Lewis, 1988). DIN : TP ratios greater than 4 are indicative of phosphorus limitation (Axler *et al.*, 1994). In the studied reservoirs, the TP concentration ranged from 0.13 to 1.85 $\mu\text{mol-P L}^{-1}$ during the stratification period and from 0.10 to 2.17 $\mu\text{mol-P L}^{-1}$ during the mixing period. The mean DIN : TP ratio ranged from 12 to 675 during the stratification period and from 63 to 392 during the mixing period. The more severe the P limitation conditions are, the higher the CH₄ production by methylphosphonates degradation is. However, we did not find a significant relationship between the DIN : TP ratio and the CH₄ concentration (Figure 5.7).

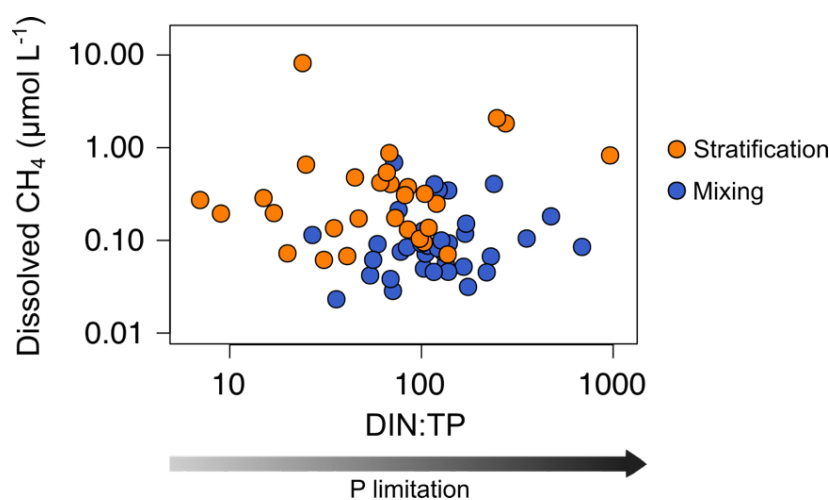


Figure 5.7. Phosphorus limitation and the dissolved CH₄ concentration in the oxic waters. Scatterplot of dissolved CH₄ concentration and the ration between dissolved inorganic nitrogen (DIN) and the total phosphorus (TP) ($\mu\text{mol N} : \mu\text{mol P}$). Note the logarithmic scale in both axes.

We also analyzed the presence and abundance of the gene *phnJ*, which encodes the enzyme complex C–P lyase that hydrolyzes the MPn's and changes in response to phosphate availability. We did not detect the *phnJ* gene in the PCR or the qPCR analysis in any of the study samples (Supplementary Figure 5.12). These results indicate that the MPn degradation was not a quantitatively relevant source of CH₄ in the oxic waters of the studied reservoirs. Our results are in concordance with Grossart *et al.* (2011), who did not detect CH₄ production by adding inorganic phosphate or methylphosphonates to lake samples in laboratory experiments. Although we used different methodologies, both studies may indicate that MPn degradation is only an important source of CH₄ in ultra-oligotrophic systems, as in Lake Matano or ocean gyres.

***In situ* CH₄-production coupled to photosynthetic organisms**

In the studied reservoirs, we analyzed the relationship between photosynthetic organisms and the dissolved CH₄ concentration using GPP (g O₂ m⁻³ d⁻¹), NEP (g O₂ m⁻³ d⁻¹), the concentration of Chl *a* (μg L⁻¹), and the abundance of photosynthetic picoeukaryotes (PPEs, cells mL⁻¹) and cyanobacteria (CYA, cells mL⁻¹). We determined GPP and NEP just once per reservoir during the stratification period (i.e., n =12).

The PPEs are essential components of the marine and freshwater phytoplankton, and they are eukaryotes with a size of 3.0 μm or less. In the freshwater, the PPEs include species from different phyla, like unicellular Chlorophyta (green algae) and Haptophyta. Using optical microscopy, we determined the main groups of photosynthetic picoeukaryotes in the studied reservoirs. PPEs were non-colonial green algae from the order Chlorococcales (class Chlorophyceae, phylum Chlorophyta) and the genus *Chrysochromulina* spp. (class Coccolithophyceae, phylum Haptophyta). The cyanobacteria detected were mainly phycoerythrin-rich picocyanobacteria, although we also detected phycocyanin-rich picocyanobacteria in one reservoir (Béznar). We show the vertical profiles of the Chl *a* concentration and the abundance of PPEs and CYA profiles of each reservoir in Figures 5.2 – 5.4 and Supplementary Figures 5.1 – 5.9. We also report the minimum, the quartiles, and the maximum values for the Chl *a* concentration and the abundance of PPEs and CYA during the stratification and the mixing periods in

Supplementary Table 5.2. The abundance of cyanobacteria ranged from 1.51×10^3 to 2.04×10^5 cells mL⁻¹ and was more than 1 order of magnitude higher than the abundance of PPEs that ranged from 32 to 7.45×10^3 cells mL⁻¹.

We found that the relationship between the gross primary production and the dissolved CH₄ concentration was only marginally significant (p-value = 0.077, n = 12) and not significant with the net ecosystem production (Table 5.3). The Chl *a* concentration showed a significant relationship with the GPP (p-value < 0.01, n = 12, adjusted R² = 0.55), but the abundance of cyanobacteria or the abundance of the photosynthetic picoeukaryotes did not show a significant relationship with the GPP (p-value = 0.911, n = 12; p-value = 0.203, n = 12, respectively). We found significant power relationships between the Chl *a* concentration, the abundance of photosynthetic picoeukaryotes, and the abundance of cyanobacteria with the concentration of dissolved CH₄ during the stratification period (Figure 5.8a, b, and c, respectively, and Table 5.3). During the mixing period, the Chl *a* concentration, and the abundance of photosynthetic picoeukaryotes were also significantly related to the dissolved CH₄ concentration (Figure 5.8 a and b). The slope of the relationship (i.e., the exponent in the power relationship) between the dissolved CH₄ and the abundance of photosynthetic picoeukaryotes, or the Chl *a* concentration, was higher during the stratification than during the mixing (Table 5.3). By comparing the stratification slopes, the effect per cell of PPEs on CH₄ concentration was slightly higher than the impact of cyanobacteria (Table 5.3). These results agree with previous studies that showed a closed link between the CH₄ concentration and the photosynthetic organisms, primary production, or chlorophyll *a* concentration (Schmidt and Conrad, 1993; Grossart *et al.*, 2011; Bogard *et al.*, 2014; Tang *et al.*, 2014).

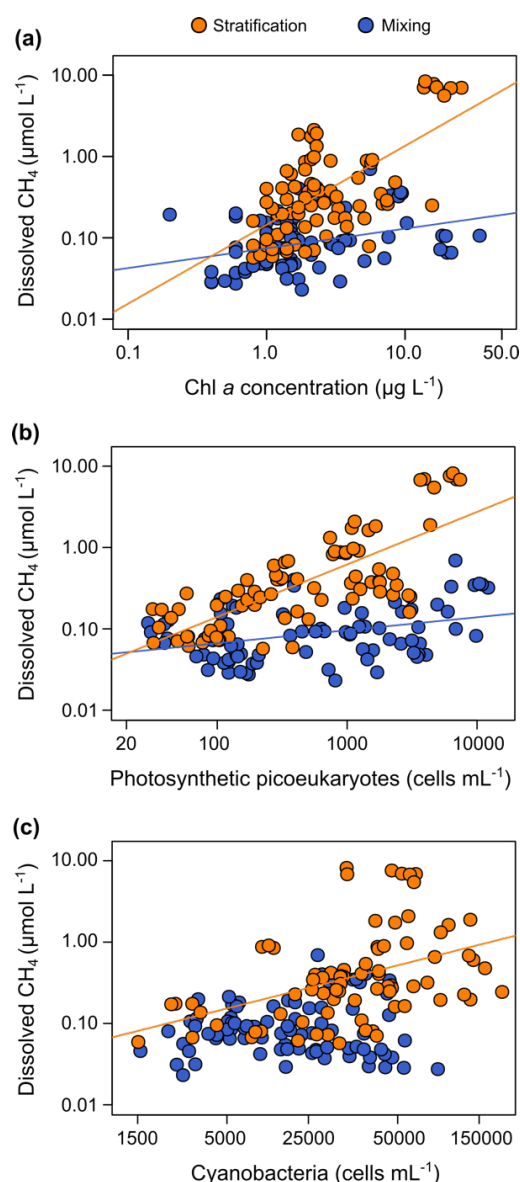


Figure 5.8. Phytoplanktonic variable coupled with the dissolved CH₄ concentration in the oxic waters.

(a) The dissolved CH₄ concentration was significantly related to the chlorophyll *a* concentration during the stratification period (p-value < 0.001), and during the mixing period (p-value < 0.01). The relationship was a power function during the stratification ($\text{CH}_4, \mu\text{mol L}^{-1} = 0.14 \text{ Chl } a^{0.97}$; $n = 78$, adjusted $R^2 = 0.40$), and during the mixing period ($\text{CH}_4, \mu\text{mol L}^{-1} = 0.07 \text{ Chl } a^{0.24}$; $n = 82$, adjusted $R^2 = 0.11$) (b) Relationships between dissolved CH₄ concentration and the abundance of photosynthetic picoeukaryotes (PPEs) during the stratification period ($\text{CH}_4, \mu\text{mol L}^{-1} = 0.0072 \text{ PPEs}^{0.65}$; $n = 78$, adjusted $R^2 = 0.55$, p-value < 0.001), and the mixing period ($\text{CH}_4, \mu\text{mol L}^{-1} = 0.032 \text{ PPEs}^{0.16}$; $n = 82$, adjusted $R^2 = 0.12$, p-value < 0.001). (c) Relationship between dissolved CH₄ concentration and the cyanobacteria abundance (CYA). A power function described the relationship between the dissolved CH₄ and the CYA during the stratification period ($\text{CH}_4, \mu\text{mol L}^{-1} = 0.0017 \text{ CYA}^{0.53}$; $n = 78$, adjusted $R^2 = 0.17$, p-value < 0.001). The relationship was not significant during the mixing period (p-value = 0.666).

In this study, we show that the PPE abundance was a better predictor of the CH₄ concentration than the abundance of cyanobacteria. In the studied reservoirs, the PPE group included members from green algae and Haptophyta, which are regular components of the marine plankton. Therefore, these results may also be relevant for marine waters. Cyanobacteria have received more attention as potential producers of CH₄ in oxic conditions than photosynthetic picoeukaryotes (Berg *et al.*, 2014; Teikari *et al.*, 2018; Bižić *et al.*, 2020). Klintzsch *et al.* (2019) demonstrated that widespread marine and freshwater haptophytes like *Emiliana huxleyi*, *Phaeocystis globosa*, and *Chrysochromulina* sp. produce CH₄ under oxic conditions. They also observed that the cell abundances were significantly related to the amount of CH₄ produced. Interestingly, *Chrysochromulina* was one of the genera of PPEs that we detected in the studied reservoirs. Grossart *et al.* (2011) also found CH₄ production in laboratory cultures of cyanobacteria and green algae.

Overall, these results indicate a clear association between the CH₄ production and the photosynthetic organisms from both Eukarya (picoeukaryotes) and Bacteria (cyanobacteria) domains. The pathways involved in the CH₄ production may be related to the central photosynthetic metabolism or the release of methylated by-products, different from methylphosphonates during the photosynthesis. Previous studies demonstrated the CH₄ production in laboratory cultures using ¹³C-labeled bicarbonate in haptophytes (Lenhart *et al.*, 2016; Klintzsch *et al.*, 2019); in marine, freshwater, and terrestrial cyanobacteria (Bižić *et al.*, 2020); and in major groups of phytoplankton (Hartmann *et al.*, 2020). In these studies, the photosynthetic organisms uptake bicarbonate in the reductive pentose phosphate cycle (Calvin–Benson cycle) (Burns and Beardall, 1987; Berg, 2011). Therefore, CH₄ production may be a common pathway in the central metabolism of photosynthesis of all the cyanobacteria and algae in freshwater and marine environments.

On the other hand, the production of CH₄ can also be related to the production of methylated compounds during photosynthesis. Lenhart *et al.* (2016) and Klintzsch *et al.* (2019) also detected the CH₄ production in cultures from the sulfur-bound methyl group of the methionine and methyl thioethers. Common substances like methionine can act as a methyl-group donor during the CH₄ production in plants and fungi (Lenhart *et al.*, 2012, 2015). Besides, algae use part of the methionine for the synthesis of dimethylsulfoniopropionate (DMSP), an abundant osmolyte, the

precursor of dimethyl sulfide (DMS), and dimethyl sulfoxide (DMSO). These methylated substances produce methane during their degradation (Damm *et al.*, 2008, 2010, 2015; Zindler *et al.*, 2013). Bižić-Ionescu *et al.* (2018) also suggested that CH₄ could be produced from methylated amines under oxic conditions. These substances, together with other organosulphur compounds, can also produce CH₄ abiotically (Althoff *et al.*, 2014; Bižić-Ionescu *et al.*, 2018). The production of DMSP, DMS, and other methylated substances like isoprene has been extensively studied in marine phytoplankton, showing that taxa as photosynthetic picoeukaryotes and the cyanobacteria are relevant sources (Yoch, 2002; Shaw *et al.*, 2003). Recent studies have also reported that freshwater algae and cyanobacteria also produced DMS and isoprene (Steinke *et al.*, 2018). Further studies are needed to quantify the potential role of all these methylated by-products as potential CH₄ sources quantitatively relevant in freshwater.

Table 5.3. Equations for the relationships between the phytoplanktonic variables and the dissolved CH₄ concentration ($\mu\text{mol L}^{-1}$) in the oxic waters. n.m. means not measured.

Driver	Period	n	Equation	Adjusted R ²	p-value
Chl <i>a</i> concentration ($\mu\text{g L}^{-1}$)	Stratification + Mixing	160	$\text{CH}_4 = 0.11 \text{ Chl } a^{0.63}$	0.23	< 0.001
	Stratification	78	$\text{CH}_4 = 0.14 \text{ Chl } a^{0.97}$	0.40	< 0.001
	Mixing	82	$\text{CH}_4 = 0.07 \text{ Chl } a^{0.24}$	0.11	< 0.01
Gross primary production (GPP; $\text{g O}_2 \text{ m}^{-3} \text{ d}^{-1}$)	Stratification	12	Marginally significant		0.077
	Mixing	n.m.			
Net ecosystem production (NEP; $\text{g O}_2 \text{ m}^{-3} \text{ d}^{-1}$)	Stratification	12	Not significantly related		0.536
	Mixing	n.m.			
Photosynthetic picoeukaryotes' (PPEs') abundance (cells mL^{-1})	Stratification + Mixing	160	$\text{CH}_4 = 0.02 \text{ PPEs}^{0.35}$	0.19	< 0.001
	Stratification	78	$\text{CH}_4 = 0.0072 \text{ PPEs}^{0.65}$	0.57	< 0.001
	Mixing	82	$\text{CH}_4 = 0.032 \text{ PPEs}^{0.16}$	0.12	< 0.001
Cyanobacteria (CYA) abundance (cells mL^{-1})	Stratification + Mixing	160	$\text{CH}_4 = 0.00099 \text{ CYA}^{0.53}$	0.19	< 0.001
	Stratification	78	$\text{CH}_4 = 0.0017 \text{ CYA}^{0.53}$	0.17	< 0.001
	Mixing	82	Not significantly related		0.666

5. 3. 2. 3. Modeling the CH₄ production in oxic waters

The explanation of the CH₄ supersaturation in oxic waters in relatively large systems relies on the interaction of several processes as the transport from anoxic

environments and the biological activity (DeSontro *et al.*, 2018). In this study, we found that vertical transport (mean depth as surrogate), water temperature, and the abundance of photosynthetic picoeukaryotes and cyanobacteria had a significant effect on the dissolved CH₄ concentration. We combined these explanatory variables with significant effects using GAMs. The GAM for the stratification period (n =78) had a fit deviance of 82.7 % and an explained variance (adjusted R²) of 81.4 % (Supplementary Table 5.3). The explanatory variables, in decreasing order, were as follows: the photosynthetic picoeukaryotes' abundance (log₁₀ PPEs), the reservoir mean depth, the cyanobacteria abundance (log₁₀ CYA), and the water temperature (Figure 5.9a). The function obtained was as follows: $\text{Log}_{10} \text{CH}_4 = -4.05 + 3.4 \cdot 10^{-1} \text{Log}_{10} \text{PPEs} + e^{(6.7/\text{mean depth})} + 1.7 \cdot 10^{-1} \text{Log}_{10} \text{CYA} + 2.7 \cdot 10^{-2} \text{Temperature}$. The abundance of PPEs was the variable explaining most of the variance of dissolved CH₄ concentration (log₁₀ CH₄) during the stratification period, with an effect higher than the cyanobacteria abundance. Figure 5.9b–e shows the partial responses of each explanatory variable.

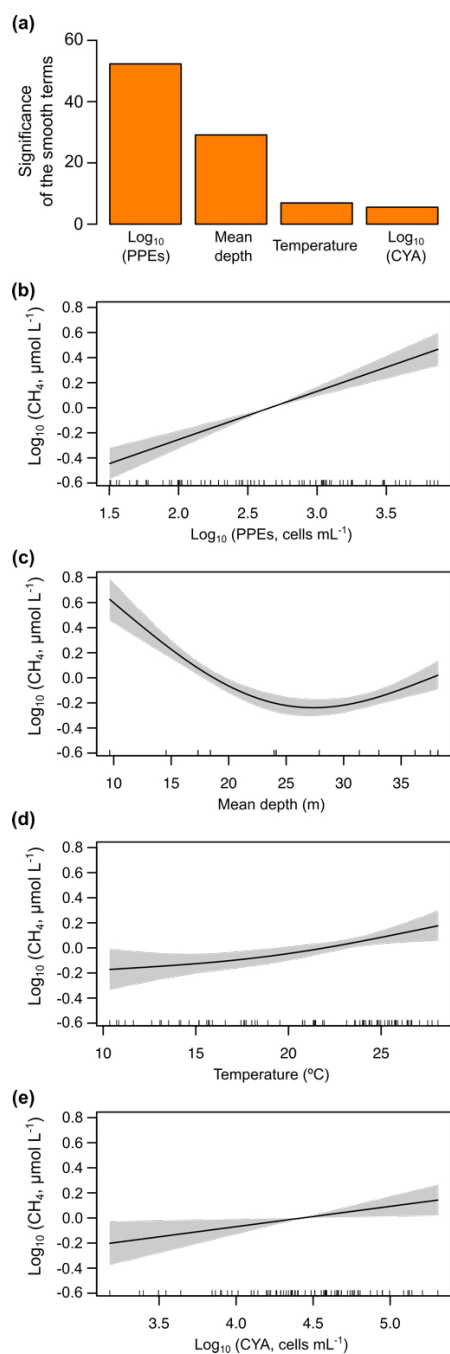


Figure 5.9. Results of the generalized additive model (GAM) fitted for the concentration of dissolved CH₄ in the oxic waters during the stratification period. (a) Bar plot showing the significance of the smooth terms from the fitted GAM (F values). (b–e) Partial response plots from the fitted GAM, showing the additive effects of the covariates on the dissolved CH₄ concentration: the photosynthetic picoeukaryotes' abundance (log₁₀ PPEs) (b), the mean depth (c), the cyanobacteria abundance (log₁₀ CYA) (d), and water temperature (e). In partial response plots, the lines are the smoothing functions,

and the shaded areas represent 95% pointwise confidence intervals. Rugs on x axis indicate the distribution of the data. More details are provided in Supplementary Table 5.3.

The GAM for the mixing period (n = 82) only included two explanatory variables: the reservoir mean depth and the abundance of the photosynthetic picoeukaryotes. The reservoir mean depth was the variable explaining most of the variance of the dissolved CH₄ concentration (log₁₀ CH₄) during the mixing period, closely followed by the abundance of PPEs (Figure 5.10a). We observed that the function of the effect of the mean depth on the CH₄ concentration changed between the two periods (Figures 5.9c and 5.10b). The function was more linear during the mixing period than during the stratification period, likely because the mixed water column enabled the more uniform distribution of the CH₄ produced in the sediment, while the thermocline acted as a barrier to the diffusion during the stratification period. The model function for the mixing period was $\log_{10} \text{CH}_4 = -2.07 + 1.5 e^{(-0.04 \text{ mean depth})} + 1.8 \cdot 10^{-1} \text{Log}_{10} \text{PPEs}$, with a fit deviance of 53.9 % and an explained variance (adjusted R²) of 52.1 % (Supplementary Table 5.3). In Figure 5.10b and c, we show the partial response plots for these two variables. The results show that the abundance of photosynthetic picoeukaryotes can be key for explaining the dissolved CH₄ concentration in oxic waters, even though they have received less attention than cyanobacteria in previous studies (Berg *et al.*, 2014; Teikari *et al.*, 2018; Bižić *et al.*, 2020). Finally, we have also included a simple model to explain the dissolved CH₄ concentration (Log₁₀CH₄) using the data of both periods (n=160) and including widely used variables like the water temperature (°C), mean depth (m), and chlorophyll *a* concentration (Chl *a*, µg L⁻¹) for future comparisons. The function of this model is $\text{Log}_{10}\text{CH}_4 = -2.03 + 0.05 \text{ Temperature} + e^{(7.64/\text{mean depth})} \cdot e^{(-0.34 \text{ Log}_{10}(\text{Chl } a))}$. This GAM model had a fit deviance of 75.2 % and an explained variance (adjusted R²) of 74 % (Supplementary Table 5.3).

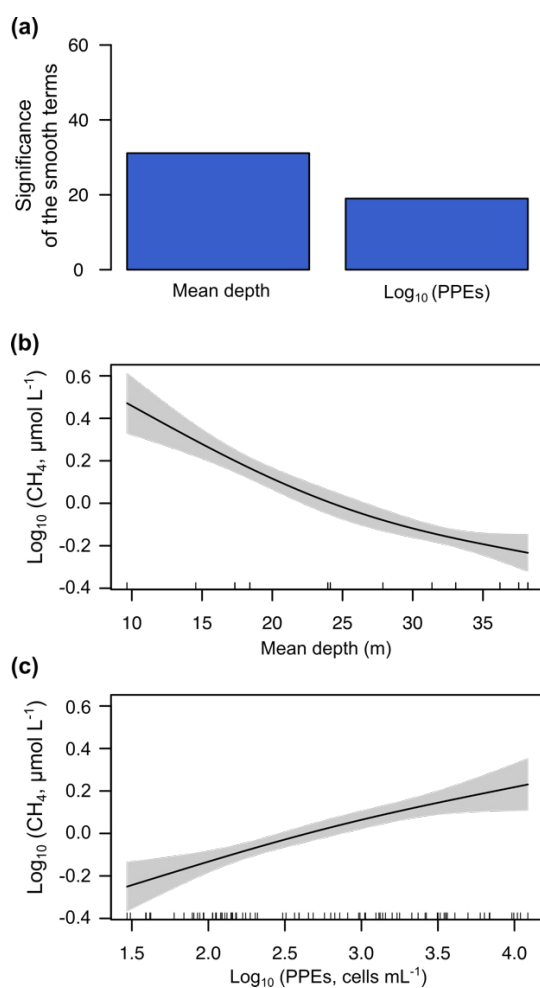


Figure 5.10. Results of the generalized additive model (GAM) fitted for the concentrations of CH₄ in the oxic waters during the mixing period. (a) Bar plot showing the significance of the smooth terms from the fitted GAM (F values). Panels (b) and (c) show partial response plots from the fitted GAM, showing the additive effects of the covariates on the dissolved CH₄ concentration: the mean depth (b) and the abundance of photosynthetic picoeukaryotes (log₁₀ PPEs) (c). In partial response plots, the lines are the smoothing functions, and the shaded areas represent 95% pointwise confidence intervals. Rugs on x axis indicate the distribution of the data. More details are provided in Supplementary Table 5.3.

Overall, during the stratification period, the *in situ* CH₄ production was coupled to the abundance of photosynthetic picoeukaryotes in oxic waters (Figure 5.9a) and mean depths. This CH₄ source, due to photosynthetic picoeukaryotes, can be crucial in large, deep lakes and reservoirs and the open ocean, since the impact of the CH₄ transport from sediments (i.e., mean depth) decreases with increasing depths. In deeper reservoirs, the thermal stratification during the summer that produced the vertical diffusion rates of CH₄ from sediments is limited. (Rudd and Hamilton, 1978)

did not detect any movement of CH₄ upwards from the hypolimnion during the stratification. Previous studies have suggested that the CH₄ produced in the oxic water column is the primary source of CH₄ in large and deep lakes (Bogard *et al.*, 2014; Donis *et al.*, 2017; DelSontro *et al.*, 2018; Günthel *et al.*, 2019). Günthel *et al.* (2019) showed that large lakes have a lower sediment area in comparison to the volume of the surface mixed layer than small lakes and that this fact determines the higher contribution of the oxic methane production to surface emission in large (>1 km²) lakes than in small ones. The photosynthetic picoeukaryotes identified in the studied reservoirs are considered indicators of eutrophic conditions, and they are bloom-forming genera (i.e., Chlorococcales and *Chrysochromulina* spp.) (Reynolds, 1984; Willén, 1987; Edvardsen and Paasche, 1998). Global future estimations suggest a rise in eutrophication and algal bloom over the next century due to climate change and the growing human population (Beaulieu *et al.*, 2019). In that situation, photosynthetic picoeukaryotes like Chlorococcales and *Chrysochromulina* spp., and cyanobacteria, would lead to an increment in CH₄ production and emissions. Further studies are needed to understand the role of the photosynthetic picoeukaryotes in the production of CH₄ in oxic waters better and to quantify their influence in the methane supersaturation and CH₄ fluxes from inland and oceanic waters.

5. 4 Conclusions

The dissolved CH₄ concentration in the studied reservoirs showed a considerable variability (i.e., up to 4 orders of magnitude) and presented a clear seasonality. Surface waters were always supersaturated in CH₄. The concentration of CH₄ was closely linked to the photosynthetic organisms. In the anoxic waters, the depth-cumulative chlorophyll *a* concentration, a proxy for the phytoplanktonic biomass exported to sediments, determined the CH₄ concentration. In the oxic waters, we considered different potential CH₄ sources, including the vertical and lateral transport of CH₄ from anoxic zones and *in situ* production. The mean depth of the reservoirs, as a surrogate of the CH₄ transport from sediment to the oxic waters, contributed in shallow systems. We did not detect methanogenic Archaea or methylphosphonates degradation target genes (i.e., *mcrA* and *phnJ* genes, respectively), which suggests that these pathways are not responsible for the *in situ* production of CH₄ in the oxic waters of the studied reservoirs. We found that

dissolved CH₄ was coupled to the abundance of photosynthetic picoeukaryotes (PPEs), and to chlorophyll *a* concentration during both periods, and to the abundance of cyanobacteria during the stratification period. These PPEs were non-colonial green algae from the order Chlorococcales (class Chlorophyceae, phylum Chlorophyta) and the genus *Chrysochromulina* spp. (class Coccolithophyceae, phylum Haptophyta). Finally, we combined all the explanatory variables with significant effects and determined their relative contribution to the CH₄ concentration using generalized additive models (GAMs). The abundance of PPEs was the variable explaining most of the variance of dissolved CH₄ concentration during the stratification period, with an effect higher than the cyanobacteria abundance. During the mixing period, the reservoir mean depth and the abundance of the PPEs were the only drivers for CH₄ concentration. Our findings show that the abundance of PPEs can be relevant for explaining the dissolved CH₄ concentration in oxic waters of large lakes and reservoirs.

Data availability

Additional figures and tables can be found in the supplementary information in Appendix 5. The datasets associated with this paper are available from Pangaea (León-Palmero *et al.*, 2020b, 2020c): dissolved concentrations of CH₄, nutrients, and biological parameters in the water column of 12 Mediterranean reservoirs in Southern Spain (<https://doi.org/10.1594/PANGAEA.912535>, last access: 14 May 2020), and primary production of 12 Mediterranean reservoirs in southern Spain (<https://doi.org/10.1594/PANGAEA.912555>, last access: 14 May 2020).

Author contribution

ELP, RMB and IR contributed equally to this work. RMB and IR designed the study and obtained the funds. ELP, RMB, and I.R. contributed to data acquisition during the reservoir samplings. ELP processed most of the chemical and biological samples. AC performed the flow cytometry and part of the molecular analysis, and AS collaborated with the dissolved CH₄ analysis using gas chromatography. ELP, RMB and IR analyzed the data and discussed the results. ELP wrote the first draft manuscript, which was complemented by significant contributions of RMB and IR.

Competing interests

The authors declare that they have no conflict of interest.

Acknowledgements

We especially thank Eulogio Corral for helping in the field, Jesús Forja and Teodora Ortega for helping with gas chromatography analysis at the University of Cádiz, and David Fernández Moreno from the Department of Botany at the University of Granada for the taxonomical identification of the phytoplankton community. We thank the Hydrological Confederations of Guadalquivir and the Agencia Andaluza del Medio Ambiente y Agua (AMAYA) for facilitating the reservoir sampling.

Financial support

This research has been supported by the Spanish Ministry of Economy and Competitiveness (grant no. CGL2014-52362-R); the University of Granada – Unidades de Excelencia (grant no. UCE.PP2017.03); the Consejería de Economía, Conocimiento, Empresas, y Universidad from Andalucía; and the European Regional Development Fund (ERDF; grant no. SOMM17/6109/UGR). Elizabeth León-Palmero and Ana Sierra were supported by PhD fellowships from the Ministry of Education, Culture and Sport (grant nos. FPU014/02917 and FPU2014-04048, respectively). Alba Contreras-Ruiz was supported by the Youth Employment Initiative (YEI) from the Junta de Andalucía and financed by the European Commission (grant no. 6017).

5. 5. References

- Althoff, F., Benzing, K., Comba, P., McRoberts, C., Boyd, D. R., Greiner, S. and Keppler, F. (2014). Abiotic methanogenesis from organosulphur compounds under ambient conditions, *Nature Communications*, 5, p. 4205. doi: 10.1038/ncomms5205.
- Álvarez-Salgado, X. A. and Miller, A. E. J. (1998). Simultaneous determination of dissolved organic carbon and total dissolved nitrogen in seawater by high temperature catalytic oxidation: conditions for precise shipboard measurements, *Marine Chemistry*, 62(3), pp. 325–333. doi: 10.1016/S0304-4203(98)00037-1.
- American Public Health Association (APHA). (1992). *Standard methods for the examination of water and wastewater* Washington, DC, USA: American Public Health Association. 18th edn. Edited by A. E. Greenberg, L. S. Clesceri, and A. D. Eaton.
- Angel, R., Matthies, D. and Conrad, R. (2011). Activation of methanogenesis in arid biological soil crusts despite the presence of oxygen, *PLOS ONE*, 6(5), p. e20453. doi: 10.1371/journal.pone.0020453.
- de Angelis, M. A. and Lee, C. (1994). Methane production during zooplankton grazing on marine phytoplankton, *Limnology and Oceanography*, 39(6), pp. 1298–1308. doi: 10.4319/lo.1994.39.6.1298.

- Angle, J. C., Morin, T. H., Solden, L. M., Narrowe, A. B., Smith, G. J., Borton, M. A., Rey-Sanchez, C., Daly, R. A., Mirfenderesgi, G., Hoyt, D. W., Riley, W. J., Miller, C. S., Bohrer, G. and Wrighton, K. C. (2017). Methanogenesis in oxygenated soils is a substantial fraction of wetland methane emissions, *Nature Communications*, 8, pp. 1–9. doi: 10.1038/s41467-017-01753-4.
- Aronow, S. (1982). Shoreline development ratio, in *Beaches and Coastal Geology*, pp. 754–755. doi: 10.1007/0-387-30843-1_417.
- Axler, R. P., Rose, C. and Tikkanen, C. A. (1994). Phytoplankton nutrient deficiency as related to atmospheric nitrogen deposition in Northern Minnesota acid-sensitive lakes, *Canadian Journal of Fisheries and Aquatic Sciences*, 51(6), pp. 1281–1296. doi: 10.1139/f94-128.
- Bastviken, D., Cole, J., Pace, M. and Tranvik, L. (2004). Methane emissions from lakes: Dependence of lake characteristics, two regional assessments, and a global estimate, *Global Biogeochemical Cycles*, 18(4), pp. 1–12. doi: 10.1029/2004GB002238.
- Bastviken, D., Tranvik, L. J., Downing, J. A., Crill, P. M. and Enrich-Prast, A. (2011). Freshwater methane emissions offset the continental carbon sink, *Science*, 331(6013), pp. 1–12. doi: 10.1126/science.1196808.
- Beaulieu, J. J., DelSontro, T. and Downing, J. A. (2019). Eutrophication will increase methane emissions from lakes and impoundments during the 21st century, *Nature Communications*, 10(1), p. 1375. doi: 10.1038/s41467-019-09100-5.
- Berg, A., Lindblad, P. and Svensson, B. H. (2014). Cyanobacteria as a source of hydrogen for methane formation, *World Journal of Microbiology and Biotechnology*, 30(2), pp. 539–545. doi: 10.1007/s11274-013-1463-5.
- Berg, I. A. (2011). Ecological aspects of the distribution of different autotrophic CO₂ fixation pathways, *Applied and Environmental Microbiology*, 77(6), pp. 1925–1936. doi: 10.1128/AEM.02473-10.
- Beverdorf, L. J., White, A. E., Björkman, K. M., Letelier, R. M. and Karl, D. M. (2010). Phosphonate metabolism by *Trichodesmium* IMS101 and the production of greenhouse gases, *Limnology and Oceanography*, 55(4), pp. 1768–1778. doi: 10.4319/lo.2010.55.4.1768.
- Bižić, M., Klintzsch, T., Ionescu, D., Hindiyeh, M. Y., Günthel, M., Muro-Pastor, A. M., Eckert, W., Urich, T., Keppler, F. and Grossart, H.-P. (2020). Aquatic and terrestrial cyanobacteria produce methane, *Science Advances*, 6(3), p. 3aax5343. doi: 10.1126/sciadv.aax5343.
- Bižić-Ionescu, M., Ionescu, D., Günthel, M., Tang, K. W. and Grossart, H.-P. (2018). Oxic methane cycling: New evidence for methane formation in oxic lake water, in Stams, A. J. M. and Sousa, D. (eds) *Biogenesis of Hydrocarbons*, pp. 1–22. doi: 10.1007/978-3-319-53114-4_10-1.
- Blees, J., Niemann, H., Erne, M., Zopfi, J., Schubert, C. J. and Lehmann, M. F. (2015). Spatial variations in surface water methane super-saturation and emission in Lake Lugano, southern Switzerland, *Aquatic Sciences*, 77(4), pp. 535–545. doi: 10.1007/s00027-015-0401-z.

- Bogard, M. J., del Giorgio, P. A., Boutet, L., Chaves, M. C. G., Prairie, Y. T., Merante, A. and Derry, A. M. (2014). Oxic water column methanogenesis as a major component of aquatic CH₄ fluxes, *Nature Communications*, 5, p. 5350. doi: 10.1038/ncomms6350.
- Boström, K. H., Simu, K., Hagström, Å. and Riemann, L. (2004). Optimization of DNA extraction for quantitative marine bacterioplankton community analysis, *Limnology and Oceanography: Methods*, 2(11), pp. 365–373. doi: 10.4319/lom.2004.2.365.
- Burns, B. D. and Beardall, J. (1987). Utilization of inorganic carbon by marine microalgae, *Journal of Experimental Marine Biology and Ecology*, 107(1), pp. 75–86. doi: 10.1016/0022-0981(87)90125-0.
- Carini, P., White, A. E., Campbell, E. O. and Giovannoni, S. J. (2014). Methane production by phosphate-starved SAR11 chemoheterotrophic marine bacteria, *Nature Communications*, 5, p. 4346. doi: 10.1038/ncomms5346.
- Cellamare, M., Rolland, A. and Jacquet, S. (2010). Flow cytometry sorting of freshwater phytoplankton, *Journal of Applied Phycology*, 22(1), pp. 87–100. doi: 10.1007/s10811-009-9439-4.
- Chistoserdova, L., Vorholt, J. A., Thauer, R. K. and Lidstrom, M. E. (1998). C1 transfer enzymes and coenzymes linking methylotrophic bacteria and methanogenic archaea, *Science*, 281(5373), pp. 99–102. doi: 10.1126/science.281.5373.99.
- Cole, J. J., Pace, M. L., Carpenter, S. R. and Kitchell, J. F. (2000). Persistence of net heterotrophy in lakes during nutrient addition and food web manipulations, *Limnology and Oceanography*, 45(8), pp. 1718–1730. doi: 10.4319/lo.2000.45.8.1718.
- Collier, J. L. (2000). Flow cytometry and the single cell in phycology, *Journal of Phycology*, 36(4), pp. 628–644. doi: 10.1046/j.1529-8817.2000.99215.x.
- Corzo, A., Jimenez-Gomez, F., Gordillo, F., Garcia-Ruiz, R. and Niell, F. (1999). *Synechococcus* and *Prochlorococcus*-like populations detected by flow cytometry in a eutrophic reservoir in summer, *Journal of Plankton Research*, 21(8), pp. 1575–1581. doi: 10.1093/plankt/21.8.1575.
- Crowe, S. A., O'Neill, A. H., Katsev, S., Hehanussa, P., Haffner, G. D., Sundby, B., Mucci, A. and Fowle, D. A. (2008). The biogeochemistry of tropical lakes: A case study from Lake Matano, Indonesia, *Limnology and Oceanography*, 53(1), pp. 319–331. doi: 10.4319/lo.2008.53.1.0319.
- Damm, E., Kiene, R. P., Schwarz, J., Falck, E. and Dieckmann, G. (2008). Methane cycling in Arctic shelf water and its relationship with phytoplankton biomass and DMSP, *Marine Chemistry*, 109(1–2), pp. 45–59. doi: 10.1016/j.marchem.2007.12.003.
- Damm, E., Helmke, E., Thoms, S., Schauer, U., Nöthig, E., Bakker, K. and Kiene, R. P. (2010). Methane production in aerobic oligotrophic surface water in the central Arctic Ocean, *Biogeosciences*, 7(3), pp. 1099–1108. doi: 10.5194/bg-7-1099-2010.
- Damm, E., Thoms, S., Beszczynska-Möller, A., Nöthig, E. M. and Kattner, G. (2015). Methane excess production in oxygen-rich polar water and a model of cellular conditions for this paradox, *Polar Science*, 9(3), pp. 327–334. doi: 10.1016/j.polar.2015.05.001.
- Deemer, B. R., Harrison, J. A., Li, S., Beaulieu, J. J., DelSontro, T., Barros, N., Bezerra-Neto, J.

- F., Powers, S. M., dos Santos, M. A. and Vonk, J. A. (2016). Greenhouse gas emissions from reservoir water surfaces: a new global synthesis, *BioScience*, 66(11), pp. 949–964. doi: 10.1093/biosci/biw117.
- DelSontro, T., del Giorgio, P. A. and Prairie, Y. T. (2018). No longer a paradox: The interaction between physical transport and biological processes explains the spatial distribution of surface water methane within and across lakes, *Ecosystems*, 21(6), pp. 1073–1087. doi: 10.1007/s10021-017-0205-1.
- Donis, D., Flury, S., Stöckli, A., Spangenberg, J. E., Vachon, D. and McGinnis, D. F. (2017). Full-scale evaluation of methane production under oxic conditions in a mesotrophic lake, *Nature Communications*, 8(1), p. 1661. doi: 10.1038/s41467-017-01648-4.
- Edwardsen, B. and Paasche, E. (1998). Bloom dynamics and physiology of *Prymnesium* and *Chrysochromulina*, *NATO ASI SERIES G ECOLOGICAL SCIENCES*, 41, pp. 193–208.
- Encinas Fernández, J., Peeters, F. and Hofmann, H. (2016). On the methane paradox: Transport from shallow water zones rather than in situ methanogenesis is the major source of CH₄ in the open surface water of lakes, *Journal of Geophysical Research: Biogeosciences*, 121(10), pp. 2717–2726. doi: 10.1002/2016JG003586.
- ESRI. (2012). *ArcGIS* Redlands, CA. Available at: www.esri.com.
- Fox, A., Kwapinski, W., Griffiths, B. S. and Schmalenberger, A. (2014). The role of sulfur- and phosphorus-mobilizing bacteria in biochar-induced growth promotion of *Lolium perenne*, *FEMS Microbiology Ecology*, 90(1), pp. 78–91. doi: 10.1111/1574-6941.12374.
- Fox, J. and Weisberg, S. (2011). *An R Companion to Applied Regression* Thousand Oaks CA: Sage. Second. Available at: <http://socserv.socsci.mcmaster.ca/jfox/Books/Companion>.
- Gasol, J. M. and Giorgio, P. A. del. (2000). Using flow cytometry for counting natural planktonic bacteria and understanding the structure of planktonic bacterial communities, *Scientia Marina*, 64(2), pp. 197–224. doi: 10.3989/scimar.2000.64n2197.
- Gomez-Garcia, M. R., Davison, M., Blain-Hartnung, M., Grossman, A. R. and Bhaya, D. (2011). Alternative pathways for phosphonate metabolism in thermophilic cyanobacteria from microbial mats, *The ISME journal*, 5(1), pp. 141–149. doi: 10.1038/ismej.2010.96.
- Grabarse, W., Mahlert, F., Duin, E. C., Goubeaud, M., Shima, S., Thauer, R. K., Lamzin, V. and Ermler, U. (2001). On the mechanism of biological methane formation: structural evidence for conformational changes in methyl-coenzyme M reductase upon substrate binding, *Journal of Molecular Biology*, 309(1), pp. 315–330. doi: 10.1006/jmbi.2001.4647.
- Gross, J. and Ligges, U. (2015). *nortest: Tests for Normality*. Available at: <https://CRAN.R-project.org/package=nortest> (Accessed: 3 June 2018).
- Grossart, H.-P., Frindte, K., Dziallas, C., Eckert, W. and Tang, K. W. (2011). Microbial methane production in oxygenated water column of an oligotrophic lake, *Proceedings of the*

- National Academy of Sciences*, 108(49), pp. 19657–19661. doi: 10.1073/pnas.1110716108.
- Günthel, M., Donis, D., Kirillin, G., Ionescu, D., Bizic, M., McGinnis, D. F., Grossart, H.-P. and Tang, K. W. (2019). Contribution of oxic methane production to surface methane emission in lakes and its global importance, *Nature Communications*, 10(1), pp. 1–10. doi: 10.1038/s41467-019-13320-0.
- Hartmann, J. F., Günthel, M., Klintzsch, T., Kirillin, G., Grossart, H.-P., Keppler, F. and Isenbeck-Schröter, M. (2020). High spatiotemporal dynamics of methane production and emission in oxic surface water, *Environmental Science & Technology*, 54(3), pp. 1451–1463. doi: 10.1021/acs.est.9b03182.
- Hastie, T. and Tibshirani, R. (1986). Generalized Additive Models, *Statistical Science*, 1(3), pp. 297–310. doi: 10.1214/ss/1177013604.
- Hastie, T. and Tibshirani, R. J. (1990). *Generalized additive models* London, UK, and New York, NY, USA: London: Chapman and Hall. 1st ed.
- Hofmann, H., Federwisch, L. and Peeters, F. (2010). Wave-induced release of methane: Littoral zones as source of methane in lakes, *Limnology and Oceanography*, 55(5), pp. 1990–2000. doi: 10.4319/lo.2010.55.5.1990.
- Jähne, B., Münnich, K. O., Bössinger, R., Dutzi, A., Huber, W. and Libner, P. (1987). On the parameters influencing air-water gas exchange, *Journal of Geophysical Research: Oceans*, 92(C2), pp. 1937–1949. doi: 10.1029/JC092iC02p01937.
- Jarrell, K. F. (1985). Extreme oxygen sensitivity in methanogenic archaeobacteria, *BioScience*, 35(5), pp. 298–302. doi: 10.2307/1309929.
- Karl, D. M. and Tilbrook, B. D. (1994). Production and transport of methane in oceanic particulate organic matter, *Nature*, 368(6473), pp. 732–734. doi: 10.1038/368732a0.
- Karl, D. M., Beversdorf, L., Björkman, K. M., Church, M. J., Martinez, A. and Delong, E. F. (2008). Aerobic production of methane in the sea, *Nature Geoscience*, 1(7), pp. 473–478. doi: 10.1038/ngeo234.
- Khatun, S., Iwata, T., Kojima, H., Fukui, M., Aoki, T., Mochizuki, S., Naito, A., Kobayashi, A. and Uzawa, R. (2019). Aerobic methane production by planktonic microbes in lakes, *Science of The Total Environment*, 696, p. 133916. doi: 10.1016/j.scitotenv.2019.133916.
- Khatun, S., Iwata, T., Kojima, H., Ikarashi, Y., Yamanami, K., Imazawa, D., Kenta, T., Shinohara, R. and Saito, H. (2020). Linking stoichiometric organic carbon–nitrogen relationships to planktonic cyanobacteria and subsurface methane maximum in deep freshwater lakes, *Water*, 12(2), p. 402. doi: 10.3390/w12020402.
- Kiene, R. P. (1991). Production and consumption of methane in aquatic systems, in Rogers, J. E. and Whitman, W. B. (eds) *Microbial Production and Consumption of Greenhouse Gases: Methane, Nitrogen Oxides, and Halomethanes*, pp. 111–146.
- Klintzsch, T., Langer, G., Nehrke, G., Wieland, A., Lenhart, K. and Keppler, F. (2019). Methane production by three widespread marine phytoplankton species: release rates, precursor compounds, and potential relevance for the environment, *Biogeosciences*, 16(20), pp. 4129–4144. doi: 10.5194/bg-16-4129-2019.

- Lenhart, K., Bunge, M., Ratering, S., Neu, T. R., Schüttmann, I., Greule, M., Kammann, C., Schnell, S., Müller, C., Zorn, H. and Keppler, F. (2012). Evidence for methane production by saprotrophic fungi, *Nature Communications*, 3, p. 1046. doi: 10.1038/ncomms2049.
- Lenhart, K., Althoff, F., Greule, M. and Keppler, F. (2015). Technical Note: Methionine, a precursor of methane in living plants, *Biogeosciences*, 12(6), pp. 1907–1914. doi: 10.5194/bg-12-1907-2015.
- Lenhart, K., Klintzsch, T., Langer, G., Nehrke, G., Bunge, M., Schnell, S. and Keppler, F. (2016). Evidence for methane production by the marine algae *Emiliania huxleyi*, *Biogeosciences*, 13(10), pp. 3163–3174. doi: 10.5194/bg-13-3163-2016.
- León-Palmero, E., Reche, I. and Morales-Baquero, R. (2019). Atenuación de luz en embalses del sur-este de la Península Ibérica, *Ingeniería del agua*, 23(1), pp. 65–75. doi: 10.4995/ia.2019.10655.
- León-Palmero, E., Morales-Baquero, R. and Reche, I. (2020a). Greenhouse gas fluxes from reservoirs determined by watershed lithology, morphometry, and anthropogenic pressure, *Environmental Research Letters*, 15(4), p. 044012. doi: 10.1088/1748-9326/ab7467.
- León-Palmero, E., Morales-Baquero, R. and Reche, I. (2020b). Dissolved concentrations of CH₄, nutrients, and biological parameters in the water column of twelve Mediterranean reservoirs in Southern Spain. Available at: <https://doi.org/10.1594/PANGAEA.912535>.
- León-Palmero, E., Morales-Baquero, R. and Reche, I. (2020c). Primary production of twelve Mediterranean reservoirs in Southern Spain. Available at: <https://doi.org/10.1594/PANGAEA.912555>.
- Liu, H., Jing, H., Wong, T. H. C. and Chen, B. (2014). Co-occurrence of phycocyanin- and phycoerythrin-rich *Synechococcus* in subtropical estuarine and coastal waters of Hong Kong, *Environmental Microbiology Reports*, 6(1), pp. 90–99. doi: 10.1111/1758-2229.12111.
- Marotta, H., Pinho, L., Gudas, C., Bastviken, D., Tranvik, L. J. and Enrich-Prast, A. (2014). Greenhouse gas production in low-latitude lake sediments responds strongly to warming, *Nature Climate Change*, 4(6), pp. 467–470. doi: 10.1038/nclimate2222.
- Michmerhuizen, C. M., Striegl, R. G. and McDonald, M. E. (1996). Potential methane emission from north-temperate lakes following ice melt, *Limnology and Oceanography*, 41(5), pp. 985–991. doi: 10.4319/lo.1996.41.5.0985.
- Mitsch, W. J., Bernal, B., Nahlik, A. M., Mander, Ü., Zhang, L., Anderson, C. J., Jørgensen, S. E. and Brix, H. (2012). Wetlands, carbon, and climate change, *Landscape Ecology*, 28(4), pp. 583–597. doi: 10.1007/s10980-012-9758-8.
- Morris, D. P. and Lewis, W. M. (1988). Phytoplankton nutrient limitation in Colorado mountain lakes, *Freshwater Biology*, 20(3), pp. 315–327. doi: 10.1111/j.1365-2427.1988.tb00457.x.
- Mortimer, C. H. (1956). *The oxygen content of air-saturated fresh waters, and aids in*

calculating percentage saturation Stuttgart, Germany: Schweizerbart Science Publishers. Available at:
http://www.schweizerbart.de/publications/detail/isbn/9783510520060/Mitteilung_n_IVL_Nr_6.

Murase, J., Sakai, Y., Sugimoto, A., Okubo, K. and Sakamoto, M. (2003). Sources of dissolved methane in Lake Biwa, *Limnology*, 4(2), pp. 91–99. doi: 10.1007/s10201-003-0095-0.

Murase, J. and Sugimoto, A. (2005). Inhibitory effect of light on methane oxidation in the pelagic water column of a mesotrophic lake (Lake Biwa, Japan), *Limnology and Oceanography*, 50(4), pp. 1339–1343. doi: 10.4319/lo.2005.50.4.1339.

Murphy, J. and Riley, J. P. (1962). A modified single solution method for the determination of phosphate in natural waters, *Analytica Chimica Acta*, 27(Supplement C), pp. 31–36. doi: 10.1016/S0003-2670(00)88444-5.

Musenze, R. S., Grinham, A., Werner, U., Gale, D., Sturm, K., Udy, J. and Yuan, Z. (2014). Assessing the spatial and temporal variability of diffusive methane and nitrous oxide emissions from subtropical freshwater reservoirs, *Environmental Science & Technology*, 48(24), pp. 14499–14507. doi: 10.1021/es505324h.

Naqvi, S. W. A., Lam, P., Narvenkar, G., Sarkar, A., Naik, H., Pratihary, A., Shenoy, D. M., Gauns, M., Kurian, S., Damare, S., Duret, M., Lavik, G. and Kuypers, M. M. M. (2018). Methane stimulates massive nitrogen loss from freshwater reservoirs in India, *Nature Communications*, 9(1), pp. 1–10. doi: 10.1038/s41467-018-03607-z.

Odum, H. T. (1956). Primary production in flowing waters, *Limnology and Oceanography*, 1(2), pp. 102–117. doi: 10.4319/lo.1956.1.2.0102.

Okuku, E. O., Bouillon, S., Tole, M. and Borges, A. V. (2019). Diffusive emissions of methane and nitrous oxide from a cascade of tropical hydropower reservoirs in Kenya, *Lakes & Reservoirs: Science, Policy and Management for Sustainable Use*, 24(2), pp. 127–135. doi: 10.1111/lre.12264.

Oswald, K., Milucka, J., Brand, A., Littmann, S., Wehrli, B., Kuypers, M. M. M. and Schubert, C. J. (2015). Light-dependent aerobic methane oxidation reduces methane emissions from seasonally stratified lakes, *PLoS one*, 10(7), pp. e0132574–e0132574. doi: 10.1371/journal.pone.0132574.

Oswald, K., Jegge, C., Tischer, J., Berg, J., Brand, A., Miracle, M. R., Soria, X., Vicente, E., Lehmann, M. F., Zopfi, J. and Schubert, C. J. (2016). Methanotrophy under versatile conditions in the water column of the ferruginous meromictic lake La Cruz (Spain), *Frontiers in microbiology*, 7, p. 1762. doi: 10.3389/fmicb.2016.01762.

Owens, N. J. P., Law, C. S., Mantoura, R. F. C., Burkill, P. H. and Llewellyn, C. A. (1991). Methane flux to the atmosphere from the Arabian Sea, *Nature*, 354(6351), pp. 293–296. doi: 10.1038/354293a0.

Peeters, F., Wüest, A., Piepke, G. and Imboden, D. M. (1996). Horizontal mixing in lakes, *Journal of Geophysical Research: Oceans*, 101(C8), pp. 18361–18375. doi: 10.1029/96JC01145.

Peeters, F., Fernandez Encinas, J. and Hofmann, H. (2019). Sediment fluxes rather than oxic methanogenesis explain diffusive CH₄ emissions from lakes and reservoirs, *Scientific*

- Reports*, 9(1), pp. 1–10. doi: 10.1038/s41598-018-36530-w.
- R Core Team. (2014). *R: A Language and Environment for Statistical Computing* Vienna, Austria: R Foundation for Statistical Computing. Available at: <http://www.R-project.org/>.
- Rasilo, T., Prairie, Y. T. and del Giorgio, P. A. (2015). Large-scale patterns in summer diffusive CH₄ fluxes across boreal lakes, and contribution to diffusive C emissions, *Global Change Biology*, 21(3), pp. 1124–1139. doi: 10.1111/gcb.12741.
- Repeta, D. J., Ferrón, S., Sosa, O. A., Johnson, C. G., Repeta, L. D., Acker, M., DeLong, E. F. and Karl, D. M. (2016). Marine methane paradox explained by bacterial degradation of dissolved organic matter, *Nature Geoscience*, 9(12), pp. 884–887. doi: 10.1038/ngeo2837.
- Reynolds, C. S. (1984). Phytoplankton periodicity: the interactions of form, function and environmental variability, *Freshwater Biology*, 14(2), pp. 111–142. doi: 10.1111/j.1365-2427.1984.tb00027.x.
- Roland, F. A. E., Darchambeau, F., Morana, C. and Borges, A. V. (2017). Nitrous oxide and methane seasonal variability in the epilimnion of a large tropical meromictic lake (Lake Kivu, East-Africa), *Aquatic Sciences*, 79(2), pp. 209–218. doi: 10.1007/s00027-016-0491-2.
- Rudd, J. W. M. and Hamilton, R. D. (1978). Methane cycling in a eutrophic shield lake and its effects on whole lake metabolism, *Limnology and Oceanography*, 23(2), pp. 337–348. doi: 10.4319/lo.1978.23.2.0337.
- Sabo, E., Roy, D., Hamilton, P. B., Hehanussa, P. E., McNeely, R. and Haffner, G. D. (2008). The plankton community of Lake Matano: factors regulating plankton composition and relative abundance in an ancient, tropical lake of Indonesia, in *Patterns and Processes of Speciation in Ancient Lakes*, pp. 225–235.
- Saunio, M., Bousquet, P., Poulter, B., Peregon, A., Ciais, P., Canadell, J. G., Dlugokencky, E. J., Etiope, G., Bastviken, D., Houweling, S., Janssens-Maenhout, G., Tubiello, F. N., Castaldi, S., Jackson, R. B., Alexe, M., Arora, V. K., Beerling, D. J., Bergamaschi, P., Blake, D. R., Brailsford, G., Brovkin, V., Bruhwiler, L., Crevoisier, C., Crill, P., Covey, K., Curry, C., Frankenberg, C., Gedney, N., Höglund-Isaksson, L., Ishizawa, M., Ito, A., Joos, F., Kim, H.-S., Kleinen, T., Krummel, P., Lamarque, J.-F., Langenfelds, R., Locatelli, R., Machida, T., Maksyutov, S., McDonald, K. C., Marshall, J., Melton, J. R., Morino, I., Naik, V., O’Doherty, S., Parmentier, F.-J., Patra, P. K., Peng, C., Peng, S., Peters, G. P., Pison, I., Prigent, C., Prinn, R., Ramonet, M., Riley, W. J., Saito, M., Santini, M., Schroeder, R., Simpson, I. J., Spahni, R., Steele, P., Takizawa, A., Thornton, B. F., Tian, H., Tohjima, Y., Viovy, N., Voulgarakis, A., van Weele, M., van der Werf, G. R., Weiss, R., Wiedinmyer, C., Wilton, D. J., Wiltshire, A., Worthy, D., Wunch, D., Xu, X., Yoshida, Y., Zhang, B., Zhang, Z. and Zhu, Q. (2016). The global methane budget 2000–2012, *Earth System Science Data*, 8, pp. 697–751.
- Schlesinger, W. H. and Bernhardt, E. S. (2013). *Biogeochemistry: An Analysis of Global Change* Academic Press.
- Schmale, O., Wäge, J., Mohrholz, V., Wasmund, N., Gräwe, U., Rehder, G., Labrenz, M. and

- Loick-Wilde, N. (2018). The contribution of zooplankton to methane supersaturation in the oxygenated upper waters of the central Baltic Sea, *Limnology and Oceanography*, 63(1), pp. 412–430. doi: 10.1002/lno.10640.
- Schmidt, U. and Conrad, R. (1993). Hydrogen, carbon monoxide, and methane dynamics in Lake Constance, *Limnology and Oceanography*, 38(6), pp. 1214–1226. doi: 10.4319/lo.1993.38.6.1214.
- Schubert, C. J. and Wehrli, B. (2018). Contribution of methane formation and methane oxidation to methane emission from freshwater systems, *Biogenesis of Hydrocarbons*. Edited by A. J. M. Stams and D. Sousa. Available at: https://doi.org/10.1007/978-3-319-53114-4_18-1.
- Schulz, M., Faber, E., Hollerbach, A., Schröder, H. G. and Güde, H. (2001). The methane cycle in the epilimnion of Lake Constance, *Archiv für Hydrobiologie*, pp. 157–176. doi: 10.1127/archiv-hydrobiol/151/2001/157.
- Schwarz, J. I. K., Eckert, W. and Conrad, R. (2008). Response of the methanogenic microbial community of a profundal lake sediment (Lake Kinneret, Israel) to algal deposition, *Limnology and Oceanography*, 53(1), pp. 113–121. doi: 10.4319/lo.2008.53.1.0113.
- Scranton, M. I. and Brewer, P. G. (1977). Occurrence of methane in the near-surface waters of the western subtropical North-Atlantic, *Deep Sea Research*, 24(2), pp. 127–138. doi: 10.1016/0146-6291(77)90548-3.
- Segers, R. (1998). Methane production and methane consumption: a review of processes underlying wetland methane fluxes, *Biogeochemistry*, 41(1), pp. 23–51. doi: 10.1023/A:1005929032764.
- Sepulveda-Jauregui, A., Hoyos-Santillan, J., Martinez-Cruz, K., Walter Anthony, K. M., Casper, P., Belmonte-Izquierdo, Y. and Thalasso, F. (2018). Eutrophication exacerbates the impact of climate warming on lake methane emission, *Science of The Total Environment*, 636, pp. 411–419. doi: 10.1016/j.scitotenv.2018.04.283.
- Seweryn, P., Van, L. B., Kjeldgaard, M., Russo, C. J., Passmore, L. A., Hove-Jensen, B., Jochimsen, B. and Brodersen, D. E. (2015). Structural insights into the bacterial carbon–phosphorus lyase machinery, *Nature*, 525(7567), pp. 68–72. doi: 10.1038/nature14683.
- Shaw, S. L., Chisholm, S. W. and Prinn, R. G. (2003). Isoprene production by *Prochlorococcus*, a marine cyanobacterium, and other phytoplankton, *Marine Chemistry*, 80(4), pp. 227–245. doi: 10.1016/S0304-4203(02)00101-9.
- Sierra, A., Jiménez-López, D., Ortega, T., Ponce, R., Bellanco, M. J., Sánchez-Leal, R., Gómez-Parra, A. and Forja, J. (2017). Distribution of N₂O in the eastern shelf of the Gulf of Cadiz (SW Iberian Peninsula), *Science of The Total Environment*, 593–594, pp. 796–808. doi: 10.1016/j.scitotenv.2017.03.189.
- Staeher, P. A., Bade, D., Bogert, M. C. V. de, Koch, G. R., Williamson, C., Hanson, P., Cole, J. J. and Kratz, T. (2010). Lake metabolism and the diel oxygen technique: State of the science, *Limnology and Oceanography: Methods*, 8(11), pp. 628–644. doi: 10.4319/lom.2010.8.0628.
- Steinke, M., Hodapp, B., Subhan, R., Bell, T. G. and Martin-Creuzburg, D. (2018). Flux of the

- biogenic volatiles isoprene and dimethyl sulfide from an oligotrophic lake, *Scientific Reports*, 8(1), pp. 1–10. doi: 10.1038/s41598-017-18923-5.
- Tang, K. W., McGinnis, D. F., Frindte, K., Brüchert, V. and Grossart, H.-P. (2014). Paradox reconsidered: Methane oversaturation in well-oxygenated lake waters, *Limnology and Oceanography*, 59(1), pp. 275–284. doi: 10.4319/lo.2014.59.1.0275.
- Tang, K. W., McGinnis, D. F., Ionescu, D. and Grossart, H.-P. (2016). Methane production in oxic lake waters potentially increases aquatic methane flux to air, *Environmental Science & Technology Letters*, 3(6), pp. 227–233. doi: 10.1021/acs.estlett.6b00150.
- Teikari, J. E., Fewer, D. P., Shrestha, R., Hou, S., Leikoski, N., Mäkelä, M., Simojoki, A., Hess, W. R. and Sivonen, K. (2018). Strains of the toxic and bloom-forming *Nodularia spumigena* (cyanobacteria) can degrade methylphosphonate and release methane, *The ISME Journal*, 12(6), pp. 1619–1630. doi: 10.1038/s41396-018-0056-6.
- Thalasso, F., Sepulveda-Jauregui, A., Gandois, L., Martinez-Cruz, K., Gerardo-Nieto, O., Astorga-España, M. S., Teisserenc, R., Lavergne, C., Tananaev, N., Barret, M. and Cabrol, L. (2020). Sub-oxycline methane oxidation can fully uptake CH₄ produced in sediments: case study of a lake in Siberia, *Scientific Reports*, 10(1), pp. 1–7. doi: 10.1038/s41598-020-60394-8.
- Thanh-Duc, N., Crill, P. and Bastviken, D. (2010). Implications of temperature and sediment characteristics on methane formation and oxidation in lake sediments, *Biogeochemistry*, 100(1), pp. 185–196. doi: 10.1007/s10533-010-9415-8.
- Tilbrook, B. D. and Karl, D. M. (1995). Methane sources, distributions and sinks from California coastal waters to the oligotrophic North Pacific gyre, *Marine Chemistry*, 49(1), pp. 51–64. doi: 10.1016/0304-4203(94)00058-L.
- del Valle, D. A. and Karl, D. M. (2014). Aerobic production of methane from dissolved water-column methylphosphonate and sinking particles in the North Pacific Subtropical Gyre, *Aquatic Microbial Ecology*, 73(2), pp. 93–105. doi: 10.3354/ame01714.
- Wang, Q., Dore, J. E. and McDermott, T. R. (2017). Methylphosphonate metabolism by *Pseudomonas* sp. populations contributes to the methane oversaturation paradox in an oxic freshwater lake, *Environmental Microbiology*, 19(6), pp. 2366–2378. doi: 10.1111/1462-2920.13747.
- West, W. E., Coloso, J. J. and Jones, S. E. (2012). Effects of algal and terrestrial carbon on methane production rates and methanogen community structure in a temperate lake sediment, *Freshwater Biology*, 57(5), pp. 949–955. doi: 10.1111/j.1365-2427.2012.02755.x.
- West, W. E., McCarthy, S. M. and Jones, S. E. (2015). Phytoplankton lipid content influences freshwater lake methanogenesis, *Freshwater Biology*, 60(11), pp. 2261–2269. doi: 10.1111/fwb.12652.
- West, W. E., Creamer, K. P. and Jones, S. E. (2016). Productivity and depth regulate lake contributions to atmospheric methane: Lake productivity fuels methane emissions, *Limnology and Oceanography*, 61(S1), pp. S51–S61. doi: 10.1002/lno.10247.
- White, A. K. and Metcalf, W. W. (2007). Microbial metabolism of reduced phosphorus

- compounds, *Annual Review of Microbiology*, 61(1), pp. 379–400. doi: 10.1146/annurev.micro.61.080706.093357.
- Wiesenburg, D. A. and Guinasso, N. L. (1979). Equilibrium solubilities of methane, carbon monoxide, and hydrogen in water and sea water, *Journal of Chemical & Engineering Data*, 24(4), pp. 356–360. doi: 10.1021/je60083a006.
- Willén, E. (1987). Phytoplankton and reversed Eutrophication in Lake Mälaren, Central Sweden, 1965–1983, *British Phycological Journal*, 22(2), pp. 193–208. doi: 10.1080/00071618700650241.
- Wood, S. N. (2006). *Generalized additive models: an introduction with R* New York, USA: Chapman and Hall/CRC.
- Wood, S. N. (2011). Fast stable restricted maximum likelihood and marginal likelihood estimation of semiparametric generalized linear models, *Journal of the Royal Statistical Society: Series B (Statistical Methodology)*, 73(1), pp. 3–36. doi: 10.1111/j.1467-9868.2010.00749.x.
- Yamamoto, S., Alcauskas, J. B. and Crozier, T. E. (1976). Solubility of methane in distilled water and seawater, *Journal of Chemical & Engineering Data*, 21(1), pp. 78–80. doi: 10.1021/je60068a029.
- Yao, M., Henny, C. and Maresca, J. A. (2016a). Freshwater bacteria release methane as a byproduct of phosphorus acquisition, *Applied and Environmental Microbiology*, 82(23), pp. 6994–7003. doi: 10.1128/AEM.02399-16.
- Yao, M., Elling, F. J., Jones, C., Nomosatryo, S., Long, C. P., Crowe, S. A., Antoniewicz, M. R., Hinrichs, K.-U. and Maresca, J. A. (2016b). Heterotrophic bacteria from an extremely phosphate-poor lake have conditionally reduced phosphorus demand and utilize diverse sources of phosphorus, *Environmental Microbiology*, 18(2), pp. 656–667. doi: 10.1111/1462-2920.13063.
- Yoch, D. C. (2002). Dimethylsulfoniopropionate: its sources, role in the marine food web, and biological degradation to dimethylsulfide, *Applied and Environmental Microbiology*, 68(12), pp. 5804–5815. doi: 10.1128/AEM.68.12.5804-5815.2002.
- Yvon-Durocher, G., Allen, A. P., Bastviken, D., Conrad, R., Gudasz, C., St-Pierre, A., Thanh-Duc, N. and del Giorgio, P. A. (2014). Methane fluxes show consistent temperature dependence across microbial to ecosystem scales, *Nature*, 507(7493), pp. 488–491. doi: 10.1038/nature13164.
- Zindler, C., Bracher, A., Marandino, C. A., Taylor, B., Torrecilla, E., Kock, A. and Bange, H. W. (2013). Sulphur compounds, methane, and phytoplankton: interactions along a north–south transit in the western Pacific Ocean, *Biogeosciences*, 10(5), pp. 3297–3311. doi: 10.5194/bg-10-3297-2013.



Chapter 6:

Dissolved N_2O driven by nitrogen and the *nirS* gene abundance in the water column of reservoirs

Chapter 6:

Dissolved N₂O driven by nitrogen and the *nirS* gene abundance in the water column of reservoirs

The Supplementary Material is available in Appendix 6

Abstract

Human activities have increased nitrogen inputs in inland waters, promoting N₂O production and emission. N₂O is a product of nitrification in oxic environments, and denitrification in anoxic environments. Lakes and reservoirs are essential sites for nitrogen processing, but the microbial pathways that produce N₂O have rarely been studied in the water column of these systems. Here we determined dissolved N₂O concentration in the water column of twelve reservoirs during the summer stratification and the winter mixing. Besides, we explored the potential microbial sources of N₂O by the quantification of target genes. Dissolved N₂O concentration varied up to three orders of magnitude (4.7 - 2441.2 nmol L⁻¹), with N₂O undersaturated and supersaturated depths. Total nitrogen (TN) concentration was correlated to the concentration of N₂O in the reservoirs. The ammonia-oxidizing archaea (i.e., the occurrence of *arch-amoA* gene) dominated over the ammonia-oxidizing bacteria (i.e., the occurrence of *bac-amoA* gene). The *amoA* gene abundance was not related to the N₂O concentration. In contrast, the abundance of the *nirS* gene was significantly related to the dissolved N₂O concentration. We detected denitrifying bacteria (i.e., the occurrence of the *nirS* gene) consistently in the water column of all reservoirs, both in anoxic and oxic conditions. The abundance

of the gene *nirS* was correlated to the concentration of total phosphorus and the concentration of depth-cumulative chlorophyll-*a*. Together, the TN concentration and the *nirS* abundance explained most of the variance of the dissolved N₂O concentration in the water column of the study reservoirs. Our findings suggest that the water column in reservoirs is also an active site for N₂O production. This production may occur both in oxic and anoxic conditions by denitrification.

6. 1. Introduction

The anthropogenic production of nitrogen fertilizer has doubled the inputs of nitrogen to the Earth's surface, increasing the export of nitrogen to inland waters (Vitousek, 1994; Howarth *et al.*, 1996; Gruber and Galloway, 2008) and boosting the production of nitrous oxide (N₂O) (Seitzinger *et al.*, 2000; Mulholland *et al.*, 2008; Beaulieu *et al.*, 2011). N₂O is a potent greenhouse gas (GHG) with 298 times the effect of CO₂ on atmospheric warming in a 100-year time horizon (IPCC, 2013), and the main driver of stratospheric ozone depletion when it is transported into the stratosphere (Ravishankara *et al.*, 2009). The studies on N₂O emissions in inland waters have mainly focused on rivers, with an estimated N₂O emission of 0.68 Tg N₂O-N y⁻¹ (Beaulieu *et al.*, 2011). The N₂O emission from lakes and reservoirs was recently estimated at ~0.3 Tg N₂O-N y⁻¹ based on a scarce dataset (DelSontro *et al.*, 2018). Reservoirs located in agricultural and urban areas may support particularly high N₂O emissions due to significant N loadings from the watersheds, exceeding punctually the climatic forcing produced by CH₄ emissions (e.g., Iznájar reservoir in León-Palmero *et al.* (2020a)). However, we still need a better understanding of the processes that lead to N₂O production in the water column of reservoirs.

N₂O is a product of nitrification and denitrification. Nitrification is a chemolithoautotrophic process that consists of the oxidation of ammonia to nitrite (i.e., ammonia oxidation), and then to nitrate (i.e., nitrite oxidation) (Figure 1.8a). Ammonia oxidation is the rate-limiting step performed by ammonia-oxidizing bacteria (AOB) and ammonia-oxidizing archaea (AOA) (Kowalchuk and Stephen, 2001; Könneke *et al.*, 2005). The global significance of this process and the relative contribution of AOB and AOA have been inferred from the abundance of the bacterial and the archaeal *amoA* genes, which encode the subunit A of the key enzyme

ammonia monooxygenase (Kowalchuk and Stephen, 2001; Francis *et al.*, 2005). During the ammonia oxidation, the intermediate product hydroxylamine (NH₂OH) can decompose to form N₂O (Anderson, 1964; Vajjala *et al.*, 2013) (Figure 1.8a). Recently, evidence of a new obligate intermediate (i.e., nitric oxide, NO) has appeared, but the details about N₂O formation are still controversial (Caranto and Lancaster, 2017; Carini *et al.*, 2018). At low oxygen concentrations, nitrifiers develop the nitrifier denitrification, and they increase the yield of N₂O produced relative to the ammonia oxidized (Goreau *et al.*, 1980; Yoshida, 1988) (Figure 1.8b). Nitrifier denitrification consists on the reduction of nitrite to nitric oxide, nitrous oxide and molecular nitrogen at low oxygen concentrations, and it is an important pathway of N₂O production in soils, and hypoxic waters in the ocean (Wrage *et al.*, 2001; Frame and Casciotti, 2010; Löscher *et al.*, 2012). AOA are present in marine waters and soils in large numbers (Francis *et al.*, 2005; Könneke *et al.*, 2005; Leininger *et al.*, 2006; Wuchter *et al.*, 2006; Prosser and Nicol, 2008; Hu *et al.*, 2014) and they contribute significantly to the N₂O production in both (Francis *et al.*, 2005; Santoro *et al.*, 2011; Löscher *et al.*, 2012; Trimmer *et al.*, 2016). However, the contribution of ammonia-oxidizing microorganisms to dissolved N₂O in reservoirs has not been studied.

Denitrification is the primary biological reduction of nitrate in aquatic environments with high rates in rivers and lakes in comparison with estuaries, coastal areas, and open ocean (Ward 1996; Piña-Ochoa and Álvarez-Cobelas 2006). Denitrifiers obtain energy from organic matter oxidation, and the subsequent reduction of nitrate to nitrite, nitric oxide, nitrous oxide, and dinitrogen (Figure 1.9). Denitrification can be an N₂O source when the rate of N₂O production exceeds the N₂O reduction to N₂ (Schlesinger, 2009). On the other hand, denitrification can be an N₂O sink depending on the rate of N₂ formation. When the nitrate used by denitrifiers comes from nitrification, there is a coupled nitrification–denitrification. The abundances of the genes that coded for the nitrite reductases (i.e., *nirS/nirK*) and the nitrous oxide reductase (i.e., *nosZ*) are widely used to infer the contribution of denitrifying bacteria to the concentration of dissolved N₂O (Hallin *et al.*, 2018). Denitrification is usually considered as facultative anaerobic respiration. Oxygen concentration appears to regulate the sequence of the denitrification enzymes, especially the *nosZ*, which is inhibited even at very low oxygen concentrations (Bonin *et al.*, 1989; Zumft, 1997). Consequently, the studies on denitrification in inland

waters are focused on anoxic waters and, particularly, in sediments (Piña-Ochoa and Álvarez-Cobelas, 2006). However, denitrifiers are also present in the water column of lakes and reservoirs (Junier *et al.*, 2008; Kim *et al.*, 2011; Pajares *et al.*, 2017). Some studies pointed out that the influence of O₂ concentration on the denitrifying activity differed from one bacterium to another, and oxic denitrifying bacteria occur in diverse environments (Lloyd *et al.*, 1987; Lloyd, 1993; Hayatsu *et al.*, 2008). Many bacteria can denitrify in oxic and anoxic conditions, with the highest N₂O/N₂ ratios in oxic conditions (Hochstein *et al.*, 1984; Lloyd *et al.*, 1987; Lloyd, 1993).

Dissimilatory nitrate reduction to ammonium (DNRA) is another heterotrophic process of nitrate reduction coupled to organic carbon oxidation (Figure 1.10a). Unlike denitrification, DNRA leads to N retention in the ecosystem. DNRA is a strict anoxic process that reduces nitrate to nitrite and then to ammonium, with concomitant formation of small amounts of N₂O (Stremińska *et al.*, 2012). In the second step, the nitrite reduction to ammonium is the critical reaction catalyzed by the enzyme nitrite reductase coded by the gene *nrfA* (Tiedje and Zehnder, 1988). DNRA is an important process in marine and lake sediments, where competes for nitrate with denitrification. DNRA dominates in environments with high content in organic matter in comparison to N availability. In contrast, high nitrate concentrations in proportion to organic matter availability may favor denitrification (Nizzoli *et al.*, 2010; Dong *et al.*, 2011; Roland *et al.*, 2018).

The nitrogen-processing microorganisms and N₂O production have been extensively studied in the ocean and soils. McCrackin and Elser (2011) suggested that lakes and reservoirs may play an important role in the N removal at the landscape scale, acting as sources of N₂O, especially in areas submitted to high N inputs. However, few studies have focused on the role of reservoirs removing N, and these few ones have focused on the sediments rather than in the water column (Piña-Ochoa and Álvarez-Cobelas, 2006). Here we present the results of a study of the dissolved N₂O concentration in the profiles of twelve Mediterranean reservoirs covering a broad spectrum of landscapes and intrinsic reservoir properties (León-Palmero *et al.*, 2019, 2020a, 2020b, and Appendix 2). We explored the potential physicochemical variables controlling the dissolved N₂O in the water column and the different microbial metabolisms involved in the N transformations through

quantitative PCR analysis. We hypothesized that the reservoirs with high N concentrations would produce higher dissolved N₂O concentrations, especially during the stratification period when anoxic conditions in deep layers occur. In the oxic waters, nitrification would be the primary source of N₂O, while denitrification would be the main source of N₂O in hypoxic and anoxic waters when N concentrations are high. In contrast, denitrification would be a net sink of N₂O in anoxic waters where there are low N concentrations.

6. 2. Material and Methods

6. 2. 1. Study reservoirs and water column sampling

We sampled twelve reservoirs between July 2016 and August 2017 in southern Spain once during the summer stratification and the winter mixing. The reservoirs were built between 1932 and 2003, and they differ in morphometry, water chemistry, trophic status, and landscape characteristics (León-Palmero *et al.*, 2019, 2020a, 2020b, and Appendix 2). The morphometry and watershed characterization of the reservoirs is detailed in Chapter 2 (see subsection 2. 1. Study reservoirs, morphometry and watershed characterization).

We performed the vertical profiles of the reservoirs using a Sea-Bird 19plus CTD profiler, coupled to a Spherical Underwater Quantum Sensor (LI-193R), and a fluorimeter Turner® SCUFA (model CYCLOPS-7) for continuous measurements of temperature (°C), dissolved oxygen ($\mu\text{mol L}^{-1}$), conductivity ($\mu\text{S cm}^{-1}$), turbidity (FTU - formazin turbidity unit), density (kg m^{-3}), photosynthetic active radiation, chlorophyll-*a* fluorescence ($\mu\text{g L}^{-1}$), specific conductance ($\mu\text{S cm}^{-1}$), and salinity (psu – practical salinity units). We performed the vertical profiles and the sampling of the water column near the dam, in the open waters of the reservoir. During the stratification and the mixing period, we selected the same location. Then, based on the temperature and oxygen profiles, we selected six to nine depths, representative of the oxic and anoxic layers and the transition between them in the different reservoirs. We took the water samples using a UWITEC sampling bottle of 5 L with a self-closing mechanism. We collected samples for the dissolved N₂O analysis in 125 or 250mL airtight Winkler bottles in duplicate (250 mL) or in triplicate (125 mL). We filled up the bottles very carefully from the bottom to avoid the formation of bubbles and minimize the loss of N₂O during field sampling. We preserved the samples with

a solution of HgCl₂ (final concentration 1 mmol L⁻¹) to inhibit biological activity and sealed the bottles with Apiezon® grease to prevent gas exchanges. We stored these samples in the dark at room temperature until analysis.

We also took samples from each depth from the chemical and biological analysis explained below. For the analysis of the major nutrients and functional genes, we selected three or four representative depths of the epilimnion, metalimnion (oxycline), and hypolimnion, and bottom layers for major nutrient analysis during the stratification period. We also selected three or four equivalent depths during the mixing period. In total, we analyzed 77 samples: 41 samples from the stratification period, and 36 samples from the mixing period. We measured barometric pressure using a multi-parameter probe (Hanna HI 9828) for the gas saturation calculations. We calculated the saturation values (%) for dissolved oxygen as the ratio of the dissolved gas measured and the gas concentration expected in equilibrium. We calculated the gas concentration in equilibrium, taking into account the differences in temperature, salinity, and barometric pressure (Mortimer, 1956).

6. 2. 2. Dissolved N₂O in the water column

We measured dissolved N₂O using headspace equilibration in a 50 ml air-tight glass syringe by duplicate or triplicate from each sample as in (Sierra *et al.*, 2017). Briefly, we analyzed the N₂O concentration using a gas chromatograph (Bruker® GC-450) equipped with an Electron Capture Detector. We daily calibrated the detectors using three standard gas mixtures with N₂O concentrations of 305, 474, 2000 ppbv, made and certified by Air Liquide (France). We calculated the (%) saturation values as the ratio between the concentration of the dissolved gas measured and the gas concentration expected in equilibrium considering the temperature, salinity, and barometric pressure of each reservoir. We calculated the gas concentration in equilibrium using the Bunsen solubilities for N₂O (Weiss and Price, 1980). We used the atmospheric gas concentrations provided by *The Global Greenhouse Gas Reference Network* website (<https://www.esrl.noaa.gov/gmd/ccgg/index.html>), which is part of the National Oceanic and Atmospheric Administration Earth System Research Laboratory in Boulder, Colorado. We calculated the 2016 global mean atmospheric concentrations for N₂O (Elkins *et al.*, 2017) from the 2016 global

monthly mean. More details are provided in Chapter 2 (see subsection 2. 3. 2. CH₄ and N₂O concentration in the water column).

6. 2. 3. Major nutrient analysis in the water column

We determined total nutrients using unfiltered water, while we filtered the samples through 0.7 µm pore-size Whatman GF/F glass-fiber filters for the dissolved nutrients. We acidified the samples for dissolved organic carbon (DOC), total dissolved nitrogen (TDN), and total nitrogen (TN) samples with phosphoric acid (final pH<2). We measured DOC, TN, and TDN by high-temperature catalytic oxidation using a Shimadzu total organic carbon analyzer (Model TOC-V CSH) coupled to nitrogen analyzer (TNM-1) (Álvarez-Salgado and Miller, 1998). We calibrated the instrument using a four-point standard curve of dried potassium hydrogen phthalate for DOC, and dried potassium nitrate for TN and TDN. We analyzed two replicates of each sample and three to five injections per replicate. We purged the DOC samples with phosphoric acid for 20 min to eliminate all the dissolved inorganic carbon.

We measured the nitrate (NO₃⁻) concentration using the ultraviolet spectrophotometric method with a Perkin Elmer UV-Lambda 40 spectrophotometer at the wavelength of 220 nm and including corrections for DOC absorbance at 275 nm (APHA, 1992). We measured the nitrite (NO₂⁻) concentration by Inductively Coupled Plasma Optical Emission Spectrometry (ICP-OES). Dissolved inorganic nitrogen (DIN) is the addition of the NO₃⁻, and NO₂⁻ concentrations. We measured total phosphorus (TP) concentration by triplicate using the molybdenum blue method (Murphy and Riley, 1962) after digestion with a mixture of potassium persulphate and boric acid at 120 °C for 30 min (APHA, 1992). More details are provided in Chapter 2 (see subsection 2. 3. Physico-chemical analysis in the water column).

6. 2. 4. Chlorophyll-*a* concentration

We determined chlorophyll-*a* concentration by filtering the particulate material of 500 to 2000 ml of water through 0.7 µm pore-size Whatman GF/F glass-fiber filters. Then, we extracted the pigments from the filters with 95% methanol in the dark at 4 °C for 24 h (APHA, 1992). We measured chlorophyll-*a* (Chl-*a*) absorption at the wavelength of 665 nm using a Perkin Elmer UV-Lambda 40

spectrophotometer, and we corrected the solution scattering at 750 nm. To obtain the cumulative chlorophyll-*a* in the whole water column (mg Chl *a* m⁻²), from the discrete depths, we summed the concentration of Chl-*a* from each stratum using the trapezoidal rule (León-Palmero *et al.*, 2020b).

6. 2. 5. Functional genes

We studied unique functional genes involved in the specific microbial transformations in the nitrogen cycle using PCR for detection and quantitative PCR (qPCR) as a proxy for the abundance of these functional groups in the water column. First, we pre-filtered the water through 3.0 µm pore-size filters and extracted DNA following the procedure developed by Boström *et al.* (2004) for environmental samples. For the PCR and qPCR analysis we chose specific primers for each gene from similar studies in freshwaters (see below).

We targeted the gene *amoA*, which encodes the catalytic subunit of ammonia monooxygenase, the first and rate-limiting step of the nitrification (Kowalchuk and Stephen, 2001). We studied the ammonia-oxidizing bacteria (AOB, bac-*amoA*) and the ammonia-oxidizing archaea (AOA, arch-*amoA*). For the bacterial *amoA*, we used specific primers tested in various aquatic and terrestrial environments (Rotthauwe *et al.*, 1997). The forward primer was amoA-1F (5'– GGGGTTTCTACTGGTGGT-3'), and the reverse primer was amoA-2R (5'– CCCCTCKGSAAAGCCTTCTTC – 3'). The specific amplicon length was 491 bp, and the annealing temperature was 60 °C. We used a pure culture of *Nitrosomonas europaea* Winogradsky 1892 (ATCC 25978) as positive control for bacterial *amoA* standard quantification. For the archaeal *amoA*, we used the specific primers described in (Francis *et al.*, 2005). The forward primer was Arch-amoAF (5'- STAATGGTCTGGCTTAGACG-3'), and the reverse primer was Arch-amoAR (5'- GCGGCCATCCATCTGTATGT-3') at a final concentration of 0.4 µmol L⁻¹. The specific amplicon length was 635 bp, and the annealing temperature was 53 °C. We used a pure culture of *Nitrososphaera viennensis* (Stieglmeier *et al.*, 2014) (strain EN76^T) for standard preparation.

To study the denitrifier abundance, we targeted the gene *nirS* in all the depths of the water column and the gene *nosZ* in the bottom layer. The gene *nirS* encodes the nitrite reductase that catalyzes the transformation of nitrite to NO during denitrification. We used the primers from (Braker *et al.*, 1998). The forward primer

was nirS-1F (5'-CCTAYTGCCGCCRCART-3'), and the reverse primer was nirS-3R (5'-GCCGCCGTCTRTGVAGGAA-3') at a final concentration of 2 $\mu\text{mol L}^{-1}$. The specific amplicon length was 260 bp, and the annealing temperature was 62 °C. We used a pure culture of *Escherichia coli* transformed with a constructed plasmid containing the *nirS* gene fragment for the standard preparation. The gene *nosZ* encodes the enzyme nitrous oxide reductase, responsible for the last step in denitrification: the N₂O reduction to N₂. We used the primers from Henry *et al.* (2006) at a final concentration of 2 $\mu\text{mol L}^{-1}$. The forward primer was nosZ1F (5'-WCSYTGTTTCMTCGACAGCCAG-3'), and the reverse primer was nosZ1R (5'-ATGTCGATCARCTGVKCRTTYTC-3'). The specific amplicon length was 259 bp and the annealing temperature was 63 °C. We used a pure culture of *Paracoccus denitrificans* (Beijerinck and Minkman 1910) Davis 1969 (ATCC 17741) as a positive control for the standard quantification.

We also studied the gene *nrfA* that encodes for the nitrite reduction to ammonium, the second step in the DNRA in the bottom layer. We used the primers established by Takeuchi (2006) at a final concentration of 0.5 $\mu\text{mol L}^{-1}$. The forward primer was nrfA6F (5'-GAYTGCCAYATGCCRAAAGT-3'), and the reverse primer was nrfA6R (5'-GCBKCTTTYGCTTCRAAGTG-3'). The annealing temperature was 54.5 °C, and the amplicon length was 222 bp. We used a pure culture of *Escherichia coli* as a positive control. More details are provided in Chapter 2 (see subsection 2. 4. 3. Functional genes: N₂O related genes).

6. 2. 6. Statistical tests

We conducted all the statistical analysis in R (R Core Team, 2019) using the packages car (Fox and Weisberg, 2011), nortest (Gross and Ligges, 2015), mgcv (Wood, 2011), readxl (Wickham and Bryan, 2019), Rcmdr (Fox and Bouchet-Valat, 2019), and outliers (Komsta, 2011). We performed the Shapiro-Wilk test of normality analysis, and the Levene's test for homogeneity of variance across groups. We performed a one-way analysis of variance test (ANOVA) when the data were normally distributed. In case the data did not meet the assumptions of normality, we used the Kruskal-Wallis rank sum test (K-W) or the Wilcoxon test. We analyzed the potential sources of dissolved N₂O using simple regression analysis, multiple regression analysis, and generalized additive models (GAMs) (Wood, 2006). GAM is a

generalized model with a linear predictor involving a sum of smooth functions of covariates (Hastie and Tibshirani, 1986, 1990). The model structure is detailed in equation 6.1:

$$y_i = f_1(x_{1i}) + f_2(x_{2i}) + \dots + f_n(x_{ni}) + \epsilon_i \quad \text{Eq. 6.1}$$

Where the $f_{1,2,\dots,n}$ are the smooth functions, and the ϵ_i are independent identically distributed $N(0, \sigma^2)$ random variables. We fit smoothing functions by penalized cubic regression splines. The cross-validation method (Generalized Cross Validation criterion, GCV) estimates the smoothness of the functions. Before model fitting, we examined the concurvity among predictors. We fitted the models to minimize the Akaike Information Criterion (AIC) and the GCV values. We provide details on these GAMs in Supplementary Table 6.2. We calculated the percentage of variance explained by the model (adjusted R^2) and the quality of the fit (deviance explained). We also fixed the effect of each predictors to assess the contribution of the other predictor on the total deviance explained. Then, the sum of the deviance explained by two predictors can be different from the deviance explained by the model due to interactive effects. We tested the multicollinearity using the Variable Inflation Factor (VIF).

6. 3. Results

6. 3. 1. Profiles description

We studied the concentration and percentage (%) of saturation of the dissolved N₂O in the water column of the twelve reservoirs during the stratification and the mixing periods. In Figures 6.1 and 6.2 and in Supplementary Figures 6.1 - 6.10, we show the profiles of the dissolved N₂O concentration and % of saturation, water temperature, dissolved oxygen (DO) concentration, chlorophyll-*a* concentration (Chl-*a*), nitrogen concentration in different forms, and the abundances of the functional genes involved in the nitrogen metabolism. The concentration of dissolved N₂O varied up to three orders of magnitude from 4.7 to 2441.2 nmol L⁻¹ during the summer stratification (n = 96), but it was less variable during the winter mixing (n = 84), ranging only from 10.9 to 47.6 nmol L⁻¹. We found N₂O undersaturation values from 37 % to supersaturation values up to 24174 % during the stratification period, and from 90 % to 392 % during the mixing period. We did

not find significant differences between the dissolved N₂O concentration during the stratification period and the mixing period ($V = 42$, p -value = 0.85).

According to our findings on N₂O fluxes in León-Palmero *et al.* (2020b), we classified a reservoir as a sink of N₂O when the emission was 0 or negative, and as a source of N₂O when the emission was positive. The eight reservoirs that acted as N₂O sinks were: San Clemente, La Bolera, Francisco Abellán, Jándula, Negratín, El Portillo, Rules, and Los Bermejales (Figure 3.2 in Chapter 3). The median for the N₂O concentration in the water column of these reservoirs was 12.3 nmol L⁻¹ ranging from 4.7 to 46.1 nmol L⁻¹. The median of saturation was 109 % ranging from 37 % to 366 %. In surface waters (i.e., 0.5 m) the median for the N₂O saturation was 105 %. We detected N₂O supersaturation and undersaturation at different depths of the same profile in both periods (Figure 6.1. and Supplementary Figures 6.1 - 6.7). In San Clemente, La Bolera, Francisco Abellán, and Jándula reservoirs, we found a peak of N₂O above the oxycline (Figure 6.1a, and Supplementary Figures 6.1a, 6.2a, 6.3a). Besides N₂O concentration and the % of saturation decreased to undersaturation values below the oxycline, reaching 37 % in San Clemente reservoir (Figure 6.1a), and 84 % in La Bolera reservoir (Supplementary Figure 6.1a). In both systems, we detected high abundances of the gene for the nitrous oxide reductase (i.e., *nosZ*), that may explain the net consumption of N₂O in the last step of denitrification. In these reservoirs acting as sinks of N₂O, the total nitrogen concentration ranged from 9.3 to 49.9 $\mu\text{mol L}^{-1}$, and the chlorophyll-*a* concentration varied from 0.4 to 10.3 $\mu\text{g L}^{-1}$.

The four reservoirs that acted as sources of N₂O were: Iznájar, Béznar, Cubillas, and Colomera (Figure 3.2 in Chapter 3). The median for the N₂O concentration was 20.3 nmol L⁻¹ (from 12.6 to 2441.2 nmol L⁻¹), and the median for the saturation value was 230 % (from 109 to 24174 %), and 193 % for surface waters (i.e., 0.5 m) (Figure 6.2, and Supplementary Figures 6.8 - 6.10). The water column of these reservoirs was always supersaturated in N₂O, with the N₂O supersaturation reaching up to 1449 % (105.5 nmol L⁻¹) in the epilimnion of Iznájar reservoir during the stratification period (Figure 6.2a). We found the highest concentrations of dissolved N₂O in the hypoxic waters, that reached up to 2441.2 nmol L⁻¹ in the hypolimnion of the Iznájar reservoir during the stratification period (Figure 6.2a). In contrast to the sink reservoirs, we detected that the concentration of dissolved N₂O increased below the oxycline,

leading to a massive accumulation of N₂O in the hypolimnion with a low concentration of oxygen (< 7.5 μmol L⁻¹). In Iznájar, Béznar and Cubillas reservoirs we detected high abundances of archaeal *amoA* gene and *nirS* gene at these sites, suggesting that the accumulation of N₂O may be produced by nitrifier denitrification (i.e., archaeal *amoA* gene), and denitrification (i.e., *nirS* gene) (Figure 6.2a, and Supplementary Figures 6.8a and 6.9a). Both processes have the highest yields of N₂O at low oxygen concentrations. In addition to the processes occurring at the water column, the diffusion from the sediments may also contribute to the accumulation in N₂O in the bottom waters, leading to maximum values in the profile in stratification and mixing periods. In this group of reservoirs, we found that the TN varied from 56.1 to 323.6 μmol L⁻¹, and the chlorophyll-*a* concentration ranged from 0.2 to 34.6 μg L⁻¹.

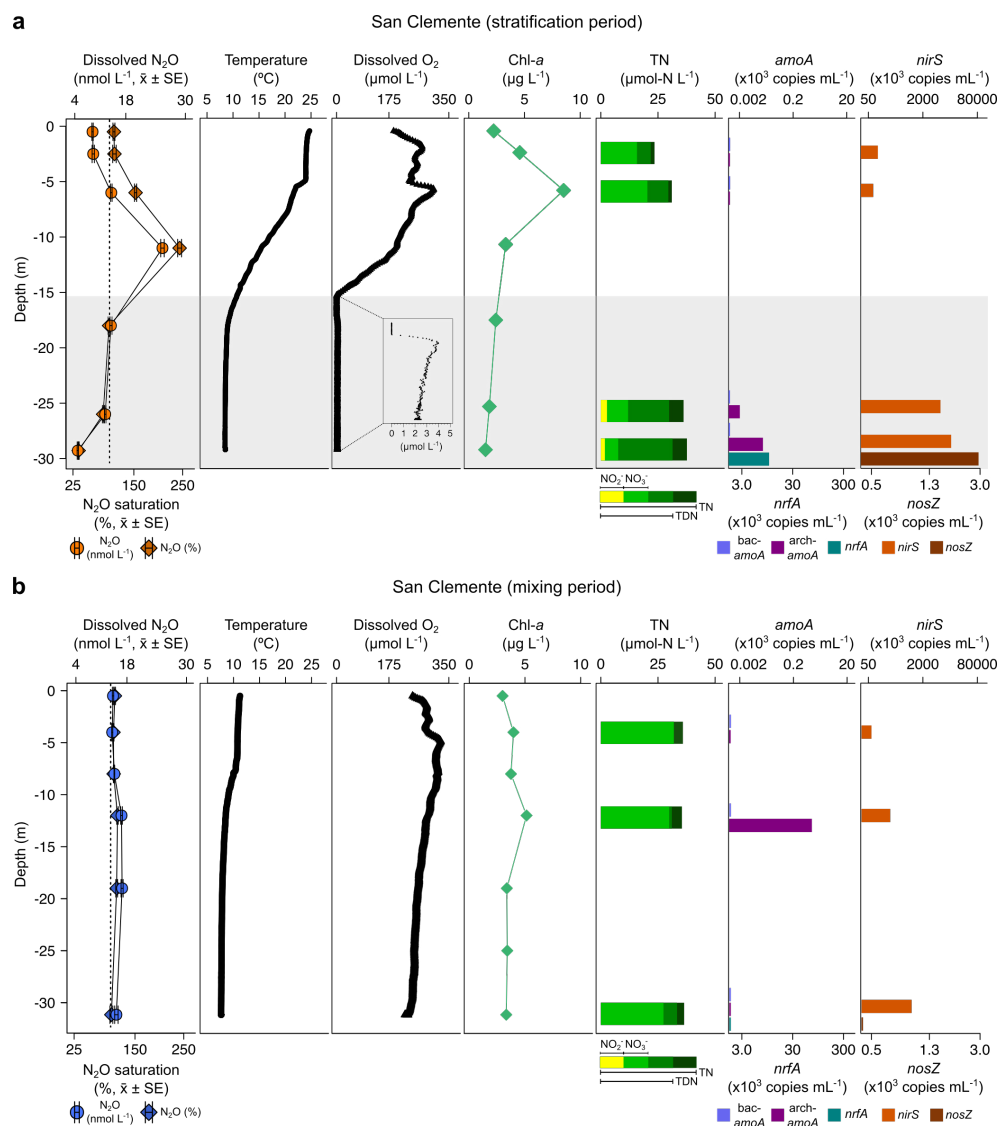


Figure 6.1. Vertical profiles of physicochemical and biological variables in San Clemente reservoir. Dissolved nitrous oxide (N₂O) concentration (nmol L⁻¹, mean ± standard error, circles), nitrous oxide saturation (%), mean ± standard error, diamonds), and atmospheric equilibrium concentration (discontinuous line); water temperature (°C); dissolved oxygen (DO) concentration (μmol L⁻¹); chlorophyll-*a* (Chl-*a*) concentration (μg L⁻¹); total nitrogen (TN) concentration (μmol-N L⁻¹); abundance of the genes *amoA* (bacterial *amoA* and archaeal *amoA*, x10³ copies mL⁻¹); abundance of the gene *nrfA* (x10³ copies mL⁻¹), and abundance of the genes *nirS* and *nosZ* (x10³ copies mL⁻¹) during the stratification period (a) and the mixing period (b). Note that the gene abundance axes are in logarithmic scale. The grey area represents the anoxic zone (DO < 7.5 μmol L⁻¹). The sampling date for the stratification period was on July 17, 2017 and March 28, 2017 for the mixing period.

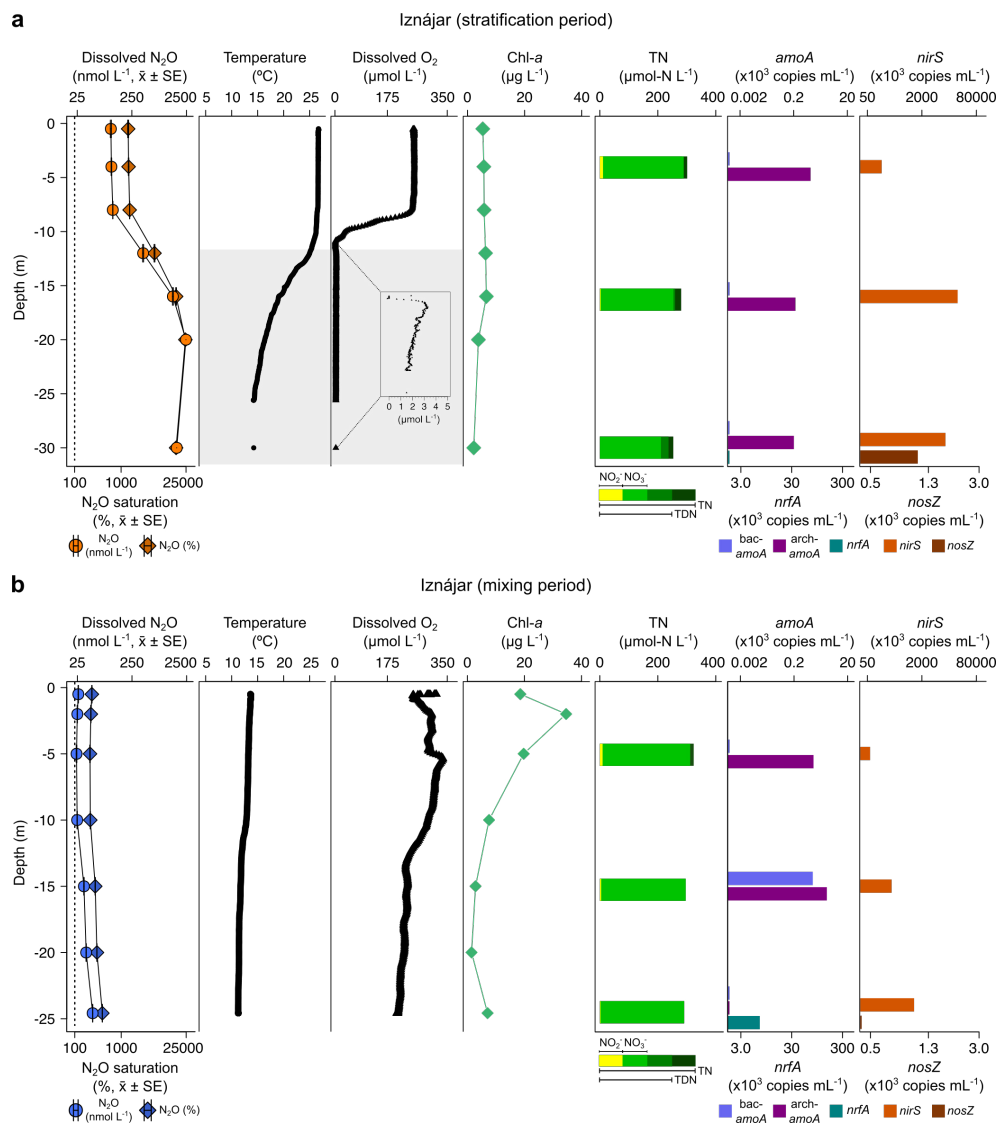


Figure 6.2. Vertical profiles of physicochemical and biological variables in Iznájar reservoir. Dissolved nitrous oxide (N₂O) concentration (nmol L⁻¹, mean ± standard error, circles), nitrous oxide saturation (% mean ± standard error, diamonds), and atmospheric equilibrium concentration (discontinuous line); water temperature (°C); dissolved oxygen (DO) concentration (μmol L⁻¹); chlorophyll-*a* (Chl-*a*) concentration (μg L⁻¹); total nitrogen (TN) concentration (μmol-N L⁻¹); abundance of the genes *amoA* (bacterial *amoA* and archaeal *amoA*, x10³ copies mL⁻¹); abundance of the gene *nrfA* (x10³ copies mL⁻¹), and abundance of the genes *nirS* and *nosZ* (x10³ copies mL⁻¹) during the stratification period (a) and the mixing period (b). Note that the N₂O, and the gene abundance axes are in logarithmic scale. The grey area represents the anoxic zone (DO < 7.5 μmol L⁻¹). The sampling date for the stratification period was on September 8 and 9, 2016 and March 15, 2017 for the mixing period. The sampling date for temperature and the dissolved oxygen was performed a day before than the sampling for N₂O and the biological variables because of logistical problems.

The dissolved N₂O concentration in the water column was significantly lower in the reservoirs acting as sinks than in the reservoirs acting as sources of N₂O (K-W = 11.76, p-value < 0.001; Figure 6.3a). We observed that the dissolved N₂O concentration declined below the oxycline in the sinks, but dissolved N₂O increased under the oxycline in the reservoirs acting as sources. We calculated the difference between the dissolved N₂O concentration above the oxycline with the dissolved N₂O concentration below the oxycline, and we found significant differences between the reservoirs acting as sinks and as sources (K-W = 5.33, p-value < 0.05; Figure 6.3b). In the reservoirs acting as sinks of N₂O there was a net consumption of N₂O below the oxycline (i.e., the difference was negative in Figure 6.3b). In contrast, we detected a higher concentration of N₂O below the oxycline of the reservoirs acting as sources of N₂O (i.e., the difference was positive in Figure 6.3b). We also detected that the TN and the total phosphorus (TP) concentrations were higher in the reservoirs acting as sources than in the reservoirs acting as sinks (t = 4.39, p-value < 0.001; t = -6.25, p-value < 0.001, respectively) (Figure 6.3.c, d). The molar ratio between the dissolved organic carbon (DOC) concentration and the dissolved inorganic nitrogen (DIN) concentration (i.e., $\mu\text{mol-C} : \mu\text{mol-N}$) was significantly higher in the reservoirs acting as sinks than in the reservoirs acting as sources (K-W = 12.62, p-value < 0.001; Figure 6.3e).

We obtained that the N₂O concentrations were related to the total nitrogen concentration following a power function ($\text{N}_2\text{O}, \text{nmol L}^{-1} = 0.93 \text{ TN } (\mu\text{mol L}^{-1})^{0.79}$, adjusted $R^2 = 0.43$, p-value < 0.001). We also found significant relationships between the total dissolved nitrogen (TDN), dissolved inorganic nitrogen (DIN), and nitrate, nitrite, and DIN concentration to the dissolved N₂O concentration. These relationships are detailed in Supplementary Table 6.1. A power function also explained the dissolved N₂O relationship in relation to the TP concentration ($\text{N}_2\text{O}, \text{nmol L}^{-1} = 25.07 \text{ TP } (\mu\text{mol-P L}^{-1})^{0.44}$, adjusted $R^2 = 0.19$, p-value < 0.001).

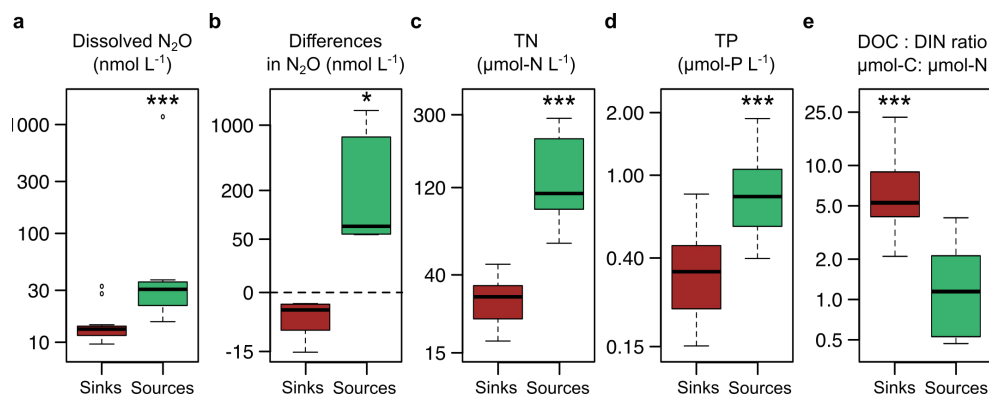


Figure 6.3. Median (line), 25-75 % percentiles (box) and max-min values without extremes (whisker) of chemical variables in the reservoirs acting as sinks (brown boxes) and as sources (green boxes) of N₂O. The whiskers extend to the most extreme data point, which is no more than range times the interquartile range from the box. (a) Dissolved nitrous oxide (N₂O) concentration (nmol L⁻¹), (b) differences in the dissolved N₂O above and under the oxycline, (c) total nitrogen (TN) concentration (μmol-N L⁻¹), (d) total phosphorus (TP) concentration (μmol-P L⁻¹), and (e) dissolved organic carbon: dissolved inorganic nitrogen ratio (C-DOC : N-DIN molar ratio). We used the t-test (i.e., normal data) or Kruskal-Wallis test (i.e., non normal data) for the comparison between sinks and sources. * Stands for statistically significant differences (* = p<0.05; *** = p<0.001). Note that the y axes are in logarithmic scale.

6. 3. 2. Microbial regulation of dissolved N₂O

Nitrification from ammonia to nitrate produces N₂O as an intermediate by-product. The archaeal *amoA* gene appeared consistently in all the study reservoirs, while the bacterial *amoA* gene appeared only in four samples. The abundance of the archaeal *amoA* gene varied from 0 to 1.9 × 10⁴ copies mL⁻¹ (median = 414 copies mL⁻¹) in the reservoirs acting as sinks and from 0 to 3.4 × 10⁴ copies mL⁻¹ (median = 295 copies mL⁻¹) in the reservoirs acting as sources. There were no significant differences in the archaeal *amoA* abundance between both groups of reservoirs (K-W = 0.90, p-value = 0.342; Figure 6.4a). We did not find any significant relationship between the abundance of the archaeal *amoA* gene and the dissolved N₂O concentration (n = 77, p-value = 0.824).

Two processes reduce nitrate to ammonium, also releasing N₂O as an intermediate by-product: DNRA and the denitrification. The abundance of the gene *nrfA* in the bottom samples of the study reservoirs varied from 0 to 3.8 × 10⁵ copies mL⁻¹ (median = 3.1 × 10³ copies mL⁻¹) in the reservoirs acting as sinks, and varied from 0 to 7.1 × 10³ copies mL⁻¹ (median = 1.8 × 10³ copies mL⁻¹) in the reservoirs acting as sources of N₂O, but the differences were not significant (K-W = 0.70, p-value = 0.40)

(Figure 6.4b). The maximum abundance of the *nrfA* gene was detected in the El Portillo reservoir during the mixing period (Supplementary Figure 6.5b). We did not find a significant relationship between the abundance of the *nrfA* gene and the dissolved N₂O concentration ($n = 24$, p -value = 0.637).

To study denitrification, we determined the abundance of the *nirS* gene in the water column and the *nosZ* gene, which is oxygen-sensitive, only at the bottom samples. The gene *nirS* was ubiquitous, appearing in large abundance in the water column of all the reservoirs in both periods. The abundance of the *nirS* gene ranged from 0 to 1.4×10^7 copies mL⁻¹ (median = 2.2×10^5 copies mL⁻¹) in the reservoirs acting as sinks, and from 0 to 1.1×10^8 copies mL⁻¹ (median = 7.0×10^5 copies mL⁻¹) in the reservoirs acting as sources. These differences between sinks and sources of N₂O were significant (K-W = 4.86, p -value < 0.05; Figure 6.4c). We detected the maximum abundances of the *nirS* gene in Iznájar, Béznar, and Cubillas reservoirs during the stratification period (Figure 6.2a and Supplementary Figures 6.8a and 6.9a). The *nirS* gene was not detected only in 8 samples out of 77. We did not include these 8 samples in the following statistical tests since they were statistical outliers ($G = 0.25$, p -value < 0.001). We obtained that the N₂O concentration depended on the *nirS* abundance following a power function ($N_2O, \text{nmol L}^{-1} = 0.27 (\textit{nirS}, \text{copies mL}^{-1})^{0.33}$, $n = 69$, adjusted $R^2 = 0.28$, p -value < 0.001).

The abundance of the gene *nosZ* ranged from 0 to 2.9×10^3 copies mL⁻¹ (median = 296 copies mL⁻¹) in the reservoirs acting as sinks, and from 0 to 1.1×10^3 copies mL⁻¹ (median = 385 copies mL⁻¹) in the reservoirs acting as sources. We did not find significant differences between sinks and sources of N₂O (K-W = 0.11, p -value = 0.74; Figure 6.4d). We detected the maximum abundance of the *nosZ* in San Clemente reservoir during the stratification period, where we also found the lowest undersaturation in N₂O (i.e., 37 %; Supplementary Figure 6.1a). We also calculated the *nosZ:nirS* ratio ($\times 100$) in the bottom samples. This ratio ranged from 0 to 1.420 (median = 0.011) in the reservoirs acting as sinks, and from 0 to 0.147 (median = 0.004) in the reservoirs acting as sources. We did not find significant differences in the *nosZ:nirS* ratio (K-W = 0.35, p -value = 0.556; Figure 6.4e).

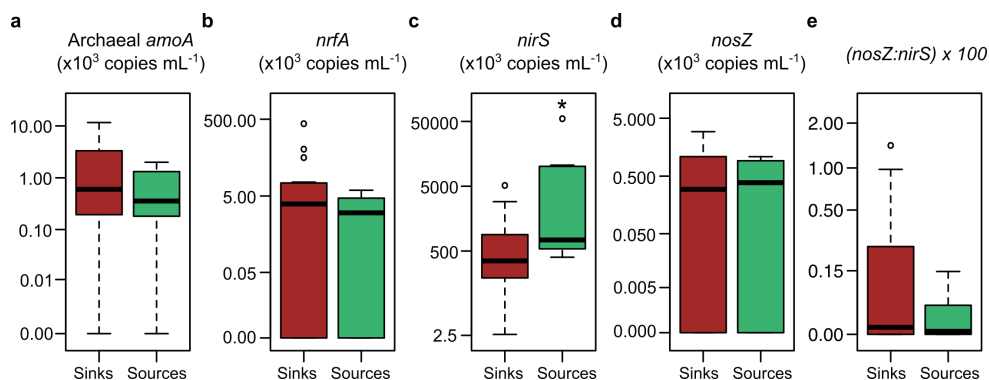


Figure 6.4. Median (line), 25-75 % percentiles (box) and max-min values without extremes (whisker) of the abundances of the functional genes in the reservoirs acting as sinks (brown boxes) and sources (green boxes) of N₂O. The whiskers extend to the most extreme data point, which is no more than range times the interquartile range from the box. (a) Abundance of the archaeal *amoA* (copies mL⁻¹), (b) abundance of the gene *nrfA* (copies mL⁻¹), (c) abundance of the gene *nirS* (copies mL⁻¹), (d) abundance of the gene *nosZ* (copies mL⁻¹), and (e) the ratio between the abundances of *nosZ* and *nirS* ((*nosZ*:*nirS*) x 100). We used the t-test (i.e., normal data) or Kruskal-Wallis test (i.e., non normal data) for the comparison between sinks and sources. * Stands for statistically significant differences (* = p<0.05). Note that the y axes are in logarithmic scale.

6. 3. 3. Modeling dissolved N₂O in the water column

The dissolved N₂O concentration in the water column of the study reservoirs was related to the nitrogen concentration and the abundance of the *nirS* gene. We combined these two explanatory variables to model the N₂O production in the water column using generalized additive models (GAMs). We found that the TN concentration and the abundance of the *nirS* gene explained the dissolved N₂O concentration with a fit deviance of 61.6 % and an explained variance (i.e., adjusted R²) of 59.6 %. The equation for the model was: $\text{Log}_{10}(\text{N}_2\text{O}, \text{nmol L}^{-1}) = 0.3 e^{0.7 \text{Log}_{10}(\text{TN}, \mu\text{mol-N L}^{-1})} + 0.01 e^{0.6 \text{Log}_{10}(\textit{nirS}, \text{copies mL}^{-1})}$ (Figure 6.5a). The N₂O concentration (log-transformed) was an exponential function of the TN, and explained a higher part of the deviance 30.5 % (Figure 6.5b). Besides, the N₂O concentration (log-transformed) was an exponential function of the abundance of the *nirS* gene (log-transformed) and explained 18.7 % (Figure 6.5c). The details of the GAM model are provided in Supplementary Table 6.2.

We also studied the main drivers of the abundance of *nirS* gene in the water column of the study reservoirs. We found a significant and negative relationship between the abundance of *nirS* gene and the dissolved oxygen concentration ($\textit{nirS}, \text{copies mL}^{-1} = 5.0 \times 10^6 e^{(-0.011 \text{DO}, \mu\text{mol L}^{-1})}$, n = 69, adjusted R² = 0.56, p-value <

0.001) (Figure 6.5d, and Supplementary Table 6.3). We also detected positive relationship between *nirS* abundance and total phosphorus concentration. The *nirS* abundance depended on the TP concentration following a power function ($nirS$, copies mL⁻¹ = 1.4×10^6 (TP, $\mu\text{mol-P L}^{-1}$)^{1.12}, n = 69, adjusted R² = 0.21, p-value < 0.001) (Figure 6.5e, and Supplementary Table 6.3). Together, the dissolved oxygen and TP concentrations explained the 62 % of the variance in the abundance of the gene *nirS* in the water column of the reservoirs (Table 6.1). In addition, the abundance of the gene *nirS* was also significantly related to the cumulative Chl-*a*, which is a proxy for the total phytoplanktonic biomass exported from the water column. Another power function explained the relationship between the *nirS* abundance and the cumulative Chl-*a* ($nirS$, copies mL⁻¹ = 5.9×10^4 (Cum Chl-*a*, mg Chl-*a* m⁻²)^{0.64}, n = 69, adjusted R² = 0.20, p-value < 0.001) (Figure 6.5f, and Supplementary Table 6.3).

Table 6.1. Linear model explaining the abundance of the gene *nirS* (copies mL⁻¹) with the dissolved oxygen (DO) concentration ($\mu\text{mol L}^{-1}$) and the total phosphorus (TP) concentration ($\mu\text{mol-P L}^{-1}$), as predictor variables.

Response variable	Predictor variable	Estimate (Std Error)	t value	p-value
Log ₁₀ (<i>nirS</i> abundance) n = 69 Adj R ² = 0.62	Intercept	6.851 (0.120)	56.83	< 0.001
	DO	-0.004 (0.000)	-8.44	< 0.001
	Log ₁₀ (TP)	0.597 (0.188)	3.18	< 0.01

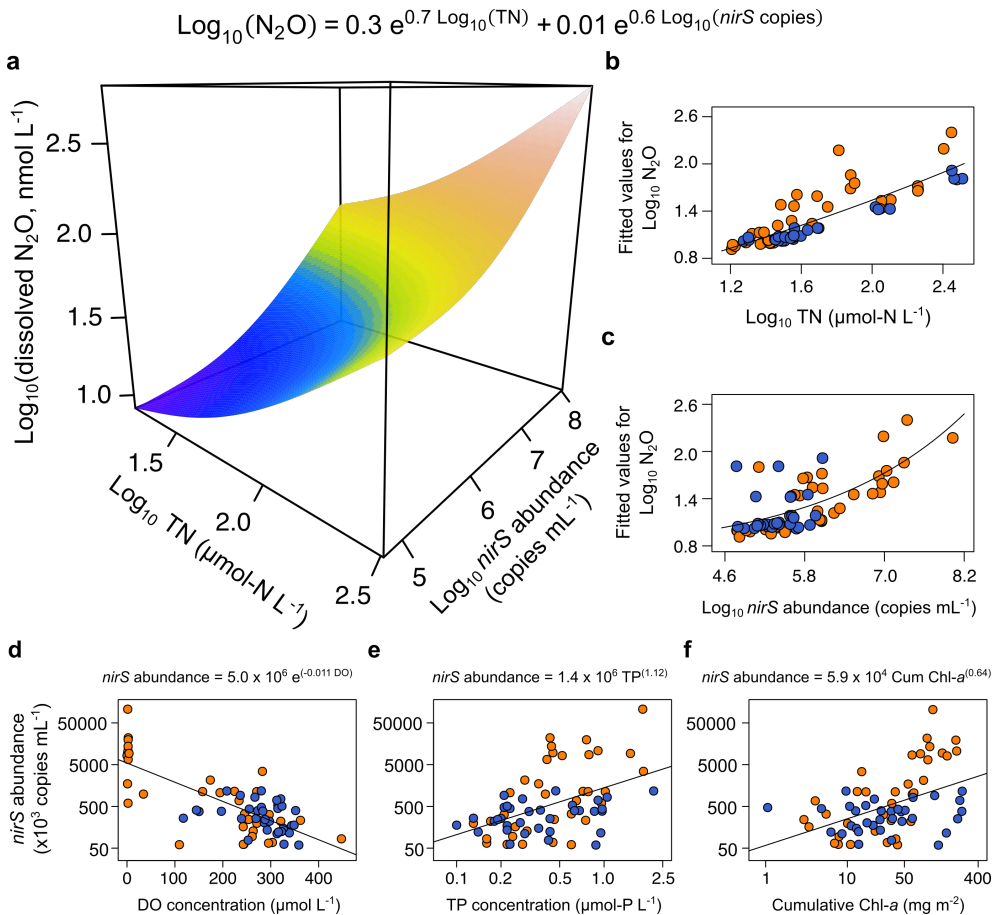


Figure 6.5. 3D-model for the main drivers of the dissolved N₂O concentration. (a) The total nitrogen (TN) concentration ($\text{Log}_{10} \text{ TN, } \mu\text{mol-N L}^{-1}$) (x-axis) and the abundance of the *nirS* gene ($\text{Log}_{10} \text{ nirS, copies mL}^{-1}$) (y-axis) determined the dissolved N₂O concentration ($\text{Log}_{10} \text{ N}_2\text{O, nmol L}^{-1}$) (z-axis), (b) partial response plot showing the exponential relationship between the fitted GAM values for the N₂O concentration and the TN concentration, (c) partial response plot showing the exponential relationship between the fitted GAM values for the N₂O concentration and the abundance of the *nirS* gene. More statistical details are provided in Supplementary Table 6.2. (d) Relationship between the dissolved oxygen (DO) concentration ($\mu\text{mol L}^{-1}$) and the abundance of the *nirS* gene ($n = 69$, adjusted $R^2 = 0.56$, p -value < 0.001), (e) Relationship between the total phosphorus (TP) concentration ($\mu\text{mol-P L}^{-1}$) and the abundance of the *nirS* gene ($n = 69$, adjusted $R^2 = 0.21$, p -value < 0.001), (e) relationship between the cumulative Chl-*a* and the abundance of the *nirS* gene ($n = 69$, adjusted $R^2 = 0.20$, p -value < 0.001). Orange dots stand for the stratification period and blue dots stand for the mixing period. Note the log-axis in panels (d), (e), and (f).

6. 4. Discussion

Profiles description

We found prominent differences in the concentration of the dissolved N₂O in the water column of the study reservoirs among depths and reservoirs. The dissolved N₂O concentration did not show significant differences between the two periods, which is coherent with the results reported in Chapter 3, where we found no significant differences between the fluxes of N₂O during the stratification period and the mixing period. The median values for the N₂O concentration and N₂O saturation were similar to the values found before in temperate and tropical lakes (Whitfield *et al.*, 2011; Roland *et al.*, 2017) and subtropical reservoirs (Liang *et al.*, 2019). However, the maximum N₂O concentration found in Iznájar reservoir was higher than the maximum values detected in previous studies in both surface and deep waters (Whitfield *et al.*, 2011; Diem *et al.*, 2012; Beaulieu *et al.*, 2014, 2015; Musenze *et al.*, 2014; Roland *et al.*, 2017; Liang *et al.*, 2019). The dissolved N₂O variability in these Mediterranean reservoirs was broader than the variability found in alpine and subtropical reservoirs (Diem *et al.*, 2012; Musenze *et al.*, 2014).

In the reservoirs acting as N₂O sinks, the surface % of saturation in N₂O was closed to the atmospheric equilibrium. In contrast, the % of saturation was higher in the reservoirs acting as sources. At the oxycline, the products of aerobic and anaerobic metabolic processes mix, and that allows the high rates of N₂O production (Beaulieu *et al.*, 2015). For example, the nitrate produced via nitrification in the epilimnion can be denitrified in the oxic-hypoxic interface (i.e., coupled nitrification-denitrification). Previous studies also detected similar peaks of dissolved N₂O in stratified lakes and reservoirs (Mengis *et al.*, 1997; Beaulieu *et al.*, 2015; Roland *et al.*, 2017). At the low oxygen concentration below the oxycline, we detected a net consumption of N₂O in the reservoirs acting as sinks, but a net production in the hypolimnion of the reservoirs acting as sources. Similar to our results, Beaulieu *et al.* (2015) found a net consumption of N₂O in the hypolimnion of reservoirs with low nitrogen content, but a net production in the hypolimnion of reservoirs with higher nitrogen content. Denitrification can act as a N₂O source and as a sink of N₂O at low oxygen concentration. Therefore, the low nitrogen concentration detected in the

reservoirs that acted as sinks may promote the reduction of N₂O to N₂ by complete denitrification.

The reservoirs that acted as sources of N₂O had a significantly higher concentration of N₂O, TN and TP, and a lower C-DOC: N-DIN ratio, than the reservoirs that acted as sinks. We also found that the N₂O concentration was a power function of the nitrogen and phosphorus content in the water column. These results suggest that the dissolved N₂O concentration was related to the eutrophication by nitrogen and phosphorus inputs. Our findings are in agreement with previous works that show that nitrogen loadings into aquatic systems can boost the production and subsequent emission of N₂O (Lemon and Lemon, 1981; Seitzinger *et al.*, 2000; Mulholland *et al.*, 2008; Baulch *et al.*, 2011; Beaulieu *et al.*, 2011, 2015). Baulch *et al.* (2011) found that nitrate and nitrite showed the best correlation to N₂O emissions, and the model was improved by including TP as a predictor variable. Wang *et al.* (2009) also reported higher saturation of N₂O in rivers with higher concentrations of TN and TP. In Chapter 3, we demonstrated that the differences in the N₂O fluxes were driven by the total nitrogen concentration, which was determined by the land-use in the watershed (i.e., agricultural and urban areas). Reservoirs located in forest dominated watersheds (i.e., lower anthropogenic land-use ratios) had a lower nitrogen concentration and negative N₂O fluxes. In contrast, reservoirs located in watersheds dominated by crops and urban areas (i.e. higher anthropogenic land-use ratios) had a higher nitrogen concentration and higher N₂O emissions (León-Palmero *et al.*, 2020a).

Microbial regulation of dissolved N₂O

N₂O is a by-product of the ammonia oxidation performed by ammonia-oxidizing archaea (AOA) and ammonia-oxidizing bacteria (AOB). In the study reservoirs, the abundance of archaeal *amoA* gene dominated over the abundance of bacterial *amoA* gene, which is in agreement with previous studies in temperate lakes (Auguet *et al.*, 2012; Small *et al.*, 2013; Palacin-Lizarbe *et al.*, 2019). In contrast, Pajares *et al.* (2017) found similar abundances of both groups in a tropical oligotrophic lake. They found a similar abundance of *amoA* gene to our study. Recent studies pointed out that AOA presented higher affinity for ammonia uptake than AOB, but lower N₂O yield than AOB, dominating in oligotrophic environments with a low ammonia supply (i.e., ocean) and producing less N₂O than AOB (Martens-

Habbena *et al.*, 2009; Hink *et al.*, 2018). Ammonia oxidation has been suggested as the primary process accounting for the N₂O production in oxic waters, but we did not find a significant relationship between the abundance of archaeal *amoA* gene and the dissolved N₂O concentration in the study reservoirs. To the best of our knowledge, this is the first study that considered the abundance of archaeal *amoA* gene to the N₂O concentration in the water column in reservoirs or lakes. In contrast, archaeal *amoA* gene has been extensively studied in the ocean and soils, where they are present in large numbers (Francis *et al.*, 2005; Könneke *et al.*, 2005; Leininger *et al.*, 2006; Wuchter *et al.*, 2006; Prosser and Nicol, 2008; Hu *et al.*, 2014) and they contribute significantly to the N₂O production (Francis *et al.*, 2005; Santoro *et al.*, 2011; Löscher *et al.*, 2012; Trimmer *et al.*, 2016).

The reduction of nitrate is coupled to the oxidation of organic carbon in two different microbial processes that may produce N₂O: DNRA and denitrification. DNRA is an anaerobic process that leads to N retention in ocean and lake sediments. Recently, Stremińska *et al.* (2012) detected that the reduction of NO₃⁻ occurs with the concomitant formation of small amounts of N₂O. However, we did not find a significant relationship between the abundance of the *nrfA* gene and the dissolved N₂O concentration. Denitrification is a facultative anaerobic respiration that promotes nitrogen loss, and it can act as a source or a sink of N₂O depending on the activity of the nitrous oxide reductase. This enzyme is especially sensitive to oxygen concentration (Bonin *et al.*, 1989; Zumft, 1997). We studied denitrifying bacteria by targeting the genes *nirS* and *nosZ*, that code for the dissimilatory nitrite reductase and nitrous oxide reductase, respectively. We only detected the *nosZ* gene in about half the bottom samples analyzed, and that may indicate that *nosZ* gene is found mostly in sediments, rather than in the water column (Smith *et al.*, 2007; Saarenheimo *et al.*, 2015; Palacin-Lizarbe *et al.*, 2019; Yin *et al.*, 2019). The gene *nirS* appeared consistently in large numbers along the water column of all systems, and it was significantly related to the dissolved N₂O concentration. The abundance of *nirS* was up to 3 orders of magnitude higher than the abundance of archaeal *amoA* gene. Our results indicate that denitrifying bacteria are ubiquitous in the water column, and denitrification may produce N₂O in the water column of the study reservoirs. The studies on N₂O production and denitrifying bacteria in inland waters have mainly focused on sediments, and the water column has received less attention (Piña-Ochoa

and Álvarez-Cobelas, 2006). Few studies have analyzed the distribution of the *nirS* gene in the water column of lakes (Junier *et al.*, 2008; Kim *et al.*, 2011; Pajares *et al.*, 2017). Based on Terminal restriction fragment length polymorphism (T-RFLP) analysis, Junier *et al.* (2008) and Kim *et al.* (2011) detected the *nirS* gene in the water column of lakes. They described the higher diversity in the epilimnion and different denitrifying communities in the water column and the sediments. The maximum abundance detected in our study was up to 3 orders of magnitude higher than the maximum detected in the tropical lake studied by Pajares *et al.* (2017).

Modeling dissolved N₂O in the water column

Our GAM model indicates that the N₂O concentration depended on the nitrogen availability and the abundance of the *nirS* gene in the water column. Nitrogen availability increases the production and emission of N₂O in inland waters, as we explained above. The abundance of the gene *nirS* depended on the dissolved, oxygen concentration, the total phosphorus concentration, and the cumulative Chl-*a*. Denitrification is considered a facultative anaerobic respiration regulated by O₂ concentration, especially the last step of reduction of N₂O to N₂ by the nitrous oxide reductase (Knowles, 1982; Bonin *et al.*, 1989; Zumft, 1997). We found a negative effect of O₂ concentration on the abundance of the *nirS* gene. The dissolved O₂ concentration may affect, but not inhibit, the activity of denitrifiers. Previous studies showed that the influence of O₂ concentration on the denitrifiers differed from one bacterium to another, and the occurrence of aerobic denitrifying bacteria in diverse environments (Lloyd *et al.*, 1987; Lloyd, 1993; Hayatsu *et al.*, 2008). Lloyd *et al.* (1987) described the aerobic denitrification as a co-respiration where bacteria may simultaneously use O₂ and NO₃⁻ as oxidizing agents and produce more N₂O than N₂ in proportion to the anaerobic conditions. Our study suggests that aerobic denitrification may be occurring in the water column of the study reservoirs. Zhou *et al.* (2019a) found that aerobic denitrification dominated the nitrogen losses in a reservoir.

We also found that phosphorus and the cumulative Chl-*a* affected the *nirS* abundance. Phosphorus is a rate-limiting nutrient in natural systems and may affect the denitrifying bacteria (Guignard *et al.*, 2017). Pajares *et al.* (2017) also reported that phosphorus concentration was positively related to the abundance of

denitrifiers. Denitrifiers are often heterotrophic microorganisms that obtain energy from organic matter oxidation. In the study reservoirs, the abundance of the *nirS* gene did not depend on dissolved organic carbon concentration (p-value = 0.759; Supplementary Table 6.3), but they depended on the depth-cumulative chlorophyll-*a* concentration, a proxy for the total phytoplanktonic biomass exported from the water column. We hypothesized that the relationship between the abundance of the gene *nirS* and the cumulative Chl-*a* may suggest that denitrification is stimulated by the autochthonous organic matter. Previous studies described that denitrification rates in the ocean are driven by organic matter exported from the photic zone, and affected by the quality and quantity of organic matter (Dalsgaard *et al.*, 2012; Babbin *et al.*, 2014). In the second place, this relationship may also suggest that denitrification in the water column is enhanced by sinking particles derived from the phytoplankton community. Zhou *et al.* (2019b) found that suspended particles potentially enhanced the production and emission of N₂O in a eutrophic lake. In addition, Zhu *et al.* (2018) detected the occurrence of nitrifiers and denitrifiers in suspended particles of the water column, where they performed the coupled nitrification-denitrification. Several studies in rivers had demonstrated that nitrification and denitrification occur in suspended particles, where both oxic and anoxic/low oxygen microenvironments can coexist, and these particles can provide, a surface to grow on, and a carbon substrate, and even increase the contact chances between bacteria and nitrogen (Xia *et al.*, 2004, 2017; Liu *et al.*, 2013; Jia *et al.*, 2016).

Overall, the water column of the study reservoirs is an active site for N₂O production and consumption. We found the coexistence of undersaturation and supersaturation of N₂O at different depths of a given reservoir. The highest and the lowest concentrations of N₂O were located in the low oxygen layers, where the production or the consumption of N₂O depended on the nitrogen content. We modeled the dissolved N₂O concentration as a function of the nitrogen concentration and the abundance of the *nirS* gene (i.e., denitrifying bacteria). The *nirS* gene appeared consistently in large numbers in the water column of all the reservoirs in both anoxic and oxic conditions. This abundance was significantly related to the dissolved N₂O concentration and affected by the phosphorus availability and the depth-cumulative Chl-*a*. Denitrification may occur in oxic and anoxic conditions, having a significant role in determining the N₂O concentration in the water column

of inland waters. In contrast, ammonia-oxidizing microorganisms may not play a relevant role in N₂O production in the study reservoirs, despite their importance in soils and ocean waters. In this chapter, we focused on microbial pathways that produce N₂O, but recent studies have revealed that abiotic reactions can also produce N₂O. In Chapter 4, we demonstrated the photoproduction of N₂O in Cubillas and Iznájar reservoirs, both reservoirs net sources of this GHG. We hypothesized that sunlight may mediate in the decomposition of NH₂OH to N₂O or in the chemodenitrification of NO₂⁻ through the Fe³⁺ reduction (Chapter 4). In the GAM model, we observed that the abundance of the *nirS* gene and TN explained about 60 %. Hence, the photoproduction of N₂O may explain part of the remaining variance in our data at surface waters. The photoproduction of N₂O may be even the main source of N₂O in the epilimnion of La Bolera reservoir during the stratification period (Supplementary Figure 6.1a), where we did not detect the *nirS* gene despite the epilimnion was supersaturated in N₂O. Aerobic denitrification and the photoproduction of N₂O may be present in surface waters globally, increasing the N₂O supersaturation and promoting N₂O emissions. Therefore, future studies should consider both microbial and abiotic processes as producers of N₂O.

6. 5. References

- Álvarez-Salgado, X. A. and Miller, A. E. J. (1998). Simultaneous determination of dissolved organic carbon and total dissolved nitrogen in seawater by high temperature catalytic oxidation: conditions for precise shipboard measurements, *Marine Chemistry*, 62(3), pp. 325–333. doi: 10.1016/S0304-4203(98)00037-1.
- American Public Health Association (APHA). (1992). *Standard methods for the examination of water and wastewater* Washington, DC, USA: American Public Health Association. 18th edn. Edited by A. E. Greenberg, L. S. Clesceri, and A. D. Eaton.
- Anderson, J. H. (1964). The metabolism of hydroxylamine to nitrite by *Nitrosomonas*, *The Biochemical journal*, 91(1), pp. 8–17. doi: 10.1042/bj0910008.
- Auguet, J.-C., Triadó-Margarit, X., Nomokonova, N., Camarero, L. and Casamayor, E. O. (2012). Vertical segregation and phylogenetic characterization of ammonia-oxidizing Archaea in a deep oligotrophic lake, *The ISME Journal*, 6(9), pp. 1786–1797. doi: 10.1038/ismej.2012.33.
- Babbin, A. R., Keil, R. G., Devol, A. H. and Ward, B. B. (2014). Organic matter stoichiometry, flux, and oxygen control nitrogen loss in the ocean, *Science*, 344(6182), pp. 406–408. doi: 10.1126/science.1248364.
- Baulch, H. M., Schiff, S. L., Maranger, R. and Dillon, P. J. (2011). Nitrogen enrichment and the emission of nitrous oxide from streams, *Global Biogeochemical Cycles*, 25(4), p. 15.

doi: 10.1029/2011GB004047.

- Beaulieu, J. J., Tank, J. L., Hamilton, S. K., Wollheim, W. M., Hall, R. O., Mulholland, P. J., Peterson, B. J., Ashkenas, L. R., Cooper, L. W., Dahm, C. N., Dodds, W. K., Grimm, N. B., Johnson, S. L., McDowell, W. H., Poole, G. C., Valett, H. M., Arango, C. P., Bernot, M. J., Burgin, A. J., Crenshaw, C. L., Helton, A. M., Johnson, L. T., O'Brien, J. M., Potter, J. D., Sheibley, R. W., Sobota, D. J. and Thomas, S. M. (2011). Nitrous oxide emission from denitrification in stream and river networks, *Proceedings of the National Academy of Sciences*, 108(1), pp. 214–219. doi: 10.1073/pnas.1011464108.
- Beaulieu, J. J., Smolenski, R. L., Nietch, C. T., Townsend-Small, A., Elovitz, M. S. and Schubauer-Berigan, J. P. (2014). Denitrification alternates between a source and sink of nitrous oxide in the hypolimnion of a thermally stratified reservoir, *Limnology and Oceanography*, 59(2), pp. 495–506. doi: 10.4319/lo.2014.59.2.0495.
- Beaulieu, J. J., Nietch, C. T. and Young, J. L. (2015). Controls on nitrous oxide production and consumption in reservoirs of the Ohio River Basin, *Journal of Geophysical Research-Biogeosciences*, 120(10), pp. 1995–2010. doi: 10.1002/2015JG002941.
- Bonin, P., Gilewicz, M. and Bertrand, J. C. (1989). Effects of oxygen on each step of denitrification on *Pseudomonas nautica*, *Canadian Journal of Microbiology*, 35(11), pp. 1061–1064. doi: 10.1139/m89-177.
- Boström, K. H., Simu, K., Hagström, Å. and Riemann, L. (2004). Optimization of DNA extraction for quantitative marine bacterioplankton community analysis, *Limnology and Oceanography: Methods*, 2(11), pp. 365–373. doi: 10.4319/lom.2004.2.365.
- Braker, G., Fesefeldt, A. and Witzel, K.-P. (1998). Development of PCR primer systems for amplification of nitrite reductase genes (*nirK* and *nirS*) to detect denitrifying bacteria in environmental samples, *Applied and Environmental Microbiology*, 64(10), pp. 3769–3775. doi: 10.1128/AEM.64.10.3769-3775.1998.
- Caranto, J. D. and Lancaster, K. M. (2017). Nitric oxide is an obligate bacterial nitrification intermediate produced by hydroxylamine oxidoreductase, *Proceedings of the National Academy of Sciences*, 114(31), pp. 8217–8222. doi: 10.1073/pnas.1704504114.
- Carini, P., Dupont, C. L. and Santoro, A. E. (2018). Patterns of thaumarchaeal gene expression in culture and diverse marine environments, *Environmental Microbiology*, 20(6), pp. 2112–2124. doi: 10.1111/1462-2920.14107.
- Dalsgaard, T., Thamdrup, B., Fariás, L. and Revsbech, N. P. (2012). Anammox and denitrification in the oxygen minimum zone of the eastern South Pacific, *Limnology and Oceanography*, 57(5), pp. 1331–1346. doi: 10.4319/lo.2012.57.5.1331.
- DelSontro, T., Beaulieu, J. J. and Downing, J. A. (2018). Greenhouse gas emissions from lakes and impoundments: Upscaling in the face of global change, *Limnology and Oceanography Letters*, 3(3), pp. 64–75. doi: 10.1002/lol2.10073.
- Diem, T., Koch, S., Schwarzenbach, S., Wehrli, B. and Schubert, C. J. (2012). Greenhouse gas emissions (CO₂, CH₄, and N₂O) from several perialpine and alpine hydropower reservoirs by diffusion and loss in turbines, *Aquatic Sciences*, 74(3), pp. 619–635. doi: 10.1007/s00027-012-0256-5.
- Dong, L. F., Sobey, M. N., Smith, C. J., Rusmana, I., Phillips, W., Stott, A., Osborn, A. M. and

- Nedwell, D. B. (2011). Dissimilatory reduction of nitrate to ammonium, denitrification or anammox, dominates benthic nitrate reduction in tropical estuaries, *Limnology and Oceanography*, 56(1), pp. 279–291. doi: 10.4319/lo.2011.56.1.0279.
- Elkins, J. W., Hall, B. D. and Nance, J. D. (2017). Nitrous Oxide data from the NOAA/ESRL halocarbons in situ program. Mauna Loa, Hawaii (MLO). Available at: <http://www.esrl.noaa.gov/gmd/obop/>.
- Fox, J. and Weisberg, S. (2011). *An R Companion to Applied Regression* Thousand Oaks CA: Sage. Second. Available at: <http://socserv.socsci.mcmaster.ca/jfox/Books/Companion>.
- Fox, J. and Bouchet-Valat, M. (2019). *Rcmdr: R Commander*. Available at: <http://socserv.socsci.mcmaster.ca/jfox/Misc/Rcmdr/>.
- Frame, C. H. and Casciotti, K. L. (2010). Biogeochemical controls and isotopic signatures of nitrous oxide production by a marine ammonia-oxidizing bacterium, *Biogeosciences*, 7(9), pp. 2695–2709. doi: <https://doi.org/10.5194/bg-7-2695-2010>.
- Francis, C. A., Roberts, K. J., Beman, J. M., Santoro, A. E. and Oakley, B. B. (2005). Ubiquity and diversity of ammonia-oxidizing archaea in water columns and sediments of the ocean, *Proceedings of the National Academy of Sciences*, 102(41), pp. 14683–14688. doi: 10.1073/pnas.0506625102.
- Goreau, T. J., Kaplan, W. A., Wofsy, S. C., McElroy, M. B., Valois, F. W. and Watson, S. W. (1980). Production of NO₂⁻ and N₂O by nitrifying bacteria at reduced concentrations of oxygen, *Appl. Environ. Microbiol.*, 40(3), pp. 526–532.
- Gross, J. and Ligges, U. (2015). *nortest: Tests for Normality*. Available at: <https://CRAN.R-project.org/package=nortest> (Accessed: 3 June 2018).
- Gruber, N. and Galloway, J. N. (2008). An Earth-system perspective of the global nitrogen cycle, *Nature*, 451(7176), pp. 293–296. doi: 10.1038/nature06592.
- Guignard, M. S., Leitch, A. R., Acquisti, C., Eizaguirre, C., Elser, J. J., Hessen, D. O., Jeyasingh, P. D., Neiman, M., Richardson, A. E., Soltis, P. S., Soltis, D. E., Stevens, C. J., Trimmer, M., Weider, L. J., Woodward, G. and Leitch, I. J. (2017). Impacts of nitrogen and phosphorus: From genomes to natural ecosystems and agriculture, *Frontiers in Ecology and Evolution*, 5. doi: 10.3389/fevo.2017.00070.
- Hallin, S., Philippot, L., Löffler, F. E., Sanford, R. A. and Jones, C. M. (2018). Genomics and ecology of novel N₂O-reducing microorganisms, *Trends in Microbiology*, 26(1), pp. 43–55. doi: 10.1016/j.tim.2017.07.003.
- Hastie, T. and Tibshirani, R. (1986). Generalized Additive Models, *Statistical Science*, 1(3), pp. 297–310. doi: 10.1214/ss/1177013604.
- Hastie, T. and Tibshirani, R. J. (1990). *Generalized additive models* London, UK, and New York, NY, USA: London: Chapman and Hall. 1st ed.
- Hayatsu, M., Tago, K. and Saito, M. (2008). Various players in the nitrogen cycle: Diversity and functions of the microorganisms involved in nitrification and denitrification, *Soil Science and Plant Nutrition*, 54(1), pp. 33–45. doi: 10.1111/j.1747-0765.2007.00195.x.
- Henry, S., Bru, D., Stres, B., Hallet, S. and Philippot, L. (2006). Quantitative detection of the *nosZ* gene, encoding nitrous oxide reductase, and comparison of the abundances of

- 16S rRNA, *narG*, *nirK*, and *nosZ* genes in soils, *Applied and Environmental Microbiology*, 72(8), pp. 5181–5189. doi: 10.1128/AEM.00231-06.
- Hink, L., Gubry-Rangin, C., Nicol, G. W. and Prosser, J. I. (2018). The consequences of niche and physiological differentiation of archaeal and bacterial ammonia oxidisers for nitrous oxide emissions, *The ISME Journal*, 12(4), pp. 1084–1093. doi: 10.1038/s41396-017-0025-5.
- Hochstein, L. I., Betlach, M. and Kritikos, G. (1984). The effect of oxygen on denitrification during steady-state growth of *Paracoccus halodenitrificans*, *Archives of Microbiology*, 137(1), pp. 74–78. doi: 10.1007/BF00425811.
- Howarth, R. W., Billen, G., Swaney, D., Townsend, A., Jaworski, N., Lajtha, K., Downing, J. A., Elmgren, R., Caraco, N., Jordan, T., Berendse, F., Freney, J., Kudeyarov, V., Murdoch, P. and Zhao-Liang, Z. (1996). Regional nitrogen budgets and riverine N & P fluxes for the drainages to the North Atlantic Ocean: Natural and human influences, *Biogeochemistry*, 35(1), pp. 75–139. doi: 10.1007/BF02179825.
- Hu, H.-W., Xu, Z.-H. and He, J.-Z. (2014). Ammonia-oxidizing archaea play a predominant role in acid soil nitrification, in Sparks, D. L. (ed.) *Advances in Agronomy, Vol 125*, pp. 261–302.
- IPCC. (2013). *Climate Change 2013: The Physical Science Basis. Contribution of Working Group I to the Fifth Assessment Report of the Intergovernmental Panel on Climate Change* Cambridge, United Kingdom and New York, NY, USA: Cambridge University Press. Edited by T. F. Stocker, D. Qin, G.-K. Plattner, M. Tignor, S. K. Allen, J. Boschung, A. Nauels, Y. Xia, V. Bex, and P. M. Midgley. Available at: <https://www.ipcc.ch/report/ar5/wg1/>.
- Jia, Z., Liu, T., Xia, X. and Xia, N. (2016). Effect of particle size and composition of suspended sediment on denitrification in river water, *Science of The Total Environment*, 541, pp. 934–940. doi: 10.1016/j.scitotenv.2015.10.012.
- Junier, P., Kim, O.-S., Witzel, K.-P., Imhoff, J. F. and Hadas, O. (2008). Habitat partitioning of denitrifying bacterial communities carrying *nirS* or *nirK* genes in the stratified water column of Lake Kinneret, Israel, *Aquatic Microbial Ecology*, 51(2), pp. 129–140. doi: 10.3354/ame01186.
- Kim, O.-S., Imhoff, J. F., Witzel, K.-P. and Junier, P. (2011). Distribution of denitrifying bacterial communities in the stratified water column and sediment–water interface in two freshwater lakes and the Baltic Sea, *Aquatic Ecology*, 45(1), pp. 99–112. doi: 10.1007/s10452-010-9335-7.
- Knowles, R. (1982). Denitrification., *Microbiological Reviews*, 46(1), pp. 43–70.
- Komsta, L. (2011). *outliers: Tests for outliers*. Available at: <https://CRAN.R-project.org/package=outliers>.
- Könneke, M., Bernhard, A. E., de la Torre, J. R., Walker, C. B., Waterbury, J. B. and Stahl, D. A. (2005). Isolation of an autotrophic ammonia-oxidizing marine archaeon, *Nature*, 437(7058), pp. 543–546. doi: 10.1038/nature03911.
- Kowalchuk, G. A. and Stephen, J. R. (2001). Ammonia-oxidizing bacteria: A model for molecular microbial ecology, *Annual Review of Microbiology*, 55(1), pp. 485–529. doi:

10.1146/annurev.micro.55.1.485.

- Leininger, S., Urich, T., Schloter, M., Schwark, L., Qi, J., Nicol, G. W., Prosser, J. I., Schuster, S. C. and Schleper, C. (2006). Archaea predominate among ammonia-oxidizing prokaryotes in soils, *Nature*, 442(7104), pp. 806–809. doi: 10.1038/nature04983.
- Lemon, E. and Lemon, D. (1981). Nitrous oxide in fresh waters of the Great Lakes Basin1, *Limnology and Oceanography*, 26(5), pp. 867–879. doi: 10.4319/lo.1981.26.5.0867.
- León-Palmero, E., Reche, I. and Morales-Baquero, R. (2019). Atenuación de luz en embalses del sur-este de la Península Ibérica, *Ingeniería del agua*, 23(1), pp. 65–75. doi: 10.4995/ia.2019.10655.
- León-Palmero, E., Morales-Baquero, R. and Reche, I. (2020a). Greenhouse gas fluxes from reservoirs determined by watershed lithology, morphometry, and anthropogenic pressure, *Environmental Research Letters*, 15(4), p. 044012. doi: 10.1088/1748-9326/ab7467.
- León-Palmero, E., Contreras-Ruiz, A., Sierra, A., Morales-Baquero, R. and Reche, I. (2020b). Dissolved CH₄ coupled to photosynthetic picoeukaryotes in oxic waters and to cumulative chlorophyll *a* in anoxic waters of reservoirs, *Biogeosciences*, 17(12), pp. 3223–3245. doi: 10.5194/bg-17-3223-2020.
- Liang, X., Xing, T., Li, J., Wang, B., Wang, F., He, C., Hou, L. and Li, S. (2019). Control of the hydraulic load on nitrous oxide emissions from cascade reservoirs, *Environmental Science & Technology*, 53(20), pp. 11745–11754. doi: 10.1021/acs.est.9b03438.
- Liu, T., Xia, X., Liu, S., Mou, X. and Qiu, Y. (2013). Acceleration of Denitrification in Turbid Rivers Due to Denitrification Occurring on Suspended Sediment in Oxic Waters, *Environmental Science & Technology*, 47(9), pp. 4053–4061. doi: 10.1021/es304504m.
- Lloyd, D., Boddy, L. and Davies, K. J. P. (1987). Persistence of bacterial denitrification capacity under aerobic conditions: The rule rather than the exception, *FEMS Microbiology Ecology*, 3(3), pp. 185–190. doi: 10.1111/j.1574-6968.1987.tb02354.x.
- Lloyd, D. (1993). Aerobic denitrification in soils and sediments: From fallacies to factx, *Trends in Ecology & Evolution*, 8(10), pp. 352–356. doi: 10.1016/0169-5347(93)90218-E.
- Löscher, C. R., Kock, A., Könneke, M., LaRoche, J., Bange, H. W. and Schmitz, R. A. (2012). Production of oceanic nitrous oxide by ammonia-oxidizing archaea, *Biogeosciences*, 9(7), pp. 2419–2429. doi: <https://doi.org/10.5194/bg-9-2419-2012>.
- Martens-Habbena, W., Berube, P. M., Urakawa, H., de la Torre, J. R. and Stahl, D. A. (2009). Ammonia oxidation kinetics determine niche separation of nitrifying archaea and bacteria, *Nature*, 461(7266), pp. 976–979. doi: 10.1038/nature08465.
- McCrackin, M. L. and Elser, J. J. (2011). Greenhouse gas dynamics in lakes receiving atmospheric nitrogen deposition, *Global Biogeochemical Cycles*, 25(4), p. GB4005. doi: 10.1029/2010GB003897.
- Mengis, M., Gächter, R. and Wehrli, B. (1997). Sources and sinks of nitrous oxide (N₂O) in deep lakes, *Biogeochemistry*, 38(3), pp. 281–301. doi: 10.1023/A:1005814020322.
- Mortimer, C. H. (1956). *The oxygen content of air-saturated fresh waters, and aids in calculating percentage saturation* Stuttgart, Germany: Schweizerbart Science

- Publishers. Available at:
http://www.schweizerbart.de/publications/detail/isbn/9783510520060/Mitteilung_n_IVL_Nr_6.
- Mulholland, P. J., Helton, A. M., Poole, G. C., Hall, R. O., Hamilton, S. K., Peterson, B. J., Tank, J. L., Ashkenas, L. R., Cooper, L. W., Dahm, C. N., Dodds, W. K., Findlay, S. E. G., Gregory, S. V., Grimm, N. B., Johnson, S. L., McDowell, W. H., Meyer, J. L., Valett, H. M., Webster, J. R., Arango, C. P., Beaulieu, J. J., Bernot, M. J., Burgin, A. J., Crenshaw, C. L., Johnson, L. T., Niederlehner, B. R., O'Brien, J. M., Potter, J. D., Sheibley, R. W., Sobota, D. J. and Thomas, S. M. (2008). Stream denitrification across biomes and its response to anthropogenic nitrate loading, *Nature*, 452(7184), p. 202. doi: 10.1038/nature06686.
- Murphy, J. and Riley, J. P. (1962). A modified single solution method for the determination of phosphate in natural waters, *Analytica Chimica Acta*, 27(Supplement C), pp. 31–36. doi: 10.1016/S0003-2670(00)88444-5.
- Musenze, R. S., Grinham, A., Werner, U., Gale, D., Sturm, K., Udy, J. and Yuan, Z. (2014). Assessing the spatial and temporal variability of diffusive methane and nitrous oxide emissions from subtropical freshwater reservoirs, *Environmental Science & Technology*, 48(24), pp. 14499–14507. doi: 10.1021/es505324h.
- Nizzoli, D., Carraro, E., Nigro, V. and Viaroli, P. (2010). Effect of organic enrichment and thermal regime on denitrification and dissimilatory nitrate reduction to ammonium (DNRA) in hypolimnetic sediments of two lowland lakes, *Water Research*, 44(9), pp. 2715–2724. doi: 10.1016/j.watres.2010.02.002.
- Pajares, S., Merino-Ibarra, M., Macek, M. and Alcocer, J. (2017). Vertical and seasonal distribution of picoplankton and functional nitrogen genes in a high-altitude warm-monomictic tropical lake, *Freshwater Biology*, 62(7), pp. 1180–1193. doi: 10.1111/fwb.12935.
- Palacin-Lizarbe, C., Camarero, L., Hallin, S., Jones, C. M., Cáliz, J., Casamayor, E. O. and Catalan, J. (2019). The DNRA-denitrification dichotomy differentiates nitrogen transformation pathways in mountain lake benthic habitats, *Frontiers in Microbiology*, 10. doi: 10.3389/fmicb.2019.01229.
- Piña-Ochoa, E. and Álvarez-Cobelas, M. (2006). Denitrification in aquatic environments: A cross-system analysis, *Biogeochemistry*, 81(1), pp. 111–130. doi: 10.1007/s10533-006-9033-7.
- Prosser, J. I. and Nicol, G. W. (2008). Relative contributions of archaea and bacteria to aerobic ammonia oxidation in the environment, *Environmental Microbiology*, 10(11), pp. 2931–2941. doi: 10.1111/j.1462-2920.2008.01775.x.
- R Core Team. (2019). *R: A Language and Environment for Statistical Computing* Vienna, Austria: R Foundation for Statistical Computing. Available at: <https://www.R-project.org/>.
- Ravishankara, A. R., Daniel, J. S. and Portmann, R. W. (2009). Nitrous oxide (N₂O): The dominant ozone-depleting substance emitted in the 21st century, *Science*, 326(5949), pp. 123–125. doi: 10.1126/science.1176985.
- Roland, F. A. E., Darchambeau, F., Morana, C. and Borges, A. V. (2017). Nitrous oxide and methane seasonal variability in the epilimnion of a large tropical meromictic lake (Lake

- Kivu, East-Africa), *Aquatic Sciences*, 79(2), pp. 209–218. doi: 10.1007/s00027-016-0491-2.
- Roland, F. A. E., Darchambeau, F., Borges, A. V., Morana, C., Brabandere, L. D., Thamdrup, B. and Crowe, S. A. (2018). Denitrification, anaerobic ammonium oxidation, and dissimilatory nitrate reduction to ammonium in an East African Great Lake (Lake Kivu), *Limnology and Oceanography*, 63(2), pp. 687–701. doi: 10.1002/lno.10660.
- Rotthauwe, J. H., Witzel, K. P. and Liesack, W. (1997). The ammonia monooxygenase structural gene *amoA* as a functional marker: molecular fine-scale analysis of natural ammonia-oxidizing populations., *Applied and Environmental Microbiology*, 63(12), pp. 4704–4712.
- Saarenheimo, J., Rissanen, A. J., Arvola, L., Nykanen, H., Lehmann, M. F. and Tirola, M. (2015). Genetic and environmental controls on nitrous oxide accumulation in lakes, *Plos One*, 10(3), p. e0121201. doi: 10.1371/journal.pone.0121201.
- Santoro, A. E., Buchwald, C., McIlvin, M. R. and Casciotti, K. L. (2011). Isotopic signature of N₂O produced by marine ammonia-oxidizing archaea, *Science*, 333(6047), pp. 1282–1285. doi: 10.1126/science.1208239.
- Schlesinger, W. H. (2009). On the fate of anthropogenic nitrogen, *Proceedings of the National Academy of Sciences*, 106(1), pp. 203–208. doi: 10.1073/pnas.0810193105.
- Seitzinger, S. P., Kroeze, C. and Styles, R. V. (2000). Global distribution of N₂O emissions from aquatic systems: natural emissions and anthropogenic effects, *Chemosphere - Global Change Science*, 2(3), pp. 267–279. doi: 10.1016/S1465-9972(00)00015-5.
- Sierra, A., Jiménez-López, D., Ortega, T., Ponce, R., Bellanco, M. J., Sánchez-Leal, R., Gómez-Parra, A. and Forja, J. (2017). Distribution of N₂O in the eastern shelf of the Gulf of Cadiz (SW Iberian Peninsula), *Science of The Total Environment*, 593–594, pp. 796–808. doi: 10.1016/j.scitotenv.2017.03.189.
- Small, G. E., Bullerjahn, G. S., Sterner, R. W., Beall, B. F. N., Brovold, S., Finlay, J. C., McKay, R. M. L. and Mukherjee, M. (2013). Rates and controls of nitrification in a large oligotrophic lake, *Limnology and Oceanography*, 58(1), pp. 276–286. doi: 10.4319/lo.2013.58.1.0276.
- Smith, C. J., Nedwell, D. B., Dong, L. F. and Osborn, A. M. (2007). Diversity and abundance of nitrate reductase genes (*narG* and *napA*), nitrite reductase genes (*nirS* and *nrfA*), and their transcripts in estuarine sediments, *Applied and Environmental Microbiology*, 73(11), pp. 3612–3622. doi: 10.1128/AEM.02894-06.
- Stieglmeier, M., Mooshammer, M., Kitzler, B., Wanek, W., Zechmeister-Boltenstern, S., Richter, A. and Schleper, C. (2014). Aerobic nitrous oxide production through N-nitrosating hybrid formation in ammonia-oxidizing archaea, *The ISME Journal*, 8(5), pp. 1135–1146. doi: 10.1038/ismej.2013.220.
- Stremińska, M. A., Felgate, H., Rowley, G., Richardson, D. J. and Baggs, E. M. (2012). Nitrous oxide production in soil isolates of nitrate-ammonifying bacteria, *Environmental Microbiology Reports*, 4(1), pp. 66–71. doi: 10.1111/j.1758-2229.2011.00302.x.
- Takeuchi, J. (2006). Habitat segregation of a functional gene encoding nitrate ammonification in estuarine sediments, *Geomicrobiology Journal*, 23(2), pp. 75–87. doi:

10.1080/01490450500533866.

- Tiedje, J. M. and Zehnder, A. J. B. (1988). Biology of anaerobic microorganisms, *Ecology of Denitrification and Dissimilarity Nitrate Reduction to Ammonium*. New York: John Wiley, p. 179.
- Trimmer, M., Chronopoulou, P.-M., Maanoja, S. T., Upstill-Goddard, R. C., Kitidis, V. and Purdy, K. J. (2016). Nitrous oxide as a function of oxygen and archaeal gene abundance in the North Pacific, *Nature Communications*, 7(1), pp. 1–10. doi: 10.1038/ncomms13451.
- Vajrala, N., Martens-Habbena, W., Sayavedra-Soto, L. A., Schauer, A., Bottomley, P. J., Stahl, D. A. and Arp, D. J. (2013). Hydroxylamine as an intermediate in ammonia oxidation by globally abundant marine archaea, *Proceedings of the National Academy of Sciences*, 110(3), pp. 1006–1011. doi: 10.1073/pnas.1214272110.
- Vitousek, P. M. (1994). Beyond global warming: Ecology and global change, *Ecology*, 75(7), pp. 1861–1876. doi: 10.2307/1941591.
- Wang, S., Liu, C., Yeager, K. M., Wan, G., Li, J., Tao, F., Lü, Y., Liu, F. and Fan, C. (2009). The spatial distribution and emission of nitrous oxide (N₂O) in a large eutrophic lake in eastern China: Anthropogenic effects, *Science of The Total Environment*, 407(10), pp. 3330–3337. doi: 10.1016/j.scitotenv.2008.10.037.
- Ward, B. B. (1996). Nitrification and denitrification: Probing the nitrogen cycle in aquatic environments, *Microbial Ecology*, 32(3), pp. 247–261. doi: 10.1007/BF00183061.
- Weiss, R. F. and Price, B. A. (1980). Nitrous oxide solubility in water and seawater, *Marine Chemistry*, 8(4), pp. 347–359. doi: 10.1016/0304-4203(80)90024-9.
- Whitfield, C. J., Aherne, J. and Baulch, H. M. (2011). Controls on greenhouse gas concentrations in polymictic headwater lakes in Ireland, *Science of The Total Environment*, 410–411, pp. 217–225. doi: 10.1016/j.scitotenv.2011.09.045.
- Wickham, H. and Bryan, J. (2019). *readxl: Read Excel Files*. Available at: <https://CRAN.R-project.org/package=readxl>.
- Wood, S. N. (2006). *Generalized additive models: an introduction with R* New York, USA: Chapman and Hall/CRC.
- Wood, S. N. (2011). Fast stable restricted maximum likelihood and marginal likelihood estimation of semiparametric generalized linear models, *Journal of the Royal Statistical Society: Series B (Statistical Methodology)*, 73(1), pp. 3–36. doi: 10.1111/j.1467-9868.2010.00749.x.
- Wrage, N., Velthof, G. L., van Beusichem, M. L. and Oenema, O. (2001). Role of nitrifier denitrification in the production of nitrous oxide, *Soil Biology and Biochemistry*, 33(12), pp. 1723–1732. doi: 10.1016/S0038-0717(01)00096-7.
- Wuchter, C., Abbas, B., Coolen, M. J. L., Herfort, L., Bleijswijk, J. van, Timmers, P., Strous, M., Teira, E., Herndl, G. J., Middelburg, J. J., Schouten, S. and Damsté, J. S. S. (2006). Archaeal nitrification in the ocean, *Proceedings of the National Academy of Sciences*, 103(33), pp. 12317–12322. doi: 10.1073/pnas.0600756103.
- Xia, X., Jia, Z., Liu, T., Zhang, S. and Zhang, L. (2017). Coupled nitrification-denitrification caused by suspended sediment (SPS) in rivers: Importance of SPS size and composition,

Environmental Science & Technology, 51(1), pp. 212–221. doi: 10.1021/acs.est.6b03886.

Xia, X. H., Yang, Z. F., Huang, G. H., Zhang, X. Q., Yu, H. and Rong, X. (2004). Nitrification in natural waters with high suspended-solid content—A study for the Yellow River, *Chemosphere*, 57(8), pp. 1017–1029. doi: 10.1016/j.chemosphere.2004.08.027.

Yin, X., Chen, L., Tang, D., Zhang, Y., Liu, G., Hua, Y., Wan, X., Zhou, W., Zhao, J. and Zhu, D. (2019). Seasonal and vertical variations in the characteristics of the nitrogen-related functional genes in sediments from urban eutrophic lakes, *Applied Soil Ecology*, 143, pp. 80–88. doi: 10.1016/j.apsoil.2019.05.027.

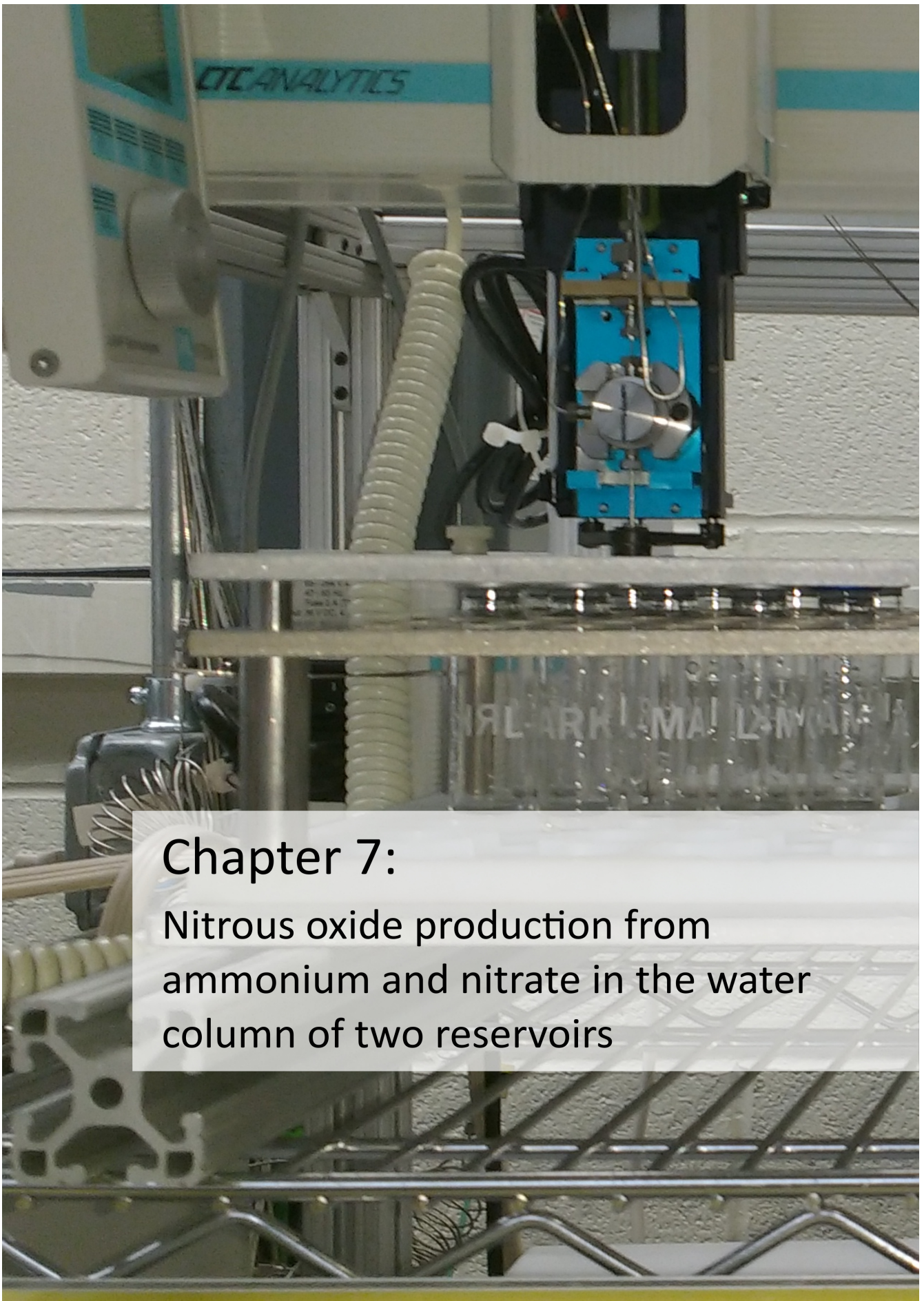
Yoshida, N. (1988). ¹⁵N-depleted N₂O as a product of nitrification, *Nature*, 335(6190), pp. 528–529. doi: 10.1038/335528a0.

Zhou, S., Zhang, Y., Huang, T., Liu, Y., Fang, K. and Zhang, C. (2019a). Microbial aerobic denitrification dominates nitrogen losses from reservoir ecosystem in the spring of Zhoucun reservoir, *Science of The Total Environment*, 651, pp. 998–1010. doi: 10.1016/j.scitotenv.2018.09.160.

Zhou, Y., Xu, X., Han, R., Li, L., Feng, Y., Yeerken, S., Song, K. and Wang, Q. (2019b). Suspended particles potentially enhance nitrous oxide (N₂O) emissions in the oxic estuarine waters of eutrophic lakes: Field and experimental evidence, *Environmental Pollution*, 252, pp. 1225–1234. doi: 10.1016/j.envpol.2019.06.076.

Zhu, W., Wang, C., Hill, J., He, Y., Tao, B., Mao, Z. and Wu, W. (2018). A missing link in the estuarine nitrogen cycle?: Coupled nitrification-denitrification mediated by suspended particulate matter, *Scientific Reports*, 8(1), pp. 1–10. doi: 10.1038/s41598-018-20688-4.

Zumft, W. G. (1997). Cell biology and molecular basis of denitrification., *Microbiology and Molecular Biology Reviews*, 61(4), pp. 533–616.



Chapter 7:

Nitrous oxide production from ammonium and nitrate in the water column of two reservoirs

Chapter 7:

Nitrous oxide production from ammonium and nitrate in the water column of two reservoirs

The Supplementary Material is available in Appendix 7

Abstract

Inland waters are quantitatively relevant sites for nitrogen processing. They reduce the excess of nitrogen loading from the agriculture and urban areas through microbial production of N₂ and the potent greenhouse gas N₂O via denitrification and nitrification. The studies on the N₂O production in inland waters have mainly focused on rivers or lake sediments, and the water column has received less attention. Here, we quantified the production of N₂O using ¹⁵N-NH₄⁺ to trace nitrification and ¹⁵N-NO₃⁻ to trace denitrification at different depths in a shallow (Cubillas) and a deep (Iznájar) reservoir. Both systems have high nitrogen inputs from their anthropized watershed. To explore the effect of oxygen availability on N₂O production, we performed the incubations at the beginning (plenty of O₂ availability) and the end (low O₂ availability) of the stratification period. The production of N₂O from ammonium ranged from 0.3 to 22.2 nmol-N L⁻¹ d⁻¹ in the Cubillas reservoir, and from 0.1 to 38.0 nmol-N L⁻¹ d⁻¹ in the Iznájar reservoir. The production of N₂O from nitrate (denitrification) varied from 6.2 to 12.5 nmol-N L⁻¹ d⁻¹ in the Cubillas reservoir, and from 3.2 to 117.7 nmol-N L⁻¹ d⁻¹ in the Iznájar reservoir. We also detected high rates of nitrification and nitrate reduction to nitrite. The production of N₂O from ammonium was related to the nitrification rates

and was a function of the *in situ* abundance of the *nirS* gene and the dissolved organic carbon concentration, suggesting a coupling nitrification-denitrification in the water column. Our findings demonstrate that the water column is, therefore, an active site for N₂O production. This production may be promoted by the autochthonous organic matter (i.e., cumulative Chl-*a* concentration) exported in the water column.

7. 1. Introduction

In recent decades, the nitrogen loading from agriculture and urban areas in the watersheds has accentuated the global problem of eutrophication in inland waters (Canfield *et al.*, 2010; Heathcote and Downing, 2012). Anthropogenic eutrophication affects biodiversity, biogeochemical cycles, and the increase in the frequency and duration of anoxia in the water column of lakes and reservoirs (Moss *et al.*, 2011; Schindler, 2012; Schilder *et al.*, 2017). Climate change intensifies the symptoms of eutrophication in inland waters, and, at the same time, eutrophication promotes climate change through the emissions of greenhouse gases (Jeppesen *et al.*, 2010; Moss *et al.*, 2011; Davidson *et al.*, 2015; Beaulieu *et al.*, 2019). Lakes and reservoirs reduce the excess of nitrogen through microbial-mediated emissions of dinitrogen gas (N₂), primarily produced during denitrification, and also through anaerobic ammonium oxidation (anammox) (Brezonik and Lee, 1968; Seitzinger, 1988; Harrison *et al.*, 2009; Rissanen *et al.*, 2013; Wenk *et al.*, 2014; Roland *et al.*, 2018). However, denitrification also produces significant amounts of nitrous oxide (N₂O), a potent greenhouse gas (GHG), with 298 times the effect of CO₂ on the atmospheric warming on a 100-year time horizon (IPCC, 2013), and the main driver of stratospheric ozone depletion (Ravishankara *et al.*, 2009).

Denitrifiers develop the sequential reduction of nitrate to nitrite, nitric oxide, nitrous oxide, and dinitrogen gas (Figure 7.1). Hence, denitrification can act as a source or sink of N₂O depending on the last step, which is catalyzed by the enzyme nitrous oxide reductase that is highly controlled by oxygen concentration (Bonin *et al.*, 1989; Zumft, 1997; Hallin *et al.*, 2018). Denitrification can represent up to 87 – 100 % of the total N₂ production in the anoxic lake water column (Roland *et al.*, 2018). N₂O production by denitrifiers has been widely studied in sediments of inland waters, demonstrating that eutrophication may increase N₂O production

rates (Seitzinger, 1988; Piña-Ochoa and Álvarez-Cobelas, 2006). Although some studies have addressed the production of N₂ by denitrification in anoxic lake waters, we still lack direct measurements on the production of N₂O by denitrifiers in the water column of lakes and reservoirs (Goering and Dugdale, 1966; Brezonik and Lee, 1968; Chan and Campbell, 1980; Hamersley *et al.*, 2009; Wenk *et al.*, 2013; Roland *et al.*, 2018).

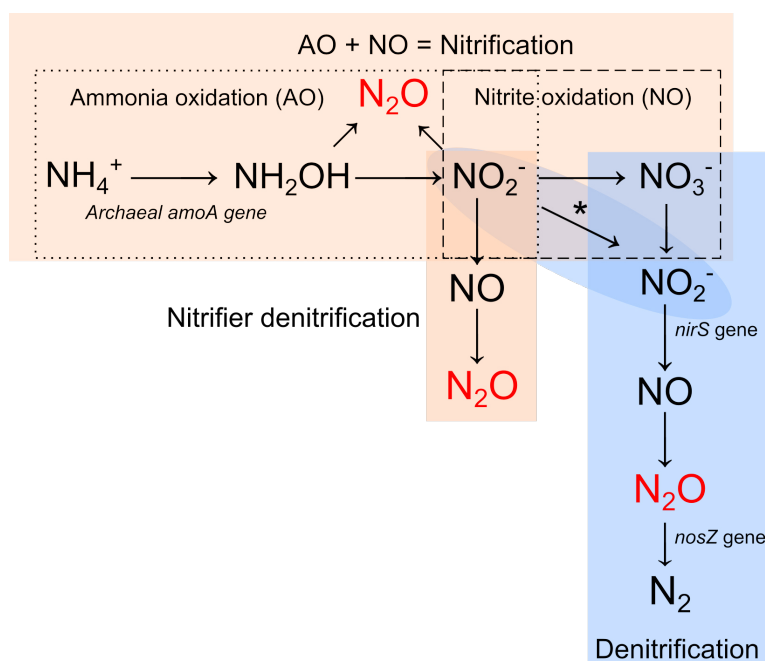


Figure 7.1. Nitrification, nitrifier denitrification, and denitrification. Outline of the three microbial pathways, with the main chemical steps, and the genes that we used as targets. *Nitrifier denitrification only reduces the nitrite, while both nitrate and nitrite can be reduced by denitrifiers.

The greenhouse gas N₂O is also by-product during the nitrification step of ammonia oxidation, which occurs in oxic and suboxic environments (Anderson, 1964; Vajjala *et al.*, 2013; Caranto and Lancaster, 2017; Carini *et al.*, 2018) (Figure 7.1). Nitrification consists of the oxidation of ammonia to nitrite (i.e., ammonia oxidation), and then to nitrate (i.e., nitrite oxidation) (Figure 7.1). Ammonia oxidation is performed by ammonia-oxidizing bacteria (AOB) and ammonia-oxidizing archaea (AOA). Nitrite oxidation step is carried out by nitrite-oxidizing bacteria (NOB) (Kowalchuk and Stephen, 2001; Könneke *et al.*, 2005). Recently, the existence of bacteria with the capacity of complete nitrification from ammonia to nitrate (complete ammonia oxidation; comammox) has been demonstrated (Daims *et al.*, 2015; van Kessel *et al.*, 2015). At low oxygen conditions, ammonia-oxidizing

organisms reduce the nitrite to nitrous oxide, a process referred to as nitrifier denitrification (Poth and Focht, 1985; Frame and Casciotti, 2010; Santoro and Casciotti, 2011) (Figure 7.1), increasing the yield of N₂O production relative to the ammonium oxidized (Goreau *et al.*, 1980; Yoshida, 1988). When the production of nitrate by nitrification is linked to its consumption by denitrification, the process is known as coupled nitrification-denitrification. That occurs in sediments, and in suspended particulate material in the water column (Xia *et al.*, 2017; Zhu *et al.*, 2018). Suspended particles in the water column promote nitrification, denitrification, or coupled nitrification-denitrification (Xia *et al.*, 2004; Liu *et al.*, 2013; Jia *et al.*, 2016; Xia *et al.*, 2017), and potentially enhance the production and emission of N₂O (Zhou *et al.*, 2019b).

The analysis of functional genes and stable isotopes are the methodological approaches more widely accepted to understand biogeochemical processes in natural ecosystems. The genes that code for the nitrite reductase (i.e., *nirS*) and the nitrous oxide reductase (i.e., *nosZ*) are target genes for the study of denitrification, and their abundances are frequently used to assess the contribution of denitrifying bacteria to the N₂O budget (Hallin *et al.*, 2018). The *amoA* genes encode the subunit A of the key enzyme ammonia monooxygenase in the ammonia oxidation. The relative contribution of AOB and AOA has been inferred based on the abundance of the bacterial and the archaeal *amoA* genes (Kowalchuk and Stephen, 2001; Francis *et al.*, 2005). On the other hand, the use of stable N isotopes allows us to examine the source, flow, and fate of N processes. There are two main approaches: the ¹⁵N natural abundance ($\delta^{15}\text{N}$) method, that uses natural ¹⁵N differences between N sources and sinks, and the ¹⁵N-enriched method, which applies an artificially enriched source of ¹⁵N (Bedard-Haughn *et al.*, 2003). Therefore, the analysis of functional genes and stable isotopes are powerful tools for determining the origin and the production rates of N₂O.

The N₂O emissions from the reservoirs depend on the net production rate (i.e., N₂O production and consumption by the last step of denitrification) and the reservoir properties such as its morphometry. The morphometry of a reservoir (i.e., mean depth and shape) determines the N₂O storage capacity in the water column. Deep reservoirs can accumulate more N₂O in the hypolimnion during the thermal stratification because they undergo high hydrostatic pressure, and the thermocline

acts as a barrier to the hypolimnetic N₂O diffusion toward the surface layers. In the hypolimnion of a thermally stratified reservoir, denitrification can be a source or sink of nitrous oxide depending on the nitrogen availability (Chapter 6, Beaulieu *et al.*, 2015). In Chapter 6, we demonstrated that the hypoxic hypolimnion of the study reservoirs might act as sources or sinks of N₂O depending on the nitrogen concentration. Reservoirs with low nitrogen concentration presented a net consumption of N₂O in the hypolimnion, while the reservoirs with high nitrogen concentration accumulated large amounts of N₂O. In contrast, shallow systems have low hydrostatic pressure, warmer waters, and less capacity to store N₂O. Therefore, the N₂O residence time in a deep reservoir may be higher than in a shallow reservoir, making it more challenging to predict N₂O emissions from N₂O concentrations. Further studies on N₂O production in the water column of lakes and reservoirs with different morphometries are required to improve our knowledge of N₂O emissions from these contrasting systems.

Chapter 3 reported that the nitrogen inputs from agriculture and urban areas from the watershed determined the N₂O fluxes from reservoirs. Besides, in a particular reservoir (i.e., Iznájar reservoir), the climatic forcing produced by N₂O emissions exceeded the one produced by CH₄ and CO₂ emissions together. In Chapter 6, we showed that ammonia-oxidizing archaea were predominant over the ammonia-oxidizing bacteria in the study reservoirs, but its abundance was not related to the N₂O concentration. We also found that the target gene for the denitrifying bacteria (i.e., *nirS*) was ubiquitous in the water column and, together with the total nitrogen concentration, determined the N₂O concentration in the water column. These results suggested that denitrification might be occurring in the water columns. Here, we studied the N₂O production rates using ¹⁵N-labeled ammonium and ¹⁵N-labeled nitrate in the water column and also determined ammonia oxidation, nitrification, and nitrate reduction rates. Based on the mentioned previous results, we selected two reservoirs (Cubillas and Iznájar) located in anthropized watersheds with high nitrogen inputs but contrasting morphometries. We hypothesized that morphometry would affect the thermal stratification and oxygen availability and determine N₂O production and storage. In the deep reservoir, the formation of a hypoxic hypolimnion will lead to higher N₂O

production by nitrifiers and denitrifiers and higher N₂O storing capacity than in the shallow reservoir.

7. 2. Material and Methods

7. 2. 1. Study reservoirs, morphometry, and vertical profiles

We sampled a shallow (i.e., Cubillas) and a deep (i.e., Iznájar) reservoir at the beginning (July) and the end (September) of the stratification period. The morphometric characterization of the reservoirs is detailed in Chapter 2 (see subsection 2. 1. Study reservoirs, morphometry and watershed characterization). We performed vertical biogeochemical profiles using a Sea-Bird 19plus CTD profiler coupled to a Spherical Underwater Quantum Sensor (LI-193R), and a fluorimeter Turner® SCUFA (model CYCLOPS-7). We obtained continuous measurements of temperature, dissolved oxygen, conductivity, turbidity, density, PAR/Irradiance, fluorescence, specific conductance, and salinity. We designed a discrete sampling of 3 depths in the water column based on the temperature and dissolved oxygen concentration profiles. These three depths are representative of the epilimnion, oxycline, and hypolimnion or bottom waters. We took the water samples using a UWITEC sampling bottle.

7. 2. 2. Chemical analysis and chlorophyll-*a* in the water column

We collected samples for dissolved N₂O analysis in air-tight Winkler bottles by duplicate, preserved with a solution of HgCl₂ (final concentration 1 mmol L⁻¹) to inhibit biological activity and sealed with Apiezon® grease to prevent gas exchange. We also took the water samples for chemical and biological analysis and preserved them by maintaining at 4° C until arriving at the laboratory. We measured the concentration of dissolved nitrous oxide (N₂O), dissolved organic carbon (DOC), nitrate (NO₃⁻), nitrite (NO₂⁻), ammonia (NH₄⁺), and chlorophyll-*a* (Chl-*a*) following the methods detailed in Chapter 2 (see subsections 2. 3. Physico-chemical analysis in the water column, and 2. 4. Biological analyses). Dissolved inorganic nitrogen (DIN) is the addition of the NO₃⁻, NH₄⁺, and NO₂⁻ concentrations. To obtain the cumulative chlorophyll-*a* concentration in the whole water column (mg Chl-*a* m⁻²), we added the Chl-*a* concentration from each stratum (León-Palmero *et al.*, 2020b).

7. 2. 3. Functional genes

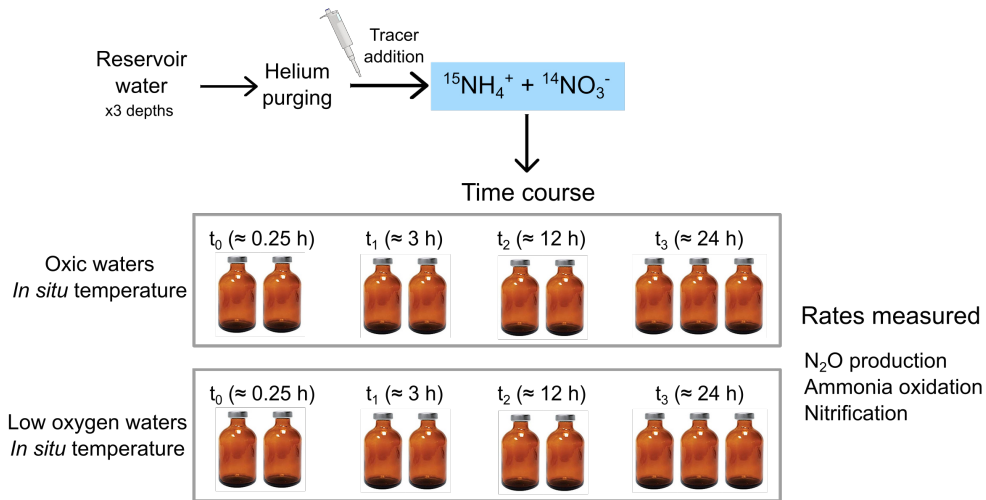
We studied functional genes involved in specific microbial nitrogen transformations using PCR for detection and quantitative PCR (qPCR) as proxy for the abundance of these groups in the water column. We studied the archaeal *amoA* gene for ammonia oxidation, the comammox *amoA* for comammox nitrification, and the bacterial *nirS* and *nosZ* genes for denitrification. More details are provided in Chapter 2 (see subsection 2. 4. 3. Functional genes).

7. 2. 4. Incubations using ¹⁵N tracers to determine N₂O production and processes involved

Incubation conditions

We took the reservoir samples and preserved them for incubations by maintaining the water at 4 °C. In the laboratory, we filled the 60 mL glass serum bottles and purged all the samples with helium for 4 minutes. Samples from low oxygen waters were sealed with butyl rubber septa, and crimped with aluminum seals immediately after filling. In these samples, we kept a 3 mL helium headspace to keep low oxygen conditions. Samples from oxic water depths were exposed to air to keep the oxic conditions. We sealed and crimped them keeping a 3 mL headspace with ambient air. We weighted the serum bottles before and after filling them, to account for the exact water volume in each sample. We compiled the incubation set-up, incubation conditions and the concentration of inorganic nitrogen added in each treatment in the Figure 7.2 and Table 7.1. In the first treatment, we injected ¹⁵N-NH₄⁺ tracer (¹⁵N-ammonium chloride >= 98 atom % ¹⁵N, Sigma Aldrich) into nine bottles from the same depth to a final concentration of 0.5 μmol L⁻¹, obtaining a fraction labeled of the substrate pools between 0.1 and 1.0. In this treatment, we also added ¹⁴N-NO₃⁻ (potassium nitrate) to a 10 % of the nitrate pool to trap the label in the product pool for nitrification rates (Figure 7.2a). In the second treatment we injected an adjusted volume of ¹⁵N-NO₃⁻ tracer (potassium ¹⁵N-nitrate, 98 atom % ¹⁵N, Sigma Aldrich) to obtain a fraction labeled of the NO₃⁻ pool about 0.10. We also added ¹⁴N-NH₄⁺ (ammonium chloride) to a final concentration of 0.5 μmol L⁻¹. We measured the NO₃⁻ concentrations before incubations to adjust the fraction labeled at 0.10 (Figure 7.2b).

a ¹⁵NH₄⁺ treatment : Incubation set up



b ¹⁵NO₃⁻ treatment : Incubation set up

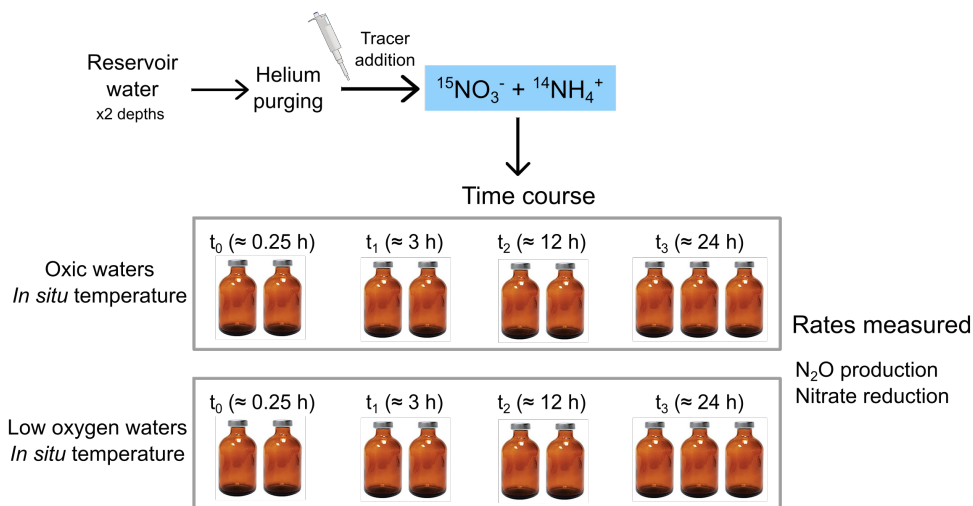


Figure 7.2. Details of the incubation set-up. (a) ¹⁵N-NH₄⁺ treatment (b) ¹⁵N-NO₃⁻ treatment

We performed the first treatment (¹⁵N-NH₄⁺ + ¹⁴N-NO₃⁻) in all the depths, but we only performed the second treatment (¹⁵N-NO₃⁻ + ¹⁴N-NH₄⁺) in the samples from the oxycline, hypolimnion and bottom waters. We incubated a set of nine bottles per depth and treatment: two bottles at t₀ (≈ 0.25 h), two at t₁ (≈ 3 h), two at t₂ (≈ 12 h), and three at t₃ (≈ 24 h), to determine a single rate (Figure 7.2). We incubated the samples at the *in situ* temperatures from 13 to 26 °C (Table 7.1). We finished the incubations by adding 0.1 mL saturated mercuric chloride (HgCl₂). Besides

incubations, we also took two serum bottles per depth without headspace or any treatment to analyze the natural isotopic composition ($\delta^{15}\text{N}$) of the nitrate, nitrite and nitrous oxide of the natural pool. All samples were stored at room temperature in the dark and shipped to the laboratory at Princeton University.

Table 7.1. Incubation conditions and concentration of inorganic nitrogen compounds added in each treatment. Concentrations are measured in $\mu\text{mol-N L}^{-1}$. NP = not performed.

Reservoir	Depth	Incubation temperature (°C)	Oxygen conditions	Treatment 1		Treatment 2	
				$^{15}\text{NH}_4^+$	$^{14}\text{NO}_3^-$	$^{14}\text{NH}_4^+$	$^{15}\text{NO}_3^-$
Cubillas (July)	Epilimnion (2 m) #1	25 ± 0.5	Oxic	0.5	35.0	NP	
	Oxycline (7 m) #2	20 ± 0.5	Oxic	0.5	30.0	0.5	30.0
	Bottom (9.5 m) #3	18 ± 0.5	Low oxygen	0.5	25.0	0.5	25.0
Cubillas (September)	Epilimnion (0.5 m) #4	24 ± 0.5	Oxic	0.5	18.0	NP	
	Epilimnion (2.5 m) #5	24 ± 0.5	Oxic	0.5	17.0	NP	
	Bottom (6.3 m) #6	24 ± 0.5	Low oxygen	0.5	13.0	0.5	13.0
Iznájar (July)	Epilimnion (3 m) #7	26 ± 0.5	Oxic	0.5	35.0	NP	
	Oxycline (8 m) #8	22 ± 0.5	Oxic	0.5	35.0	0.5	35.0
	Hypolimnion (20 m) #9	13 ± 0.5	Low oxygen	0.5	35.0	0.5	35.0
Iznájar (September)	Epilimnion (5 m) #10	26 ± 0.5	Oxic	0.5	33.0	NP	
	Oxycline (11 m) #11	26 ± 0.5	Low oxygen	0.5	31.0	0.5	31.0
	Hypolimnion (23 m) #12	15 ± 0.5	Low oxygen	0.5	34.0	0.5	34.0

$^{15}\text{N-N}_2\text{O}$ production

The total N₂O in each incubation bottle was extracted by purging with helium for 35 min at 38 mL min⁻¹. Then, N₂O was trapped by liquid nitrogen and isolated from interference by gas chromatography (Ji *et al.*, 2015; Frey *et al.*, 2020). We detected the nitrogen mass 44 (i.e., $^{44}\text{N}_2\text{O}$ coming from $^{14}\text{N}^{14}\text{N}^{16}\text{O}$), 45 (i.e., $^{45}\text{N}_2\text{O}$ coming from $^{14}\text{N}^{15}\text{N}^{16}\text{O}$ or $^{15}\text{N}^{14}\text{N}^{16}\text{O}$), and 46 (i.e., $^{46}\text{N}_2\text{O}$ coming from $^{15}\text{N}^{15}\text{N}^{16}\text{O}$), and the isotope ratios 45/44, 46/44 with a GC-IRMS system (Delta V Plus, Thermo). We measured 20 mL glass vial with a known amount of N₂O gas every two to three samples to calibrate for the N₂O concentration. The N₂O reference had the following isotopic composition: $\delta^{15}\text{N} = 1.75 \pm 0.10 \text{ ‰}$ and $\delta^{18}\text{O} = 1.9 \pm 0.19 \text{ ‰}$ present in $^{45}\text{N}_2\text{O}$ and $^{46}\text{N}_2\text{O}$. We also included internal isotope standards for $^{15}\text{N}_2\text{O}$, that we prepared by mixing natural abundance KNO₃ of known $\delta^{15}\text{N}$ values with 99 % Na¹⁵NO₃ (Cambridge Isotope Laboratories) and converted to N₂O using the denitrifier method (Sigman *et al.*, 2001; Granger and Sigman, 2009;

Weigand *et al.*, 2016). We converted the total N₂O concentration and ⁴⁵N₂O/⁴⁴N₂O and ⁴⁶N₂O/⁴⁴N₂O ratios to moles of ⁴⁴N₂O, ⁴⁵N₂O and ⁴⁶N₂O. The mass spectrometer detection limit of the N₂O production is 0.005 nmol-N L⁻¹ d⁻¹. We calculated the N₂O production rates for each treatment from the slope of the increase in mass 45 and 46 during the linear phase over time. The N₂O production (R_{15-N_2O} , nmol-N L⁻¹ d⁻¹) was calculated according to the following the equation 7.1 (Ji *et al.*, 2015):

$$R_{15-N_2O} = (F_N)^{-1} \left(\frac{\Delta^{45}N_2O}{\Delta t} + 2 \frac{\Delta^{46}N_2O}{\Delta t} \right) \quad \text{Eq. 7.1}$$

Where $\Delta^{45}N_2O$ and $\Delta^{46}N_2O$ represent the variation in the concentration of $\Delta^{45}N_2O$ and $\Delta^{46}N_2O$ over the incubation time (Δt), and the F_N represents the fraction of ¹⁵N in the initial substrate pool (NH₄⁺ or NO₃⁻), which is assumed to be constant over the incubation time. Natural abundance 1000 ppm N₂O carrier gas (50 μ L in He) was injected before measurement to trap the produced labeled N₂O and to ensure a sufficient mass for isotope analysis.

¹⁵N-NO₂⁻ production

After N₂O analysis, to determine the rates of NH₄⁺ oxidation and NO₃⁻ reduction (first step of denitrification) we analyzed the samples incubated with ¹⁵NH₄⁺ and ¹⁵NO₃⁻ for ¹⁵NO₂⁻ production, respectively. The method is based on the isotopic analysis of the nitrous oxide (N₂O) generated from the ¹⁵NO₂⁻. We adjusted the individual sample size to contain 20 nmol of N₂O, and transferred the samples into 20mL glass vials to be He purged for 10 min. We converted the NO₂⁻ to N₂O using sodium azide in acetic acid (McIlvin and Altabet, 2005). The nitrogen isotope ratio of the nitrous oxide (N₂O) generated was measured on a Delta V Plus (Thermo) as described above. Net production of ¹⁵NO₂⁻ (R_{NO_2} , nmol-N L⁻¹ d⁻¹) were calculated following the equation 7.2:

$$R_{NO_2} = \left(F_{NH_4^+} \right)^{-1} \frac{\Delta[^{15}NO_2^-]}{\Delta t} \quad \text{Eq. 7.2}$$

Where $\Delta[^{15}NO_2^-]$ represents the variation in the concentration of ¹⁵NO₂⁻, the $F_{NH_4^+}$ represents the fraction of ¹⁵NH₄⁺ in the initial substrate pool, and the Δt is the incubation time. We analyzed two time points, and two or three replicates per time point.

¹⁵N-NO₃⁻ production

We measured the ¹⁵NO₃⁻ production by the increase in ¹⁵NO₃⁻ in the samples incubated with ¹⁵NH₄⁺ using the denitrifier method (Sigman *et al.*, 2001; Granger and Sigman, 2009; Weigand *et al.*, 2016). The method is based on the isotopic analysis of the nitrous oxide (N₂O) generated from the nitrate using the denitrifier method with the denitrifying bacteria that lack N₂O-reductase activity (i.e., *Pseudomonas chlororaphis*). The nitrogen isotope ratio of the nitrous oxide (N₂O) generated was measured on a Delta V Plus (Thermo) as described above. Net production of ¹⁵NO₃⁻ ($R_{NO_3^-}$, nmol-N L⁻¹ d⁻¹) were calculated following the equation 7.3:

$$R_{NO_3^-} = \left(F_{NH_4^+} \right)^{-1} \frac{\Delta[^{15}NO_3^-]}{\Delta t} \quad \text{Eq. 7.3}$$

Where $\Delta[^{15}NO_3^-]$ represents the variation in the concentration of ¹⁵NO₃⁻, the $F_{NH_4^+}$ represents the fraction of ¹⁵NH₄⁺ in the initial substrate pool, and the Δt is the incubation time. We analyzed two time points, and two or three replicates per time point.

Determination of N₂O yields

The N₂O yield during NH₄⁺ oxidation to NO₂⁻ (Yield_{Amox}, %) was defined as the ratio of the production rates during the incubation with ¹⁵N-NH₄⁺ (equation 7.4):

$$\text{Yield}_{Amox} = \frac{R_{^{15}\text{-N}_2\text{O}}}{R_{NO_2^-}} \times 100 \quad \text{Eq. 7.4}$$

The N₂O yield during nitrification (i.e., NH₄⁺ oxidation to NO₃⁻) (Yield_{Nit}, %) was defined as the ratio of the production rates during the incubation with ¹⁵N-NH₄⁺ (equation 7.5):

$$\text{Yield}_{Nit} = \frac{R_{^{15}\text{-N}_2\text{O}}}{R_{NO_3^-}} \times 100 \quad \text{Eq. 7.5}$$

The N₂O yield during denitrification (Yield_{Denit}, %) was calculated considering that N₂O is not a side product during nitrate reduction to nitrite in the incubation with ¹⁵N-NO₃⁻, but rather the next intermediate during denitrification (equation 7.6):

$$\text{Yield}_{Denit} = \frac{R_{^{15}\text{-N}_2\text{O}}}{R_{NO_2^-} + R_{^{15}\text{-N}_2\text{O}}} \times 100 \quad \text{Eq. 7.6}$$

Scaling up to the reservoir level

The hydraulic residence time (d) was obtained by dividing the mean volume (m³) during the study period by the mean water inflow or the mean disburshed volume per day (m³ d⁻¹), whichever is larger.

$$\text{Hydraulic residence time} = \frac{\text{Mean volume}}{\text{Flow per day}} \quad \text{Eq. 7.7}$$

We also calculated the total DIN loss (mol-N) in each reservoir from July to September following equation 7.8:

$$\text{Total DIN loss} = (\text{DIN}_{\text{July}} - \text{DIN}_{\text{Sept}}) \times \text{reservoir volume} \quad \text{Eq. 7.8}$$

Where DIN_{July} and DIN_{Sept} represent the mean concentration of DIN (mol-N L⁻¹) in the water column of each reservoir in July and in September, respectively. The reservoir volume (L⁻¹) is the average between the volume in July and the volume in September. We obtained the DIN loss percentage (%), DIN loss per day (kg-N d⁻¹) and DIN loss per surface (g-N d⁻¹ m⁻²) following the equations 7.9, 7.10, and 7.11:

$$\text{DIN loss percentage} = \frac{\text{DIN}_{\text{July}} - \text{DIN}_{\text{Sept}}}{\text{DIN}_{\text{July}}} \times 100 \quad \text{Eq. 7.9}$$

$$\text{DIN loss per day} = \frac{\text{Total DIN loss} \times 14.0067 \times 10^{-3}}{\text{time}} \quad \text{Eq. 7.10}$$

$$\text{DIN loss per surface} = \frac{\text{Total DIN loss} \times 14.0067}{\text{time} \times \text{reservoir area}} \quad \text{Eq. 7.11}$$

Where 14.0067 is the molar mass of nitrogen (g mol-N⁻¹), and 10⁻³ is the factor to convert grams to kilograms. Time are the days between the sampling in July and the sampling in September, and the reservoir area is measured in m². Similarly, we also calculated the mean N₂O production per day (kg-N d⁻¹), and the mean N₂O prod. per surface (g-N d⁻¹ m⁻²) following the equations 7.12, and 7.13:

$$\begin{aligned} \text{Mean N}_2\text{O prod. per day} = \\ \text{Mean N}_2\text{O prod.} \times 14.0067 \times 10^{-12} \times \text{reservoir volume} \end{aligned} \quad \text{Eq. 7.12}$$

$$\text{Mean N}_2\text{O prod. per surface} = \frac{\text{Mean N}_2\text{O prod. per day} \times 10^3}{\text{reservoir area}} \quad \text{Eq. 7.13}$$

Where the mean N₂O prod. (nmol-N L⁻¹ d⁻¹) is the mean for the total N₂O production in the water column for each reservoir. This total N₂O production was obtained as the sum of the production of N₂O from ammonia, and from nitrate at each layer. 10⁻¹² and 10³ are conversion factors. The reservoir volume (L⁻¹) is the average between the volume in July and the volume in September, and the time are the days between the sampling in July and the sampling in September. Finally, we calculated the N₂O production per DIN loss (%) from the DIN loss per day (kg-N d⁻¹) and the mean N₂O production per day (kg-N d⁻¹) as follows (Eq. 7.14):

$$\text{N}_2\text{O per DIN loss} = \frac{\text{Mean total N}_2\text{O prod.}}{\text{DIN loss per day}} \times 100 \quad \text{Eq. 7.14}$$

7. 2. 5. Statistical tests

We conducted all the statistical analysis in R (R Core Team, 2014) using the packages car (Fox and Weisberg, 2011), nortest (Gross and Ligges, 2015), mgcv (Wood, 2011), readxl (Wickham and Bryan, 2019), and Rcmdr (Fox and Bouchet-Valat, 2019). We performed the Shapiro-Wilk test of normality analysis, and the Levene's test for homogeneity of variance across groups. We performed a one-way analysis of variance test (ANOVA, F), and the t-test (t) when the data were normally distributed. We used the Welch t-test (t) when the data were normally distributed but there was not homogeneity of variance across groups. In case the data did not meet the assumptions of normality, we used the Kruskal-Wallis rank sum test (K-W) or the Wilcoxon test. We used the Grubbs test (G) to detect outliers.

7. 3. Results

7. 3. 1. Characterization of the vertical profiles

Dissolved N₂O concentration during the stratification period

Cubillas is a small and shallow reservoir, which changed from a volume of 17 hm³ in July to 11 hm³ in September. This decline in the water level was evident in the vertical profiles of temperature and dissolved oxygen concentration (Figure 7.3a). The hydraulic residence time during these months was 83 days. Dissolved N₂O concentration varied from 0.11 to 6.38 μmol-N L⁻¹ in July, increasing exponentially from the epilimnion to the bottom. However, dissolved N₂O distribution was mostly homogeneous in September, and varied from 0.22 to 0.42

$\mu\text{mol-N L}^{-1}$, due to the absence of thermal stratification caused by the decline in water level (Figure 7.3a, Supplementary Table 7.1). The maximum value for the N₂O concentration was located in the bottom waters of the Cubillas reservoir in July at suboxic conditions (0 - 11 $\mu\text{mol L}^{-1}$ of dissolved oxygen) (Figure 7.3a). The water column was always supersaturated in N₂O (Supplementary Table 7.1). The DOC concentration varied from 217.6 to 247.7 $\mu\text{mol-C L}^{-1}$, and the chlorophyll-*a* concentration ranged from 5.4 to 18.1 $\mu\text{g L}^{-1}$ (Supplementary Table 7.1).

Iznájar is a big and deep reservoir, which changed from a volume of 575 hm^3 in July to 480 hm^3 in September. The hydraulic residence time was 255 days. During the study period, Iznájar experienced a thermal stratification, and we observed the appearance of an anoxic hypolimnion (i.e., 4 - 6 $\mu\text{mol L}^{-1}$ of dissolved oxygen). In parallel with thermal stratification and oxygen consumption in the hypolimnion, we noticed an increase in the dissolved N₂O concentration (Figure 7.3b, Supplementary Table 7.1). Dissolved N₂O concentration ranged from 0.05 to 0.26 $\mu\text{mol-N L}^{-1}$ in July, and from 0.20 to 3.60 $\mu\text{mol-N L}^{-1}$ in September (Figure 7.3b, Supplementary Table 7.1). We measured the maximum value for the N₂O concentration in the hypolimnion of the Iznájar reservoir in September. We detected that the dissolved N₂O increased at both moments with depth, and the water column was always supersaturated in N₂O (Supplementary Table 7.1). The DOC concentration varied from 186.0 to 228.0 $\mu\text{mol-C L}^{-1}$, and the chlorophyll-*a* concentration from 3.8 to 12.4 $\mu\text{g L}^{-1}$ (Supplementary Table 7.1).

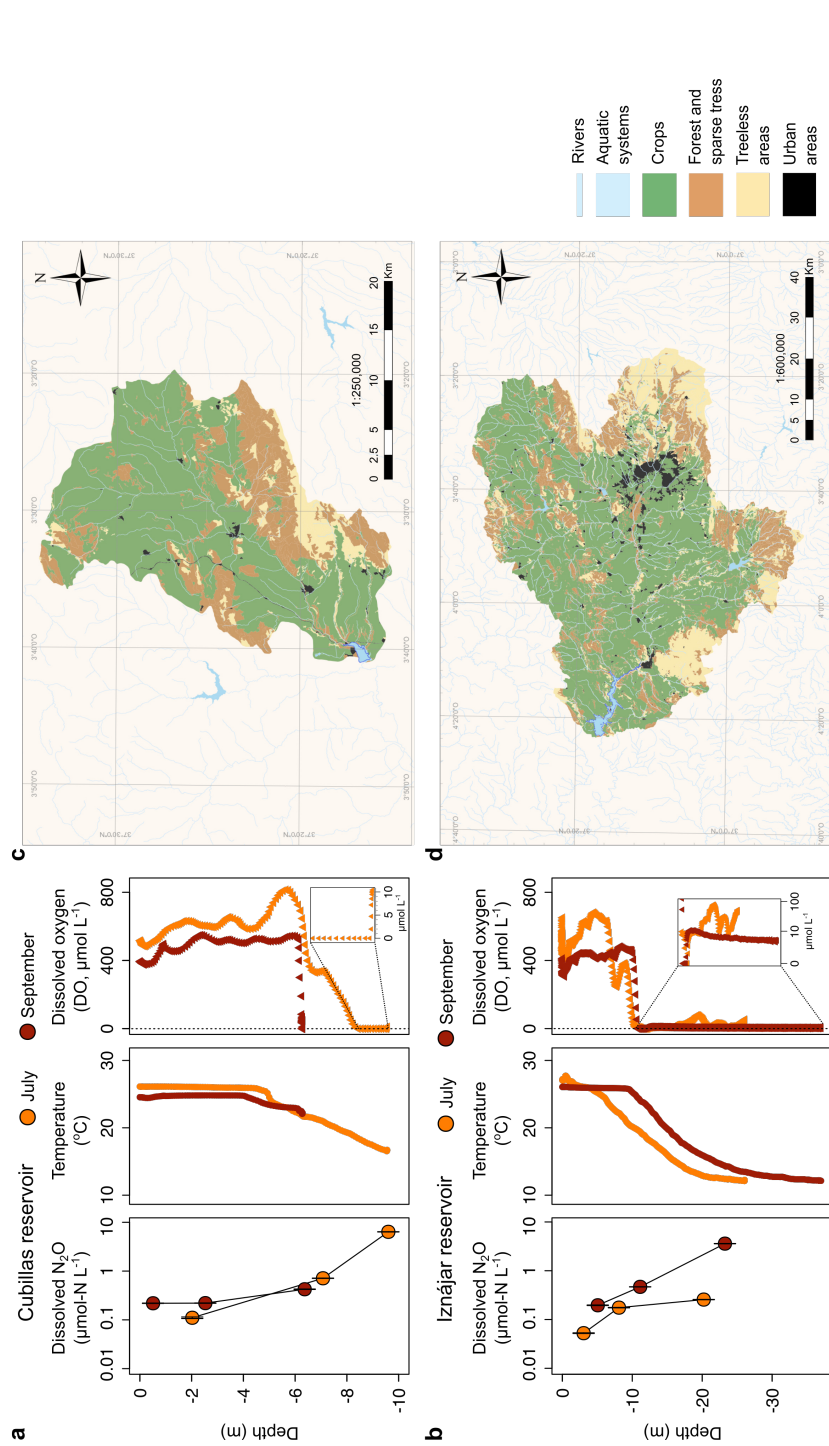


Figure 7.3. Vertical profiles of dissolved N₂O, water temperature and dissolved oxygen concentration, and land-use in the watershed of Cubillas and Iznájar reservoirs. Dissolved N₂O concentration (μmol-N L⁻¹, mean ± standard error), water temperature (°C), and dissolved oxygen (DO) concentration (μmol L⁻¹) during the July and September sampling in Cubillas reservoir (a) and Iznájar reservoir (b). Land-use characterization in the watershed of Cubillas reservoir (c) and Iznájar reservoir (d). Note the different scales in the maps.

For both systems, we detected that the higher concentrations of dissolved N₂O were located at depths with suboxic conditions. We found a significant and negative relationship between the dissolved N₂O concentration and the dissolved oxygen concentration (Dissolved N₂O, $\mu\text{mol-N L}^{-1} = 1.17 e^{(-0.004 \text{ DO, } \mu\text{mol L}^{-1})}$, $n = 12$, $\text{adj } R^2 = 0.50$, $p\text{-value} < 0.01$). The dissolved N₂O also depended on the cumulative Chl-*a* concentration ($\text{mg Chl-}a \text{ m}^{-2}$) following a power function (Dissolved N₂O, $\mu\text{mol-N L}^{-1} = 0.013 (\text{Cum Chl-}a, \text{mg m}^{-2})^{0.86}$, $n = 12$, $\text{adj } R^2 = 0.30$, $p\text{-value} < 0.05$). These relationships are shown in Supplementary Figure 7.1.

Cubillas and Iznájar are located in watersheds dominated by agriculture and urban areas (Figure 7.3c and d). Agriculture areas occupied the 64 % (417 km²) and the 58 % (2752 km²) of the Cubillas and Iznájar watersheds, respectively. Urban areas occupied the 1 % (6 km²) and the 3 % (153 km²) of the Cubillas and Iznájar watersheds (León-Palmero *et al.*, 2020a). As shown in Chapter 3 and in Appendix 2, agriculture and urban areas determined the nitrogen concentration in the reservoirs.

Changes in concentration and natural isotopic composition of the inorganic nitrogen compounds ($\delta^{15}\text{N}$)

We studied the concentration of the inorganic nitrogen compounds, and their natural isotopic composition in the study reservoirs. We show the values in July and September in both reservoirs in Figure 7.4 and in Supplementary Table 7.1 and 7.2. We also show the relationships between the concentrations and the natural isotopic compositions of the nitrogen species in Supplementary Figure 7.2. We detected that the nitrate concentration decreased from July to September in both reservoirs (Figure 7.4 and Supplementary Figure 7.2.). The decrease was especially evident in Cubillas, where the mean concentration was reduced from 343.3 $\mu\text{mol-N L}^{-1}$ in July to 189.4 $\mu\text{mol-N L}^{-1}$ September. The consumption of nitrate in the water column produces the progressive enrichment in ¹⁵N of the remaining nitrate pool, because denitrifiers discriminate against the heavier isotope in the nitrate pool. We observed that the $\delta^{15}\text{N-NO}_3^-$ was consistently positive (i.e., ¹⁵N enriched pool) in all the samples analyzed, and it varied from 8.86 to 13.35 ‰. In the Iznájar reservoir, the concentration of nitrate from July to September also

decreased, but $\delta^{15}\text{N-NO}_3^-$ increased, suggesting that denitrification is consuming the lighter nitrate during these months.

The concentration of nitrite showed the maximum values closed to the oxycline in both reservoirs. In general, the consumption of nitrite enriches in ^{15}N the remaining NO_2^- pool, while the production of nitrite may decrease its $\delta^{15}\text{N-NO}_2^-$. In the study reservoirs the $\delta^{15}\text{N-NO}_2^-$ varied more than the $\delta^{15}\text{N-NO}_3^-$, from negative values (i.e., ^{15}N depleted pool due to nitrite production) to positive values (i.e., ^{15}N enriched pool due to nitrite consumption). The minimum value of $\delta^{15}\text{N-NO}_2^-$ (-36.83 ‰) was found in the epilimnion of Cubillas in July, and the maximum value (23.01 ‰) in the bottom waters of Cubillas in September. In general, the $\delta^{15}\text{N-NO}_2^-$ increased with depth, showing changes in few meters, from ^{15}N depleted to ^{15}N -enriched values, except for the Iznájar reservoir in the July sampling. Ammonia concentration was undetectable at some depths, with the maximum values located in the bottom waters of the Cubillas reservoir at both moments. In the Iznájar reservoir, the maximum values were in the oxycline in July and the in hypolimnion in September.

Ammonia oxidizers and denitrifiers produce N₂O depleted in ^{15}N relative to the substrate, but the consumption of N₂O increases the relative abundance of the ^{15}N and ^{18}O in the N₂O pool. The $\delta^{15}\text{N-N}_2\text{O}$ in the Cubillas reservoir ranged from -0.01 ‰ in the oxycline in July to 7.16 ‰ in the epilimnion in September. The $\delta^{15}\text{N-N}_2\text{O}$ in the Iznájar reservoir ranged from -10.44 ‰ in the hypolimnion in July to 0.05 ‰ in the hypolimnion in September. The $\delta^{18}\text{O-N}_2\text{O}$ ranged from 10.93 ‰ in the bottom waters of the Cubillas reservoir in July to 28.14 ‰ in the bottom waters of the Cubillas reservoir in September. In general, the increase in the N₂O concentration with depth was coupled to the $\delta^{15}\text{N-N}_2\text{O}$ decreased, except for the profile of Iznájar in September, where we detected the opposite trend. From July to September, there was an increase in the $\delta^{15}\text{N-N}_2\text{O}$ and in the $\delta^{18}\text{O-N}_2\text{O}$ in the bottom waters of Cubillas and in the hypolimnion of Iznájar, suggesting a net consumption of N₂O during these months.

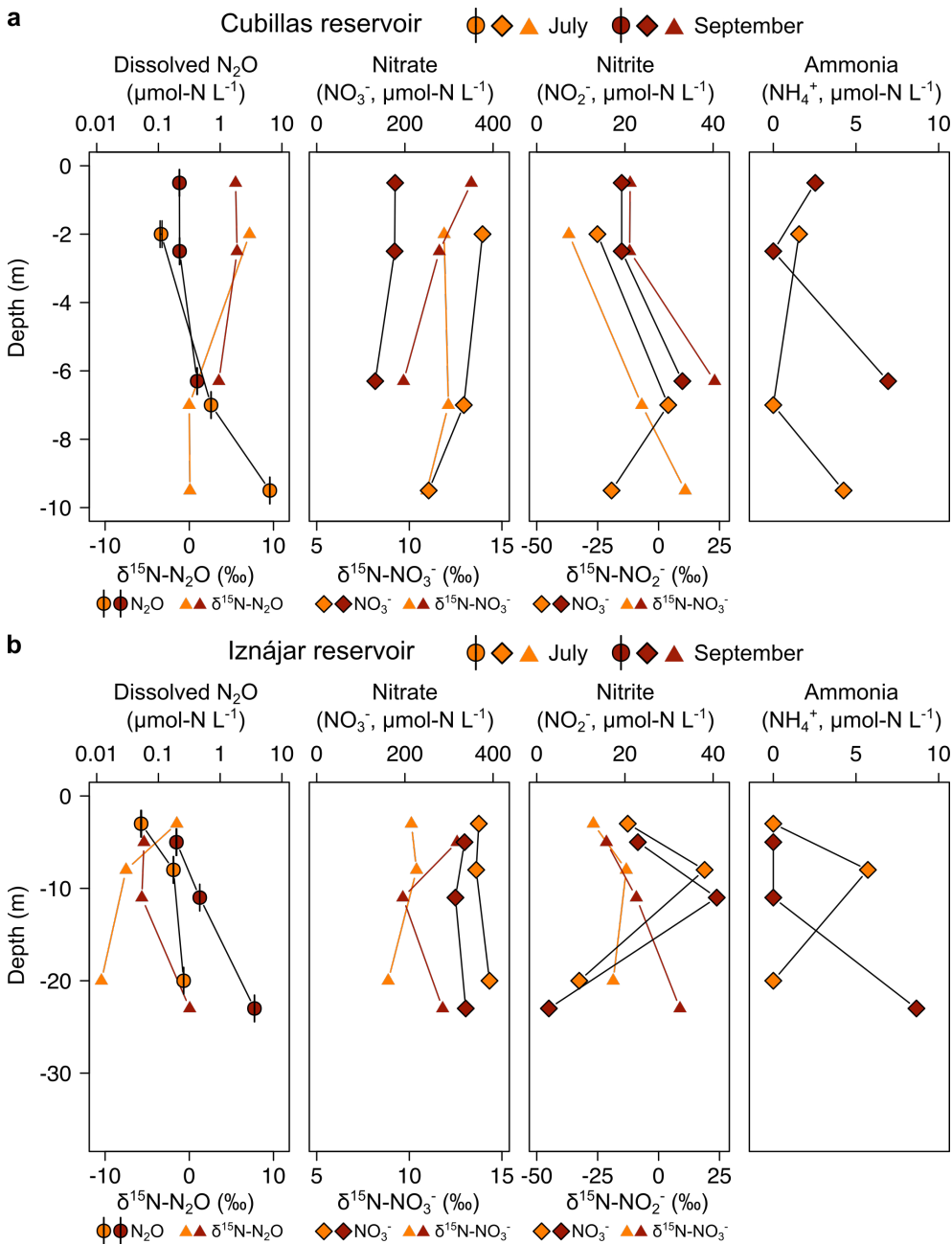


Figure 7.4. Vertical profiles of dissolved N₂O, and inorganic nitrogen concentration and their isotopic composition in Cubillas and Iznájar reservoirs. Dissolved N₂O concentration ($\mu\text{mol-N L}^{-1}$) and $\delta^{15}\text{N-N}_2\text{O}$ (‰); nitrate (NO_3^-) concentration ($\mu\text{mol-N L}^{-1}$) and $\delta^{15}\text{N-NO}_3^-$ (‰); nitrite (NO_2^-) concentration ($\mu\text{mol-N L}^{-1}$) and $\delta^{15}\text{N-NO}_2^-$ (‰); and ammonia (NH_4^+) concentration ($\mu\text{mol-N L}^{-1}$) during the July and September sampling in Cubillas reservoir (a) and Iznájar reservoir (b). Values are provided in Supplementary Table 7.1 and 7.2.

We did not find a relationship between the $\delta^{15}\text{N-NO}_3^-$ and the dissolved N₂O concentration ($n = 12$, p -value = 0.85; Figure 7.5a), but we found a significant relationship between the $\delta^{15}\text{N-NO}_2^-$ and the dissolved N₂O concentration ($n = 12$, $\text{adj } R^2 = 0.37$, p -value < 0.01; Figure 7.5b). The dissolved N₂O concentration depended on the $\delta^{15}\text{N-NO}_2^-$ following an exponential function (dissolved N₂O, $\mu\text{mol-N L}^{-1} = 0.67 \times 10^{0.026 \delta^{15}\text{N-NO}_2^- (\text{‰})}$). This significant relationship suggests that the N₂O production had an evident signature in the ¹⁵N enrichment in the nitrite pool, but not in nitrate pool.

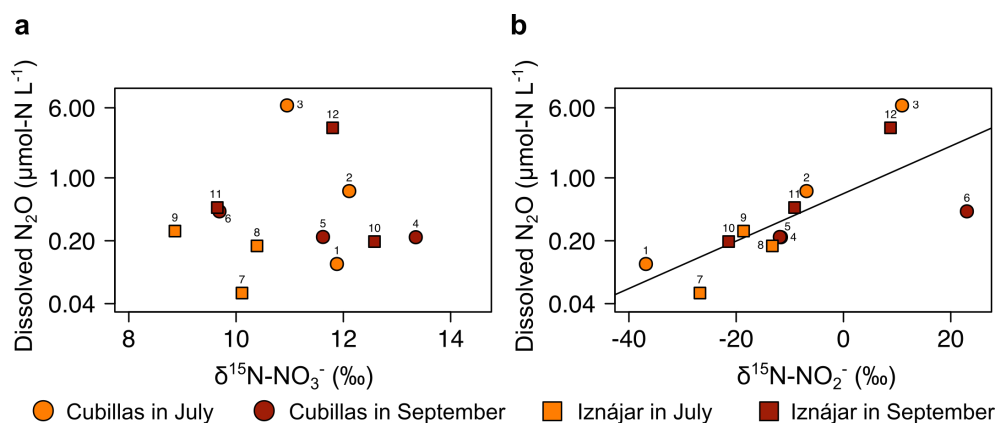


Figure 7.5. The dissolved N₂O concentration ($\mu\text{mol-N L}^{-1}$) as function of the natural isotopic composition of nitrate and nitrite. (a) Scatterplot of the nitrogen isotopic composition of the nitrate pools ($\delta^{15}\text{N-NO}_3^-$) and the concentration of the N₂O; (b) relationship between the nitrogen isotopic composition of the nitrite pools ($\delta^{15}\text{N-NO}_2^-$) and the concentration of the N₂O. Note the logarithmic scales in the y-axis. Table 7.1. shows the correspondence between samples and numbers.

Abundance of the functional genes

We analyzed the *in situ* abundance of the target genes for the ammonia-oxidizing archaea (AOA, archaeal *amoA* gene), and for denitrification (*nirS* and *nosZ* genes). The *nosZ* gene, only active under anoxic conditions, was analyzed only in the deepest point of each profile. We show the abundances of these genes in both reservoirs in Figure 7.7 and 7.8 and in Supplementary Table 7.3. The abundance of the archaeal *amoA* varied from 0 to 2.7×10^3 copies mL^{-1} . In the Cubillas reservoir, we only detected the archaeal *amoA* gene in the oxycline in July, where we observed the maximum value of nitrite but the minimum of ammonia concentration. In September, we detected the archaeal *amoA* gene in the three depths, and its abundance decreased with depth. In the Iznájar reservoir we

detected the archaeal *amoA* gene in all the depths, with the minimum abundance located in the oxycline of July sampling. The *nirS* abundance ranged from 4.5×10^4 to 5.3×10^5 copies mL⁻¹ in Cubillas, and from 8.1×10^4 to 4.7×10^6 copies mL⁻¹ in Iznájar. We observed that the *nirS* abundance appeared in all the samples, and increased with depth and during the thermal stratification in Iznájar from July to September. The abundance of *nosZ* gene varied from 800 to 2.1×10^3 copies mL⁻¹, and the abundance was higher at the end of stratification period (in September) than at the beginning (in July) in both reservoirs.

We found that archaeal *amoA* was not related to the dissolved N₂O concentration ($n = 12$, p -value = 0.42), whereas we obtained that the N₂O concentration was related to the *nirS* abundance following a power function (Dissolved N₂O, $\mu\text{mol-N L}^{-1} = 2.5 \times 10^{-4} (\textit{nirS}, \text{copies mL}^{-1})^{0.60}$, $n = 12$, $\text{adj R}^2 = 0.32$, p -value < 0.05) (Figure 7.6a). We also found that the *nirS* abundance was a power function of the cumulative Chl-*a* concentration ($\textit{nirS}, \text{copies mL}^{-1} = 2.5 \times 10^3 (\text{Cum Chl-}a, \text{mg m}^{-2})^{1.15}$, $n = 12$, $\text{adj R}^2 = 0.56$, p -value < 0.01) (Figure 7.6b). We did not find a significant relationship between the abundance of the archaeal *amoA* gene and the $\delta^{15}\text{N-NO}_2^-$ ($n = 12$, p -value = 0.728; Figure 7.6c). We found that the relationship between the abundance of the *nirS* gene and the $\delta^{15}\text{N-NO}_2^-$ was marginally significant in the Cubillas samples ($n = 6$, p -value = 0.077) (Figure 7.6d). In the Iznájar samples, the $\delta^{15}\text{N-NO}_2^-$ was related to the abundance of the *nirS* gene following an exponential function ($\textit{nirS}, \text{copies mL}^{-1} = 2.1 \times 10^6 10^{0.05 \delta^{15}\text{N-NO}_2^- (\%)}$, $n = 6$, $\text{adj R}^2 = 0.94$, p -value < 0.001) (Figure 7.6d).

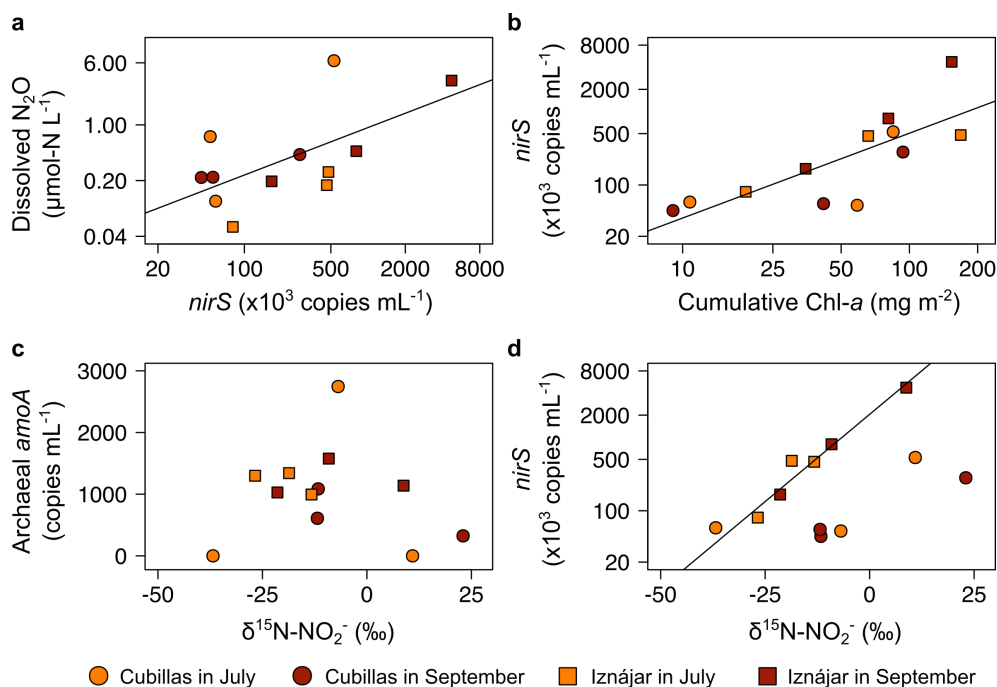


Figure 7.6. Relationship between dissolved N₂O, the cumulative Chl-*a*, the natural isotopic composition of the nitrite (δ¹⁵N-NO₂⁻), and the abundance of the genes. (a) Relationship between the abundance of the gene *nirS* (copies mL⁻¹) and the dissolved N₂O concentration (μmol-N L⁻¹); (b) relationship between the cumulative Chl-*a* (mg m⁻²) and the abundance of the gene *nirS*; (c) scatterplot of the δ¹⁵N-NO₂⁻, and the abundance of the gene archaeal *amoA*; (d) relationship between the δ¹⁵N-NO₂⁻ and the abundance of the gene *nirS*. The regression line in (d) was drawn for the Iznájar samples. Note the logarithmic scale in the x-axis of (a) and (b); and in the y-axis of (a), (b), and (d).

7.3.2. ¹⁵N-labelling incubations

Distribution of the nitrification rates and N₂O production using ¹⁵N-NH₄⁺

We show the distribution of the nitrification rates and N₂O production in Figures 7.7 and 7.8, and in Supplementary Table 7.4. Complete nitrification includes two steps, the oxidation of ammonia to nitrite, and then to nitrate, with the concomitant formation of N₂O. We only detected a significant ammonia oxidation rate in 4 of the 12 depths tested, 2 of these rates were negative (i.e., nitrite consumption) and the other 2 rates were positive (i.e., nitrite production). We detected a net consumption of nitrite in the epilimnion of Cubillas in September (-38.9 nmol-N L⁻¹ d⁻¹), and in the oxycline of Iznájar in July sampling (-712.8 nmol-N L⁻¹ d⁻¹), both oxic depths. We detected a significant nitrite production in low oxygen waters during the September sampling: in the bottom waters of Cubillas reservoir

(336.8 nmol-N L⁻¹ d⁻¹), and in the hypolimnion of Iznájar reservoir (215.8 nmol-N L⁻¹ d⁻¹).

In contrast, we detected significant nitrification rates (i.e., NO₃⁻ production from NH₄⁺) in all depths of both reservoirs except in the hypolimnion of Iznájar in September, where we detected the maximum ammonia oxidation rate of this reservoir (Figures 7.7 and 7.8). The nitrification rates varied from 6.1 x 10³ to 5.6 x 10⁴ nmol-N L⁻¹ d⁻¹ in Cubillas, and from 0.0 to 3.7 x 10³ nmol-N L⁻¹ d⁻¹ in the Iznájar reservoir. The sample in which the nitrification rate was 0 was not included in the statistical analysis, because was identified as outlier (G = 0.96, p-value < 0.001). The nitrification rates in July (mean = 2.5 x 10⁴) were an order of magnitude higher than the nitrification rates in September (mean = 8.7 x 10³) (n = 11, F = 5.44, p-value < 0.05). The nitrification rates were also higher in Cubillas (mean = 2.2 x 10⁴) than in Iznájar (mean = 1.2 x 10⁴) (n = 11, F = 5.79, p-value < 0.05). Our results show that we did not detect a significant nitrite production from NH₄⁺ in many depths, but we detected an important nitrate production from NH₄⁺. This fact suggests that a complete nitrification, likely by comammox bacteria, could be happening at these sites. We tested the presence of the comammox amoA genes through PCR resolved on 1.5 % agarose gel electrophoresis, but we did not observe any band at the expected size (415 bp) (Supplementary Figure 7.3).

The production of N₂O from ammonia ranged from 0.3 to 22.2 nmol-N L⁻¹ d⁻¹ in the Cubillas reservoir, and from 0.1 to 38.0 nmol-N L⁻¹ d⁻¹ in the Iznájar reservoir (Figures 7.7 and 7.8). In general, the production of N₂O increased with depth in both reservoirs, and the variation was up to 3 orders of magnitude in the same vertical profile. We measured the highest productions in low oxygen environments (< 10 μmol L⁻¹): in the bottom waters of Cubillas in July (i.e., 22.2 nmol-N L⁻¹ d⁻¹), and in the hypolimnion of Iznájar in September (i.e., 38.0 nmol-N L⁻¹ d⁻¹). We did not find significant differences between the production of N₂O in July and September (n = 12, F = 0.01, p-value = 0.919), or between the reservoirs (n = 12, F = 0.12, p-value = 0.739). The N₂O yield (Yield_{Nit}, %) during nitrification varied from 0.002 to 0.041 % in Cubillas reservoir, and from 0.002 to 0.032 % in Iznájar reservoir. The maximum yields were located in the bottom waters of Cubillas in July (0.039 %) and in September (0.041 %) (Supplementary Table 7.4).

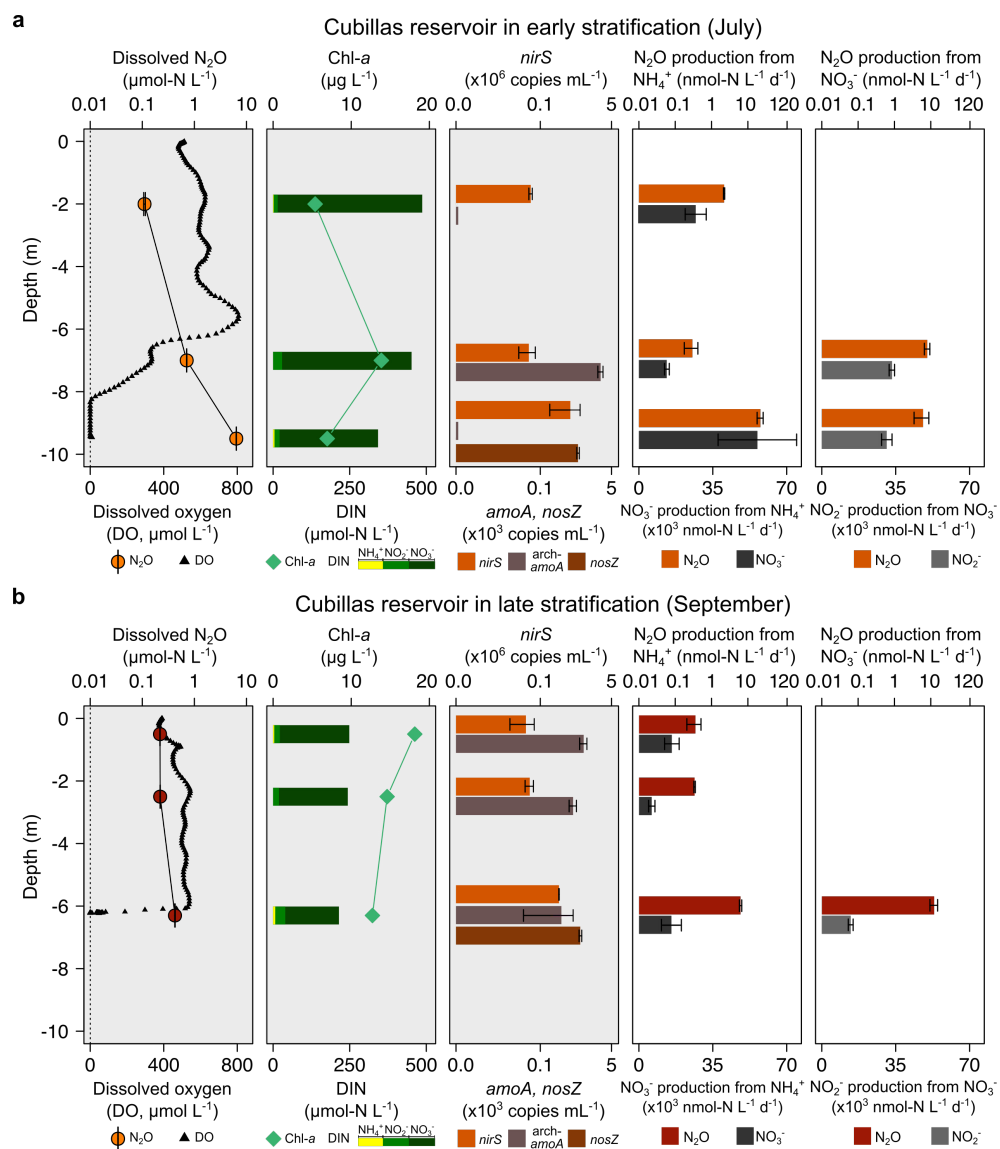


Figure 7.7. Vertical profiles of the dissolved N₂O concentration, dissolved oxygen, concentration of chlorophyll-*a* and dissolved inorganic nitrogen, the abundances of target genes, and the production rates measured using ¹⁵N-labelled substrates in Cubillas reservoir. Dissolved N₂O concentration (μmol-N L⁻¹, mean ± standard error), and dissolved oxygen (DO) concentration (μmol L⁻¹); chlorophyll-*a* (Chl-*a*) concentration (μg L⁻¹), and dissolved inorganic nitrogen (DIN) concentration (μmol-N L⁻¹), abundance of the gene *nirS* (x 10⁶ copies mL⁻¹), and archaeal *amoA*, and *nosZ* (x 10³ copies mL⁻¹); the production rates of N₂O (nmol-N L⁻¹ d⁻¹) and NO₃⁻ (x 10³ nmol-N L⁻¹ d⁻¹) from NH₄⁺, and production rates of N₂O (nmol-N L⁻¹ d⁻¹) and NO₂⁻ (x 10³ nmol-N L⁻¹ d⁻¹) from NO₃⁻ in July (a) and September (b). Note that the dissolved N₂O, the gene abundances, and the production of N₂O are in logarithmic scale. The grey background stands for the variables measured *in situ*, and the white background stands for the measurements derived from the incubations. We summarized the production rates in Supplementary Table 7.4 and 7.5.

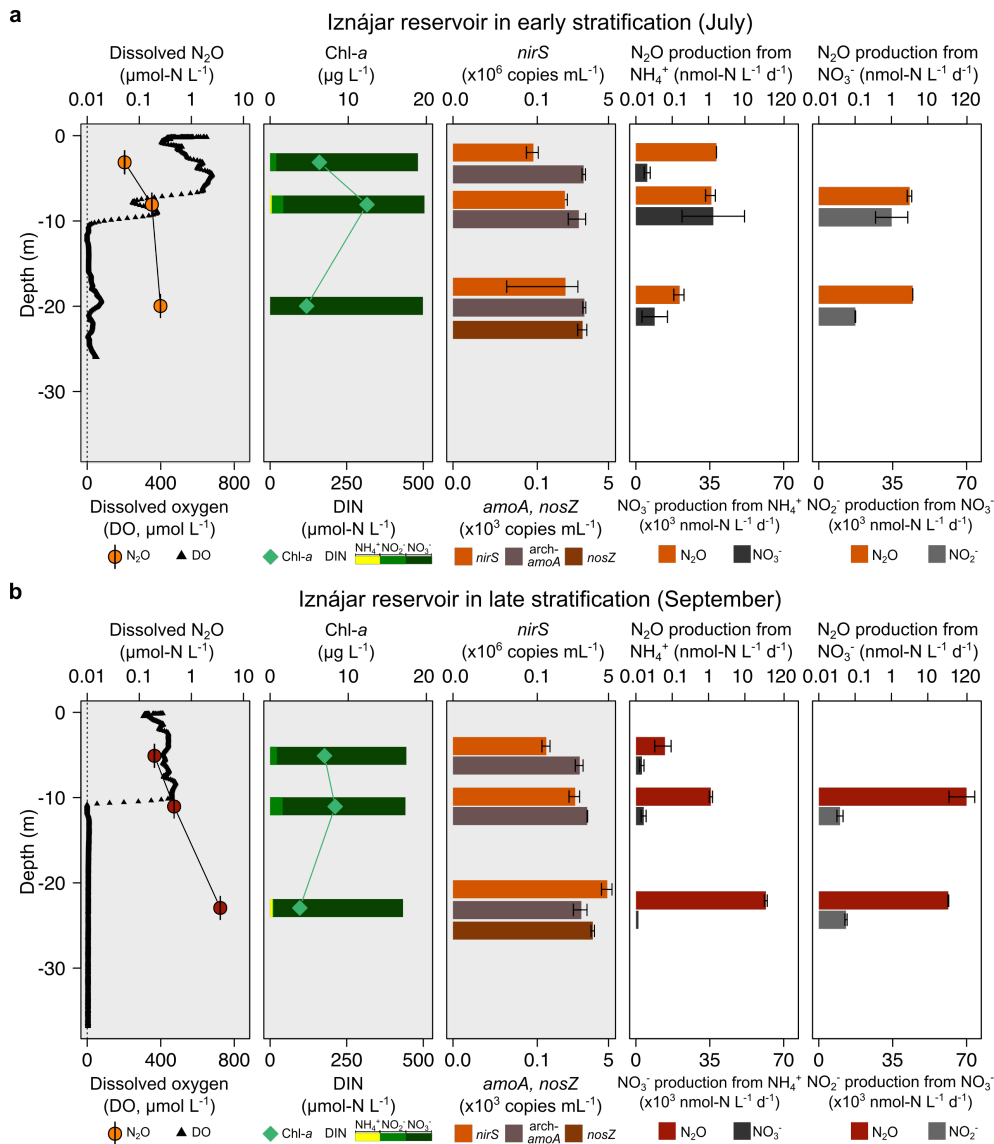


Figure 7.8. Vertical profiles of the dissolved N₂O concentration, dissolved oxygen, concentration of chlorophyll-*a* and dissolved inorganic nitrogen, the abundances of target genes, and the production rates measured using ¹⁵N-labelled substrates in Iznájár reservoir. Dissolved N₂O concentration (μmol-N L⁻¹, mean ± standard error), and dissolved oxygen (DO) (μmol L⁻¹); chlorophyll-*a* (Chl-*a*) concentration (μg L⁻¹), and dissolved inorganic nitrogen (DIN) concentration (μmol-N L⁻¹), abundance of the gene *nirS* (x 10⁶ copies mL⁻¹), and archaeal *amoA*, and *nosZ* (x 10³ copies mL⁻¹); the production rates of N₂O (nmol-N L⁻¹ d⁻¹) and NO₃⁻ (x 10³ nmol-N L⁻¹ d⁻¹) from NH₄⁺, and production rates of N₂O (nmol-N L⁻¹ d⁻¹) and NO₂⁻ (x 10³ nmol-N L⁻¹ d⁻¹) from NO₃⁻ in July (a) and September (b). Note that the dissolved N₂O, the gene abundances, and the production of N₂O are in logarithmic scale. The grey background stands for the variables measured *in situ*, and the white background stands for the measurements derived from the incubations. We summarized the production rates in Supplementary Table 7.4 and 7.5.

We found that the production of N₂O from ammonia was related to the *in situ* ammonia concentration following an exponential function (N₂O production, nmol-N L⁻¹ d⁻¹ = 0.39 × e^{0.47 Ammonia, μmol-N L⁻¹}, n = 12, adj R² = 0.54, p-value < 0.01) (Figure 7.9a). We also detected that the production of N₂O was significantly related to the nitrification rates (N₂O production, nmol-N L⁻¹ d⁻¹ = 0.26 × e^{7 × 10⁻⁵ Nitrification rates, nmol-N L⁻¹ d⁻¹}, n = 11, adj R² = 0.43, p-value < 0.05) (Figure 7.9b).

We also studied the relationships between the rate of production of N₂O in the incubations and the *in situ* abundances of the ammonia oxidizing archaea (archaeal *amoA* gene) and the nitrifying bacteria (*nirS* gene). The abundance of the archaeal *amoA* gene and the N₂O production was not significantly related (n = 12, p-value = 0.163) (Figure 7.9c), but we found that the abundance of the gene *nirS* was significantly related to the N₂O production (N₂O production, nmol-N L⁻¹ d⁻¹ = 9.2 × 10⁻⁵ (*nirS*, copies mL⁻¹)^{0.78}, n = 12, adj R² = 0.29, p-value < 0.05) (Figure 7.9d). Besides, the abundance of the gene *nirS* and the concentration of dissolved organic carbon (DOC, μmol-C L⁻¹) explained the 60 % of the variance in the production of N₂O from ammonia according to multiple linear regression model showed in Table 7.2.

Table 7.2. Linear model explaining the production of N₂O from NH₄⁺ (nmol-N L⁻¹ d⁻¹) with the abundance of the gene *nirS* (copies mL⁻¹) and the dissolved organic carbon (DOC) concentration (μmol-C L⁻¹) as predictor variables.

Response variable	Predictor variable	Estimate (Std Error)	t value	p-value
Log ₁₀ (N ₂ O production) n = 12 Adj R ² = 0.60	Intercept	-15.51 (4.05)	-3.829	< 0.01
	Log ₁₀ (<i>nirS</i>)	1.65 (0.38)	4.316	< 0.01
	DOC	0.03 (0.01)	2.999	< 0.05

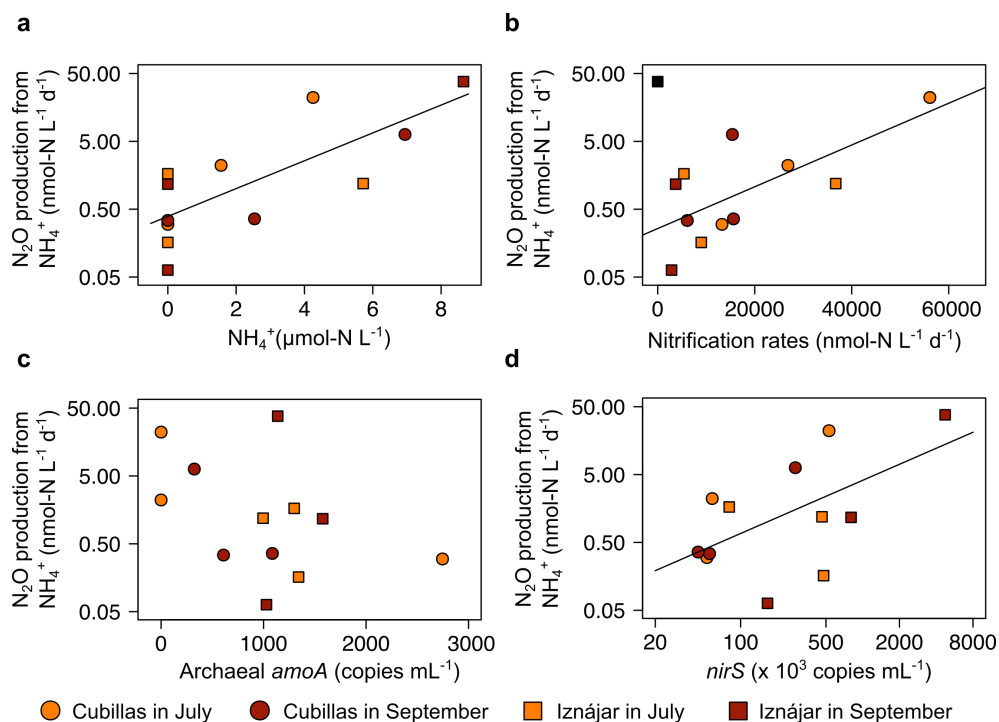


Figure 7.9. Drivers of the production of N₂O from NH₄⁺. (a) Exponential function that relates the *in situ* ammonia concentration (μmol-N L⁻¹) and the rate of production of N₂O during the incubations (nmol-N L⁻¹ d⁻¹), (b) relationship between the nitrification rates (nmol-N L⁻¹ d⁻¹) and the production of N₂O in the incubations, (c) scatterplot of the production of N₂O and the *in situ* abundance of the gene archaeal *amoA* (copies mL⁻¹), (d) relationship between the *in situ* abundance of the gene *nirS* (x 10³ copies mL⁻¹), and the production of N₂O. Note the logarithmic scales in the x-axis in (d), and in the y-axis in (a), (b), (c), and (d).

Distribution of the nitrate reduction rates and N₂O production using ¹⁵N-NO₃⁻

We show the distribution of the nitrate reduction rates and N₂O production in Figures 7.7 and 7.8, and in Supplementary Table 7.5. We also calculated the rates of nitrate reduction to nitrite (first step of denitrification) in all the depths analyzed (n = 7). The nitrate reduction rates varied from 1.4 x 10⁴ to 3.3 x 10⁴ nmol-N L⁻¹ d⁻¹ in Cubillas, and from 1.0 x 10⁴ to 3.5 x 10⁴ nmol-N L⁻¹ d⁻¹ in Iznájjar reservoir. We found that the rates were significantly higher in July (mean = 2.9 x 10⁴ nmol-N L⁻¹ d⁻¹) than in September (mean = 1.2 x 10⁴ nmol-N L⁻¹ d⁻¹) (n = 7, F = 11.96, p-value < 0.05), but we did not detect significant differences between the reservoirs (n = 7, F = 0.84, p-value = 0.411). This decrease in the nitrate reduction rates from July to September coincided with the decrease in the nitrate concentration.

The production of N₂O from nitrate varied from 6.2 to 12.5 nmol-N L⁻¹ d⁻¹ in Cubillas reservoir, and from 3.2 to 117.7 nmol-N L⁻¹ d⁻¹ in Iznájjar reservoir (Figure

7.7 and 7.8). The higher production (117.7 nmol-N L⁻¹ d⁻¹) was obtained in the oxycline of Iznájar reservoir in September in anoxic conditions, where we also observed a reduction in the nitrate concentration (i.e., 314.6 μmol-N L⁻¹) with respect to epilimnion and hypolimnion (i.e., 335.3, and 338.0 μmol-N L⁻¹). We detected production of N₂O in the oxycline of Cubillas (8.0 nmol-N L⁻¹ d⁻¹) and in the oxycline of Iznájar (3.2 nmol-N L⁻¹ d⁻¹) in July, which were incubated in oxic conditions. At these depths, the production measured did not differ much of the production obtained in the following anoxic depth (bottom waters and the hypolimnion, respectively). We did not find significant differences between the production in July and September (n = 7, F = 3.39, p-value = 0.140), or between the reservoirs (n = 7, F = 0.74, p-value = 0.439). The N₂O yield during denitrification (yield_{denit}, %) varied from 0.020 to 0.091 % in Cubillas reservoir, and from 0.009 to 1.156 % in Iznájar reservoir. The maximum yield was located in the oxycline of Iznájar reservoir in September. We found that the production of N₂O from NO₃⁻ was significantly higher than the production of N₂O from NH₄⁺ (n = 7, t = -3.07, p-value < 0.01). We did not detect a significant relationship between the N₂O production from nitrate and the *in situ* nitrate concentration (n = 7, p-value = 0.757) (Supplementary Figure 7.4a), or the *in situ* abundances of the *nirS* gene (n = 7, p-value = 0.320) (Supplementary Figure 7.4b).

7. 4. Discussion

During the study period, we observed that the accumulation of the dissolved N₂O produced in each reservoir was affected by the changes in the mean depth, and the stratification of the water column. The water-level drawdown from July to September in Cubillas decreased the hydrostatic pressure and the solubility of N₂O in the bottom waters, and that changed the N₂O storage capacity of these waters, and likely produced the massive release of N₂O from July to September. Previous studies showed that the mean depth determined the storage capacity, and fluxes of CH₄ (Keller and Stallard, 1994; West *et al.*, 2016; León-Palmero *et al.*, 2020a, 2020b), and the water-level drawdown can increase the emission of CH₄ in shallow reservoirs (Harrison *et al.*, 2017; Beaulieu *et al.*, 2018). In contrast, during the study period the water column of Iznájar experienced a thermal stratification and the formation of a sharp oxygen gradient and an anoxic hypolimnion. We observed a

great accumulation of N₂O in the hypolimnion during this period, as we also found in Chapter 6. However, the highest production of N₂O was not located in the hypolimnion, but in the oxycline. Therefore, this high production of N₂O at the oxycline may contribute significantly to the high emissions of N₂O found in Iznájar reservoir previously (León-Palmero *et al.*, 2020a). Other studies in ocean waters also found that the highest rates of N₂O production were located near the oxic-anoxic interface, where there is a strong potential for N₂O fluxes to the atmosphere (Ji *et al.*, 2015, 2018; Frey *et al.*, 2020).

The trends that we observed in the natural isotopic composition of the nitrogen species suggested that denitrification may be occurring in the water column of the reservoirs, as previous studies have shown (Sugimoto *et al.*, 2008; Hirota *et al.*, 2009; Sigman *et al.*, 2009; Xiong *et al.*, 2009; Valiente *et al.*, 2018). Our results suggest that the production of N₂O determined the enrichment in ¹⁵N of the nitrite pool, and that the increase in the $\delta^{15}\text{N-NO}_2^-$ was coupled to the abundance of the denitrifying bacteria in the reservoirs, as was made evident by the abundance of the *nirS* gene. This gene encodes the nitrite reductase that catalyzes the transformation of nitrite to NO during denitrification. Besides, the abundance of the *nirS* gene in the water column was correlated to the dissolved N₂O concentration, as we also detected in Chapter 6. These results suggest that the production of N₂O by denitrifiers was the main pathway in the study systems, and the production of N₂O had an important isotopic signature in the NO₂⁻ pools. Lennon and Houlton (2017) found that the $\delta^{15}\text{N-NO}_3^-$ was strongly correlated to the *nirS* abundance in soils, and that highlights the widespread importance of isotopic discrimination by denitrifiers.

We quantified the N₂O production rates from ¹⁵N labeled ammonia and nitrate. During the incubations, we also measured the ammonia oxidation and nitrification rates, and the nitrate reduction rates. The detection of high nitrification rates, but no significant ammonia oxidation in most of the samples may suggest that a complete nitrification by comammox bacteria is occurring at these depths. However, the PCR results showed no evidence of the presence of comammox bacteria. We used the primers developed by Pjevac *et al.* (2017) for the detection of comammox *Nitrospira*, but other genera may exist and we haven't detected them using these primers. Comammox was demonstrated few years ago (Daims *et al.*,

2015; van Kessel *et al.*, 2015), and the diversity of these bacteria is still unknown. Another possibility to explain these results is that the nitrite production by ammonia oxidation is so tightly coupled to the nitrite consumption that we were not able to detect the changes in concentration. Kowalchuk and Stephen (2001) pointed out that ammonia oxidation is the rate-limiting step for nitrification in most systems, as nitrite is rarely found to accumulate in the environment. However, the gene *amoA* showed low abundances, or it was even undetectable. It is likely that the ammonia oxidizers are not very abundant in these reservoirs, or we are not detecting them with the primers that we used. It is important to notice that we pre-filtered the reservoir water (pore size = 3 µm) before DNA extraction. Therefore, comammox bacteria or ammonia oxidizing archaea may be present attached to particles > 3 µm, and we did not detect them during the analysis. If appearing in particles, that may support the tight coupling between reactions.

Across different pelagic environments, nitrification rates vary several orders of magnitude, with the lower rates in the ocean waters (0.4 - 10 nmol-N L⁻¹ d⁻¹) and the higher rates in eutrophic lakes, as lake Mendota (1.7 10³ - 2.6 x 10⁴ nmol-N L⁻¹ d⁻¹) (Small *et al.*, 2013). The nitrification rates found in this study were similar to the nitrification rates found in Lake Mendota by Hall (1986). The rates of N₂O production from ammonium were significantly related to the *in situ* concentration of ammonium and to the nitrification rates. In fact, Small *et al.* (2013) found that nitrification rates were limited by the ammonium availability. Carini and Joye (2008) found that the concentration of N₂O was significantly related to the nitrification rates in Mono Lake. In Chapter 6 we studied the abundance of the ammonia oxidizing archaea and the ammonia oxidizing bacteria, and we determined that the main oxidizing organisms in the study reservoirs were the ammonia oxidizing archaea. Here, we found that production of N₂O from ammonia was not related to the *in situ* archaeal *amoA* gene, but it was significantly related to the *in situ* abundance of the *nirS* gene, and to the DOC concentration. That suggests that the high rates of N₂O production from ammonia may be produced in a coupled nitrification-denitrification process. In addition, the rates of nitrification were also very high, and coupled to the N₂O production from ammonia, and that may support the hypothesis of the nitrification-denitrification coupling. Zhu *et al.* (2018) pointed out that coupled nitrification-denitrification not only occurs in sediments, but it can also

takes place in suspended particulate material in the water column. Besides, several studies in rivers have demonstrated that nitrification, denitrification, or coupled nitrification-denitrification occur in suspended particles (Xia *et al.*, 2004; Liu *et al.*, 2013; Jia *et al.*, 2016; Xia *et al.*, 2017). In this study we did not quantify the particulate material in the incubations, but we observed the particulate organic matter suspended in the bottles with the naked eye (Supplementary Figure 7.5).

In the incubations with ¹⁵N labeled nitrate we found that the nitrate to nitrite reduction rates (first step of denitrification) were at least one order of magnitude higher than the rate of nitrate reduction (to ammonia and organic nitrogen) detected in the hypolimnion of Lake Mendota (Brezonik and Lee, 1968); and up to 3 orders of magnitude higher than the rates detected in the ocean (Füssel *et al.*, 2012; Ji *et al.*, 2015). Besides, these rates were at least one order of magnitude higher than the rates of N₂ production (i.e., complete denitrification) found in previous studies (Brezonik and Lee, 1968; Chan and Campbell, 1980; Roland *et al.*, 2018). We detected that nitrate reduction rates were significantly higher in July than in September, which is in accordance with Deemer *et al.* (2011), who found that hypolimnion N₂ production was higher in early stratification than in late stratification.

The N₂O production rates from nitrate were higher than the rates found in ocean waters (Ji *et al.*, 2015), and closed to the results obtained in the Chesapeake Bay by Ji *et al.* (2018). Our results were lower than the rates measured in the Potomac River, which had a nutrient budget dominated by sewage inputs (McElroy *et al.*, 1978). The N₂O production rates from nitrate varied up to 2 orders of magnitude, and they were higher than the N₂O production from ammonia, as found by other studies in the ocean water column (Ji *et al.*, 2015). Interestingly, in the hypolimnion of Iznájar in September the production of N₂O from nitrate (i.e., $36.9 \pm 0.9 \text{ nmol-N L}^{-1} \text{ d}^{-1}$) was similar to the production from ammonia (i.e., $38.0 \pm 3.4 \text{ nmol-N L}^{-1} \text{ d}^{-1}$), that supports the coupled nitrification-denitrification hypothesis stated above. At this depth, we did not detect a significant net nitrification rate (i.e., nitrate production from ammonia), and that may also indicate that the nitrate is consumed quickly after being produced.

The N₂O production from nitrate was not significantly related to the *in situ* concentration of nitrate, probably because these reservoirs are eutrophic systems

and they are not limited by the nitrate availability. The N₂O production from nitrate increased when the *in situ* dissolved oxygen concentration decreased, but the production was not inhibited by oxygen. Denitrifying bacteria are diverse, and many of them can denitrify in oxic and anoxic conditions, with the highest N₂O/N₂ ratios in oxic conditions (Hochstein *et al.*, 1984; Lloyd *et al.*, 1987; Lloyd, 1993). The occurrence of the denitrifying bacteria (i.e., gene *nirS*) was consistent in the water column of the two reservoirs, and it reached the maximum abundances in the suboxic waters. In Chapter 6 we also detected that *nirS* gene was present in the water column of all reservoirs, both in anoxic and oxic conditions. However, we did not find a significant relationship between the abundance of the gene *nirS*, and the N₂O production from nitrate, likely because we calculated only 7 production rates for the nitrate treatment. Besides, denitrifiers can reduce both nitrate and nitrite to N₂O. In the natural abundance analysis, we found that the N₂O production had a clear signature in the ¹⁵N enrichment in the nitrite pool. Both the dissolved N₂O concentration and the abundance of the gene *nirS* were related to the δ¹⁵N-NO₂⁻. Frey *et al.* (2020) found that the gene *nirS* was significantly correlated to N₂O production from NO₂⁻ but not from NO₃⁻. Nitrite is a key compound for the denitrifying community, but we did not quantify the production of N₂O from nitrite. Therefore, the rates of N₂O production from denitrification are likely underestimated in this study.

In summary, we propose that N₂O is produced by coupled nitrification-denitrification (from ammonia), and by denitrification (from nitrate). The *in situ* gene abundances, the *in situ* natural abundances of the nitrogen isotopes, and the incubation N₂O rates are coherent among them, and they suggest that denitrification is occurring in the water column of these reservoirs. In addition, we found that the export of the autochthonous organic matter may have a relevant role in N₂O production by denitrification, and by coupled nitrification-denitrification in the study reservoirs. We studied the cumulative Chl-*a* concentration, which is a proxy for the vertical export of the autochthonous organic matter produced by primary producers in the whole water column. The cumulative Chl-*a* concentration was significantly related to the abundance of the gene *nirS*, and to the dissolved N₂O concentration. In addition, the total N₂O production, obtained as the sum of the N₂O production from ammonium and from nitrate, was also significantly related

to the abundance of the gene *nirS* (n = 12, adj R² = 0.42, p-value < 0.05) (Supplementary Figure 7.6a), and to the cumulative Chl-*a* concentration (n = 12, adj R² = 0.32, p-value < 0.05) (Supplementary Figure 7.6b). According to these results, in Chapter 6 we also found that the abundance of the gene *nirS* in the water column of twelve reservoirs was correlated to the cumulative Chl-*a* concentration. In Figure 7.10 we compared the relationships found in Chapter 6 and in Chapter 7. Interestingly, the slopes of these relationships, which corresponds to the exponent of the power function, were similar. These results suggest that the abundance of *nirS*, and, as consequence, the production of N₂O by denitrification, and coupled nitrification-denitrification in the water column, is likely enhanced by particulate material derived from the phytoplankton community.

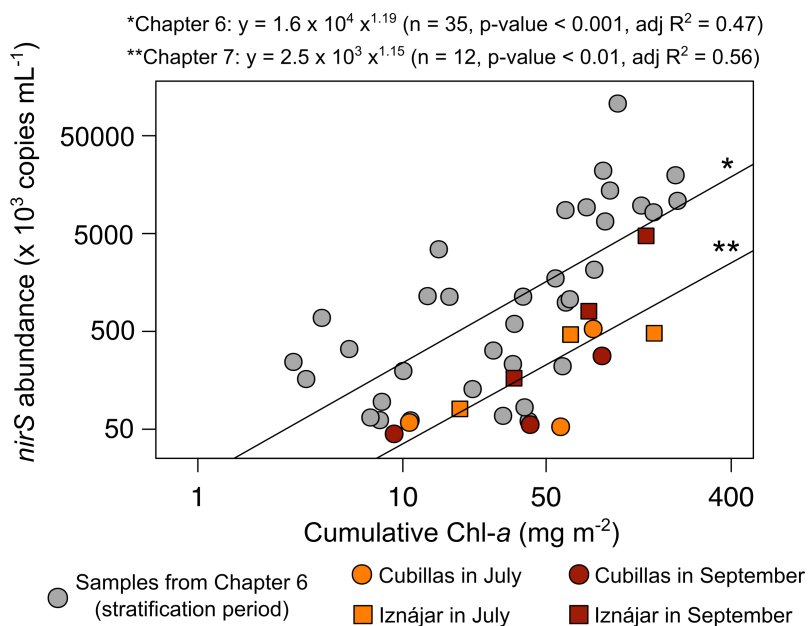


Figure 7.10. Comparison of the relationships between the cumulative Chl-*a* concentration and the abundance of the *nirS* gene in Chapter 6 and in Chapter 7. Note that both axes are in logarithmic scale.

Zhou *et al.* (2019b) found that suspended particles potentially enhanced the production and emission of N₂O in a eutrophic lake. In addition, several studies in marine waters have described that denitrification was affected by the quantity and quality of organic matter (Ward *et al.*, 2008; Babbin *et al.*, 2014). Dalsgaard *et al.* (2012) found that the high denitrification rates were all found at marine stations with high chlorophyll levels in the overlying water, suggesting a subducted and potentially decaying algal bloom. In general, this organic matter export represent a

high quality carbon source, but also sinking particles with a surface for microorganisms to grow on, an environment where both oxic and anoxic/low oxygen microenvironments coexist, and they even increase the contact chances between bacteria and nitrogen (Xia *et al.*, 2004; Liu *et al.*, 2013; Jia *et al.*, 2016; Xia *et al.*, 2017).

Scaling up to the reservoir level: how much nitrogen the reservoirs lost?

Microbial activity in the water column and sediments of reservoirs can reduce the excess of nitrogen through emissions of N₂, primarily produced during denitrification, and also through anaerobic ammonium oxidation (anammox), and, importantly, through emissions of N₂O, which were quantified in this study. From July to September we detected a reduction in the concentration of DIN in the water column of both reservoirs, that confirmed that nitrogen is processed and removed in these systems. We calculated the total DIN loss in each reservoir from July to September, and we compared this DIN loss with the total N₂O production (the sum of the production of N₂O from ammonia, and from nitrate) (Table 7.3). The loss of nitrogen has been calculated using the DIN concentration measured in July and in September, without taking into account whether the reservoirs received inputs of N from their watersheds during that period.

Table 7.3. Total DIN loss, and N₂O produced from July to September in Cubillas and Iznájar reservoirs.

Reservoir	Period	DIN loss			N ₂ O production		N ₂ O production per DIN loss
		days	kg-N d ⁻¹	g-N m ⁻² d ⁻¹	%	kg-N d ⁻¹	g-N m ⁻² d ⁻¹
Cubillas	64	468	0.24	45	1.9	9.8 x 10 ⁻⁴	0.4
Iznájar	61	5337	0.20	11	251.4	9.6 x 10 ⁻³	4.7

From July to September, Cubillas lost 468 kg-N per day, while Iznájar reservoir lost 5337 kg-N per day, and that represented a 45 % and 11 % of decrease in the DIN concentration during the study period. Cubillas is a smaller reservoir than Iznájar, and that explains the higher percentage of the DIN loss despite the lower net loss than Iznájar. In terms of reservoir surface, the nitrogen loss was slightly higher in Cubillas. We detected that the N₂O production was two orders of magnitude higher in Iznájar than in Cubillas in terms of kg-N per day, but the difference decreased normalizing by the area. In the water column of Iznájar the

percentage of the N₂O production per DIN loss was higher than in Cubillas, and represented the 4.7 %, and 0.4 %, respectively.

Zhou *et al.* (2019) described a decrease of the 79 % and the 97 % in the total nitrogen and the nitrate concentration respectively in the water column of Zhoucun reservoir during spring (2 months), and they related the nitrogen losses to aerobic denitrification occurring in the water column. Brezonik and Lee (1968) estimated that the hypolimnion of lake Mendota lost 312 kg N per day, which accounted for the 11 % of the nitrogen inputs.

Conclusions

Overall, we show the importance of the nitrogen loss and the production of N₂O in the water column of reservoirs affected by nitrogen loadings from agriculture and urban areas. *In situ* data suggested that denitrification is an important pathway in the study reservoirs, and that was confirmed by the incubations. We suggested that a coupled nitrification-denitrification may be also occurring in the water column. The production of N₂O from nitrate showed the highest rates of N₂O production. Together, the rates of N₂O production by a coupled nitrification-denitrification from ammonium, and denitrification from nitrate may explain that the dissolved N₂O concentration in the study reservoirs depended of the abundance of the *nirS* gene, and in Chapter 6. The rates presented here are likely an underestimation, because we did not measure the N₂O production from nitrite by denitrifiers. In addition, N₂O can be also produced by abiotic reactions. We demonstrated the N₂O photoproduction in the surface waters of these two reservoirs in Chapter 4. This abiotic production should be measured to account for the total N₂O production. Finally, we observed that the concentration and production of N₂O increased at low-oxygen conditions, and depended on the cumulative Chl-*a* concentration of the water column. Future scenarios with anthropogenic eutrophication increasing the frequency and duration of water column anoxia in lakes and reservoirs (Moss *et al.*, 2011), may also increase the production and fluxes of N₂O. Further studies should focus on the water column of lakes and reservoirs as relevant sites for N₂O production.

7. 5. References

- Anderson, J. H. (1964). The metabolism of hydroxylamine to nitrite by *Nitrosomonas*, *The Biochemical journal*, 91(1), pp. 8–17. doi: 10.1042/bj0910008.
- Babbin, A. R., Keil, R. G., Devol, A. H. and Ward, B. B. (2014). Organic matter stoichiometry, flux, and oxygen control nitrogen loss in the ocean, *Science*, 344(6182), pp. 406–408. doi: 10.1126/science.1248364.
- Beaulieu, J. J., Nietch, C. T. and Young, J. L. (2015). Controls on nitrous oxide production and consumption in reservoirs of the Ohio River Basin, *Journal of Geophysical Research-Biogeosciences*, 120(10), pp. 1995–2010. doi: 10.1002/2015JG002941.
- Beaulieu, J. J., Balz, D. A., Birchfield, M. K., Harrison, J. A., Nietch, C. T., Platz, M. C., Squier, W. C., Waldo, S., Walker, J. T., White, K. M. and Young, J. L. (2018). Effects of an experimental water-level drawdown on methane emissions from a eutrophic reservoir, *Ecosystems (New York, N.y.)*, 21(4), pp. 657–674. doi: 10.1007/s10021-017-0176-2.
- Beaulieu, J. J., DelSontro, T. and Downing, J. A. (2019). Eutrophication will increase methane emissions from lakes and impoundments during the 21st century, *Nature Communications*, 10(1), p. 1375. doi: 10.1038/s41467-019-09100-5.
- Bedard-Haughn, A., van Groenigen, J. W. and van Kessel, C. (2003). Tracing ¹⁵N through landscapes: Potential uses and precautions, *Journal of Hydrology*, 272(1), pp. 175–190. doi: 10.1016/S0022-1694(02)00263-9.
- Bonin, P., Gilewicz, M. and Bertrand, J. C. (1989). Effects of oxygen on each step of denitrification on *Pseudomonas nautica*, *Canadian Journal of Microbiology*, 35(11), pp. 1061–1064. doi: 10.1139/m89-177.
- Brezonik, P. L. and Lee, G. F. (1968). Denitrification as a nitrogen sink in Lake Mendota, Wisconsin, *Environmental Science & Technology*, 2(2), pp. 120–125.
- Canfield, D. E., Glazer, A. N. and Falkowski, P. G. (2010). The evolution and future of Earth's nitrogen cycle, *Science*, 330(6001), pp. 192–196. doi: 10.1126/science.1186120.
- Caranto, J. D. and Lancaster, K. M. (2017). Nitric oxide is an obligate bacterial nitrification intermediate produced by hydroxylamine oxidoreductase, *Proceedings of the National Academy of Sciences*, 114(31), pp. 8217–8222. doi: 10.1073/pnas.1704504114.
- Carini, P., Dupont, C. L. and Santoro, A. E. (2018). Patterns of thaumarchaeal gene expression in culture and diverse marine environments, *Environmental Microbiology*, 20(6), pp. 2112–2124. doi: 10.1111/1462-2920.14107.
- Carini, S. A. and Joye, S. B. (2008). Nitrification in Mono Lake, California: Activity and community composition during contrasting hydrological regimes, *Limnology and Oceanography*, 53(6), pp. 2546–2557. doi: 10.4319/lo.2008.53.6.2546.
- Chan, Y. K. and Campbell, N. E. R. (1980). Denitrification in Lake 227 during summer stratification, *Canadian Journal of Fisheries and Aquatic Sciences*, 37(3), pp. 506–512. doi: 10.1139/f80-065.
- Daims, H., Lebedeva, E. V., Pjevac, P., Han, P., Herbold, C., Albertsen, M., Jehmlich, N.,

- Palatinszky, M., Vierheilig, J., Bulaev, A., Kirkegaard, R. H., von Bergen, M., Rattei, T., Bendinger, B., Nielsen, P. H. and Wagner, M. (2015). Complete nitrification by *Nitrospira* bacteria, *Nature*, 528(7583), pp. 504–509. doi: 10.1038/nature16461.
- Dalsgaard, T., Thamdrup, B., Farías, L. and Revsbech, N. P. (2012). Anammox and denitrification in the oxygen minimum zone of the eastern South Pacific, *Limnology and Oceanography*, 57(5), pp. 1331–1346. doi: 10.4319/lo.2012.57.5.1331.
- Davidson, T. A., Audet, J., Svenning, J.-C., Lauridsen, T. L., Søndergaard, M., Landkildehus, F., Larsen, S. E. and Jeppesen, E. (2015). Eutrophication effects on greenhouse gas fluxes from shallow-lake mesocosms override those of climate warming, *Global Change Biology*, 21(12), pp. 4449–4463. doi: 10.1111/gcb.13062.
- Deemer, B. R., Harrison, J. A. and Whitling, E. W. (2011). Microbial dinitrogen and nitrous oxide production in a small eutrophic reservoir: An *in situ* approach to quantifying hypolimnetic process rates, *Limnology and Oceanography*, 56(4), pp. 1189–1199. doi: 10.4319/lo.2011.56.4.1189.
- Fox, J. and Weisberg, S. (2011). *An R Companion to Applied Regression* Thousand Oaks CA: Sage. Second. Available at: <http://socserv.socsci.mcmaster.ca/jfox/Books/Companion>.
- Fox, J. and Bouchet-Valat, M. (2019). *Rcmdr: R Commander*. Available at: <http://socserv.socsci.mcmaster.ca/jfox/Misc/Rcmdr/>.
- Frame, C. H. and Casciotti, K. L. (2010). Biogeochemical controls and isotopic signatures of nitrous oxide production by a marine ammonia-oxidizing bacterium, *Biogeosciences*, 7(9), pp. 2695–2709. doi: <https://doi.org/10.5194/bg-7-2695-2010>.
- Francis, C. A., Roberts, K. J., Beman, J. M., Santoro, A. E. and Oakley, B. B. (2005). Ubiquity and diversity of ammonia-oxidizing archaea in water columns and sediments of the ocean, *Proceedings of the National Academy of Sciences*, 102(41), pp. 14683–14688. doi: 10.1073/pnas.0506625102.
- Frey, C., Bange, H. W., Achterberg, E. P., Jayakumar, A., Löscher, C. R., Arévalo-Martínez, D. L., León-Palmero, E., Sun, M., Sun, X., Xie, R. C., Oleynik, S. and Ward, B. B. (2020). Regulation of nitrous oxide production in low-oxygen waters off the coast of Peru, *Biogeosciences*, 17(8), pp. 2263–2287. doi: 10.5194/bg-17-2263-2020.
- Füssel, J., Lam, P., Lavik, G., Jensen, M. M., Holtappels, M., Günter, M. and Kuypers, M. M. (2012). Nitrite oxidation in the Namibian oxygen minimum zone, *The ISME Journal*, 6(6), pp. 1200–1209. doi: 10.1038/ismej.2011.178.
- Goering, J. J. and Dugdale, V. A. (1966). Estimates of the rates of denitrification in a subarctic lake, *Limnology and Oceanography*, 11(1), pp. 113–117. doi: 10.4319/lo.1966.11.1.0113.
- Goreau, T. J., Kaplan, W. A., Wofsy, S. C., McElroy, M. B., Valois, F. W. and Watson, S. W. (1980). Production of NO₂⁻ and N₂O by nitrifying bacteria at reduced concentrations of oxygen, *Appl. Environ. Microbiol.*, 40(3), pp. 526–532.
- Granger, J. and Sigman, D. M. (2009). Removal of nitrite with sulfamic acid for nitrate N and O isotope analysis with the denitrifier method, *Rapid Communications in Mass Spectrometry*, 23(23), pp. 3753–3762. doi: 10.1002/rcm.4307.

- Gross, J. and Ligges, U. (2015). *nortest: Tests for Normality*. Available at: <https://CRAN.R-project.org/package=nortest> (Accessed: 3 June 2018).
- Hall, G. H. (1986). Nitrification in lakes, in Prosser, J. I. (ed.) *Nitrification*, pp. 127–156.
- Hallin, S., Philippot, L., Löffler, F. E., Sanford, R. A. and Jones, C. M. (2018). Genomics and ecology of novel N₂O-reducing microorganisms, *Trends in Microbiology*, 26(1), pp. 43–55. doi: 10.1016/j.tim.2017.07.003.
- Hamersley, M. R., Woebken, D., Boehrer, B., Schultze, M., Lavik, G. and Kuypers, M. M. M. (2009). Water column anammox and denitrification in a temperate permanently stratified lake (Lake Ransnitzer, Germany), *Systematic and Applied Microbiology*, 32(8), pp. 571–582. doi: 10.1016/j.syapm.2009.07.009.
- Harrison, J. A., Maranger, R. J., Alexander, R. B., Giblin, A. E., Jacinthe, P.-A., Mayorga, E., Seitzinger, S. P., Sobota, D. J. and Wollheim, W. M. (2009). The regional and global significance of nitrogen removal in lakes and reservoirs, *Biogeochemistry*, 93(1–2), pp. 143–157. doi: 10.1007/s10533-008-9272-x.
- Harrison, J. A., Deemer, B. R., Birchfield, M. K. and O'Malley, M. T. (2017). Reservoir water-level drawdowns accelerate and amplify methane emission, *Environmental Science & Technology*, 51(3), pp. 1267–1277. doi: 10.1021/acs.est.6b03185.
- Heathcote, A. J. and Downing, J. A. (2012). Impacts of eutrophication on carbon burial in freshwater lakes in an intensively agricultural landscape, *Ecosystems*, 15(1), pp. 60–70. doi: 10.1007/s10021-011-9488-9.
- Hirota, A., Ijiri, A., Komatsu, D. D., Ohkubo, S. B., Nakagawa, F. and Tsunogai, U. (2009). Enrichment of nitrous oxide in the water columns in the area of the Bering and Chukchi Seas, *Marine Chemistry*, 116(1), pp. 47–53. doi: 10.1016/j.marchem.2009.09.001.
- Hochstein, L. I., Betlach, M. and Kritikos, G. (1984). The effect of oxygen on denitrification during steady-state growth of *Paracoccus halodenitrificans*, *Archives of Microbiology*, 137(1), pp. 74–78. doi: 10.1007/BF00425811.
- IPCC. (2013). *Climate Change 2013: The Physical Science Basis. Contribution of Working Group I to the Fifth Assessment Report of the Intergovernmental Panel on Climate Change* Cambridge, United Kingdom and New York, NY, USA: Cambridge University Press. Edited by T. F. Stocker, D. Qin, G.-K. Plattner, M. Tignor, S. K. Allen, J. Boschung, A. Nauels, Y. Xia, V. Bex, and P. M. Midgley. Available at: <https://www.ipcc.ch/report/ar5/wg1/>.
- Jeppesen, E., Moss, B., Bennion, H., Carvalho, L., DeMeester, L., Feuchtmayr, H., Friberg, N., Gessner, M. O., Hefting, M., Lauridsen, T. L. and others. (2010). Interaction of climate change and eutrophication, *Climate change impacts on freshwater ecosystems*, pp. 119–151.
- Ji, Q., Babbín, A. R., Jayakumar, A., Oleynik, S. and Ward, B. B. (2015). Nitrous oxide production by nitrification and denitrification in the Eastern Tropical South Pacific oxygen minimum zone, *Geophysical Research Letters*, 42(24), p. 10,755–10,764. doi: 10.1002/2015GL066853.
- Ji, Q., Frey, C., Sun, X., Jackson, M., Lee, Y.-S., Jayakumar, A., Cornwell, J. C. and Ward, B. B.

- (2018). Nitrogen and oxygen availabilities control water column nitrous oxide production during seasonal anoxia in the Chesapeake Bay, *Biogeosciences*, 15(20), p. 6127.
- Jia, Z., Liu, T., Xia, X. and Xia, N. (2016). Effect of particle size and composition of suspended sediment on denitrification in river water, *Science of The Total Environment*, 541, pp. 934–940. doi: 10.1016/j.scitotenv.2015.10.012.
- Keller, M. and Stallard, R. F. (1994). Methane emission by bubbling from Gatun Lake, Panama, *Journal of Geophysical Research: Atmospheres*, 99(D4), pp. 8307–8319. doi: 10.1029/92JD02170.
- van Kessel, M. A. H. J., Speth, D. R., Albertsen, M., Nielsen, P. H., Op den Camp, H. J. M., Kartal, B., Jetten, M. S. M. and Lücker, S. (2015). Complete nitrification by a single microorganism, *Nature*, 528(7583), pp. 555–559. doi: 10.1038/nature16459.
- Könneke, M., Bernhard, A. E., de la Torre, J. R., Walker, C. B., Waterbury, J. B. and Stahl, D. A. (2005). Isolation of an autotrophic ammonia-oxidizing marine archaeon, *Nature*, 437(7058), pp. 543–546. doi: 10.1038/nature03911.
- Kowalchuk, G. A. and Stephen, J. R. (2001). Ammonia-oxidizing bacteria: A model for molecular microbial ecology, *Annual Review of Microbiology*, 55(1), pp. 485–529. doi: 10.1146/annurev.micro.55.1.485.
- Lennon, E. F. E. and Houlton, B. Z. (2017). Coupled molecular and isotopic evidence for denitrifier controls over terrestrial nitrogen availability, *The ISME Journal*, 11(3), pp. 727–740. doi: 10.1038/ismej.2016.147.
- León-Palmero, E., Morales-Baquero, R. and Reche, I. (2020a). Greenhouse gas fluxes from reservoirs determined by watershed lithology, morphometry, and anthropogenic pressure, *Environmental Research Letters*, 15(4), p. 044012. doi: 10.1088/1748-9326/ab7467.
- León-Palmero, E., Contreras-Ruiz, A., Sierra, A., Morales-Baquero, R. and Reche, I. (2020b). Dissolved CH₄ coupled to photosynthetic picoeukaryotes in oxic waters and to cumulative chlorophyll *a* in anoxic waters of reservoirs, *Biogeosciences*, 17(12), pp. 3223–3245. doi: 10.5194/bg-17-3223-2020.
- Liu, T., Xia, X., Liu, S., Mou, X. and Qiu, Y. (2013). Acceleration of denitrification in turbid rivers due to denitrification occurring on suspended sediment in oxic waters, *Environmental Science & Technology*, 47(9), pp. 4053–4061. doi: 10.1021/es304504m.
- Lloyd, D., Boddy, L. and Davies, K. J. P. (1987). Persistence of bacterial denitrification capacity under aerobic conditions: The rule rather than the exception, *FEMS Microbiology Ecology*, 3(3), pp. 185–190. doi: 10.1111/j.1574-6968.1987.tb02354.x.
- Lloyd, D. (1993). Aerobic denitrification in soils and sediments: From fallacies to factx, *Trends in Ecology & Evolution*, 8(10), pp. 352–356. doi: 10.1016/0169-5347(93)90218-E.
- Löscher, C. R., Kock, A., Könneke, M., LaRoche, J., Bange, H. W. and Schmitz, R. A. (2012). Production of oceanic nitrous oxide by ammonia-oxidizing archaea, *Biogeosciences*, 9(7), pp. 2419–2429. doi: <https://doi.org/10.5194/bg-9-2419-2012>.

- McElroy, M. B., Elkins, J. W., Wofsy, S. C., Kolb, C. E., Durán, A. P. and Kaplan, W. A. (1978). Production and release of N₂O from the Potomac Estuary, *Limnology and Oceanography*, 23(6), pp. 1168–1182. doi: 10.4319/lo.1978.23.6.1168.
- McIlvin, M. R. and Altabet, M. A. (2005). Chemical conversion of nitrate and nitrite to nitrous oxide for nitrogen and oxygen isotopic analysis in freshwater and seawater, *Analytical Chemistry*, 77(17), pp. 5589–5595. doi: 10.1021/ac050528s.
- Moss, B., Kosten, S., Meerhoff, M., Battarbee, R. W., Jeppesen, E., Mazzeo, N., Havens, K., Lacerot, G., Liu, Z., Meester, L. D., Paerl, H. and Scheffer, M. (2011). Allied attack: climate change and eutrophication, *Inland Waters*, 1(2), pp. 101–105. doi: 10.5268/IW-1.2.359.
- Piña-Ochoa, E. and Álvarez-Cobelas, M. (2006). Denitrification in aquatic environments: A cross-system analysis, *Biogeochemistry*, 81(1), pp. 111–130. doi: 10.1007/s10533-006-9033-7.
- Pjevac, P., Schaubberger, C., Poghosyan, L., Herbold, C. W., van Kessel, M. A. H. J., Daebeler, A., Steinberger, M., Jetten, M. S. M., Lücker, S., Wagner, M. and Daims, H. (2017). *amoA*-targeted polymerase chain reaction primers for the specific detection and quantification of comammox *Nitrospira* in the Environment, *Frontiers in Microbiology*, 8. doi: 10.3389/fmicb.2017.01508.
- Poth, M. and Focht, D. D. (1985). ¹⁵N kinetic analysis of N₂O production by *Nitrosomonas europaea*: an examination of nitrifier denitrification, *Applied and Environmental Microbiology*, 49(5), pp. 1134–1141.
- R Core Team. (2014). *R: A Language and Environment for Statistical Computing* Vienna, Austria: R Foundation for Statistical Computing. Available at: <http://www.R-project.org/>.
- Ravishankara, A. R., Daniel, J. S. and Portmann, R. W. (2009). Nitrous oxide (N₂O): The dominant ozone-depleting substance emitted in the 21st century, *Science*, 326(5949), pp. 123–125. doi: 10.1126/science.1176985.
- Rissanen, A. J., Tirola, M., Hietanen, S. and Ojala, A. (2013). Interlake variation and environmental controls of denitrification across different geographical scales, *Aquatic Microbial Ecology*, 69(1), pp. 1–16. doi: 10.3354/ame01619.
- Roland, F. A. E., Darchambeau, F., Borges, A. V., Morana, C., Brabandere, L. D., Thamdrup, B. and Crowe, S. A. (2018). Denitrification, anaerobic ammonium oxidation, and dissimilatory nitrate reduction to ammonium in an East African Great Lake (Lake Kivu), *Limnology and Oceanography*, 63(2), pp. 687–701. doi: 10.1002/lno.10660.
- Santoro, A. E., Buchwald, C., McIlvin, M. R. and Casciotti, K. L. (2011). Isotopic signature of N₂O produced by marine ammonia-oxidizing archaea, *Science*, 333(6047), pp. 1282–1285. doi: 10.1126/science.1208239.
- Santoro, A. E. and Casciotti, K. L. (2011). Enrichment and characterization of ammonia-oxidizing archaea from the open ocean: phylogeny, physiology and stable isotope fractionation, *The ISME Journal*, 5(11), pp. 1796–1808. doi: 10.1038/ismej.2011.58.
- Schilder, J., van Hardenbroek, M., Bodelier, P., Kirilova, E. P., Leuenberger, M., Lotter, A. F. and Heiri, O. (2017). Trophic state changes can affect the importance of methane-


- derived carbon in aquatic food webs, *Proceedings of the Royal Society B: Biological Sciences*, 284(1857), p. 20170278. doi: 10.1098/rspb.2017.0278.
- Schindler, D. W. (2012). The dilemma of controlling cultural eutrophication of lakes, *Proceedings of the Royal Society B: Biological Sciences*, 279(1746), pp. 4322–4333. doi: 10.1098/rspb.2012.1032.
- Seitzinger, S. P. (1988). Denitrification in freshwater and coastal marine ecosystems: Ecological and geochemical significance, *Limnology and Oceanography*, 33(4part2), pp. 702–724. doi: 10.4319/lo.1988.33.4part2.0702.
- Sigman, D. M., Casciotti, K. L., Andreani, M., Barford, C., Galanter, M. and Böhlke, J. K. (2001). A bacterial method for the nitrogen isotopic analysis of nitrate in seawater and freshwater, *Analytical Chemistry*, 73(17), pp. 4145–4153. doi: 10.1021/ac010088e.
- Sigman, D. M., Karsh, K. L. and Casciotti, K. L. (2009). Nitrogen isotopes in the ocean, in Steele, J. H. (ed.) *Encyclopedia of Ocean Sciences (Second Edition)*, pp. 40–54. doi: 10.1016/B978-012374473-9.00632-9.
- Small, G. E., Bullerjahn, G. S., Sterner, R. W., Beall, B. F. N., Brovold, S., Finlay, J. C., McKay, R. M. L. and Mukherjee, M. (2013). Rates and controls of nitrification in a large oligotrophic lake, *Limnology and Oceanography*, 58(1), pp. 276–286. doi: 10.4319/lo.2013.58.1.0276.
- Sugimoto, R., Kasai, A., Miyajima, T. and Fujita, K. (2008). Nitrogen isotopic discrimination by water column nitrification in a shallow coastal environment, *Journal of Oceanography*, 64(1), pp. 39–48. doi: 10.1007/s10872-008-0003-7.
- Trimmer, M., Chronopoulou, P.-M., Maanoja, S. T., Upstill-Goddard, R. C., Kitidis, V. and Purdy, K. J. (2016). Nitrous oxide as a function of oxygen and archaeal gene abundance in the North Pacific, *Nature Communications*, 7(1), pp. 1–10. doi: 10.1038/ncomms13451.
- Vajjala, N., Martens-Habbena, W., Sayavedra-Soto, L. A., Schauer, A., Bottomley, P. J., Stahl, D. A. and Arp, D. J. (2013). Hydroxylamine as an intermediate in ammonia oxidation by globally abundant marine archaea, *Proceedings of the National Academy of Sciences*, 110(3), pp. 1006–1011. doi: 10.1073/pnas.1214272110.
- Valiente, N., Carrey, R., Otero, N., Soler, A., Sanz, D., Muñoz-Martín, A., Jirsa, F., Wanek, W. and Gómez-Alday, J. J. (2018). A multi-isotopic approach to investigate the influence of land use on nitrate removal in a highly saline lake-aquifer system, *The Science of the Total Environment*, 631–632, pp. 649–659. doi: 10.1016/j.scitotenv.2018.03.059.
- Ward, B. B., Tuit, C. B., Jayakumar, A., Rich, J. J., Moffett, J. and Naqvi, S. W. A. (2008). Organic carbon, and not copper, controls denitrification in oxygen minimum zones of the ocean, *Deep Sea Research Part I: Oceanographic Research Papers*, 55(12), pp. 1672–1683. doi: 10.1016/j.dsr.2008.07.005.
- Weigand, M. A., Foriel, J., Barnett, B., Oleynik, S. and Sigman, D. M. (2016). Updates to instrumentation and protocols for isotopic analysis of nitrate by the denitrifier method, *Rapid Communications in Mass Spectrometry*, 30(12), pp. 1365–1383. doi: 10.1002/rcm.7570.

- Wenk, C. B., Brees, J., Zopfi, J., Veronesi, M., Bourbonnais, A., Schubert, C. J., Niemann, H. and Lehmann, M. F. (2013). Anaerobic ammonium oxidation (anammox) bacteria and sulfide-dependent denitrifiers coexist in the water column of a meromictic south-alpine lake, *Limnology and Oceanography*, 58(1), pp. 1–12. doi: 10.4319/lo.2013.58.1.0001.
- Wenk, C. B., Zopfi, J., Gardner, W. S., McCarthy, M. J., Niemann, H., Veronesi, M. and Lehmann, M. F. (2014). Partitioning between benthic and pelagic nitrate reduction in the Lake Lugano south basin, *Limnology and Oceanography*, 59(4), pp. 1421–1433. doi: 10.4319/lo.2014.59.4.1421.
- West, W. E., Creamer, K. P. and Jones, S. E. (2016). Productivity and depth regulate lake contributions to atmospheric methane: Lake productivity fuels methane emissions, *Limnology and Oceanography*, 61(S1), pp. S51–S61. doi: 10.1002/lno.10247.
- Wickham, H. and Bryan, J. (2019). *readxl: Read Excel Files*. Available at: <https://CRAN.R-project.org/package=readxl>.
- Wilson, S. T., del Valle, D. A., Segura-Noguera, M. and Karl, D. M. (2014). A role for nitrite in the production of nitrous oxide in the lower euphotic zone of the oligotrophic North Pacific Ocean, *Deep Sea Research Part I: Oceanographic Research Papers*, 85, pp. 47–55. doi: 10.1016/j.dsr.2013.11.008.
- Wood, S. N. (2011). Fast stable restricted maximum likelihood and marginal likelihood estimation of semiparametric generalized linear models, *Journal of the Royal Statistical Society: Series B (Statistical Methodology)*, 73(1), pp. 3–36. doi: 10.1111/j.1467-9868.2010.00749.x.
- Xia, X., Jia, Z., Liu, T., Zhang, S. and Zhang, L. (2017). Coupled nitrification-denitrification caused by suspended sediment (SPS) in rivers: Importance of SPS size and composition, *Environmental Science & Technology*, 51(1), pp. 212–221. doi: 10.1021/acs.est.6b03886.
- Xia, X. H., Yang, Z. F., Huang, G. H., Zhang, X. Q., Yu, H. and Rong, X. (2004). Nitrification in natural waters with high suspended-solid content—A study for the Yellow River, *Chemosphere*, 57(8), pp. 1017–1029. doi: 10.1016/j.chemosphere.2004.08.027.
- Xiong, Z. Q., Khalil, M. a. K., Xing, G., Shearer, M. J. and Butenhoff, C. (2009). Isotopic signatures and concentration profiles of nitrous oxide in a rice-based ecosystem during the drained crop-growing season, *Journal of Geophysical Research: Biogeosciences*, 114(G2). doi: 10.1029/2008JG000827.
- Yoshida, N. (1988). ¹⁵N-depleted N₂O as a product of nitrification, *Nature*, 335(6190), pp. 528–529. doi: 10.1038/335528a0.
- Zhou, S., Zhang, Y., Huang, T., Liu, Y., Fang, K. and Zhang, C. (2019a). Microbial aerobic denitrification dominates nitrogen losses from reservoir ecosystem in the spring of Zhoucun reservoir, *Science of The Total Environment*, 651, pp. 998–1010. doi: 10.1016/j.scitotenv.2018.09.160.
- Zhou, Y., Xu, X., Han, R., Li, L., Feng, Y., Yeerken, S., Song, K. and Wang, Q. (2019b). Suspended particles potentially enhance nitrous oxide (N₂O) emissions in the oxic estuarine waters of eutrophic lakes: Field and experimental evidence, *Environmental Pollution*, 252, pp. 1225–1234. doi: 10.1016/j.envpol.2019.06.076.

Chapter 7 | N₂O production in eutrophic reservoirs

Zhu, W., Wang, C., Hill, J., He, Y., Tao, B., Mao, Z. and Wu, W. (2018). A missing link in the estuarine nitrogen cycle?: Coupled nitrification-denitrification mediated by suspended particulate matter, *Scientific Reports*, 8(1), pp. 1–10. doi: 10.1038/s41598-018-20688-4.

Zumft, W. G. (1997). Cell biology and molecular basis of denitrification., *Microbiology and Molecular Biology Reviews*, 61(4), pp. 533–616.



Chapter 8: General Discussion

Chapter 8 | General Discussion

Chapter 8: General Discussion

The Supplementary Material is available in Appendix 8

This dissertation presents the first inventory of direct and simultaneous fluxes of the greenhouse gases (CO₂, CH₄, and N₂O) in reservoirs located in the Mediterranean biome. In this region, reservoirs are the preponderant aquatic ecosystems, but their GHG fluxes had been seldom measured (Deemer *et al.*, 2016). We presented the variability and the environmental drivers of these fluxes in twelve reservoirs covering a broad spectrum of lithology, land-use, and anthropic influence during the stratification and mixing period in Chapter 3. We also described the daily patterns of CO₂, CH₄, and N₂O in two eutrophic reservoirs with contrasted morphometries (i.e., Cubillas and Iznájar) in Chapter 4. Next, we explored the drivers of dissolved CH₄ and N₂O in the water column of the twelve reservoirs during both periods in Chapters 5 and 6, respectively. Besides the GHG fluxes and dissolved concentrations, we determined the GHG production in the water column of two reservoirs (i.e., Cubillas and Iznájar) in Chapter 4 and Chapter 7. We measured the abiotic GHG photoproduction in Chapter 4, and, for the first time, we demonstrated the N₂O photoproduction. We also measured the microbial N₂O production in the water column of these two reservoirs during the stratification. In the following subsections, we connect all the results of the different chapters to provide a holistic view of the regulation GHG emissions from reservoirs in the Mediterranean biome.

8. 1. The C footprint of reservoirs

Recent studies have documented the role of the reservoirs as a globally significant GHG source (Barros *et al.*, 2011; Deemer *et al.*, 2016). In this Ph.D. work, we measured the fluxes of CO₂, CH₄, and N₂O in twelve reservoirs during the summer stratification and the winter mixing in southeastern Spain and their environmental drivers. We found that some reservoirs were sinks (influx rates < 0), and other were sources (outflux rates > 0) for CO₂ and N₂O fluxes, but all reservoirs were CH₄ sources (León-Palmero *et al.*, 2020a). To determine the net carbon footprint considering these three GHGs, we converted the CH₄ and N₂O fluxes in CO₂ equivalents using their warming potentials (IPCC, 2013) and summed the CO₂, CH₄, and N₂O fluxes in this unit (Figure 8.1 and Supplementary Table 8.1). We observed that most of the study reservoirs had a positive C footprint in the study time (i.e., acted as GHG sources). The concept of C footprint is addressed in more detail in the Box 8.1.

We only found that the Jándula reservoir in both periods and the Rules reservoir during the stratification had a negative C footprint in the study time (i.e., acted as GHG sinks at this time scale). In these cases, the CO₂ inflow overcompensated the CH₄ emissions. The N₂O inflow partly compensated the emissions of CO₂ and CH₄, as shown in Figure 8.1. In the San Clemente reservoir, we observed that the sink produced by the N₂O inflow was almost the same magnitude of CO₂ equivalents that the CH₄ emissions. The Jándula reservoir was the only net sink. The Rules reservoir was a net GHG source because the emission during the mixing period was higher than the sink during the stratification period. Our study improves the global dataset for GHG fluxes by including the fluxes from reservoirs in the Mediterranean biome. We also emphasized the need of studying the three main greenhouse gases to determine the C footprint of existing reservoirs.

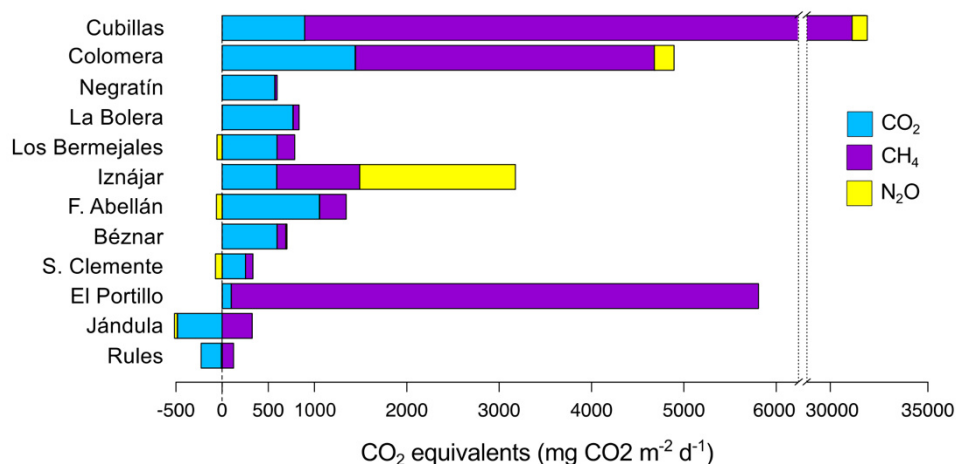
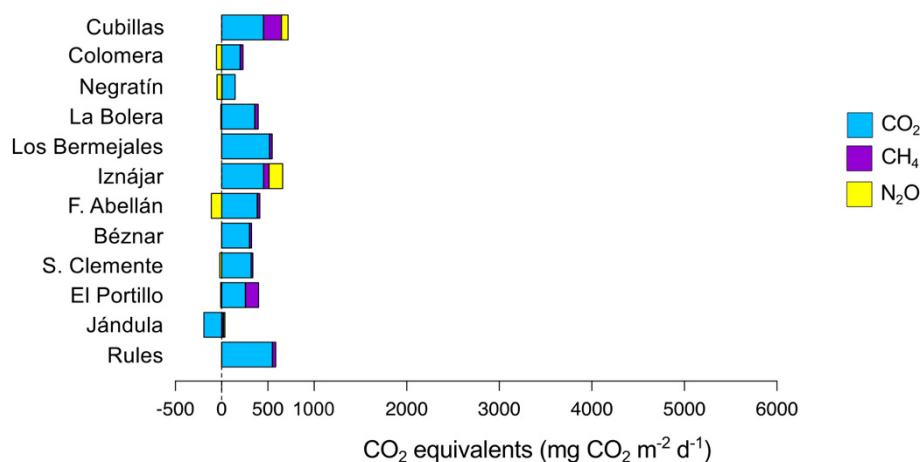
a Fluxes of GHG in CO₂ equivalents during the stratification period**b** Fluxes of GHG in CO₂ equivalents during the mixing period

Figure 8.1. The study reservoirs act as GHG sinks (<0 values) or sources (>0 values). Fluxes of CO₂, CH₄ and N₂O expressed in CO₂ equivalents (mg CO₂ m⁻² d⁻¹) during the stratification (a) and mixing (b) periods. Note the x-axis has a break in the panel (a). The data are provided in Supplementary Table 8.1. The CO₂ equivalents were calculated by multiplying the mass-based flux by the 100-year global warming potential of each gas (1 for CO₂, 34 for CH₄ and 298 for N₂O) (IPCC, 2013).

Here, we have presented the direct fluxes of CO₂, CH₄, and N₂O during the stratification and mixing periods. In Chapters 5 and 6, we show that some reservoirs presented relevant accumulations of DIC, CH₄, and N₂O in the hypolimnion. During the stratification period, hypoxic waters and sediments are important sites for the production of CH₄ and N₂O. A fraction of the GHG produced in the deep waters and sediments moves upwards by diffusion and ebullition, but other fraction remains accumulated in the hypolimnion (Figure 8.2). The storage of the GHG in deep waters is especially significant in deep reservoirs with a robust thermal

stratification, which makes it difficult the GHG diffusion. For this reason, the mean depth of reservoirs has a significant role in GHG emissions, as discussed in Chapters 3, 5, and 7. Besides, CH_4 can be oxidized to CO_2 by methane-oxidizing microorganisms, and N_2O can be reduced to N_2 by denitrifiers if the proper conditions are present during the storage time. These GHGs stored in deep waters may be emitted to the atmosphere via other pathways, such as the autumn overturn, or by degassing at the dam outflow or further downstream (i.e., indirect emissions in Figure 8.2). These indirect emissions should be addressed to account for the total C footprint of reservoirs.

During the autumn overturn, the dissolved gases stored in deep waters are redistributed over the water column, likely resulting in high diffusive fluxes to the atmosphere. Previous works detected higher fluxes of CO_2 and CH_4 during the overturn period, but they also demonstrated that most of the accumulated CH_4 was oxidized in the water column during the overturn in lakes (Kankaala *et al.*, 2007; López Bellido *et al.*, 2009; Schubert *et al.*, 2012; Encinas Fernández *et al.*, 2014). However, less is known about the N_2O fluxes during the overturn. We hypothesize that the reservoirs may have positive or negative fluxes of N_2O during the overturn, depending on the N_2O saturation found in the water column. The reservoirs with large accumulations of N_2O in the hypolimnion may increase their emissions during the autumn overturn. For instance, the N_2O supersaturation in the Iznájar hypolimnion during the stratification reached up to 1449 % (Figure 6.2a), which will likely produce a large emission of N_2O . In contrast, we observed that the water column of other reservoirs presented undersaturation and supersaturation in N_2O at different depths. For instance, the percentage of N_2O saturation in the water column of the San Clemente reservoir varied between 37 % (i.e., in the hypolimnion) and 244 % (in the thermocline) (Figure 6.1a). Therefore, the overturn will cause the N_2O mixing of the supersaturated layers (epilimnion and thermocline) and the undersaturated layers (hypolimnion), likely decreasing the N_2O emissions during this period. These indirect emissions will only be well quantified through studies with high temporal resolution.

Another source of indirect GHG emissions from reservoirs is the gas release immediately below the turbines and emissions further downstream. Unlike natural

lakes, reservoirs have water intakes that connect the deep section of the water column and the downstream river, which provides water to the turbines to generate electricity (Figure 8.2). The turbulence and reduced pressure when the GHGs-rich water passes through the turbines and the pipes cause the degasification and direct emission of GHG to the atmosphere at the dam outflow (i.e., degassing emissions) or the emission from the river surface below (i.e., downstream emission). Previous works have demonstrated that degassing and downstream emissions represent a relatively small fraction of the CO₂ emissions (Teodoru *et al.*, 2012), but a significant fraction for CH₄ emissions (Abril *et al.*, 2005; Kemenes *et al.*, 2007; Diem *et al.*, 2012; Teodoru *et al.*, 2012; Maeck *et al.*, 2013; Okuku *et al.*, 2019) and N₂O emissions (Okuku *et al.*, 2019). Overall, a better knowledge of the direct and indirect GHG emissions from reservoirs must accurately assess the C footprint of reservoirs and hydropower.

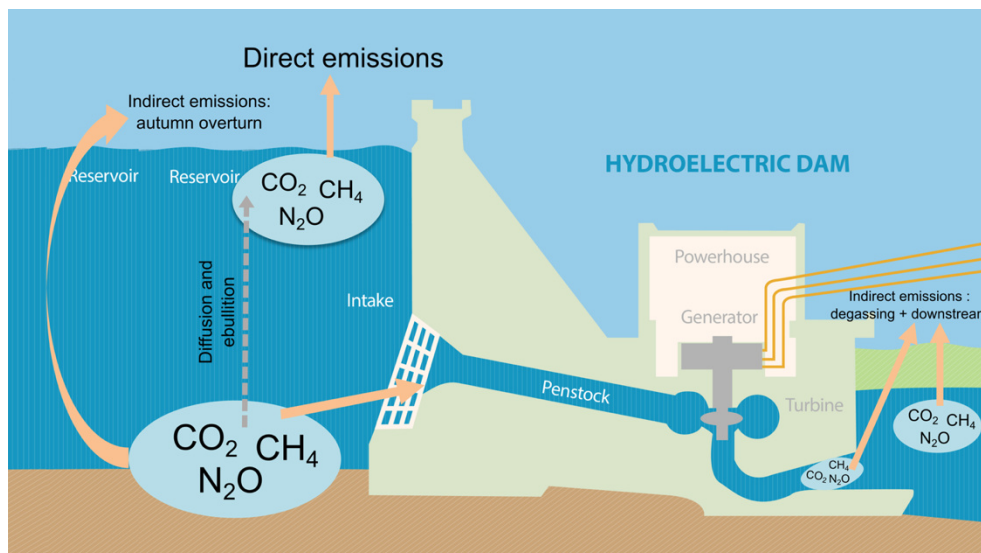


Figure 8.2. Direct and indirect emissions of GHG in a hydropower reservoir.

On the other hand, it is also necessary to understand the environmental drivers of the GHG emissions in reservoirs to improve global GHG estimations and reduce and prevent the impact of the existing and projected reservoirs. Previous studies pointed out that GHG emissions were related to the age of the reservoirs (Abril *et al.*, 2005; Barros *et al.*, 2011; Teodoru *et al.*, 2012). Reservoirs may present the highest emissions of CO₂ and CH₄ during the early years after the flooding event, due to the decomposition of the flooded vegetation and soil organic matter,

but C emissions would stabilize after this first stage (Abril *et al.*, 2005; Tremblay *et al.*, 2005; Barros *et al.*, 2011). In contrast, Teodoru *et al.* (2012) found the highest emissions of CO₂, but the lower CH₄ emissions during the first years after the flooding event. To test the effect of the age of the reservoirs in their emissions we selected twelve reservoirs that covered a wide range of ages, from 14 years (i.e., Rules reservoir) to 85 years (i.e., Jándula). We did not detect significant relationships between the CO₂, CH₄, or N₂O fluxes in the study reservoirs and the age of the reservoirs (Supplementary Figure 8.1). We also tested if the decomposition of the flooded vegetation and organic carbon in soils affected the concentration of organic carbon and the GHG concentration in the bottom waters of the reservoirs. We found that organic carbon concentration (i.e., DOC) increased with the age of the reservoir (Supplementary Figure 8.2a), but the age did not affect the concentration of DIC, dissolved CH₄, or dissolved N₂O in bottom waters (Supplementary Figure 8.2b, c, d). The reservoirs studied in this dissertation are located in the stabilization region described by Teodoru *et al.* (2012) (i.e., five years from the flooding event, red area in Figure 8.3), and that may explain the absence of relationship between emissions and the age of the reservoirs. Regarding the flood event, it is important to notice that different landscapes contain different types of vegetation and amounts of organic carbon stored in soils, and that will affect the GHG emissions during the first years. For instance, a reservoir that flood peatlands will presumably emit more C to the atmosphere, because these ecosystems store large amounts of organic carbon in the peat (Kelly *et al.*, 1997; Louis *et al.*, 2000).

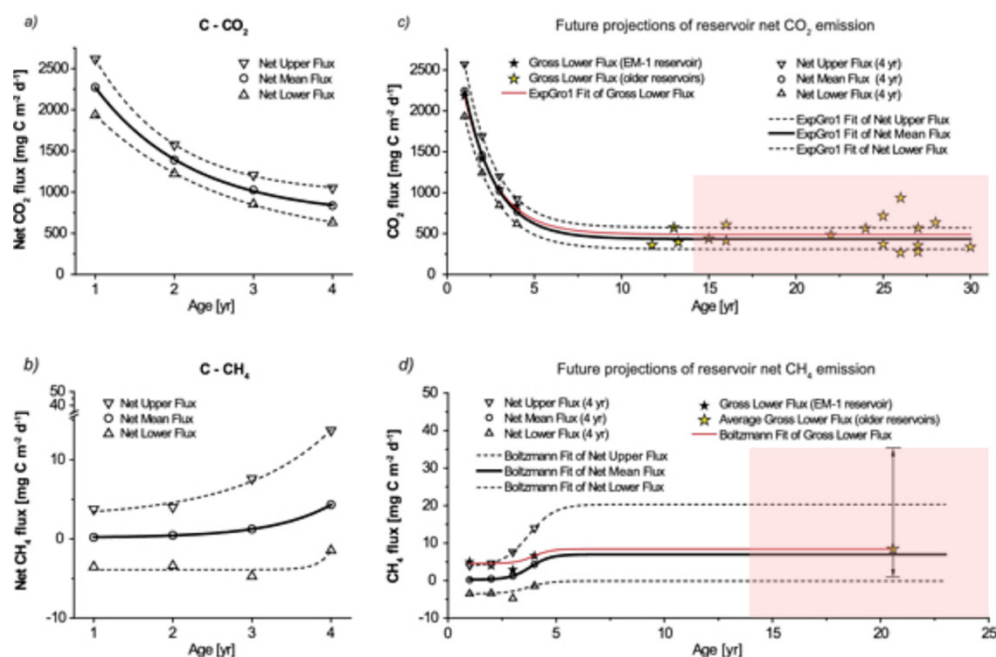


Figure 8.3. Emissions of CO₂ and CH₄ from a reservoir at different ages. Range variability (upper, mean and lower) of (a) net CO₂ and (b) net CH₄ fluxes for a reservoir calculated over the initial four years' period; and future projection of (c) net CO₂ and (d) net CH₄ emissions over the expected life span of the reservoir (100 years). The red shaded areas represent the age of the study reservoirs (14 – 85 years). Modified from (Teodoru *et al.*, 2012).

The watershed lithology and land-use determined the CO₂ and N₂O fluxes in the study reservoirs, respectively, while the reservoir water temperature and mean depth explained the CH₄ emissions (León-Palmero *et al.*, 2020a). In the case of the reservoirs acting as sinks at any period, we found that the non-calcareous rocks covered up to 73 % of the Rules watershed and the 91 % of the Jándula watershed that determined the CO₂ inflow. Both reservoirs had low CH₄ and N₂O fluxes because they were deep systems with a mean depth higher than 35 m, and agricultural or urban areas did not dominated the watersheds. Agricultural and urban areas increased the nitrogen and phosphorus concentration significantly in the study reservoirs (León-Palmero *et al.*, 2020a, and Appendix 2), and that promoted the eutrophication, and the production of CH₄ and N₂O, as we showed in the Chapters 5, 6, and 7. Therefore, we suggest that mitigation measures to reduce the GHG emissions in the already constructed reservoirs could be related to the control of the nutrient inputs from the watersheds (Deemer *et al.*, 2016; Beaulieu *et al.*, 2019; León-Palmero *et al.*, 2020a). In addition, for the construction of the

more than 3500 hydroelectric dams planned globally (Zarfl *et al.*, 2015), we advocate to consider the carbon intensity of hydropower (i.e., GHG emissions per unit of electricity generated), and the strategic dam planning. Future reservoirs should consider that siliceous bedrocks, forestal landscapes, and deep canyons could minimize GHG emissions and C footprints. Almeida *et al.* (2019) also suggested that the strategic dam planning would significantly reduce the GHG emissions of new reservoirs in the Amazon basin, where hundreds of dams have been planned for hydropower production. The GHG emissions per unit of electricity generated by hydropower may be comparable with solar and wind energy or even exceed the fossil-fuel power plants depending on the construction sites (Almeida *et al.*, 2019).

Box 8.1. The Carbon Footprint Concept

There are different definitions of carbon footprint that may be applied to reservoirs. In a limnological context, the net reservoir carbon footprint has been understood as the difference of the GHG emissions from the pre-construction and post-construction conditions of a reservoir in a 100 years lifecycle (see for instance (The UNESCO/IHA Greenhouse Gas Emissions from Freshwater Reservoirs Research Project, 2010; Teodoru *et al.*, 2012; Prairie *et al.*, 2018). However, in a more general and socio-economical context, carbon footprint has also been defined as the amount of GHG emissions in terms of CO₂ equivalent (CO₂-eq) (see, for instance, <https://www.footprintnetwork.org/our-work/climate-change/>; (Deemer *et al.*, 2016). In this last meaning, the carbon footprint is the total GHG emissions caused directly and indirectly by an individual, organization, event or product, and is expressed as a carbon dioxide equivalent (CO₂e). A carbon footprint accounts for all six Kyoto GHG emissions: the primary emissions of CO₂, CH₄, and N₂O and the emissions of hydrofluorocarbons (HFCs), perfluorocarbons (PFCs), and sulfur hexafluoride (SF₆). During this study, we considered the second definition, and we addressed the C footprint of reservoirs as the sum of the emissions of CO₂, CH₄, and N₂O.

8. 2. Are the GHG fluxes in Chapter 3 representative on a daily scale?

The GHG fluxes presented in Chapter 3 (León-Palmero *et al.*, 2020a) are based on daytime measurements, from 10 to 16 hours (local time). However, in Chapter 4, we demonstrated that GHG emissions had a large daily variability being higher during daytime than nighttime. Then, these fluxes could have been an overestimation because they were taken exclusively during the daytime. For this reason, we compared if the measurements taken from 10 to 16 h local time (which correspond to the 8 to 14 h solar time in summer) were significantly different or not from the GHG fluxes measured during the complete daily cycle in the Cubillas reservoir in the summers of 2016 and 2018 and the Iznájar reservoir in the summer of 2018. We extracted the GHG fluxes in the 8 to 14 h (solar time) period from the daily datasets of Chapter 4, and we compared these fluxes with the GHG fluxes from the entire daily period. We did not find significant differences in the GHG fluxes (Figure 8.4 and Supplementary Table 8.2). Therefore, we can assume that the average of the GHG fluxes obtained from 8 to 14 h is not significantly different from the average fluxes measured during the daily cycle. Therefore, the GHG fluxes presented in (León-Palmero *et al.*, 2020a) were not significantly overestimated. However, future studies should consider that time interval is an accurate proxy for the measurements of CO₂, N₂O, and CH₄ fluxes in reservoirs.

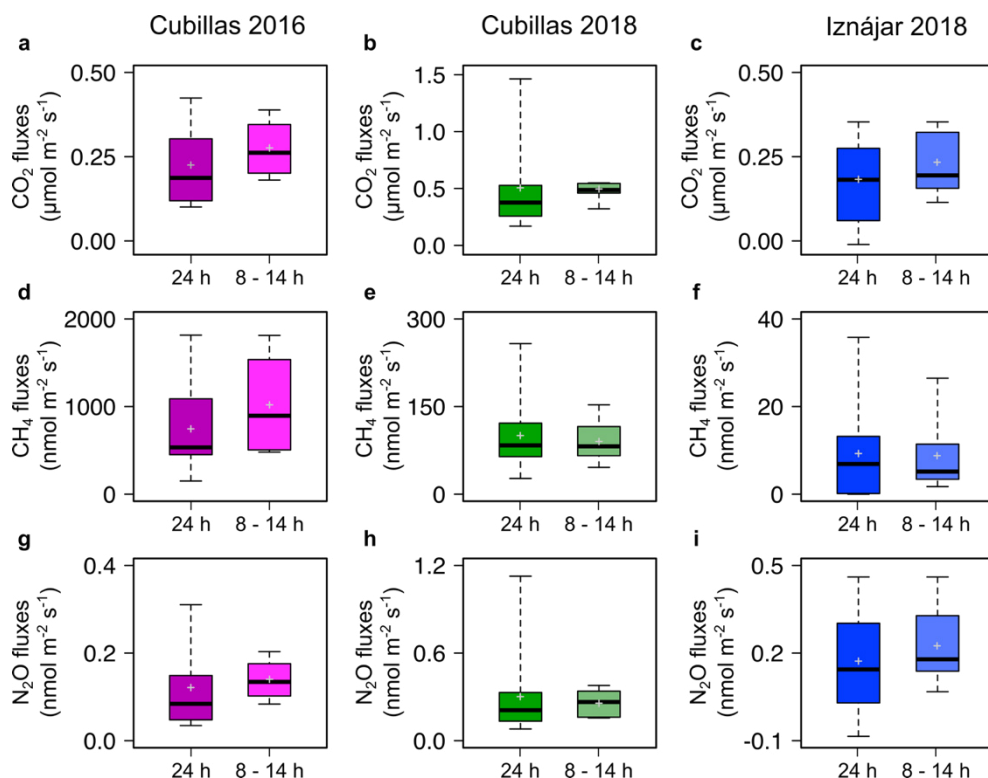


Figure 8.4. Median (line), 25 - 75 % percentiles (box) and max-min values (whisker) of GHG fluxes using the entire daily cycle measurements, and only the interval from 8 to 14 h solar time. The grey crosses stand for the mean fluxes. (a, b, c) CO₂ fluxes, (d, e, f) CH₄ fluxes, and (g, h, i) N₂O fluxes. In a, d, and g are the GHG fluxes in the Cubillas reservoir in 2016, in b, e, and h are the GHG fluxes in the Cubillas reservoir in 2018, and in c, f, and i are the GHG fluxes in the Iznájar reservoir in 2018. Note the different scales. We used the t-test (i.e., normal data) or Wilcoxon signed-rank test (i.e., non normal data) for the comparison between the time periods. Statistical details are provided in Supplementary Table 8.2.

8. 3. Change of drivers depending on scale

To understand ecological phenomena is necessary to observe their behavior across multiple spatial and temporal scales (Estes *et al.*, 2018). Estes *et al.* (2018) stated that the scale at which ecosystems are observed shapes our understanding of their functioning, and different ecological patterns can emerge at different scales. Consistent with this statement, we found different environmental drivers in GHG fluxes, depending on the study scale. The wind speed and water temperature were the main drivers of GHG fluxes at daily scale (Chapter 4). The wind-derived turbulence promotes the emission of GHGs, but it does not promote the GHGs production, while the water temperature can promote both the emission (reducing

gas solubility) and biological production. The explanatory power of a parameter depends on its variability range. For instance, the water temperature was the main driver of GHG fluxes when the wind-speed variability decreased in the Iznájar reservoir. We also detected that the diffusive fluxes of CO₂, CH₄, and N₂O were significantly correlated among them on the daily scale because wind speed and water temperature promoted the emission of the three gases (Table 4.1).

On the other hand, in Chapter 3 we studied the reservoir variability in the CO₂, CH₄, and N₂O fluxes of and between the stratification and mixing periods. We found that the environmental drivers of the CO₂, CH₄, and N₂O fluxes were different for each corresponding GHG. Therefore, the three GHG fluxes were not tightly coupled as were at the daily scale (Supplementary Table 8.3). We only found a significant correlation between the fluxes of CO₂ and CH₄ ($n = 21$, p -value < 0.05) when we considered the emissions (i.e., fluxes > 0) instead of all the fluxes. In (León-Palmero *et al.*, 2020a), we found that the respiration rate was the second driver of the CO₂ fluxes in the GAM model (Figure 3.3), and the respiration rate was significantly related to the concentration of chlorophyll-*a* in surface waters (Figure 3.3e). We also showed that the surface Chl-*a* was significantly related to the surface concentration of CH₄ (Figure 3.4e), which determined the flux of CH₄ to the atmosphere (Figure 3.4d). Therefore, that may be the link behind the correlation between the emissions of CO₂ and CH₄. The discussion about the variability in the GHG fluxes and concentrations at different scales has been extended in the supplementary material.

8. 4. Comparison between microbial production and photoproduction of N₂O

Nitrous oxide is produced by microbial and abiotic reactions. In Chapter 7 we measured the production of N₂O from ¹⁵N-NH₄⁺ and from ¹⁵N-NO₃⁻ in the Cubillas and Iznájar reservoirs at the beginning (July) and end (September) of the stratification period at 3 different depths. In addition, in Chapter 4 we measured the abiotic production of N₂O induced by sunlight (i.e., photoproduction). This new pathway was demonstrated in Cubillas and Iznájar reservoirs, in the experiments performed in June 2018, and in September 2018. Here, we compare the rates of microbial production of N₂O, and the rates of N₂O photoproduction (Table 8.1).

Note that the microbial N₂O production presented in Table 8.1 as been calculated as the sum of the production of N₂O from ammonia and from nitrate, but in the epilimnion we only included the N₂O production from ammonia. In addition, microbial N₂O production can also occur from nitrite. Therefore, as discussed in Chapter 7, the microbial N₂O production rate is underestimated. It is also important to note that the microbial production occurs along the water column increasing with depth, while the photoproduction of N₂O only occurs in the surface waters, where the UV light intensity is high enough.

We found that the rates of N₂O photoproduction were higher than the microbial production in the surface waters of both reservoirs. The N₂O photoproduction was so high that it even exceeded microbial production at other layers such as oxycline or hypolimnion in Cubillas. These results demonstrate that the N₂O photoproduction, although only occurs on the surface waters, can contribute significantly to the N₂O total production, and consequently to N₂O fluxes.

Table 8.1. Biotic and photoproduction in the surface waters of Cubillas and Iznájar reservoirs. The experiments were performed in June, July, and September 2018.

Microbial production			Photoproduction	
Reservoir	Date	N ₂ O production (nmol N-N ₂ O L ⁻¹ d ⁻¹)	Date	N ₂ O production (nmol N-N ₂ O L ⁻¹ d ⁻¹)
Cubillas	July 2018	Epilimnion: 2.2 Oxycline: 8.3 Bottom: 28.3	June 2018 (250 mL vials)	2.4 – 2.7
	September 2018	Epilimnion: 0.3 Bottom: 18.8	September 2018 (100 mL vials)	32.9 - 65.6
Iznájar	July 2018	Epilimnion: 1.7 Oxycline: 4.4 Hypolimnion: 4.1		
	September 2018	Epilimnion: 0.1 Oxycline: 118.9 Hypolimnion: 74.9	September 2018 (100 mL vials)	24.8 - 43.9

8. 5. Connecting eutrophication and GHG emissions

Almost 40 years ago, Margalef (1983) explained that inland waters are forced by the terrestrial ecosystems in their watersheds receiving inorganic and organic carbon, major nutrients (N and P), and micronutrients. The eutrophication of inland waters is a response to this external forcing, and limnologists have extensively studied it. Eutrophication is a common phenomenon occurring in inland and coastal waters globally, and it is characterized by the excessive plant and algal growth (Chislock *et al.*, 2013). Eutrophication occurs naturally when sediments fill a lake over centuries (Carpenter, 1981), but also occur when human activities, such as agriculture, industry, and sewage disposal, increase the loading of limiting nutrients into inland waters, and, in this case, is termed cultural eutrophication (Carpenter *et al.*, 1998). Phosphorus (P) is often the limiting nutrient in inland waters (Schindler, 1977), while nitrogen (N) is more commonly the limiting nutrient in estuarine and coastal marine waters (Ryther and Dunstan, 1971; Nixon, 1995). Human activities increase the loading of both nutrients, but P is retained in the soils more efficiently than N during runoff (Appendix 2). Some consequences of cultural eutrophication include cyanobacteria blooms, hypoxia events, and the degradation of drinking water supplies, fisheries, and recreational areas (Chislock *et al.*, 2013).

In response to this forcing caused by the anthropogenic N and P inputs, inland waters modify their functioning by accelerating some processes and displacing a fraction of the materials to their boundaries: the atmosphere and the sediments. The system deviates from its previous situation less than expected, thanks to several regulation mechanisms (Margalef, 1983). Here we propose that the production and emission of CO₂, CH₄, and N₂O is also an important part of the response of inland waters to this external forcing. We show this response in Figure 8.5, which is inspired by the model proposed by Margalef for perturbed ecosystems in his book “Limnología” (Margalef, 1983).

The N and P loadings from the watershed produce the eutrophication and the increase in the gross primary production (GPP) in inland waters to the limit defined by the light absorption of chlorophyll. The increase in GPP incorporates CO₂ into the system (i.e., organic C) and increases the production of CH₄ in oxic waters, which is linked to the photoautotrophic carbon fixation of algae and Cyanobacteria

(Lenhart *et al.*, 2016; Klintzsch *et al.*, 2019; Bižić *et al.*, 2020; Hartmann *et al.*, 2020; León-Palmero *et al.*, 2020b). Consequently, the concomitant CO₂ production by respiration (i.e., organic C mineralization) also increases. In the study systems, the respiration rate during the stratification period was a function of the chlorophyll-*a* concentration in surface waters, and the respiration rate was one of the variables driving the CO₂ fluxes (León-Palmero *et al.*, 2020a).

Margalef (1983) also explained that a perturbed lake or reservoir removes a C and P fraction to the sediment, and an O and N fraction to the atmosphere. A significant fraction of the organic matter produced in the photic zone follows the sediment's detrital pathway as particulate C, N, and P. The microbial community will partly degrade these organic C, and another part will be sequestered by sediment burial. In this study, we demonstrated that the production that follows the detrital pathway, which was accounted as cumulative Chl-*a*, promoted the sediments CH₄ production (León-Palmero *et al.*, 2020b), and the N₂O production in the water column (Chapter 6). This autochthonous production stimulated the production of GHG more than the allochthonous inputs. Recent studies showed that the global C-sequestration in lakes and reservoirs sediments has increased due to higher nutrient availability (Anderson *et al.*, 2020). In addition, inland waters also receive significant inputs of inorganic C from their watersheds, and these inputs can determine the emissions of CO₂ (León-Palmero *et al.*, 2020a). Thus, the increase in erosion in the watershed may increase of CO₂ emissions. Overall, the CO₂ and CH₄ emissions in inland waters determine the release of an important fraction of C to the atmosphere, while the organic C burial determines the movement to the sediment. The excess of P is also displaced to the sediment that acts as a P trap. A fraction of P can return to the water column at reductive conditions (i.e., anoxic conditions). The concentration of P in water depends on the solubility of the Ca and Fe compounds.

Margalef (1983) explained that an O and N fraction is transferred to the atmosphere when the system is forced. The decomposition of the allochthonous and autochthonous organic matter consumes the oxygen in the water column and produces hypoxia events during the stratification period. These hypoxia events promote denitrification and archaeal methanogenesis, with the subsequent

formation of N_2O , CH_4 , and CO_2 (denitrification and methanogenesis also produce CO_2). Inland waters can obtain the N through N_2 fixation from the atmosphere, which is the biggest pool of N. At low N concentration, denitrification can act as an N_2O sink, and that reduces N_2O to N_2 , that is emitted to the atmosphere. However, denitrification may also act as a source of N_2O at high N concentrations. Inland waters derive the excess of nitrogen to the atmosphere by producing high amounts of N_2O and N_2 . It might be an equilibrium concentration of N for each system, which should depend on the physico-chemical characteristics of the water, similarly to P concentration. In contrast to P, the main N movement is between the water column and the atmosphere, instead of the sediment. Therefore, denitrification acts as a regulation mechanism to release the excess of N back into the atmosphere, from where it was extracted first of all. Globally, half of the global terrestrial denitrification occurs in inland waters, with most of the nitrogen that is denitrified coming from land (Seitzinger *et al.*, 2006).

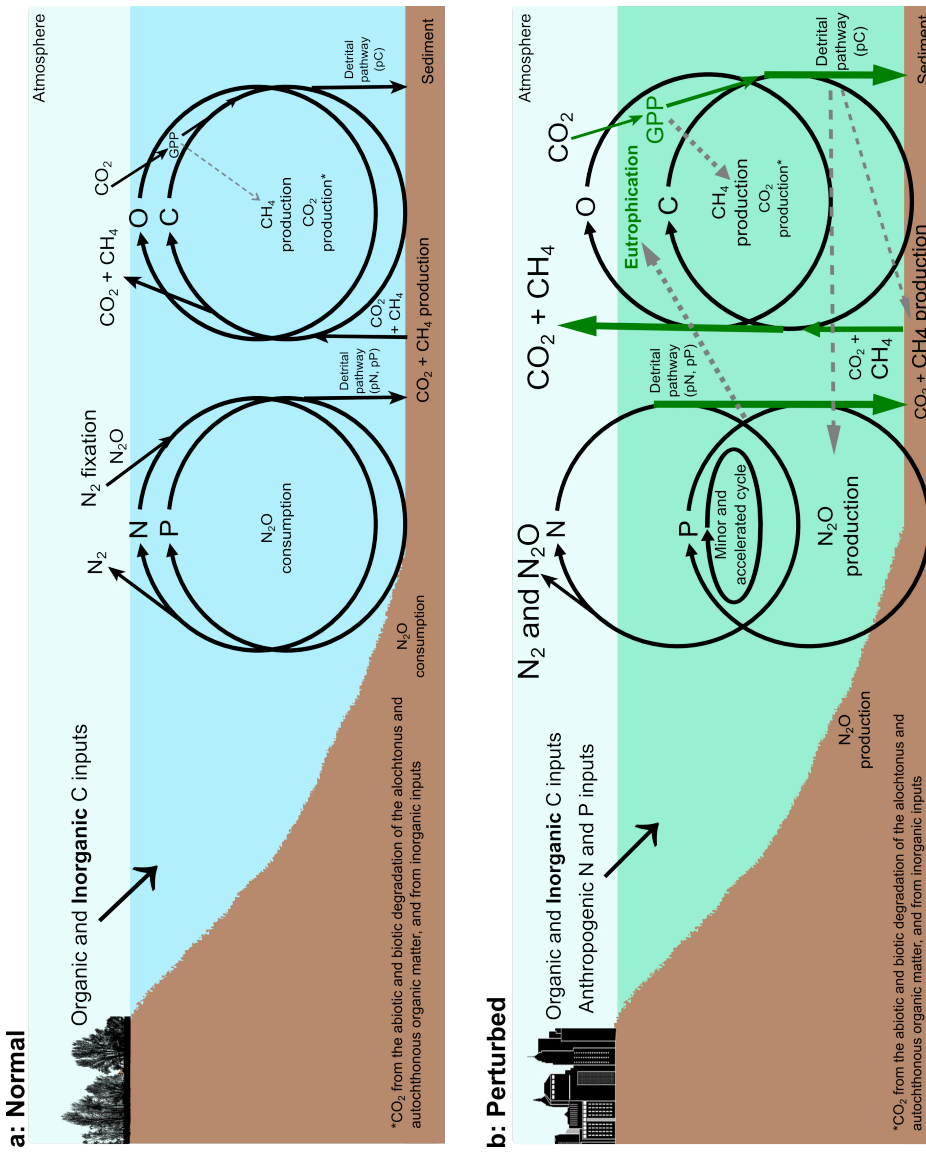


Figure 8.5. Nitrogen (N), phosphorus (P), carbon (C), and oxygen (O) cycles in an unperturbed (normal) (a), and in a perturbed (b) lake or reservoir. Inspired in the model of Margalef (1983).

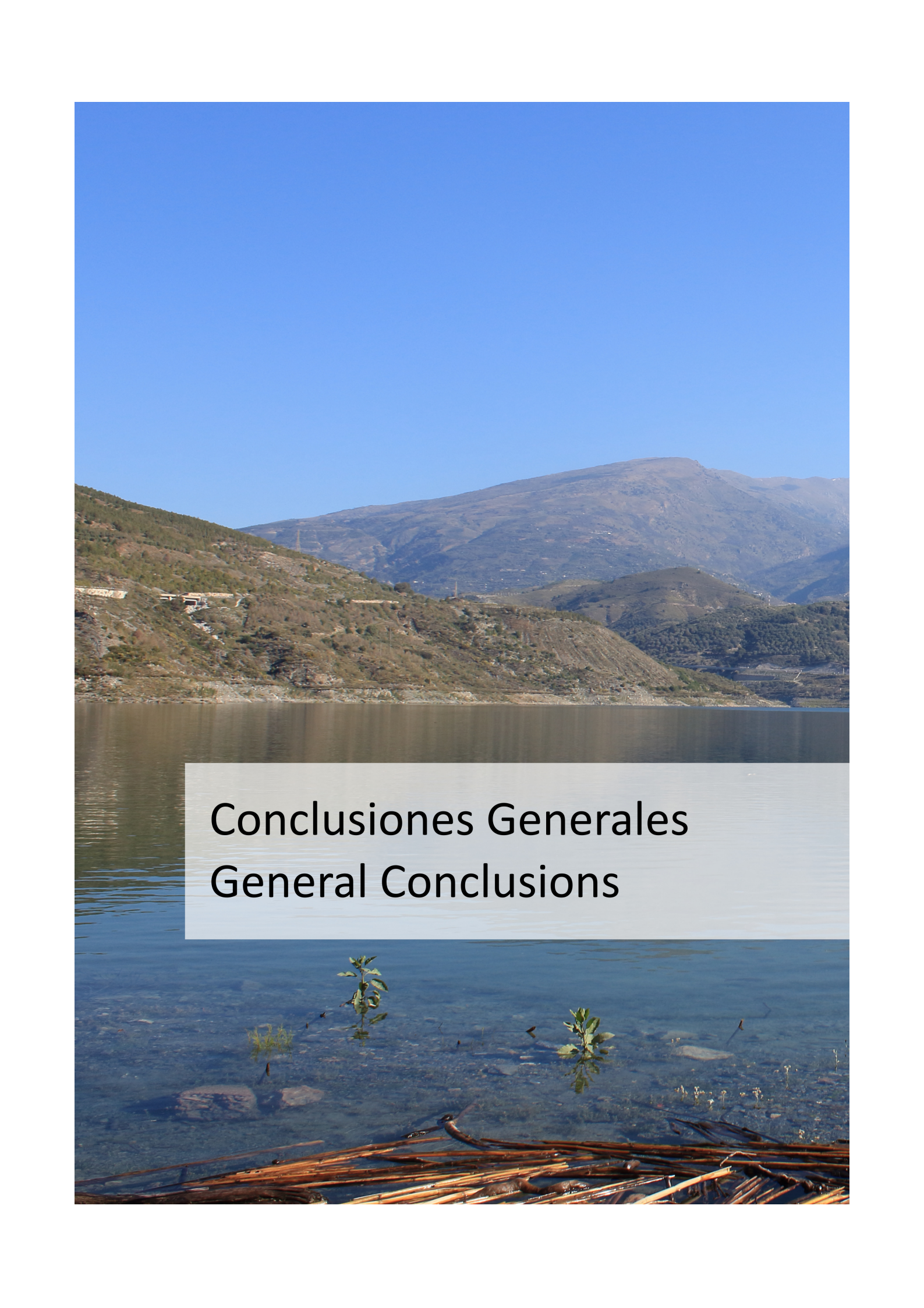
8. 6 References

- Abril, G., Guérin, F., Richard, S., Delmas, R., Galy-Lacaux, C., Gosse, P., Tremblay, A., Varfalvy, L., Santos, M. A. D. and Matvienko, B. (2005). Carbon dioxide and methane emissions and the carbon budget of a 10-year old tropical reservoir (Petit Saut, French Guiana), *Global Biogeochemical Cycles*, 19(4). doi: 10.1029/2005GB002457.
- Almeida, R. M., Shi, Q., Gomes-Selman, J. M., Wu, X., Xue, Y., Angarita, H., Barros, N., Forsberg, B. R., García-Villacorta, R., Hamilton, S. K., Melack, J. M., Montoya, M., Perez, G., Sethi, S. A., Gomes, C. P. and Flecker, A. S. (2019). Reducing greenhouse gas emissions of Amazon hydropower with strategic dam planning, *Nature Communications*, 10(1), pp. 1–9. doi: 10.1038/s41467-019-12179-5.
- Anderson, N. J., Heathcote, A. J., Engstrom, D. R. and Globocarb data contributors. (2020). Anthropogenic alteration of nutrient supply increases the global freshwater carbon sink, *Science Advances*, 6(16), p. eaaw2145. doi: 10.1126/sciadv.aaw2145.
- Barros, N., Cole, J. J., Tranvik, L. J., Prairie, Y. T., Bastviken, D., Huszar, V. L. M., del Giorgio, P. and Roland, F. (2011). Carbon emission from hydroelectric reservoirs linked to reservoir age and latitude, *Nature Geoscience*, 4(9), pp. 593–596. doi: 10.1038/ngeo1211.
- Beaulieu, J. J., DelSontro, T. and Downing, J. A. (2019). Eutrophication will increase methane emissions from lakes and impoundments during the 21st century, *Nature Communications*, 10(1), p. 1375. doi: 10.1038/s41467-019-09100-5.
- Bižić, M., Klintzsch, T., Ionescu, D., Hindiyeh, M. Y., Günthel, M., Muro-Pastor, A. M., Eckert, W., Urich, T., Keppler, F. and Grossart, H.-P. (2020). Aquatic and terrestrial cyanobacteria produce methane, *Science Advances*, 6(3), p. 3aax5343. doi: 10.1126/sciadv.aax5343.
- Carpenter, S. R. (1981). Submersed vegetation: An internal factor in lake ecosystem succession, *The American Naturalist*, 118(3), pp. 372–383.
- Carpenter, S. R., Caraco, N. F., Correll, D. L., Howarth, R. W., Sharpley, A. N. and Smith, V. H. (1998). Nonpoint pollution of surface waters with phosphorus and nitrogen, *Ecological Applications*, 8(3), pp. 559–568. doi: 10.1890/1051-0761(1998)008[0559:NPOSWW]2.0.CO;2.
- Chislock, M. F., Doster, E. and Zitomer, R. A. (2013). Eutrophication: causes, consequences, and controls in aquatic ecosystems, *Nature Education Knowledge*, 4(4), p. 10.
- Deemer, B. R., Harrison, J. A., Li, S., Beaulieu, J. J., DelSontro, T., Barros, N., Bezerra-Neto, J. F., Powers, S. M., dos Santos, M. A. and Vonk, J. A. (2016). Greenhouse gas emissions from reservoir water surfaces: a new global synthesis, *BioScience*, 66(11), pp. 949–964. doi: 10.1093/biosci/biw117.
- Diem, T., Koch, S., Schwarzenbach, S., Wehrli, B. and Schubert, C. J. (2012). Greenhouse gas emissions (CO₂, CH₄, and N₂O) from several perialpine and alpine hydropower reservoirs by diffusion and loss in turbines, *Aquatic Sciences*, 74(3), pp. 619–635. doi: 10.1007/s00027-012-0256-5.
- Encinas Fernández, J., Peeters, F. and Hofmann, H. (2014). Importance of the autumn overturn and anoxic conditions in the hypolimnion for the annual methane emissions

- from a temperate lake, *Environmental Science & Technology*, 48(13), pp. 7297–7304. doi: 10.1021/es4056164.
- Estes, L., Elsen, P. R., Treuer, T., Ahmed, L., Caylor, K., Chang, J., Choi, J. J. and Ellis, E. C. (2018). The spatial and temporal domains of modern ecology, *Nature Ecology & Evolution*, 2(5), pp. 819–826. doi: 10.1038/s41559-018-0524-4.
- Hartmann, J. F., Günthel, M., Klintzsch, T., Kirillin, G., Grossart, H.-P., Keppler, F. and Isenbeck-Schröter, M. (2020). High spatiotemporal dynamics of methane production and emission in oxic surface water, *Environmental Science & Technology*, 54(3), pp. 1451–1463. doi: 10.1021/acs.est.9b03182.
- IPCC. (2013). *Climate Change 2013: The Physical Science Basis. Contribution of Working Group I to the Fifth Assessment Report of the Intergovernmental Panel on Climate Change* Cambridge, United Kingdom and New York, NY, USA: Cambridge University Press. Edited by T. F. Stocker, D. Qin, G.-K. Plattner, M. Tignor, S. K. Allen, J. Boschung, A. Nauels, Y. Xia, V. Bex, and P. M. Midgley. Available at: <https://www.ipcc.ch/report/ar5/wg1/>.
- Kankaala, P., Taipale, S., Nykänen, H. and Jones, R. I. (2007). Oxidation, efflux, and isotopic fractionation of methane during autumnal turnover in a polyhumic, boreal lake, *Journal of Geophysical Research: Biogeosciences*, 112(G2). doi: 10.1029/2006JG000336.
- Kelly, C. A., Rudd, J. W. M., Bodaly, R. A., Roulet, N. P., St.Louis, V. L., Heyes, A., Moore, T. R., Schiff, S., Aravena, R., Scott, K. J., Dyck, B., Harris, R., Warner, B. and Edwards, G. (1997). Increases in fluxes of greenhouse gases and methyl mercury following flooding of an experimental reservoir, *Environmental Science & Technology*, 31(5), pp. 1334–1344. doi: 10.1021/es9604931.
- Kemenes, A., Forsberg, B. R. and Melack, J. M. (2007). Methane release below a tropical hydroelectric dam, *Geophysical Research Letters*, 34(12). doi: 10.1029/2007GL029479.
- Klintzsch, T., Langer, G., Nehrke, G., Wieland, A., Lenhart, K. and Keppler, F. (2019). Methane production by three widespread marine phytoplankton species: release rates, precursor compounds, and potential relevance for the environment, *Biogeosciences*, 16(20), pp. 4129–4144. doi: 10.5194/bg-16-4129-2019.
- Lenhart, K., Klintzsch, T., Langer, G., Nehrke, G., Bunge, M., Schnell, S. and Keppler, F. (2016). Evidence for methane production by the marine algae *Emiliania huxleyi*, *Biogeosciences*, 13(10), pp. 3163–3174. doi: 10.5194/bg-13-3163-2016.
- León-Palmero, E., Morales-Baquero, R. and Reche, I. (2020a). Greenhouse gas fluxes from reservoirs determined by watershed lithology, morphometry, and anthropogenic pressure, *Environmental Research Letters*, 15(4), p. 044012. doi: 10.1088/1748-9326/ab7467.
- León-Palmero, E., Contreras-Ruiz, A., Sierra, A., Morales-Baquero, R. and Reche, I. (2020b). Dissolved CH₄ coupled to photosynthetic picoeukaryotes in oxic waters and to cumulative chlorophyll *a* in anoxic waters of reservoirs, *Biogeosciences*, 17(12), pp. 3223–3245. doi: 10.5194/bg-17-3223-2020.
- López Bellido, J., Tulonen, T., Kankaala, P. and Ojala, A. (2009). CO₂ and CH₄ fluxes during

- spring and autumn mixing periods in a boreal lake (Pääjärvi, southern Finland), *Journal of Geophysical Research: Biogeosciences*, 114(G4). doi: 10.1029/2009JG000923.
- Louis, V. L. St., Kelly, C. A., Duchemin, É., Rudd, J. W. M. and Rosenberg, D. M. (2000). Reservoir surfaces as sources of greenhouse gases to the atmosphere: A global estimate: Reservoirs are sources of greenhouse gases to the atmosphere, and their surface areas have increased to the point where they should be included in global inventories of anthropogenic emissions of greenhouse gases, *BioScience*, 50(9), pp. 766–775. doi: 10.1641/0006-3568(2000)050[0766:RSASOG]2.0.CO;2.
- Maeck, A., DelSontro, T., McGinnis, D. F., Fischer, H., Flury, S., Schmidt, M., Fietzek, P. and Lorke, A. (2013). Sediment trapping by dams creates methane emission hot spots, *Environmental Science & Technology*, 47(15), pp. 8130–8137. doi: 10.1021/es4003907.
- Margalef, R. (1983). Capítulo 18: Ecosistemas forzados, in *Limnología*, p. 1010.
- Nixon, S. W. (1995). Coastal marine eutrophication: A definition, social causes, and future concerns, *Ophelia*, 41(1), pp. 199–219. doi: 10.1080/00785236.1995.10422044.
- Okuku, E. O., Bouillon, S., Tole, M. and Borges, A. V. (2019). Diffusive emissions of methane and nitrous oxide from a cascade of tropical hydropower reservoirs in Kenya, *Lakes & Reservoirs: Science, Policy and Management for Sustainable Use*, 24(2), pp. 127–135. doi: 10.1111/lre.12264.
- Prairie, Y. T., Alm, J., Beaulieu, J., Barros, N., Battin, T., Cole, J., del Giorgio, P., DelSontro, T., Guérin, F., Harby, A., Harrison, J., Mercier-Blais, S., Serça, D., Sobek, S. and Vachon, D. (2018). Greenhouse gas emissions from freshwater reservoirs: What does the atmosphere see?, *Ecosystems*, 21(5), pp. 1058–1071. doi: 10.1007/s10021-017-0198-9.
- Ryther, J. H. and Dunstan, W. M. (1971). Nitrogen, phosphorus, and eutrophication in the coastal marine environment, *Science*, 171(3975), pp. 1008–1013. doi: 10.1126/science.171.3975.1008.
- Schindler, D. W. (1977). Evolution of phosphorus limitation in lakes, *Science*, 195(4275), pp. 260–262. doi: 10.1126/science.195.4275.260.
- Schubert, C. J., Diem, T. and Eugster, W. (2012). Methane emissions from a small wind shielded lake determined by eddy covariance, flux chambers, anchored funnels, and boundary model calculations: A comparison, *Environmental Science & Technology*, 46(8), pp. 4515–4522. doi: 10.1021/es203465x.
- Seitzinger, S., Harrison, J. A., Böhlke, J. K., Bouwman, A. F., Lowrance, R., Peterson, B., Tobias, C. and Drecht, G. V. (2006). Denitrification across landscapes and waterscapes: A synthesis, *Ecological Applications*, 16(6), pp. 2064–2090. doi: 10.1890/1051-0761(2006)016[2064:DALAWA]2.0.CO;2.
- Teodoru, C. R., Bastien, J., Bonneville, M.-C., Giorgio, P. A. del, Demarty, M., Garneau, M., Hélie, J.-F., Pelletier, L., Prairie, Y. T., Roulet, N. T., Strachan, I. B. and Tremblay, A. (2012). The net carbon footprint of a newly created boreal hydroelectric reservoir, *Global Biogeochemical Cycles*, 26(2). doi: 10.1029/2011GB004187.

- The UNESCO/IHA Greenhouse Gas Emissions from Freshwater Reservoirs Research Project. (2010). *GHG Measurement Guidelines for Freshwater Reservoirs* London, UK: International Hydropower Association (IHA). Edited by J. A. Goldenfum.
- Tremblay, A., Therrien, J., Hamlin, B., Wichmann, E. and LeDrew, L. J. (2005). GHG emissions from boreal reservoirs and natural aquatic ecosystems, in Tremblay, A., Varfalvy, L., Roehm, C., and Garneau, M. (eds) *Greenhouse Gas Emissions — Fluxes and Processes: Hydroelectric Reservoirs and Natural Environments*, pp. 209–232. doi: 10.1007/978-3-540-26643-3_9.
- Zarfl, C., Lumsdon, A. E., Berlekamp, J., Tydecks, L. and Tockner, K. (2015). A global boom in hydropower dam construction, *Aquatic Sciences*, 77(1), pp. 161–170. doi: 10.1007/s00027-014-0377-0.



Conclusiones Generales General Conclusions

Conclusiones Generales

-
1. La heterogeneidad en las características de las cuencas de captación y morfométricas de los embalses estudiados resultaron en una variación de varios órdenes de magnitud en los flujos de los gases de efecto invernadero entre los sitios, con valores, a menudo, más elevados durante el período de estratificación que durante el período de mezcla. Algunos embalses actuaron como sumideros, y otros como fuentes de CO_2 y N_2O , pero todos los embalses fueron fuentes de CH_4 .
 2. Los embalses localizados en cuencas de captación con una litología de naturaleza calcárea fueron fuentes netas de CO_2 ; en cambio, los embalses actuaron como sumideros de CO_2 cuando la litología de la cuenca fue mayormente de naturaleza silíceo. Los embalses localizados en cuencas de captación dominadas por zonas de uso agrícola y urbano fueron fuentes netas de N_2O , mientras que los embalses situados en cuencas con más de un 40 % de área forestal actuaron como sumideros de N_2O . Finalmente, la profundidad media del embalse y la temperatura del agua determinaron las emisiones de CH_4 en los embalses.
 3. Los flujos diarios de CO_2 , N_2O , y CH_4 difusivo y ebulitivo variaron varios órdenes de magnitud. Los flujos de CO_2 , N_2O , y CH_4 difusivo mostraron un patrón diario consistente, con emisiones mayores durante el día que durante la noche.

Conclusiones Generales

Estas emisiones estuvieron acopladas al ciclo solar diario, la velocidad del viento, la temperatura del agua y la saturación de oxígeno.

4. La radiación solar indujo la producción abiótica de N_2O y de carbono inorgánico disuelto, con una contribución relevante a la producción diaria de N_2O y CO_2 .

5. Independientemente de la profundidad, la concentración de oxígeno o el estado trófico, la columna de agua de los embalses estuvo siempre supersaturada de CH_4 , tanto en el período de estratificación, como en el período de mezcla. La concentración de CH_4 disuelto varió hasta cuatro órdenes de magnitud

6. En las aguas anóxicas, la concentración de CH_4 estuvo correlacionada con la concentración de clorofila-*a* acumulada en profundidad, que es una aproximación a la biomasa fitoplanctónica exportada hacia los sedimentos. Por lo tanto, el detritus de origen fitoplanctónico podría ser una fuente de carbono de alta calidad para las arqueas metanógenas de los sedimentos.

7. En las aguas oxigénicas, la concentración de CH_4 dependió mayormente de la abundancia de los picoeucariotas fotosintéticos. La profundidad media de los embalses, como indicador del transporte vertical de CH_4 desde los sedimentos hacia las aguas oxigénicas, también explicó parcialmente estas concentraciones.

8. En la columna de agua de los embalses, la concentración de N_2O disuelto varió hasta tres órdenes de magnitud, con profundidades subsaturadas y supersaturadas en el mismo perfil. El hipolimnion anóxico actuó como fuente de N_2O cuando los embalses tenían elevadas concentraciones de nitrógeno total, en cambio actuó como sumidero de N_2O cuando los embalses tenían bajas concentraciones de nitrógeno total.

9. En la columna de agua de los embalses estudiados, la concentración de nitrógeno total y la abundancia del gen *nirS*, que es una aproximación a la abundancia de las bacterias desnitrificantes, determinaron la concentración de N_2O disuelto. El gen *nirS* fue ubicuo en la columna de agua y dependió de la concentración total de fósforo y de la concentración de clorofila-*a* acumulada en profundidad.

10. En los embalses eutróficos de Cubillas e Iznájar, la concentración de nitrato en la columna de agua disminuyó significativamente durante la estratificación desde julio a septiembre, particularmente en el embalse más somero (es decir, Cubillas). El N_2O producido en el hipolimnion durante la estratificación se acumuló en el embalse más profundo (es decir, Iznájar), pero se fue liberando con el descenso del nivel del agua en el embalse de Cubillas.

11. La producción de N_2O a partir de amonio y nitrato varió notablemente entre profundidades en un mismo sistema, con las máximas producciones en las aguas con baja concentración de oxígeno. Los resultados sugieren que la producción de N_2O a partir de la oxidación de amonio podría ocurrir por acoplamiento de la nitrificación y la desnitrificación y por desnitrificación a partir de nitrato. La materia orgánica autóctona exportada en la columna de agua (es decir, la concentración de clorofila-*a* acumulada en profundidad) parece promover la producción de N_2O , y también explicó la abundancia *in situ* del gen *nirS*.

12. La tasa de fotoproducción de N_2O por volumen fue mayor que la tasa de producción biológica de N_2O a partir de amonio en las aguas superficiales de Cubillas e Iznájar. La fotoproducción de N_2O incluso superó la tasa de producción biológica de N_2O a partir de amonio y nitrato en otras capas como la oxiclina o el hipolimnion en Cubillas. Estos resultados demuestran que la fotoproducción de N_2O , aunque solo ocurra en aguas superficiales, puede contribuir de forma muy significativa a la producción total de N_2O y, como consecuencia, a los flujos de N_2O .

Conclusiones Generales

-
1. The heterogeneous watershed and morphometric characteristics of the study reservoirs was reflected in the variation of several orders of magnitude of their greenhouse gas fluxes among sites, with higher values usually during the stratification than during the mixing period. Some reservoirs acted as sinks and others as sources of CO₂ and N₂O, but all the study reservoirs were sources of CH₄.
 2. Reservoirs located in calcareous watersheds were net CO₂ sources; by contrast they were CO₂ sinks when the lithology was mostly siliceous. Reservoirs located in watersheds dominated by agricultural and urban areas were net N₂O sources; by contrast they were N₂O sinks when the landscape had more than 40 % of forestal coverage. Finally, the mean depth and water temperature of the reservoirs determined their CH₄ emissions.
 3. The daily fluxes of CO₂, N₂O, and the diffusive and ebullitive CH₄ varied by several orders of magnitude. The fluxes of CO₂, N₂O, and diffusive CH₄ showed a coherent daily pattern, with higher emissions during the daytime than during the nighttime. These emissions were coupled with the daily solar cycle, wind speed, water temperature, and oxygen saturation.

General Conclusions

4. Solar radiation induced the abiotic production of N_2O , and dissolved inorganic carbon, with a relevant contribution to the daily N_2O and CO_2 production.

5. Regardless of the depth, the oxygen concentration, or the trophic state, the water column of the reservoirs was consistently supersaturated in CH_4 both in the stratification and mixing periods. The dissolved CH_4 concentration ranged up to four orders of magnitude.

6. In anoxic waters, the CH_4 concentration was correlated to the depth-cumulative chlorophyll-*a* concentration, which is a proxy for the phytoplanktonic biomass exported to sediments. Therefore, phytoplankton detritus may be a high-quality carbon source for methanogenic archaea in sediments.

7. In oxic waters, the CH_4 concentration depended mainly on the photosynthetic picoeukaryotes abundance. The mean depth of the reservoirs, as a surrogate of the vertical CH_4 transport from sediment to the oxic waters, also partially explain these concentrations.

8. In the water column of reservoirs, the dissolved N_2O concentration ranged up to three orders of magnitude, with N_2O undersaturated and supersaturated depths in the same profile. The anoxic hypolimnion acted as a N_2O source when the reservoirs contained high concentrations of total nitrogen; by contrast it acted as a N_2O sink when the reservoirs contained low concentration of nitrogen.

9. In the water column of the study reservoirs, the total nitrogen concentration, and the abundance of the gene *nirS*, which is a proxy for the abundance of the denitrifying bacteria, determined the dissolved N_2O concentration. The gene *nirS* was ubiquitous in the water column, and depended on the total phosphorus concentration, and the depth-cumulative chlorophyll-*a* concentration.

10. In the two eutrophic reservoirs Cubillas and Iznájar, the nitrate concentration in the water column decreased significantly during the stratification from July to September, particularly in the shallowest reservoir (i.e., Cubillas). The N_2O produced in the hypolimnion during the stratification was stored in the deepest reservoir (i.e., Iznájar), but was released with the water level drawdown in the Cubillas reservoir.

11. The production of N_2O from ammonium and nitrate varied notably among depths, with the maximum productions located at the low oxygen depths. The results suggest that N_2O production from ammonium may occur by a coupled nitrification-denitrification, and by denitrification from nitrate. The autochthonous organic matter exported in the water column (i.e., cumulative chlorophyll-*a* concentration) appears to promote N_2O production, which also explained the *in situ* abundance of the gene *nirS*.

12. The rate of N_2O photoproduction per volume was higher than the biological production of N_2O from ammonium in surface waters of Cubillas and Iznájar reservoirs. The N_2O photoproduction even exceeded the biological N_2O production from ammonium and nitrate at other layers such as oxycline or hypolimnion in Cubillas. These results demonstrate that the N_2O photoproduction, although only occurs on the surface waters, can contribute significantly to the N_2O total production and, consequently, N_2O emissions.

General Conclusions

Peer review and scientific outreach publications

Publications in peer review journals included in this dissertation:

León-Palmero, E., Contreras-Ruiz, A., Sierra, A., Morales-Baquero, R. and Reche, I.

(2020). Dissolved CH₄ coupled to photosynthetic picoeukaryotes in oxic waters and to cumulative chlorophyll *a* in anoxic waters of reservoirs, *Biogeosciences*, 17(12), pp. 3223–3245. doi: [10.5194/bg-17-3223-2020](https://doi.org/10.5194/bg-17-3223-2020).

This article was highlighted in the SCOPE Newsletter special issue addressing the links between phosphorus, nutrients and climate change, produced by the Sustainable Phosphorus Alliance, and the European Sustainable Phosphorus Platform.

León-Palmero, E., Morales-Baquero, R. and Reche, I. (2020). Greenhouse gas fluxes

from reservoirs determined by watershed lithology, morphometry, and anthropogenic pressure, *Environmental Research Letters*, 15(4), p. 044012. doi: [10.1088/1748-9326/ab7467](https://doi.org/10.1088/1748-9326/ab7467).

León-Palmero, E., Reche, I. and Morales-Baquero, R. (2019). Atenuación de luz en embalses del sur-este de la Península Ibérica, *Ingeniería del agua*, 23(1), pp. 65–75. doi: [10.4995/ia.2019.10655](https://doi.org/10.4995/ia.2019.10655).

Scientific outreach and public communication activities:

Interview for the report: González, V. (2020). Metano: ¿una bomba de relojería climática? (Methane: a climatic time bomb?), *Muy Interesante*, September, pp. 74–81.

Article: León-Palmero, E (2020). Verde que te quiero verde..., ¡pero no tanto! : la paradoja del metano (Green I love you green... but not that much! : the methane paradox), *Ecomandanga*, España. Available at: <https://ecomandanga.org/2020/09/16/verde-que-te-quiero-verde-pero-no-tanto-la-paradoja-del-metano/>

Radio interview in the programme "Investigadores por el Mundo" (2020): Gases de efecto invernadero en embalses (Greenhouse gases in reservoirs). Available at: <https://go.ivoox.com/rf/56322396>

Divulgative video: León-Palmero, E (2020). Los embalses como emisores de gases de efecto invernadero (Reservoirs as sources of greenhouse gases). Available at: <https://www.youtube.com/watch?v=UD2cLJeaRU&feature=youtu.be>

Publications

Article: León-Palmero, E., Reche, I. and Baquero, R. M. (2020). *Medimos la contribución de los embalses mediterráneos al cambio climático (We measured the contribution of Mediterranean reservoirs to climate change)*,

The Conversation España. ISSN 2201-5639. Available at:

<http://theconversation.com/medimos-la-contribucion-de-los-embalses-mediterraneos-al-cambio-climatico-139687>

Talk to general public (2020): Emisiones de gases de efecto invernadero en embalses (Greenhouse gas fluxes in reservoirs). DIVULGA TU CIENCIA EN BAENA, Ayuntamiento de Baena, Córdoba

Talk (3) to high school students (2020): Pasado, presente y futuro de la mujer en ciencia (#11F) (Past Present, and Future of Women in Science). Sagrada Familia (SA.FA.), Baena (Córdoba).

Talk in DESGRANANDO CIENCIA 6 outreach event (2019): La pizza más romántica y cara del cine: sobre el impacto ambiental de la producción de alimentos (The most romantic and expensive pizza in cinema: on the environmental impact of food production). Available at: <https://youtu.be/vdYHvpWVzM8?t=4847>

A landscape photograph showing a wide expanse of water in the foreground, with a rocky, forested hill in the background under a cloudy sky. The water is dark green and has small ripples. The sky is overcast with soft, grey clouds. The hill in the background is covered in dark green trees and has a rocky, brownish appearance. The overall scene is calm and serene.

Appendixes:

Appendix 1 | Atenuación de luz en embalses del sur-este de la Península Ibérica

Appendix 1:

Atenuación de luz en embalses del sur-este de la Península Ibérica

Light attenuation in Southern Iberian Peninsula reservoirs

Elizabeth León-Palmero¹, Rafael Morales-Baquero¹ & Isabel Reche^{1,2}

¹Instituto del Agua y Departamento de Ecología, Universidad de Granada, E-18071 Granada, Spain

²Research Unit Modeling Nature (MNat), Universidad de Granada, E-18071 Granada, Spain

Resumen

Este trabajo estudia de forma pareada los valores del coeficiente de extinción vertical de la luz (K_d) y de la profundidad de visión del disco de Secchi (SD) en un conjunto de 12 embalses del sureste de la Península Ibérica que difieren en sus características de paisaje, físicas, químicas y tróficas. Se analizan las relaciones encontradas para evaluar la utilidad del SD como predictor de la zona fótica (Z_{eu}) calculada mediante K_d y se propone la expresión Z_{eu} (m) \approx 2 SD (m) + 6 como la mejor estima de la zona fótica en estos embalses. Además se investiga la influencia de la clorofila-*a*, turbidez y carbono orgánico disuelto (DOC) sobre la transparencia del agua de los embalses. Tanto la concentración de DOC como la turbidez afectan a dichas propiedades. Finalmente, se analiza la capacidad de SD como predictor de K_d .

Palabras clave | extinción de luz en agua; disco de Secchi; transparencia; zona fótica; embalses.

Abstract

This study evaluates the extinction coefficient of light (K_d) and the Secchi disk depth (SD) in 12 reservoirs located in the southern Iberian Peninsula. These systems show differences in landscape, physical, chemical and trophic properties. The relationships found were analyzed to evaluate the utility of the SD as predictor of the photic zone (Z_{eu}) measured with K_d . A new equation is proposed here as a better estimation for the photic zone in these reservoirs: Z_{eu} (m) \approx 2 SD (m) + 6. The influence of the chlorophyll-*a*, turbidity and dissolved organic carbon (DOC) concentration on the water transparency is studied. Both DOC concentration and turbidity affect water transparency. Finally, the capacity of SD as a K_d predictor is also assessed.

Key words | light extinction in water; Secchi disk; transparency; photic zone; reservoirs.

Introducción

La gestión eficaz de las masas de aguas continentales superficiales requiere la obtención de información sobre los elementos de la calidad del agua, según el uso humano que se hace de ella, como tradicionalmente se ha considerado, pero también sobre los aspectos necesarios para la conservación de sus propiedades naturales, como obliga la Directiva 2000/60/CE (Directiva Marco del Agua) a los estados miembros de la Comunidad Europea. Recabar esta información supone un considerable esfuerzo económico, reflejado en el desarrollo por los organismos competentes de redes de seguimiento de la calidad y estado ecológico de las masas de agua continentales, que implican programas de muestreo periódicos y la instalación de estaciones de medida automatizadas. En este contexto, es evidente el interés de la investigación y desarrollo de metodologías que optimicen la adquisición de la información mencionada (Canteras *et al.*, 1999; Prats-Rodríguez *et al.*, 2014). En el presente trabajo nos centramos en la estima de la penetración de la luz solar en los embalses, uno de los parámetros fundamentales para comprender su funcionamiento como ecosistemas.

La penetración de la radiación solar fotosintéticamente activa (PAR) en los ecosistemas acuáticos determina su estructura vertical en cuanto a la capacidad neta de producir materia orgánica (zona trofogénica, en la parte iluminada) o descomponerla (zona trofolítica, en la parte oscura). Esta penetración depende de la absorción luminosa debida al agua misma, pero especialmente de la absorción debida a los componentes disueltos y a los componentes en suspensión (vivos o inertes). Ambos componentes determinan también la calidad del agua. Por eso, desde hace tiempo se han establecido relaciones entre la penetración de la luz en los sistemas acuáticos, su transparencia, y diversos criterios para establecer la calidad de las aguas (Carlson, 1977).

La transparencia de los sistemas acuáticos se mide habitualmente mediante la profundidad de visión del disco de Secchi (SD) o mediante espectroradiómetros subacuáticos para calcular el coeficiente de extinción vertical de la luz (K_d). Ambos métodos se han usado para determinar la profundidad de compensación, o profundidad donde la producción primaria iguala a la respiración, que marca el límite de la zona fótica (Z_{eu}). La dispersión y absorción de la luz debida a los componentes en suspensión y la absorción debida a los componentes disueltos pueden afectar de forma diferente a SD y K_d . Así, aunque se han tratado de establecer equivalencias generales entre SD y K_d (Poole y Atkins, 1929; Holmes, 1970; French *et al.*, 1982) la variabilidad de los componentes disueltos y en suspensión en distintos cuerpos de agua, incluso dentro de una misma región geográfica, no han permitido validar los valores propuestos para el producto de $K_d \cdot SD$ que, de ser constante, validaría la hipótesis de ser parámetros inversamente proporcionales. Sin embargo, debido a la simplicidad de las medidas con el disco de Secchi, aún se siguen usando como aproximaciones en algunos estudios (Tundisi y Tundisi, 2011; Rodríguez, 2016).

El propósito de este trabajo es estudiar la transparencia de un conjunto de 12 embalses del sur-este de la Península Ibérica, que difieren en sus características paisajísticas, físico-químicas y tróficas, para: a) evaluar la variabilidad óptica natural mediante medidas pareadas de K_d y SD; b) estudiar las relaciones entre K_d y SD en el conjunto de embalses y la utilidad del SD para establecer la zona fótica y c) analizar las relaciones entre K_d y SD y constituyentes del agua ópticamente

relevantes como la turbidez, la clorofila-*a* (Clorofila-*a*) y la concentración de materia orgánica disuelta medida como carbono orgánico disuelto (DOC).

Material y Métodos

La Figura 1 muestra la localización de los embalses estudiados y la Tabla 1 alguna de sus características morfométricas y de sus correspondientes cuencas de captación. La selección de los embalses se realizó con la intención tener un amplio espectro de condiciones paisajísticas, tróficas, de tamaño y edad. Los embalses se muestrearon una vez durante los meses de febrero a abril de 2017, época en la que todos ellos estaban mezclados. Tres de los embalses fueron muestreados, además, en septiembre y octubre de 2016, época en la que estaban estratificados.



Figura 1 | Localización de los embalses estudiados.

Tabla 1 | Algunas características de los embalses estudiados y de sus cuencas de captación: superficie cultivada (Sup. Cult.) y superficie arbolada (Sup. Arb.). La edad ha sido referida al año del muestreo (2017).

Embalse	Edad	Altitud	Volumen	Superficie	C. Captación	Sup. Cult.	Sup. Arb.
	(años)	(m)	(hm ³)	(km ²)	(km ²)	(km ²)	(km ²)
Cubillas	61	640	19	1.94	647	417	166
Colomera	27	810	40	2.76	237	146	65
Negratín	33	618	567	23.51	3765	1698	1304
La Bolera	50	950	53	2.89	163	5	139
Los Bermejales	59	852	103	5.95	281	84	133
Iznájar	48	425	981	26.13	4714	2752	984
Francisco Abellán	26	942	58	2.43	193	27	117
Béznar	31	486	53	1.60	347	110	122
San Clemente	27	1050	118	3.76	153	18	101
El Portillo	18	920	33	1.18	113	4	62
Jándula	85	350	322	8.43	2245	427	1350
Rules	14	239	111	3.06	1078	254	350

En cada embalse, en un punto generalmente cercano a la presa, se estudió la capa mezclada de la columna de agua, tomando medidas de: penetración de la luz PAR ($\mu\text{Einteins m}^{-2} \text{s}^{-1}$), mediante un sensor esférico LI-COR® (modelo LI-193R) y turbidez (FTU) mediante un sensor Seapoint. Estos dos sensores estaban montados en una sonda perfiladora multiparamétrica SeaBird® (modelo SBE 19plus, SEACAT Profiler) dotada de sensor de profundidad, temperatura y registrador continuo de datos, de modo que fue posible obtener perfiles verticales simultáneos de las medidas obtenidas con los sensores más la temperatura. Gracias al registro continuo de datos, se pudo obtener un valor de turbidez promedio como:

$$\text{Turbidez} = \frac{1}{N} \sum_{i=1}^N (x_i) \quad (1)$$

donde x_i es cada uno de los datos de la muestra, y N el número total de datos tomados por la sonda.

Paralelamente, se midió la transparencia del agua con un disco de Secchi blanco de 20 cm. El coeficiente de absorción luminosa PAR con la profundidad (K_d) se calculó como la pendiente de la recta que resulta de la transformación semilogarítmica de la ley de Lambert-Beer, de modo que

$$\ln I_z = \ln I_0 - K_d z \quad (2)$$

donde I_z es la intensidad luminosa a la profundidad de z metros e I_0 es la intensidad luminosa justo debajo de la superficie del agua. Admitiendo que el 1 % de la radiación recibida en superficie es el límite para la producción primaria, la zona fótica (Z_{eu}) se estableció como

$$Z_{eu} = \ln(0.01) / K_d \quad (3)$$

La concentración de clorofila-*a* (μg Clorofila-*a* L^{-1}) y de carbono orgánico disuelto (DOC) se midieron a partir de muestras de agua obtenidas a diferentes profundidades (de 6 a 8 puntos) con una botella UWITEC de 5 L de capacidad. Las profundidades se establecieron de acuerdo con los perfiles térmico y luminoso obtenidos procurando reflejar la heterogeneidad vertical observada. Para la clorofila se filtraron entre 500 y 2000 mL de muestra usando filtros de fibra de vidrio Whatman GF/F y 0.7 μm de tamaño de poro. La concentración de DOC se midió mediante oxidación catalítica a alta temperatura en un analizador de carbono orgánico total Shimadzu (modelo TOC-V CSH). Las muestras se acidificaron y purgaron durante 20 minutos para eliminar el carbono inorgánico. A partir de los filtros se extrajeron los pigmentos usando metanol 95% en oscuridad a 4 °C durante 24 horas (APHA 1992). La absorción de los pigmentos se midió a 665 nm y 750 nm usando un espectrofotómetro Perkin Elmer UV-Lambda 40. Para obtener un valor integrado a partir de los valores discretos de la columna de agua se hizo una media ponderada teniendo en cuenta las profundidades muestreadas, de forma que

$$\text{Chl-}a = \frac{1}{Z} \sum_{k=1}^n X_{ik} \left(Z_{k+1} - \frac{Z_{k-1}}{2} \right) \quad (4)$$

donde Z_k son las n profundidades muestreadas; X_{ij} es la concentración de clorofila-*a* (μg Clorofila-*a* L^{-1}) a la profundidad Z_k . Z es la profundidad máxima considerada.

Las características físicas de los embalses, como el año de construcción, superficie y volumen fueron tomados del Ministerio de Agricultura y Pesca, Alimentación y Medio Ambiente (MAPAMA; www.embalses.net). El análisis de las cuencas de captación se realizó mediante ArcGIS® (ESRI Maps versión 10.2) bajo la licencia de la Universidad de Granada. Se utilizaron bases de datos públicas provenientes de la Infraestructura de Datos Espaciales (IDE) del Ministerio de

Agricultura y Pesca, Alimentación y Medio Ambiente (MAPAMA; <http://www.mapama.gob.es/es/cartografia-y-sig/ide/>); el Instituto de Estadística y Cartografía de Andalucía (DEAndalucía; <http://www.ideandalucia.es/portal/web/ideandalucia/>); la Confederación Hidrográfica del Segura (CHSEGURA; <https://www.chsegura.es/chs/index.html>) y Junta de Comunidades de Castilla-La Mancha (IDE-JCCM; <https://castillalamancha.maps.arcgis.com/home/index.html>).

Resultados

La transparencia de los embalses varió notablemente con valores de SD comprendidos entre el mínimo de 1 m en Cubillas y el máximo de 9 m en Rules (Tabla 2). Igualmente, la extinción vertical de la luz difiere ampliamente con valores de K_d entre 0.18 m^{-1} en El Portillo y 0.82 m^{-1} en Cubillas. Consecuentemente, la zona fótica de los embalses también cambia marcadamente, desde 5.6 m en Cubillas hasta 25.6 m en El Portillo. Por tanto, el producto $K_d \cdot \text{SD}$ varió entre 0.82 y 2.16.

Tabla 2 | Profundidad de visión del disco de Secchi (SD), coeficiente de absorción de la luz (K_d), zona eufótica (Z_{eu}), concentración de clorofila, turbidez y carbono orgánico disuelto (DOC) medidos en los embalses estudiados. En los embalses muestreados dos veces, el primer valor corresponde al periodo estratificado y el segundo al de mezcla.

Embalse	SD	K_d	Z_{eu}	Clorofila- <i>a</i>	Turbidez	DOC
	(m)	(m^{-1})	(m)	($\mu\text{g L}^{-1}$)	(FTU)	(mg L^{-1})
Cubillas	1	0.82	5.6	9.08	9.02	2.80
Colomera	2.1	0.57	8.1	0.47	8.94	1.44
Negratín	3.7	0.3	15.1	11.05	3.81	1.71
La Bolera	6	0.24	19	0.73	1.79	1.35
Los Bermejales	3.3	0.31	14.7	11.20	3.55	1.19
Iznájar	4.0 - 2.0	0.34 - 0.65	13.8 - 7.0	5.64 - 1.19	2.27 - 1.66	1.65 - 2.00
Francisco Abellán	2.5 - 2.5	0.33 - 0.37	13.9 - 12.5	2.24 - 1.00	3.26 - 4.45	1.18 - 1.50
Béznar	4.0 - 2.0	0.36 - 0.52	12.8 - 8.8	11.46 - 3.95	1.93 - 3.16	0.89 - 1.60
San Clemente	3.7	0.31	14.9	1.22	2.49	1.63
El Portillo	8	0.18	25.6	1.84	0.78	0.96
Jándula	6	0.34	13.4	1.03	0.99	4.95
Rules	9	0.24	19.2	2.10	0.98	0.79

Para estudiar el valor de las medidas de SD como predictoras de la zona fótica analizamos la regresión lineal entre ellas y Z_{eu} como variable dependiente. La relación obtenida muestra una buena linealidad con un coeficiente de determinación R^2 de 0.71 (Figura 2).

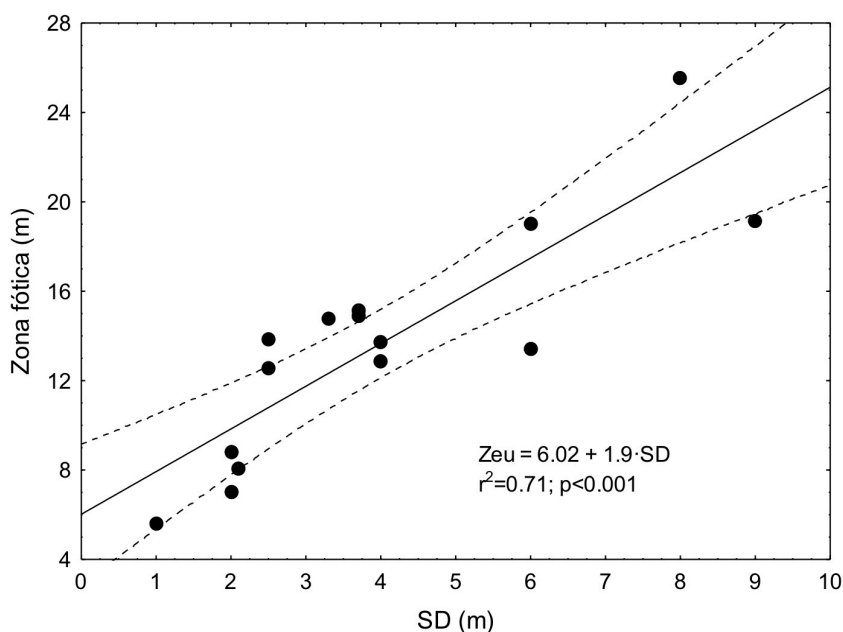


Figura 2 | Relación entre la profundidad de visión del disco de Secchi y la zona fótica. Las líneas discontinuas representan la región de confianza al 95%.

Las variables estudiadas como determinantes de SD y K_d también difirieron entre embalses. La clorofila- a alcanza un mínimo de $0.47 \mu\text{g L}^{-1}$ durante la mezcla en Colomera, y un máximo de $11.46 \mu\text{g L}^{-1}$ en Béznar durante la estratificación (Tabla 2). La turbidez alcanza un mínimo de 0.78 FTU en el embalse del Portillo y un máximo de 9.02 FTU en el embalse de Cubillas, mientras el DOC varía entre 0.79mg L^{-1} en Rules y un máximo de 4.95mg L^{-1} en el embalse de Jándula; sin embargo, este valor se desmarca claramente del rango observado en el resto de embalses (Tabla 2) y será considerado como un valor atípico.

Tanto el DOC como la turbidez muestran un efecto significativo sobre SD, negativo ($p < 0.01$), y sobre K_d , positivo ($p < 0.005$). La clorofila- a no mostró efecto alguno sobre SD ni sobre K_d . La Figura 3 muestra las relaciones entre SD y K_d como variables dependientes de la clorofila- a , de la turbidez y del DOC.

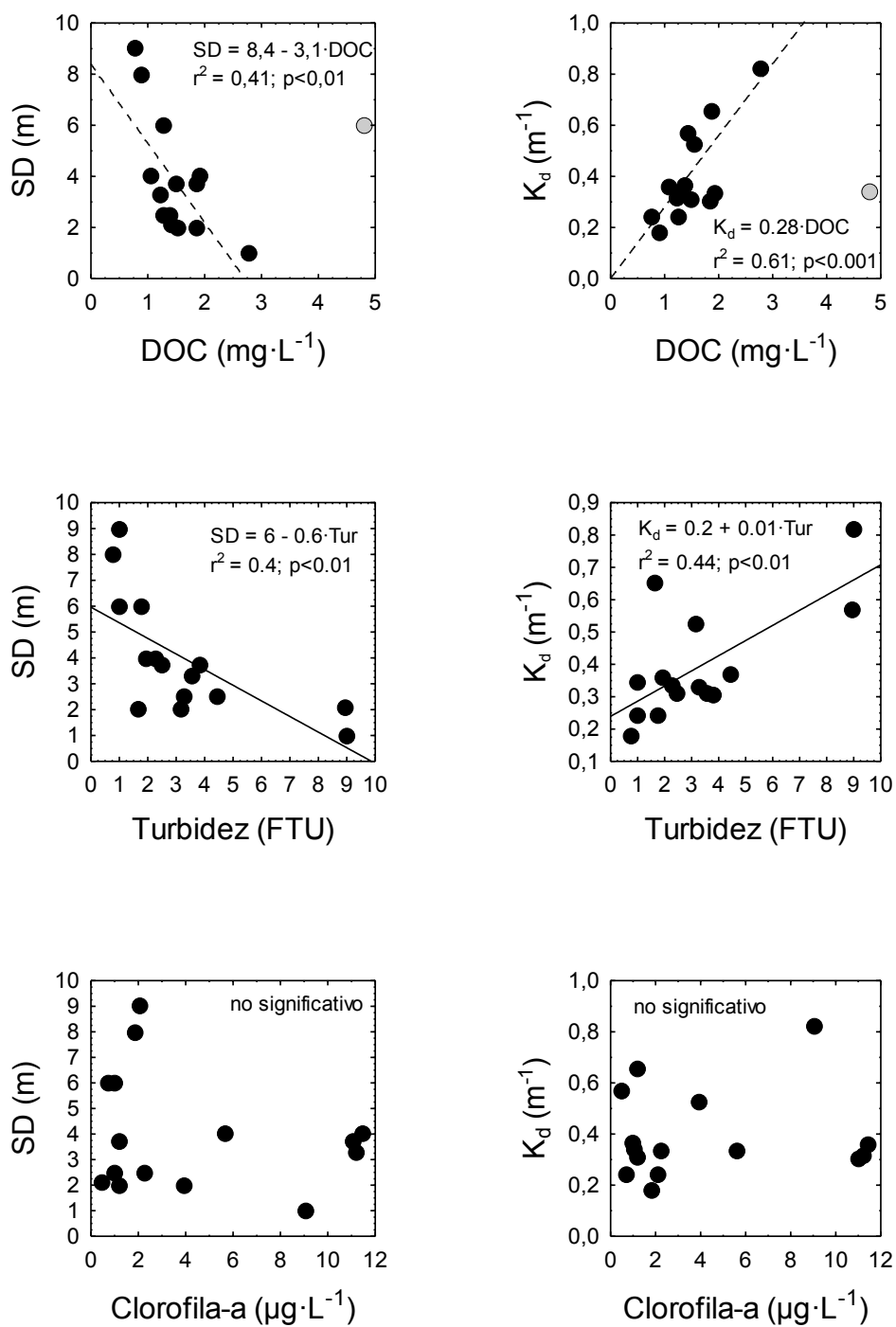


Figura 3 | Relaciones entre SD y K_d como variables dependientes del DOC, la turbidez y la Clorofila-*a*. Las regresiones con el DOC, en línea discontinua, no incluyen al embalse de Jándula, cuyo valor es considerado un valor atípico.

Para analizar la posible influencia de las características de los embalses y de sus cuencas de captación, mostradas en la Tabla 1, sobre las variables determinantes de la transparencia del agua (turbidez, Clorofila-*a* y DOC), se realizaron sendos análisis de regresión simple entre ellas. Solamente el año de construcción de los embalses y la superficie de terreno arbolado en la cuenca de captación mostraron efectos significativos positivos sobre el DOC (Tabla 3). La edad del embalse es un parámetro que afecta al contenido en carbono orgánico disuelto. A mayor edad, mayor es la concentración de DOC observada en estos embalses. Este hecho puede estar relacionado con un mayor periodo de acumulación de DOC procedente de la escorrentía. De igual forma, una mayor cobertura arbolada en la cuenca de captación supone un mayor contenido en DOC (Tabla 3).

Tabla 3 | Resultados de los análisis de regresión lineal efectuados para evaluar el efecto de la edad del embalse y de la superficie arbolada de las cuencas de captación sobre el contenido de DOC de los embalses (b=coeficiente de regresión, R²=coeficiente de determinación).

Fuente de variación	b	Intercepción	Significación (p)	R ²
Edad del embalse	0.043	0.032	<0.0005	0.65
Área arbolada	0.001	1.192	<0.05	0.35

Relación K_d- SD

La Figura 4 muestra la relación observada entre SD y K_d. El mejor ajuste se obtuvo tras la transformación logarítmica según la recta de regresión: log K_d = a – b·log SD, siendo a = -0.113 y b = -0.615 (r² = 0.8; p < 0.001), que es equivalente a la siguiente ecuación potencial

$$K_d = \frac{0.771}{SD^{0.615}} \tag{5}$$

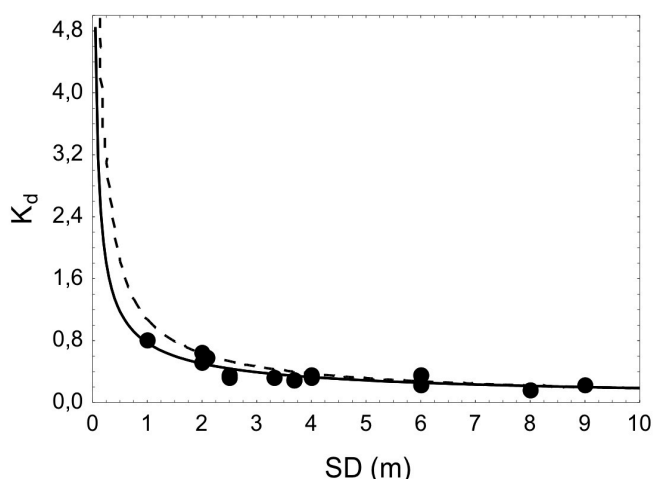


Figura 4 | Relación entre el coeficiente de absorción de luz y la profundidad de visión del disco de Secchi. La línea continua corresponde al ajuste obtenido en el presente trabajo (ecuación 3) y la línea discontinua al obtenido en 1991 (ver texto).

Discusión

Transparencia y zona fótica

A pesar de ser sólo 12 los embalses recogidos en este estudio, presentan un amplio rango de profundidades de visión del disco de Secchi (entre 1 y 9 m) mayor, por ejemplo, que el registrado en 23 lagos, representativos de la diversidad de 167 lagos, del Parque Suwałki de Polonia (entre 1.1 y 6 m) (Borowiak y Borowiak 2016). Sin embargo, el coeficiente de absorción K_d en esos lagos, varió mucho más (entre 0.44 y 2.0 m^{-1}) que entre nuestros embalses (entre 0.18 y 0.85 m^{-1}). Este hecho pone de manifiesto que K_d y SD se ven afectados de forma diferente por los constituyentes de las aguas naturales que determinan sus propiedades ópticas y que pueden ser diferentes entre distintos lagos. Por eso, el producto $K_d \cdot SD$ no resulta ser un valor generalizable como se pretendió históricamente. El primer valor que se propuso fue de 1.7 (Poole y Atkins 1929), posteriormente 1.44 (Holmes, 1970) y más tarde 1.16 (French *et al.*, 1982). Como se puede apreciar en la Tabla 2, en nuestro caso, el valor de $K_d \cdot SD$ en cada embalse varía entre 0.82 y 2.16, rango que supera ampliamente los valores propuestos.

Más recientemente Koenings y Edmundson (1991) sugieren que los cambios en el producto $K_d \cdot SD$ dan información sobre las cargas de los constituyentes del agua que modifican la penetración PAR en las aguas naturales y proponen un uso diagnóstico de este producto, ya que incrementos en la turbidez bajan $K_d \cdot SD$

mientras incrementos en el color del agua lo suben. En nuestro caso la variación de $K_d \cdot SD$ concuerda bien con esta idea; los valores mas bajos corresponden con embalses como Cubillas y Colomera con altos valores de turbidez mientras que los valores mas altos de $K_d \cdot SD$ corresponden a embalses como Rules o Jándula con bajos valores de turbidez (Tabla 2).

Para los ecosistemas acuáticos, en los que la luz regula la mayoría de los procesos internos, la profundidad de la zona fótica (Z_{eu}) es una importante divisoria ecológica definida por el coeficiente de absorción de la luz K_d . Sin embargo, el cálculo de K_d exige instrumentación y procesamiento de los datos. Por eso, se han tratado de utilizar las medidas del disco de Secchi, más simples, como predictoras de la Z_{eu} , estableciendo relaciones empíricas entre medidas pareadas de SD y la Z_{eu} calculada mediante K_d . Así, la Directiva Marco del Agua (DMA) de la Unión Europea propone la relación $Z_{eu} \sim 2.5 \cdot SD$ (Poikane, 2009). Nuestros resultados (Figura 2) ofrecen una relación algo diferente $Z_{eu} = 1.91 \cdot SD + 6.02$ que predice mejor la zona fótica de nuestros embalses, ya que la relación de la DMA la subestima generalmente (Figura 5). Así pues, simplificando, proponemos la relación $Z_{eu} \sim 2 \cdot SD + 6$ como aproximación para el cálculo de la zona fótica en los embalses del sureste de la Península Ibérica.

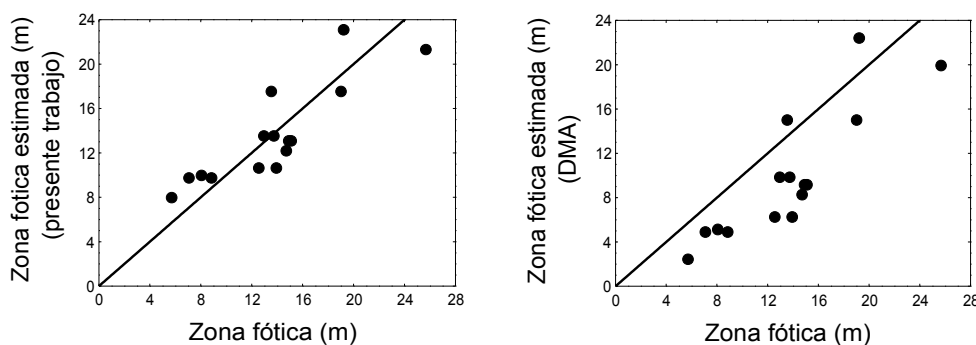


Figura 5 | Relación entre la zona fótica calculada y la estimada según la función obtenida en este trabajo y la recomendada en la Directiva Marco del Agua. Las líneas indican la relación 1:1.

Variables determinantes de K_d y SD

De las tres variables estudiadas como determinantes de las propiedades ópticas de los embalses : Clorofila-*a*, turbidez y DOC; la turbidez y el DOC mostraron una influencia clara sobre K_d y SD. Estudios clásicos, como el trabajo de Morris *et al.* (1995) en 65 lagos concluyeron que una gran proporción de la variación de K_d (87 – 96 %) era debida a las diferencias en la concentraciones de DOC. Se sabe que la

materia orgánica disuelta es también un factor fundamental en la absorción de la luz de los sistemas acuáticos continentales (Scully y Lean 1994). En nuestros embalses la influencia del DOC (como estimador de la materia orgánica disuelta), aumentando K_d y disminuyendo SD, también queda de manifiesto. La concentración de DOC medida en el embalse de Jándula es la mayor que hemos medido, y se desmarca claramente del resto de los embalses en su influencia sobre las propiedades ópticas, absorbiendo menos luz de la que debería (Figura 2). Puesto que la antigüedad y la cantidad de área arbolada incrementan la cantidad de DOC (Tabla 3) el hecho de que Jándula sea el embalse más antiguo y con mayor área de arbolado en su cuenca de captación sugiere que la fotodegradación (blanqueo por radiación solar) (Reche *et al.*, 2000) pueda tener algún papel en la alteración de las propiedades ópticas del DOC de este embalse.

En nuestro trabajo también es importante el efecto de la turbidez, aunque con pendientes de la regresión un orden de magnitud menor. Otros estudios recientes muestran a la turbidez como el principal factor que afecta a ambas propiedades ópticas. Así, en 26 lagos y embalses del noreste de China el principal factor que explica las variaciones en K_d (que osciló entre 0.45 y 15.04 m^{-1}) fue la turbidez y solamente en lagos excepcionalmente claros se encuentra que K_d dependa de la Clorofila o de la materia orgánica disuelta de naturaleza cromofórica (Ma *et al.*, 2016). Igualmente en el trabajo de Borowiak y Borowiak (2016), citado previamente, también la turbidez fue la variable que mejor explicó la variación en K_d . El hecho de que las propiedades ópticas de nuestros embalses muestren una dependencia clara de la cantidad de material en suspensión, que determina la turbidez, a pesar de tener unos valores de absorción de luz mucho menores y menos variables que en estos trabajos, subraya la importancia de estos materiales como condicionantes de la calidad del agua en nuestra área.

La clorofila-*a* como indicador de la cantidad de fitoplancton es también un factor principal en la absorción de luz de los sistemas acuáticos. Sin embargo, en nuestro estudio la concentración de clorofila-*a* tiene escasa variabilidad entre embalses, entre 0.5 $\mu g L^{-1}$ y 11.5 $\mu g L^{-1}$ aproximadamente (Tabla 2), que es un margen escaso para que se manifieste. Así, trabajos en los que la influencia de la clorofila-*a* es patente tienen mayores rangos de variación entre sistemas como, por ejemplo, en 31 lagos polacos en los que la clorofila-*a* varió entre 1.5 $\mu g L^{-1}$ y 174.4

$\mu\text{g L}^{-1}$ (Dzieszko y Zwoliński 2015). Entre nuestros embalses es destacable el cambio producido en el embalse de Cubillas. En el año 1988/89 este embalse tenía unos valores medios de clorofila-*a* de $33 \mu\text{g L}^{-1}$ y llegaba a tener máximos superiores a $80 \mu\text{g L}^{-1}$ (Morales-Baquero *et al.*, 1991) que contrastan con el valor mucho menor observado en este trabajo (Tabla 2).

Por último, destacar que los datos que se recogen en este trabajo se refieren en su mayoría a la época de mezcla. Esto podría justificar en parte la importancia de la turbidez, y al mismo tiempo, que la concentración de clorofila-*a* no muestre una relación significativa con K_d y SD. Futuros trabajos, en los que se incluyan ambas condiciones (mezcla y estratificación) podrán discernir mejor esta cuestión.

Relación K_d - SD

Dada la simplicidad de las medidas con el disco de Secchi, su uso como predictor de K_d se puede optimizar obteniendo relaciones empíricas en grupos de aguas naturales homogéneas en cuanto a las características que afectan a las propiedades ópticas (Devlin *et al.*, 2009). Estos autores obtienen coeficientes de regresión para la relación logarítmica entre SD y K_d , en aguas marinas de transición (estuarios) (-1.029) y aguas libres y/o costeras (-0.861), estas con menor cantidad de material particulado en suspensión. El coeficiente de regresión obtenido por nosotros (-0.615) es menor que el obtenido por estos autores indicando, probablemente, una menor influencia del material particulado en suspensión. En un trabajo anterior (Morales-Baquero *et al.*, 1991) se realizó un seguimiento mensual, durante un año, de las propiedades ópticas de cuatro embalses del río Genil, dos de los cuales, Cubillas y Los Bermejales también están en el presente trabajo. En aquella ocasión el coeficiente de regresión obtenido para la relación logarítmica entre SD y K_d fue de -0.765 pero con rangos mucho mayores de variación en SD y K_d , que tuvieron valores tan bajos de SD como 0.2 m y tan altos de K_d que alcanzó 5.1 m^{-1} , debido fundamentalmente a las condiciones tróficas del embalse de Cubillas, mucho peores en aquellos años. En la Figura 4, hemos dibujado también la función correspondiente y, como se puede apreciar, ambas ofrecen buenos ajustes, sobre todo para valores de SD superiores a 1 m. Esto permite avalar el uso de estas ecuaciones en nuestros embalses.

Conclusiones

La medida simultánea del coeficiente de extinción vertical de la luz (K_d) y de la profundidad de visión del disco de Secchi (SD) en 12 embalses del sureste peninsular permite constatar que el producto de $K_d \cdot SD$ varía ampliamente entre los sistemas estudiados, indicando que ambos parámetros resultan afectados diferencialmente por los constituyentes de las aguas naturales que determinan sus propiedades ópticas. En concreto, de los tres de estos constituyentes estudiados en el presente trabajo: clorofila-*a*, turbidez y carbono orgánico disuelto (DOC), la turbidez y, especialmente, el DOC afectan a dichas propiedades ópticas. Este último muestra una mayor influencia sobre el K_d que sobre el SD, de acuerdo con los coeficientes de determinación en las ecuaciones de regresión que relacionan el DOC con K_d ($r^2 = 0.56$) y con SD ($r^2 = 0.42$). Nuestros resultados indican que la antigüedad del embalse y la cantidad de superficie arbolada en la cuenca de captación aumentan la concentración de DOC, lo que debe ser tenido en cuenta cuando se evalúe la influencia de este importante constituyente de las aguas naturales sobre la penetración de la luz en los embalses.

A pesar de la diferente influencia de los constituyentes de las aguas naturales sobre K_d y SD, y asumiendo cierta homogeneidad regional en las características que afectan a las propiedades ópticas de las aguas de los embalses estudiados, la robusta regresión obtenida para la relación logarítmica de K_d sobre SD, con coeficiente de determinación $r^2 = 0.8$ y coeficiente de regresión $b = -0.615$, permiten usar a SD como estimador de K_d en estos embalses, especialmente cuando los valores de SD son superiores a 1 m.

Finalmente, la relación obtenida entre SD y Z_{eu} en el conjunto de los embalses estudiados permite proponer la aproximación $Z_{eu} \text{ (m)} \approx 2 \text{ SD (m)} + 6$ como una mejor estima de la zona fótica en los embalses del sureste de la Península Ibérica.

Agradecimientos

La financiación para el presente trabajo fue obtenida del Ministerio de Economía y Competitividad, referencia: CGL2014-52362-R y fondos FEDER. E.L-P. cuenta con un contrato predoctoral de Formación del Profesorado Universitario

(FPU014/02917). Los autores agradecen a los revisores los comentarios recibidos sobre el texto original al que han ayudado a mejorar.

Referencias

- American Public Health Association (APHA). (1992). *Standard methods for the examination of water and wastewater*. 18th edn. Editor por A. E. Greenberg, L. S. Clesceri, y A. D. Eaton. Washington, DC, USA: American Public Health Association.
- Borowiak, D. y Borowiak, M. (2016). Comparative studies of underwater light regimes in lakes of the East-Suwałki Lakeland, *Limnological Review*, 16(4), pp. 173–183. doi: 10.1515/limre-2016-0019.
- Canteras, J. C., Pérez, L., León, P. y Lorda, T. (1999). Efecto de la radiación luminosa en la desaparición de *Escherichia coli* (T90) en medio acuático. Estudio experimental, *Ingeniería del agua*, 6(3), pp. 269–274. doi: 10.4995/ia.1999.2791.
- Carlson, R. E. (1977). A trophic state index for lakes, *Limnology and Oceanography*, 22(2), pp. 361–369. doi: 10.4319/lo.1977.22.2.0361.
- Devlin, M. J., Barry, J., Mills, D. K., Gowen, R. J., Foden, J., Sivyler, D., Greenwood, N., Pearce, D. y Tett, P. (2009). Estimating the diffuse attenuation coefficient from optically active constituents in UK marine waters, *Estuarine, Coastal and Shelf Science*, 82(1), pp. 73–83. doi: 10.1016/j.ecss.2008.12.015.
- Dziesko, P. y Zwoliński, Z. (2015). Trophic diversity of Poznań Lakeland lakes, *Limnological Review*. Sciendo, 15(2), pp. 61–69. doi: 10.2478/limre-2015-0007.
- French, R. H., Cooper, J. J. y Vigg, S. (1982). Secchi Disc Relationships, *Journal of the American Water Resources Association*, 18(1), pp. 121–123. doi: 10.1111/j.1752-1688.1982.tb04538.x.
- Holmes, R. W. (1970). The Secchi Disk in Turbid Coastal Waters, *Limnology and Oceanography*, 15(5), pp. 688–694. doi: 10.4319/lo.1970.15.5.0688.
- Koenings, J. P. y Edmundson, J. A. (1991). Secchi disk and photometer estimates of light regimes in Alaskan lakes: Effects of yellow color and turbidity, *Limnology and Oceanography*, 36(1), pp. 91–105. doi: 10.4319/lo.1991.36.1.0091.
- Ma, J., Song, K., Wen, Z., Zhao, Y., Shang, Y., Fang, C. y Du, J. (2016). Spatial Distribution of Diffuse Attenuation of Photosynthetic Active Radiation and Its Main Regulating Factors in Inland Waters of Northeast China, *Remote Sensing*, 8(11), p. 964. doi: 10.3390/rs8110964.
- Morales-Baquero, R., Conde-Porcuna, J. M., Pérez-Martínez, C. y Cruz-Pizarro, L. (1991). Vertical light attenuation in four reservoirs of Genil river (Granada, Spain), *Proceedings of the 17th International Congress on Large Dams (ICOLD)*, 64, pp. 137–148.
- Morris, D. P., Zagarese, H., Williamson, C. E., Balseiro, E. G., Hargreaves, B. R., Modenutti, B., Moeller, R. y Queimalinos, C. (1995). The attenuation of solar UV radiation in lakes and the role of dissolved organic carbon, *Limnology and Oceanography*, 40(8), pp. 1381–1391. doi: 10.4319/lo.1995.40.8.1381.

- Poikane, S. (2009). *Water Framework Directive. Intercalibration Technical Report. Part 2: Lakes*. Luxemburgo: Office for Official Publications of the European Communities. Disponible en: <https://op.europa.eu/en/publication-detail/-/publication/7c03183f-a1b8-4608-9d6d-7bde9fa12e02/language-en>.
- Poole, H. H. y Atkins, W. R. G. (1929). Photo-electric Measurements of Submarine Illumination throughout the Year, *Journal of the Marine Biological Association of the United Kingdom*. Cambridge University Press, 16(1), pp. 297–324. doi: 10.1017/S0025315400029829.
- Prats-Rodríguez, J., Morales-Baquero, R., Dolz-Ripollés, J. y Armengol-Bachero, J. (2014). Aportaciones de la limnología a la gestión de embalses Contributions from limnology to reservoir management, *Ingeniería del agua*, 18(1), pp. 83–97. doi: 10.4995/ia.2014.3145.
- Reche, I., Pace, M. L. y Cole, J. J. (2000). Modeled Effects of Dissolved Organic Carbon and Solar Spectra on Photobleaching in Lake Ecosystems, *Ecosystems*, 3(5), pp. 419–432. doi: 10.1007/s100210000038.
- Rodríguez, J. (2016). *Ecología*. 2nd edn. Madrid: Ediciones Pirámide (Ciencia Y Técnica).
- Scully, N. M. y Lean, D. R. S. (1994). The attenuation of ultraviolet radiation in temperate lakes, *Ergebnisse der Limnologie*, 43, pp. 135–135.
- Tundisi, J. G. y Tundisi, T. M. (2011). *Limnology*. Boca Raton, FL, USA: CRC Press. Disponible en: <https://www.routledge.com/Limnology/Tundisi-Tundisi/p/book/9781138072046>.

Appendix 1 | Atenuación de luz en embalses del sur-este de la Península Ibérica

Appendix 2:

El uso del suelo en las cuencas de captación condiciona la calidad del agua en embalses del sudeste peninsular ibérico

Land-use on the watershed determines the quality of water in Southern Iberian Peninsula reservoirs

Resumen

Se examinan los contenidos de nitrógeno total (NT), fósforo total (PT) y las relaciones NT/PT, en 12 embalses del sur-este de la Península Ibérica, con objeto de indagar la influencia del uso del suelo en las cuencas de captación sobre el estado trófico de estos sistemas. Los embalses mostraron relaciones NT/PT que indican limitación por P o co-limitación según el sistema considerado. Según los análisis de regresión en árbol univariados efectuados, sólo el porcentaje de áreas cultivadas clasifica significativamente a los embalses por sus contenidos en P y N, mientras el porcentaje de áreas urbanas agrupa, además, a los embalses por los contenidos en N. La relación positiva encontrada entre el porcentaje de áreas cultivadas y el estado trófico de los embalses, cuantificado según el índice de Carlson (TSI), indica un deterioro en la calidad del agua en los embalses inducido por la actividad agrícola.

Abstract

We examined total nitrogen (TN) concentration, total phosphorus (TP) concentration, and the TN/PT ratios in 12 reservoirs located in the southern Iberian Peninsula, to study the influence of land-use in the watershed of the reservoirs on the trophic status of these systems. The TN/TP ratios indicated limitation by P or co-limitation according to the system considered. Only the percentage of agriculture areas significantly classifies the reservoirs by their P and N concentrations, while the percentage of urban areas also groups the reservoirs by their N contents, according to the univariate tree regression analyses. We found a positive relationship between the percentage of agriculture areas and the trophic state of the reservoirs (according to the Carlson index, TSI), that indicates a deterioration in water quality in the reservoirs induced by agricultural activity.

Introducción

Las características físicas, químicas y biológicas de las aguas continentales superficiales determinan su calidad, y por tanto, condicionan el uso que de ellas hace la sociedad. Dichas características dependen de una pléyade de factores climáticos, geológicos, morfométricos, etc., que, entre otros efectos, condicionan los aportes de nutrientes desde la cuenca de captación a los lagos y los embalses y, en consecuencia, su estado trófico (Vollenweider, 1989). Esto permite vincular el deterioro de la calidad del agua de dichos sistemas con las perturbaciones humanas en el paisaje que incrementan la concentración de nutrientes en la escorrentía, deterioro conocido como eutrofización. Este es uno de los problemas ambientales que tienen más prevalencia globalmente, a pesar de los esfuerzos de décadas de investigación y de la adopción de medidas preventivas (Smith y Schindler, 2009).

En los embalses los efectos de las perturbaciones del paisaje pueden ser especialmente pronunciados ya que tienden a tener mayor cuenca de captación y mayor proporción área de la cuenca de captación/área superficial de la lámina de agua (AC/AS) que en los lagos naturales, incrementando la materia orgánica, inorgánica y nutrientes que reciben (Thornton *et al.*, 1990; Tong y Chen, 2002; Prats-Rodríguez *et al.*, 2014; Knoll *et al.*, 2015; Hayes *et al.*, 2017). El estudio de las perturbaciones mencionadas es importante precisamente en la Península Ibérica

donde los embalses son muy numerosos (más de 1200, sólo en España) y representan una reserva hídrica fundamental para las necesidades de la sociedad. Los principales nutrientes que determinan el estado trófico de lagos y embalses son nitrógeno (N) y fósforo (P), pero la disponibilidad relativa de uno u otro tiene importantes efectos en las comunidades biológicas, tanto cuantitativos como cualitativos, y consecuentemente, en la calidad del agua. Así, la relación entre el N total (NT) y el P total (PT) tiende a ser alta en sistemas oligotróficos y baja en sistemas eutróficos (Downing y McCauley, 1992).

La actividad humana altera profundamente la forma en la que los suelos exportan el N y el P. De forma natural, los terrenos tienden a retener el P, de ciclo biogeoquímico simple y fácilmente capturado por los organismos, y exportar en mayor medida el N, de ciclo biogeoquímico más complejo y con formas móviles en los suelos. Así, la escorrentía de los suelos en terrenos no fertilizados tiene relaciones NT/PT, en masa, del orden de 274, pero entre 20 y 60 en cultivos fertilizados y de sólo alrededor de 5 en las aguas residuales o la escorrentía urbana (Downing y McCauley, 1992). Esta secuencia de valores refleja el incremento en la disponibilidad del P que se provoca con la fertilización de los cultivos para la producción de alimentos, y el consumo y descomposición en las áreas urbanas de los alimentos producidos, que libera el P retenido por los organismos. Por otra parte, desde el logro de la síntesis del amoníaco por el proceso Haber-Bosch, la disponibilidad de N para la fertilización de los cultivos es prácticamente ilimitada y ha ocasionado un aumento de los compuestos nitrogenados en los ecosistemas terrestres como nunca antes se ha registrado en la historia de la Biosfera (Rockström *et al.*, 2009). Por tanto, según lo expuesto, cabe esperar diferencias en los aportes de N y P a los embalses en función del uso del suelo que hace la actividad humana en sus cuencas de captación.

El objeto de este trabajo es el de examinar las relaciones NT/PT en 12 embalses del sur-este de la Península Ibérica, que difieren en su edad y sus características físicas, químicas y tróficas, para indagar la influencia del uso del suelo en las cuencas de captación sobre los aportes de N y P y el estado trófico de estos sistemas.

Material y Métodos

La Figura 1 muestra la localización de los embalses estudiados y la Tabla 1 algunas de sus características morfométricas y de las cuencas de captación. Entre julio de 2016 y julio de 2017 cada embalse se muestreó en dos periodos: uno durante la estratificación estival y el otro durante la mezcla otoñal. En cada ocasión, se tomaron medidas pelágicas superficiales de NT, PT, clorofila-*a* y la transparencia del agua con un disco de Secchi blanco de 20 cm. Las muestras para nitrógeno total se acidificaron con ácido fosfórico (pH final < 2) y se analizaron mediante oxidación catalítica a alta temperatura con un analizador Shimadzu (modelo TOC-V SCH) acoplado a un analizador de nitrógeno (TNM-1) (Álvarez-Salgado y Miller, 1998). La concentración de fósforo total se midió por triplicado usando el método de azul de molibdeno tras digestión con una mezcla de persulfato potásico y ácido bórico a 120 °C (APHA, 1992). La concentración de clorofila-*a* se determinó filtrando de 500 a 2000 ml de agua por un filtro de fibra de vidrio GF/F de 0.7 µm de luz de poro. El material particulado retenido se sometió a extracción con metanol al 95 % en la oscuridad a 4 °C durante 24 h. La absorción de los pigmentos obtenidos se midió con un espectrofotómetro Perkin-Elmer UV-Lambda 40 a 665 nm con corrección de luz dispersada a 750 nm (American Public Health Association (APHA), 1992).



Figura 1 | Localización de los embalses estudiados.

Tabla 1 | Algunas características de los embalses estudiados y de sus cuencas de captación.

Embalse	Año de construcción	Altitud (m)	Volumen (hm ³)	Superficie (ha)	Sup. captación (km ²)	% Calizas y dolomías	% síliceos	% carbonatados	% urbano	% cultivos
Cubillas	1956	640	19	194	626	97	0.62	2.42	1.00	64
Colomera	1990	810	40	249	245	95	5.03	0.00	0.94	62
Negratín	1984	618	567	2170	3877	50	5.80	7.56	0.58	45
La Bolera	1967	950	53	265	163	47	0.00	47.89	0.00	3
Los Bermejales	1958	852	103	562	375	17	47.26	0.00	0.38	30
Iznájar	1969	425	981	2522	5000	74	11.28	2.44	3.25	58
Francisco Abellán	1991	942	58	231	184	37	22.37	27.79	0.93	14
Béznar	1986	486	53	170	347	17	52.44	14.89	2.48	32
San Clemente	1990	1050	118	622	574	68	0.00	23.77	0.12	12
El Portillo	1999	920	33	143	113	71	0.00	27.57	0.04	4
Rules	2003	239	111	309	732	14	72.92	7.43	1.12	24
Jándula	1932	350	322	1350	1547	41	90.57	0.00	1.13	19

El análisis de las cuencas de captación se realizó mediante el software ArcGIS® (ESRI, 2012) bajo la licencia de la Universidad de Granada, utilizando las bases de datos de: Ministerio de Agricultura y Pesca, Alimentación y Medio Ambiente; Infraestructura de Datos Espaciales de Andalucía (IDEA Andalucía) y Red de Información Ambiental de Andalucía (REDIAM). Así, se pudieron determinar los porcentajes de superficies en las respectivas cuencas de captación con diferentes litologías, por un lado, y usos del suelo, por otro.

Para buscar las variables de la cuenca de captación de los embalses (variables predictoras) que más influyen en sus contenidos de NT y PT (como variables dependientes), e identificar los valores umbrales de las variables predictoras que mejor discriminan los embalses según sus contenidos de las variables dependientes, se construyeron árboles de regresión univariados. Estos árboles de regresión son un método de separación dicotómica en el que un conjunto de objetos, en nuestro caso embalses, es dividido progresivamente en los subconjuntos que reducen la variabilidad de la variable dependiente de forma más significativa. Este tipo de regresión permite conocer de forma muy intuitiva las interacciones entre las variables predictoras y proporciona una clara imagen de la estructura de los datos (Crawley, 2002). Otra ventaja de los árboles de regresión es que son insensibles a los valores atípicos y a la multicolinealidad. Para realizar estos árboles usamos el programa Statistica® con validación cruzada, para evitar el exceso de ajuste, deteniendo el número de divisiones en el árbol más simple que muestra la mejor precisión promedio en la clasificación. Las 7 variables que se usaron como predictoras fueron: 3 según la naturaleza de los suelos, % calizas y dolomías, % suelos silíceos y % suelos carbonatados; 2 según el uso del suelo, % área urbana (con tres categorías: <0.5 ; $0.5 < x < 1.5$ y $1.5 <$) y % áreas cultivadas; y 2 como variables morfogénicas, edad del embalse y relación AC/AS. Las variables dependientes se transformaron logarítmicamente para normalizar sus distribuciones. También usamos el programa R (R Core Team, 2019) y los paquetes readxl (Wickham y Bryan, 2019), car (Fox y Weisberg, 2019), rpart (Therneau y Atkinson, 2019) y rpart.plot (Milborrow, 2019) para el análisis de datos.

La calidad de las aguas de los embalses se estableció mediante el índice de estado trófico (Carlson, 1977).

Resultados

Las variables estudiadas presentan un amplio rango de valores entre los embalses. El NT varía entre 169.5 y 4532.6 $\mu\text{g-N mL}^{-1}$, mientras el PT oscila entre 4.0 y 57.3 $\mu\text{g-P L}^{-1}$. Los promedios de ambas variables en los embalses, durante los periodos de mezcla y estratificación, no mostraron diferencias significativas entre ambos periodos, de acuerdo con los test estadísticos pareados que hemos hecho. Este resultado indica que los contenidos de N y P son propios de cada sistema, más allá de las diferencias estacionales. La relación NT/PT (en masa) varió entre 10.1 y 453.9 lo que sugiere grandes diferencias en la limitación por N o P entre los embalses. La Figura 2 muestra que todos nuestros embalses se sitúan por encima de la relación NT/PT = 9 que es el valor por debajo del cual los lagos muestran claras señales de limitación por N (Guildford y Hecky 2000). La mayor parte de nuestros embalses se situó por encima de la relación NT/PT = 22, indicando limitación por P.

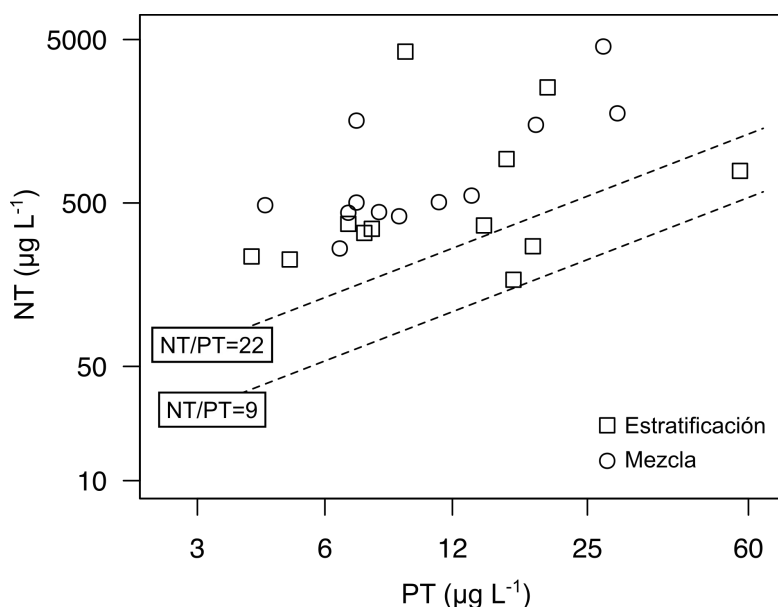


Figura 2 | Concentraciones de NT y PT en los embalses estudiados. Las líneas discontinuas muestran las relaciones NT/PT umbrales para la limitación de N ($\text{NT/PT} < 9$) o P ($\text{NT/PT} > 22$) según Guildford y Hecky (2000).

Los análisis de regresión en árbol realizados para explicar los contenidos en NT y PT de los embalses, usando siete variables de la cuenca de captación como predictoras (ver métodos), muestra que, en el caso del NT, sólo entran en el modelo el porcentaje del área dedicado a cultivo y el porcentaje de áreas urbanas. El análisis (Figure 3a), origina un árbol de tres ramas en el que la primera división,

que reduce la varianza original en un 43 %, se produce por el porcentaje de cultivos en la cuenca de captación, que diferencia tres embalses ($n=3 \times 2=6$), con más del 52 % de cultivos, del resto. Estos embalses presentan los contenidos en NT más elevados. La segunda división se produce por el porcentaje de áreas urbanas en la cuenca y separa a un embalse que tiene más del 1.5 % de áreas urbanas de los otros 8, que presentan, como grupo, el promedio de contenido en NT más bajo. En el caso del PT, el análisis (Figure 3b) produce un árbol de sólo dos ramas, que se dividen por el porcentaje de área cultivada en las cuencas de captación, única variable predictora que entra en el modelo. La división, que supone una reducción de la varianza original del 71 %, separa 5 embalses, que presentan más del 31 % de su cuenca de captación ocupada por cultivos, del resto y tienen el promedio de PT más elevado.

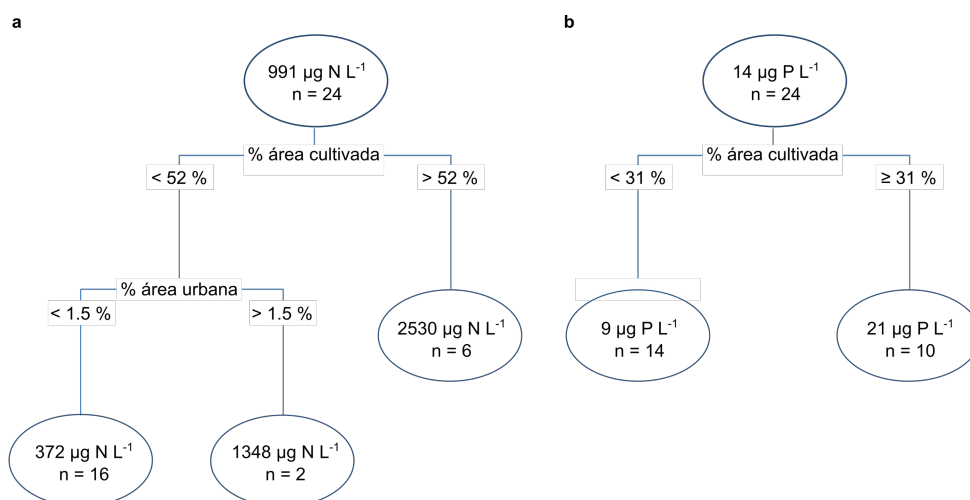


Figura 3 | Análisis de regresión en árbol que muestra las variables significativas predictoras de los contenidos de NT (a) y PT (b) en los embalses estudiados (en estratificación y en mezcla). La altura de las ramas se corresponde con la reducción relativa de la varianza en cada división. En cada una de estas se muestra el valor medio del nutriente en el grupo formado y el número de elementos que lo forma.

Las Figuras 4 y 5 muestran el efecto de los cultivos y las áreas urbanas sobre los contenidos de NT y PT en los embalses. Los análisis de regresión efectuados muestran un efecto positivo muy significativo sobre los contenidos de ambos nutrientes (Figure 4), aunque el efecto del área cultivada se manifiesta más acusadamente sobre el NT (el coeficiente de regresión es 0.013 en el N, frente al 0.006 del P) y, además, los cultivos explican mejor la variabilidad del NT que del PT (coeficiente de determinación de 0.5 en el N frente a 0.2 del P). Como

consecuencia, conforme aumenta el porcentaje de cultivos en las cuencas tienden a subir en las razones NT/PT en los embalses. Las áreas urbanas, a pesar del pequeño porcentaje que ocupan de las cuencas de captación, también presentan un efecto considerable sobre los contenidos de NT y PT (Figure 5). Es notable el caso del N; los embalses con más del 1.5 % de áreas urbanas en las cuencas presentan un fuerte incremento en NT.

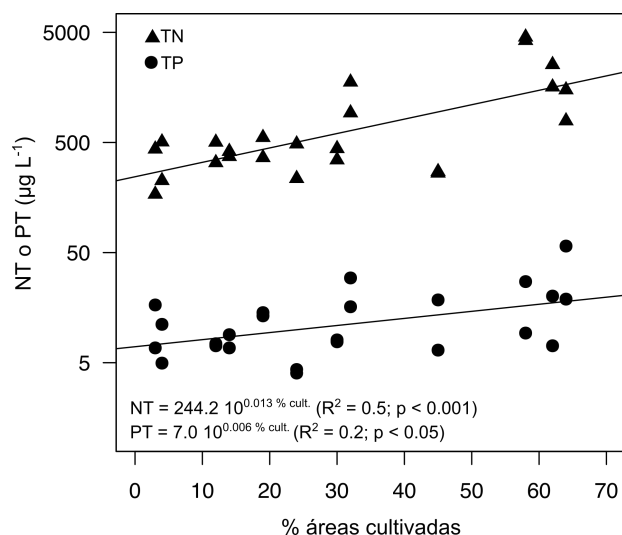


Figura 4 | Relación entre el % de cultivos en las cuencas de captación y los contenidos en NT y PT en los embalses. El eje y está en escala logarítmica.

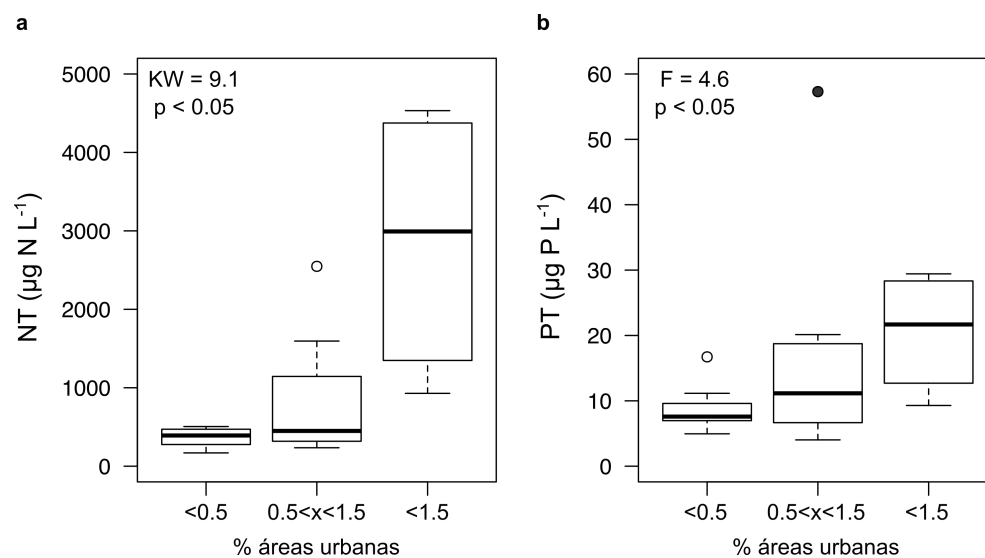


Figura 5 | Valores medianos, percentiles y extremos de NT (a) y PT (b) en los embalses, agrupados según tres categorías del % de áreas urbanas en las cuencas. Los grupos son significativamente diferentes de acuerdo con los test de Kruskal- Wallis (KW) y ANOVA (F) realizados. El valor máximo alcanzado en Cubillas ($57.3 \mu\text{g-P L}^{-1}$) fue considerado un valor atípico (B).

El porcentaje de cultivos en las cuencas es la única variable predictora que entra en los modelos de regresión en árbol tanto para el N como para el P. Su efecto sobre la calidad del agua de los embalses, cuantificada según el índice de estado trófico (TSI) de Carlson (1977), se muestra en la Figura 6. Como se puede apreciar, el aumento de la proporción de cultivos en las cuencas de captación incrementa de forma significativa el estado trófico de los embalses que varían desde la oligotrofia hacia la eutrofia.

Discusión

Aunque nuestro estudio comprende sólo 12 embalses, su diversidad de tipos y cuencas de captación, ya observados previamente (León-Palmero *et al.*, 2019), cubren un espectro suficientemente amplio que permite explorar las relaciones entre las variables de la cuenca y los nutrientes. Así, las concentraciones de NT que encontramos en nuestros embalses tienen un rango de variabilidad comparable al de conjuntos de sistemas lenticos mucho más amplios, como los rangos de variación de NT en 109 embalses de Ohio ($130 - 5300 \mu\text{g N L}^{-1}$), aunque con menos variabilidad de PT en nuestro caso que en dichos embalses ($11 - 715 \mu\text{g P L}^{-1}$) (Knoll *et al.*, 2015). Las relaciones TN/TP de nuestros embalses (entre 10.1 y 452.9) también muestran una amplia variabilidad. Si tomamos como referencia los límites indicados por Guildford y Hecky (2000) (Figure 2), los valores encontrados sugieren tanto limitación por N en unos embalses, y co-limitación en otros. Es interesante señalar que los valores más bajos de TN/TP aparecen en la época de estratificación. En esta época, el aislamiento del epilimnion induce el agotamiento de los nutrientes en esa zona, en especial del más escaso, y como nuestras muestras son superficiales.

Según los resultados de los análisis de regresión en árbol efectuados, los contenidos en N y P de los embalses están fuertemente condicionados por la actividad humana. De todas las variables de la cuenca de captación que hemos considerado, sólo las dos que reflejan la intervención humana: porcentaje de áreas cultivadas y porcentaje de áreas urbanas son las que producen la mejor división de los embalses, y de ellas el porcentaje de cultivo es la única que entra en los modelos de regresión tanto para el N como para el P. Estudios recientes también señalan fuertes relaciones entre el uso antrópico del suelo y los contenidos de N y P

de las aguas continentales. Así, un análisis regional de la calidad del agua superficial en el estado de Ohio (USA) demostró que la agricultura y las aguas urbanas producen mucho más N y P que otras superficies de las cuencas de captación (Tong y Chen, 2002). Por otro lado, el porcentaje de suelo agrícola es la principal variable de la cuenca que predice el estado trófico de 109 embalses de ese estado americano (Knoll *et al.*, 2015).

La actividad agrícola se manifiesta en nuestros resultados, que muestran aumentos en los contenidos de P y N en los embalses según se incrementa el porcentaje de áreas agrícolas en la cuenca. Este resultado es esperable dado que la fertilización de los cultivos introduce N y P. Sin embargo, las pendientes de las regresiones obtenidas muestran que el N aumenta más que el P para un mismo aumento de la superficie de la cuenca dedicada a cultivos, sugiriendo que se retiene en la cuenca más P que nitrógeno durante la escorrentía. En esta misma línea, la revisión de Downing y McCauley (1992) sobre las proporciones TN:TP de diferentes fuentes potenciales de estos nutrientes, encuentra que los fertilizantes tienen relaciones TN:TP en torno a 7.9, una proporción que se ajusta a las necesidades de los cultivos, pero la escorrentía de los terrenos agrícolas tiene razones TN:TP entre 20 y 60, reflejando, probablemente, la mayor movilidad de los compuestos de N frente a los de P y la mayor retención de este por los suelos.

El porcentaje de áreas urbanas, también ha mostrado un efecto significativo sobre las concentraciones de N y P en los embalses estudiados, aunque esta variable no entra como predictora de los contenidos de P en los embalses en la división producida por el análisis de regresión en árbol que hemos realizado. Este resultado puede sorprender, dado que las relaciones NT:PT de las aguas residuales urbanas, entre 2.8 y 10 (Downing y McCauley, 1992), indican que los aportes urbanos son más ricos en P que la escorrentía agrícola. Sin embargo, la proporción de áreas urbanas en las cuencas de captación es muy pequeña y, además, los núcleos urbanos no suelen estar cerca de los embalses. Ambos factores, junto con la comentada mayor capacidad de retención del P que muestran los suelos, pueden explicar la pérdida de peso de las áreas urbanas al predecir el P que se encuentra en los embalses.

El efecto de las áreas cultivadas en las cuencas de captación se manifiesta finalmente en la calidad de las aguas de los embalses, como demuestra la relación

que hemos encontrado entre esa variable predictora y el índice de estado trófico de Carlson (1977). Este índice agrupa, en un solo valor, tres variables relacionadas con la calidad del agua: transparencias del agua, concentración de PT y concentración de clorofila-*a*, y se ha usado para establecer las principales categorías tróficas: oligotrófico (TSI<40), mesotrófico (40<TSI<50) y eutrófico (50<TSI) (Carlson, 1977). Nuestros resultados reflejan claramente la influencia de las áreas cultivadas, cuya proporción en las cuencas (entre el 3 % y el 64 %, Tabla 1) explica un 24 % de la variabilidad en el estado trófico de los embalses (Figure 6).

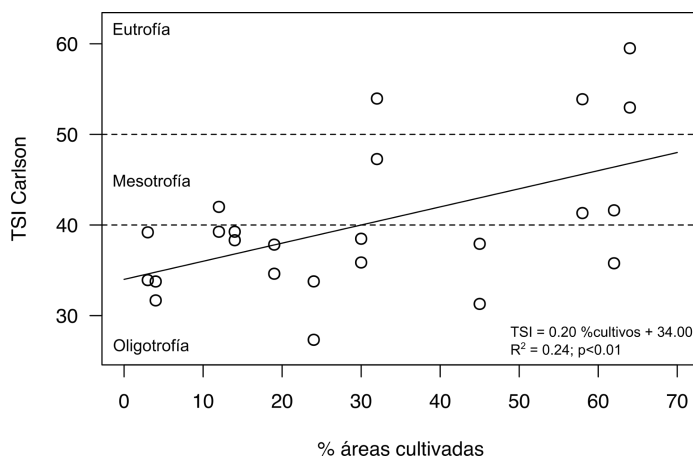


Figura 6 | Índice de estado trófico (TSI) de Carlson en función del porcentaje de área cultivada en la cuenca de captación de cada embalse.

Conclusiones

Teniendo en cuenta lo restringido del área peninsular donde se sitúan los sistemas estudiados, el sudeste ibérico aparece como un área heterogénea en tipos de paisaje que ha permitido establecer relaciones entre las características de los embalses y las de las cuencas que los alimentan. Las áreas agrícolas, donde se producen los alimentos, y los núcleos urbanos, donde se concentra, consume y degrada lo producido en vastas extensiones de terreno, son dos intervenciones humanas de primer orden en las cuencas de captación de las aguas continentales, cuyos efectos hemos podido apreciar en los 12 embalses estudiados. Estas actividades implican la incorporación de N y P de fuentes externas a las cuencas de captación, rompiendo los ciclos biogeoquímicos naturales de estos elementos, que tienden a acumularse en los embalses. La rotura es especialmente aguda en el caso del N. El proceso Haber-Bosch, de síntesis del amoníaco, ha proporcionado a la

humanidad una fuente inagotable de este elemento y propiciado el uso desmedido de los fertilizantes. Por su parte el transporte del P, desde los pocos depósitos mundiales de rocas fosfatadas, hasta los lugares donde se producen y distribuyen los fertilizantes, supone la rotura del ciclo natural de este elemento. En este caso, el recurso es limitado y no tiene sustituto para la producción de alimentos. En consecuencia, los resultados del presente trabajo respaldan la necesidad de mejorar la eficacia en la fertilización de los cultivos y de recuperar los nutrientes en las plantas de tratamiento de las aguas residuales. En el caso del P, es necesario el desarrollo de una ingeniería que permita recuperar este elemento en una forma que sea fácilmente utilizable para la confección de fertilizantes.

Agradecimientos

La financiación para el presente trabajo fue obtenida del Ministerio de Economía y Competitividad, referencia: CGL2014-52362-R. E.L-P. cuenta con un contrato predoctoral de Formación del Profesorado Universitario (FPU014/02917) del Ministerio de Educación.

Referencias

- Álvarez-Salgado, X. A. y Miller, A. E. J. (1998). Simultaneous determination of dissolved organic carbon and total dissolved nitrogen in seawater by high temperature catalytic oxidation: conditions for precise shipboard measurements, *Marine Chemistry*, 62(3), pp. 325–333. doi: 10.1016/S0304-4203(98)00037-1.
- American Public Health Association (APHA) (1992). *Standard methods for the examination of water and wastewater* Washington, DC, USA: American Public Health Association. 18th edn. Edited by A. E. Greenberg, L. S. Clesceri, y A. D. Eaton.
- Carlson, R. E. (1977). A trophic state index for lakes, *Limnology and Oceanography*, 22(2), pp. 361–369. doi: 10.4319/lo.1977.22.2.0361.
- Crawley, M. J. (2002). *Statistical Computing: An Introduction to Data Analysis using S-Plus* Chichester, UK: Wiley.
- Downing, J. A. y McCauley, E. (1992). The nitrogen: phosphorus relationship in lakes, *Limnology and Oceanography*, 37(5), pp. 936–945. doi: 10.4319/lo.1992.37.5.0936.
- ESRI. (2012). *ArcGIS* Redlands, CA. Available at: www.esri.com.
- Fox, J. y Weisberg, S. (2019). *An R Companion to Applied Regression* Thousand Oaks CA: Sage. Third. Available at: <https://socialsciences.mcmaster.ca/jfox/Books/Companion/>.
- Guildford, S. J. y Hecky, R. E. (2000). Total nitrogen, total phosphorus, and nutrient limitation in lakes and oceans: Is there a common relationship?, *Limnology and Oceanography*,

- 45(6), pp. 1213–1223. doi: 10.4319/lo.2000.45.6.1213.
- Hayes, N. M., Deemer, B. R., Corman, J. R., Razavi, N. R. y Strock, K. E. (2017). Key differences between lakes and reservoirs modify climate signals: A case for a new conceptual model, *Limnology and Oceanography Letters*, 2(2), pp. 47–62. doi: 10.1002/lol2.10036.
- Knoll, L. B., Hagenbuch, E. J., Stevens, M. H., Vanni, M. J., Renwick, W. H., Denlinger, J. C., Hale, R. S. y González, M. J. (2015). Predicting eutrophication status in reservoirs at large spatial scales using landscape and morphometric variables, *Inland Waters*, 5(3), pp. 203–214. doi: 10.5268/IW-5.3.812.
- León-Palmero, E., Reche, I. y Morales-Baquero, R. (2019). Atenuación de luz en embalses del sur-este de la Península Ibérica, *Ingeniería del agua*, 23(1), pp. 65–75. doi: 10.4995/ia.2019.10655.
- Milborrow, S. (2019). *rpart.plot: Plot 'rpart' Models: An Enhanced Version of 'plot.rpart'*. Available at: <https://CRAN.R-project.org/package=rpart.plot>.
- Prats-Rodríguez, J., Morales-Baquero, R., Dolz-Ripollés, J. y Armengol-Bachero, J. (2014). Aportaciones de la limnología a la gestión de embalses Contributions from limnology to reservoir management, *Ingeniería del agua*, 18(1), pp. 83–97. doi: 10.4995/ia.2014.3145.
- R Core Team. (2019). *R: A Language and Environment for Statistical Computing* Vienna, Austria: R Foundation for Statistical Computing. Available at: <https://www.R-project.org/>.
- Rockström, J., Steffen, W., Noone, K., Persson, Å., Chapin lii, F. S., Lambin, E. F., Lenton, T. M., Scheffer, M., Folke, C., Schellnhuber, H. J., Nykvist, B., de Wit, C. A., Hughes, T., van der Leeuw, S., Rodhe, H., Sörlin, S., Snyder, P. K., Costanza, R., Svedin, U., Falkenmark, M., Karlberg, L., Corell, R. W., Fabry, V. J., Hansen, J., Walker, B., Liverman, D., Richardson, K., Crutzen, P. y Foley, J. A. (2009). A safe operating space for humanity, *Nature*, 461, pp. 472–475. doi: 10.1038/461472a.
- Smith, V. H. y Schindler, D. W. (2009). Eutrophication science: where do we go from here?, *Trends in Ecology & Evolution*, 24(4), pp. 201–207. doi: 10.1016/j.tree.2008.11.009.
- Therneau, T. y Atkinson, B. (2019). *rpart: Recursive Partitioning and Regression Trees*. Available at: <https://CRAN.R-project.org/package=rpart>.
- Thornton, K. W., Kimmel, B. L. y Payne, F. E. (1990). *Reservoir Limnology: Ecological Perspectives* John Wiley & Sons.
- Tong, S. T. Y. y Chen, W. (2002). Modeling the relationship between land use and surface water quality, *Journal of Environmental Management*, 66(4), pp. 377–393. doi: 10.1006/jema.2002.0593.
- Vollenweider, R. A. (1989). Eutrophication, in Meybeck, M., Chapman, D. V., and Helmer, R. (eds) *Global Freshwater Quality: A First Assessment*, pp. 107–120.
- Wickham, H. y Bryan, J. (2019). *readxl: Read Excel Files*. Available at: <https://CRAN.R-project.org/package=readxl>.

Appendix 3:

Supplementary Material for Chapter 3

Greenhouse gas fluxes from reservoirs determined by watershed lithology, morphometry, and anthropogenic pressure

Elizabeth León-Palmero¹, Rafael Morales-Baquero¹ and Isabel Reche^{1,2}

¹Instituto del Agua and Departamento de Ecología, Universidad de Granada, E-18071 Granada, Spain

²Research Unit Modeling Nature (MNat), Universidad de Granada, E-18071 Granada, Spain

Supplementary Material:

Detailed methods

Supplementary Tables 3.1 - 3.6

Supplementary Figures 3.1 - 3.25

Detailed Methods

Reservoir morphometry and watershed characterization

We collected data on reservoir area, capacity, age, and location from the open databases: Infraestructura de Datos Espaciales de Andalucía (IDEAndalucia; <http://www.ideandalucia.es/portal/web/ideandalucia/>) and the Ministerio para la Transición Ecológica (<https://www.embalses.net/>) (Supplementary table 3.1).

We obtained the lithology and land-use maps using ArcGIS® 10.2 software (ESRI, 2012) under the Universidad de Granada license. First, we delimited the watershed of each reservoir using the rivers and hydrographical demarcations, and, second, we calculated the area for each different type of lithology and land-use within watersheds (supplementary figures 1-24). We used the databases: Infraestructura de Datos Espaciales (IDE) from the Ministerio de Agricultura, Pesca y Alimentación (MAPA; <https://www.mapa.gob.es/es/cartografia-y-sig/ide/default.aspx>); the Infraestructura de Datos Espaciales de Andalucía (IDEAndalucia; <http://www.ideandalucia.es/portal/web/ideandalucia/>); the Instituto Geológico y Minero de España (IGME; <http://www.igme.es/default.asp>); the Confederación Hidrográfica del Segura (CHSEGURA; <https://www.chsegura.es/chs/>); and The Junta de Comunidades de Castilla-La Mancha (IDE-JCCM; <https://castillalamancha.maps.arcgis.com/home/index.html>). We defined the next categories: water-covered area; carbonate-rich rocks; limestones, marls, and dolomites; gravels, conglomerates, sands and silts; and non-calcareous rocks. The soils with high capacity to solubilize dissolved inorganic carbon are carbonate-rich rocks and limestones, marls, and dolomites. In contrast, non-calcareous rocks include igneous rocks like basalt and metamorphic rocks like marble, schist, quartzite, phyllite, gneiss, and slate have less capacity to leach dissolved inorganic carbon. The land-use categories were: crops, forest, urban, treeless area, and water covered area. The forestry area includes trees, plantation trees, sparse trees, and dispersed trees.

Dissolved CH₄ and N₂O in the water column

We collected surface water (0.5 m) in air-tight Winkler bottles by duplicate, preserved with a solution of HgCl₂ (final concentration 1 mM) to inhibit biological activity and sealed with Apiezon® grease to prevent gas exchange. We stored the samples in the dark until analysis in the laboratory. Measurements of CH₄ and N₂O

were performed by headspace equilibration in a 50 ml air-tight glass syringe by duplicate (Sierra *et al.*, 2017b, 2017a). Then, we analyzed simultaneously the concentration of dissolved CH₄ and N₂O of each sample using a gas chromatograph (GC; Bruker® GC-450) equipped with Hydrogen Flame Ionization Detector (FID) and Electron Capture Detector (ECD). The detectors were calibrated daily using three standard gas mixtures, which were made and certified by Air Liquide (France). We calculated the saturation values (%) at the temperature, salinity, and barometric pressure of each reservoir, as the ratio of the dissolved gas measured and the gas concentration expected in equilibrium. The gas concentration in equilibrium was calculated using the functions for the Bunsen solubility for CH₄ (Yamamoto *et al.*, 1976; Wiesenburg and Guinasso, 1979) and for N₂O (Weiss and Price, 1980). We obtained the atmospheric gas concentrations from *The Global Greenhouse Gas Reference Network website* (<https://www.esrl.noaa.gov/gmd/ccgg/index.html>), part of NOAA's Earth System Research Laboratory in Boulder, Colorado. We calculated the 2016 global mean concentrations for CH₄ (Dlugokencky, 2019) and N₂O (Elkins *et al.*, 2017) from the 2016 global monthly mean. The differences among these values and the local atmospheric concentrations are assumed to be small compared with the high dissolved concentrations in the study sites.

Statistical tests

We performed all the statistical analysis in R (R Core Team, 2014) using the packages *car* (Fox and Weisberg, 2011), *nortest* (Gross and Ligges, 2015), and *mgcv* (Wood, 2011). We compared the CO₂ fluxes between stratification and mixing using a two-tailed T-test for paired samples. We compared the CH₄ and N₂O fluxes between stratification and mixing using a Wilcoxon test because these fluxes did not fit normality (supplementary table 3). We analyzed the drivers of fluxes using generalized additive models (GAMs) (Wood, 2006). GAM is a generalized model with a linear predictor involving a sum of smooth functions of covariates (Hastie and Tibshirani, 1986, 1990). The model structure is:

$$y_i = f_1(x_{1i}) + f_2(x_{2i}) + \dots + f_n(x_{ni}) + \epsilon_i \quad \text{Eq. 3.3}$$

Where f_j are the smooth functions, and the ϵ_i are independent identically distributed $N(0, \sigma^2)$ random variables. We fit smoothing functions using penalized cubic regression splines. The smoothness of the functions was estimated using the

cross-validation method (Generalized Cross Validation criterion, GCV). We fitted the models based on minimizing the AIC (Akaike Information Criterion) and the GCV values. We provide details on these GAMs in Supplementary Table 5. We calculated the percentage of variance explained by the model ($\text{adj } R^2$) and the quality of the fit (deviance explained). We also fixed the effect of each predictor to assess the contribution of the other predictor on the deviance explained. Then, the sum of the deviance explained by two predictors can be different from the deviance explained by the model due to interactive effects.

Supplementary Table 3. 1. Construction year, basic morphometry and lithology and land-use watershed analysis in the study reservoirs.

Reservoir	Construction year	Mean depth (m)	Reservoir area (km ²)	Reservoir capacity (hm ³)	Watershed area (km ²)	Lithology: Non-calcareous rocks (km ²)	Lithology: limestones, marls and dolomites (km ²)	Lithology: carbonate-rich rocks (km ²)	Land-Use: urban area (km ²)	Land-Use: crops (km ²)	Land-Use: forest (km ²)	Anthropogenic land-use ratio
Cubillas #1	1956	9.66	1.94	18.74	646.57	3.98	623.6	15.57	6.46	416.83	166.14	2.55
Colomera #2	1990	14.56	2.76	40.18	236.56	11.91	224.65	0	2.23	145.9	64.98	2.28
Negratín #3	1984	24.12	23.51	567.12	3764.62	218.42	2506.13	284.59	21.91	1698.15	1303.95	1.32
La Bolera #4	1967	18.40	2.89	53.19	162.78	0	79.39	77.96	0	4.76	138.81	0.03
Bermejales #5	1958	17.33	5.95	103.12	281.03	132.8	85.24	0	1.07	83.63	133.37	0.64
Iznájar #6	1969	37.55	26.13	981.12	4713.87	531.95	3704.91	115.22	153	2751.98	983.64	2.95
FcoAbellán #7	1991	23.95	2.43	58.21	192.82	43.14	93.42	53.59	1.8	27.33	116.67	0.25
Béznar #8	1986	33.06	1.60	52.90	347.23	182.09	57.39	51.7	8.62	109.85	122.46	0.97
San Clemente #9	1990	31.36	3.76	117.92	152.95	0	111.26	36.35	0.19	18.03	101.38	0.18
El Portillo #10	1999	27.88	1.18	32.90	113.12	0	81.94	31.19	0.04	4.04	62.48	0.07
Jándula #11	1932	38.20	8.43	321.99	2244.8	2026.32	210.89	0	25.36	427.42	1350.03	0.34
Rules #12	2003	36.20	3.06	110.78	1078.36	786.38	155.86	80.08	12.06	254.13	349.91	0.76

Supplementary Table 3.2. CO₂, CH₄ and N₂O fluxes and corresponding climatic forcing of the study reservoirs during the stratification and the mixing periods.

Reservoir	Period	CO ₂ fluxes (mean ± SE, mg C m ⁻² d ⁻¹)	CO ₂ contribution to climatic forcing (%)	CH ₄ fluxes (mean ± SE, mg C m ⁻² d ⁻¹)	CH ₄ contribution to climatic forcing (%)	N ₂ O fluxes (mean ± SE, μg N m ⁻² d ⁻¹)	N ₂ O contribution to climatic forcing (%)	Total climatic forcing in CO ₂ equivalents (mg CO ₂ m ⁻² d ⁻¹)	Total climatic forcing in CO ₂ equivalents (kg CO ₂ d ⁻¹)
Cubillas #1	Stratification	244.4 ± 37.1	2.81	678.84 ± 226.35	96.67	352 ± 84	0.52	31884.03	61855.02
Colomera #2	Stratification	393.1 ± 138.7	29.42	71.39 ± 48.64	66.21	456 ± 192	4.36	4895.50	13511.58
Negratín #3	Stratification	155.8 ± 50.7	96.10	0.51 ± 0.23	3.90	0 ± 0	0.00	593.95	13963.87
La Bolera #4	Stratification	209.5 ± 8.5	92.35	1.40 ± 0.11	7.65	0 ± 0	0.00	831.15	2402.02
Bermejales #5	Stratification	162.5 ± 20.5	75.72	4.21 ± 1.15	24.28	-118 ± 82	0.00	786.56	4680.06
Iznájar #6	Stratification	161.1 ± 34.5	18.60	19.78 ± 5.62	28.29	3601 ± 1032	53.11	3174.52	82950.25
FcoAbellán #7	Stratification	287.6 ± 27.4	78.57	6.33 ± 0.81	21.43	-132 ± 101	0.00	1341.09	3258.84
Béznar #8	Stratification	162.3 ± 37.7	84.87	2.06 ± 0.43	13.38	26 ± 60	1.76	700.55	1120.89
San Clemente #9	Stratification	69.0 ± 2.6	75.95	1.76 ± 0.15	24.05	-154 ± 126	0.00	332.71	1250.99
El Portillo #10	Stratification	26.6 ± 10.6	1.68	125.73 ± 11.83	98.32	0 ± 0	0.00	5806.13	6851.23

Jándula #11	Stratification	-132.0 ± 11.3	0.00	7.18 ± 1.26	100.00	-63 ± 63	0.00	325.97	2747.92
Rules #12	Stratification	-62.0 ± 4.6	0.00	2.74 ± 0.27	100.00	-20 ± 20	0.00	124.53	381.07
Cubillas #1	Mixing	123.1 ± 32.5	62.49	4.41 ± 1.56	27.78	150 ± 119	9.73	721.65	1400.00
Colomera #2	Mixing	54.6 ± 6.4	87.32	0.64 ± 0.16	12.68	-120 ± 112	0.00	229.25	632.73
Negratin #3	Mixing	39.6 ± 2.8	97.00	0.10 ± 0.01	3.00	-107 ± 88	0.00	149.44	3513.34
La Bolera #4	Mixing	97.8 ± 16.5	91.05	0.78 ± 0.14	8.95	-18 ± 18	0.00	393.61	1137.53
Bermejales #5	Mixing	141.3 ± 15.0	94.80	0.63 ± 0.10	5.20	0 ± 0	0.00	546.19	3249.81
Iznájar #6	Mixing	123.4 ± 16.1	68.79	1.29 ± 0.24	8.89	313 ± 67	22.32	657.56	17182.08
Fco Abellán #7	Mixing	104.9 ± 0.0	94.05	0.54 ± 0.00	5.95	-238 ± 0	0.00	408.76	993.29
Béznar #8	Mixing	82.7 ± 11.7	93.51	0.46 ± 0.02	6.49	0 ± 0	0.00	324.06	518.50
San Clemente #9	Mixing	87.0 ± 8.0	94.85	0.38 ± 0.05	5.15	-43 ± 43	0.00	335.99	1263.33
El Portillo #10	Mixing	69.6 ± 20.1	64.55	3.09 ± 0.82	35.45	-22 ± 22	0.00	395.14	466.27
Jándula #11	Mixing	-52.5 ± 10.6	0.00	0.34 ± 0.08	53.60	28 ± 28	46.40	28.68	241.73
Rules #12	Mixing	149.6 ± 21.3	94.09	0.76 ± 0.15	5.91	0 ± 0	0.00	582.68	1783.01

Supplementary Table 3.3. Normality tests and paired data comparisons of the CO₂, CH₄ and N₂O fluxes between the stratification and the mixing periods. We performed the Lilliefors (Kolmogorov-Smirnov) test for normality analysis. For paired data comparison, we performed paired t-test for the comparison of the CO₂ fluxes (i.e. for normal distributed data) and Wilcoxon signed-rank test for CH₄ and N₂O fluxes (i.e. for non-normal distributed data). P-value <0.05 means significant differences between the stratification and mixing periods.

Fluxes	Transformation	Lilliefors (Kolmogorov-Smirnov) Test For Normality		Paired data comparison			
		D	p-value	T- test (t)	Wilcoxon test (V)	df	p-value
CO ₂		0.16029	>0.05	1.36		11	0.2015
CH ₄	Log ₁₀ (CH ₄ flux+1)	0.21321	< 0.01		78	11	0.0025
N ₂ O	Log ₁₀ (N ₂ O flux + 240)	0.21452	< 0.01		53	11	0.2892

Supplementary Table 3.4. Physico-chemical and biological characterization of study reservoirs

Reservoir	Period	DOC (mean \pm SD, mg C L ⁻¹) in the epilimnion	DIC (mean \pm SD, mg C L ⁻¹) in the epilimnion	Surface Chl- <i>a</i> concentration (μ g L ⁻¹)	Respiration rate mg C m ⁻² d ⁻¹	Surface CH ₄ saturation (mean \pm SD, ng L ⁻¹)	Surface CH ₄ saturation (mean \pm SD, %)	Surface oxygen concentration (mg L ⁻¹)	Surface oxygen saturation (%)	Surface water temperature (°C)
Cubillas #1	Stratification	2.12 \pm 0.06	29.79 \pm 0.12	16.1	4566.00	121776.2 \pm 3551.3	339999 \pm 9915	8.892	120.584	28.43
Colomera #2	Stratification	1.28 \pm 0.06	26.36 \pm 0.00	2.2	1759.77	26101.6 \pm 257.7	72626 \pm 717	7.46	101.166	26.05
Negratín #3	Stratification	1.41 \pm 0.05	28.06 \pm 0.07	1.1	2742.82	949.3 \pm 20.7	2576 \pm 56	7.656	100.613	25.83
La Bolera #4	Stratification	1.57 \pm 0.17	37.35 \pm 0.42	0.9	1291.35	2574.8 \pm 99.9	4589 \pm 178	8.475	115.148	25.67
Bermejales #5	Stratification	1.31 \pm 0.01	30.78 \pm 0.03	1.0	2534.24	6380.0 \pm 1101.1	17423 \pm 3007	7.747	102.994	24.85
Iznájar #6	Stratification	1.65 \pm 0.01	24.99 \pm 0.67	5.3	5810.44	14030.7 \pm 711.3	37944 \pm 1924	8.384	109.93	26.85
FcoAbellán #7	Stratification	1.18 \pm 0.01	35.70 \pm 0.04	2.0	1126.92	5855.4 \pm 30.4	15153 \pm 79	7.774	98.434	21.48
Béznar #8	Stratification	0.89 \pm 0.01	42.23 \pm 0.01	6.9	7629.82	4191.0 \pm 42.1	6926 \pm 70	7.569	90.51	21.34

San Clemente #9	Stratification	1.58 ± 0.02	34.95 ± 0.51	2.2	511.85	7062.3 ± 996.5	19431 ± 2742	7.131	95.665	24.79
El Portillo #10	Stratification	1.13 ± 0.00	31.46 ± 0.06	1.9	359.18	13591.3 ± 102.2	37817 ± 284	6.996	94.814	25.77
Jándula #11	Stratification	4.45 ± 0.00	20.68 ± 0.01	1.6	1651.77	9637.6 ± 132.7	26070 ± 359	5.381	70.63	27.26
Rules #12	Stratification	1.26 ± 0.04	28.35 ± 0.47	3.1	3307.66	2800.0 ± 169.3	7222 ± 437	6.821	85.548	25.55
Cubillas #1	Mixing	2.80 ± 0.20	42.70 ± 0.21	7.9	ND	5295.8 ± 15.7	9690 ± 29	7.302	67.144	9.81
Colomera #2	Mixing	1.44 ± 0.01	30.28 ± 0.02	0.2	ND	3080.0 ± 276.6	5997 ± 539	10.18	99.18	11.75
Negratín #3	Mixing	1.71 ± 0.08	32.50 ± 0.12	0.6	ND	440.6 ± 9.5	827 ± 18	9.289	87.184	9.80
La Bolera #4	Mixing	1.35 ± 0.02	43.17 ± 0.08	1.5	ND	2511.1 ± 128.0	5400 ± 275	8.032	85.887	14.91
Bermejales #5	Mixing	1.19 ± 0.04	38.78 ± 0.02	1.0	ND	760.0 ± 10.7	1530 ± 22	7.817	78.583	13.64
Iznájar #6	Mixing	2.00 ± 0.10	38.18 ± 0.09	18.6	ND	1703.6 ± 62.1	3444 ± 126	8.376	83.922	15.67
FcoAbellán #7	Mixing	1.50 ± 0.02	41.94 ± 0.04	1.1	ND	1037.3 ± 33.5	2144 ± 69	8.066	83.17	11.76

Béznar #8	Mixing	1.60 ± 0.08	52.95 ± 0.00	20.2	ND	1052.4 ± 74.3	2047 ± 145	7.982	77.516	11.75
San Clemente #9	Mixing	1.63 ± 0.05	39.79 ± 0.03	3.0	ND	1325.5 ± 15.3	2686 ± 31	9.23	93.539	11.64
El Portillo #10	Mixing	0.96 ± 0.05	36.05 ± 0.10	0.6	ND	3186.6 ± 63.2	6552 ± 130	7.791	79.944	12.79
Jándula #11	Mixing	4.95 ± 0.04	17.69 ± 0.01	1.6	ND	771.2 ± 28.8	1664 ± 62	7.377	78.584	17.65
Rules #12	Mixing	0.79 ± 0.01	28.78 ± 0.09	1.0	ND	767.5 ± 9.9	1567 ± 20	7.145	72.228	16.06

Reservoir	Period	TN (mean \pm SD, mg N L ⁻¹) in the epilimnion	Wind speed (m s ⁻¹)	Surface N ₂ O (mean \pm SD, ng·L ⁻¹)	Surface N ₂ O saturation (mean \pm SD, %)	TDN (mean \pm SD, mg N L ⁻¹) in the epilimnion	NO ₃ ⁻ (mean \pm SD, mg N L ⁻¹) in the epilimnion	NO ₂ ⁻ (mg N L ⁻¹) in the epilimnion	NH ₄ ⁺ (mg N L ⁻¹) in the epilimnion	TP (mean \pm SD, µg P L ⁻¹) in the epilimnion
Cubillas #1	Stratification	0.79 \pm 0.06	2.99	760.9 \pm 44.6	244.3 \pm 14.3	0.65 \pm 0.00	0.59 \pm 0.00	0.03	0.05	57.22 \pm 1.84
Colomera #2	Stratification	2.55 \pm 0.07	3.93	726.1 \pm 34.4	228.1 \pm 10.8	2.47 \pm 0.01	2.46 \pm 0.00	0.04	0.06	20.06 \pm 2.67
Negratín #3	Stratification	0.27 \pm 0.01	2.41	334.1 \pm 20.9	103.8 \pm 6.5	0.22 \pm 0.01	0.18 \pm 0.00	0.08	0.06	18.56 \pm 0.93
La Bolera #4	Stratification	0.17 \pm 0.04	1.99	358.3 \pm 8.7	111.4 \pm 2.7	0.12 \pm 0.00	0.07 \pm 0.00	0.00	0.10	16.86 \pm 2.95
Bermejales #5	Stratification	0.35 \pm 0.00	2.10	312.8 \pm 1.7	95.3 \pm 0.5	0.30 \pm 0.00	0.24 \pm 0.00	0.00	0.07	7.67 \pm 0.79
Iznájar #6	Stratification	4.22 \pm 0.08	3.17	4539.6 \pm 171.1	1418.7 \pm 53.5	3.97 \pm 0.01	3.89 \pm 0.00	0.16	0.06	9.22 \pm 0.83
FcoAbellán #7	Stratification	0.37 \pm 0.08	1.97	378.3 \pm 11.4	105.5 \pm 3.2	0.32 \pm 0.02	0.26 \pm 0.00	0.00	0.07	6.83 \pm 1.42
Béznar #8	Stratification	0.93 \pm 0.01	1.48	598.1 \pm 20.4	157.2 \pm 5.4	0.87 \pm 0.00	0.79 \pm 0.00	0.08	1.05	16.00 \pm 1.01
San Clemente #9	Stratification	0.33 \pm 0.04	1.11	359.8 \pm 13.6	109.1 \pm 4.1	0.31 \pm 0.03	0.22 \pm 0.00	0.00	0.00	7.44 \pm 0.98

El Portillo #10	Stratification	0.23 ± 0.00	1.95	362.9 ± 25.0	112.1 ± 7.7	0.24 ± 0.02	0.15 ± 0.00	0.00	0.00	5.06 ± 0.44
Jándula #11	Stratification	0.36 ± 0.01	2.14	323.0 ± 20.7	100.3 ± 6.4	0.38 ± 0.00	0.16 ± 0.00	0.00	0.00	14.33 ± 0.69
Rules #12	Stratification	0.24 ± 0.01	4.11	438.9 ± 14.0	127.8 ± 4.1	0.24 ± 0.01	0.13 ± 0.01	0.00	0.00	4.11 ± 0.60
Cubillas #1	Mixing	1.50 ± 0.01	2.08	872.5 ± 19.6	150.3 ± 3.4	1.50 ± 0.03	1.12 ± 0.00	0.06	0.00	18.83 ± 0.42
Colomera #2	Mixing	1.60 ± 0.00	1.02	616.4 ± 30.1	115.2 ± 5.6	1.56 ± 0.02	1.51 ± 0.00	0.02	0.00	7.08 ± 0.59
Negratín #3	Mixing	0.26 ± 0.00	1.38	513.6 ± 9.0	93.4 ± 1.6	0.24 ± 0.03	0.21 ± 0.00	0.00	0.00	6.50 ± 0.35
La Bolera #4	Mixing	0.44 ± 0.00	1.43	485.8 ± 12.1	102.8 ± 2.6	0.39 ± 0.02	0.36 ± 0.00	0.00	0.00	6.72 ± 0.25
Bermejales #5	Mixing	0.44 ± 0.03	1.98	529.0 ± 13.2	102.9 ± 2.6	0.42 ± 0.01	0.38 ± 0.00	0.00	0.00	7.94 ± 2.31
Iznájar #6	Mixing	4.53 ± 0.00	2.11	1143.5 ± 18.8	233.4 ± 3.8	4.18 ± 0.05	4.23 ± 0.00	0.13	0.00	27.11 ± 3.67
FcoAbellán #7	Mixing	0.41 ± 0.03	2.55	500.2 ± 9.5	100.3 ± 1.9	0.36 ± 0.02	0.32 ± 0.02	0.01	0.00	8.89 ± 0.87
Béznar #8	Mixing	1.77 ± 0.43	0.92	577.2 ± 21.2	108.6 ± 4.0	1.37 ± 0.01	1.32 ± 0.00	0.08	0.00	29.50 ± 0.58
San Clemente	Mixing	0.50 ± 0.00	1.66	560.2 ± 13.6	108.7 ± 2.6	0.44 ± 0.01	0.45 ± 0.00	0.00	0.00	7.11 ± 0.42

#9																					
El Portillo #10	Mixing	0.51 ± 0.03	1.56	481.5 ± 8.9	95.6 ± 1.8	0.46 ± 0.01	0.38 ± 0.00	0.00	0.00	11.17 ± 5.39											
Jándula #11	Mixing	0.55 ± 0.01	2.91	598.1 ± 19.7	131.8 ± 4.3	0.49 ± 0.01	0.34 ± 0.00	0.00	0.00	13.44 ± 1.40											
Rules #12	Mixing	0.48 ± 0.01	2.73	539.8 ± 24.6	111.3 ± 5.1	0.44 ± 0.02	0.43 ± 0.00	0.00	0.00	4.39 ± 0.59											

Supplementary Table 3.5. Results of the Generalized Additive Models (GAMs) fitted to fluxes of CO₂ (mg C m⁻² d⁻¹) CH₄ (mg C m⁻² d⁻¹) and N₂O N-N₂O ug m⁻² d⁻¹. S.E. = Standard Error; EDF = Estimated Degrees of Freedom. See the main text for the parameters names.

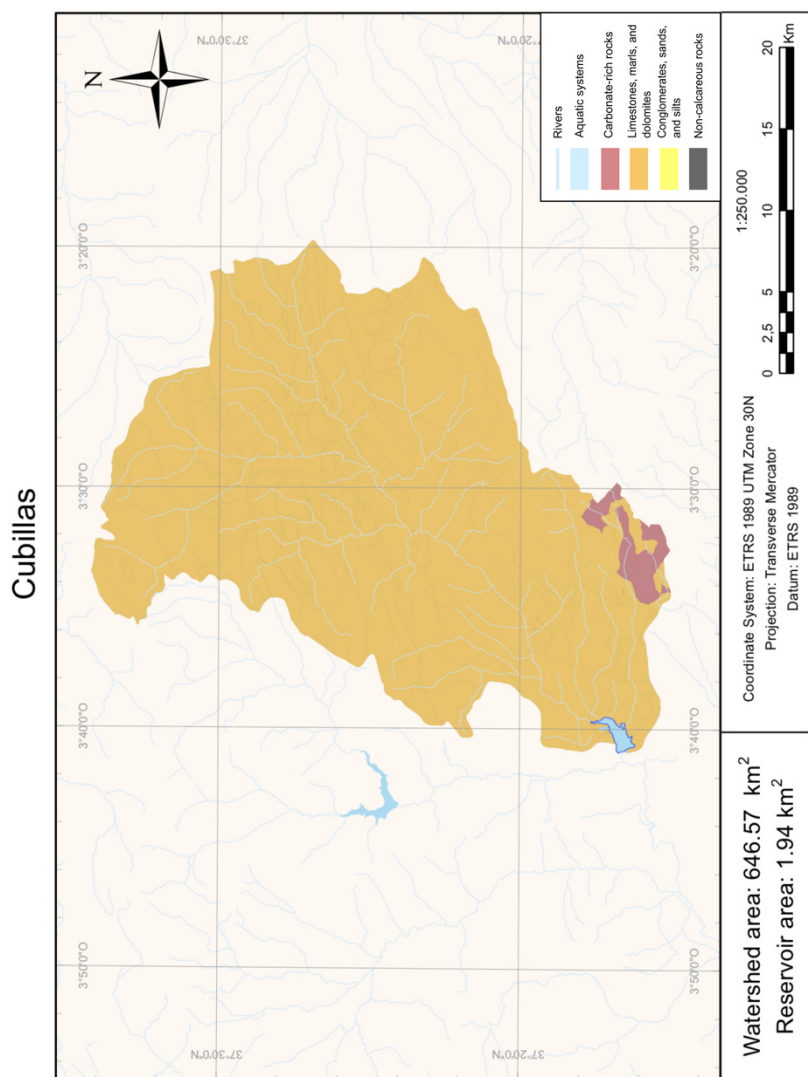
	Drivers	Estimate (±SE)	EDF	t-value	F-value	P-value	Deviance explained
Log ₁₀ (CO ₂ flux + 150), n = 12 R ² _{adj} = 0.91 Deviance explained = 93.4% GCV = 0.02 AIC = -12.14	Intercept	2.36 (0.03)		68.99		<0.001	
	Non-calcareous surface in the watershed (km ²)		1.00		114.77	<0.001	90.7%
	Log ₁₀ (Daily Respiration rate, mg C·m ⁻² ·d ⁻¹)		1.88		6.75	<0.05	9.4%
Log ₁₀ (CH ₄ flux) n = 24 R ² _{adj} = 0.59 Deviance explained = 65.0 % GCV = 0.25 AIC = 35.83	Intercept	0.676(0.09)		7.22		<0.001	
	Surface water temperature (°C)		1.00		21.23	<0.001	38.1%
	Mean depth (log ₁₀ mean depth, m)		2.37		4.62	<0.05	27.6%
Log ₁₀ (N ₂ O flux + 240) n = 23 R ² _{adj} = 0.69 Deviance explained = 72.9% GCV = 0.04 AIC = -6.30	Intercept	2.41 (0.04)		61.39		<0.001	
	Total nitrogen concentration (TN, mg N·L ⁻¹)		1.00		30.42	<0.001	42.7 %
	Wind speed (m·s ⁻¹)		1.50		8.35	<0.01	18.3 %

Supplementary Table 3.6. Linear regressions among land-use in the watershed, nitrogen concentration (in different chemical forms) and N₂O fluxes. n.s. = no significant

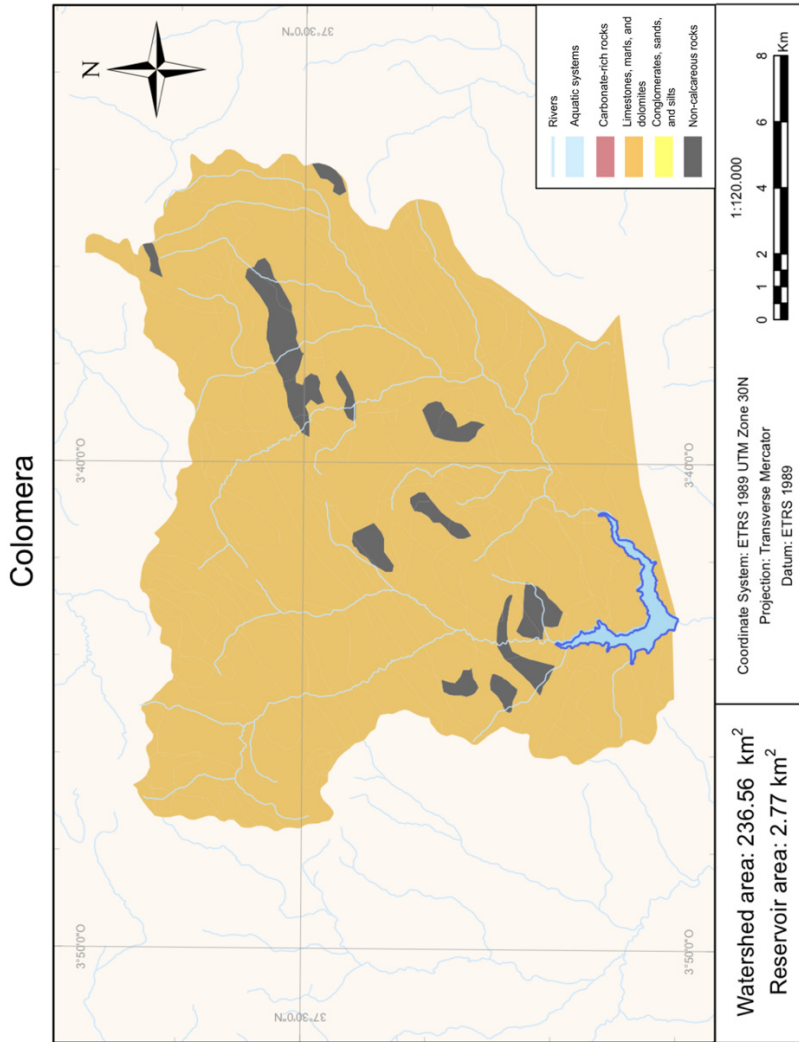
Predictor variable	Response variable	n	Slope estimate (std error)	Adj R ²	p-value
Crop area (km ²) as log ₁₀ (crop area+1)	Total nitrogen concentration (TN, mg N L ⁻¹)	24	0.71 (0.25)	0.23	<0.01
	Total dissolved nitrogen concentration (TDN, mg N L ⁻¹)	24	0.67 (0.24)	0.23	<0.01
	Dissolved inorganic nitrogen (DIN, mg N L ⁻¹)	24	0.69 (0.26)	0.22	<0.05
	Nitrate concentration (NO ₃ ⁻ , mg N L ⁻¹)	24	0.66 (0.24)	0.22	<0.05
	Nitrite concentration (NO ₂ ⁻ , mg N L ⁻¹)	24	0.03 (0.01)	0.33	<0.01
Ammonia concentration (NH ₄ ⁺ , mg N L ⁻¹)	Ammonia concentration (NH ₄ ⁺ , mg N L ⁻¹)	24	n.s.	n.s.	n.s.
	Total nitrogen concentration (TN, mg N L ⁻¹)	24	1.10 (0.31)	0.34	<0.01
	Total dissolved nitrogen concentration (TDN, mg N L ⁻¹)	24	1.02 (0.29)	0.33	<0.01
	Dissolved inorganic nitrogen (DIN, mg N L ⁻¹)	24	1.08 (0.31)	0.32	<0.01
	Nitrate concentration (NO ₃ ⁻ , mg N L ⁻¹)	24	1.01 (0.30)	0.31	<0.01
Urban area (km ²) as log ₁₀ (urban area+1)	Nitrite concentration (NO ₂ ⁻ , mg N L ⁻¹)	24	0.05 (0.01)	0.45	<0.001
	Ammonia concentration (NH ₄ ⁺ , mg N L ⁻¹)	24	n.s.	n.s.	n.s.
	Total nitrogen concentration (TN, mg N L ⁻¹)	24	n.s.	n.s.	n.s.
	Total dissolved nitrogen concentration (TDN, mg N L ⁻¹)	24	n.s.	n.s.	n.s.
	Dissolved inorganic nitrogen (DIN, mg N L ⁻¹)	24	n.s.	n.s.	n.s.
Forest area (km ²) as log ₁₀ (Forest area+1)	Nitrate concentration (NO ₃ ⁻ , mg N L ⁻¹)	24	n.s.	n.s.	n.s.
	Nitrite concentration (NO ₂ ⁻ , mg N L ⁻¹)	24	n.s.	n.s.	n.s.
	Nitrite concentration (NO ₂ ⁻ , mg N L ⁻¹)	24	n.s.	n.s.	n.s.

	Ammonia concentration (NH_4^+ , mg N L^{-1})	24	n.s.	n.s.	n.s.
Crop area (%)	Total nitrogen concentration (TN, mg N L^{-1})	24	0.035 (0.009)	0.38	<0.001
	Total dissolved nitrogen concentration (TDN, mg N L^{-1})	24	0.034 (0.008)	0.40	<0.001
	Dissolved inorganic nitrogen (DIN, mg N L^{-1})	24	0.035 (0.009)	0.37	<0.01
	Nitrate concentration (NO_3^- , mg N L^{-1})	24	0.033 (0.009)	0.37	<0.001
	Nitrite concentration (NO_2^- , mg N L^{-1})	24	0.001 (0.000)	0.36	<0.01
	Ammonia concentration (NH_4^+ , mg N L^{-1})	24	n.s.	n.s.	n.s.
Urban area (%)	Total nitrogen concentration (TN, mg N L^{-1})	24	0.990 (0.163)	0.61	<0.001
	Total dissolved nitrogen concentration (TDN, mg N L^{-1})	24	0.907 (0.159)	0.58	<0.001
	Dissolved inorganic nitrogen (DIN, mg N L^{-1})	24	1.024 (0.153)	0.66	<0.001
	Nitrate concentration (NO_3^- , mg N L^{-1})	24	0.911 (0.162)	0.57	<0.001
	Nitrite concentration (NO_2^- , mg N L^{-1})	24	0.040 (0.006)	0.69	<0.001
	Ammonia concentration (NH_4^+ , mg N L^{-1})	24	n.s.	n.s.	n.s.
Forest area (%)	Total nitrogen concentration (TN, mg N L^{-1})	24	-0.037 (0.011)	0.32	<0.01
	Total dissolved nitrogen concentration (TDN, mg N L^{-1})	24	-0.035 (0.010)	0.32	<0.01
	Dissolved inorganic nitrogen (DIN, mg N L^{-1})	24	-0.037 (0.011)	0.33	<0.01
	Nitrate concentration (NO_3^- , mg N L^{-1})	24	-0.035 (0.010)	0.31	<0.01
	Nitrite concentration (NO_2^- , mg N L^{-1})	24	-0.001 (0.000)	0.37	<0.01
	Ammonia concentration (NH_4^+ , mg N L^{-1})	24	n.s.	n.s.	n.s.
Anthropogenic land-use ratio	Total nitrogen concentration (TN, mg N L^{-1})	24	0.94 (0.16)	0.60	<0.001

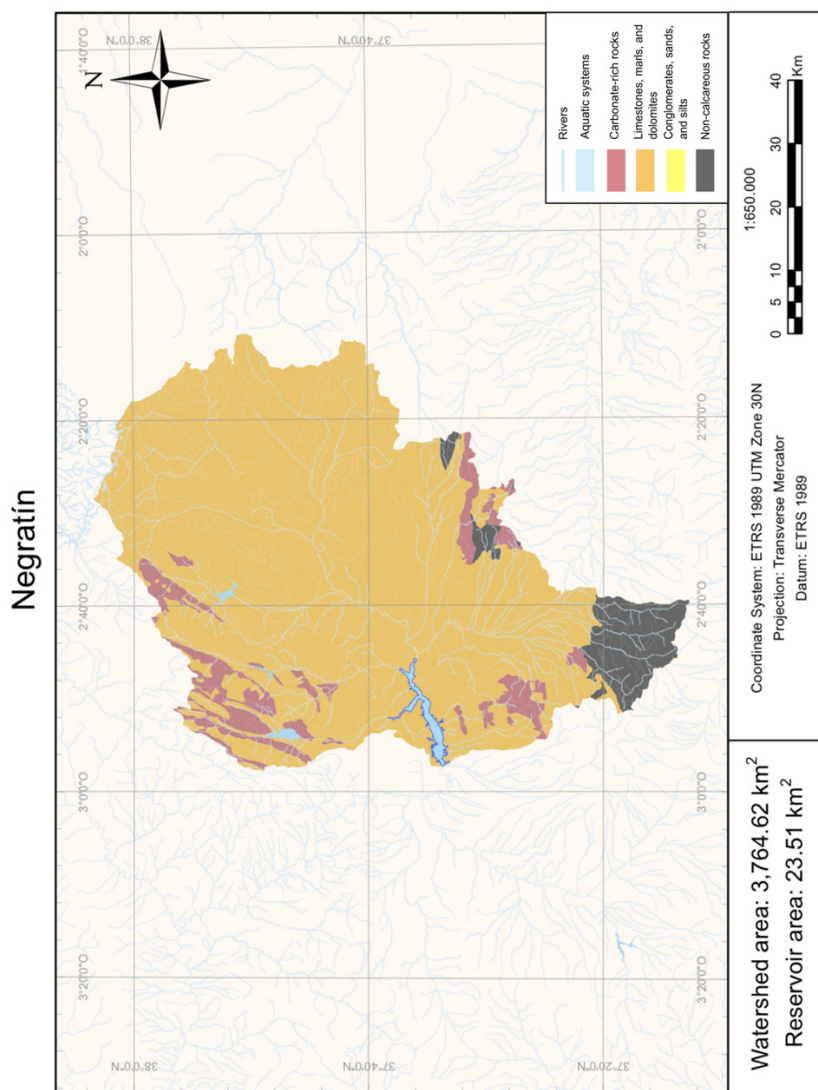
	Total dissolved nitrogen concentration (TDN, mg N L ⁻¹)	24	0.89 (0.14)	0.61	<0.001
	Dissolved inorganic nitrogen (DIN, mg N L ⁻¹)	24	0.92 (0.16)	0.58	<0.001
	Nitrate concentration (NO ₃ ⁻ , mg N L ⁻¹)	24	0.88 (0.15)	0.59	<0.001
	Nitrite concentration (NO ₂ ⁻ , mg N L ⁻¹)	24	0.03 (0.01)	0.52	<0.001
	Ammonia concentration (NH ₄ ⁺ , mg N L ⁻¹)	24	n.s.	n.s.	n.s.
	Total nitrogen concentration (TN, mg N L ⁻¹)	23	0.21 (0.04)	0.52	<0.001
	Total dissolved nitrogen concentration (TDN, mg N L ⁻¹)	23	0.22 (0.04)	0.53	<0.001
	Dissolved inorganic nitrogen (DIN, mg N L ⁻¹)	23	0.48 (0.12)	0.39	<0.001
	Nitrate concentration (NO ₃ ⁻ , mg N L ⁻¹)	23	0.22 (0.04)	0.51	<0.001
	Nitrite concentration (NO ₂ ⁻ , mg N L ⁻¹)	23	0.21 (0.04)	0.51	<0.001
	Ammonia concentration (NH ₄ ⁺ , mg N L ⁻¹)	23	n.s.	n.s.	n.s.
	Crop area (%)	23	0.008 (0.003)	0.23	<0.05
	Urban area (%)	23	0.209 (0.061)	0.33	<0.01
	Forest area (%)	23	-0.008 (0.003)	0.19	<0.05
	Anthropogenic land-use ratio	23	0.221 (0.055)	0.40	<0.001
	Anthropogenic land-use ratio	12	0.374 (0.068)	0.72	<0.001



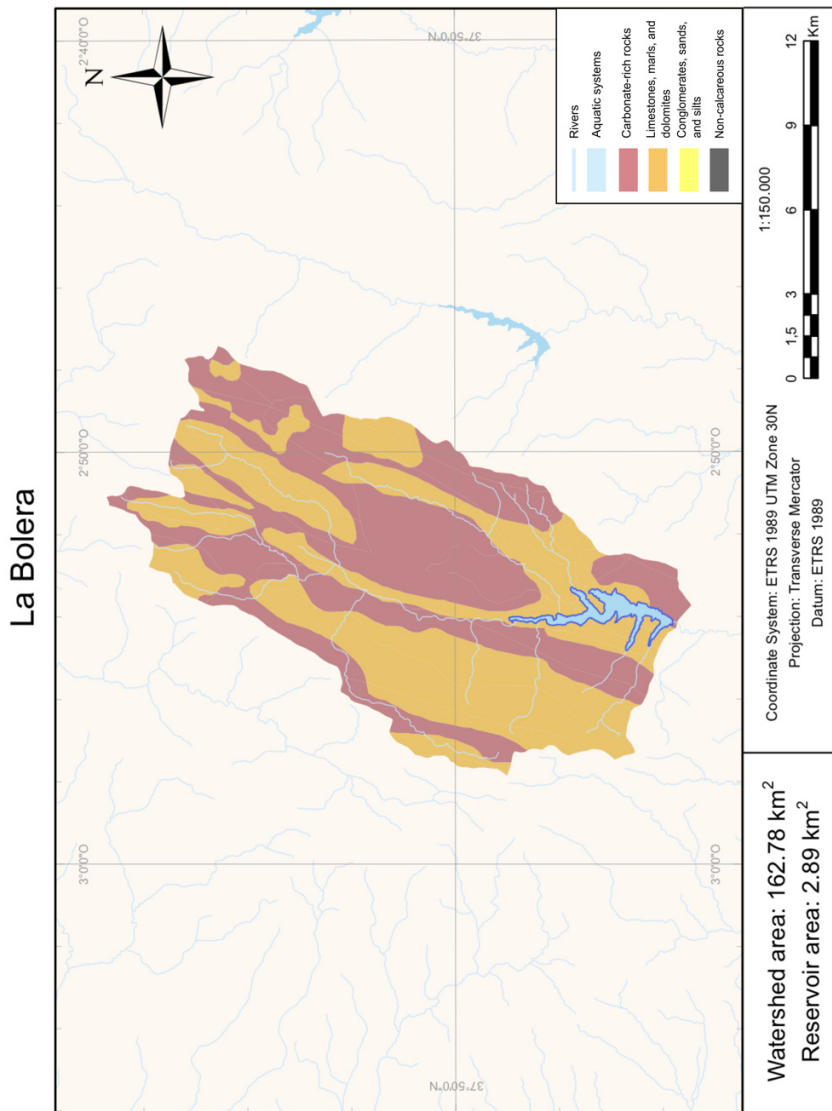
Supplementary Figure 3.1. Map of lithology analysis in the Cubillas reservoir watershed using GIS, showing aquatic systems in blue, carbonate-rich rocks in pink, limestones, marls and dolomites in brown; conglomerates, sands and silts in yellow and non-calcareous rocks in grey. Note that *O* means *W* (west) on the map coordinates.



Supplementary Figure 3.2. Map of lithology analysis in the Colomera reservoir watershed using GIS, showing aquatic systems in blue, carbonate-rich rocks in pink, limestones, marls and dolomites in brown; conglomerates, sands and silts in yellow and non-calcareous rocks in grey. Note that *O* means *W* (west) on the map coordinates.

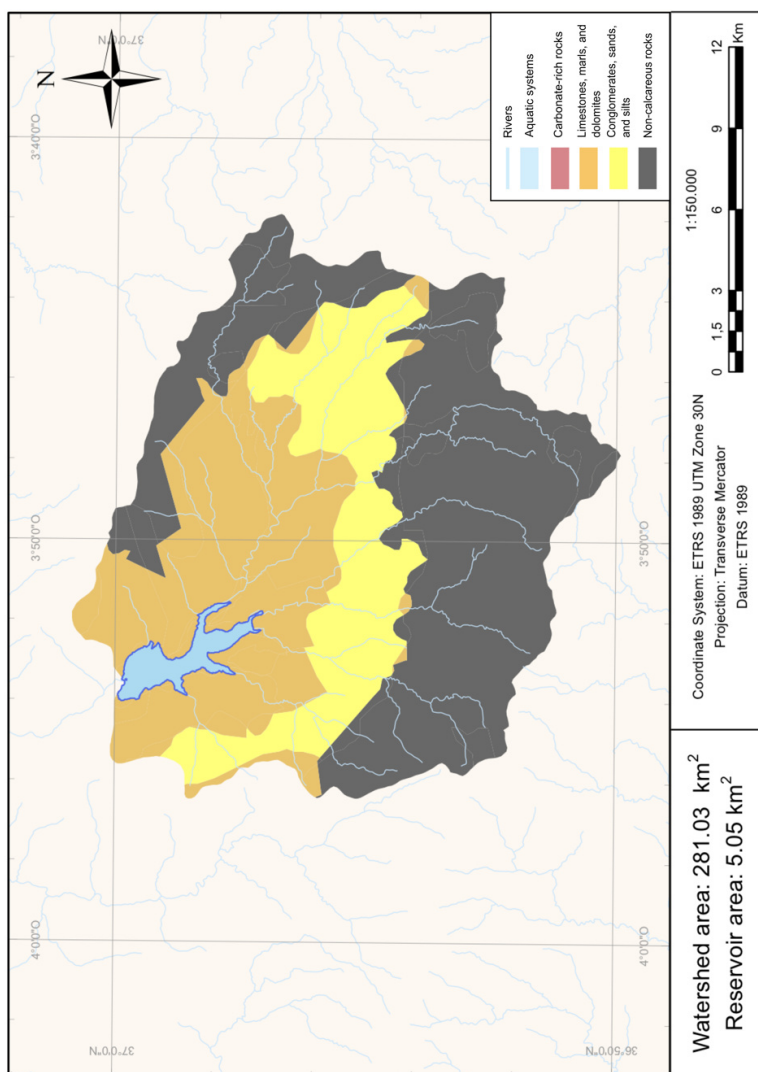


Supplementary Figure 3.3. Map of lithology analysis in the Negratín reservoir watershed using GIS, showing aquatic systems in blue, carbonate-rich rocks in pink, limestones, marls and dolomites in brown; conglomerates, sands and silts in yellow and non-calcareous rocks in grey. Note that O means W (west) on the map coordinates.



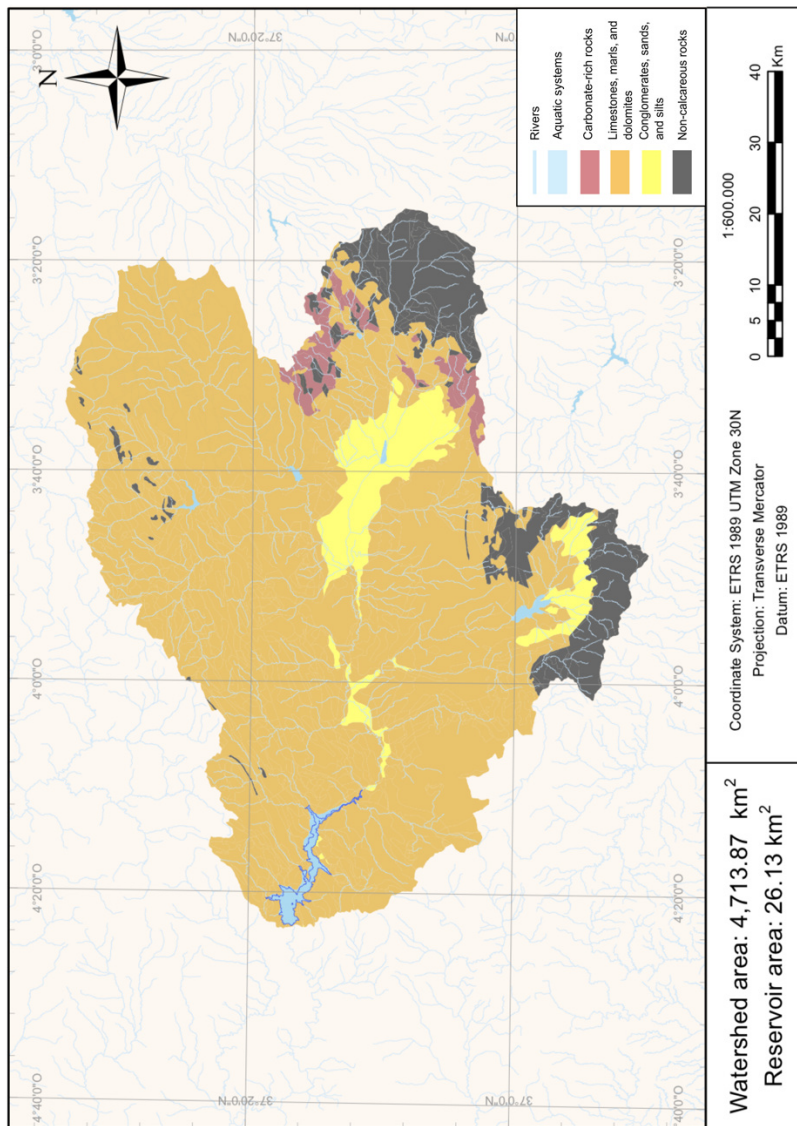
Supplementary Figure 3.4. Map of lithology analysis in the La Bolera reservoir watershed using GIS, showing aquatic systems in blue, carbonate-rich rocks in pink, limestones, marls and dolomites in brown; conglomerates, sands and silts in yellow and non-calcareous rocks in grey. Note that O means W (west) on the map coordinates.

Los Bermejales



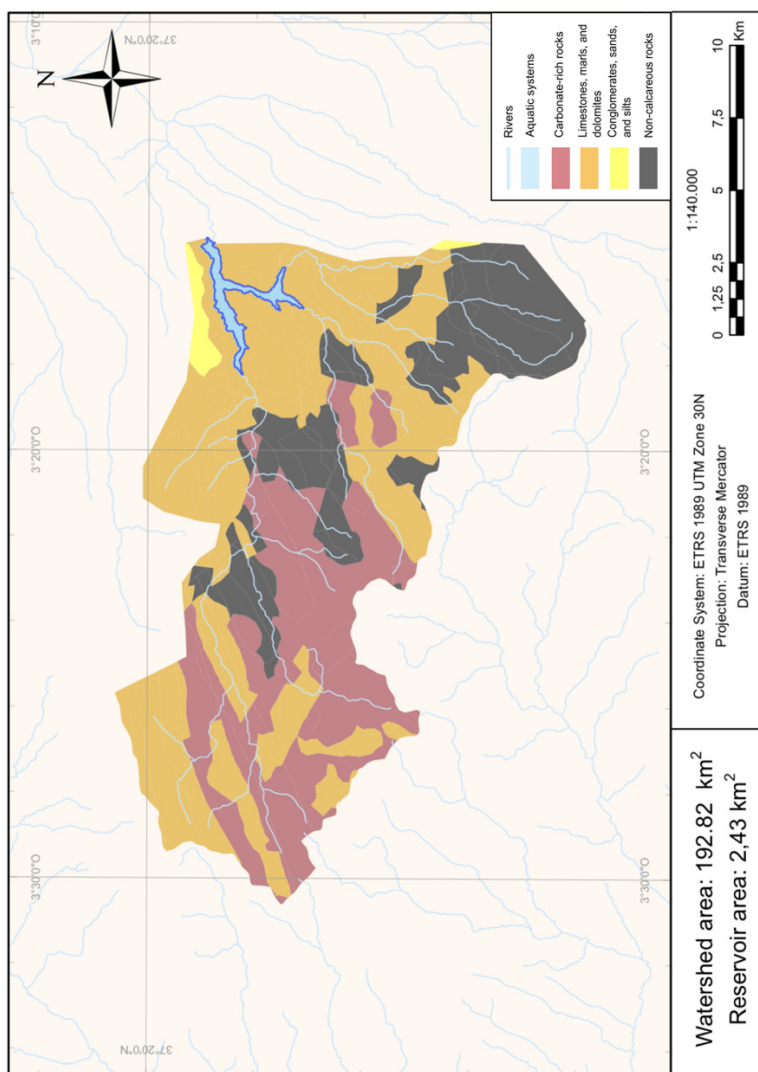
Supplementary Figure 3.5. Map of lithology analysis in Los Bermejales reservoir watershed using GIS, showing aquatic systems in blue, carbonate-rich rocks in pink, limestones, marls and dolomites in brown; conglomerates, sands and silts in yellow and non-calcareous rocks in grey. Note that O means W (west) on the map coordinates.

Iznájar

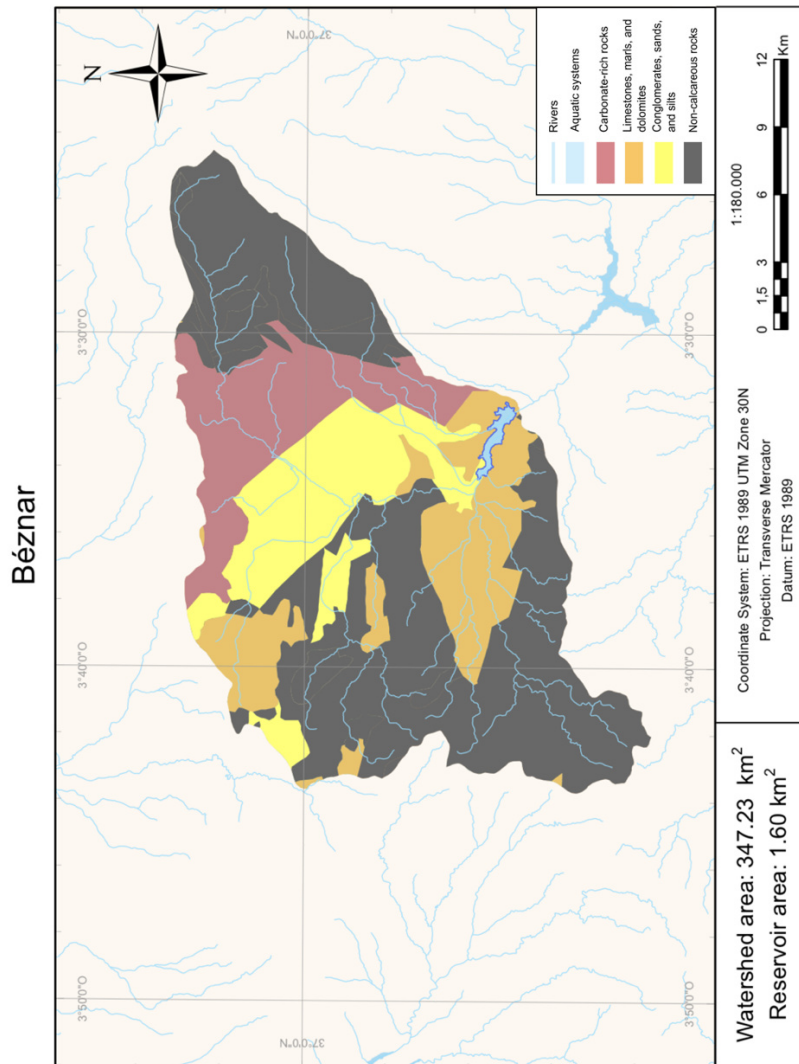


Supplementary Figure 3.6. Map of lithology analysis in the Iznájar reservoir watershed using GIS, showing aquatic systems in blue, carbonate-rich rocks in pink, limestones, marls and dolomites in brown; conglomerates, sands and silts in yellow and non-calcareous rocks in grey. Note that O means W (west) on the map coordinates.

Francisco Abellán

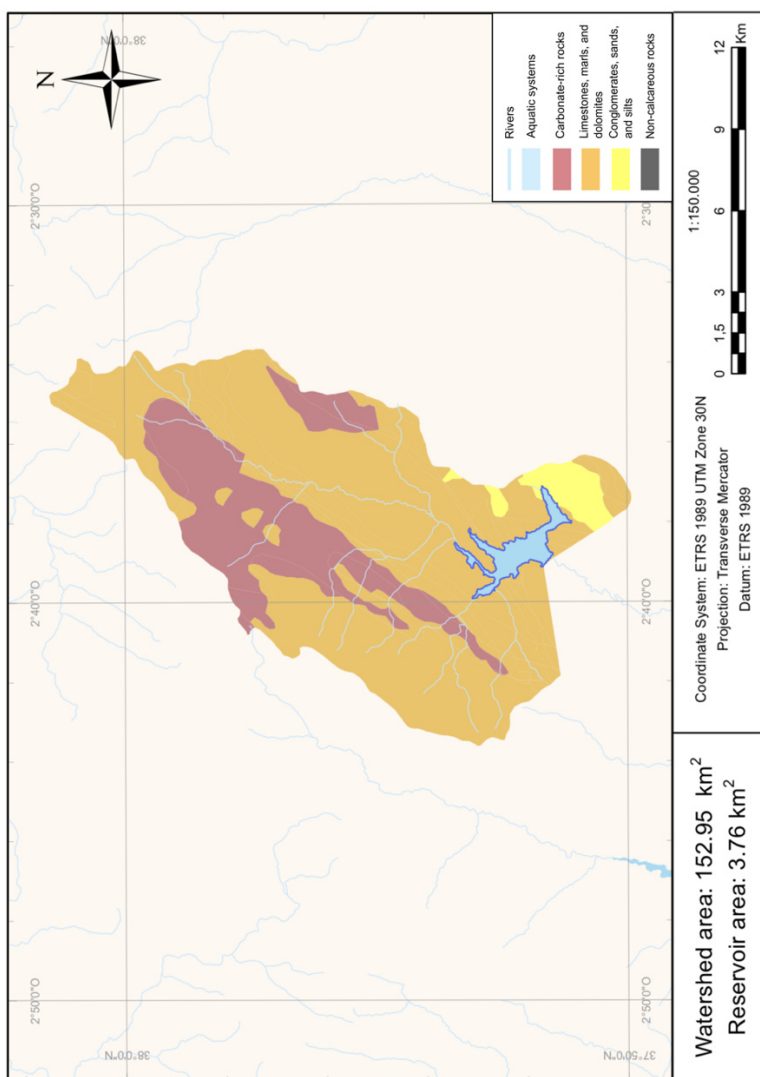


Supplementary Figure 3.7. Map of lithology analysis in the Francisco Abellán reservoir watershed using GIS, showing aquatic systems in blue, carbonate-rich rocks in pink, limestones, marls and dolomites in brown, conglomerates, sands and silts in yellow and non-calcareous rocks in grey. Note that O means W (west) on the map coordinates.



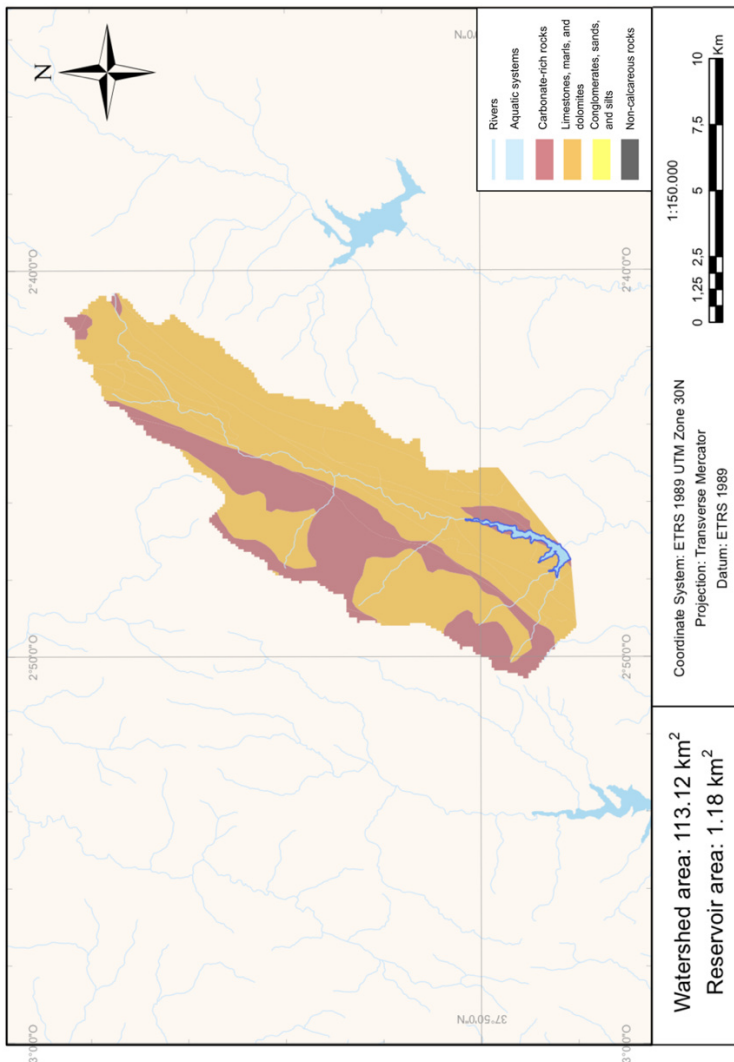
Supplementary Figure 3.8. Map of lithology analysis in the Béznar reservoir watershed using GIS, showing aquatic systems in blue, carbonate-rich rocks in pink, limestones, marls and dolomites in brown; conglomerates, sands and silts in yellow and non-calcareous rocks in grey. Note that O means W (west) on the map coordinates

San Clemente

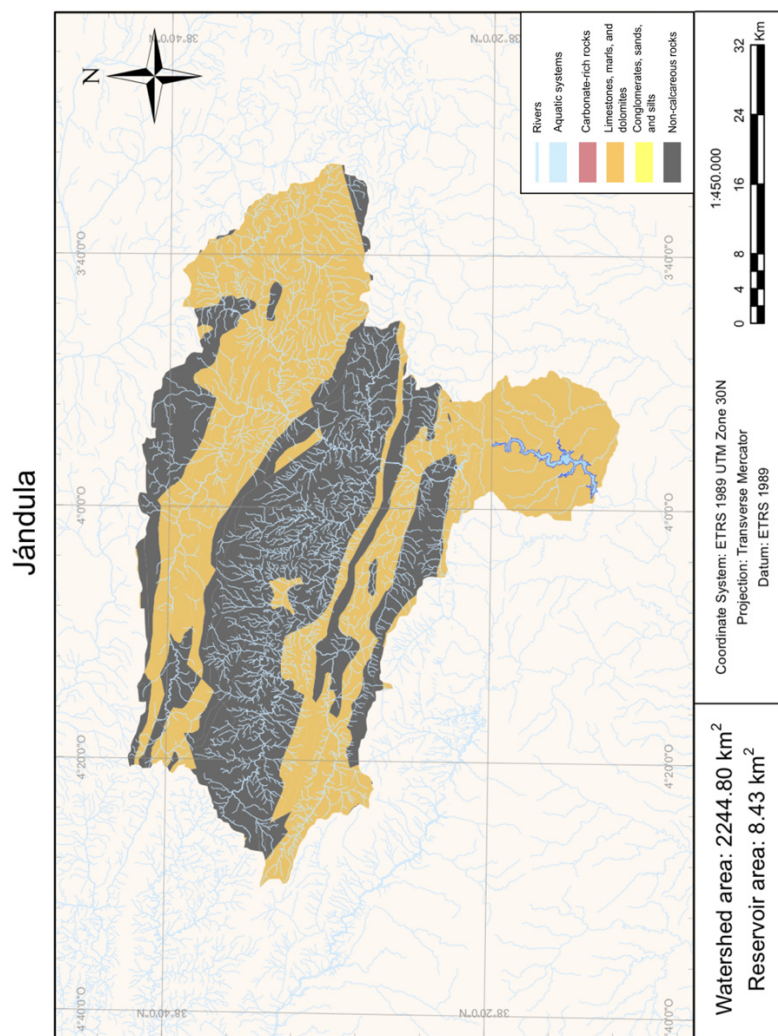


Supplementary Figure 3.9. Map of lithology analysis in the San Clemente reservoir watershed using GIS, showing aquatic systems in blue, carbonate-rich rocks in pink, limestones, marls and dolomites in brown; conglomerates, sands and silts in yellow and non-calcareous rocks in grey. Note that *O* means *W* (west) on the map coordinates.

El Portillo

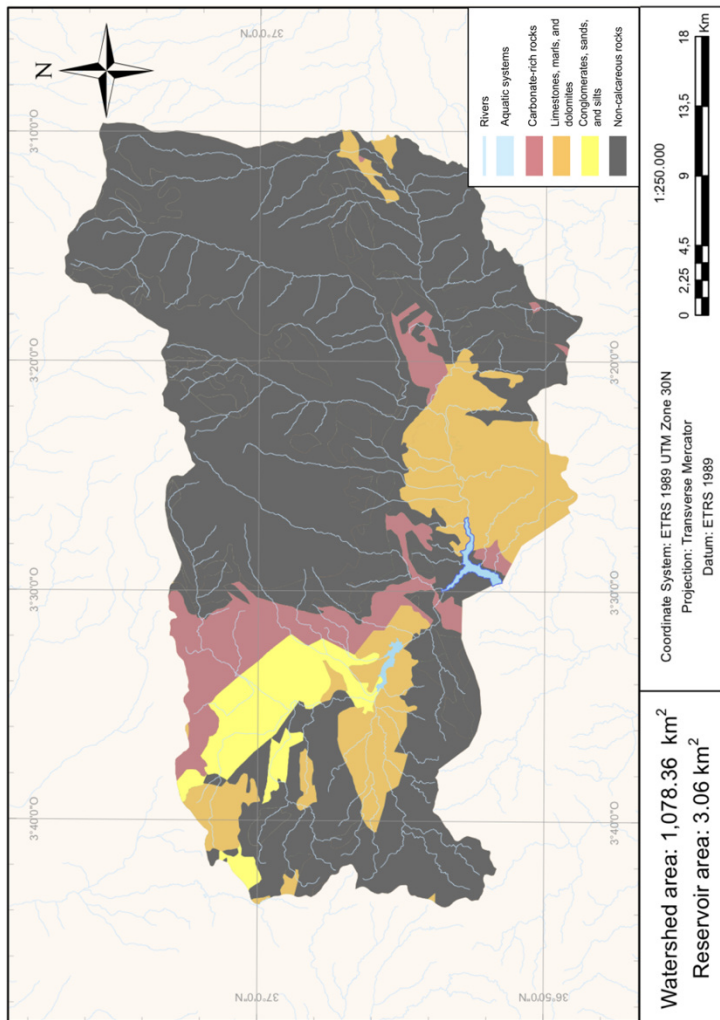


Supplementary Figure 3.10. Map of lithology analysis in the El Portillo reservoir watershed using GIS, showing aquatic systems in blue, carbonate-rich rocks in pink, limestones, marls and dolomites in brown; conglomerates, sands and silts in yellow and non-calcareous rocks in grey. Note that *O* means *W* (west) on the map coordinates.

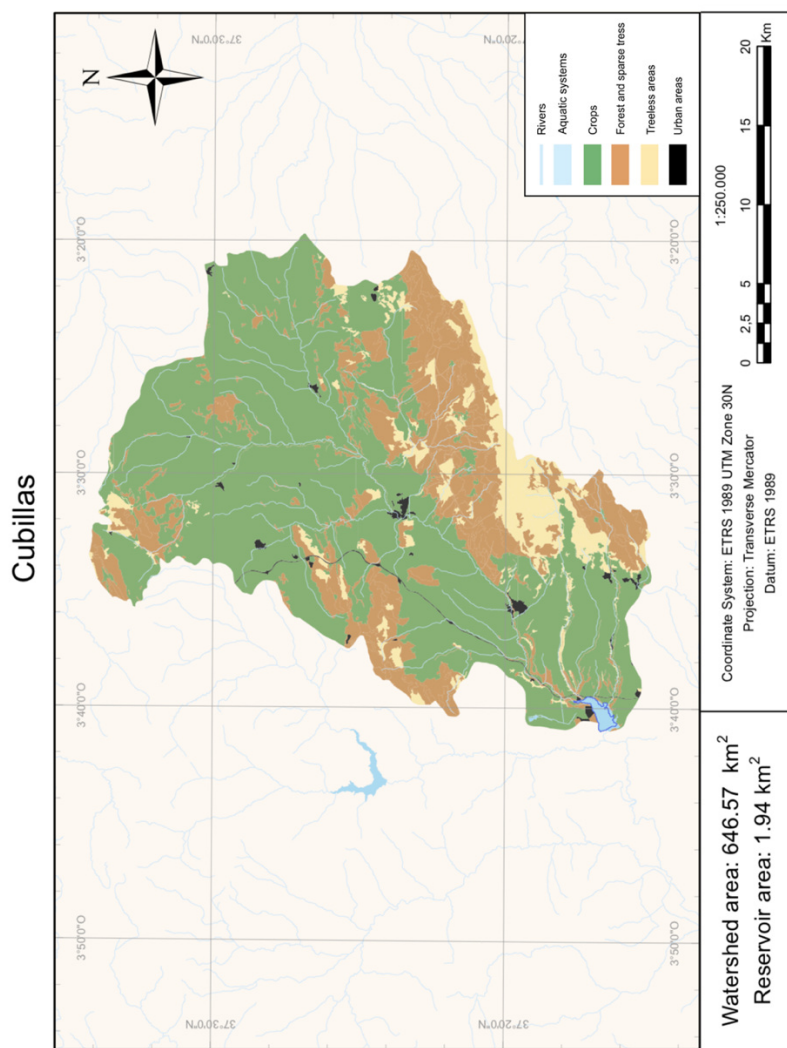


Supplementary Figure 3.11. Map of lithology analysis in the Jándula reservoir watershed using GIS, showing aquatic systems in blue, carbonate-rich rocks in pink, limestones, marls and dolomites in brown; conglomerates, sands and silts in yellow and non-calcareous rocks in grey. Note that *O* means *W* (west) on the map coordinates.

Rules

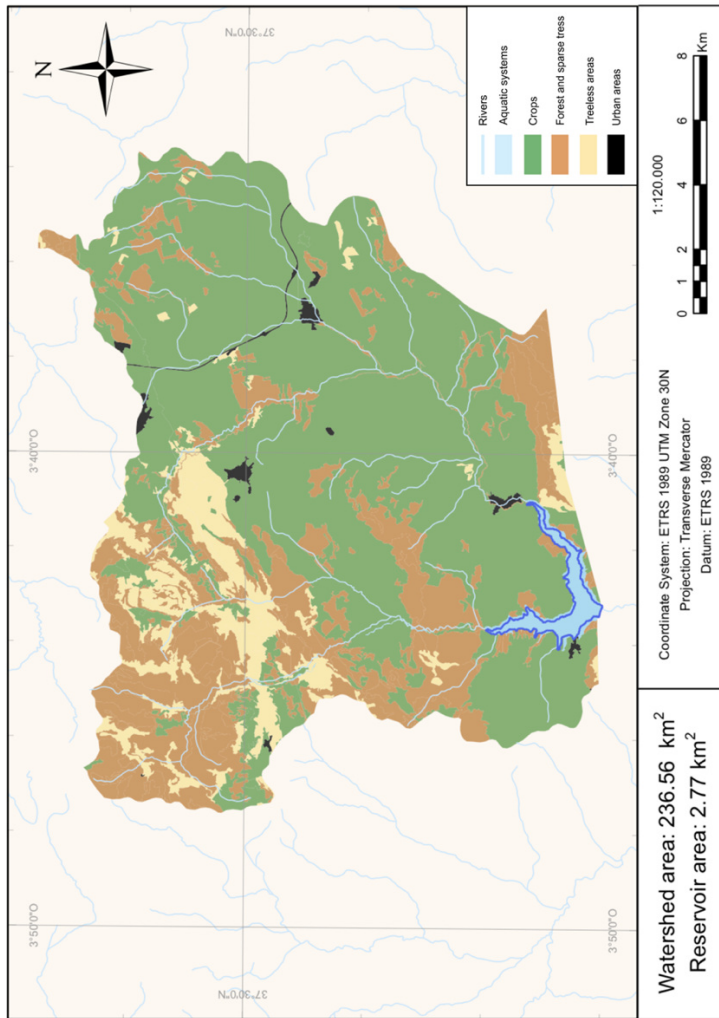


Supplementary Figure 3.12. Map of lithology analysis in the Rules reservoir watershed using GIS, showing aquatic systems in blue, carbonate-rich rocks in pink, limestones, marls and dolomites in brown; conglomerates, sands and silts in yellow and non-calcareous rocks in grey. Note that O means W (west) on the map coordinates.

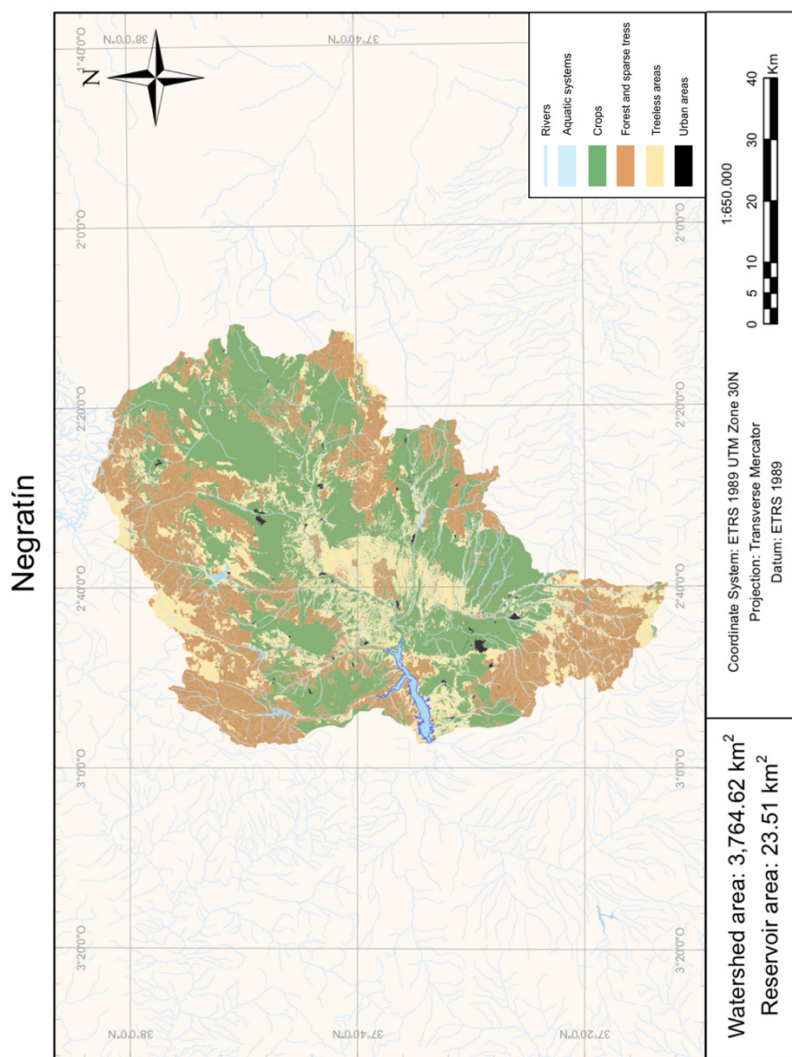


Supplementary Figure 3.13. Map of land-use analysis in the Cubillas reservoir watershed using GIS, showing aquatic systems in blue, crops in green, forest and sparse trees areas in brown, treeless areas in lemon-white and urban areas in black. Note that O means W (west) on the map coordinates.

Colomera

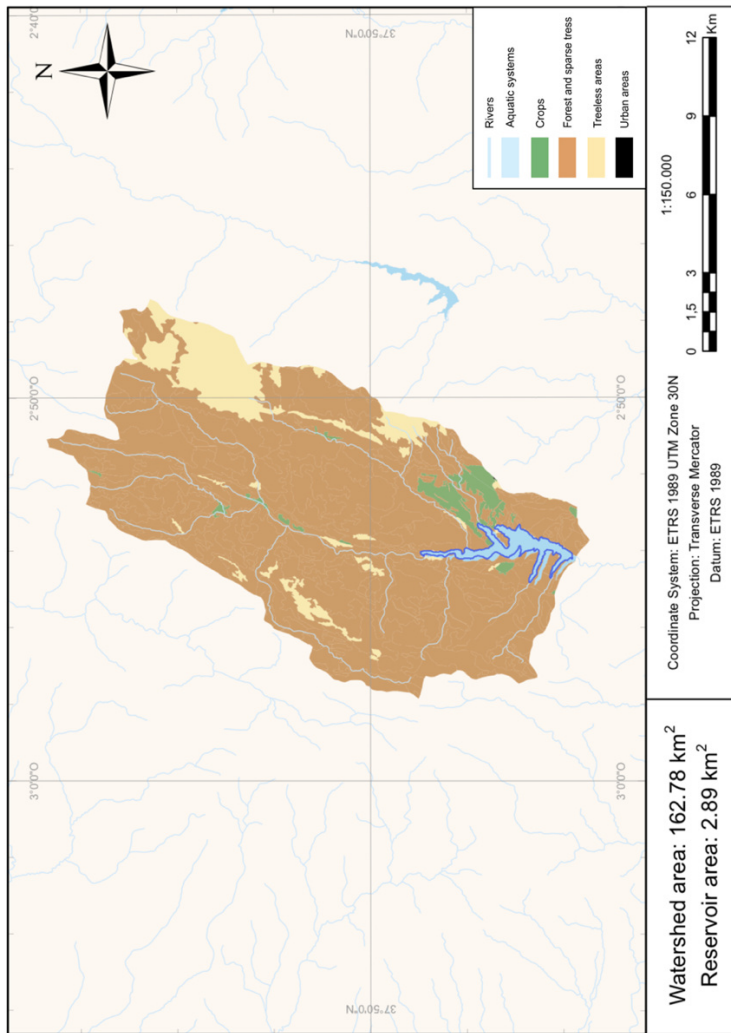


Supplementary Figure 3.14. Map of land-use analysis in the Colomera reservoir watershed using GIS, showing aquatic systems in blue, crops in green, forest and sparse trees areas in brown, treeless areas in lemon-white and urban areas in black. Note that O means W (west) on the map coordinates.

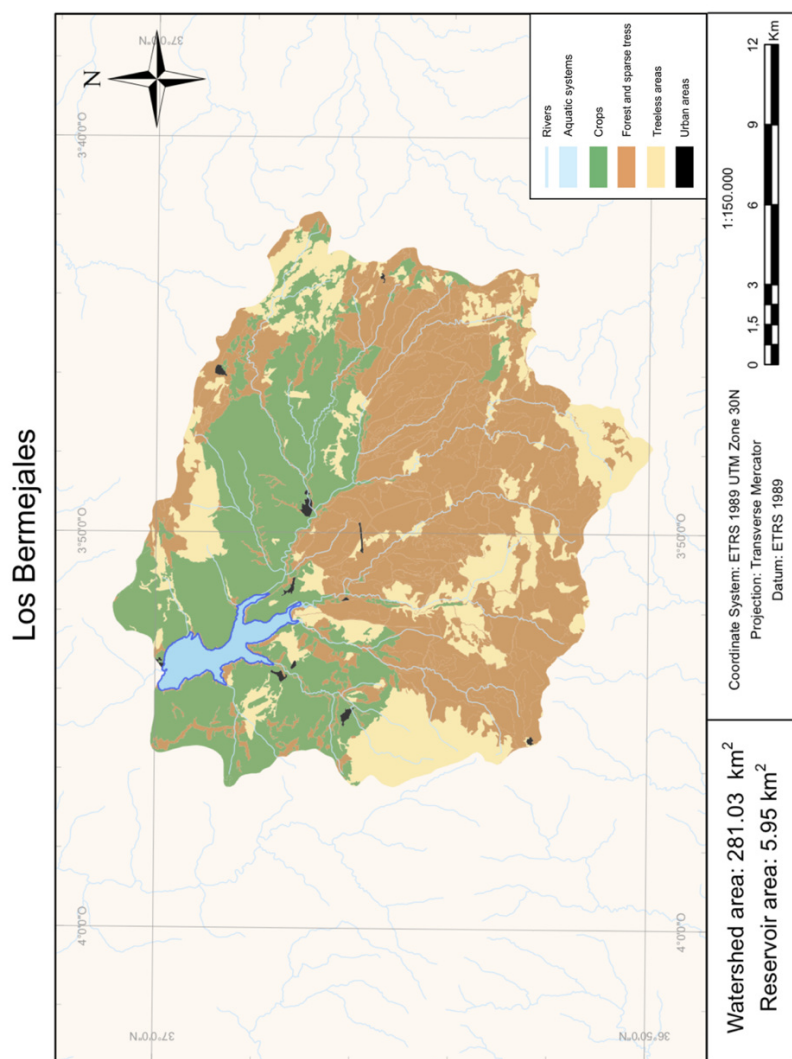


Supplementary Figure 3.15. Map of land-use analysis in the Negratín reservoir watershed using GIS, showing aquatic systems in blue, crops in green, forest and sparse trees areas in brown, treeless areas in lemon-white and urban areas in black. Note that O means W (west) on the map coordinates.

La Bolera

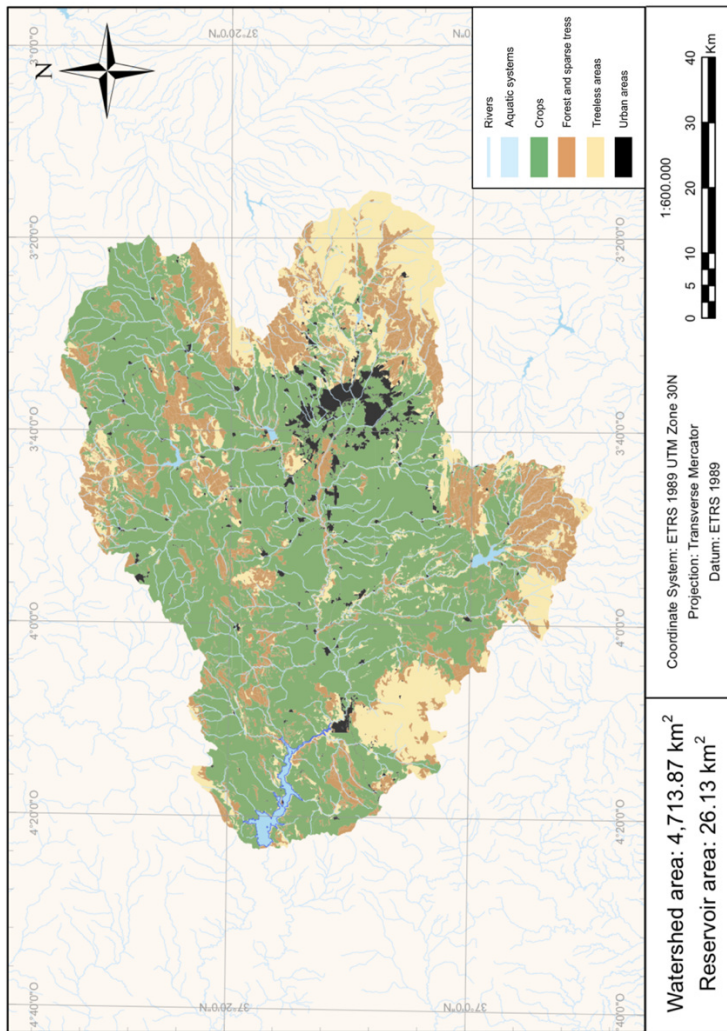


Supplementary Figure 3.16. Map of land-use analysis in the La Bolera reservoir watershed using GIS, showing aquatic systems in blue, crops in green, forest and sparse trees areas in brown, treeless areas in lemon-white and urban areas in black. Note that O means W (west) on the map coordinates.

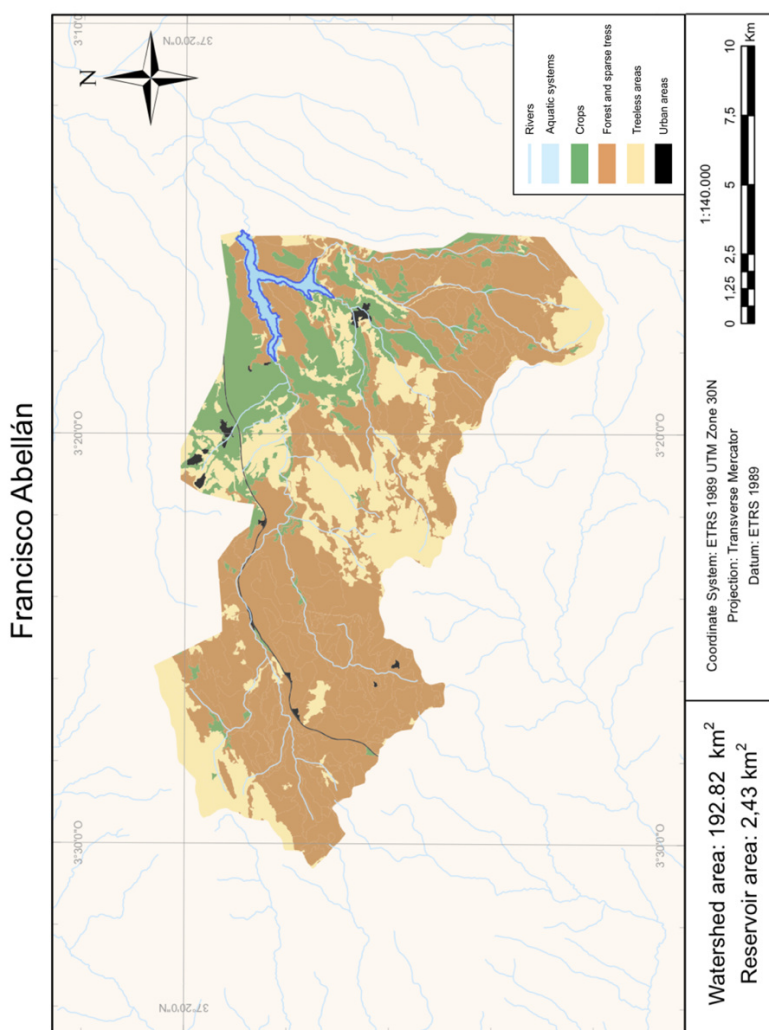


Supplementary Figure 3.17. Land-use analysis map on Los Bermejales reservoir watershed using GIS, showing aquatic systems in blue, crops in green, forest and sparse trees areas in brown, treeless areas in lemon-white and urban areas in black. Note that O means W (west) on the map coordinates.

Iznájar

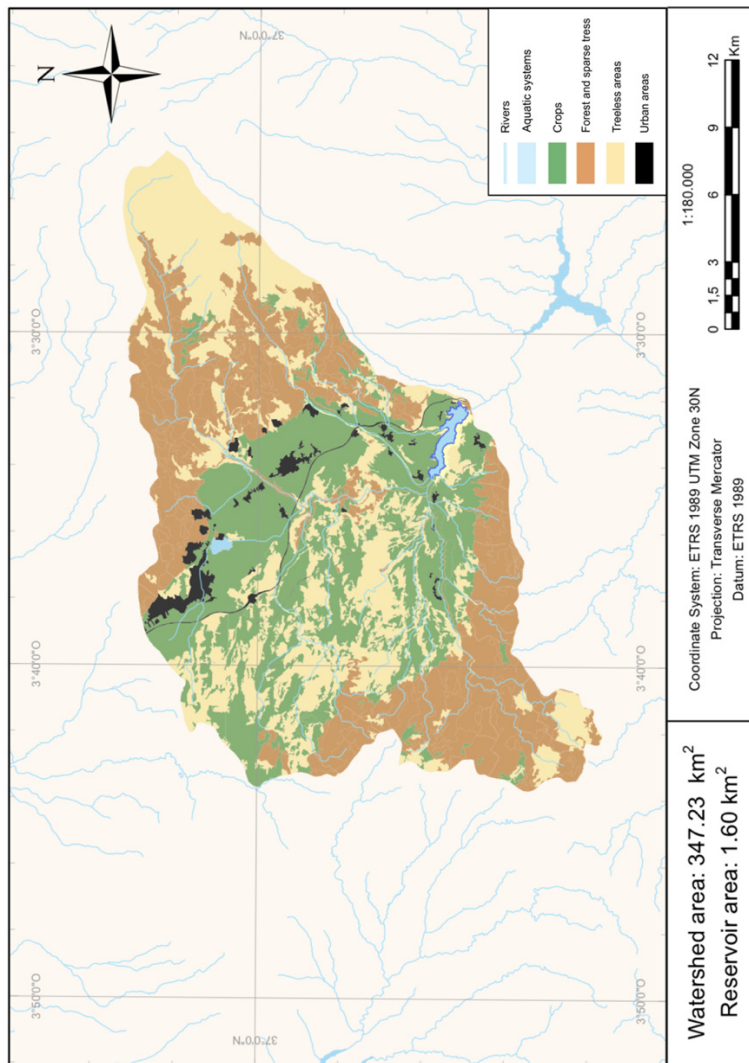


Supplementary Figure 3.18. Map of land-use analysis in the Iznájar reservoir watershed using GIS, showing aquatic systems in blue, crops in green, forest and sparse trees areas in brown, treeless areas in lemon-white and urban areas in black. Note that O means W (west) on the map coordinates.



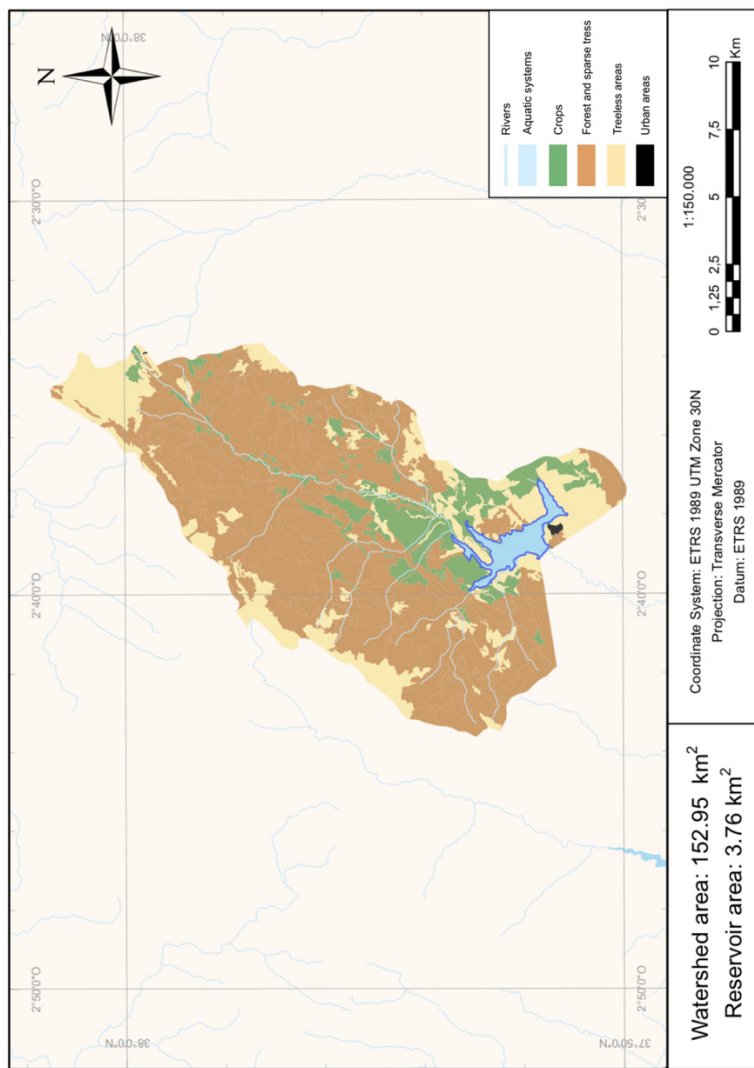
Supplementary Figure 3.19. Map of land-use analysis in the Francisco Abellán reservoir watershed using GIS, showing aquatic systems in blue, crops in green, forest and sparse trees areas in brown, treeless areas in lemon-white and urban areas in black. Note that O means W (west) on the map coordinates.

Béznar

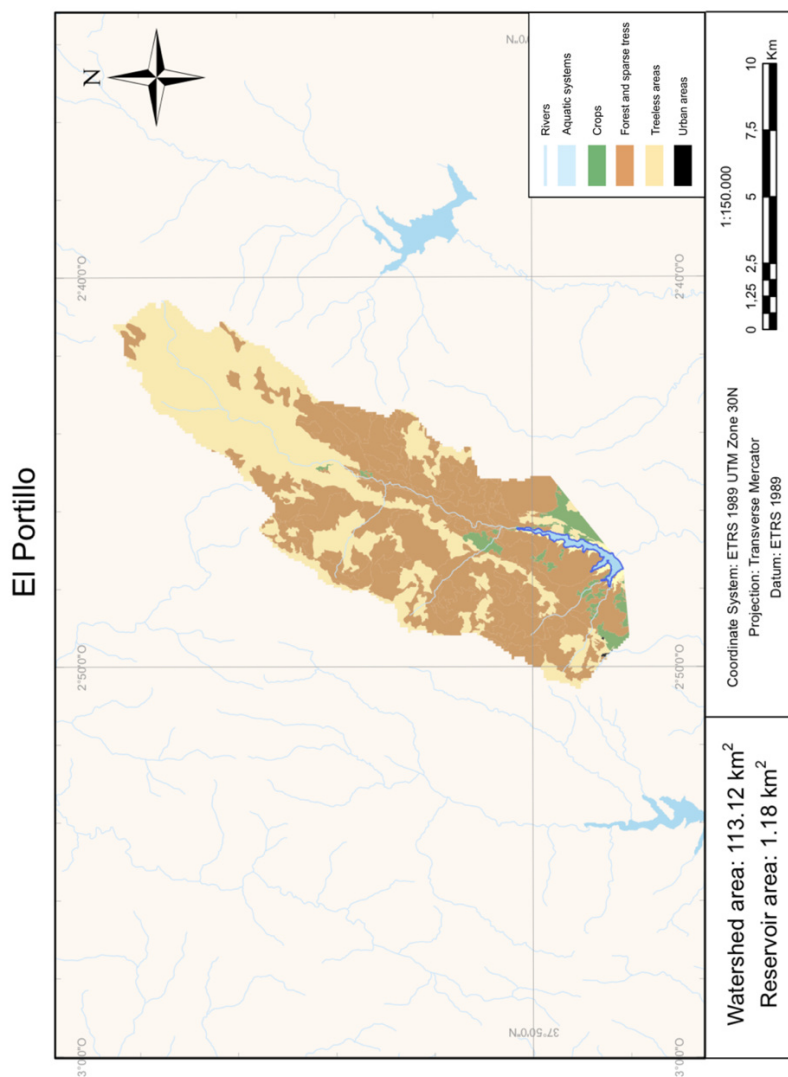


Supplementary Figure 3.20. Map of land-use analysis in the Béznar reservoir watershed using GIS, showing aquatic systems in blue, crops in green, forest and sparse trees areas in brown, treeless areas in lemon-white and urban areas in black. Note that O means W (west) on the map coordinates.

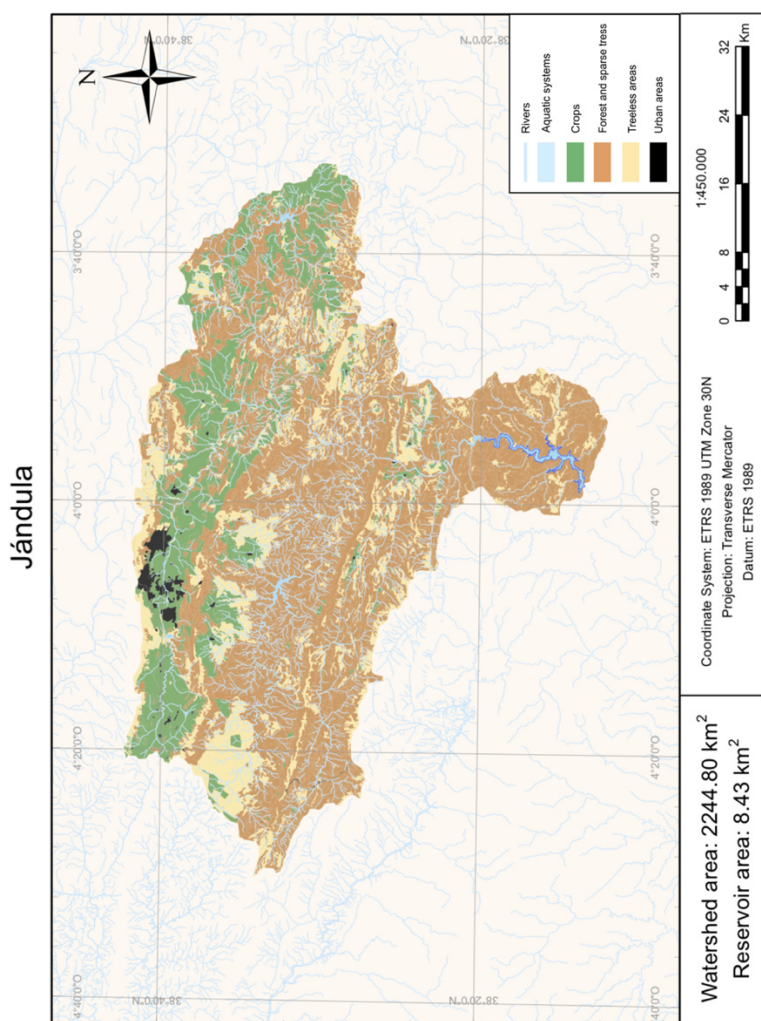
San Clemente



Supplementary Figure 3.21. Map of land-use analysis in the San Clemente reservoir watershed using GIS, showing aquatic systems in blue, crops in green, forest and sparse trees areas in brown, treeless areas in lemon-white and urban areas in black. Note that O means W (west) on the map coordinates.

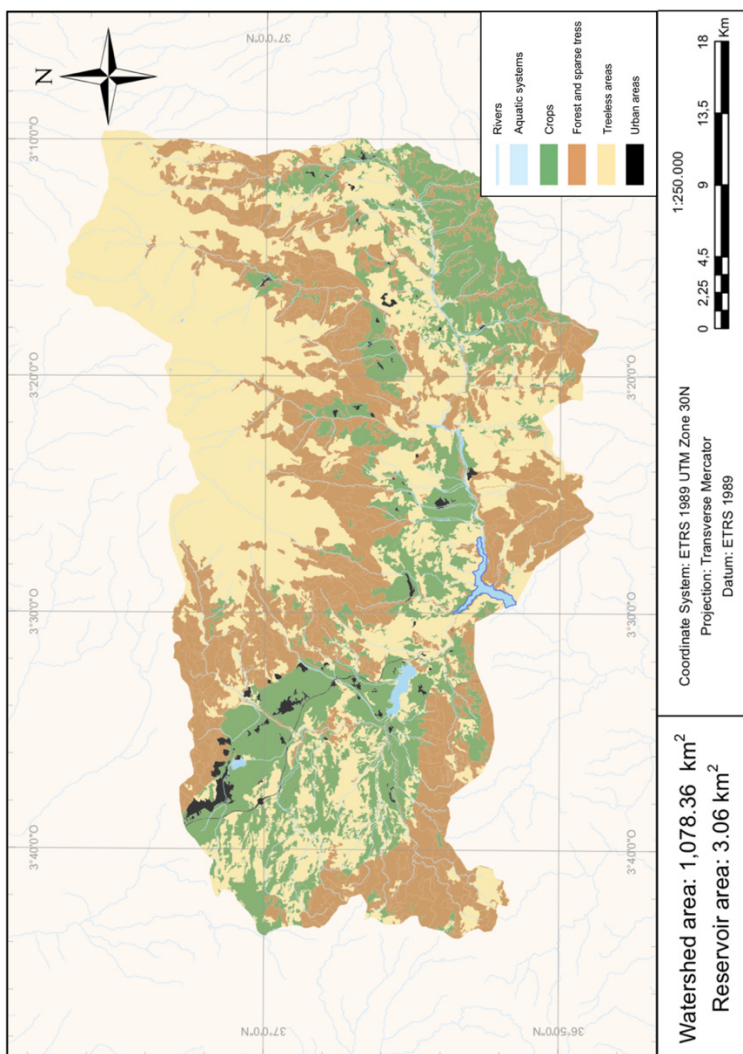


Supplementary Figure 3.22. Map of land-use analysis in the El Portillo reservoir watershed using GIS, showing aquatic systems in blue, crops in green, forest and sparse trees areas in brown, treeless areas in lemon-white and urban areas in black. Note that O means W (west) on the map coordinates.



Supplementary Figure 3.23. Map of land-use analysis in the Jándula reservoir watershed using GIS, showing aquatic systems in blue, crops in green, forest and sparse trees areas in brown, treeless areas in lemon-white and urban areas in black. Note that O means W (west) on the map coordinates.

Rules



Supplementary Figure 3.24. Map of land-use analysis in the Rules reservoir watershed using GIS, showing aquatic systems in blue, crops in green, forest and sparse trees areas in brown, treeless areas in lemon-white and urban areas in black. Note that O means W (west) on the map coordinates

References

- Dlugokencky, E. J. (2019). *Trends in Atmospheric Methane. Globally averaged marine surface monthly mean data*. NOAA/ESRL. Available at: www.esrl.noaa.gov/gmd/ccgg/trends_ch4/.
- Elkins, J. W., Hall, B. D. and Nance, J. D. (2017). Nitrous Oxide data from the NOAA/ESRL halocarbons in situ program. Mauna Loa, Hawaii (MLO). Available at: <http://www.esrl.noaa.gov/gmd/obop/>.
- ESRI. (2012). *ArcGIS*. Redlands, CA. Available at: www.esri.com.
- Fox, J. and Weisberg, S. (2011). *An R Companion to Applied Regression*. Second. Thousand Oaks CA: Sage. Available at: <http://socserv.socsci.mcmaster.ca/jfox/Books/Companion>.
- Gross, J. and Ligges, U. (2015). *nortest: Tests for Normality*. Available at: <https://CRAN.R-project.org/package=nortest> (Accessed: 3 June 2018).
- Hastie, T. J. and Tibshirani, R. J. (1990). *Generalized Additive Models*. CRC Press.
- Hastie, T. and Tibshirani, R. (1986). Generalized Additive Models, *Statistical Science*, 1(3), pp. 297–310. doi: 10.1214/ss/1177013604.
- R Core Team. (2014). *R: A Language and Environment for Statistical Computing*. Vienna, Austria: R Foundation for Statistical Computing. Available at: <http://www.R-project.org/>.
- Sierra, A., Jiménez-López, D., Ortega, T., Ponce, R., Bellanco, M. J., Sánchez-Leal, R., Gómez-Parra, A. and Forja, J. (2017a). Spatial and seasonal variability of CH₄ in the eastern Gulf of Cadiz (SW Iberian Peninsula), *Science of The Total Environment*, 590–591, pp. 695–707. doi: 10.1016/j.scitotenv.2017.03.030.
- Sierra, A., Jiménez-López, D., Ortega, T., Ponce, R., Bellanco, M. J., Sánchez-Leal, R., Gómez-Parra, A. and Forja, J. (2017b). Distribution of N₂O in the eastern shelf of the Gulf of Cadiz (SW Iberian Peninsula), *Science of The Total Environment*, 593–594, pp. 796–808. doi: 10.1016/j.scitotenv.2017.03.189.
- Weiss, R. F. and Price, B. A. (1980). Nitrous oxide solubility in water and seawater, *Marine Chemistry*, 8(4), pp. 347–359. doi: 10.1016/0304-4203(80)90024-9.
- Wiesenburg, D. A. and Guinasso, N. L. (1979). Equilibrium solubilities of methane, carbon monoxide, and hydrogen in water and sea water, *Journal of Chemical & Engineering Data*, 24(4), pp. 356–360. doi: 10.1021/je60083a006.
- Wood, S. N. (2006). *Generalized additive models: an introduction with R*. New York, USA: Chapman and Hall/CRC.
- Wood, S. N. (2011). Fast stable restricted maximum likelihood and marginal likelihood estimation of semiparametric generalized linear models, *Journal of the Royal Statistical Society: Series B (Statistical Methodology)*, 73(1), pp. 3–36. doi: 10.1111/j.1467-9868.2010.00749.x.

Appendix 3 | Supplementary Material for Chapter 3

Yamamoto, S., Alcauskas, J. B. and Crozier, T. E. (1976). Solubility of methane in distilled water and seawater, *Journal of Chemical & Engineering Data*, 21(1), pp. 78–80. doi: 10.1021/je60068a029.

Appendix 4:

Supplementary Material for Chapter 4

Daily patterns of greenhouse gas emissions in reservoirs:
evidence of CO₂ and N₂O photoproduction

Supplementary Material:

Supplementary Tables 4.1 - 4.8

Supplementary Table 4.1. Emissions of CO₂ ($\mu\text{mol m}^{-2} \text{s}^{-1}$), N₂O ($\text{nmol m}^{-2} \text{s}^{-1}$), and CH₄ by diffusion and ebullition ($\text{nmol m}^{-2} \text{s}^{-1}$). Mean, minimum and maximum values are provided.

Sampling	CO ₂ emissions	N ₂ O emissions	Diffusive CH ₄ emissions	Ebullitive CH ₄ emissions		
	Mean (min - max)	Mean (min - max)	Mean (min - max)	Mean (min - max)	% of the total CH ₄	
Cubillas 2016	Day	0.27 (0.12 - 0.42)	0.16 (0.03 - 0.31)	306.88 (0.00 - 989.15)	495.94 (0.00 - 1815.32)	55 (0 - 100)
	Night	0.15 (0.10 - 0.21)	0.06 (0.03 - 0.11)	103.64 (26.53 - 168.66)	560.08 (132.54 - 919.99)	81 (56 - 95)
Cubillas 2018	Day	0.61 (0.26 - 1.46)	0.41 (0.13 - 1.13)	50.66 (17.05 - 142.89)	64.92 (1.05 - 206.79)	54 (1 - 80)
	Night	0.24 (0.17 - 0.39)	0.13 (0.08 - 0.24)	23.82 (11.31 - 36.47)	52.76 (15.67 - 96.96)	66 (48 - 89)
Iznájar 2018	Day	0.24 (0.11 - 0.35)	0.26 (0.07 - 0.46)	6.37 (1.73 - 14.61)	6.01 (0.00 - 21.07)	33 (0 - 80)
	Night	0.07 (-0.01 - 0.27)	0.05 (-0.09 - 0.28)	1.71 (0.00 - 8.74)	3.65 (0.00 - 27.06)	17 (0 - 77)

Supplementary Table 4.2. Statistical details of the circular-linear correlation between solar time (h, circular variable) and greenhouse gas fluxes (linear variable). r = correlation coefficient.

Sampling	GHG fluxes	n	r	p-value
Cubillas 2016	CO ₂ emissions ($\mu\text{mol m}^{-2} \text{s}^{-1}$)	13	0.425	0.161
Cubillas 2018		24	0.633	< 0.001
Iznájar 2018		24	0.790	< 0.001
Cubillas 2016	N ₂ O emissions ($\text{nmol m}^{-2} \text{s}^{-1}$)	13	0.613	< 0.05
Cubillas 2018		24	0.588	< 0.001
Iznájar 2018		24	0.831	< 0.001
Cubillas 2016	Total CH ₄ emissions ($\text{nmol m}^{-2} \text{s}^{-1}$)	13	0.393	0.210
Cubillas 2018		24	0.212	0.388
Iznájar 2018		24	0.525	< 0.01
Cubillas 2016	Diffusive CH ₄ emissions ($\text{nmol m}^{-2} \text{s}^{-1}$)	13	0.454	0.123
Cubillas 2018		24	0.501	< 0.01
Iznájar 2018		24	0.721	< 0.001
Cubillas 2016	Ebullitive CH ₄ emissions ($\text{nmol m}^{-2} \text{s}^{-1}$)	13	0.476	0.100
Cubillas 2018		24	0.107	0.787
Iznájar 2018		24	0.325	0.107

Supplementary Table 4.3. Statistical details of the Spearman's correlation between greenhouse gas fluxes. CO₂ emissions are provided in $\mu\text{mol m}^{-2} \text{s}^{-1}$, and N₂O and CH₄ are provided in $\text{nmol m}^{-2} \text{s}^{-1}$. rho = correlation coefficient.

Sampling	Variable 1	Variable 2	S	rho	p-value
Cubillas 2016	CO ₂	N ₂ O	48	0.868	< 0.001
		Diffusive CH ₄	180	0.505	0.081
	N ₂ O	Ebullitive CH ₄	242	0.335	0.263
		Diffusive CH ₄	150	0.588	< 0.05
		Ebullitive CH ₄	338	0.071	0.821
Cubillas 2018	CO ₂	N ₂ O	140	0.939	< 0.001
		Diffusive CH ₄	458	0.801	< 0.001
	N ₂ O	Ebullitive CH ₄	2086	0.093	0.665
		Diffusive CH ₄	574	0.750	< 0.001
		Ebullitive CH ₄	2226	0.032	0.882
Iznájar 2018	CO ₂	N ₂ O	194	0.916	< 0.001
		Diffusive CH ₄	270	0.883	< 0.001
	N ₂ O	Ebullitive CH ₄	1257	0.454	< 0.05
		Diffusive CH ₄	451	0.804	< 0.001
		Ebullitive CH ₄	1383	0.400	0.054

Supplementary Table 4.4. Physical, chemical, and biological parameters in Cubillas and Iznájar reservoirs. We provide the mean, minimum, and maximum values for wind speed, air temperature, surface water temperature, the oxygen saturation during the 24-hour sampling. For the rest of parameters, we provide discrete measurements for surface waters made in Cubillas in July 2016, in June and September 2018 in Cubillas, and in July and September and Iznájar.

	Cubillas 2016 (July)	Cubillas 2018 (June and September)	Iznájar 2018 (July and September)
Wind speed (m s^{-1} , mean; min-max)	2.3 (0.0 - 5.5)	1.7 (0.0 - 5.7)	2.2 (0.0 - 4.0)
Air temperature ($^{\circ}\text{C}$, mean; min-max)	27.8 (19.5 - 33.1)	25.7 (17.1 - 35.3)	27.9 (20.9 - 33.9)
Surface water temperature ($^{\circ}\text{C}$, mean; min-max)	28.52 (27.27 - 29.75)	25.68 (24.98 - 26.85)	26.59 (25.01 - 28.78)
Oxygen saturation (%, mean; min-max)	120.66 (106.99 - 132.35)	117.85 (113.85 - 124.20)	133.01 (124.35 - 141.47)
Surface dissolved CH_4 concentration ($\mu\text{mol L}^{-1}$, mean \pm SD)	8.87 ± 0.43	1.80 ± 0.11 (June) 3.67 ± 0.59 (Sept.)	0.20 ± 0.01 (July) 0.19 ± 0.01 (Sept.)
Surface dissolved N_2O concentration (nmol L^{-1} , mean \pm SD)	17.4 ± 0.6	33.0 ± 0.2 (June) 84.6 ± 4.6 (Sept.)	27.1 ± 0.7 (July) 83.4 ± 1.1 (Sept.)
Surface DOC concentration (mmol-C L^{-1} , mean \pm SD)	0.18 ± 0.01	0.25 ± 0.00 (June) 0.23 ± 0.00 (Sept.)	0.23 ± 0.00 (July) 0.21 ± 0.01 (Sept.)
Surface DIC concentration (mmol-C L^{-1} , mean \pm SD)	2.48 ± 0.01	2.86 ± 0.01 (June) 2.57 ± 0.03 (Sept.)	1.89 ± 0.01 (July) 2.29 ± 0.01 (Sept.)
Surface nitrate concentration ($\mu\text{mol-N L}^{-1}$)	42.2	375.5 (June) 177.7 (Sept.)	367.3 (July) 334.9 (Sept.)
Surface nitrite concentration ($\mu\text{mol-N L}^{-1}$)	2.1	13.8 (June) 19.3 (Sept.)	20.6 (July) 22.9 (Sept.)
Surface ammonia concentration ($\mu\text{mol-N L}^{-1}$)	3.2	0.0 (June) 0.0 (Sept.)	0.0 (July) 0.0 (Sept.)
Surface Chl- <i>a</i> concentration ($\mu\text{g L}^{-1}$)	13.7	5.4 (June) 18.1 (Sept.)	6.3 (July) 7.0 (Sept.)

Supplementary table 4.5. Statistical details of the circular-linear correlation between solar time (h, circular variable) and environmental drivers (linear variable). r = correlation coefficient.

Sampling	Driver	n	r	p-value
Cubillas 2016	Wind speed (m s^{-1})	13	0.621	< 0.05
Cubillas 2018		24	0.672	< 0.001
Iznájar 2018		24	0.849	< 0.001
Cubillas 2016	Water temperature ($^{\circ}\text{C}$)	13	0.970	< 0.001
Cubillas 2018		24	0.957	< 0.001
Iznájar 2018		24	0.642	< 0.001
Cubillas 2016	Dissolved oxygen saturation (%)	13	0.983	< 0.001
Cubillas 2018		24	0.940	< 0.001
Iznájar 2018		24	0.957	< 0.001
Cubillas 2016	Ambient temperature ($^{\circ}\text{C}$)	13	0.829	< 0.001
Cubillas 2018		24	0.964	< 0.001
Iznájar 2018		24	0.98	< 0.001
Cubillas 2016	Atmospheric pressure (mbar)	13	0.883	< 0.001
Cubillas 2018		24	0.763	< 0.001
Iznájar 2018		24	0.918	< 0.001

Supplementary table 4.6. Results for the ANOVA and Kruskal-Wallis (KW) rank sum tests in the experiments on GHG photoproduction. df = degrees of freedom. SS = sum of squares in ANOVA test. MS = mean of squares in ANOVA test. F = F value in ANOVA test. χ^2 = Chi-squared value in the Kruskal-Wallis test.

Variable	Effect	df	SS	MS	F	χ^2	p-value
DIC (Cubillas, September 2018)	Light treatment effect	2				1.44	0.487
	Incubation time effect	1				0.24	0.624
DIC (Iznájar, September 2018)	Light treatment effect	1	7.93	7.93	10.30		0.024
	Incubation time effect	2	2.15	1.07	1.40		0.330
	Interaction	1	0.97	0.97	1.26		0.313
	Residuals	5	3.85	0.77			
a_{325} (Cubillas, September 2018)	Light treatment effect	1	4.12	4.12	26.14		0.007
	Incubation time effect	2	0.24	0.12	0.77		0.520
	Interaction	1	0.02	0.02	0.11		0.760
	Residuals	4	0.63	0.16			
a_{325} (Iznájar, September 2018)	Light treatment effect	1	0.27	0.27	16.85		0.009
	Incubation time effect	2	0.22	0.11	6.81		0.037
	Interaction	1	0.35	0.35	22.01		0.005
	Residuals	5	0.08	0.02			
Slope 275 - 295 (Cubillas, September 2018)	Light treatment effect	1	0.00	0.00	99.47		0.001
	Incubation time effect	2	0.00	0.00	7.61		0.043
	Interaction	1	0.00	0.00	1.26		0.324
	Residuals	4	0.00	0.00			
Slope 275 - 295 (Iznájar, September 2018)	Light treatment effect	1	0.00	0.00	25.43		0.004
	Incubation time effect	2	0.00	0.00	0.83		0.489
	Interaction	1	0.00	0.00	7.23		0.043

Appendix 4 | Supplementary Material for Chapter 4

	Residuals	5	0.00	0.00		
Slope 350 - 400 (Cubillas, September 2018)	Light treatment effect	1	0.00	0.00	40.79	0.003
	Incubation time effect	2	0.00	0.00	1.50	0.327
	Interaction	1	0.00	0.00	1.43	0.298
	Residuals	4	0.00	0.00		
Slope 350 - 400 (Iznájar, September 2018)	Light treatment effect	1	0.00	0.00	12.65	0.016
	Incubation time effect	2	0.00	0.00	4.33	0.081
	Interaction	1	0.00	0.00	1.19	0.324
	Residuals	5	0.00	0.00		
Slope ratio (S_R) (Cubillas, September 2018)	Light treatment effect	1	1.16	1.16	129.06	< 0.001
	Incubation time effect	2	0.00	0.00	0.11	0.899
	Interaction	1	0.00	0.00	0.18	0.697
	Residuals	4	0.04	0.01		
Slope ratio(S_R) (Iznájar, September 2018)	Light treatment effect	1	0.00	0.00	12.65	0.016
	Incubation time effect	2	0.00	0.00	4.33	0.081
	Interaction	1	0.00	0.00	1.19	0.324
	Residuals	5	0.00	0.00		
Dissolved N_2O (Cubillas, June 2018)	Light treatment effect	1			19.76	< 0.001
	Incubation time effect	2			9.49	0.009
Dissolved N_2O (Cubillas, September 2018)	Light treatment effect	1			12.63	< 0.001
	Incubation time effect	2			4.56	0.102
Dissolved N_2O (Iznájar, September 2018)	Light treatment effect	1			13.71	< 0.001
	Incubation time effect	2			9.60	0.008
Dissolved CH_4 (Cubillas, June 2018)	Light treatment effect	1	0.01	0.01	3.19	0.09
	Incubation time effect	2	0.03	0.02	4.07	0.03

Supplementary Material for Chapter 4 | Appendix 4

	Interaction	1	0.02	0.02	5.51	0.03
	Residuals	25	0.10	0.00		
Dissolved CH ₄ (Iznájar, September 2018)	Light treatment effect	1			2.02	0.155
	Incubation time effect	2			13.06	0.001
Dissolved CH ₄ (Cubillas, June 2018)	Light treatment effect	1	0.00	0.00	2.11	0.17
	Incubation time effect	2	0.00	0.00	2.30	0.14
	Interaction	1	0.00	0.00	3.44	0.09
	Residuals	13	0.00	0.00		

Supplementary table 4.7. DIC production rates ($R_{\text{DIC-Area}}$ and $R_{\text{DIC-Volume}}$) in the Iznájar experiment.

Incubation	$R_{\text{DIC-Area}}$ (mmol-C m ⁻² d ⁻¹)	$R_{\text{DIC-Volume}}$ (mmol-C m ⁻³ d ⁻¹)	% of the initial pool per day
$t_0 - t_1$	0.74 ± 0.31	91 ± 39	3.99
$t_0 - t_2$	0.17 ± 0.03	21 ± 3	0.91
Mean	0.45	56	2.45

Supplementary table 4.8. N₂O production rates ($R_{\text{N}_2\text{O-Area}}$ and $R_{\text{N}_2\text{O-Volume}}$) in the three experiments performed. The experiments were performed in 250 mL bottles in June, but we used 100 mL bottles in the experiments developed in September.

Experiment	Incubation	$R_{\text{N}_2\text{O-Area}}$ (nmol m ⁻² d ⁻¹)	$R_{\text{N}_2\text{O-Volume}}$ (μmol m ⁻³ d ⁻¹)	% of the initial pool per day	Production per N unit (μmol N-N ₂ O m ⁻³ d ⁻¹ ; μmol N-DIN m ⁻³)
Cubillas (June 2018)	$t_0 - t_1$	18.5 ± 4.0	1.35 ± 0.30	4.10	7.0 10 ⁻⁶
	$t_0 - t_2$	16.7 ± 1.7	1.22 ± 0.12	3.70	6.3 10 ⁻⁶
	Mean	17.6	1.29	3.90	6.6 10 ⁻⁶
Cubillas (September 2018)	$t_0 - t_1$	168.1 ± 91.7	16.43 ± 8.97	19.42	1.7 10 ⁻⁴
	$t_0 - t_2$	335.4 ± 7.8	32.80 ± 0.76	38.75	3.3 10 ⁻⁴
	Mean	251.8	24.62	29.08	2.5 10 ⁻⁴
Iznájar (September 2018)	$t_0 - t_1$	126.7 ± 13.9	12.39 ± 1.36	14.86	6.9 10 ⁻⁵
	$t_0 - t_2$	224.5 ± 120.1	21.95 ± 11.75	26.32	1.2 10 ⁻⁴
	Mean	175.6	17.17	20.59	9.6 10 ⁻⁵

Appendix 5:

Supplementary material for Chapter 5

Dissolved CH₄ coupled to photosynthetic picoeukaryotes
in oxic waters and to cumulative chlorophyll *a* in anoxic
waters of reservoirs

Elizabeth León-Palmero¹, Alba Contreras-Ruiz¹, Ana Sierra², Rafael Morales-
Baquero¹, and Isabel Reche^{1,3}

¹Departamento de Ecología and Instituto del Agua, Universidad de Granada, 18071,
Granada, Spain

²Departamento de Química Física and Instituto Universitario de Investigación
Marina (INMAR), Facultad de Ciencias del Mar y Ambientales, Universidad de Cádiz,
Puerto Real, 11510, Cádiz, Spain

³Research Unit “Modeling Nature” (MNat), Universidad de Granada, 18071
Granada, Spain

Supplementary Material:

Supplementary Tables 5.1 - 5.3

Supplementary Figures 5.1 - 5.13

Supplementary Table 5.1. Summary of the results. We show the minima (min), lower quartile (Q1), median (Q2), upper quartile (Q3), and maxima values for the dissolved CH₄ concentration (μmol L⁻¹), saturation in CH₄ (%), water temperature (°C), dissolved oxygen (DO) concentration (μmol L⁻¹), oxygen saturation (O₂ saturation, %), concentration of chlorophyll *a* (Chl *a*, μg L⁻¹), and the abundance of photosynthetic picoeukaryotes (PPEs, cells mL⁻¹), and cyanobacteria (CYA, cells mL⁻¹) in the mixing layer (epilimnion), and below the mixing layer during the stratification period, and in the mixing layer during the mixing period.

	CH ₄ (μmol L ⁻¹)	CH ₄ .sat. (%)	Temp. (°C)	DO (μmol L ⁻¹)	O ₂ sat. (%)	Chl <i>a</i> (μg L ⁻¹)	PPEs (cells mL ⁻¹)	CYAs, (cells mL ⁻¹)
Stratification period	Min	0.06	20.77	0.00	0.00	0.8	32	1.51 10 ³
	Q ₁	0.25	23.73	227.03	91.67	1.7	287	1.73 10 ⁴
	Q ₂	0.44	1.94 10 ⁴	24.82	241.18	100.88	2.3	1.07 10 ³
	Q ₃	1.27	5.64 10 ⁴	25.86	261.70	108.29	6.2	2.34 10 ³
	Max	8.18	3.63 10 ⁵	28.06	296.69	127.42	25.6	9.41 10 ³
Below mixing layer (n= 49)	Min	0.07	2.22 10 ³	8.48	0.00	0.8	32	3.14 10 ³
	Q ₁	0.16	5.94 10 ³	11.71	2.61	0.94	1.5	108
	Q ₂	0.29	1.01 10 ⁴	15.16	120.33	44.34	2.2	272
	Q ₃	7.21	1.83 10 ⁵	17.72	261.74	88.19	3.2	741
	Max	213.64	7.08 10 ⁶	24.76	447.56	169.64	14.7	4.38 10 ³
Mixing period	Min	0.02	710	7.63	117.57	0.2	29	1.56 10 ³
	Q ₁	0.05	1.57 10 ³	9.22	262.63	81.59	1.0	123
	Q ₂	0.08	2.50 10 ³	10.40	301.85	92.80	1.5	421
	Q ₃	0.15	4.44 10 ³	11.58	319.70	99.15	3.4	2.29 10 ³
	Max	0.69	2.00 10 ⁴	16.77	358.60	114.11	34.6	1.22 10 ⁴

Supplementary Table 5.2. Statistical details of the relationships between the dissolved CH₄ concentration (μmol L⁻¹) and the study drivers in anoxic and oxic waters.

Driver	Period	n	Equation	Adj. R ²	p-value	
Anoxic waters (DO < 7.5 μmol L ⁻¹)	Water temperature (°C)	17	Not significantly related		0.66	
	DOC concentration (μmol-C L ⁻¹)	12	Not significantly related		0.10	
	Cumulative chlorophyll <i>a</i> (mg m ⁻²)	17	CH ₄ = 3.0 10 ⁻⁴ (Cumulative Chl <i>a</i>) ^{2,28}	0.40	< 0.01	
Oxic waters (DO > 7.5 μmol L ⁻¹)	Mean depth (m)	78	CH ₄ = 0.04 e ^(50.0/mean depth)	0.95	< 0.001	
	Shallowness index (m ⁻¹)	Mixing	82	CH ₄ = 0.037 e ^(22.9/mean depth)	0.54	< 0.001
		Stratification	78	Not significantly related		0.134
	DIN: TP ratio (μmol-N:μmol-P)	Mixing	82	Not significantly related		0.114
		Stratification	29	Not significantly related		0.147
	DIN: SRP ratio (μmol-N:μmol-P)	Mixing	36	Not significantly related		0.274
		Stratification	25	Not significantly related		0.104
	Chl <i>a</i> concentration (μg L ⁻¹)	Mixing	25	Not significantly related		0.163
		Stratification + Mixing	160	CH ₄ = 0.11 Chl <i>a</i> ^{0.63}	0.23	< 0.001
	Stratification	78	CH ₄ = 0.14 Chl <i>a</i> ^{0.97}	0.40	< 0.001	

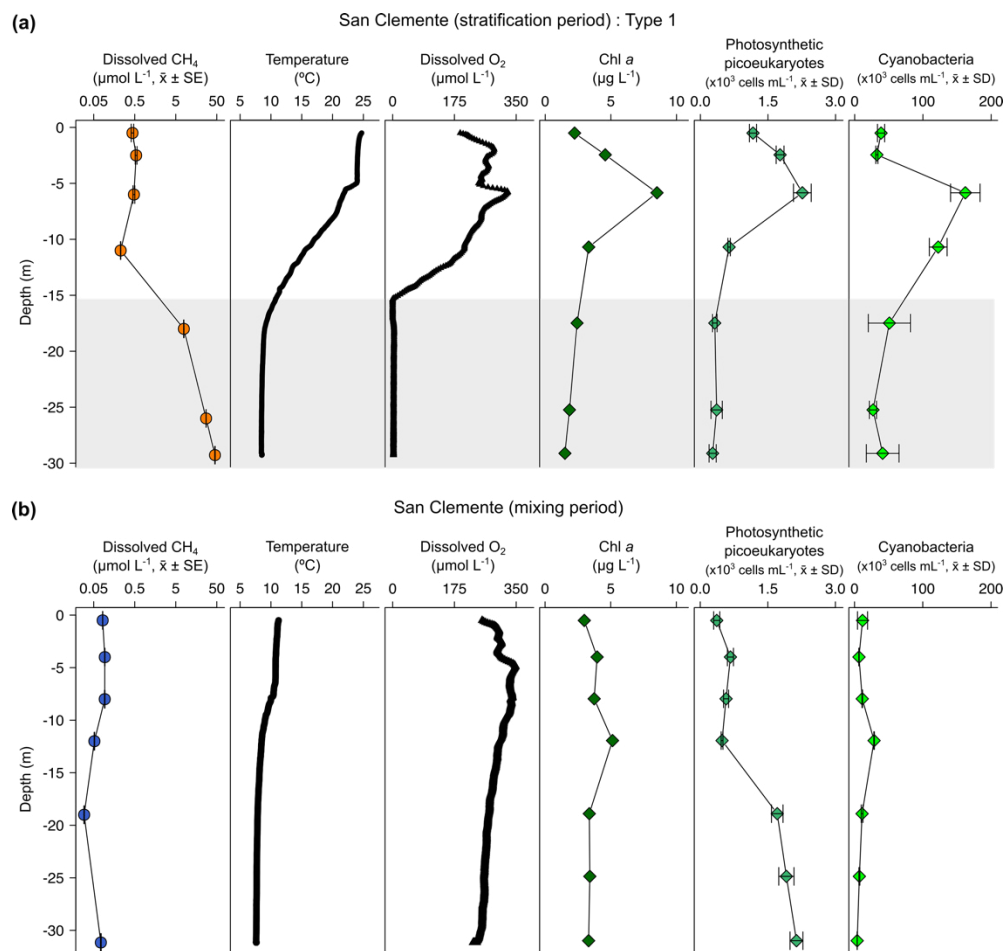
Appendix 5 | Supplementary Material for Chapter 5

	Mixing	82	$\text{CH}_4 = 0.07 \text{ ChI } a^{0.24}$	0.11	< 0.01
Gross primary production (GPP, $\text{g O}_2 \text{ m}^{-3} \text{ d}^{-1}$)	Stratification	12	Marginally significant		0.077
	Mixing		Not measured		
Net ecosystem production (NEP, $\text{g O}_2 \text{ m}^{-3} \text{ d}^{-1}$)	Stratification	12	Not significantly related		0.536
	Mixing		Not measured		
Photosynthetic picoeukaryotes abundance (PPEs, cells mL^{-1})	Stratification + Mixing	160	$\text{CH}_4 = 0.02 \text{ PPEs}^{0.35}$	0.19	< 0.001
	Stratification	78	$\text{CH}_4 = 0.0072 \text{ PPEs}^{0.65}$	0.57	< 0.001
	Mixing	82	$\text{CH}_4 = 0.032 \text{ PPEs}^{0.16}$	0.12	< 0.001
Cyanobacteria abundance (CYA, cells mL^{-1})	Stratification + Mixing	160	$\text{CH}_4 = 0.00099 \text{ CYA}^{0.53}$	0.19	< 0.001
	Stratification	78	$\text{CH}_4 = 0.0017 \text{ CYA}^{0.53}$	0.17	< 0.001
	Mixing	82	Not significantly related		0.666

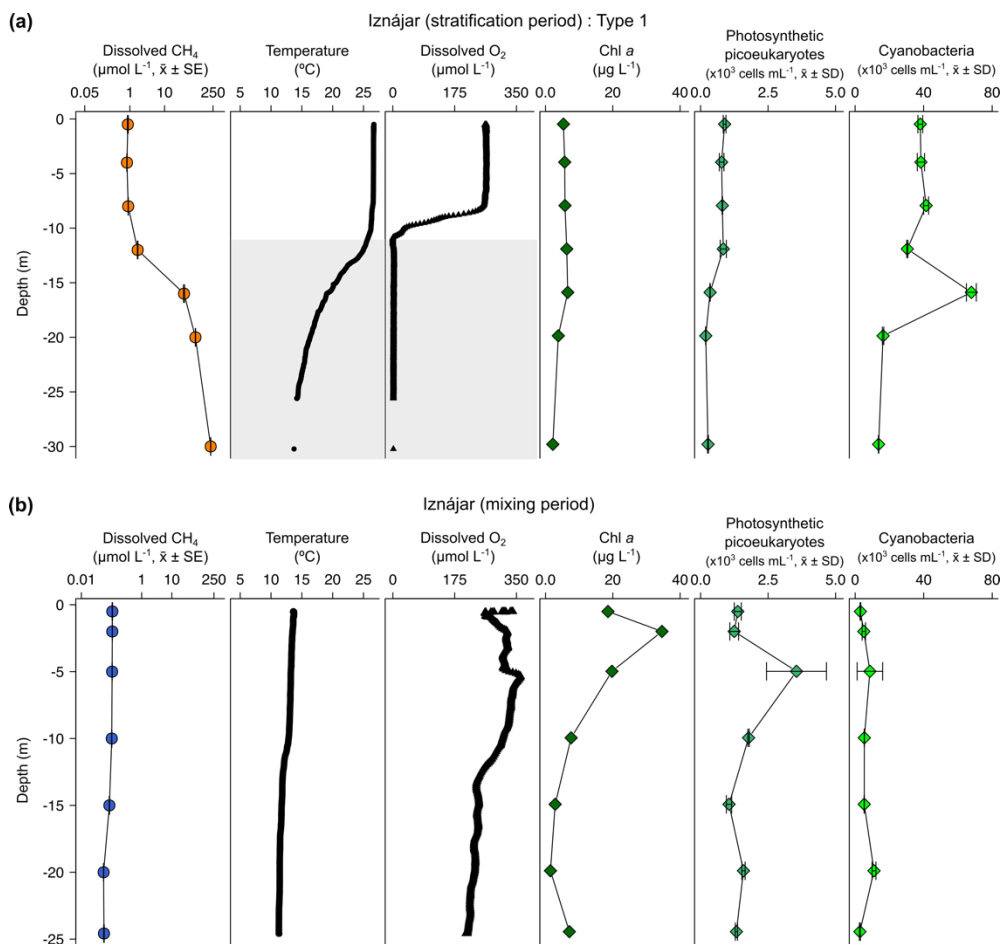
Supplementary Table 5.3. Results of the Generalized Additive Models (GAMs) fitted the concentrations of dissolved CH₄ (μmol L⁻¹) in the oxic samples (dissolved oxygen > 7.5 μmol L⁻¹) during the stratification period, the mixing period and the simple version of the model with the two periods. S.E. = Standard Error; EDF = Estimated Degrees of Freedom.

		Drivers	Estimate (±SE)	EDF	t-value	F-value	P-value	
Log ₁₀ (CH ₄) during the stratification period n = 78 R ² _{adj} = 0.81 Deviance explained = 82.7 % GCV = 0.06 AIC = 8.45	Intercept		0.43 (0.03)		-15.6		<0.001	
	Log ₁₀ (Photosynthetic picoeukaryotes abundance, PPEs, cells mL ⁻¹)			1.00		52.32	<0.001	
	Mean depth (m)			1.95		29.12	<0.001	
	Water temperature (°C)			1.41		6.92	<0.01	
	Log ₁₀ (Cyanobacteria abundance, CYA, cells mL ⁻¹)			1.00		5.53	<0.05	
Function			Log ₁₀ CH ₄ = - 4.05 + 0.34 Log ₁₀ PPEs + e ^(6.7/mean depth) + 0.17 Log ₁₀ CYA + 2.7 10 ⁻² Temperature					
Log ₁₀ (CH ₄) during the mixing period n = 82 R ² _{adj} = 0.52 Deviance explained = 53.9 % GCV = 0.05 AIC = -3.68	Intercept		-1.06 (0.03)		-42.2		<0.001	
	Mean depth (m)			1.77		31.12	<0.001	
	Log ₁₀ (Photosynthetic picoeukaryotes abundance, PPEs, cells mL ⁻¹)			1.00		19.00	<0.001	
	Function			Log ₁₀ (CH ₄) = - 2.07 + 1.5 e ^(-0.04 mean depth) + 0.18 Log ₁₀ PPEs				

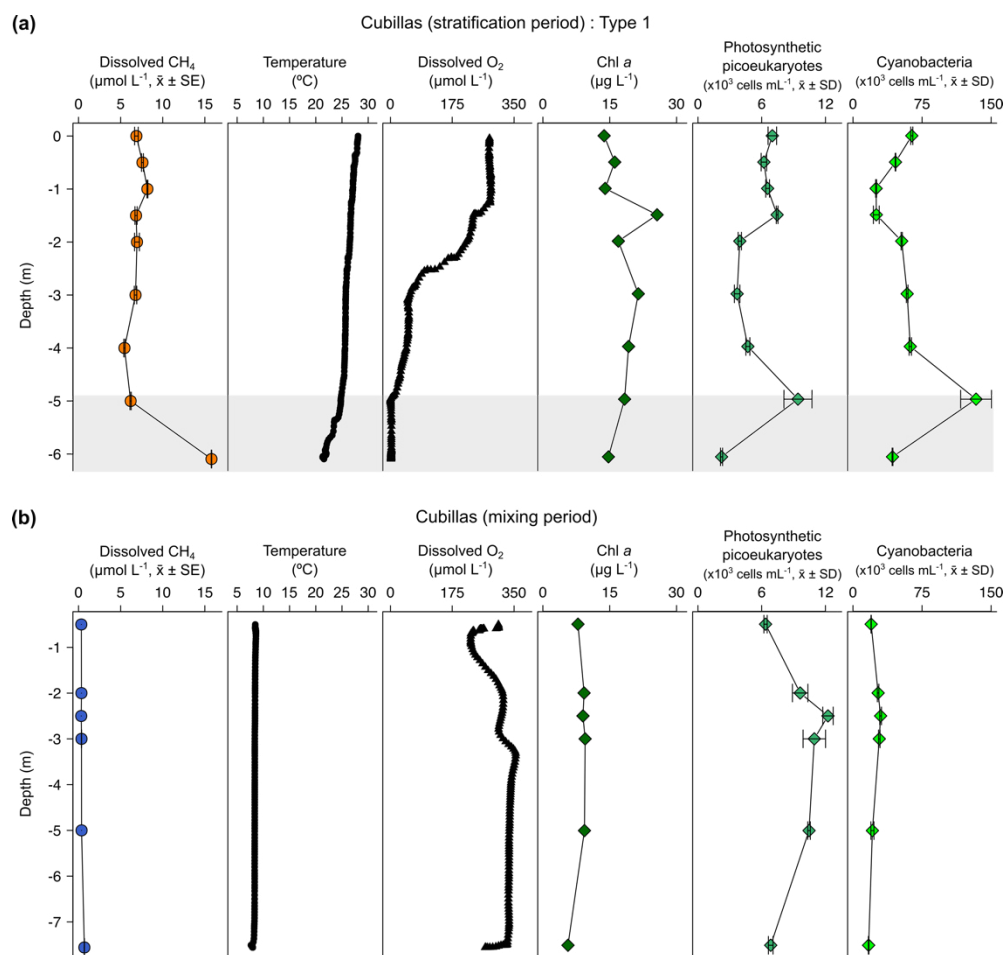
Log ₁₀ (CH ₄) during both periods	Intercept	-0.75 (0.02)	-33.9	<0.001
n = 160	Temperature (°C)		1.64	<0.001
R ² _{adj} = 0.74	Mean depth (m)		1.81	<0.001
Deviance explained = 75.2 %	Log ₁₀ (Chlorophyll <i>a</i> concentration, Chl <i>a</i> , µg L ⁻¹)		1.89	<0.001
GCV = 0.08	Function	$\text{Log}_{10} \text{CH}_4 = -2.03 + 0.05 \text{ Temperature} + e^{(7.64/\text{mean depth}) - e^{(-0.34 \text{ Log}_{10}(\text{Chl } a)}}$		
AIC = 56.91				



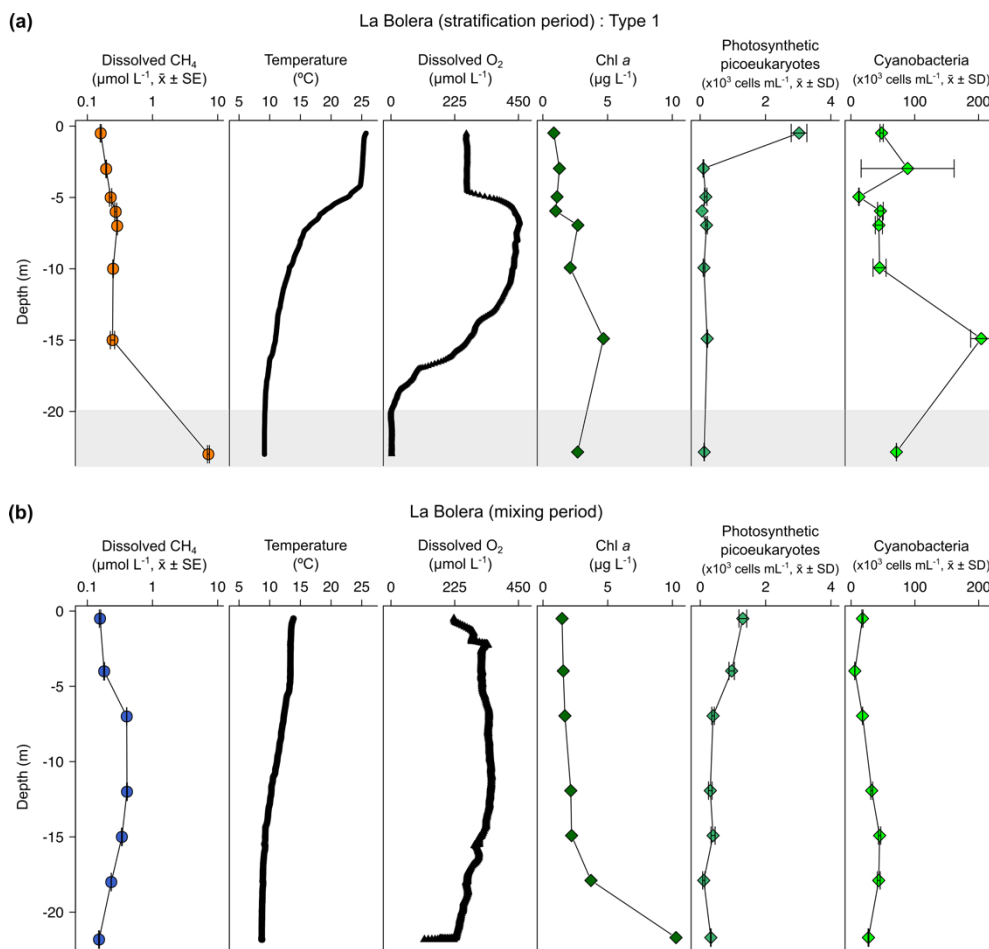
Supplementary Figure 5.1. Vertical profiles of physicochemical and biological variables in San Clemente reservoir. Dissolved methane (CH₄) concentration ($\mu\text{mol L}^{-1}$, mean \pm standard error), temperature ($^{\circ}\text{C}$), dissolved oxygen (DO) concentration ($\mu\text{mol L}^{-1}$), chlorophyll *a* (Chl-*a*) concentration ($\mu\text{g L}^{-1}$), abundance of photosynthetic picoeukaryotes ($\times 10^3$ cells mL^{-1} , mean \pm standard deviation) and abundance of cyanobacteria ($\times 10^3$ cells mL^{-1} , mean \pm standard deviation) during the stratification period (a) and the mixing period (b). The grey area represents the anoxic zone (DO < 7.5 $\mu\text{mol L}^{-1}$). Note the logarithmic scales in the x axis of the dissolved CH₄ profiles. The sampling for the stratification period was on July 17, 2017 and March 28, 2017 for the mixing period.



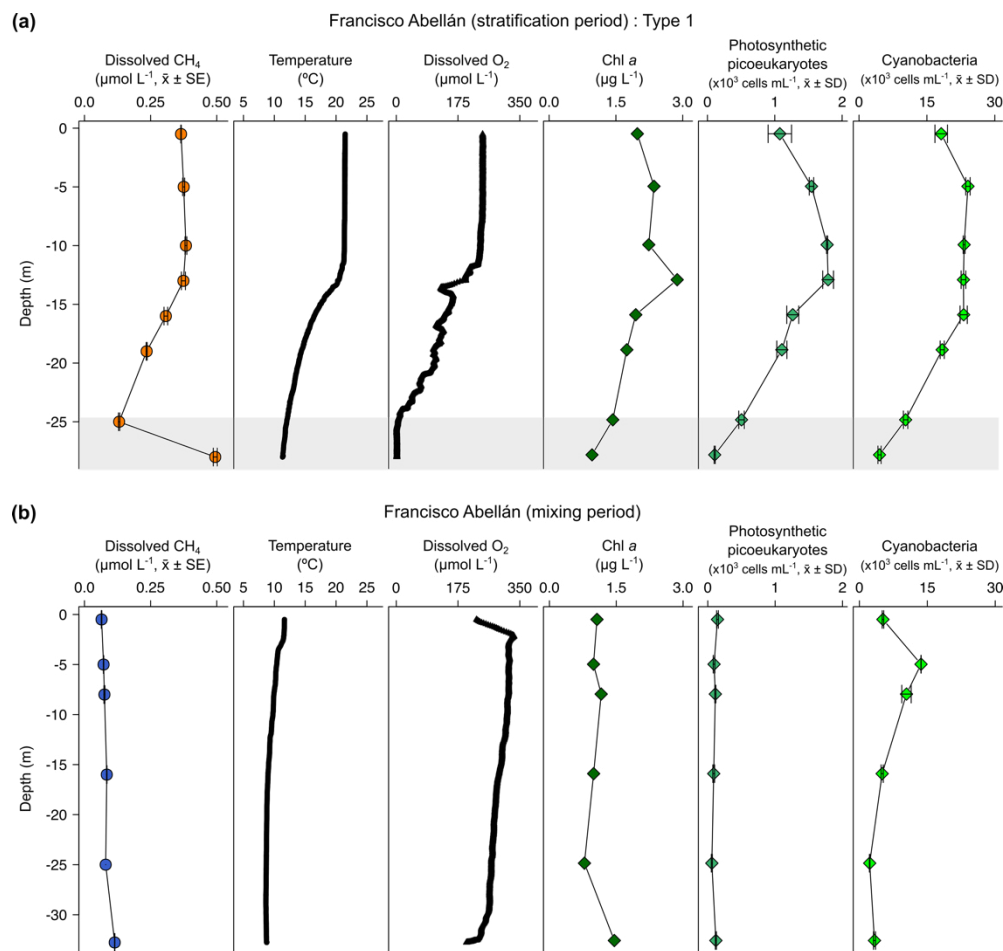
Supplementary Figure 5.2. Vertical profiles of physicochemical and biological variables in Iznájar reservoir. Dissolved methane (CH₄) concentration (μmol L⁻¹, mean ± standard error), temperature (°C), dissolved oxygen (DO) concentration (μmol L⁻¹), chlorophyll *a* (Chl-*a*) concentration (μg L⁻¹), abundance of photosynthetic picoeukaryotes (x10³ cells mL⁻¹, mean ± standard deviation) and abundance of cyanobacteria (x10³ cells mL⁻¹, mean ± standard deviation) during the stratification period (a) and the mixing period (b). The grey area represents the anoxic zone (DO < 7.5 μmol L⁻¹). Note the logarithmic scales in the x axis of the dissolved CH₄ profiles. The sampling for the stratification period was on September 8 and 9, 2016 and March 15, 2017 for the mixing period. The sampling for temperature and the dissolved oxygen was developed a day before than the sampling for CH₄ and the biological variables because of logistical problems.



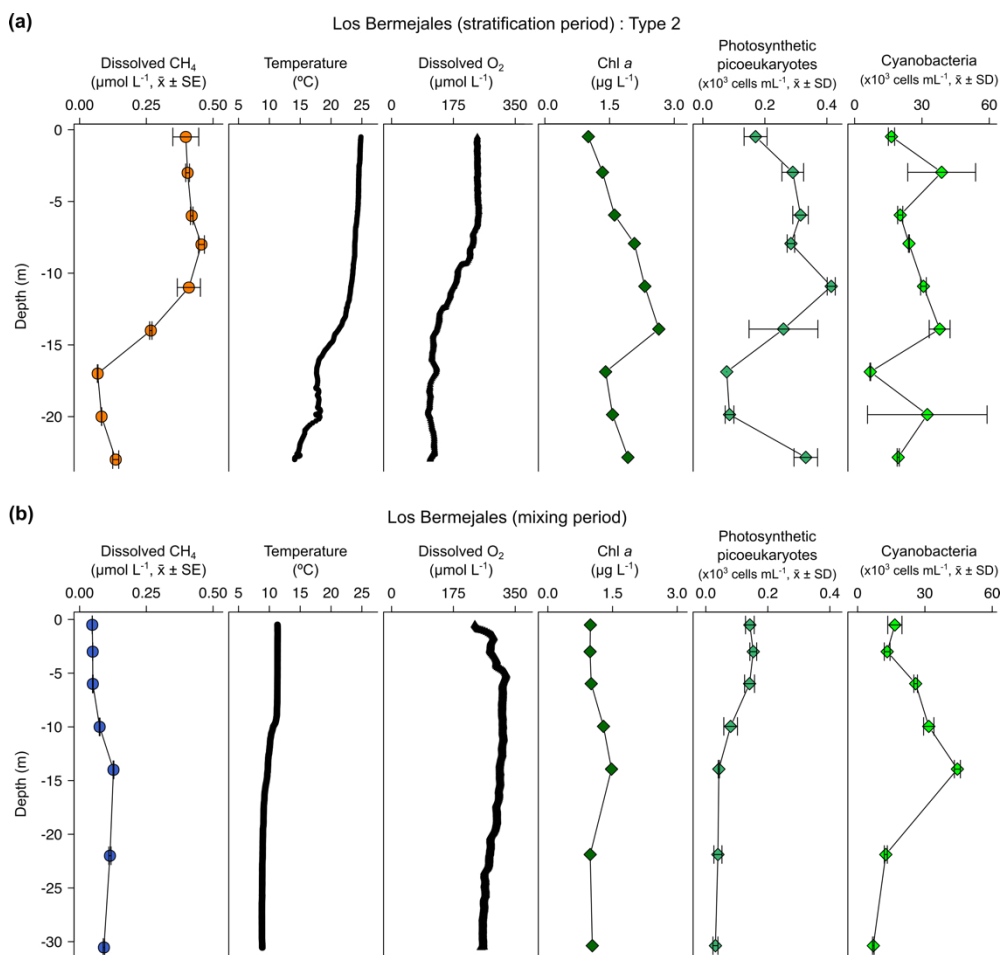
Supplementary Figure 5.3. Vertical profiles of physicochemical and biological variables in Cubillas reservoir. Dissolved methane (CH₄) concentration (μmol L⁻¹, mean ± standard error), temperature (°C), dissolved oxygen (DO) concentration (μmol L⁻¹), chlorophyll *a* (Chl-*a*) concentration (μg L⁻¹), abundance of photosynthetic picoeukaryotes (x10³ cells mL⁻¹, mean ± standard deviation) and abundance of cyanobacteria (x10³ cells mL⁻¹, mean ± standard deviation) during the stratification period (a) and the mixing period (b). The grey area represents the anoxic zone (DO < 7.5 μmol L⁻¹). The sampling for the stratification period was on July 14, 2016 and February 2, 2017 for the mixing period.



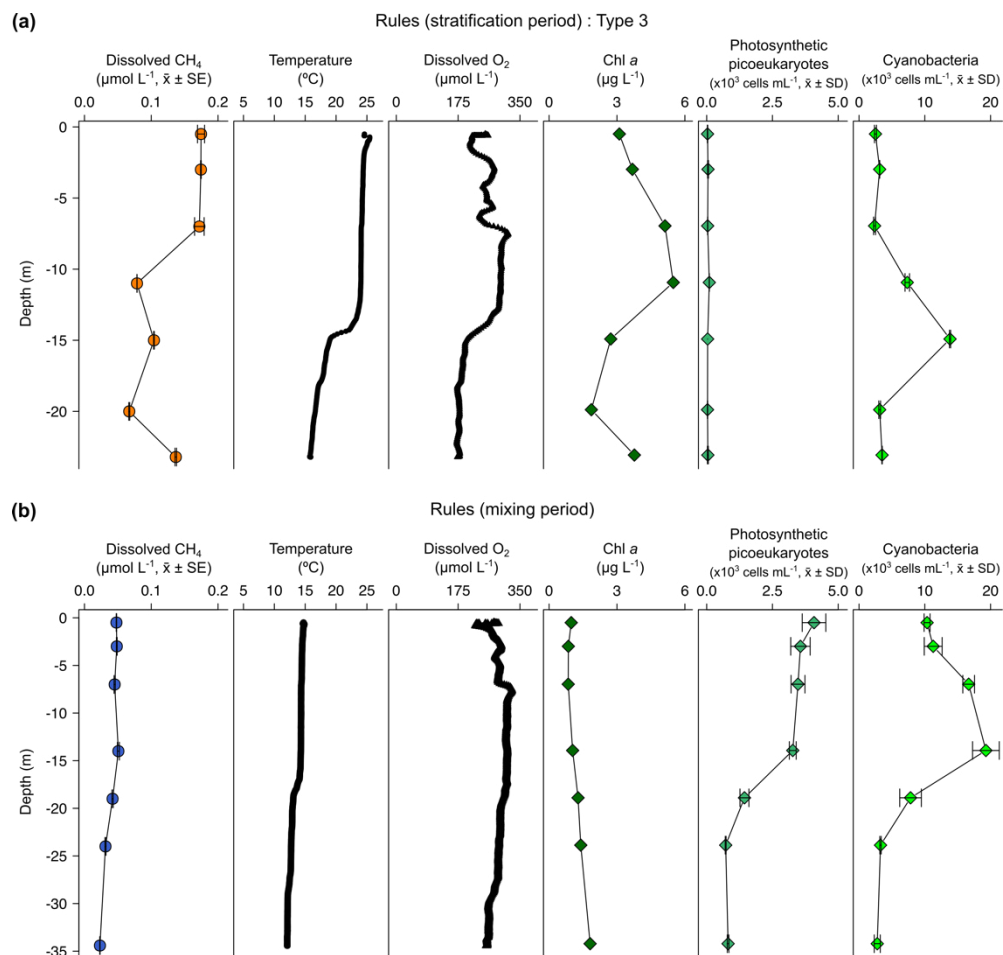
Supplementary Figure 5.4. Vertical profiles of physicochemical and biological variables in La Bolera reservoir. Dissolved methane (CH₄) concentration (μmol L⁻¹, mean ± standard error), temperature (°C), dissolved oxygen (DO) concentration (μmol L⁻¹), chlorophyll *a* (Chl-*a*) concentration (μg L⁻¹), abundance of photosynthetic picoeukaryotes (x10³ cells mL⁻¹, mean ± standard deviation) and abundance of cyanobacteria (x10³ cells mL⁻¹, mean ± standard deviation) during the stratification period (a) and the mixing period (b). The grey area represents the anoxic zone (DO < 7.5 μmol L⁻¹). Note the logarithmic scales in the x axis of the dissolved CH₄ profiles. The sampling for the stratification period was on July 28, 2016 and April 8, 2017 for the mixing period.



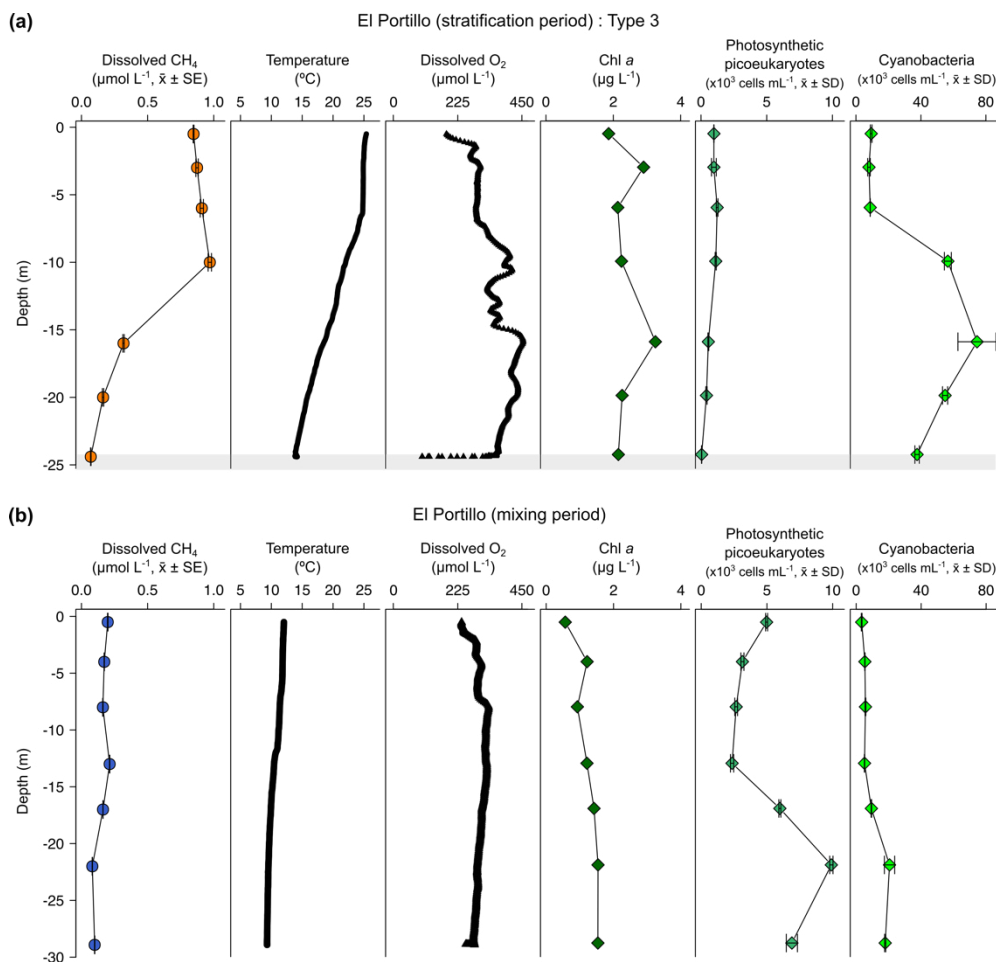
Supplementary Figure 5.5. Vertical profiles of physicochemical and biological variables in Francisco Abellán reservoir. Dissolved methane (CH₄) concentration (μmol L⁻¹, mean ± standard error), temperature (°C), dissolved oxygen (DO) concentration (μmol L⁻¹), chlorophyll *a* (Chl-*a*) concentration (μg L⁻¹), abundance of photosynthetic picoeukaryotes (x10³ cells mL⁻¹, mean ± standard deviation) and abundance of cyanobacteria (x10³ cells mL⁻¹, mean ± standard deviation) during the stratification period (a) and the mixing period (b). The grey area represents the anoxic zone (DO < 7.5 μmol L⁻¹). The sampling for the stratification period was on September 28, 2016 and March 21, 2017 for the mixing period.



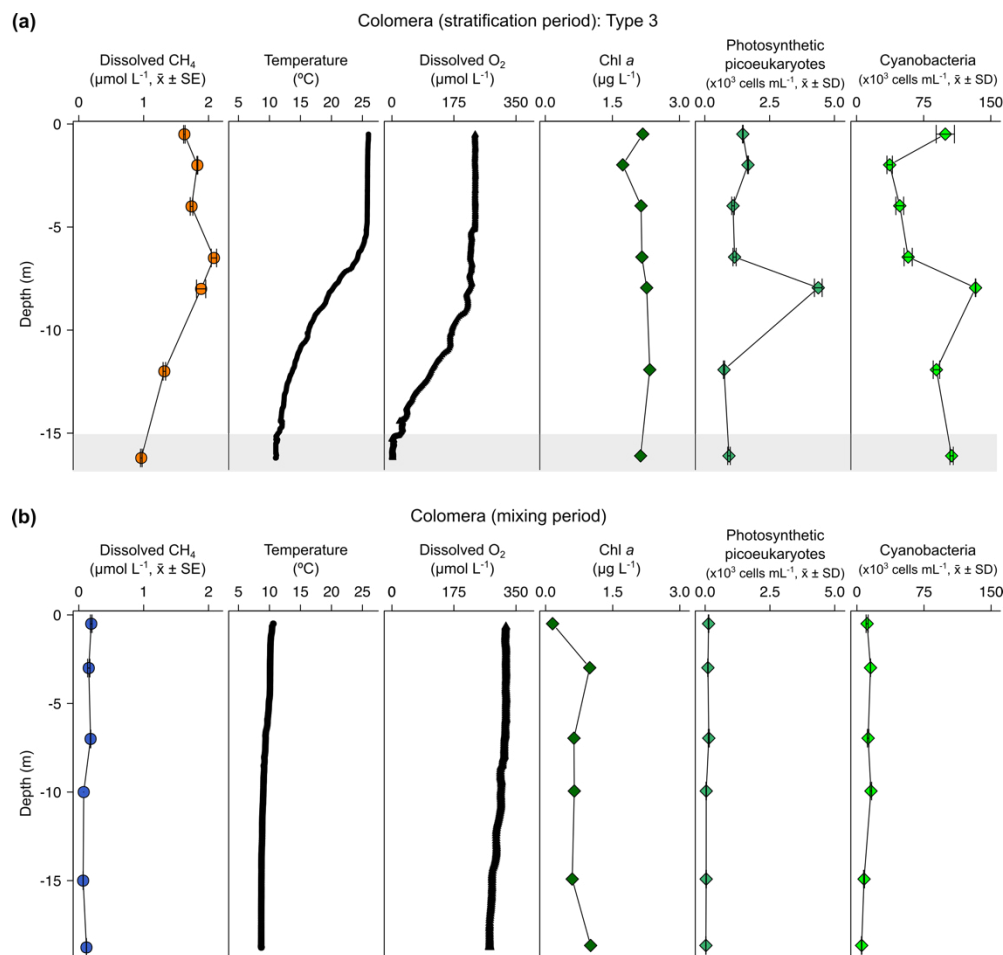
Supplementary Figure 5.6. Vertical profiles of physicochemical and biological variables in Los Bermejales reservoir. Dissolved methane (CH₄) concentration (μmol L⁻¹, mean ± standard error), temperature (°C), dissolved oxygen (DO) concentration (μmol L⁻¹), chlorophyll *a* (Chl-*a*) concentration (μg L⁻¹), abundance of photosynthetic picoeukaryotes (x10³ cells mL⁻¹, mean ± standard deviation) and abundance of cyanobacteria (x10³ cells mL⁻¹, mean ± standard deviation) during the stratification period (a) and the mixing period (b). The sampling for the stratification period was on September 7, 2016 and March 17, 2017 for the mixing period.



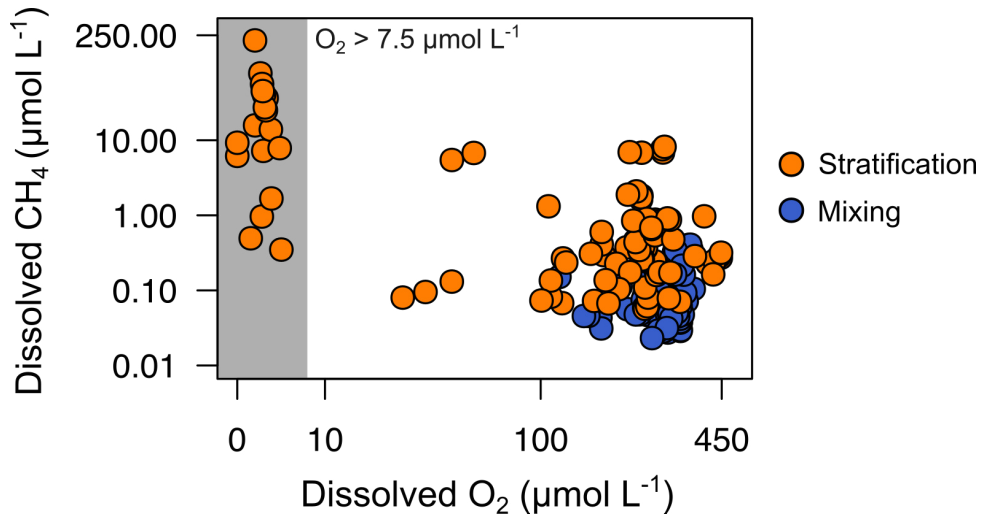
Supplementary Figure 5.7. Vertical profiles of physicochemical and biological variables in Rules reservoir. Dissolved methane (CH₄) concentration (μmol L⁻¹, mean ± standard error), temperature (°C), dissolved oxygen (DO) concentration (μmol L⁻¹), chlorophyll *a* (Chl-*a*) concentration (μg L⁻¹), abundance of photosynthetic picoeukaryotes (x10³ cells mL⁻¹, mean ± standard deviation) and abundance of cyanobacteria (x10³ cells mL⁻¹, mean ± standard deviation) during the stratification period (a) and the mixing period (b). The sampling for the stratification period was on July 10, 2017 and April 7, 2017 for the mixing period.



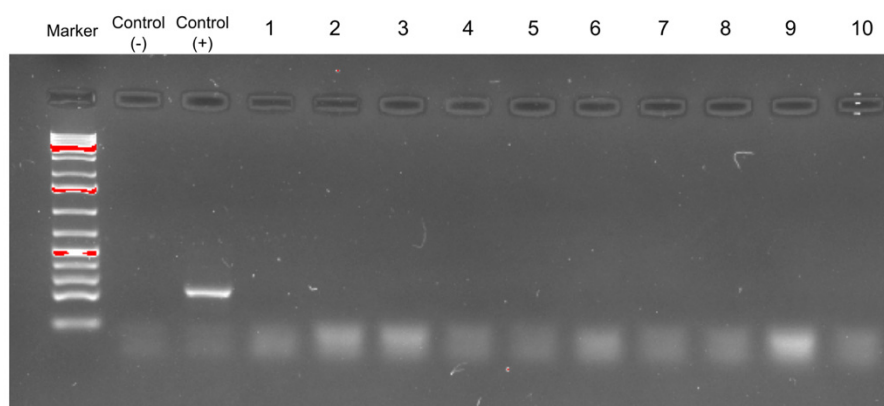
Supplementary Figure 5.8. Vertical profiles of physicochemical and biological variables in El Portillo reservoir. Dissolved methane (CH₄) concentration (μmol L⁻¹, mean ± standard error), temperature (°C), dissolved oxygen (DO) concentration (μmol L⁻¹), chlorophyll *a* (Chl-*a*) concentration (μg L⁻¹), abundance of photosynthetic picoeukaryotes (x10³ cells mL⁻¹, mean ± standard deviation) and abundance of cyanobacteria (x10³ cells mL⁻¹, mean ± standard deviation) during the stratification period (a) and the mixing period (b). The grey area represents the anoxic zone (DO < 7.5 μmol L⁻¹). The sampling for the stratification period was on July 18, 2017 and March 30, 2017 for the mixing period.



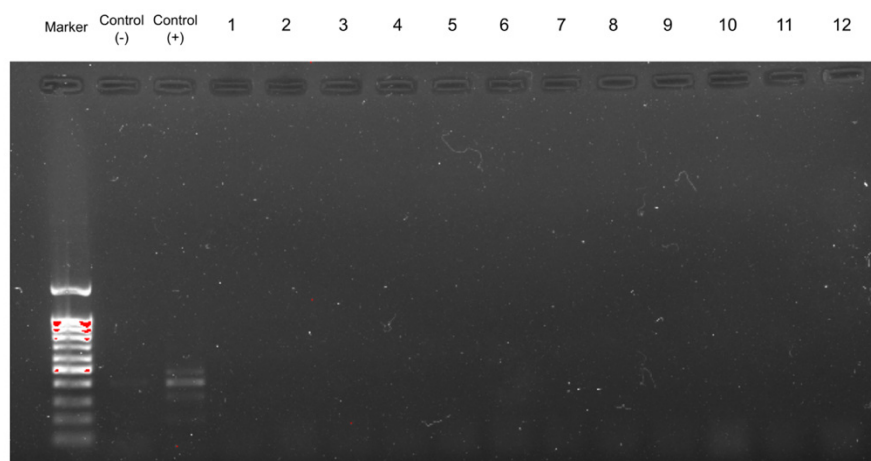
Supplementary Figure 5.9. Vertical profiles of physicochemical and biological variables in Colomera reservoir. Dissolved methane (CH₄) concentration (μmol L⁻¹, mean ± standard error), temperature (°C), dissolved oxygen (DO) concentration (μmol L⁻¹), chlorophyll *a* (Chl-*a*) concentration (μg L⁻¹), abundance of photosynthetic picoeukaryotes (x10³ cells mL⁻¹, mean ± standard deviation) and abundance of cyanobacteria (x10³ cells mL⁻¹, mean ± standard deviation) during the stratification period (a) and the mixing period (b). The grey area represents the anoxic zone (DO < 7.5 μmol L⁻¹). The sampling for the stratification period was on July 22, 2016 and March 8, 2017 for the mixing period.



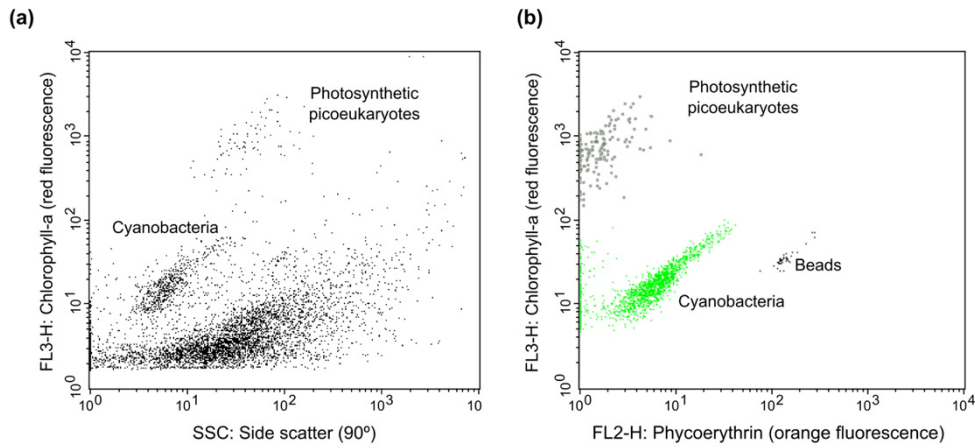
Supplementary Figure 5.10. Relationship between the dissolved oxygen (O_2 , $\mu\text{mol L}^{-1}$) and the dissolved methane (CH_4 , $\mu\text{mol L}^{-1}$) concentrations. The plot shows the two well differentiated groups. Note that the log scale in both axes.



Supplementary Figure 5.11. Results of the PCR for the gene *mcrA* in oxic waters. Agarose gel electrophoresis (1.5 %) showing part of the results of the PCR performed for the gene *mcrA*. We tested all the samples (77), but here we show only 10 of them. In this order: the marker, the controls, and samples (1-10) from oxic waters. The samples displayed are from the stratification period (1-5), and from the mixing period (6-10), and they correspond to the following depths: 1: Colomera reservoir (6.5 m); 2: Negratín reservoir (16 m); 3: Los Bermejales reservoir (6 m); 4: Iznájar reservoir (4); 5: Francisco Abellán (16 m); 6: Iznájar reservoir (5 m); 7: Francisco Abellán reservoir (16 m); 8: San Clemente reservoir (12 m); 9: El Portillo reservoir (22 m); and 10: Jándula reservoir (8 m). More details in the Methods section.



Supplementary Figure 5.12. Results of the PCR for the gene *phnJ* in oxic waters. Agarose gel electrophoresis (1.5 %) showing part of the results of the PCR performed for the gene *phnJ*. We tested all the samples (77), but here we show only 12 of them. In this order: the marker, the controls, and samples (1-12) from oxic waters. The samples displayed are from the mixing period: 1: Cubillas reservoir (7.6 m); 2: Colomera reservoir (7 m); 3: Colomera reservoir (19 m); 4: Negratín reservoir (2 m); 5: Negratín reservoir (22 m); 6: Negratín reservoir (38 m); 7: La Bolera reservoir (12 m); 8: La Bolera reservoir (22 m); 9: Los Bermejales reservoir (6 m); 10: Los Bermejales reservoir (14 m); 11: Los Bermejales reservoir (30.5 m); and 12: Iznájar reservoir (5 m). More details in the Methods section.



Supplementary Figure 5.13. Flow cytometric signatures of cyanobacteria and photosynthetic picoeukaryotes populations in the epilimnion of Bézinar reservoir. (a) Side scatter (SSC) on the x-axis and chlorophyll *a* (red fluorescence, FL3) on the y-axis. (b) Phycoerythrin (the orange fluorescence, FL2) on the x-axis and chlorophyll *a* (red fluorescence, FL3) on the y-axis. Populations selected in the plot A were colored on the plot B. We used yellow-green 0.92 μm latex beads (Polysciences) as an internal standard.

Appendix 6:

Supplementary Material for Chapter 6

Dissolved N₂O driven by nitrogen and the *nirS* gene abundance in the water column of reservoirs

Supplementary Material:

Supplementary Tables 6.1 - 6.3

Supplementary Figures 6.1 - 6.10

Supplementary Table 6.1. Effect of the physico-chemical drivers on the dissolved N₂O concentration (nmol L⁻¹) in the water column.

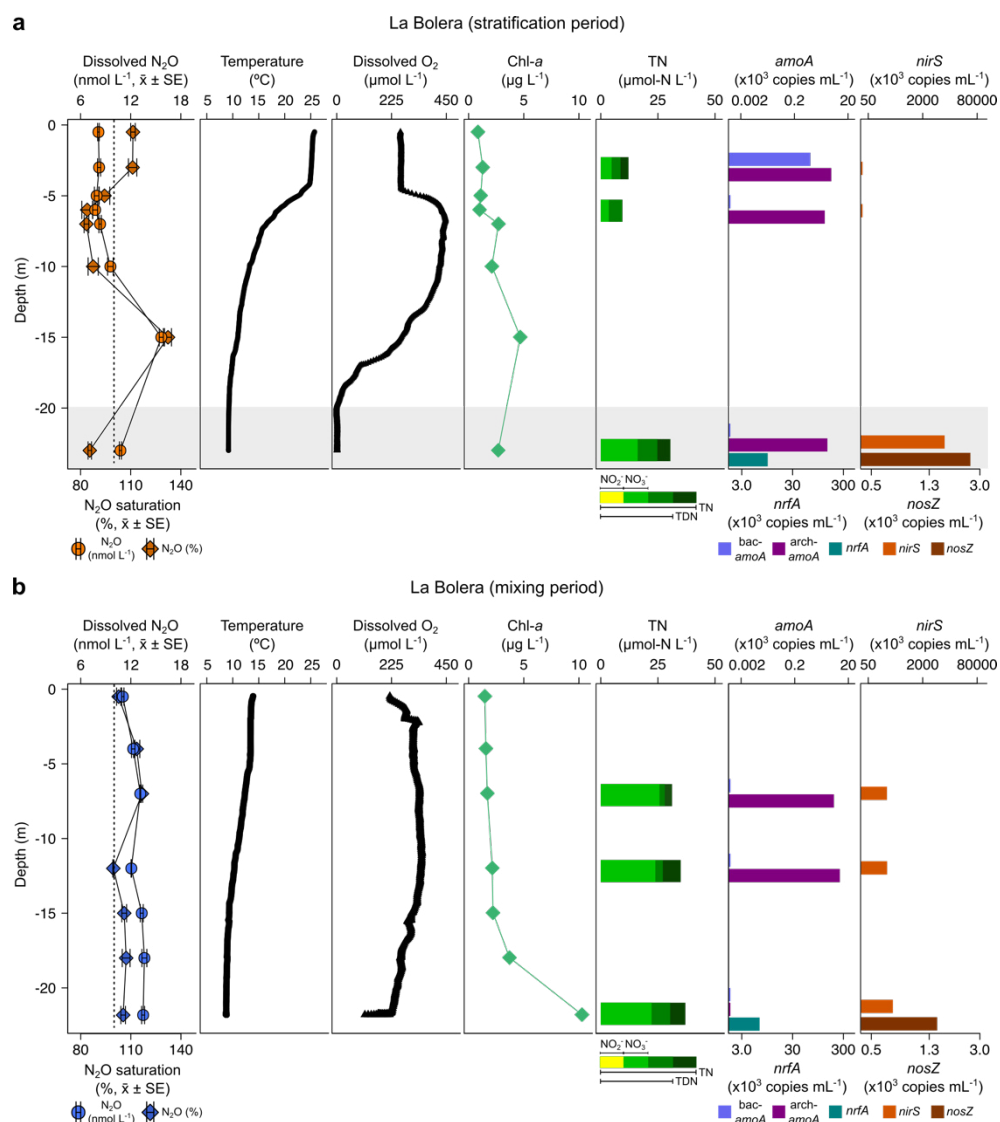
Driver	Equation	n	adj. R ²	p-value
Water temperature (°C)	Not significantly related	178		0.335
Dissolved oxygen concentration (DO, μmol L ⁻¹)	$N_2O = 44.51 \times 10^{-0.002 \text{ DO}}$	178	0.24	< 0.001
Total nitrogen concentration (TN, μmol-N L ⁻¹)	$N_2O = 0.93 \text{ TN}^{0.79}$	77	0.43	< 0.001
Total dissolved nitrogen concentration (TDN, μmol-N L ⁻¹)	$N_2O = \text{TDN}^{0.79}$	77	0.44	< 0.001
Dissolved inorganic nitrogen concentration (DIN, μmol-N L ⁻¹)	$N_2O = 1.87 \text{ DIN}^{0.66}$	77	0.43	< 0.001
Nitrate concentration (NO ₃ ⁻ , μmol-N L ⁻¹)	$N_2O = 1.88 (\text{NO}_3^-)^{0.66}$	77	0.43	< 0.001
Nitrite concentration (NO ₂ ⁻ , μmol-N L ⁻¹)	Not significantly related	24		0.768
Dissolved organic carbon concentration (DOC, μmol-C L ⁻¹)	Not significantly related	77		0.301
Total phosphorus concentration (TP, μmol-P L ⁻¹)	$N_2O = 25.07 \text{ TP}^{0.44}$	75	0.19	< 0.001
DOC : DIN molar ratio (μmol-C : μmol-N)	$N_2O = 36.47 \text{ DOC:DIN}^{-0.52}$	77	0.31	< 0.001
DIN : TP molar ratio (μmol-N : μmol-P)	$N_2O = 2.37 \text{ DIN:TP}^{0.47}$	77	0.20	< 0.001

Supplementary Table 6.2. Results of the Generalized Additive Models (GAMs) fitted to the dissolved N_2O concentration (nmol L^{-1}) as function of the concentration of total nitrogen (TN, $\mu\text{mol L}^{-1}$), and the abundance of the gene *nirS* (copies mL^{-1}) in the water column. S.E. = Standard Error; EDF = Estimated Degrees of Freedom.

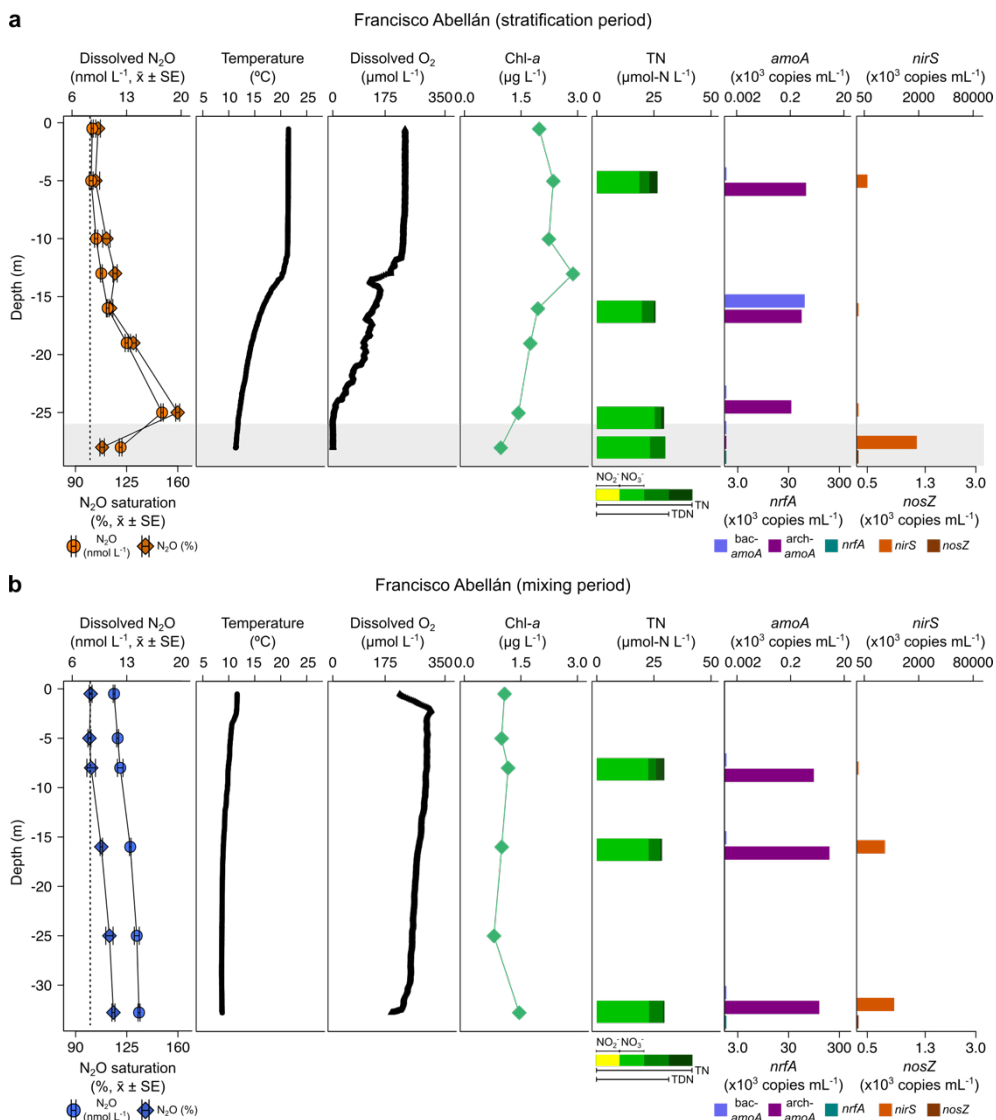
	Predictor variable	Estimate (\pm SE)	EDF	t-value	F-value	p-value
Log_{10} (dissolved N_2O , nmol L^{-1}) n = 69 $R^2_{\text{adj}} = 0.60$ Deviance explained = 61.6 % GCV = 0.09 AIC = 27.87	Intercept	1.30 (0.03)		38.31		<0.001
	Log_{10} (TN, $\mu\text{mol-N L}^{-1}$)		1.68		22.33	<0.001
	Log_{10} (<i>nirS</i> copies mL^{-1})		1.80		13.64	<0.001

Supplementary Table 6.3. Relationships among the abundance of the gene *nirS* (copies mL⁻¹) and the physico-chemical and biological variables in the water column of the study reservoirs.

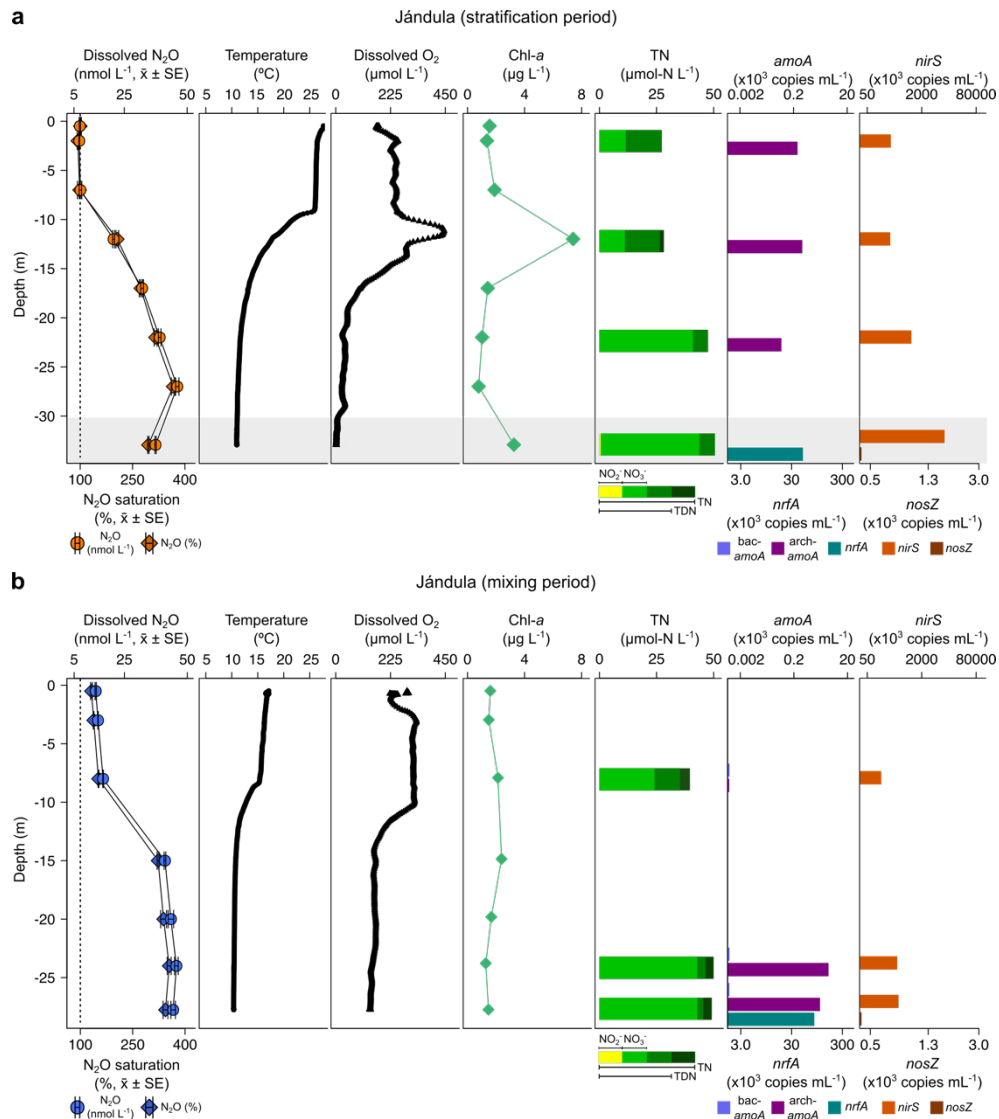
Driver	Equation	n	adj R ²	p-value
Water temperature (°C)	Not significantly related	69		0.358
Dissolved oxygen concentration (DO, μmol L ⁻¹)	$= 5.0 \times 10^6 \text{ Copies } e^{-0.011 \text{ DO}}$	69	0.56	< 0.001
Total nitrogen concentration (TN, μmol-N L ⁻¹)	$= 6.3 \times 10^4 \text{ Copies } \text{TN}^{0.54}$	69	0.06	< 0.05
Total dissolved nitrogen concentration (TDN, μmol-N L ⁻¹)	$= 6.7 \times 10^4 \text{ Copies } \text{TDN}^{0.54}$	69	0.06	0.379
Dissolved inorganic nitrogen concentration (DIN, μmol-N L ⁻¹)	Not significantly related	69		0.106
Nitrate concentration (NO ₃ ⁻ , μmol-N L ⁻¹)	Not significantly related	69		0.145
Nitrite concentration (NO ₂ ⁻ , μmol-N L ⁻¹)	$= 4.0 \times 10^5 \text{ Copies } (\text{NO}_2^- + 1)^{0.53}$	69	0.04	< 0.05
Dissolved organic carbon concentration (DOC, μmol-C L ⁻¹)	Not significantly related	69		0.762
Total phosphorus concentration (TP, μmol-P L ⁻¹)	$= 1.4 \times 10^6 \text{ Copies } \text{TP}^{1.12}$	69	0.21	< 0.001
DOC : DIN molar ratio (μmol-C : μmol-N)	Not significantly related	69		0.102
Chl- <i>a</i> concentration (μg L ⁻¹)	Not significantly related	69		0.417
Cumulative Chl- <i>a</i> (mg m ⁻²)	$5.9 \times 10^4 \text{ Copies } = \text{Cum Chl-}a^{0.64}$	69	0.20	< 0.001



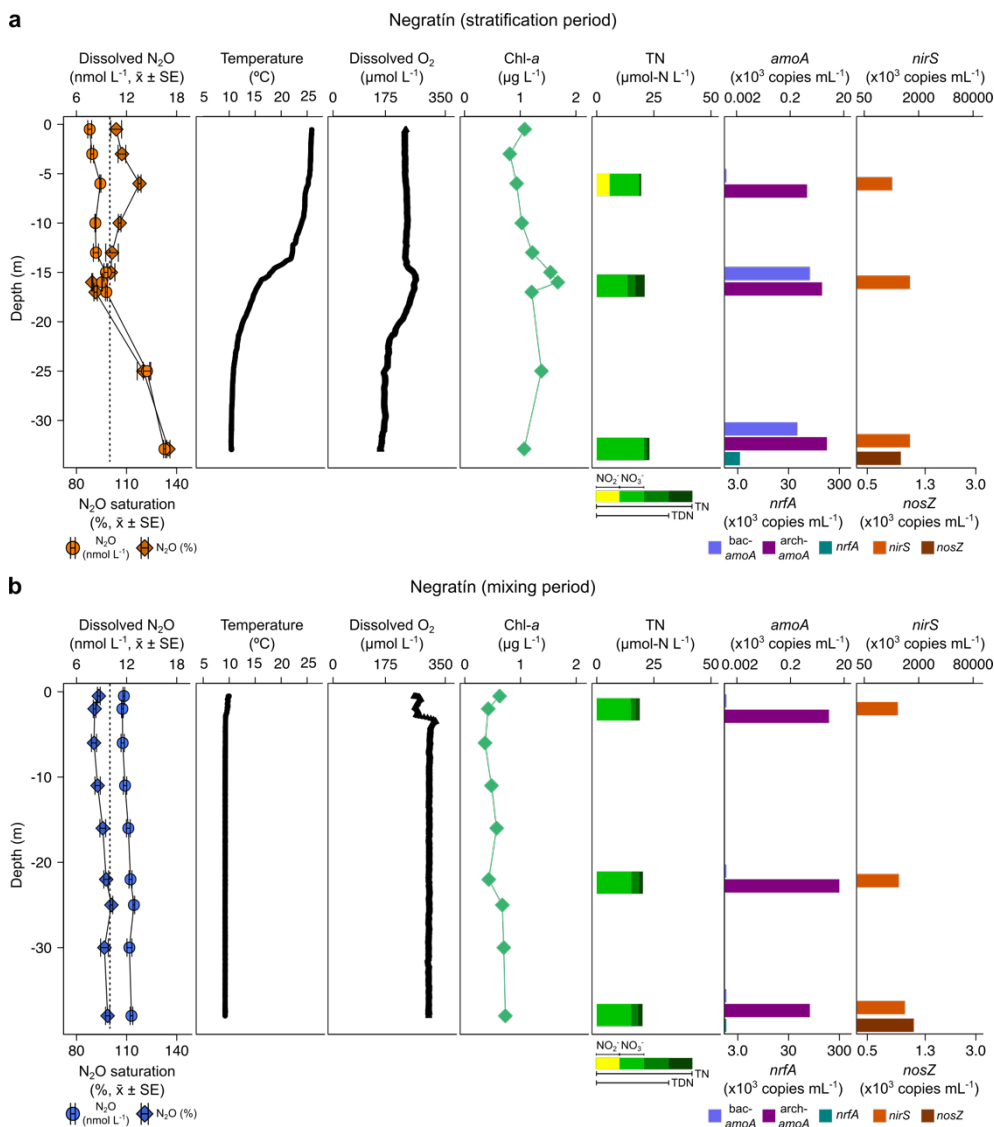
Supplementary Figure 6.1. Vertical profiles of physicochemical and biological variables in La Bolera reservoir. Dissolved nitrous oxide (N_2O) concentration ($nmol L^{-1}$, mean \pm standard error, circles), nitrous oxide saturation (%), and atmospheric equilibrium concentration (discontinuous line); water temperature ($^{\circ}C$); dissolved oxygen (DO) concentration ($\mu mol L^{-1}$); chlorophyll-*a* (Chl-*a*) concentration ($\mu g L^{-1}$); total nitrogen (TN) concentration ($\mu mol-N L^{-1}$); abundance of the genes *amoA* (bacterial *amoA* and archaeal *amoA*, $\times 10^3$ copies mL^{-1}); abundance of the gene *nrfA* ($\times 10^3$ copies mL^{-1}), and abundance of the genes *nirS* and *nosZ* ($\times 10^3$ copies mL^{-1}) during the stratification period (a) and the mixing period (b). Note that the gene abundance axes are in logarithmic scale. The grey area represents the anoxic zone ($DO < 7.5 \mu mol L^{-1}$). The sampling date for the stratification period was on July 28, 2016 and April 8, 2017 for the mixing period.



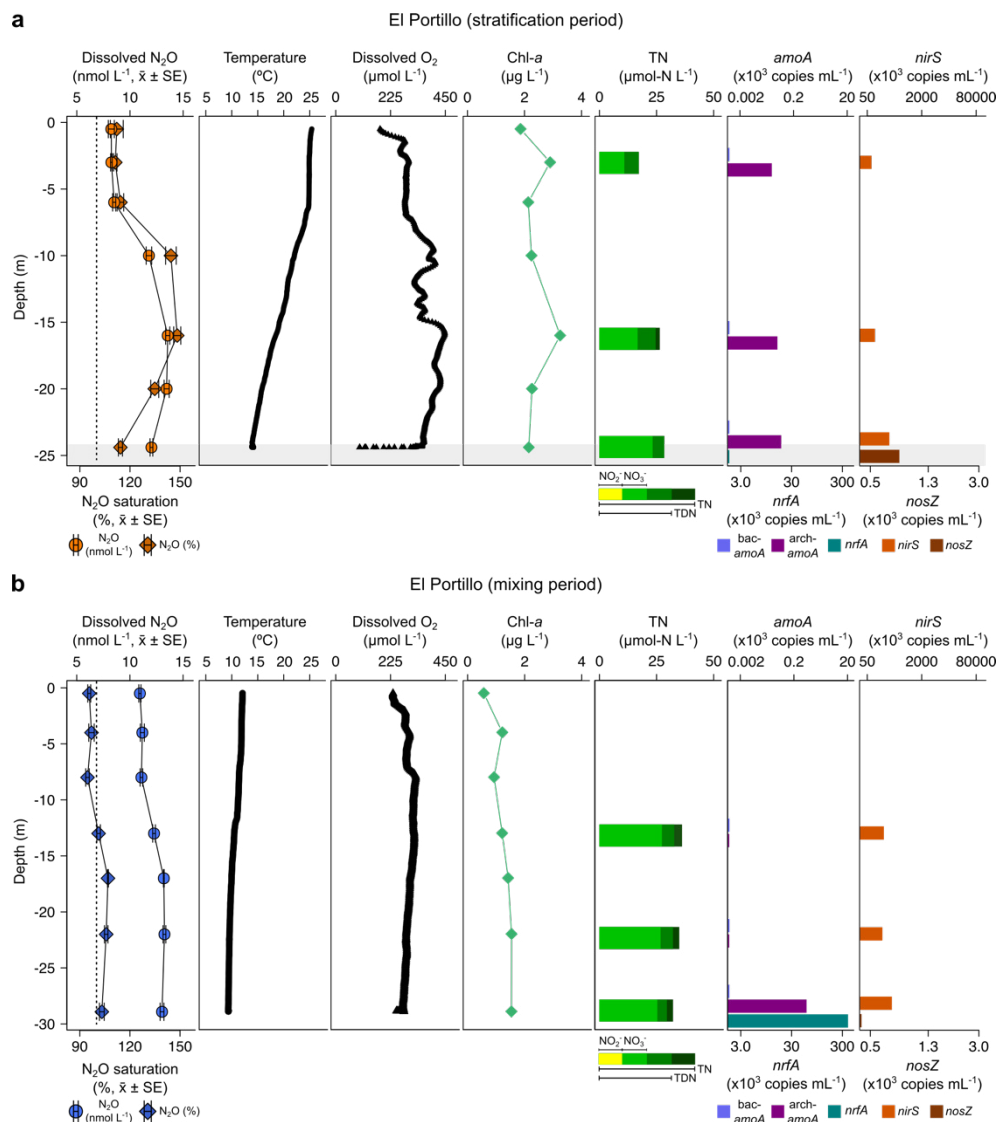
Supplementary Figure 6.2. Vertical profiles of physicochemical and biological variables in Francisco Abellán reservoir. Dissolved nitrous oxide (N_2O) concentration ($nmol L^{-1}$, mean \pm standard error, circles), nitrous oxide saturation (%), mean \pm standard error, diamonds), and atmospheric equilibrium concentration (discontinuous line); water temperature ($^{\circ}C$); dissolved oxygen (DO) concentration ($\mu mol L^{-1}$); chlorophyll-*a* (Chl-*a*) concentration ($\mu g L^{-1}$); total nitrogen (TN) concentration ($\mu mol-N L^{-1}$); abundance of the genes *amoA* (bacterial *amoA* and archaeal *amoA*, $\times 10^3$ copies mL^{-1}); abundance of the gene *nrfA* ($\times 10^3$ copies mL^{-1}), and abundance of the genes *nirS* and *nosZ* ($\times 10^3$ copies mL^{-1}) during the stratification period (a) and the mixing period (b). Note that the gene abundance axes are in logarithmic scale. The grey area represents the anoxic zone ($DO < 7.5 \mu mol L^{-1}$). The sampling date for the stratification period was on September 28, 2016 and March 21, 2017 for the mixing period.



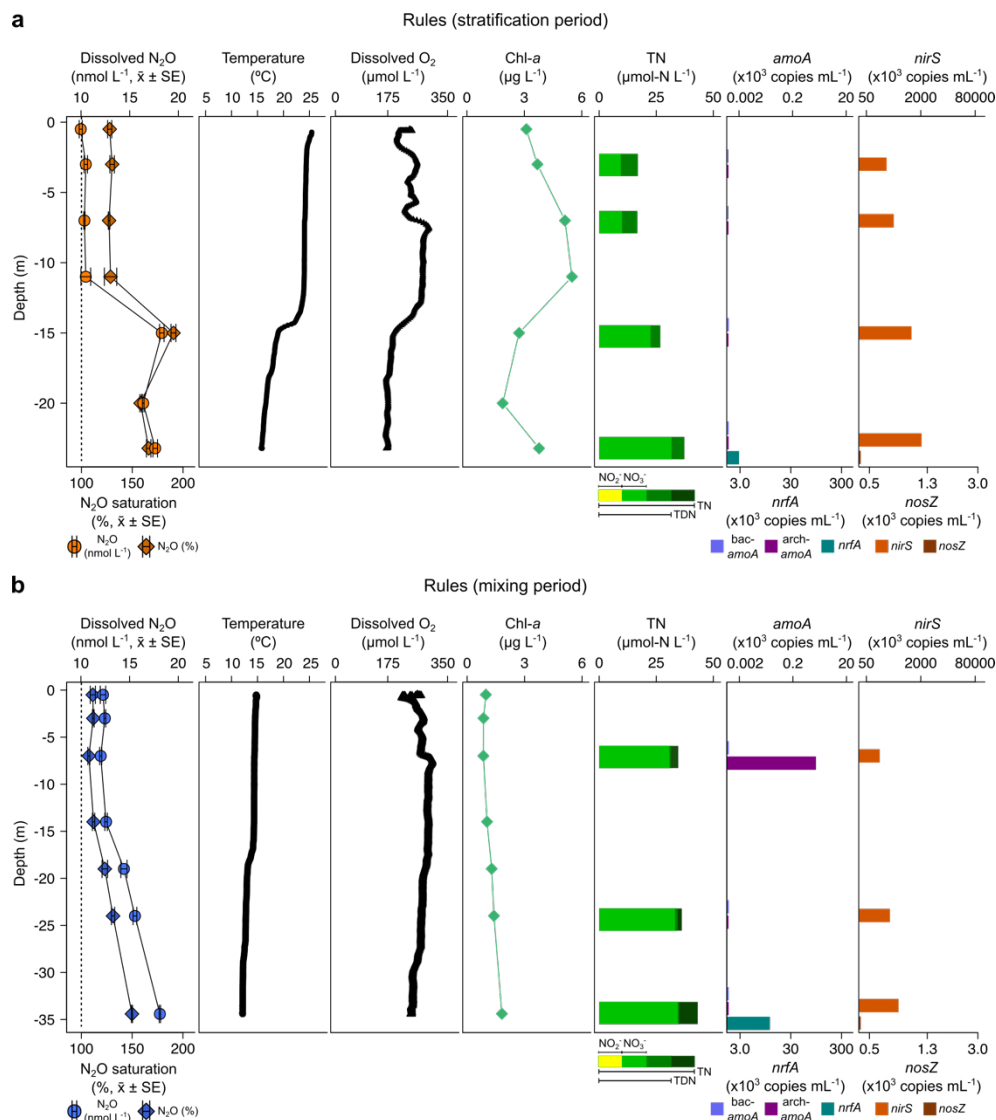
Supplementary Figure 6.3. Vertical profiles of physicochemical and biological variables in Jándula reservoir. Dissolved nitrous oxide (N_2O) concentration (nmol L^{-1} , mean \pm standard error, circles), nitrous oxide saturation (%), mean \pm standard error, diamonds), and atmospheric equilibrium concentration (discontinuous line); water temperature ($^{\circ}\text{C}$); dissolved oxygen (DO) concentration ($\mu\text{mol L}^{-1}$); chlorophyll-*a* (Chl-*a*) concentration ($\mu\text{g L}^{-1}$); total nitrogen (TN) concentration ($\mu\text{mol-N L}^{-1}$); abundance of the genes *amoA* (bacterial *amoA* and archaeal *amoA*, $\times 10^3$ copies mL^{-1}); abundance of the gene *nrfA* ($\times 10^3$ copies mL^{-1}), and abundance of the genes *nirS* and *nosZ* ($\times 10^3$ copies mL^{-1}) during the stratification period (a) and the mixing period (b). Note that the gene abundance axes are in logarithmic scale. The grey area represents the anoxic zone ($\text{DO} < 7.5 \mu\text{mol L}^{-1}$). The sampling date for the stratification period was on 24 July and 5 April 2017 for the mixing period.



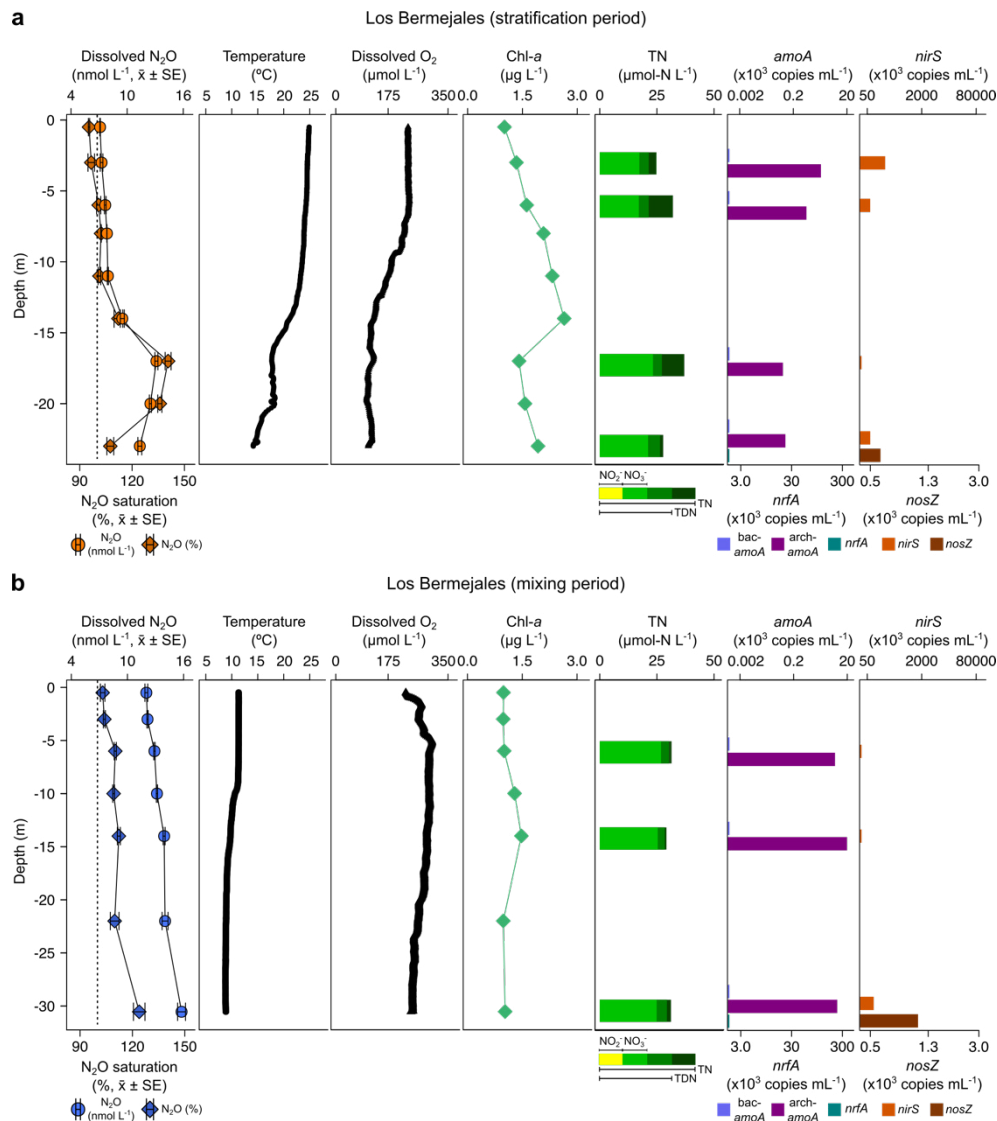
Supplementary Figure 6.4. Vertical profiles of physicochemical and biological variables in Negratín reservoir. Dissolved nitrous oxide (N₂O) concentration (nmol L⁻¹, mean ± standard error, circles), nitrous oxide saturation (%), and atmospheric equilibrium concentration (discontinuous line); water temperature (°C); dissolved oxygen (DO) concentration (µmol L⁻¹); chlorophyll-*a* (Chl-*a*) concentration (µg L⁻¹); total nitrogen (TN) concentration (µmol-N L⁻¹); abundance of the genes *amoA* (bacterial *amoA* and archaeal *amoA*, x 10³ copies mL⁻¹); abundance of the gene *nrfA* (x 10³ copies mL⁻¹), and abundance of the genes *nirS* and *nosZ* (x 10³ copies mL⁻¹) during the stratification period (a) and the mixing period (b). Note that the gene abundance axes are in logarithmic scale. The sampling date for the stratification period was on 27 July 2016 and 16 February 2017 for the mixing period.



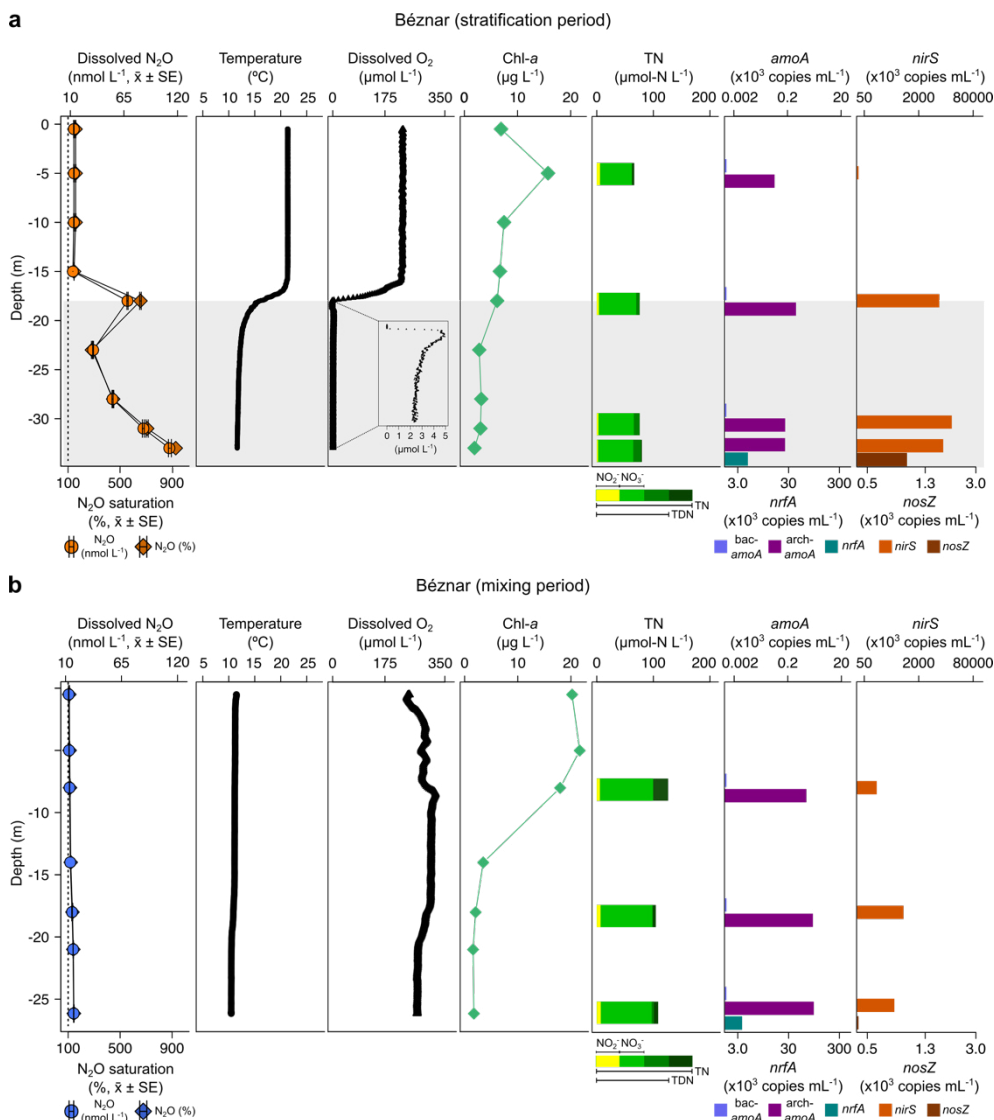
Supplementary Figure 6.5. Vertical profiles of physicochemical and biological variables in El Portillo reservoir. Dissolved nitrous oxide (N_2O) concentration (nmol L^{-1} , mean \pm standard error, circles), nitrous oxide saturation (%), and atmospheric equilibrium concentration (discontinuous line); water temperature ($^{\circ}\text{C}$); dissolved oxygen (DO) concentration ($\mu\text{mol L}^{-1}$); chlorophyll-*a* (Chl-*a*) concentration ($\mu\text{g L}^{-1}$); total nitrogen (TN) concentration ($\mu\text{mol-N L}^{-1}$); abundance of the genes *amoA* (bacterial *amoA* and archaeal *amoA*, $\times 10^3$ copies mL^{-1}); abundance of the gene *nrfA* ($\times 10^3$ copies mL^{-1}), and abundance of the genes *nirS* and *nosZ* ($\times 10^3$ copies mL^{-1}) during the stratification period (a) and the mixing period (b). Note that the gene abundance axes are in logarithmic scale. The grey area represents the anoxic zone ($\text{DO} < 7.5 \mu\text{mol L}^{-1}$). The sampling date for the stratification period was on July 18, 2017 and March 30, 2017 for the mixing period.



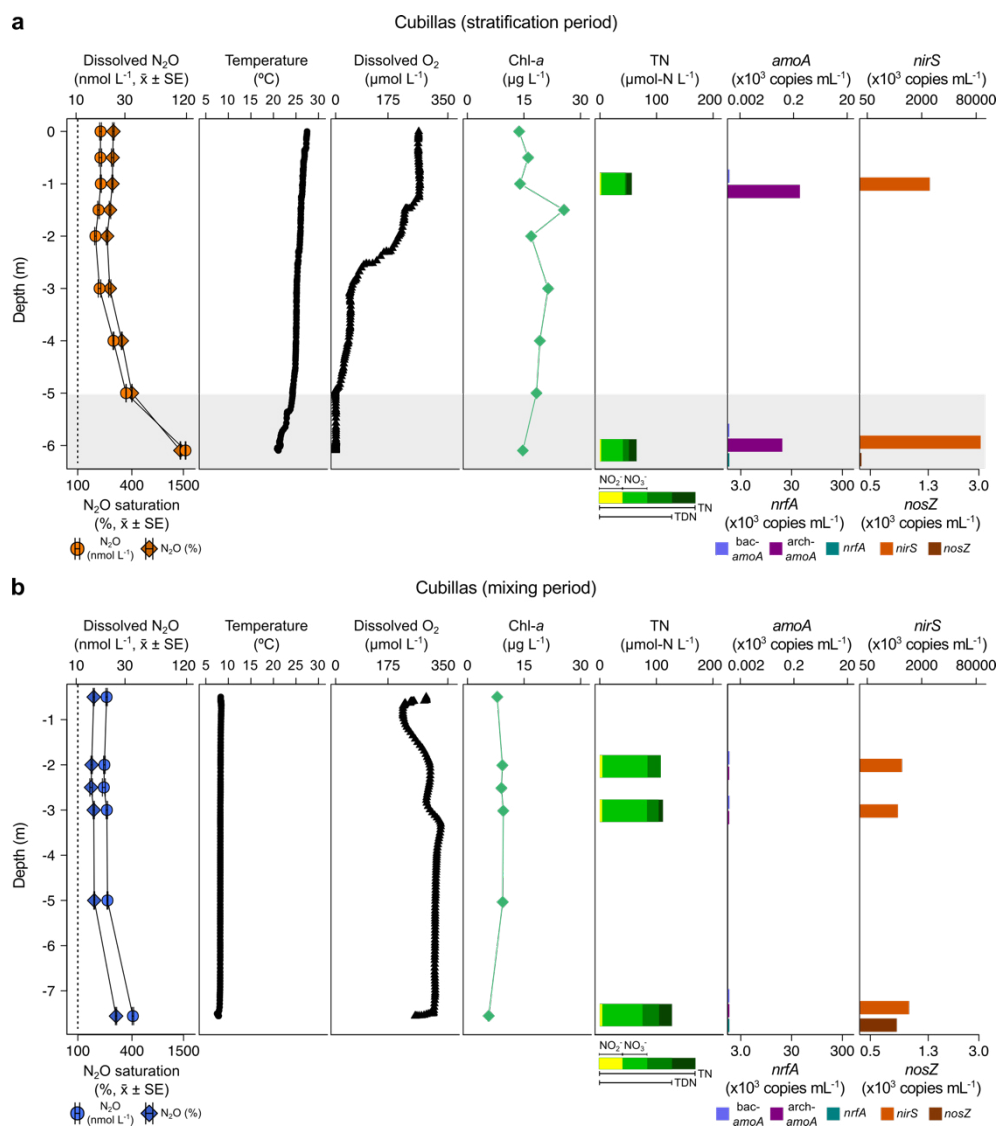
Supplementary Figure 6.6. Vertical profiles of physicochemical and biological variables in Rules reservoir. Dissolved nitrous oxide (N_2O) concentration ($nmol L^{-1}$, mean \pm standard error, circles), nitrous oxide saturation (%), mean \pm standard error, diamonds), and atmospheric equilibrium concentration (discontinuous line); water temperature ($^{\circ}C$); dissolved oxygen (DO) concentration ($\mu mol L^{-1}$); chlorophyll-*a* (Chl-*a*) concentration ($\mu g L^{-1}$); total nitrogen (TN) concentration ($\mu mol-N L^{-1}$); abundance of the genes *amoA* (bacterial *amoA* and archaeal *amoA*, $x 10^3$ copies mL^{-1}); abundance of the gene *nrfA* ($x 10^3$ copies mL^{-1}), and abundance of the genes *nirS* and *nosZ* ($x 10^3$ copies mL^{-1}) during the stratification period (a) and the mixing period (b). Note that the gene abundance axes are in logarithmic scale. The sampling date for the stratification period was on July 10, 2017 and April 7, 2017 for the mixing period.



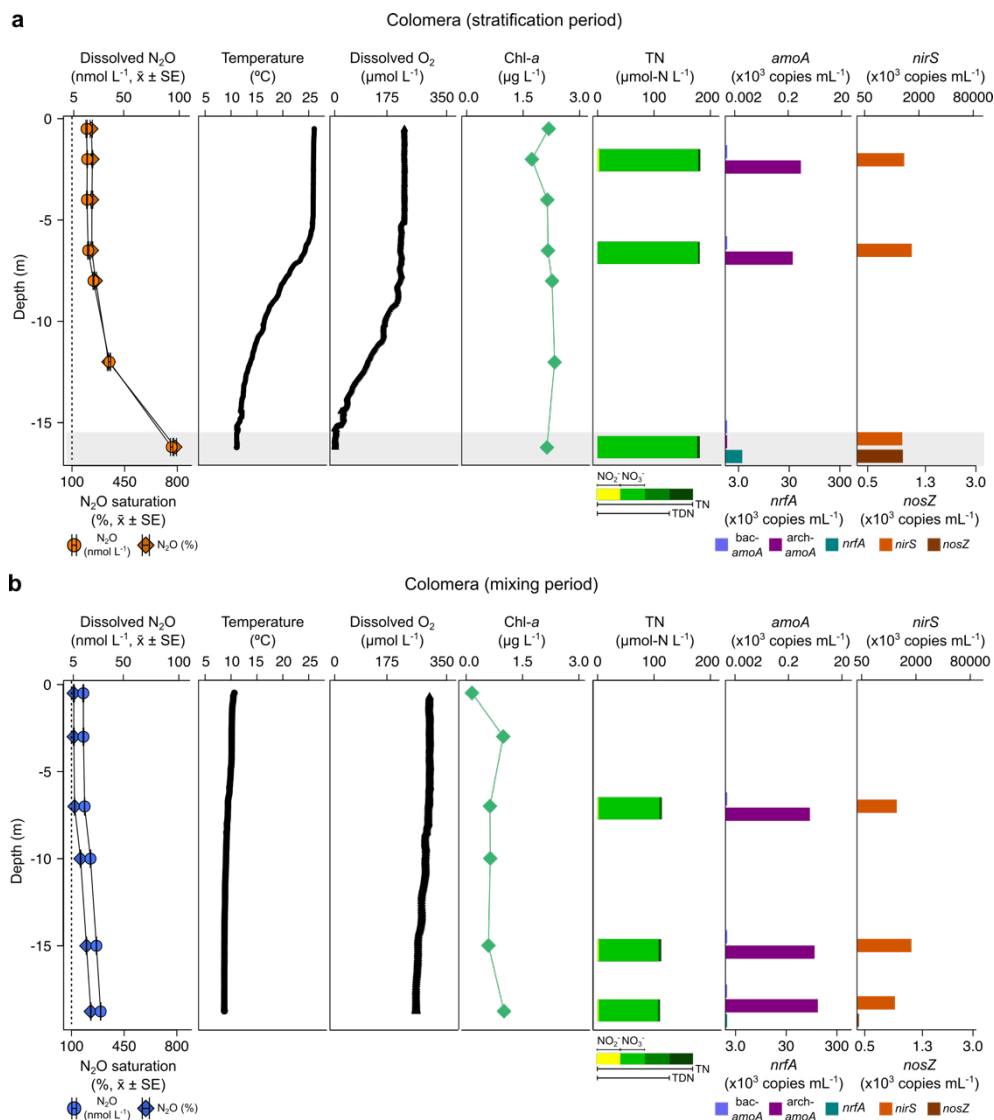
Supplementary Figure 6.7. Vertical profiles of physicochemical and biological variables in Los Bermejales reservoir. Dissolved nitrous oxide (N_2O) concentration ($nmol L^{-1}$, mean \pm standard error, circles), nitrous oxide saturation (%), mean \pm standard error, diamonds), and atmospheric equilibrium concentration (discontinuous line); water temperature ($^{\circ}C$); dissolved oxygen (DO) concentration ($\mu mol L^{-1}$); chlorophyll-*a* (*Chl-a*) concentration ($\mu g L^{-1}$); total nitrogen (*TN*) concentration ($\mu mol-N L^{-1}$); abundance of the genes *amoA* (bacterial *amoA* and archaeal *amoA*, $\times 10^3$ copies mL^{-1}); abundance of the gene *nrfA* ($\times 10^3$ copies mL^{-1}), and abundance of the genes *nirS* and *nosZ* ($\times 10^3$ copies mL^{-1}) during the stratification period (a) and the mixing period (b). Note that the gene abundance axes are in logarithmic scale. The sampling date for the stratification period was on September 7, 2016 and March 17, 2017 for the mixing period.



Supplementary Figure 6.8. Vertical profiles of physicochemical and biological variables in Bézarn reservoir. Dissolved nitrous oxide (N_2O) concentration (nmol L^{-1} , mean \pm standard error, circles), nitrous oxide saturation (%), mean \pm standard error, diamonds), and atmospheric equilibrium concentration (discontinuous line); water temperature ($^{\circ}\text{C}$); dissolved oxygen (DO) concentration ($\mu\text{mol L}^{-1}$); chlorophyll-*a* (Chl-*a*) concentration ($\mu\text{g L}^{-1}$); total nitrogen (TN) concentration ($\mu\text{mol-N L}^{-1}$); abundance of the genes *amoA* (bacterial *amoA* and archaeal *amoA*, $\times 10^3$ copies mL^{-1}); abundance of the gene *nrfA* ($\times 10^3$ copies mL^{-1}), and abundance of the genes *nirS* and *nosZ* ($\times 10^3$ copies mL^{-1}) during the stratification period (a) and the mixing period (b). Note that the gene abundance axes are in logarithmic scale. The grey area represents the anoxic zone ($\text{DO} < 7.5 \mu\text{mol L}^{-1}$). The sampling date for the stratification period was on 7 October 2016 and 23 February 2017 for the mixing period.



Supplementary Figure 6.9. Vertical profiles of physicochemical and biological variables in Cubillas reservoir. Dissolved nitrous oxide (N_2O) concentration (nmol L^{-1} , mean \pm standard error, circles), nitrous oxide saturation (%), mean \pm standard error, diamonds), and atmospheric equilibrium concentration (discontinuous line); water temperature ($^{\circ}\text{C}$); dissolved oxygen (DO) concentration ($\mu\text{mol L}^{-1}$); chlorophyll-*a* (Chl-*a*) concentration ($\mu\text{g L}^{-1}$); total nitrogen (TN) concentration ($\mu\text{mol-N L}^{-1}$); abundance of the genes *amoA* (bacterial *amoA* and archaeal *amoA*, $\times 10^3$ copies mL^{-1}); abundance of the gene *nrfA* ($\times 10^3$ copies mL^{-1}), and abundance of the genes *nirS* and *nosZ* ($\times 10^3$ copies mL^{-1}) during the stratification period (a) and the mixing period (b). Note that the N_2O , and the gene abundance axes are in logarithmic scale. The grey area represents the anoxic zone ($\text{DO} < 7.5 \mu\text{mol L}^{-1}$). The sampling date for the stratification period was on July 14, 2016 and February 2, 2017 for the mixing period.



Supplementary Figure 6.10. Vertical profiles of physicochemical and biological variables in Colomera reservoir. Dissolved nitrous oxide (N₂O) concentration (nmol L⁻¹, mean ± standard error, circles), nitrous oxide saturation (%), and atmospheric equilibrium concentration (discontinuous line); water temperature (°C); dissolved oxygen (DO) concentration (µmol L⁻¹); chlorophyll-*a* (Chl-*a*) concentration (µg L⁻¹); total nitrogen (TN) concentration (µmol-N L⁻¹); abundance of the genes *amoA* (bacterial *amoA* and archaeal *amoA*, x 10³ copies mL⁻¹); abundance of the gene *nrfA* (x 10³ copies mL⁻¹), and abundance of the genes *nirS* and *nosZ* (x 10³ copies mL⁻¹) during the stratification period (a) and the mixing period (b). Note that the gene abundance axes are in logarithmic scale. The grey area represents the anoxic zone (DO < 7.5 µmol L⁻¹). The sampling date for the stratification period was on July 22, 2016 and March 8, 2017 for the mixing period.

Appendix 7:

Supplementary Material for Chapter 7

Nitrous oxide production from ammonium and nitrate in the water column of two reservoirs

Supplementary Material:

Supplementary Tables 7.1 - 7.5

Supplementary Figures 7.1 - 7.6

Supplementary Table 7.1. Dissolved N₂O concentration ($\mu\text{mol-N L}^{-1}$), and saturation (%), dissolved organic carbon (DOC) concentration ($\mu\text{mol-C L}^{-1}$), nitrate (NO_3^-), nitrite (NO_2^-), and ammonia (NH_4^+) concentrations ($\mu\text{mol-N L}^{-1}$), and chlorophyll-*a* (Chl-*a*) concentration ($\mu\text{g L}^{-1}$) measured during the July and September sampling in Cubillas and Iznájar reservoirs. SE = standard error. SD = standard deviation.

Reservoir	Depth	Dissolved N ₂ O ± SE	N ₂ O saturation ± SE	DOC ± SD	NO ₃ ⁻	NO ₂ ⁻	NH ₄ ⁺	Chl- <i>a</i>
Cubillas (July)	Epilimnion (2 m) #1	0.11 ± 0.00	739 ± 27	247.7 ± 4.6	376.0	13.8	1.6	5.4
	Oxycline (7 m) #2	0.71 ± 0.01	4075 ± 29	227.4 ± 6.5	333.6	29.8	0.0	13.9
	Bottom (9.5 m) #3	6.38 ± 0.04	31822 ± 207	246.4 ± 8.6	254.0	17.0	4.3	6.9
Cubillas (September)	Epilimnion (0.5 m) #4	0.22 ± 0.00	1404 ± 11	246.5 ± 1.1	177.8	19.3	2.5	18.1
	Epilimnion (2.5 m) #5	0.22 ± 0.00	1424 ± 10	235.9 ± 5.8	176.7	19.3	0.0	14.6
	Bottom (6.3 m) #6	0.42 ± 0.00	2565 ± 27	217.6 ± 0.2	132.7	33.0	6.9	12.7
Iznájar (July)	Epilimnion (3 m) #7	0.05 ± 0.00	357 ± 5	228.0 ± 9.5	367.6	20.6	0.0	6.3
	Oxycline (8 m) #8	0.18 ± 0.00	1059 ± 10	191.0 ± 0.5	361.6	38.1	5.7	12.4
	Hypolimnion (20 m) #9	0.26 ± 0.00	1137 ± 7	198.5 ± 0.6	391.8	9.6	0.0	4.7
Iznájar (September)	Epilimnion (5 m) #10	0.20 ± 0.00	1308 ± 17	217.3 ± 3.0	335.3	22.9	0.0	7.0
	Oxycline (11 m) #11	0.47 ± 0.00	3072 ± 8	192.1 ± 2.8	314.6	40.8	0.0	8.3
	Hypolimnion (23 m) #12	3.60 ± 0.00	16585 ± 105	186.0 ± 8.3	338.0	2.8	8.7	3.8

Supplementary Table 7.2. Concentrations ($\mu\text{mol-N L}^{-1}$) and isotopic composition of the nitrate ($\delta^{15}\text{N-NO}_3^-$, ‰), the nitrite ($\delta^{15}\text{N-NO}_2^-$, ‰) and the N_2O pools ($\delta^{15}\text{N-N}_2\text{O}$ and $\delta^{18}\text{O-N}_2\text{O}$, ‰) in July and September in Cubillas and Iznájar reservoir.

Reservoir	Depth	NO_3^-	$\delta^{15}\text{N-NO}_3^-$	NO_2^-	$\delta^{15}\text{N-NO}_2^-$	N_2O	$\delta^{15}\text{N-N}_2\text{O}$	$\delta^{18}\text{O-N}_2\text{O}$
Cubillas (July)	Epilimnion (2 m) #1	376.0	11.88	13.8	-36.83	0.11	7.16	21.33
	Oxycline (7 m) #2	333.6	12.11	29.8	-6.89	0.71	-0.01	21.68
	Bottom (9.5 m) #3	254.0	10.95	17.0	10.92	6.38	0.08	10.93
Cubillas (September)	Epilimnion (0.5 m) #4	177.8	13.35	19.3	-11.66	0.22	5.50	21.77
	Epilimnion (2.5 m) #5	176.7	11.62	19.3	-11.86	0.22	5.68	21.66
	Bottom (6.3 m) #6	132.7	9.69	33.0	23.01	0.42	3.51	28.14
Iznájar (July)	Epilimnion (3 m) #7	367.6	10.11	20.6	-26.76	0.05	-1.48	11.34
	Oxycline (8 m) #8	361.6	10.39	38.1	-13.26	0.18	-7.51	14.34
	Hypolimnion (20 m) #9	391.8	8.86	9.6	-18.63	0.26	-10.44	20.08
Iznájar (September)	Epilimnion (5 m) #10	335.3	12.58	22.9	-21.41	0.20	-5.38	13.73
	Oxycline (11 m) #11	314.6	9.65	40.8	-9.12	0.47	-5.64	14.13
	Hypolimnion (23 m) #12	338.0	11.80	2.8	8.77	3.60	0.05	21.64

Supplementary Table 7.3. In situ abundance of the gene archaeal *amoA* (mean \pm SD, copies mL⁻¹), *nrfA* (mean \pm SD, copies mL⁻¹), *nirS* (mean \pm SD, copies mL⁻¹), and *nosZ* (mean \pm SD, copies mL⁻¹) detected in July and September in Cubillas and Iznájar reservoirs. SD = standard deviation. NP = not performed.

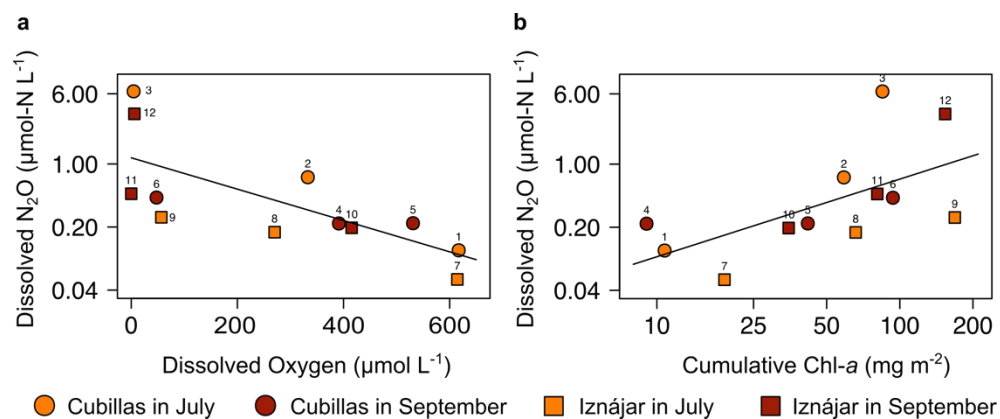
Reservoir	Depth	Archaeal <i>amoA</i> \pm SD (copies mL ⁻¹)	<i>nrfA</i> \pm SD (copies mL ⁻¹)	<i>nirS</i> \pm SD (copies mL ⁻¹)	<i>nosZ</i> \pm SD (copies mL ⁻¹)
Cubillas (July)	Epilimnion (2 m) #1	0	NP	$5.9 \times 10^4 \pm 5.5 \cdot 10^3$	NP
	Oxycline (7 m) #2	$2.7 \times 10^3 \pm 385$	NP	$5.3 \times 10^4 \pm 2.3 \cdot 10^4$	NP
	Bottom (9.5 m) #3	0	0	$5.3 \times 10^5 \pm 3.6 \cdot 10^5$	800 ± 54
Cubillas (September)	Epilimnion (0.5 m) #4	$1.1 \times 10^3 \pm 214$	NP	$4.5 \times 10^4 \pm 2.7 \cdot 10^4$	NP
	Epilimnion (2.5 m) #5	609 ± 120	NP	$5.6 \times 10^4 \pm 1.3 \cdot 10^4$	NP
	Bottom (6.3 m) #6	324 ± 285	$5.1 \times 10^3 \pm 1.5 \cdot 10^2$	$2.8 \times 10^5 \pm 3.2 \cdot 10^3$	913 ± 68
Iznájar (July)	Epilimnion (3 m) #7	$1.3 \times 10^3 \pm 120$	NP	$8.1 \times 10^4 \pm 2.6 \cdot 10^4$	NP
	Oxycline (8 m) #8	995 ± 441	NP	$4.6 \times 10^5 \pm 6.1 \cdot 10^4$	NP
	Hypolimnion (20 m) #9	$1.3 \times 10^3 \pm 110$	0	$4.8 \times 10^5 \pm 4.6 \cdot 10^5$	$1.2 \times 10^3 \pm 302$
Iznájar (September)	Epilimnion (5 m) #10	$1.1 \times 10^3 \pm 216$	NP	$1.7 \times 10^5 \pm 3.6 \cdot 10^4$	NP
	Oxycline (11 m) #11	$1.6 \times 10^3 \pm 24$	NP	$8.0 \times 10^5 \pm 2.3 \cdot 10^5$	NP
	Hypolimnion (23 m) #12	$1.1 \times 10^3 \pm 406$	0	$4.7 \times 10^6 \pm 1.3 \cdot 10^6$	$2.1 \cdot 10^3 \pm 198$

Supplementary Table 7.4. Summary of the production rates measured during the incubations with ¹⁵N-labelled ammonia. All the rates are supplied in nmol-N L⁻¹ d⁻¹. The yield is supplied in %.

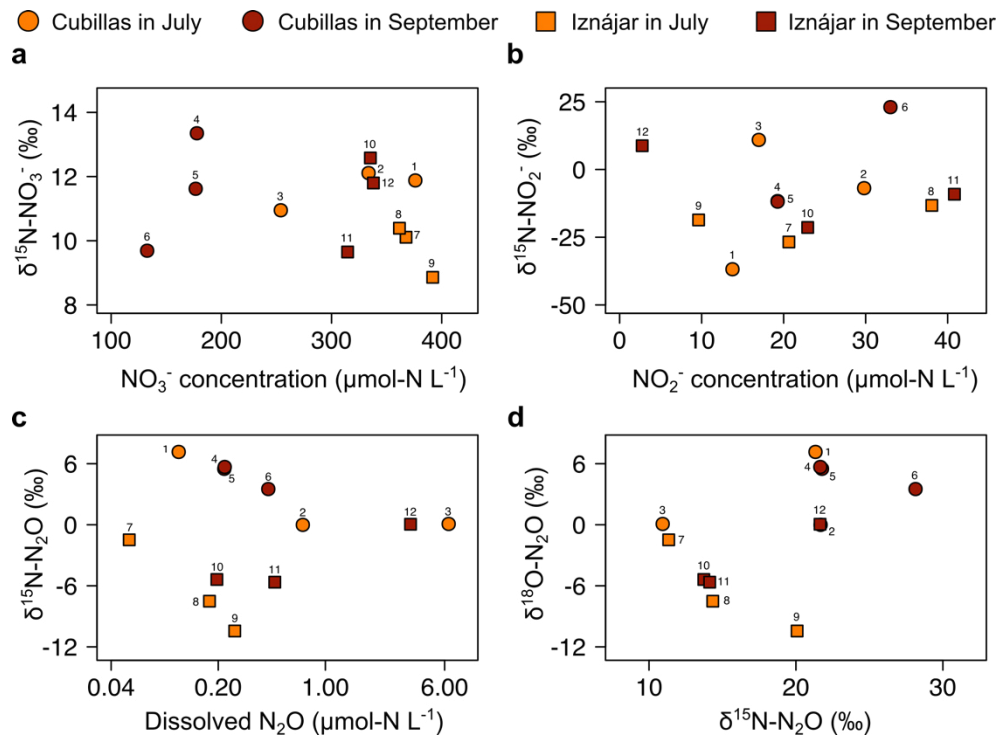
Reservoir	Depth	N ₂ O production from NH ₄ ⁺	Ammonia oxidation (NO ₂ ⁻ from NH ₄ ⁺)	Nitrification (NO ₃ ⁻ from NH ₄ ⁺)	N ₂ O yield from nitrification
Cubillas (July)	Epilimnion (2 m) #1	2.2 ± 0.1	0.0	26851.0 ± 4979.6	0.008
	Oxycline (7 m) #2	0.3 ± 0.1	0.0	13252.7 ± 1133.0	0.002
	Bottom (9.5 m) #3	22.2 ± 4.2	0.0	56110.5 ± 18597.3	0.039
Cubillas (September)	Epilimnion (0.5 m) #4	0.4 ± 0.2	0.0	15620.3 ± 3446.7	0.002
	Epilimnion (2.5 m) #5	0.3 ± 0.0	-38.9 ± 14.7	6094.8 ± 1508.7	0.006
	Bottom (6.3 m) #6	6.3 ± 0.5	336.8 ± 255.3	15394.9 ± 4710.3	0.041
	Epilimnion (3 m) #7	1.7 ± 0.0	0.0	5406.3 ± 1431.3	0.031
Iznájar (July)	Oxycline (8 m) #8	1.2 ± 0.4	-712.8 ± 26.3	36706.9 ± 14785.9	0.003
	Hypolimnion (20 m) #9	0.2 ± 0.1	0.0	8981.3 ± 6030.7	0.002
	Epilimnion (5 m) #10	0.1 ± 0.0	0.0	2856.3 ± 1002.6	0.002
Iznájar (September)	Oxycline (11 m) #11	1.2 ± 0.1	0.0	3702.8 ± 1178.2	0.032
	Hypolimnion (23 m) #12	38.0 ± 3.4	215.8 ± 38.0	0.0	0.0

Supplementary Table 7.5. Summary of the production rates measured during the incubations with ¹⁵N-labelled nitrate. All the rates are supplied in nmol-N L⁻¹ d⁻¹. The yield is supplied in %.

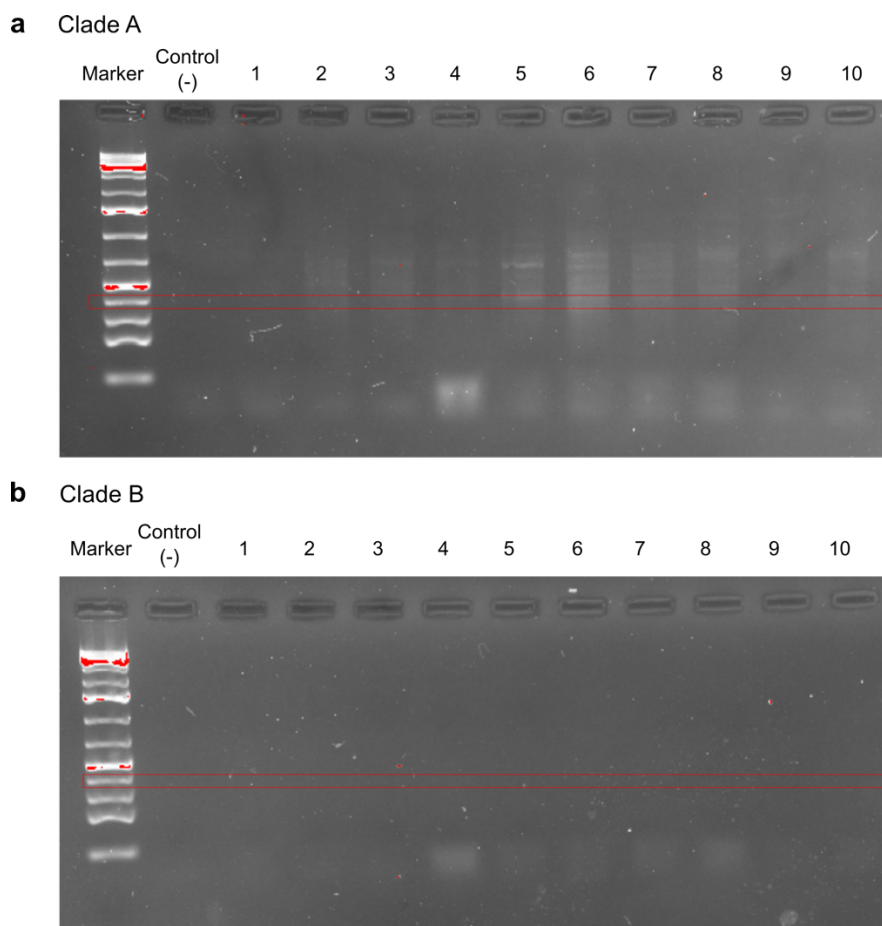
Reservoir	Depth	N ₂ O production from NO ₃	Nitrate reduction (NO ₂ from NO ₃)	N ₂ O yield from denitrification
Cubillas (July)	Epilimnion (2 m) #1	NP	NP	NP
	Oxycline (7 m) #2	8.0 ± 1.4	33182.2 ± 1284.1	0.024
	Bottom (9.5 m) #3	6.2 ± 2.7	30791.6 ± 2477.1	0.020
Cubillas (September)	Epilimnion (0.5 m) #4	NP	NP	NP
	Epilimnion (2.5 m) #5	NP	NP	NP
	Bottom (6.3 m) #6	12.5 ± 3.0	13696.4 ± 1150.9	0.091
Iznájar (July)	Epilimnion (3 m) #7	NP	NP	NP
	Oxycline (8 m) #8	3.2 ± 0.5	34555.4 ± 7634.0	0.009
	Hypolimnion (20 m) #9	3.9 ± 0.0	17354.2 ± 125.5	0.023
Iznájar (September)	Epilimnion (5 m) #10	NP	NP	NP
	Oxycline (11 m) #11	117.7 ± 79.1	10068.0 ± 1456	1.156
	Hypolimnion (23 m) #12	36.9 ± 0.9	12920.9 ± 520.0	0.285



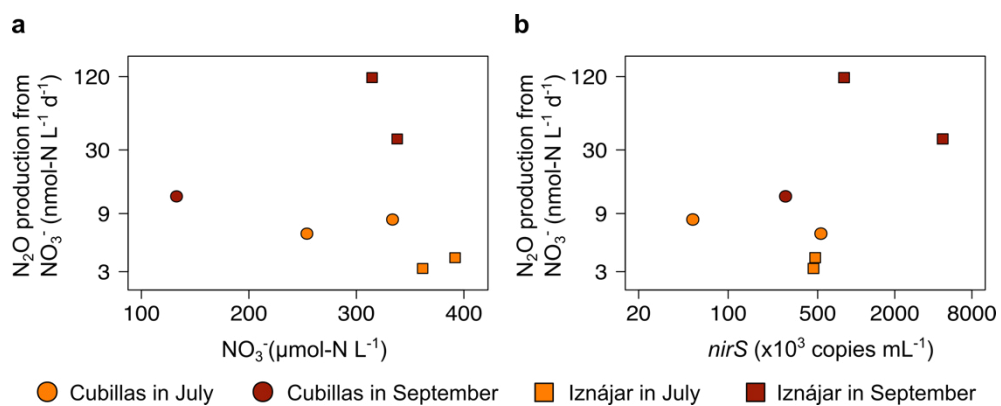
Supplementary Figure 7.1. (a) The dissolved N_2O concentration ($\mu\text{mol-N L}^{-1}$) was an exponential function of the dissolved oxygen ($\mu\text{mol-N L}^{-1}$): dissolved N_2O , $\mu\text{mol-N L}^{-1} = 1.17 e^{(-0.004 \text{ DO}, \mu\text{mol L}^{-1})}$ ($n = 12$, adj $R^2 = 0.50$, p-value < 0.01); (b) The dissolved N_2O also depended on the cumulative Chl-*a* concentration ($\text{mg Chl-}a \text{ m}^{-2}$) following a power function: dissolved N_2O , $\mu\text{mol-N L}^{-1} = 0.013 (\text{Cum Chl-}a, \text{mg m}^{-2})^{0.86}$ ($n = 12$, adj $R^2 = 0.30$, p-value < 0.05). Note the logarithmic scales in the y-axis in (a) and (b), and in x-axis in (b). The tables show the correspondence between samples and numbers.



Supplementary Figure 7.2. Relationships between the concentrations of the nitrate, nitrite, and the dissolved N_2O ($\mu\text{mol-N L}^{-1}$), and their natural isotopic compositions. (a) Scatterplot of the concentration of NO_3^- and its nitrogen isotopic composition ($\delta^{15}\text{N}-\text{NO}_3^-$, ‰); (b) scatterplot of the concentration of NO_2^- and its nitrogen isotopic composition ($\delta^{15}\text{N}-\text{NO}_2^-$, ‰); (c) scatterplot of the concentration of N_2O and its nitrogen isotopic composition ($\delta^{15}\text{N}-\text{N}_2\text{O}$, ‰); and (d) the nitrogen isotopic composition ($\delta^{15}\text{N}-\text{N}_2\text{O}$) versus the oxygen isotopic composition of N_2O ($\delta^{18}\text{O}-\text{N}_2\text{O}$). Note the logarithmic scales in the x-axis in (c). Supplementary table 7.1. shows the correspondence between samples and numbers. Values are provided in supplementary table 7.1 and 7.2.



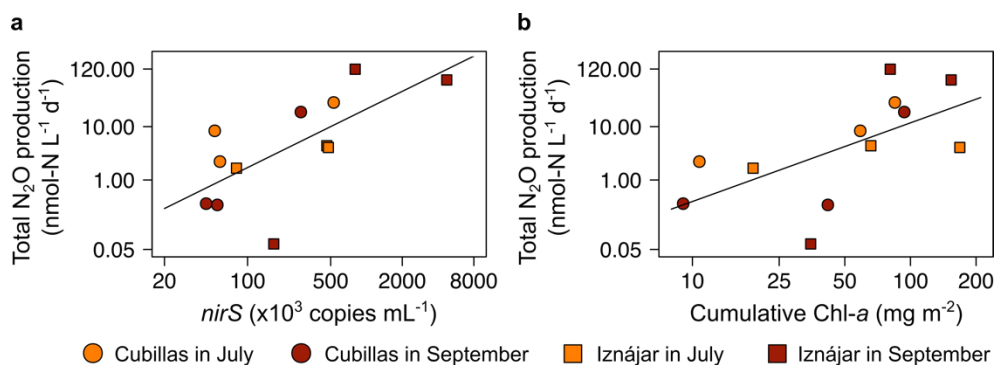
Supplementary Figure 7.3. Results of the PCR for the comammox *amoA* genes. PCR results resolved on 1.5 % agarose gel electrophoresis. We used the two degenerate PCR primer pars from Pjevac *et al.* (2017) to target the clade A (a) or the clade B (b) of comammox bacteria, with an expected amplicon length of 415 bp. The red boxes stand for the \approx 400 bp bands. In this order: the DNA marker, the negative controls, and samples (1-10). The samples displayed correspond to the following depths: 1: Cubillas epilimnion in July (2 m); 2: Iznájar epilimnion in July (3 m); 3: Iznájar oxycline in July (8 m); 4: Iznájar hypolimnion in July (20); 5: Cubillas epilimnion in September (0.5 m); 6: Cubillas epilimnion in September (2.5 m); 7: Cubillas oxycline-bottom in September (6.3 m); 8: Iznájar epilimnion in September (5 m); 9: Iznájar oxycline in September (11 m); and 10: Iznájar hypolimnion in September (23 m). We provide more details in the Methods section.



Supplementary Figure 7.4. Drivers of the production of N_2O from NO_3^- . (a) Scatterplot of the production of N_2O from NO_3^- ($\text{nmol-N L}^{-1} \text{d}^{-1}$) in the incubation and the in situ concentration of NO_3^- ($\mu\text{mol-N L}^{-1}$), (b) scatterplot of the production of N_2O and the in situ abundance of the gene *nirS* ($\times 10^3$ copies mL^{-1}). Note the logarithmic scales in the x-axis in (b), and in the y-axis in (a) and (b).



Supplementary Figure 7.5. Picture of an incubation bottle, where the suspended particulate material can be seen.



Supplementary Figure 7.6. Drivers of the N₂O production rates. (a) Relationship between the abundance of the gene *nirS* (copies mL⁻¹) and the total N₂O production rates (nmol-N L⁻¹ d⁻¹). The total production of N₂O depended on the abundance of the gene *nirS* following a power function (total N₂O production, μmol-N L⁻¹ d⁻¹ = 5.6 × 10⁻⁶ (*nirS*, copies mL⁻¹)^{1.10}, n = 12, adj R² = 0.42, p-value < 0.05); (b) Relationship between the cumulative Chl-*a* concentration (mg m⁻²) and the total N₂O production rates. Note that the x and y axes are in logarithmic scales. Total production of N₂O was also a power function on the cumulative Chl-*a* concentration (total N₂O production, μmol-N L⁻¹ d⁻¹ = 0.01 (cumulative Chl-*a*, mg m⁻²)^{1.47}, n = 12, adj R² = 0.32, p-value < 0.05)

References:

Pjevac, P., Schauburger, C., Poghosyan, L., Herbold, C. W., van Kessel, M. A. H. J., Daebeler, A., Steinberger, M., Jetten, M. S. M., Lucker, S., Wagner, M. and Daims, H. (2017). *amoA*-targeted polymerase chain reaction primers for the specific detection and quantification of comammox *Nitrospira* in the Environment, *Frontiers in Microbiology*, 8. doi: 10.3389/fmicb.2017.01508.

Appendix 8:
Supplementary Material for Chapter 8
General Discussion

Supplementary Material:

Supplementary Tables 8.1 - 8.3

Supplementary Figures 8.1 and 8.2

Extended discussion: Variability in the GHG
fluxes and concentrations at different scales

Supplementary Table 8.1. CO₂, CH₄ and N₂O fluxes and corresponding CO₂ equivalents (eq.) in the study reservoirs during the stratification and the mixing periods. The CO₂ eq. were calculated by multiplying the mass-based flux by the 100-year global warming potential of each gas (1 for CO₂, 34 for CH₄ and 298 for N₂O) (IPCC 2013).

Reservoir	Period	CO ₂ fluxes (mean ± SE, mg C m ⁻² d ⁻¹)	CO ₂ fluxes (mg CO ₂ m ⁻² d ⁻¹)	CH ₄ fluxes (mean ± SE, mg C m ⁻² d ⁻¹)	CH ₄ in CO ₂ eq. (mg CO ₂ m ⁻² d ⁻¹)	N ₂ O fluxes (mean ± SE, µg N m ⁻² d ⁻¹)	N ₂ O in CO ₂ eq. (mg CO ₂ m ⁻² d ⁻¹)	Total CO ₂ eq. (mg CO ₂ m ⁻² d ⁻¹)	Total CO ₂ eq. (kg CO ₂ d ⁻¹)
Cubillas #1	Stratification	244.4 ± 37.1	895.7	678.84 ± 226.35	30823.31	352 ± 84	165.03	31884.03	61855.02
Colomera #2	Stratification	393.1 ± 138.7	1440.4	71.39 ± 48.64	3241.40	456 ± 192	213.67	4895.50	13511.58
Negratín #3	Stratification	155.8 ± 50.7	570.8	0.51 ± 0.23	23.17	0 ± 0	0.00	593.95	13963.87
La Bolera #4	Stratification	209.5 ± 8.5	767.6	1.40 ± 0.11	63.59	0 ± 0	0.00	831.15	2402.02
Los Bermejales #5	Stratification	162.5 ± 20.5	595.5	4.21 ± 1.15	191.02	-118 ± 82	-55.25	731.32	4351.33
Iznájar #6	Stratification	161.1 ± 34.5	590.5	19.78 ± 5.62	898.11	3601 ± 1032	1685.93	3174.52	82950.25
Francisco Abellán #7	Stratification	287.6 ± 27.4	1053.7	6.33 ± 0.81	287.38	-132 ± 101	-61.68	1279.40	3108.95
Béznar #8	Stratification	162.3 ± 37.7	594.5	2.06 ± 0.43	93.71	26 ± 60	12.30	700.55	1120.89
San Clemente #9	Stratification	69.0 ± 2.6	252.7	1.76 ± 0.15	80.03	-154 ± 126	-72.12	260.59	979.83
El Portillo #10	Stratification	26.6 ± 10.6	97.3	125.73 ± 11.83	5708.84	0 ± 0	0.00	5806.13	6851.23
Jándula #11	Stratification	-132.0 ± 11.3	-483.6	7.18 ± 1.26	325.97	-63 ± 63	-29.66	-187.25	-1578.53
Rules #12	Stratification	-62.0 ± 4.6	-227.2	2.74 ± 0.27	124.53	-20 ± 20	-9.35	-111.97	-342.63

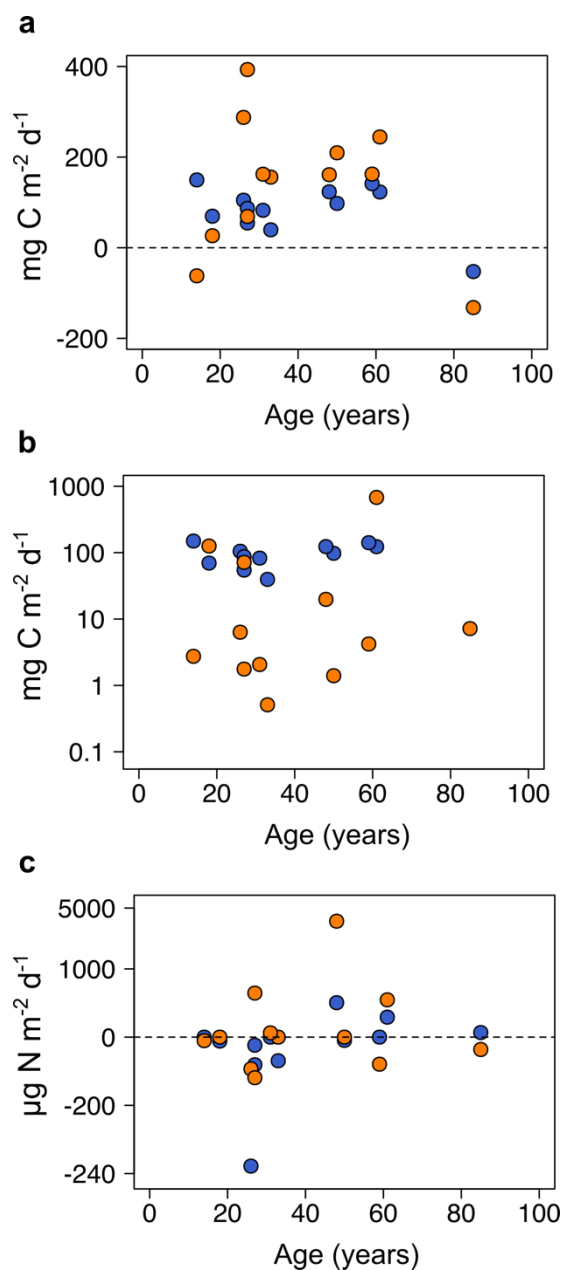
Cubillas #1	Mixing	123.1 ± 32.5	451.0	4.41 ± 1.56	200.44	150 ± 119	70.24	721.65	1400.00
Colomera #2	Mixing	54.6 ± 6.4	200.2	0.64 ± 0.16	29.07	-120 ± 112	-56.08	173.17	477.94
Negratín #3	Mixing	39.6 ± 2.8	145.0	0.10 ± 0.01	4.48	-107 ± 88	-50.03	99.41	2337.12
La Bolera #4	Mixing	97.8 ± 16.5	358.4	0.78 ± 0.14	35.21	-18 ± 18	-8.57	385.04	1112.77
Los Bermejales #5	Mixing	141.3 ± 15.0	517.8	0.63 ± 0.10	28.40	0 ± 0	0.00	546.19	3249.81
Iznájar #6	Mixing	123.4 ± 16.1	452.3	1.29 ± 0.24	58.48	313 ± 67	146.75	657.56	17182.08
Francisco Abellán #7	Mixing	104.9 ± 0.0	384.4	0.54 ± 0.00	24.31	-238 ± 0	-111.47	297.29	722.43
Béznar #8	Mixing	82.7 ± 11.7	303.0	0.46 ± 0.02	21.03	0 ± 0	0.00	324.06	518.50
San Clemente #9	Mixing	87.0 ± 8.0	318.7	0.38 ± 0.05	17.29	-43 ± 43	-20.31	315.68	1186.96
El Portillo #10	Mixing	69.6 ± 20.1	255.0	3.09 ± 0.82	140.10	-22 ± 22	-10.43	384.71	453.96
Jándula #11	Mixing	-52.5 ± 10.6	-192.4	0.34 ± 0.08	15.37	28 ± 28	13.30	-163.75	-1380.40
Rules #12	Mixing	149.6 ± 21.3	548.2	0.76 ± 0.15	34.44	0 ± 0	0.00	582.68	1783.01

Supplementary Table 8.2. Normality, homogeneity of variances, and data comparisons tests of the CO₂, CH₄ and N₂O fluxes between the 24 hours' period and the 8 – 14h period in Cubillas 2016, Cubillas 2018, and Iznájar 2018. We performed the Shapiro-Wilk test for normality analysis, and the F test to compare the variances. For data comparison, we performed t-test for normal distributed data, and Wilcoxon signed-rank test for non-normal distributed data.

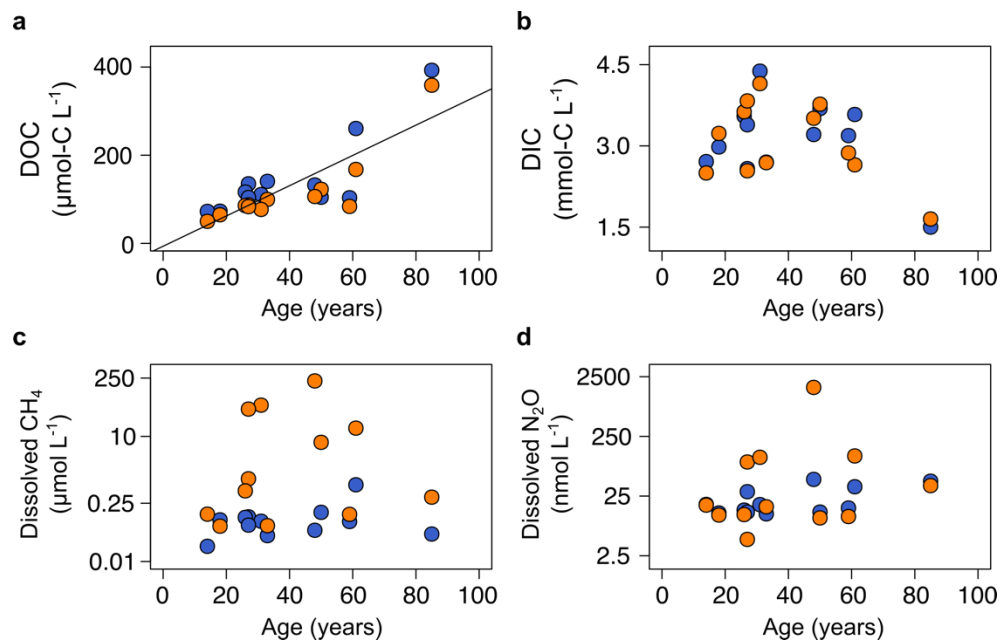
Fluxes	Location	Time period	Normality test		Homogeneity of variances test			Data comparison			
			W	p-value	F	p-value	T- test (t)	Wilcoxon test (W)	df	p-value	
CO ₂	Cubillas 2016	24 hours	0.85	< 0.05							
		8 – 14 h	0.96	0.793	1.73	0.721		18		0.395	
	Cubillas 2018	24 hours	0.75	< 0.001	16.87	< 0.01		50		0.265	
		8 – 14 h	0.86	0.178							
	Iznájar 2018	24 hours	0.91	< 0.05	1.51	0.691		55		0.391	
		8 – 14 h	0.91	0.450							
CH ₄	Cubillas 2016	24 hours	0.90	0.135	0.64	0.494	-0.79	4.25		0.472	
		8 – 14 h	0.88	0.356							
	Cubillas 2018	24 hours	0.90	< 0.05	1.91	0.487		77		0.815	
		8 – 14 h	0.95	0.733							
	Iznájar 2018	24 hours	0.84	< 0.01	1.29	0.849		67		0.815	
		8 – 14 h	0.79	< 0.05							
N ₂ O	Cubillas 2016	24 hours	0.82	< 0.05	3.70	0.309		17		0.335	
		8 – 14 h	0.99	0.951							
	Cubillas 2018	24 hours	0.71	< 0.001	8.63	< 0.05		60		0.551	
		8 – 14 h	0.87	0.240							
	Iznájar 2018	24 hours	0.95	0.269	1.17	0.95	-0.77	8.20		0.461	
		8 – 14 h	0.93	0.550							

Supplementary Table 8.3. Statistical details of the Spearman's correlation between greenhouse gas fluxes. CO₂ and CH₄ fluxes are provided in mg C·m⁻²·d⁻¹, and N₂O is provided in µg N·m⁻²·d⁻¹. Only fluxes > 0 are considered in emissions. rho = correlation coefficient.

Flux 1	Flux 2	n	S	rho	p-value
CO ₂ fluxes	CH ₄ fluxes	24	1562	0.321	0.126
CO ₂ fluxes	N ₂ O fluxes	24	1476	0.358	0.085
CH ₄ fluxes	N ₂ O fluxes	24	1657	0.280	0.186
CO ₂ emissions	CH ₄ emissions	21	860	0.442	< 0.05
CO ₂ emissions	N ₂ O emissions	6	22	0.371	0.497
CH ₄ emissions	N ₂ O emissions	7	18	0.679	0.110



Supplementary Figure 8.1. Scatterplot of the GHG fluxes and the age of the reservoir. (a) CO₂ fluxes, mg C m⁻² d⁻¹ (n = 24, p-value = 0.347) (b) CH₄ fluxes, mg C m⁻² d⁻¹ (n = 24, p-value = 0.758) (c) N₂O fluxes, µg C m⁻² d⁻¹ (n = 24, p-value = 0.294). The orange dots stand for the fluxes during the stratification period, and the blue dots for the fluxes during the mixing period. Note the logarithmic scales in the y axis of (b) and (c).



Supplementary Figure 8.2. Scatterplot of the dissolved organic carbon (DOC), dissolved inorganic carbon (DIC), CH_4 , and N_2O in bottom waters and the age of the reservoir. (a) DOC, $\mu\text{mol-C L}^{-1}$ ($n = 24$, p -value < 0.001 , adjusted $R^2 = 0.64$); (b) DIC, mmol-C L^{-1} ($n=24$, p -value = 0.069); (c) dissolved CH_4 , $\mu\text{mol L}^{-1}$ ($n = 24$, p -value = 0.600); (d) dissolved N_2O , nmol L^{-1} ($n = 24$, p -value = 0.184). The orange dots stand for the values during the stratification period, and the blue dots for the values during the mixing period. Note the logarithmic scales in the y axis of (c) and (d).

Extended discussion: Variability in the GHG fluxes and concentrations at different scales

We analyzed the GHG flux variability at different scales: inter-periods (i.e., stratification vs mixing), inter-systems (i.e., the variance in the GHG fluxes among the study reservoirs in each period), and daily (i.e., the variance in the GHG fluxes during the daily cycles) (Supplementary Table 8.4). By analyzing the variance at these different scales we can understand the ecological patterns and detect the main variability sources, where more scientific effort should be paid in future studies. We detected that the variance in the GHG fluxes between the stratification and the mixing period were significantly different. We found that the variances among reservoirs were higher during the stratification period than during the mixing period for the three GHG fluxes. In the CO₂ fluxes, we detected that the variance between the two study periods in each reservoir ranged from 162.3 to 5.7×10^4 (mg C m⁻² d⁻¹)², and the median value was 4.7×10^3 mg C m⁻² d⁻¹. The median value for the variance among reservoirs, and the daily cycle were similar, and higher than the median of the variance in each reservoir between the two periods. In the Cubillas and Iznájar reservoirs, we detected that variances in the CO₂ fluxes at daily scales were higher than the variances between the stratification and the mixing period. We found that the variance in the CH₄ fluxes between the two study periods in each reservoir ranged from 0.08 to 2.27×10^5 (mg C m⁻² d⁻¹)², and the median value was 11.60 mg C m⁻² d⁻¹. The variance among reservoirs obtained in the summer stratification (i.e., 3.74×10^4 (mg C m⁻² d⁻¹)²) was up to four orders of magnitude higher than the variance in the winter mixing (i.e., 1.68 (mg C m⁻² d⁻¹)²). In the Cubillas and Iznájar reservoirs the variances in the CH₄ fluxes at daily scales were similar than the variances between the stratification and the mixing period of these reservoirs. By comparing the median values, the higher variance was obtained among reservoirs. In the N₂O fluxes, we observed that the variance between the two study periods in each reservoir ranged from 167.44 to 5.40×10^6 (μg N m⁻² d⁻¹)², and the median value was 5.68×10^3 μg N m⁻² d⁻¹. Like CO₂ fluxes, we obtained that the median value for the variance among reservoirs, and the daily cycle were similar and higher than the median of the variance in each reservoir between the two periods. In the Iznájar reservoir, the variance between the two periods was higher than the variance during the daily cycle, but it was similar in the Cubillas reservoir.

Supplementary Table 8.4. Variances in the GHG fluxes in the study reservoirs between the periods, among the reservoirs, and the variance during the daily cycle.

Variances	Location	CO ₂ flux (mg C m ⁻² d ⁻¹) ²	CH ₄ flux (mg C m ⁻² d ⁻¹) ²	N ₂ O flux (μg N m ⁻² d ⁻¹) ²
Inter-period scales: Variances between periods in each reservoir	Cubillas	7.4 × 10 ³	2.27 × 10 ⁵	2.05 × 10 ⁴
	Colomera	5.7 × 10 ⁴	2.50 × 10 ³	1.66 × 10 ⁵
	Negratín	6.8 × 10 ³	0.08	5.71 × 10 ³
	La Bolera	6.2 × 10 ³	0.20	167.44
	Los Bermejales	225.2	6.41	6.96 × 10 ³
	Iznájar	710.7	170.97	5.40 × 10 ⁶
	Francisco Abellán	1.7 × 10 ⁴	16.78	5.65 × 10 ³
	Béznar	3.2 × 10 ³	1.28	345.19
	San Clemente	162.3	0.95	6.12 × 10 ³
	El Portillo	926.8	7.52 × 10 ³	248.02
	Jándula	3.2 × 10 ³	23.40	4.21 × 10 ³
	Rules	2.2 × 10 ⁴	1.97	199.37
		Median	4.7 × 10 ³	11.60
	Minimum	162.3	0.08	167.44
	Maximum	5.7 × 10 ⁴	2.27 × 10 ⁵	5.40 × 10 ⁶
Inter-system scales: Variances among reservoirs during each period:	Stratification	2.1 × 10 ⁴	3.74 × 10 ⁴	1.10 × 10 ⁶
	Mixing	3.0 × 10 ³	1.68	1.88 × 10 ⁴
	Median	1.2 × 10 ⁴	1.87 × 10 ⁴	5.58 × 10 ⁵
Daily scales: Variances during the daily cycle	Cubillas 2016	1.6 × 10 ⁴	2.77 × 10 ⁵	5.52 × 10 ⁴
	Cubillas 2018	1.3 × 10 ⁵	3.00 × 10 ³	4.77 × 10 ⁵
	Iznájar 2018	1.5 × 10 ⁴	199.12	1.43 × 10 ⁵
	Median	1.6 × 10 ⁴	3.00 × 10 ³	1.43 × 10 ⁵

We also studied the variability in the dissolved CH₄ and N₂O in the water column at different scales: within-system (i.e., variability in the water column of each reservoir), inter-system (i.e., by comparing the mean of the dissolved CH₄ and N₂O in the water column among the study reservoirs in each period, and comparing the mean of the dissolved CH₄ and N₂O in each reservoir between the stratification and the mixing periods) (Supplementary Table 8.5). We found that the variances in the dissolved CH₄ in the water column of the reservoirs varied from 2.17 × 10³ to 6.21 × 10⁹ (nmol L⁻¹)² (median = 1.48 × 10⁵ nmol L⁻¹ during the stratification period, and from 31.81 to 2.07 × 10⁴ (median = 594.15 nmol L⁻¹ during the mixing period). The variances

in the dissolved N₂O ranged from 5.58 to 8.90 × 10⁵ (nmol L⁻¹)² (median = 27.48 nmol L⁻¹) during the stratification period, and from 0.25 to 239.44 (nmol L⁻¹)² (median = 2.86 nmol L⁻¹) during the mixing period. We found that the variability in the dissolved CH₄ and N₂O in the water column was higher in the stratification period than in the mixing period. Thermal stratification reduces gas diffusion from hypolimnion, increasing the concentration differences among depths. The variability in CH₄ and N₂O concentrations among reservoirs was also higher during the stratification period than during the mixing period. The variability between the stratification period and the mixing period ranged from 3.32 × 10³ to 1.80 × 10⁹ (nmol L⁻¹)² in the dissolved CH₄ and varied from 0.01 to 6.15 × 10⁵ (nmol L⁻¹)² in the dissolved N₂O. We detected the higher variability in the dissolved CH₄ and N₂O at the inter-system scale than at within-system or inter-period scales.

Supplementary Table 8.5. Variance in the concentration of dissolved CH₄ and N₂O in the water column of the study reservoirs. We used the integrated mean of the dissolved CH₄ and the dissolved N₂O to calculate the variances among the reservoirs between the two periods, and the variances among the reservoirs.

Variance	Location	Dissolved CH ₄ (nmol L ⁻¹) ²		Dissolved N ₂ O (nmol L ⁻¹) ²	
		Stratification	Mixing	Stratification	Mixing
Variances in the water column: within-system scale	Cubillas	9.46 × 10 ⁶	2.07 × 10 ⁴	1.09 × 10 ³	44.83
	Colomera	1.44 × 10 ⁵	2.82 × 10 ³	789.24	43.92
	Negratín	6.83 × 10 ³	31.81	9.02	0.25
	La Bolera	6.09 × 10 ⁶	1.28 × 10 ⁴	7.15	0.89
	Los Bermejales	2.51 × 10 ⁴	1070.51	5.58	1.69
	Iznájar	6.21 × 10 ⁹	545.02	8.90 × 10 ⁵	75.70
	Francisco Abellán	1.20 × 10 ⁴	297.90	9.41	1.81
	Béznar	4.17 × 10 ⁸	200.24	1.35 × 10 ³	3.92
	San Clemente	3.15 × 10 ⁸	643.28	40.17	1.01
	El Portillo	1.53 × 10 ⁵	2.34 × 10 ³	5.88	1.10
	Jándula	6.93 × 10 ⁴	80.28	257.49	239.44
	Rules	2.17 × 10 ³	104.14	14.78	5.11
	Median	1.48 × 10 ⁵	594.15	27.48	2.86
	Minimum	2.17 × 10 ³	31.81	5.58	0.25
Maximum	6.21 × 10 ⁹	2.07 × 10 ⁴	8.90 × 10 ⁵	239.44	
Median between periods		9.42 × 10 ³		9.22	

Variances among reservoirs during each period: inter-system scale	Among reservoirs	2.88×10^8	1.28×10^4	1.05×10^5	51.01
	Median		1.44×10^8		5.24×10^4
Variances between periods: inter-period scales	Cubillas		2.50×10^7		21.84
	Colomera		1.09×10^6		90.48
	Negratín		7.04×10^3		0.61
	La Bolera		7.05×10^5		1.50
	Los Bermejales		1.93×10^4		9.02
	Iznájar		1.80×10^9		6.15×10^5
	Francisco Abellán		2.62×10^4		1.76
	Béznar		6.33×10^7		230.65
	San Clemente		5.11×10^7		0.01
	El Portillo		9.39×10^4		0.41
	Jándula		3.22×10^4		10.71
	Rules		3.32×10^3		0.25
	Median		3.99×10^5		5.39
	Minimum		3.32×10^3		0.01
Maximum		1.80×10^9		6.15×10^5	

GHG emissions and concentrations in reservoirs have a large variability at temporal, and spatial scales. In the three GHG fluxes, we detected that the variance among reservoirs was higher during the stratification than during the mixing. Besides, the inter-season variances were significantly different among the study reservoirs. In CO₂ and N₂O fluxes the variance at spatial and daily scales were higher than the variance at the inter-season scale. The highest inter-season variance was detected in the CH₄ fluxes. The dissolved CH₄ and N₂O showed a considerable variation along the water column of the study reservoirs. We found higher variance in both dissolved gases at the inter-system scale, than at within-system or inter-season scales. Rey-Sanchez *et al.* (2018) studied the fluxes of CO₂ and CH₄ in a Lake Erie estuarine marsh, and they found a variance of $6.89 \times 10^5 \text{ (mg C m}^{-2} \text{ d}^{-1})^2$ for CO₂ fluxes, and $1.03 \times 10^5 \text{ (mg C m}^{-2} \text{ d}^{-1})^2$ for CH₄ fluxes at daily scales. These values are higher than the median of the variance found at daily scales. (Zhang *et al.*, 2019) found that the change of amplitude of diffusive flux at daily scale was much larger than the change occurring

on a monthly timescale in a eutrophic pond, and both variances were lower than the variances of this study. In contrast to our inter-period results, Yang *et al.* (2011) found higher variance at the inter-period than at the daily scale in N₂O fluxes in three rivers.

References:

- Rey-Sanchez, A. C., Morin, T. H., Stefanik, K. C., Wrighton, K. and Bohrer, G. (2018). Determining total emissions and environmental drivers of methane flux in a Lake Erie estuarine marsh, *Ecological Engineering*, 114, pp. 7–15. doi: 10.1016/j.ecoleng.2017.06.042.
- Yang, L., Yan, W., Ma, P. and Wang, J. (2011). Seasonal and diurnal variations in N₂O concentrations and fluxes from three eutrophic rivers in Southeast China, *Journal of Geographical Sciences*, 21(5), p. 820. doi: 10.1007/s11442-011-0882-1.
- Zhang, C., Cheng, S., Li, Y., Zhang, W. and Xiao, S. (2019). Diel methane flux from a subtropical eutrophic pond in November based on continuous monitoring, *Acta Geochimica*. doi: 10.1007/s11631-019-00317-1.

